CAMBRIDGE TEXTS IN APPLIED MATHEMATICS

An Introduction to Magnetohydrodynamics

P.A. DAVIDSON

Magnetic fields influence many natural and man-made flows. They are routinely used in industry to heat, pump, stir and levitate liquid metals. There is the terrestrial magnetic field which is maintained by fluid motion in the earth's core, the solar magnetic field which generates sunspots and solar flares, and the galactic field which influences the formation of stars. This is an introductory text on magnetohydrodynamics (MHD) – the study of the interaction of magnetic fields and conducting fluids.

This book is intended to serve as an introductory text for advanced undergraduate and postgraduate students in physics, applied mathematics and engineering. The material in the text is heavily weighted towards incompressible flows and to terrestrial (as distinct from astrophysical) applications. The final sections of the text also contain an outline of the latest advances in the metallurgical applications of MHD and so are relevant to professional researchers in applied mathematics, engineering and metallurgy.

Dr. P.A. Davidson is a Reader in Fluid Mechanics at the University of Cambridge, where his current research is in fluid mechanics in process metallurgy, turbulence and stability theory. He is the author of over 50 publications, and was awarded the Institute of Materials prize in 1996 for the best paper on non-ferrous metallurgy.

An Introduction to Magnetohydrodynamics

Cambridge Texts in Applied Mathematics

Complex Variables: Introduction and Applications
M.J. Ablowitz and A. S. Fokas

The Space-Time Ray Method
V.M. Babich, I. Molotkov and V.S. Buldyrev

Scaling, Self-Similarity and Intermediate Asymptotics
G.I. Barenblatt

Rarefied Gas Dynamics
Carlo Cercignani

High Speed Flow
C.J. Chapman

Introduction to Numerical Linear Algebra and Optimisation
Philippe G. Ciarlet

Applied Analysis of the Navier–Stokes Equations
C.R. Doering and J.D. Gibbon

Nonlinear Systems
P.G. Drazin

Solitons
P.G. Drazin and R.S. Johnson

Mathematical Models in the Applied Sciences
A. Fowler

Stability, Instability and Chaos
Paul Glendinning

Perturbation Methods
E.J. Hinch

Symmetry Methods for Differential Equations
Peter E. Hydon

A First Course in the Numerical Analysis of Differential Equations
A. Iserles

A Modern Introduction to the Mathematical Theory of Water Waves
R.S. Johnson

The Thermomechanics of Plasticity and Fracture
Gerard A. Maugin

Viscous Flow
H. Ockendon and J.R. Ockendon

Thinking About Ordinary Differential Equations
R. O'Malley

The Kinematics of Mixing
J.M. Ottino

Integral Equations
David Porter and David S.G. Stirling

Boundary Integral and Singularity Methods for Linearized Viscous Flow
C. Pozrikidis

Maximum and Minimum Principles
M.J. Sewell

An Introduction to Magnetohydrodynamics

P. A. DAVIDSON
University of Cambridge

CAMBRIDGE
UNIVERSITY PRESS

CAMBRIDGE UNIVERSITY PRESS
Cambridge, New York, Melbourne, Madrid, Cape Town, Singapore, São Paulo

Cambridge University Press
The Edinburgh Building, Cambridge CB2 2RU, UK

Published in the United States of America by Cambridge University Press, New York

www.cambridge.org
Information on this title: www.cambridge.org/9780521791496

First published 2001

A catalogue record for this publication is available from the British Library

Library of Congress Cataloguing in Publication data
Davidson, P. A. (Peter Alan), 1957–
An introduction to magnetohydrodynamics / P.A. Davidson.
p. cm. — (Cambridge texts in applied mathematics)
Includes bibliographical references.
ISBN 0-521-79149-9—ISBN 0-521-79487-0 (pb)
1. Magnetohydrodynamics. I. Title. II. Series.
QA920.D38 2000
538′.6—dc21
00-033733

ISBN-13 978-0-521-79149-6 hardback
ISBN-10 0-521-79149-9 hardback

ISBN-13 978-0-521-79487-9 paperback
ISBN-10 0-521-79487-0 paperback

Transferred to digital printing 2006

For my family

Contents

Preface

Prefaces are rarely inspiring and, one suspects, seldom read. They generally consist of a dry, factual account of the content of the book, its intended readership and the names of those who assisted in its preparation. There are, of course, exceptions, of which Den Hartog's preface to a text on mechanics is amongst the wittiest. Musing whimsically on the futility of prefaces in general, and on the inevitable demise of those who, like Heaviside, use them to settle old scores, Den Hartog's preface contains barely a single relevant fact. Only in the final paragraph does he touch on more conventional matters with the observation that he has 'placed no deliberate errors in the book, but he has lived long enough to be quite familiar with his own imperfections'.

We, for our part, shall stay with a more conventional format. This work is more of a text than a monograph. Part A (the larger part of the book) is intended to serve as an introductory text for (advanced) undergraduate and post-graduate students in physics, applied mathematics and engineering. Part B, on the other hand, is more of a research monograph and we hope that it will serve as a useful reference for professional researchers in industry and academia. We have at all times attempted to use the appropriate level of mathematics required to expose the underlying phenomena. Too much mathematics can, in our opinion, obscure the interesting physics and needlessly frighten the student. Conversely, a studious avoidance of mathematics inevitably limits the degree to which the phenomena can be adequately explained.

It is our observation that physics graduates are often well versed in the use of Maxwell's equations, but have only a passing acquaintance with fluid mechanics. Engineering graduates often have the opposite background. Consequently, we have decided to develop, more or less from first principles, those aspects of electromagnetism and fluid mechanics

which are most relevant to our subject, and which are often treated inadequately in elementary courses.

The material in the text is heavily weighted towards incompressible flows and to engineering (as distinct from astrophysical) applications. There are two reasons for this. The first is that there already exist several excellent texts on astrophysical, geophysical and plasma MHD, whereas texts oriented towards engineering applications are somewhat thinner on the ground. Second, in recent years we have witnessed a rapid growth in the application of MHD to metallurgical processes. This has spurred a great deal of fruitful research, much of which has yet to find its way into textbooks or monographs. It seems timely to summarise elements of this research. We have not tried to be exhaustive in our coverage of the metallurgical MHD, but we hope to have captured the key advances.

The author is indebted to the late D. Crighton, without whose support this text would never have seen the light of day, to H.K. Moffatt and J.C.R. Hunt for their constant advice over the years, to K. Graham for typing the manuscript, and to C. Davidson for her patience. Above all, the author would like to thank Stephen Davidson who painstakingly read each draft, querying every ambiguity and exposing the many inconsistencies in the original text.

Part A:
The Fundamentals of MHD

> Nothing can be more fatal to progress than a too confident reliance on mathematical symbols; for the student is only too apt to take the easier course, and consider the formula and not the fact as the physical reality.
>
> *Kelvin (1879)*

Introduction: The Aims of Part A

Magnetohydrodynamics (MHD for short) is the study of the interaction between magnetic fields and moving, conducting fluids. In the following seven chapters we set out the fundamental laws of MHD. The discussion is restricted to incompressible flows, and we have given particular emphasis to the elucidation of physical principles rather than detailed mathematical solutions to particular problems.

We presuppose little or no background in fluid mechanics or electromagnetism, but rather develop these topics from first principles. Nor do we assume any knowledge of tensors, the use of which we restrict (more or less) to Chapter 7, in which an introduction to tensor notation is provided. We do, however, make extensive use of vector analysis and the reader is assumed to be fluent in vector calculus.

The subjects covered in Part A are:

1. A qualitative overview of MHD
2. The governing equations of electrodynamics
3. The governing equations of fluid mechanics
4. The kinematics of MHD: advection and diffusion of a magnetic field
5. Dynamics at low magnetic Reynolds' number
6. Dynamics at high magnetic Reynolds' number
7. MHD turbulence at low and high magnetic Reynolds' numbers

One point is worth emphasising from the outset. The governing equations of MHD consist simply of Newton's laws of motion and the pre-Maxwell form of the laws of electrodynamics. The reader is likely to be familiar with elements of both sets of laws and many of the phenomena associated with them. Thus, while the mathematical formulation of MHD may often seem daunting, the underlying physical phenomena

are usually fairly straightforward. It pays, therefore, when confronted with a welter of mathematical detail, to follow the advice of Kelvin and keep asking the question: 'What is really going on?'

In line with this principle, we start, in §1.3, not with fully fledged MHD, but rather with a simple laboratory experiment. This consists of a static magnetic field at right angles to a conducting rod which in turn slides along two conducting rails. Such an apparatus is commonly used in high schools to illustrate Faraday's law of induction. However, when the *dynamics* of the sliding rod are investigated we discover a lot more than just Faraday's law. In fact, this simple experiment illustrates many of the key physical phenomena to be found in MHD. That is to say, a magnetic field, **B**, and a moving, conducting medium interact in such a way as to restrain the relative motion of the field and medium.

We start our formal analysis in Chapters 2 and 3, where we set out the governing equations of MHD. These consist of the Navier–Stokes equation and a simplified version of Maxwell's equations from which Gauss's law is omitted and displacement currents are neglected.

In Chapter 4 we consider one half of the coupling between **B** and the medium. Specifically, we look at the influence of a prescribed fluid velocity, **u**, on the magnetic field without worrying about the origin of the velocity field or the back-reaction of the Lorentz force on the fluid. In effect, we take **u** to be prescribed, dispense with the Navier–Stokes equation, and focus on the rôle of **u** when using Maxwell's equations.

We finally introduce dynamics in Chapters 5 and 6. We start, in Chapter 5, by considering weakly conducting or slowly moving fluids in which the magnetic field greatly influences the motion of the conductor but there is little back-reaction on the imposed magnetic field. This typifies much of liquid-metal MHD. Next, in Chapter 6, we consider highly conducting, or rapidly moving, fluids in which the two-way coupling of **B** and **u** is strong. Here interest focuses on stability theory, which is important in plasma containment, and on dynamo theory, a phenomenon which is of considerable importance in geophysics. We end, in Chapter 7, with a discussion of MHD turbulence.

Throughout Part A emphasis is placed on physical phenomena, rather than mathematical rigor, or engineering applications. This is not so much because we particularly share Rutherford's view of the commanding rôle of physics,[1] although he had a point, but rather that it provides a convenient way of introducing the diverse range of phenomena we call MHD.

[1]Ernest Rutherford is reputed to have said: 'Science is divided into two categories, physics and stamp collecting.'

1

A Qualitative Overview of MHD

> The neglected borderland between two branches of knowledge is often that which best repays cultivation, or, to use a metaphor of Maxwell's, the greatest benefits may be derived from a cross-fertilisation of the sciences.
>
> *Rayleigh (1884)*

1.1 What is MHD?

Magnetic fields influence many natural and man-made flows. They are routinely used in industry to heat, pump, stir and levitate liquid metals. There is the terrestrial magnetic field which is maintained by fluid motion in the earth's core, the solar magnetic field which generates sunspots and solar flares, and the galactic magnetic field which is thought to influence the formation of stars from interstellar clouds. The study of these flows is called magnetohydrodynamics (MHD). Formally, MHD is concerned with the mutual interaction of fluid flow and magnetic fields. The fluids in question must be electrically conducting and non-magnetic, which limits us to liquid metals, hot ionised gases (plasmas) and strong electrolytes.

The mutual interaction of a magnetic field, $\mathbf{B}$, and a velocity field, $\mathbf{u}$, arises partially as a result of the laws of Faraday and Ampère, and partially because of the Lorentz force experienced by a current-carrying body. The exact form of this interaction is analysed in detail in the following chapters, but perhaps it is worth stating now, without any form of proof, the nature of this coupling. It is convenient, although somewhat artificial, to split the process into three parts.

(i) The relative movement of a conducting fluid and a magnetic field causes an e.m.f. (of order $|\mathbf{u} \times \mathbf{B}|$) to develop in accordance with Faraday's law of induction. In general, electrical currents will ensue, the current density being of order $\sigma(\mathbf{u} \times \mathbf{B})$, σ being the electrical conductivity.

(ii) These induced currents must, according to Ampère's law, give rise to a second, induced magnetic field. This adds to the original magnetic

field and the change is usually such that the fluid appears to 'drag' the magnetic field lines along with it.

(iii) The combined magnetic field (imposed plus induced) interacts with the induced current density, $\mathbf{J}$, to give rise to a Lorentz force (per unit volume), $\mathbf{J} \times \mathbf{B}$. This acts on the conductor and is generally directed so as to inhibit the relative movement of the magnetic field and the fluid.

Note that these last two effects have similar consequences. In both cases the relative movement of fluid and field tends to be reduced. Fluids can 'drag' magnetic field lines (effect (ii)) and magnetic fields can pull on conducting fluids (effect (iii)). It is this partial 'freezing together' of the medium and the magnetic field which is the hallmark of MHD.

These effects are, perhaps, more familiar in the context of conventional electrodynamics. Consider a wire loop which is pulled through a magnetic field, as shown in Figure 1.1. As the wire loop is pulled to the right, an e.m.f. of order $|\mathbf{u} \times \mathbf{B}|$ is generated which drives a current as shown (effect (i)). The magnetic field, associated with the induced current perturbs the original magnetic field, and the net result is that the magnetic field lines seem to be dragged along by the wire (effect (ii)). The current also gives rise to a Lorentz force, $\mathbf{J} \times \mathbf{B}$, which acts on the wire in a direction opposite to that of the motion (effect (iii)). Thus it is necessary to provide a force to move the wire. In short, the wire appears to drag the field lines while the magnetic field reacts back on the wire, tending to oppose the relative movement of the two.

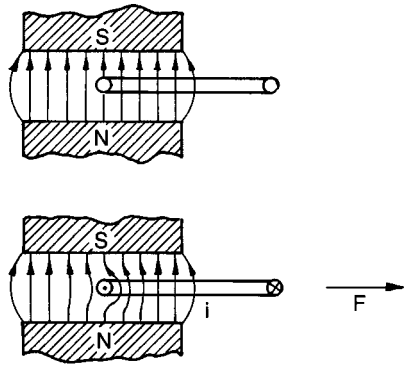

Figure 1.1 Interaction of a magnetic field and a moving wire loop.

Let us consider effect (ii) in a little more detail. As we shall see later, the extent to which a velocity field influences an imposed magnetic field depends on the product of (i) the typical velocity of the motion, (ii) the conductivity of the fluid, and (iii) a characteristic length scale, l, of the motion. Clearly, if the fluid is non-conducting or the velocity negligible there will be no significant induced magnetic field. Conversely, if σ or $\mathbf{u}$ are (in some sense) large, then the induced magnetic field may substantially alter the imposed field. (Consider the wire shown in Figure 1.1. If it is a poor conductor, or moves very slowly, then the induced current, and the associated magnetic field, will be weak.) The reason why l is important is a little less obvious, but may be clarified by the following argument. The e.m.f. generated by a relative movement of the imposed magnetic field and the medium is of order $|\mathbf{u} \times \mathbf{B}|$ and so, by Ohm's law, the induced current density is of the order of $\sigma(|\mathbf{u} \times \mathbf{B}|)$. However, a modest current density spread over a large area can produce a high magnetic field, whereas the same current density spread over a small area induces only a weak magnetic field. It is therefore the product $\sigma \mathbf{u} l$ which determines the ratio of the induced field to the applied magnetic field. In the limit $\sigma \mathbf{u} l \to \infty$ (typical of so-called ideal conductors) the induced and imposed magnetic fields are of the same order. In such cases it turns out that the combined magnetic field behaves as if it were locked into the fluid. Conversely, when $\sigma \mathbf{u} l \to 0$, the imposed magnetic field remains relatively unperturbed. Astrophysical MHD tends to be closer to the first situation, not so much because of the high conductivity of the plasmas involved, but because of the vast characteristic length scale. Liquid-metal MHD, on the other hand, generally lies closer to the second limit, with $\mathbf{u}$ leaving $\mathbf{B}$ unperturbed. Nevertheless, it should be emphasised that effect (iii) is still strong in liquid metals, so that an imposed magnetic field can substantially alter the velocity field.

Perhaps it is worth taking a moment to consider the case of liquid metals in a little more detail. They have a reasonable conductivity ($\sim 10^6 \Omega^{-1} \mathrm{m}^{-1}$), but the velocity involved in a typical laboratory or industrial process is small (~ 1 m/s). As a consequence, the induced current densities are generally rather modest (a few Amps per cm^2). When this is combined with a small length-scale (~ 0.1 m in the laboratory), the induced magnetic field is usually found to be negligible by comparison with the imposed field. There is very little 'freezing together' of the fluid and the magnetic field. However, the imposed magnetic field is often strong enough for the Lorentz force, $\mathbf{J} \times \mathbf{B}$, to dominate the motion of the fluid. We tend to think of the coupling as being one way: $\mathbf{B}$ controls $\mathbf{u}$

through the Lorentz force, but **u** does not substantially alter the imposed field, **B**. There are, however, exceptions. Perhaps the most important of these is the earth's dynamo. Here, motion in the liquid-metal core of the earth twists, stretches and intensifies the terrestrial magnetic field, maintaining it against the natural processes of decay. It is the large length-scales which are important here. While the induced current densities are weak, they are spread over a large area and so their combined effect is to induce a substantial magnetic field.

In summary then, the freezing together of the magnetic field and the medium is usually strong in astrophysics, significant in geophysics, weak in metallurgical MHD and utterly negligible in electrolytes. However, the influence of **B** on **u** can be important in all four situations.

1.2 A Brief History of MHD

The laws of magnetism and fluid flow are hardly a twentieth-century innovation, yet MHD became a fully fledged subject only in the late 1930s or early 1940s. The reason, probably, is that there was little incentive for nineteenth century engineers to capitalise on the possibilities offered by MHD. Thus, while there were a few isolated experiments by nineteenth-century physicists such as Faraday (he tried to measure the voltage across the Thames induced by its motion through the earth's magnetic field), the subject languished until the turn of the century. Things started to change, however, when astrophysicists realised just how ubiquitous magnetic fields and plasmas are throughout the universe. This culminated in 1942 with the discovery of the Alfvén wave, a phenomenon which is peculiar to MHD and important in astrophysics. (A magnetic field line can transmit transverse inertial waves, just like a plucked string.) Around the same time, geophysicists began to suspect that the earth's magnetic field was generated by dynamo action within the liquid-metal of its core, an hypothesis first put forward in 1919 by Larmor in the context of the sun's magnetic field. A period of intense research followed and continues to this day.

Plasma physicists, on the other hand, acquired an interest in MHD in the 1950s as the quest for controlled thermonuclear fusion gathered pace. They were particularly interested in the stability, or lack of stability, of plasmas confined by magnetic fields, and great advances in stability theory were made as a result.

The development of MHD in engineering was slower and did not really get going until the 1960s. However, there was some early pioneering work by the engineer J. Hartmann, who invented the electromagnetic pump in 1918. Hartmann also undertook a systematic theoretical and experimental investigation of the flow of mercury in a homogeneous magnetic field. In the introduction to the 1937 paper describing his researches he observed:

> The invention [his pump] is, as will be seen, no very ingenious one, the principle utilised being borrowed directly from a well-known apparatus for measuring strong magnetic fields. Neither does the device represent a particularly effective pump, the efficiency being extremely low due mainly to the large resistivity of mercury and still more to the contact resistance between the electrodes and the mercury. In spite hereof considerable interest was in the course of time bestowed on the apparatus, firstly because of a good many practical applications in cases where the efficiency is of small moment and then, during later years, owing to its inspiring nature. As a matter of fact, the study of the pump revealed to the author what he considered a new field of investigation, that of flow of a conducting liquid in a magnetic field, a field for which the name Hg-dynamics was suggested.

The name, of course, did not stick, but we may regard Hartmann as the father of liquid-metal MHD, and indeed the term 'Hartmann flow' is now used to describe duct flows in the presence of a magnetic field. Despite Hartmann's early researches, it was only in the early 1960s that MHD began to be exploited in engineering. The impetus for change came largely as a result of three technological innovations: (i) fast-breeder reactors use liquid sodium as a coolant and this needs to be pumped; (ii) controlled thermonuclear fusion requires that the hot plasma be confined away from material surfaces by magnetic forces; and (iii) MHD power generation, in which ionised gas is propelled through a magnetic field, was thought to offer the prospect of improved power station efficiencies. This last innovation turned out to be quite impracticable, and its failure was rather widely publicised in the scientific community. However, as the interest in power generation declined, research into metallurgical MHD took off. Two decades later, magnetic fields are routinely used to heat, pump, stir and levitate liquid metals in the metallurgical industries. The key point is that the Lorentz force provides a non-intrusive means of controlling the flow of metals. With constant commercial pressure to produce cheaper, better and more consistent materials, MHD provides

a unique means of exercising greater control over casting and refining processes.

1.3 From Electrodynamics to MHD: A Simple Experiment

Now the only difference between MHD and conventional electrodynamics lies in the fluidity of the conductor. This makes the interaction between **u** and **B** more subtle and difficult to quantify. Nevertheless, many of the important features of MHD are latent in electrodynamics and can be exposed by simple laboratory experiments. An elementary grasp of electromagnetism is then all that is required to understand the phenomena. Just such an experiment is described below. First, however, we shall discuss those features of MHD which the experiment is intended to illustrate.

1.3.1 Some important parameters in electrodynamics and MHD

Let us introduce some notation. Let μ be the permeability of free space, σ and ρ denote the electrical conductivity and density of the conducting medium, respectively, and l be a characteristic length scale. Three important parameters in MHD are:

$$\text{Magnetic Reynolds number,} \quad R_m = \mu\sigma u l \tag{1.1}$$

$$\text{Alfvèn velocity,} \quad v_a = B/\sqrt{\rho\mu} \tag{1.2}$$

$$\text{Magnetic damping time,} \quad \tau = \left[\sigma B^2/\rho\right]^{-1} \tag{1.3}$$

The first of these parameters may be considered as a dimensionless measure of the conductivity, while the second and third quantities have the dimensions of speed and time, respectively, as their names suggest.

Now we have already hinted that magnetic fields behave very differently depending on the conductivity of the medium. In fact, it turns out to be R_m, rather than σ, which is important. Where R_m is large, the magnetic field lines act rather like elastic bands frozen into the conducting medium. This has two consequences. First, the magnetic flux passing through any closed material loop (a loop always composed of the same material particles) tends to be conserved during the motion of the fluid. This is indicated in Figure 1.1. Second, as we shall see, small disturbances of the medium tend to result in near-elastic oscillations, with the magnetic field

providing the restoring force for the vibration. In a fluid, this results in Alfvén waves, which turn out to have a frequency of $\omega \sim v_a/l$

When R_m is small, on the other hand, **u** has little influence on **B**, the induced field being negligible by comparison with the imposed field. The magnetic field then behaves quite differently. We shall see that it is dissipative in nature, rather than elastic, damping mechanical motion by converting kinetic energy into heat via Joule dissipation. The relevant time scale is now the damping time, τ, rather than l/v_a.

All of this is dealt with more fully in Chapters 4–6. The purpose of this chapter is to show that a familiar high-school experiment is sufficient to expose these two very different types of behaviour, and to highlight the important rôles played by R_m, v_a and τ.

1.3.2 A brief reminder of the laws of electrodynamics

Let us start with a reminder of the elementary laws of electromagnetism. (A more detailed discussion of these laws is given in Chapter 2.) The laws which concern us here are those of Ohm, Faraday and Ampère. We start with Ohm's law (Figure 1.2(i)).

This is an empirical law which, for stationary conductors, takes the form $\mathbf{J} = \sigma\mathbf{E}$, where **E** is the electric field and **J** the current density. We interpret this as **J** being proportional to the Coulomb force $\boldsymbol{f} = q\mathbf{E}$ which acts on the free charge carriers, q being their charge. If, however, the conductor is moving in a magnetic field with velocity **u**, the free charges will experience an additional force, $q\mathbf{u} \times \mathbf{B}$, and Ohm's law becomes

$$\mathbf{J} = \sigma(\mathbf{E} + \mathbf{u} \times \mathbf{B}) \tag{1.4}$$

The quantity $\mathbf{E} + \mathbf{u} \times \mathbf{B}$, which is the total electromagnetic force per unit charge, arises frequently in electrodynamics and it is convenient to give it a label. We use

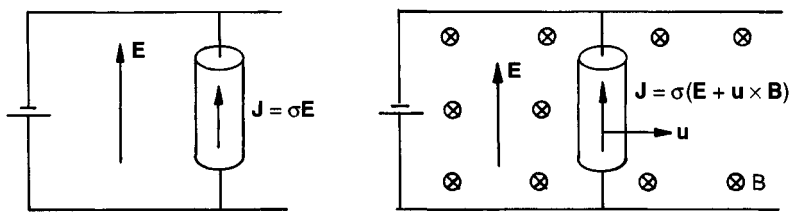

Figure 1.2 (i) Ohm's law in stationary and moving conductors.

$$\mathbf{E}_r = \mathbf{E} + \mathbf{u} \times \mathbf{B} = \mathbf{f}/q$$

Formally, $\mathbf{E}_r$ is the electric field measured in a frame of reference moving with velocity $\mathbf{u}$ relative to the laboratory frame (see Chapter 2). However, for the present purposes it is more useful to think of $\mathbf{E}_r$ as $\mathbf{f}/q$. Some authors refer to $\mathbf{E}_r$ as the *effective electric field.* In terms of $\mathbf{E}_r$, (1.4) becomes $\mathbf{J} = \sigma\mathbf{E}_r$.

Faraday's law (Figure 1.2 (ii)) tells us about the e.m.f. which is generated in a conductor as a result of: (i) a time-dependent magnetic field; or (ii) the motion of a conductor within a magnetic field. In either case Faraday's law may be written as

$$\text{emf} = \oint_C \mathbf{E}_r \cdot d\mathbf{l} = -\frac{d}{dt}\int_S \mathbf{B} \cdot d\mathbf{S} \tag{1.5}$$

Here C is a closed curve composed of line elements $d\mathbf{l}$. The curve may be fixed in space, or else move with the conducting medium (if the medium does indeed move). S is any surface which spans C. (We use the right-hand screw convention to define the positive directions of $d\mathbf{l}$ and $d\mathbf{S}$.) The subscript on $\mathbf{E}_r$ indicates that we must use the 'effective' electric field for each line element $d\mathbf{l}$:

$$\mathbf{E}_r = \mathbf{E} + \mathbf{u} \times \mathbf{B} \tag{1.6}$$

where $\mathbf{E}$, $\mathbf{u}$ and $\mathbf{B}$ are measured in the laboratory frame and $\mathbf{u}$ is the velocity of the line element $d\mathbf{l}$.

Next, we need Ampère's law (Figure 1.3). This (in a round-about way) tells us about the magnetic field associated with a given distribution of current, $\mathbf{J}$. If C is a closed curve drawn in space, and S is any surface spanning that curve, then Ampère's circuital law states that

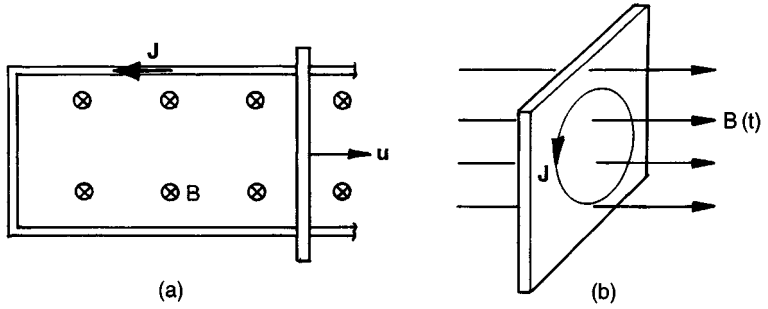

Figure 1.2 (ii) Faraday's law (a) e.m.f. generated by movement of a conductor; (b) e.m.f. generated by a time-dependent magnetic field.

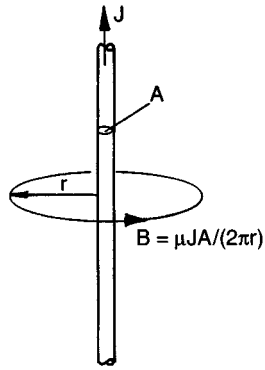

Figure 1.3 Ampère's law applied to a wire.

$$\oint_C \mathbf{B} \cdot d\mathbf{l} = \mu \int_S \mathbf{J} \cdot d\mathbf{S} \tag{1.7}$$

Finally, there is the Lorentz force, **F**. This acts on all conductors carrying a current in a magnetic field. It has its origins in the force acting on individual charge carriers, $\mathbf{f} = q(\mathbf{u} \times \mathbf{B})$ and it is easy to show that the force per unit volume of the conductor is given by

$$\mathbf{F} = \mathbf{J} \times \mathbf{B} \tag{1.8}$$

1.3.3 A familiar high-school experiment

We now turn to the laboratory experiment. Consider the apparatus illustrated in Figure 1.4. This is frequently used to illustrate Faraday's law of induction. It consists of a horizontal, rectangular circuit sitting in a vertical magnetic field, $\mathbf{B}_0$. The circuit is composed of a frictionless, conducting slide which is free to move horizontally between two rails. We take the rails and slide to have a common thickness Δ and to be made from the same material. To simplify matters, we shall also suppose that the depth of the apparatus is much greater than its lateral dimensions, L and W, so that we may treat the problem as two-dimensional. Also, we take Δ to be much smaller than L or W.

We now show that, if the slide is given a tap, and it has a high conductivity, it simply vibrates as if held in place by a (magnetic) spring. On the other hand, if the conductivity is low, it moves forward as if immersed in treacle, slowing down on a time scale of τ. Suppose that, at $t = 0$, the

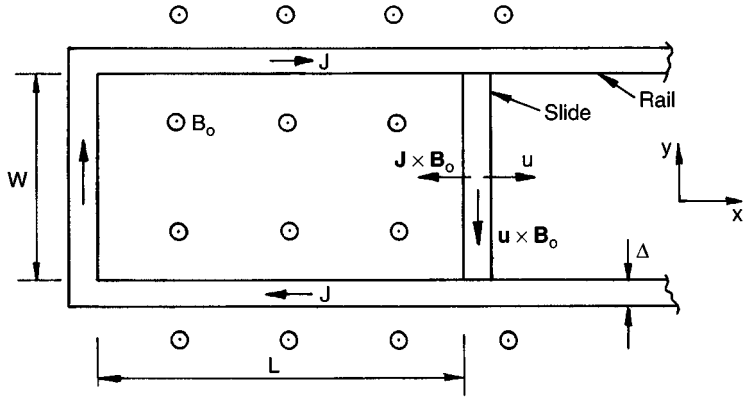

Figure 1.4 A simple experiment for illustrating MHD phenomena.

slide is given a forward motion, **u**. This movement of the slide will induce a current density, **J**, as shown. This, in turn, produces an induced field $\mathbf{B}_i$ which is negligible outside the closed current path but is finite and uniform within the current loop. It may be shown, from Ampère's law, that $\mathbf{B}_i$ is directed downward and has a magnitude and direction given by

$$\mathbf{B}_i = -(\mu \Delta J)\hat{\mathbf{e}}_z \tag{1.9}$$

Note that the direction of $\mathbf{B}_i$ is such as to try to maintain a constant flux in the current loop (Lenz's law) (Figure 1.5). Next we combine (1.4) and (1.5) to give

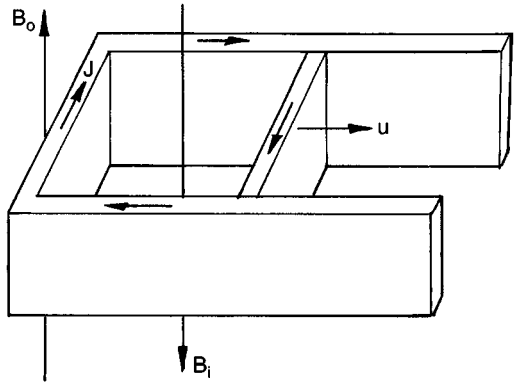

Figure 1.5 Direction of the magnetic field induced by current in the slide.

$$\frac{1}{\sigma}\oint_C \mathbf{J}\cdot d\mathbf{l} = -\frac{d}{dt}\int_S \mathbf{B}\cdot d\mathbf{S} \tag{1.10}$$

where C is the material circuit comprising the slide and the return path for $\mathbf{J}$. This yields

$$\frac{d\Phi}{dt} = \frac{d}{dt}[LW(B_0 - \mu\Delta J)] = 2J(L+W)/\sigma \tag{1.11}$$

Here $\Phi = (B_0 - \mu\Delta J)LW$ is the flux through the circuit (see Figure 1.6). Finally, the Lorentz force (per unit depth) acting on the slide is

$$\mathbf{F} = -J(B_0 - \mu\Delta J/2)\Delta W\hat{\mathbf{e}}_x \tag{1.12}$$

where the expression in parentheses represents the average field within the slide (Figure 1.7). The equation of motion for the slide is therefore

$$\rho\frac{d^2L}{dt^2} = \rho\frac{du}{dt} = -J(B_0 - \mu\Delta J/2) \tag{1.13}$$

where ρ is the density of the metal.

Equations (1.11) and (1.13) are sufficient to determine the two unknown functions $L(t)$ and $J(t)$. Let us introduce some simplifying notation: $B_I = \mu\Delta J$, $l = \Delta W/L$, $T = \mu\sigma\Delta W$ and $R_m = \mu\sigma ul$. Evidently, B_I is the magnitude of the induced field and T is a measure of the conductivity, σ, which happens to have the dimensions of time. Our two equations may be rewritten as

$$\frac{d}{dt}[L(B_0 - B_I)] = \frac{2(L+W)B_I}{T} \tag{1.14}$$

and

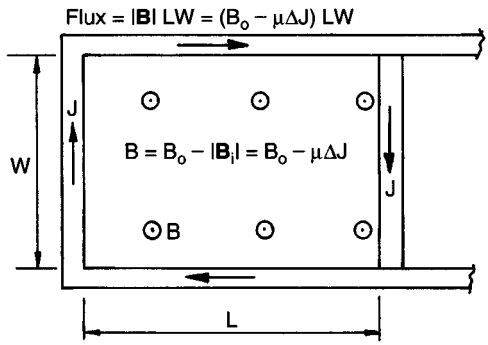

Figure 1.6 Relationship between flux and current.

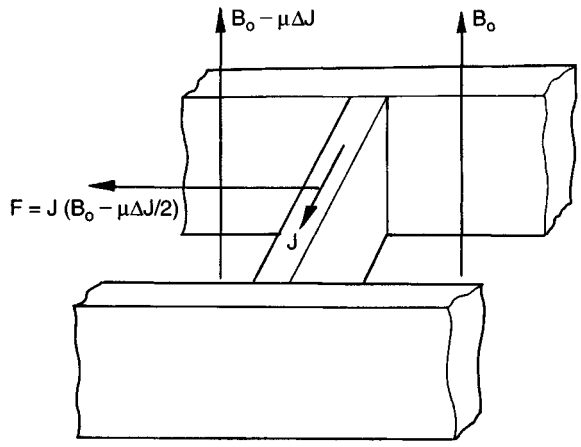

Figure 1.7 Forces acting on the slide.

$$2\rho\mu\Delta\frac{d^2L}{dt^2} = 2\rho\mu\Delta\frac{du}{dt} = (B_0 - B_I)^2 - B_0^2 \tag{1.15}$$

Now we might anticipate that the solutions of (1.14) and (1.15) will depend on the conductivity of the apparatus as represented by T, and so we consider two extreme cases:

1. high conductivity limit; $\frac{u}{L} \gg \frac{1}{T}$ $(R_m = \mu\sigma ul \gg 1)$
2. low conductivity limit; $\frac{u}{L} \ll \frac{1}{T}$ $(R_m = \mu\sigma ul \ll 1)$

In the high conductivity limit, the right-hand side of (1.14) may be neglected and so the flux Φ linking the current path is conserved during the motion. In such cases we may look for solutions of (1.15) of the form $L = L_0 + \eta$, where η is an infinitesimal change of L and $L_0 = \Phi/B_0W$. Multiplying through (1.15) by L^2W, noting that Φ is constant and equal to L_0B_0W, and retaining only leading order terms in η, yields

$$\frac{d^2\eta}{dt^2} + \frac{B_0^2}{\rho\mu\Delta L_0}\eta = 0 \tag{1.16}$$

Thus, when the magnetic Reynolds number is high, the slide oscillates in an elastic manner, with an angular frequency of $\omega \sim v_a/\sqrt{\Delta L_0}$, v_a, being the Alfvén velocity. In short, if we tap the slide it will vibrate (Figure 1.8). It seems to be held in place by the magnetic field.

Now consider the low conductivity limit, $R_m \ll 1$ (Figure 1.9). In this case the induction equation (1.14) tells us that $B_I \ll B_0$ and so the left-

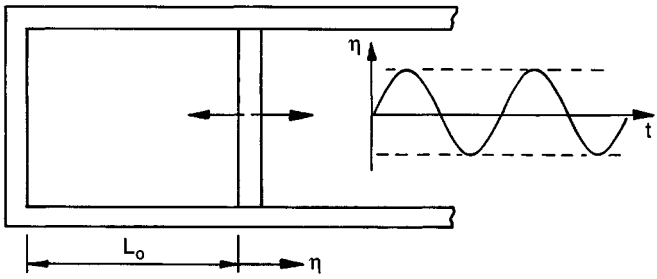

Figure 1.8 Oscillation of the slide when $R_m \gg 1$.

hand side of (1.14) reduces to uB_0. Substituting for B_I (in terms of u) in the equation of motion (1.15) yields

$$\frac{du}{dt} + \frac{W}{2(L+W)}\left(\frac{\sigma B_0^2}{\rho}\right)u = 0 \tag{1.17}$$

Again we look for solutions of the form $L_0 + \eta$, with $\eta \ll L_0$ and $L_0 = L(t=0)$. This time u declines exponentially on a time scale of $\tau = (\sigma B_0^2/\rho)^{-1}$, the magnetic damping time. The magnetic field now appears to play a dissipative rôle. Indeed, it is not difficult to show that

$$\frac{dE}{dt} = -\int (J^2/\sigma)dV \tag{1.18}$$

where the volume integral is taken over the entire conductor and E is the kinetic energy of the slide. Thus the mechanical energy of the slide is lost to heat via Ohmic dissipation.

Let us summarise our findings. When $R_m \gg 1$, and the slide is abruptly displaced from its equilibrium position, it oscillates in an elastic manner at a frequency proportional to the Alfvén velocity. During the oscillation

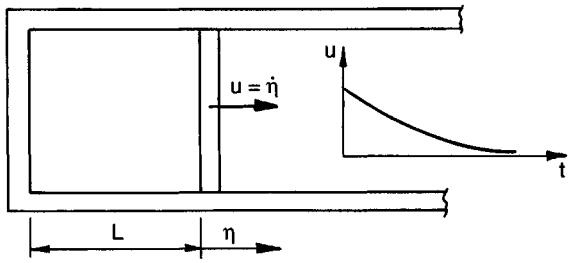

Figure 1.9 Motion of the slide when $R_m \ll 1$.

the magnetic flux trapped between the slide and the rails remains constant. If $R_m \ll 1$, on the other hand, and the slide is given a push, it moves forward as if it were immersed in treacle. Its kinetic energy decays exponentially on a time scale of $\tau = (\sigma B_0^2/\rho)^{-1}$, the energy being lost to heat via Ohmic dissipation. Also, when R_m is small, the induced magnetic field is negligible.

We shall see that precisely the same behaviour occurs in fluids. The counterpart of the vibration is an Alfvén wave (Figure 1.10), which is a common feature of astrophysical MHD. In liquid-metal MHD, on the other hand, the primary rôle of **B** is to dissipate mechanical energy on a time scale of τ.

We have yet to explain these two types of behaviour. Consider first the high R_m case. Here the key equation is Faraday's law (1.10),

$$\frac{1}{\sigma}\oint_C \mathbf{J} \cdot d\mathbf{l} = -\frac{d}{dt}\int_S \mathbf{B} \cdot d\mathbf{S}$$

As $\sigma \to \infty$, the flux, Φ, enclosed by the slide and rails must be conserved. If the slide is pushed forward, $J = B_I/\mu\Delta$ must rise to conserve Φ. The Lorentz force therefore increases until the slide is halted. At this point the Lorentz force $\mathbf{J} \times \mathbf{B}$ is finite but $\mathbf{u}$ is zero and so the slide starts to return. The induced field B_I, and hence J, now falls to maintain the magnetic flux. Eventually the slide returns to its equilibrium position and the Lorentz force falls to zero. However, the inertia of the slide carries it over its neutral point and the whole process now begins in reverse. It is the conservation of flux, combined with the inertia of the conductor,

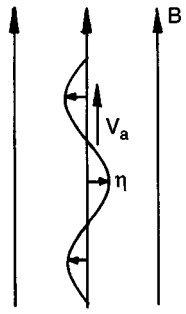

Figure 1.10 Alfvén waves. A magnetic field behaves like a plucked string, transmitting a transverse inertial wave with a phase velocity of v_a.

which leads to oscillations in this experiment, and to Alfvén waves in plasmas (Figure 1.11).

Now consider the case where $R_m \ll 1$. It is Ohm's law which plays the critical rôle here. The high resistivity of the circuit means that the currents, and hence induced field, are small. We may consider $\mathbf{B}$ to be approximately equal to the imposed field, $\mathbf{B}_0$. Since $\mathbf{B}$ is now almost constant, the electric field must be irrotational

$$\nabla \times \mathbf{E} = -\frac{\partial \mathbf{B}}{\partial t} \approx 0$$

Ohm's law and the Lorentz force per unit volume now simplify to

$$\mathbf{J} = \sigma[-\nabla V + \mathbf{u} \times \mathbf{B}_0], \qquad \mathbf{F} = \mathbf{J} \times \mathbf{B}_0 \tag{1.19a,b}$$

where V is the electrostatic potential. Integrating Ohm's law around the closed current loop eliminates V and yields a simple relationship between u and J:

$$2J(L + W) = \sigma W B_0 u$$

The Lorentz force per unit mass becomes

$$\frac{\mathbf{F}}{\rho} = -\frac{W}{2(L+W)}\left(\frac{\sigma B_0^2}{\rho}\right)\mathbf{u} \sim -\frac{\mathbf{u}}{\tau}$$

from which

$$\frac{d\mathbf{u}}{dt} \sim -\frac{\mathbf{u}}{\tau} \tag{1.20}$$

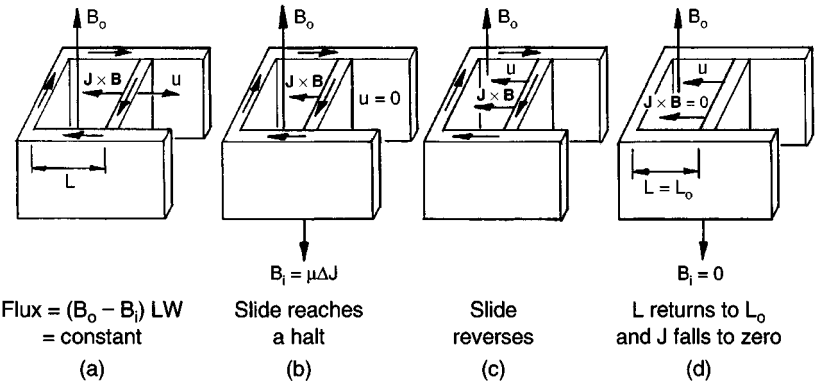

Figure 1.11 Mechanism for oscillation of the slide.

Thus the slide slows down exponentially on a time scale of τ. The rôle of the induced current here is quite different to the high R_m case. The fact that J creates an induced field is irrelevant. It is the contribution of J to the Lorentz force $\mathbf{J} \times \mathbf{B}_0$ which is important. This always acts to retard the motion. As we shall see, the two equations $\mathbf{J} = \sigma[-\nabla V + \mathbf{u} \times \mathbf{B}_0]$ and $\mathbf{F} = \mathbf{J} \times \mathbf{B}_0$ are the hallmark of low-R_m MHD.

This familiar high-school experiment encapsulates many of the phenomena which will be explored in the subsequent chapters. The main difference is that fluids have, of course, none of the rigidity of electrodynamic machines, and so they behave in more subtle and complex ways. Yet it is precisely this subtlety which makes MHD so intriguing.

1.3.4 A summary of the key results for MHD

1. When the medium is highly conducting ($R_m \gg 1$), Faraday's law tells us that the flux through any closed material loop is conserved. When the material loop contracts or expands, currents flow so as to keep the flux constant. These currents lead to a Lorentz force which tends to oppose the contraction or expansion of the loop. The result is an elastic oscillation with a characteristic frequency of $\sim v_a/l$, v_a being the Alfvén velocity.
2. When the medium is a poor conductor (($R_m \ll 1$), the magnetic field induced by motion is negligible by comparison with the imposed field, B_0. The Lorentz force and Ohm's law simplify to

$$\mathbf{F} = \mathbf{J} \times \mathbf{B}_0, \qquad \mathbf{J} = \sigma[-\nabla V + \mathbf{u} \times \mathbf{B}_0]$$

   The Lorentz force is now dissipative in nature, converting mechanical energy into heat on a time scale of the magnetic damping time, τ.

Statements 1 and 2 are, in effect, a summary of Chapters 4–6.

1.4 Some Simple Applications of MHD

We close this introductory chapter with a brief overview of the scope of MHD, and of this book. In fact, MHD operates on every scale, from the vast to the minute. For example, magnetic fields pervade interstellar space and aid the formation of stars by removing excess angular momentum from collapsing interstellar clouds. Closer to home, sunspots and solar flares are magnetic in origin, sunspots being caused by buoyant

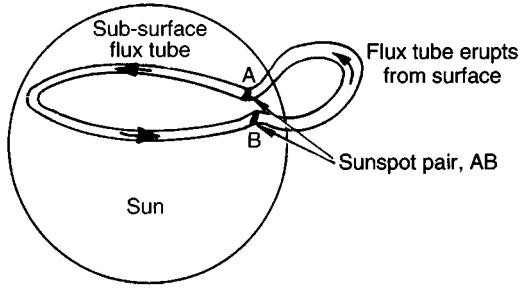

Figure 1.12 Sunspot formation.

magnetic flux tubes, perhaps 10^4 km in diameter and 10^5 km long, erupting from the surface of the sun (Figure 1.12). Sunspots are discussed in Chapter 4.

Back on earth, the terrestrial magnetic field is now known to be maintained by fluid motion in the core of the earth (Figure 1.13). This process, called dynamo action, is reviewed in Chapter 6.

MHD is also an intrinsic part of controlled thermonuclear fusion. Here plasma temperatures of around 10^8 K must be maintained, and magnetic forces are used to confine the hot plasma away from the reactor walls. A simple example of a confinement scheme is shown in Figure 1.14. Unfortunately, such schemes are prone to hydrodynamic instabilities, the nature of which is discussed in Chapter 6.

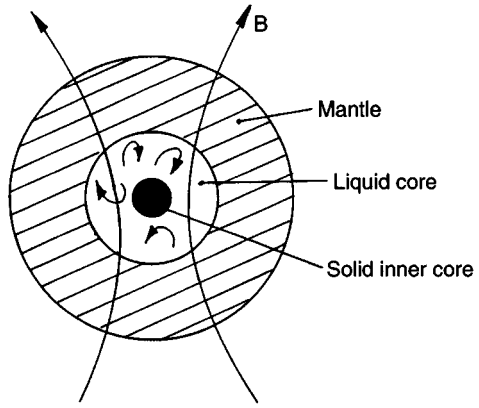

Figure 1.13 Motion in the earth's core maintains the terrestrial magnetic field.

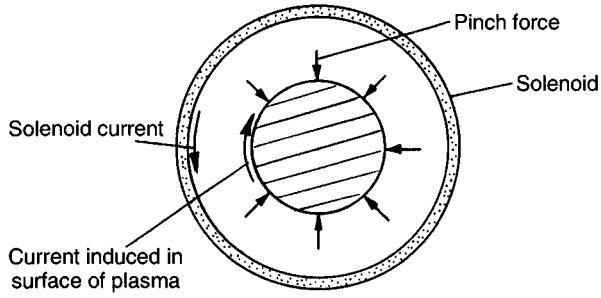

Figure 1.14 Plasma confinement. A current in the solenoid which surrounds the plasma induces an opposite current in the surface of the plasma and the resulting Lorentz force pinches radially inward.

In the metallurgical industries, magnetic fields are routinely used to heat, pump, stir and levitate liquid metals. Perhaps the earliest application of MHD is the electromagnetic pump (Figure 1.15). This simple device consists of mutually perpendicular magnetic and electric fields arranged normal to the axis of a duct. Provided the duct is filled with a conducting liquid, so that currents can flow, the resulting Lorentz force provides the necessary pumping action. First proposed back in 1832, the electromagnetic pump has found its ideal application in fast-breeder nuclear reactors, where it is used to pump liquid sodium coolant through the reactor core.

Perhaps the most widespread application of MHD in engineering is the use of electromagnetic stirring. A simple example is shown in Figure 1.16. Here the liquid metal which is to be stirred is placed in a rotating magnetic field. In effect, we have an induction motor, with the liquid metal taking the place of the rotor. This is routinely used in casting operations to homogenise the liquid zone of a partially solidified ingot. The resulting motion has a profound influence on the solidification process, ensuring good mixing of the alloying elements and the continual fragmentation of

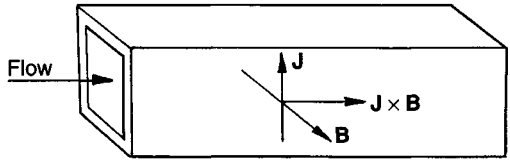

Figure 1.15 The electromagnetic pump.

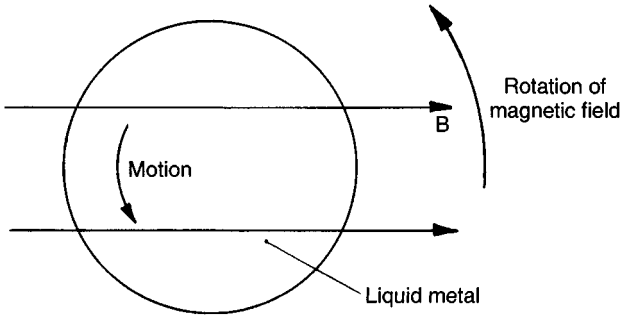

Figure 1.16 Magnetic stirring of an ingot.

the snowflake-like crystals which form in the melt. The result is a fine-structured, homogeneous ingot. This is discussed in detail in Chapter 8.

Perversely, in yet other casting operations, magnetic fields are used to dampen the motion of liquid metal. Here we take advantage of the ability of a static magnetic field to convert kinetic energy into heat via Joule dissipation (as discussed in the last section). A typical example is shown in Figure 1.17, in which an intense, static magnetic field is imposed on a casting mould. Such a device is used when the fluid motion within the mould has become so violent that the free surface of the liquid is disturbed, causing oxides and other pollutants to be entrained into the bulk. The use of magnetic damping promotes a more quiescent process, thus minimising contamination. The damping of jets and vortices is discussed in Chapters 5 and 9.

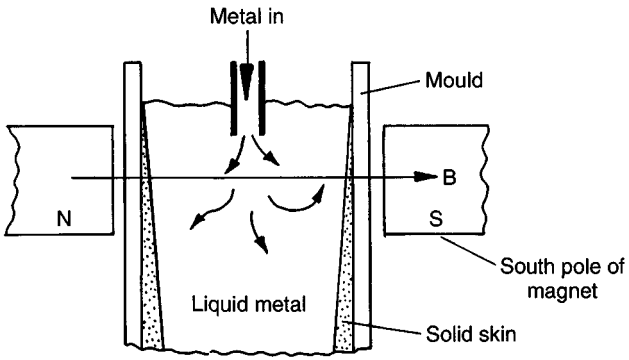

Figure 1.17 Magnetic damping of motion during casting.

Another common application of MHD in metallurgy is magnetic levitation or confinement. This relies on the fact that a high-frequency induction coil repels conducting material by inducing opposing currents in any adjacent conductor (opposite currents repel each other). Thus a 'basket' formed from a high-frequency induction coil can be used to levitate and melt highly reactive metals, or a high-frequency solenoid can be used to form a non-contact magnetic valve which modulates and guides a liquid metal jet (Figure 1.18). Such applications are discussed in Chapter 12.

MHD is also important in electrolysis, particularly in those electrolysis cells used to reduce aluminium oxide to aluminium. These cells consist of broad but shallow layers of electrolyte and liquid aluminium, with the electrolyte lying on top. A large current (perhaps 200 kAmps) passes vertically downward through the two layers, continually reducing the oxide to metal. The process is highly energy intensive, largely because of the high electrical resistance of the electrolyte. For example, in the USA, around 3% of all generated electricity is used for aluminium production. It has long been known that stray magnetic fields can destabilise the interface between the electrolyte and aluminium, in effect through the generation of interfacial gravity waves (Figure 1.19). In order to avoid this instability, the electrolyte layer must be maintained at a depth above some critical threshold, and this carries with it a severe energy penalty. This instability turns out to involve a rather subtle mechanism, in which interfacial oscillations absorb energy from the ambient magnetic field,

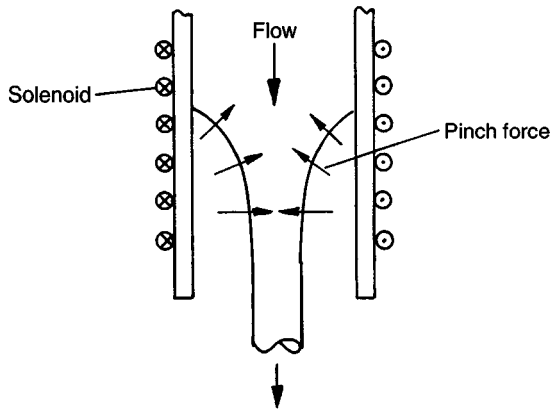

Figure 1.18 An electromagnetic valve.

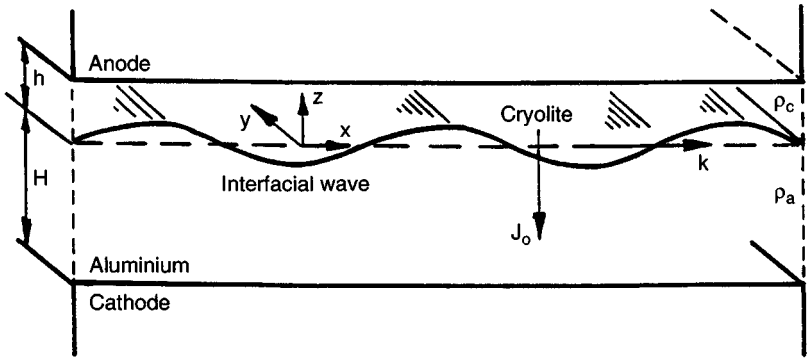

Figure 1.19 Instabilities in an aluminium reduction cell.

converting it into kinetic energy. The stability of aluminium reduction cells is discussed in Chapter 11.

There are many other applications of MHD in engineering and metallurgy which, in the interests of brevity, we have not described here. These include electromagnetic (non-contact) casting of aluminium, vacuum-arc remelting of titanium and nickel-based super alloys (a process which resembles a gigantic electric welding rod – see Chapter 10), electromagnetic removal of non-metallic inclusions from melts, electromagnetic launchers (which have the same geometry as Figure 1.4, but where the slide is now a projectile and current is forced down the rails accelerating the slide) and the so-called 'cold-crucible' induction melting process, in which the melt is protected from the crucible walls by a thin solid crust of its own material. This latter technology is currently finding favour in the nuclear industry, where it is used to vitrify highly active nuclear waste.

All-in-all, it would seem that MHD has now found a substantial and permanent place in the world of materials processing. However, it would be wrong to pretend that every engineering venture in MHD has been a success, and so we end this section on a lighter note, describing one of MHD's less notable developments: that of MHD propulsion for military submarines.

Stealth is all important in the military arena and so, in an attempt to eliminate the detectable (and therefore unwanted) cavitation noise associated with propellers, MHD pumps were once proposed as a propulsion mechanism for submarines. The idea is that sea-water is drawn into ducts at the front of the submarine, passed through MHD pumps

within the submarine hull, and then expelled at the rear of the vessel in the form of high-speed jets. It is an appealing idea, dating back to the 1960s, and in principle it works, as demonstrated recently in Japan by the surface ship *Yamato*. Indeed, this idea has even found its way into popular fiction! The concept found renewed favour with the military authorities in the 1980s (the armaments race was at fever pitch) and serious design work commenced. Unfortunately, however, there is a catch. It turns out that the conductivity of sea-water is so poor that the efficiency of such a device is, at best, a few per cent, nearly all of the energy going to heat the water. Worse still, the magnetic field required to produce a respectable thrust is massive, at the very limits of the most powerful superconducting magnets. So, while in principle it is possible to eliminate propeller cavitation, in the process a (highly detectable) magnetic signature is generated, to say nothing of the thermal and chemical signatures induced by electrolysis in the ducts. To locate an MHD submarine, therefore, you simply have to borrow a Gauss meter, buy a thermometer, invest in litmus paper, or just follow the trail of dead fish!

Submarine propulsion apart, engineering MHD has scored some notable successes in recent years, particularly in its application to metallurgy. It is this which forms the basis of Part B of this text.

Suggested Reading

J A Shercliff: *A textbook of magnetohydrodynamics, 1965*, Pergamon Press. (Chapter 1 gives a brief history of MHD.)

Examples

1.1 A bar of small but finite conductivity slides at a constant velocity u along conducting rails in a region of uniform magnetic field. The resistance in the circuit is R and the inductance is negligible. Calculate: (i) the current I flowing in the circuit; (ii) the power required to move the bar; and (iii) the Ohmic losses in the circuit.

1.2 A square metal bar of length l and mass m slides without friction down parallel conducting rails of negligible resistance. The rails are connected to each other at the bottom by a resistanceless rail parallel to the bar, so that the bar and rails form a closed loop. The plane of the rails makes an angle θ with the horizontal, and a uniform vertical field, B, exists throughout the region. The bar has a small but finite

conductivity and has a resistance of R. Show that the bar acquires a steady velocity of $u = mgR\sin\theta/(Bl\cos\theta)^2$.

1.3 A steel rod is 0.5 m long and has a diameter of 1 cm. It has a density and conductivity of 7×10^3 kg/m^3 and 10^6 mho/m, respectively. It lies horizontally with its ends on two parallel rails, 0.5 m apart. The rails are perfectly conducting and are inclined at an angle of 15° to the horizontal. The rod slides up the rails with a coefficient of friction of 0.25, propelled by a battery which maintains a constant voltage difference of 2 V between the rails. There is a uniform, unperturbed vertical magnetic field of 0.75 T. Find the velocity of the bar when travelling steadily.

1.4 When Faraday's and Ohm's laws are combined, we obtain (1.10). Consider an isolated flux tube sitting in a perfectly conducting fluid, and let C_m be a material curve (a curve always composed of the same material) which at some initial instant encircles the flux tube, lying on the surface of the tube. Show that the flux enclosed by C_m will remain constant as the flow evolves, and that this is true of each and every curve enclosing the tube at $t = 0$. This suggests that the tube itself moves with the fluid, as if frozen into the medium. Now suppose that the diameter of the flux tube is very small. What does this tell us about magnetic field lines in a perfectly conducting fluid?

1.5 Consider a two-dimensional flow consisting of an (initially) thin jet propagating in the x-direction and sitting in a uniform magnetic field which points in the y-direction. The magnetic Reynolds number is low. Show that the Lorentz force (per unit volume) acting on the fluid is $-\sigma u_x B^2 \hat{\mathbf{e}}_x$. Now consider a fluid particle sitting on the axis of the jet. It has an axial acceleration of $u_x(\partial u_x/\partial x)$. Show that the jet is annihilated within a finite distance of $L \sim u_0\tau$, where u_0 is the initial value of u_x (τ is the magnetic damping time).

1.6 Calculate the magnetic Reynolds number for motion in the core of the earth, using the radius of the core, $R_c = 3500$ km as the characteristic length-scale and $u \sim 2 \times 10^{-4}$ m/s as a typical velocity. Take the conductivity of iron as 0.5×10^6 mho/m. Now calculate the magnetic Reynolds number for motion in the outer regions of the sun taking $l \sim 10^3$ km, $u \sim 1$ km/s and $\sigma = 10^4$ mho/m. Explain why it is difficult to model solar and geo-dynamos using scaled laboratory experiments with liquid metals.

1.7 Magnetic forces are sometimes used to levitate objects. For example, if a metal object is situated near a coil carrying an alternating current

I, eddy currents will flow in the object and there will result a repulsive force. Show that the force in the x-direction is $\frac{1}{2}I^2(\partial L/\partial x)$ if the object is allowed to move in the x-direction (L is the effective inductance of the coil).

2

The Governing Equations of Electrodynamics

> From a long view of history of mankind – seen from, say, ten thousand years from now – there can be little doubt that the most significant event of the 19th Century will be judged as Maxwell's discovery of the laws of electrodynamics.
>
> *R P Feynman (1964)*

We are concerned here with conducting, non-magnetic materials. For simplicity, we shall assume that all material properties, such as the conductivity, σ, are spatially uniform, and that the medium is incompressible. The topics which concern us are the Lorentz force, Ohm's law, Ampère's law and Faraday's law. We shall examine these one at a time.

2.1 The Electric Field and the Lorentz Force

A particle moving with velocity $\mathbf{u}$ and carrying a charge q is, in general, subject to three electromagnetic forces:

$$\mathbf{f} = q\mathbf{E}_s + q\mathbf{E}_i + q\mathbf{u} \times \mathbf{B} \tag{2.1}$$

The first is the electrostatic force, or Coulomb force, which arises from the mutual repulsion or attraction of electric charges ($\mathbf{E}_s$ is the electrostatic field). The second is the force which the charge experiences in the presence of a time-varying magnetic field, $\mathbf{E}_i$ being the electric field induced by the changing magnetic field. The third contribution is the Lorentz force which arises from the motion of the charge in a magnetic field. Now Coulomb's law tells us that $\mathbf{E}_s$ is irrotational, and Gauss's law fixes the divergence of $\mathbf{E}_s$. Together these laws yield

$$\nabla \cdot \mathbf{E}_s = \rho_e/\varepsilon_0, \qquad \nabla \times \mathbf{E}_s = 0 \tag{2.2a,b}$$

Here ρ_e is the total charge density (free charges plus bound charges) and ε_0 is the permittivity of free space. In view of (2.2b), we may introduce the electrostatic potential, V, defined by $\mathbf{E}_s = -\nabla V$. It follows from (2.2a) that $\nabla^2 V = -\rho_e/\varepsilon_0$.

The induced electric field, on the other hand, has zero divergence, while its curl is finite and governed by Faraday's law.

$$\nabla \cdot \mathbf{E}_i = 0, \qquad \nabla \times \mathbf{E}_i = -\frac{\partial \mathbf{B}}{\partial t} \tag{2.3}$$

It is convenient to define the total electric field as $\mathbf{E} = \mathbf{E}_s + \mathbf{E}_i$, and so we have

$$\begin{array}{ll} \nabla \cdot \mathbf{E} = \rho_e/\varepsilon_0, & \nabla \times \mathbf{E} = -\dfrac{\partial \mathbf{B}}{\partial t} \\ \text{(Gauss's law)} & \text{(Faraday's law)} \end{array} \tag{2.4}$$

$$\begin{array}{l} \mathbf{f} = q(\mathbf{E} + \mathbf{u} \times \mathbf{B}) \\ \text{(electrostatic force plus Lorentz force)} \end{array} \tag{2.5}$$

Equations (2.4) uniquely determine the electric field since the requirements are that the divergence and curl of the field be known (and suitable boundary conditions are specified). It is customary to use equation (2.5) to define the electric field **E** and the magnetic field **B**. Thus, for example, the electric field **E** is the force per unit charge on a small test charge *at rest* in the observer's frame of reference.

Due attention must be given to frames of reference. Suppose that in the laboratory frame there is an electric field and a magnetic field. The electric field, **E**, is defined by the force per unit charge on a charge at rest in that frame. If the charge is moving, the force due to the electric field is still given by $\mathbf{f} = q\mathbf{E}$ but the additional force $q\mathbf{u} \times \mathbf{B}$ appears, which is used to define **B**. If, however, we use a frame of reference in which the charge is instantaneously *at rest* (but moving with velocity **u** relative to the laboratory frame), then the force on the charge can only be interpreted as due to an electric field, say $\mathbf{E}_r$ (the subscript r indicates 'relative to a moving frame'). Newton's second law then gives, for the two frames, $\mathbf{f} = q(\mathbf{E} + \mathbf{u} \times \mathbf{B})$ and $\mathbf{f}_r = q\mathbf{E}_r$. However, Newtonian relativity (which is all that is required for MHD) tells us that $\mathbf{f} = \mathbf{f}_r$. It follows that the electric fields in the two frames are related by

$$\mathbf{E}_r = \mathbf{E} + \mathbf{u} \times \mathbf{B} \tag{2.6}$$

The magnetic fields **B** and $\mathbf{B}_r$ are equal.

We close this section by noting that **B** is a pseudo-vector and not a true vector. That is to say, the sense of **B** is somewhat arbitrary, to the extent that **B** reverses direction if we move from a right-handed coordinate system (the usual convention) to a left-handed one. This may be seen as follows. Suppose we transform our coordinate system according to $\mathbf{x} \to \mathbf{x}' = -\mathbf{x}$. (This is referred to as an inversion of the coordinates, or else as a reflection about the origin.) We have moved from a right-handed coordinate system to a left-handed one in which $x' = -x$, $y' = -y$,

$z' = -z$, $\mathbf{i}' = -\mathbf{i}$, $\mathbf{j}' = -\mathbf{j}$ and $\mathbf{k}' = -\mathbf{k}$. Now the components of a true vector, such as force, **f**, or velocity, **u**, transform like $f_x' = -f_x$ etc., which leaves the physical direction of the vector unchanged since

$$\mathbf{f} = f_x\mathbf{i}_x + f_y\mathbf{i}_y + f_z\mathbf{i}_z = (-f_x')(-\mathbf{i}_x') + (-f_y')(-\mathbf{i}_y') + (-f_z')(-\mathbf{i}_z')$$

Thus, after an inversion of the coordinates, a true vector (such as **f** or **u**) has the same magnitude and direction as before, although the numerical values of its components change sign. Now consider the definition of **B**: $\mathbf{f} = q(\mathbf{u} \times \mathbf{B})$. Under an inversion of the coordinates the components of **u** and **f** both change sign and so those of **B** cannot. Thus the magnetic field transforms according to $B_x' = B_x$, etc. By implication, the physical direction of **B** reverses. (Such vectors are called pseudo-vectors.) So, if one morning we all agreed to change convention from a right-handed coordinate system to a left-handed one, all the magnetic field lines would reverse direction! The fact that **B** is a pseudo-vector is important in dynamo theory.

2.2 Ohm's Law and the Volumetric Lorentz Force

In a stationary conductor it is found that the current density, **J**, is proportional to the force experienced by the free charges. This is reflected in the conventional form of Ohm's law, $\mathbf{J} = \sigma\mathbf{E}$. In a conducting fluid the same law applies, only now we must use the electric field measured in a frame moving with the local velocity of the conductor:

$$\mathbf{J} = \sigma\mathbf{E}_r = \sigma(\mathbf{E} + \mathbf{u} \times \mathbf{B}) \tag{2.7}$$

Note that **u** will, in general, vary with position.

Now the Lorentz force (2.5) is important not just because it lies behind Ohm's law, but also because the forces exerted on the free charges are ultimately transmitted to the conductor. In MHD we are less concerned with the forces on individual charges than the bulk force acting on the medium, but this is readily found. If (2.5) is summed over a unit volume of the conductor then $\sum q$ becomes the charge density, ρ_e, and $\sum q\mathbf{u}$ becomes the current density, **J**. The volumetric version of (2.5) is therefore

$$\mathbf{F} = \rho_e\mathbf{E} + \mathbf{J} \times \mathbf{B} \tag{2.8}$$

where **F** is the force per unit volume acting on the conductor. However, in conductors travelling at the sort of speeds we are interested in (much less

than the speed of light), the first term in (2.8) is negligible. We may demonstrate this as follows. Conservation of charge requires that

$$\nabla \cdot \mathbf{J} = -\frac{\partial \rho_e}{\partial t} \tag{2.9}$$

(This simply says that the rate at which charge is decreasing inside a small volume must equal the rate at which charge flows out across the surface of that volume.) By taking the divergence of both sides of (2.7), and using Gauss's law and (2.9), we find that

$$\frac{\partial \rho_e}{\partial t} + \frac{\rho_e}{\tau_e} + \sigma \nabla \cdot (\mathbf{u} \times \mathbf{B}) = 0, \qquad \tau_e = \varepsilon_0/\sigma$$

The quantity τ_e is called the charge relaxation time, and for a typical conductor has a value of around 10^{-18} s. It is extremely small! To appreciate where its name comes from, consider the situation where $\mathbf{u} = 0$. In this case, $\partial \rho_e/\partial t + \rho_e/\tau_e = 0$ and so

$$\rho_e = \rho_e(0) \exp[-t/\tau_e]$$

Any net charge density which, at $t = 0$, lies in the interior of a conductor will move rapidly to the surface under the action of the electrostatic repulsion forces. It follows that ρ_e is always zero in stationary conductors, except during some minuscule period when a battery, say, is turned on. Now consider the case where $\mathbf{u}$ is non-zero. We are interested in events which take place on a time-scale much longer than τ_e (we exclude events like batteries being turned on) and so we may neglect $\partial \rho_e/\partial t$ by comparison with ρ_e/τ_e. We are left with the pseudo-static equation

$$\rho_e = -\varepsilon_0 \nabla \cdot (\mathbf{u} \times \mathbf{B}) \tag{2.10}$$

Thus, when there is motion, we can sustain a finite charge density in the interior of the conductor. However, it turns out that ρ_e is very small, i.e. too low to produce any significant electric force, $\rho_e \mathbf{E}$. That is, from (2.10) we have $\rho_e \sim \varepsilon_0 uB/l$, while Ohm's law requires $\mathbf{E} \sim \mathbf{J}/\sigma$, and so

$$\rho_e \mathbf{E} \sim [\varepsilon_0 uB/l][J/\sigma] \sim \frac{u\tau_e}{l} JB$$

Here l is a typical length-scale for the flow. Evidently, since $u\tau_e/l \sim 10^{-18}$, the Lorentz force completely dominates (2.8) and we may write

$$\mathbf{F} = \mathbf{J} \times \mathbf{B} \tag{2.11}$$

Note also that (2.10) is equivalent to ignoring $\partial \rho_e/\partial t$ in the charge conservation equation (2.9). That is to say, the charge density is so small that (2.9) simplifies to

$$\nabla \cdot \mathbf{J} = 0 \tag{2.12}$$

2.3 Ampère's Law

The Ampère–Maxwell equation tells us something about the magnetic field generated by a given distribution of current. It is

$$\nabla \times \mathbf{B} = \mu\left[\mathbf{J} + \varepsilon_0 \frac{\partial \mathbf{E}}{\partial t}\right] \tag{2.13}$$

The last term in (2.13) may be unfamiliar. It does not, for example, appear in Ampère's circuital law (1.7). This new term was introduced by Maxwell as a correction to Ampère's law and is called the displacement current. To see why it is necessary, we take the divergence of (2.13). Noting that $\nabla \cdot \nabla \times (\cdot) = 0$ and using Gauss' law, this yields

$$\nabla \cdot \mathbf{J} = -\varepsilon_0 \frac{\partial}{\partial t} \nabla \cdot \mathbf{E} = -\frac{\partial \rho_e}{\partial t}$$

This is just the charge conservation equation which, without the displacement current, would be violated. However, Maxwell's correction is not needed in MHD. That is, we have already noted that $\partial \rho_e / \partial t$ is negligible in conductors, and so we might anticipate that the contribution of $\varepsilon_0 \frac{\partial \mathbf{E}}{\partial t}$ to (2.13) is also small in MHD. This is readily confirmed:

$$\varepsilon_0 \frac{\partial \mathbf{E}}{\partial t} \sim \frac{\varepsilon_0}{\sigma} \frac{\partial \mathbf{J}}{\partial t} \sim \tau_e \frac{\partial \mathbf{J}}{\partial t} \ll \mathbf{J}$$

We are therefore at liberty to use the pre-Maxwell form of (2.13), which is simply the differential form of Ampère's law:

$$\nabla \times \mathbf{B} = \mu \mathbf{J} \tag{2.14}$$

This is consistent with (2.12), since the divergence of (2.14) yields

$$\nabla \cdot \mathbf{J} = 0$$

Finally, we note that in infinite domains, (2.14) may be inverted using the Biot–Savart law. That is, when the current density is a known function of position, the magnetic field may be calculated directly from

$$\mathbf{B}(\mathbf{x}) = \frac{\mu}{4\pi} \int \frac{\mathbf{J}(\mathbf{x}') \times \mathbf{r}}{r^3} d^3\mathbf{x}', \qquad \mathbf{r} = \mathbf{x} - \mathbf{x}' \tag{2.15}$$

This comes from the fact that a small element of material located at $\mathbf{x}'$ and carrying a current density of $\mathbf{J}(\mathbf{x}')$ induces a magnetic field at point $\mathbf{x}$ which is given by (see Figure 2.1)

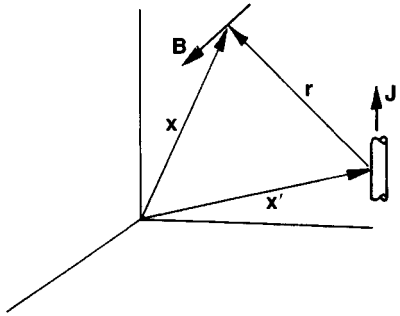

Figure 2.1 Coordinate system used in the Biot–Savart law.

$$d\mathbf{B}(\mathbf{x}) = \frac{\mu}{4\pi}\frac{\mathbf{J}(\mathbf{x}') \times \mathbf{r}}{r^3} d^3\mathbf{x}'$$

Note that (2.15), which is equivalent to (2.14)[1], reveals the true character of Ampère's law. It really tells us about the structure of the magnetic field associated with a given current distribution.

Example: Force-free fields

Magnetic fields of the form $\nabla \times \mathbf{B} = \alpha\mathbf{B}$, $\alpha =$ constant, are known as *force-free* fields, since $\mathbf{J} \times \mathbf{B} = 0$. (More generally, fields of the form $\nabla \times \mathbf{G} = \alpha\mathbf{G}$ are known as *Beltrami* fields.) They are important in plasma MHD where we frequently require the Lorentz force to vanish. Show that, for a force-free field,

$$(\nabla^2 + \alpha^2)\mathbf{B} = 0$$

Deduce that there are no force-free fields, other than $\mathbf{B} = 0$, for which $\mathbf{J}$ is localised in space and $\mathbf{B}$ is everywhere differentiable and $0(x^{-3})$ at infinity.

2.4 Faraday's Law in Differential Form

Faraday's law is sometimes stated in integral form and sometimes in differential form. You have already met both. In Section 2.1 we stated it to be

[1] In fact, (2.15) is a stronger statement than (2.14) as it determines both the divergence and the curl of **B**.

$$\nabla \times \mathbf{E} = -\frac{\partial \mathbf{B}}{\partial t}$$

This tells us about the electric field induced by a time-varying magnetic field. However, in Chapter 1 we gave the integral version,

$$\text{e.m.f.} = \oint_C \mathbf{E}_r \cdot d\mathbf{l} = -\frac{d}{dt}\int_S \mathbf{B} \cdot d\mathbf{S} \tag{2.16}$$

where $\mathbf{E}_r$ is the electric field measured in a frame of reference moving with $d\mathbf{l}$ (see equation (2.6)). In fact, it is easily seen that (2.16) is a more powerful statement than the differential form of Faraday's law. In words, it states that the e.m.f. around a closed loop is equal to the total rate of change of flux of $\mathbf{B}$ through that loop. In (2.16), the flux may change because $\mathbf{B}$ is changing with time, or because the loop is moving uniformly in an inhomogeneous field, or because the loop is changing shape. Whatever the cause, (2.16) gives the induced e.m.f. We shall return to the integral version of Faraday's law in Section 2.7, where we discuss its full significance. In the meantime, we shall show that the differential form of Faraday's law is a special case of (2.16).

Suppose that the loop is rigid and at rest in a laboratory frame. Then the e.m.f. can arise only from a magnetic field which is time-dependent. In this case (2.16) becomes

$$\oint_C \mathbf{E} \cdot d\mathbf{l} = \oint_S (\nabla \times \mathbf{E}) \cdot d\mathbf{S} = -\int_S (\partial \mathbf{B}/\partial t) \cdot d\mathbf{S}$$

Since this is true for any and all (fixed) surfaces, we may equate the integrands in the surface integrals. We then obtain the differential form of Faraday's law:

$$\nabla \times \mathbf{E} = -\frac{\partial \mathbf{B}}{\partial t} \tag{2.17}$$

In this form, Faraday's law becomes one of Maxwell's equations (see Section 2.5). Note, however, that (2.17) is a weaker statement than (2.16). It only tells us about the electric field induced by a time-varying magnetic field.

Now (2.17) ensures that $\partial \mathbf{B}/\partial t$ is solenoidal, since $\nabla \cdot (\nabla \times \mathbf{E}) = 0$. In fact, it transpires that we can make an even stronger statement about $\mathbf{B}$. It turns out that $\mathbf{B}$ is itself solenoidal,

$$\nabla \cdot \mathbf{B} = 0 \tag{2.18}$$

This allows us to introduce another field, **A**, called the vector potential, defined by

$$\nabla \times \mathbf{A} = \mathbf{B}, \qquad \nabla \cdot \mathbf{A} = 0 \tag{2.19a,b}$$

This definition automatically ensures that **B** is solenoidal, since $\nabla \cdot \nabla \times \mathbf{A} = 0$. If we substitute for **A** in Faraday's equation we obtain

$$\nabla \times \mathbf{E} = -\nabla \times (\partial \mathbf{A}/\partial t)$$

from which

$$\mathbf{E} = -\frac{\partial \mathbf{A}}{\partial t} - \nabla V \tag{2.20}$$

where V is an arbitrary scalar function. However, we also have, from (2.2) and (2.3),

$$\mathbf{E} = \mathbf{E}_i + \mathbf{E}_s, \qquad \nabla \times \mathbf{E}_s = 0, \qquad \nabla \cdot \mathbf{E}_i = 0$$

and so we might anticipate that $\mathbf{E}_i = -\partial \mathbf{A}/\partial t$ and $\mathbf{E}_s = -\nabla V$ where V is now the electrostatic potential. This is readily confirmed by taking the divergence of (2.20) which, given (2.19b), shows that all of the divergence of **E** is captured by ∇V in (2.20), as required by (2.2) and (2.3).

Example: The divergence of **B**

Faraday's law implies that $(\partial/\partial t)(\nabla \cdot \mathbf{B}) = 0$. If this is also true relative to all sets of axes moving uniformly relative to one another, show that $\nabla \cdot \mathbf{B} = 0$.

2.5 The Reduced Form of Maxwell's Equations for MHD

We have mentioned Maxwell's equations several times. When combined with the force law (2.5) and the law of charge conservation (2.9), they embody all that we know about electrodynamics, and so it seems appropriate that, at some point, we should write them down. For materials which are neither magnetic nor dielectric, Maxwell's equations state that:

$$\nabla \cdot \mathbf{E} = \rho_e/\varepsilon_0 \qquad \text{(Gauss' law)}$$

$$\nabla \cdot \mathbf{B} = 0 \qquad \text{(Solenoidal nature of } \mathbf{B}\text{)}$$

$$\nabla \times \mathbf{E} = -\frac{\partial \mathbf{B}}{\partial t} \qquad \text{(Faraday's law in differential form)}$$

$$\nabla \times \mathbf{B} = \mu\left(\mathbf{J} + \varepsilon_0 \frac{\partial \mathbf{E}}{\partial t}\right) \qquad \text{(Ampère–Maxwell equation)}$$

In addition, we have

$$\nabla \cdot \mathbf{J} = -\partial \rho_e / \partial t \quad \text{(charge conservation)},$$

$$\mathbf{F} = q(\mathbf{E} + \mathbf{u} \times \mathbf{B})$$

For our purposes these may be simplified considerably. In MHD, the charge density ρ_e plays no significant part. For example, we have seen that the electric force, $q\mathbf{E}$, is minute by comparison with the Lorentz force, and that the contribution of $\partial \rho_e / \partial t$ to the charge conservation equation is also negligible. Apparently ρ_e is significant only in Gauss's law and so we simply drop Gauss's law and ignore ρ_e. Also, we have seen that in MHD the displacement currents are negligible by comparison with the current density, $\mathbf{J}$, and so the Ampère–Maxwell equation reduces to the differential form of Ampère's law. We may now summarise the (pre-Maxwell) form of the electrodynamic equations used in MHD:

Ampère's law plus charge conservation,

$$\boxed{\nabla \times \mathbf{B} = \mu \mathbf{J}}, \quad \boxed{\nabla \cdot \mathbf{J} = 0} \tag{2.21}$$

Faraday's law plus the solenoidal constraint on $\mathbf{B}$,

$$\boxed{\nabla \times \mathbf{E} = -\frac{\partial \mathbf{B}}{\partial t}}, \quad \boxed{\nabla \cdot \mathbf{B} = 0} \tag{2.22}$$

Ohm's law plus the Lorentz Force,

$$\boxed{\mathbf{J} = \sigma(\mathbf{E} + \mathbf{u} \times \mathbf{B})}, \quad \boxed{\mathbf{F} = \mathbf{J} \times \mathbf{B}} \tag{2.23}$$

Equations (2.21)–(2.23) encapsulate all that we need to know about electromagnetism for MHD.

Example 1: A paradox

Although electrostatic forces are of no importance in MHD, they can lead to some unexpected effects in those cases where they are significant, as we now show. Consider a hollow plastic sphere which is mounted on a frictionless spindle and is free to rotate. Charged metal pellets are embedded in the surface of the sphere and a wire loop is placed near its centre, the axis of the loop being parallel to the rotation axis. The loop is connected to a battery, so that a current

flows and a dipole-like magnetic field is created. We now ensure that everything is stationary and (somehow) disconnect the battery. The magnetic field declines and so, by Faraday's law, we induce an electric field which is azimuthal, i.e. **E** takes the form of rings which are concentric with the axis of the wire loop. This electric field now acts on the charges to produce a torque on the sphere, causing it to spin up. At the end of the process we have gained some angular momentum in the sphere, but at the cost of the magnetic field. Apparently, we have contravened the principle of conservation of angular momentum! Can you unravel this paradox? (Hint: consult Feynman's 'Lectures on Physics' Vol. 2.)

The earth has a large negative charge on its surface, which gives rise to an average surface electric field of around 100 V/m. It also has a dipole magnetic field, and rotates about an axis which is more-or-less aligned with the magnetic axis. Do you think the rotation rate of the earth changes when the earth's magnetic field reverses (as it occasionally does)?

Example 2: The Poynting vector

Use Faraday's law and Ampère's law to show that

$$\frac{d}{dt}\int_V (\mathbf{B}^2/2\mu)dV = -\int_V \mathbf{J}\cdot\mathbf{E}dV - \oint_S [(\mathbf{E}\times\mathbf{B})/\mu]\cdot d\mathbf{S}$$

Now use Ohm's law to confirm that

$$\int_V \mathbf{J}\cdot\mathbf{E}dV = \frac{1}{\sigma}\int_V \mathbf{J}^2 dV + \int_V (\mathbf{J}\times\mathbf{B})\cdot\mathbf{u}dV$$

Combining the two we obtain

$$\frac{d}{dt}\int (\mathbf{B}^2/2\mu)dV = -\frac{1}{\sigma}\int_V \mathbf{J}^2 dV - \int_V (\mathbf{J}\times\mathbf{B})\cdot\mathbf{u}dV - \oint_S \mathbf{P}\cdot d\mathbf{S}$$

where $\mathbf{P} = (\mathbf{E}\times\mathbf{B})/\mu$ is called the Poynting vector. The integrals on the right represent Joule dissipation, the rate of loss of magnetic energy due to the rate of working of the Lorentz force on the medium, and the rate at which electromagnetic energy flows out through the surface S, the Poynting vector being the electromagnetic energy flux density.

2.6 A Transport Equation for B

If we combine Ohm's law, Faraday's equation and Ampère's law we obtain an expression relating **B** to **u**.

$$\frac{\partial \mathbf{B}}{\partial t} = -\nabla \times \mathbf{E} = -\nabla \times [(\mathbf{J}/\sigma) - \mathbf{u} \times \mathbf{B}] = \nabla \times [\mathbf{u} \times \mathbf{B} - \nabla \times \mathbf{B}/\mu\sigma]$$

Noting that $\nabla \times \nabla \times \mathbf{B} = -\nabla^2 \mathbf{B}$ (since **B** is solenoidal), this simplies to

$$\boxed{\frac{\partial \mathbf{B}}{\partial t} = \nabla \times (\mathbf{u} \times \mathbf{B}) + \lambda \nabla^2 \mathbf{B}}, \qquad \lambda = (\mu\sigma)^{-1} \tag{2.24}$$

This is sometimes called the induction equation, although, as we shall see, a more descriptive name would be the advection–diffusion equation for **B**. The quantity λ is called the magnetic diffusivity. Like all diffusivities it has the units m^2/s. Equation (2.24) is, in effect, a transport equation for **B**, in the sense that if **u** is known then it dictates the spatial and temporal evolution of **B** from some specified initial condition. We shall spend much of Chapter 4 unpicking the physical implications of (2.24): it is one of the key equations in MHD.

Example: Decay of force-free fields

Show that if, at $t = 0$, there exists a *force-free* field, $\nabla \times \mathbf{B} = \alpha \mathbf{B}$, in a stationary fluid, then that field will decay as $\mathbf{B} \sim \exp(-\lambda \alpha^2 t)$, remaining as a force-free field.

2.7 On the Remarkable Nature of Faraday and of Faraday's Law

We shall now show that the integral version of Faraday's law, (2.16), is a quite remarkable result, encompassing not just one physical law, but two! Moreover, as we shall see, Faraday's law in its most general form embodies many of the key phenomena of MHD. We start, however, with a historical footnote.

2.7.1 An historical footnote

Faraday played a crucial part in the development of MHD for three reasons. First, his law of induction, discovered in 1831, shows that magnetic field lines in a perfectly conducting fluid must move with the fluid, as if frozen into the medium. This result is usually attributed to the 20th

century astrophysicist Alfvén, but really it follows directly from Faraday's law. Second, he performed the first experiment in MHD when he tried to measure the voltage induced by the Thames flowing through the earth's magnetic field.[2] Third, he invented magnetic fields!

Prior to the work of Faraday, the scientific and mathematical communities were convinced that the laws of electromagnetism should be formulated in terms of action at a distance. The notion of a field did not exist. For example, Ampère had discovered that two current-carrying wires attract each other, and so, by analogy with Newton's law of gravitational attraction, it seemed natural to try and describe this force in terms of some kind of inverse square law. In this view, nothing of significance exists *between* the wires.

Faraday had a different vision, in which the medium between the wires plays a rôle. In his view, a wire which carries a current introduces a field into the medium surrounding it. This field (the magnetic field) exists whether or not a second wire is present. When the second wire is introduced it experiences a force by virtue of this field. Moreover, in Faraday's view the field is not just some convenient mathematical intermediary. It has real physical significance, possessing energy, momentum and so on.

Of course, it is Faraday's view which now prevails, which is all the more remarkable because Faraday had no formal education and, as a consequence, little mathematical skill. James Clerk Maxwell was greatly impressed by Faraday, and in the preface to his classic treatise on Electricity and Magnetism he wrote:

> Before I began the study of electricity I resolved to read no mathematics on the subject till I had first read through Faraday's Experimental Researches in Electricity. I was aware that there was supposed to be a difference between Faraday's way of conceiving phenomena and that of the mathematicians, so that neither he nor they were satisfied with each other's language...
>
> As I proceeded with the study of Faraday, I perceived that his method of conceiving the phenomena was also a mathematical one, though not exhibited in the conventional form of mathematical symbols...

[2] In Faradays words: 'I made experiments therefore (by favour) at Waterloo bridge, extending a copper wire nine hundred and sixty feet in length upon the parapet of the bridge, and dropping from its extremities other wires with extensive plates of metal attached to them to complete contact with the water. Thus the wire and the water made one conducting circuit; and as the water ebbed and flowed with the tide, I hoped to obtain currents.' (1832)

> For instance, Faraday, in his mind's eye, saw lines of force traversing space where the mathematicians saw centres of force attracting at a distance: Faraday sought the seat of the phenomena in real actions going on in the medium, they were satisfied that they had found it in a power of action at a distance...
>
> When I translated what I considered to be Faraday's ideas into mathematical form, I found that in general the results of the two methods coincided, so that the same phenomena were accounted for, and the same laws of action deduced by both methods, but that Faraday's methods resembled those in which we begin with the whole and arrive at the parts by analysis, while the ordinary mathematical methods were founded on the principle of beginning with the parts and building up the whole by synthesis. I also found that several of the most fertile methods of research discovered by the mathematicians could be expressed much better in terms of the ideas derived by Faraday than in their original form...
>
> If by anything I have written I may assist any student in understanding Faraday's modes of thought and expression, I shall regard it as the accomplishment of one of my principle aims – to communicate to others the same delight which I have found myself in reading Faraday's 'Researches'.
>
> *(1873)*

When Maxwell transcribed Faraday's ideas into mathematical form, correcting Ampère's law in the process, he arrived at the famous laws which now bear his name. Kelvin was similarly taken by Faradays physical insight:

> One of the most brilliant steps made in philosophical exposition of which any instance existed in the history of science was that in which Faraday stated, in three or four words, intensely full of meaning, the law of magnetic attraction or repulsion... Mathematicians were content to investigate the general expression of the resultant force experienced by a globe of soft iron in all such cases; but Faraday, without any mathematics, devined the result of the mathematical investigations. Indeed, the whole language of the magnetic field and 'lines of force' is Faraday's. It must be said for the mathematicians that they greedily accepted it, and have ever since been most zealous in using it to the best advantage.'
>
> *(1872)*

The central rôle played by fields acquires special significance in relativistic mechanics where, because of the finite velocity of propagation of interactions, it is not meaningful to talk of direct interactions of particles

(or currents) located at distant points. We can speak only of the field established by one particle and of the subsequent influence of this field on other particles. Of course, Faraday could not have foreseen this! Einstein explicitly noted the important role played by Faraday and Maxwell in his popular introduction to Relativity:

> during the second half of the 19th century, in conjunction with the researches of Faraday and Maxwell, it became more and more clear that the description of electromagnetic processes in terms of fields was vastly superior to a treatment on the basis of the mechanical concepts of material points.... One psychological effect of this immense success was that the field concept, as opposed to the mechanistic framework of classical physics, gradually won greater independence.
>
> *(1916)*

Of course, Faraday's contribution to magnetism did not stop with the introduction of fields. He also discovered electromagnetic induction. In fact, in 1831, in no more than ten full days of research, Faraday unravelled all of the essential features of electromagnetic induction. Even more remarkable, the integral equation now attributed to Faraday encompasses not just one physical law, but two, as we now show. First, however, we need an important kinematic result.

2.7.2 An important kinematic equation

Suppose that $\mathbf{G}$ is a solenoidal field, $\nabla \cdot \mathbf{G} = 0$, and S_m is a surface which is embedded in a conducting medium, i.e. S_m is locked into the medium and moves as the fluid moves. (The subscript m indicates that it is a *material surface*.) Then it may be shown that

$$\boxed{\frac{d}{dt}\int_{S_m} \mathbf{G}\cdot d\mathbf{S} = \int_{S_m}\left[\frac{\partial \mathbf{G}}{\partial t} - \nabla\times(\mathbf{u}\times\mathbf{G})\right]\cdot d\mathbf{S}} \qquad (2.25a)$$

A formal proof of (2.25) will be given in a moment. First, however, we might try to get a qualitative feel for its origins. The idea behind (2.25a) is the following. The flux of $\mathbf{G}$ through S_m changes for two reasons. First, even if S_m were fixed in space there is a change in flux whenever $\mathbf{G}$ is time-dependent. This is the first term on the right of (2.25a). Second, if the boundary of S_m moves it may expand at points to include additional flux, or perhaps contract at other points to exclude flux. It happens that, in a

time δt, the surface adjacent to the line element $d\mathbf{l}$ increases by an amount $d\mathbf{S} = (\mathbf{u} \times d\mathbf{l})\delta t$, and so the increase in flux due to movement of the boundary C_m is

$$\delta \int_{S_m} \mathbf{G} \cdot d\mathbf{S} = \oint_{C_m} \mathbf{G} \cdot (\mathbf{u} \times d\mathbf{l})\delta t = -\oint_{C_m} (\mathbf{u} \times \mathbf{G}) \cdot d\mathbf{l}\, \delta t$$

Using Stoke's theorem, the last line integral may be converted into a surface integral, which accounts for the second term on the right of (2.25a). Of course, we have yet to show that $d\mathbf{S} = (\mathbf{u} \times d\mathbf{l})\delta t$.

The formal proof of (2.25) proceeds as follows. The change in flux through S_m in a time δt is

$$\delta \int_{S_m} \mathbf{G} \cdot d\mathbf{S} = (\delta t) \int_{S_m} (\partial \mathbf{G}/\partial t) \cdot d\mathbf{S} + \oint_{S_m} \mathbf{G} \cdot \delta \mathbf{S}$$

where $\delta\mathbf{S}$ is the element of area swept out by the line element $d\mathbf{l}$ in time δt. However, $\delta\mathbf{S} = d\mathbf{l}' \times d\mathbf{l}$, where $d\mathbf{l}'$ is the infinitesimal displacement of the element $d\mathbf{l}$ in time δt (Figure 2.2). Since $d\mathbf{l}' = \mathbf{u}\delta t$, we have $\delta\mathbf{S} = (\mathbf{u} \times d\mathbf{l})\delta t$ and so

$$\delta \int_{S_m} \mathbf{G} \cdot d\mathbf{S} = (\delta t) \int_{S_m} (\partial \mathbf{G}/\partial t) \cdot d\mathbf{S} - \oint_{C_m} \mathbf{u} \times \mathbf{G} \cdot d\mathbf{l}(\delta t)$$

(We have used the cyclic properties of the scalar triple product to rearrange the terms in the line integral.) Finally, the application of Stoke's theorem to the line integral gets us back to (2.25), and this completes the proof.

Now (2.25) should not be passed over lightly: it is a very useful result. The reason is that often in MHD (or conventional fluid mechanics) we find that certain vector fields obey a transport equation of the form

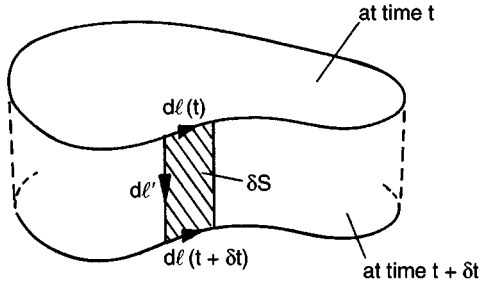

Figure 2.2 Movement of the material surface in a time δt.

$$\frac{\partial \mathbf{G}}{\partial t} = \nabla \times [\mathbf{u} \times \mathbf{G}]$$

This is true of $\nabla \times \mathbf{u}$ in an unforced, inviscid flow (see Chapter 3) and of $\mathbf{B}$ in a perfect conductor (see equation (2.24)). In such cases, (2.25) tells us that the flux of $\mathbf{B}$ (or $\nabla \times \mathbf{u}$) through any material surface, S_m, is conserved as the flow evolves. We shall return to this idea time and again in subsequent chapters.

Note that it is not necessary to invoke the idea of a continuously moving medium and of material surfaces in order to arrive at (2.25). If we consider any curve, C, moving in space with a prescribed velocity, $\mathbf{u}$, then

$$\frac{d}{dt}\int_S \mathbf{G} \cdot d\mathbf{S} = \int_S \left[\frac{\partial \mathbf{G}}{\partial t} - \nabla \times (\mathbf{u} \times \mathbf{G})\right] \cdot d\mathbf{S} \tag{2.25b}$$

where S is any surface which spans the curve C.

2.7.3 The full significance of Faraday's law

We now return to electrodynamics. Recall that the differential form of Faraday's law is

$$\nabla \times \mathbf{E} = -\partial \mathbf{B}/\partial t \tag{2.26}$$

As noted earlier, this is a weaker statement than the integral version (2.16), since it tells us only about the e.m.f. induced by a time-dependent field. Let us now see if we can *deduce* the more general version of Faraday's law, (2.16), from (2.26).

Suppose we have a curve, C, which deforms in space with a prescribed velocity $\mathbf{u}(\mathbf{x})$. (This could be, but need not be, a material curve.) Then, at each point on the curve, (2.26) gives

$$\nabla \times (\mathbf{E} + \mathbf{u} \times \mathbf{B}) = -\left\{\frac{\partial \mathbf{B}}{\partial t} - \nabla \times (\mathbf{u} \times \mathbf{B})\right\}$$

We now integrate this over any surface S which spans C and invoke the kinematic equation (2.25b). The result is

$$\oint_C (\mathbf{E} + \mathbf{u} \times \mathbf{B}) \cdot d\mathbf{l} = -\frac{d}{dt}\int_S \mathbf{B} \cdot d\mathbf{S}$$

So far we have used only Faraday's law in differential form. We now invoke the idea of the Lorentz force. This tells us that, in a frame of reference moving with velocity $\mathbf{u}$, the electric field is $\mathbf{E}_r = \mathbf{E} + \mathbf{u} \times \mathbf{B}$.

Given that **E** transforms in this way, we may rewrite our integral equation as

$$\oint_C \mathbf{E}_r \cdot d\mathbf{l} = -\frac{d}{dt}\int_S \mathbf{B} \cdot d\mathbf{S}$$

Note that this applies to any curve C. For example, C may be fixed in space, move with the fluid, or execute some motion quite different to that of the fluid. It does not matter. The final step is to introduce the idea of an e.m.f. We define the e.m.f. to be the closed integral of $\mathbf{E}_r$, from which

$$\text{e.m.f.} = \oint_C \mathbf{E}_r \cdot d\mathbf{l} = -\frac{d}{dt}\int_S \mathbf{B} \cdot d\mathbf{S} \tag{2.27}$$

We have arrived at the integral version of Faraday's law. Note, however, that to get from (2.26) to (2.27) we had to invoke the force law $\mathbf{F} = q(\mathbf{u} \times \mathbf{B})$. Note also that if C and S happen to be material curves and surfaces embedded in a fluid, then (2.27) becomes

$$\text{e.m.f.} = \oint_{C_m} \mathbf{E}_r \cdot d\mathbf{l} = -\frac{d}{dt}\int_{S_m} \mathbf{B} \cdot d\mathbf{S} \tag{2.28}$$

Now it is intriguing that the integral version of Faraday's law describes the e.m.f. generated in two very different situations, i.e. when **E** is induced by a time-dependent magnetic field, and when $\mathbf{E}_r$ is induced (at least in part) by motion of the circuit within a magnetic field. The two extremes are shown in Figure 2.3. If **B** is constant, and the e.m.f. is

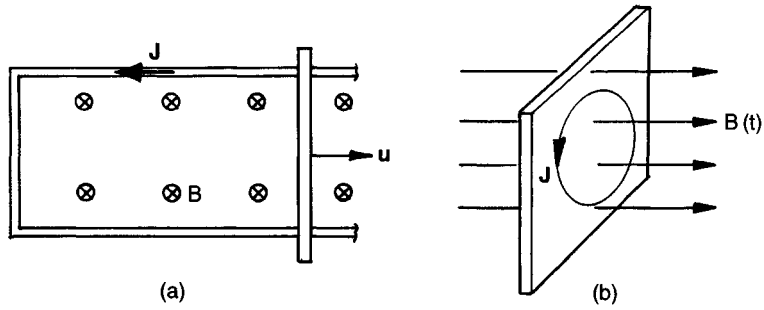

Figure 2.3 An e.m.f. can be generated either by movement of the conducting medium (motional e.m.f.) or else by variation of the magnetic field (transformer e.m.f.).

due solely to movement of the circuit, then $\oint \mathbf{E}_r \cdot d\mathbf{l}$ is called a *motional* e.m.f. If the circuit is fixed and $\mathbf{B}$ is time-dependent, then $\oint \mathbf{E} \cdot d\mathbf{l}$ is termed a *transformer* e.m.f. In either case, however, the e.m.f. is equal to (minus) the rate of change of flux. Now motional e.m.f. is due essentially to the Lorentz force, $q\mathbf{u} \times \mathbf{B}$, while transformer e.m.f. results from the Maxwell equation $\nabla \times \mathbf{E} = -\partial \mathbf{B}/\partial t$, which is usually regarded as a separate physical law. Yet both are described by the integral equation (2.27). Faraday's law is therefore an extraordinary result. It embodies two quite different phenomena. It seems that it just so happens that motional e.m.f. and transformer e.m.f. can both be described by the same flux rule! (At a deeper level both Maxwell's equations and the Lorentz force can, with some additional assumptions, be deduced from Coulomb's law plus the Lorentz transformation of special relativity, and so it is not just coincidence that Faraday's equation embraces two apparently distinct physical laws. Nevertheless, from a classical viewpoint, it represents a remarkably convenient equation.)

2.7.4 *Faraday's law in ideal conductors: Alfvén's theorem*

From Ohm's law, $\mathbf{J} = \sigma \mathbf{E}_r$, and (2.28) we have

$$\boxed{\frac{1}{\sigma} \oint_{C_m} \mathbf{J} \cdot d\mathbf{l} = -\frac{d}{dt} \int_{S_m} \mathbf{B} \cdot d\mathbf{S}} \tag{2.29}$$

for any material surface, S_m. Now suppose that $\sigma \to \infty$. Then

$$\frac{d}{dt} \int_{S_m} \mathbf{B} \cdot d\mathbf{S} = 0 \qquad \sigma \to \infty \tag{2.30}$$

We have arrived at a key result in MHD. That is to say, *in a perfect conductor, the flux through any material surface S_m is preserved as the flow evolves.* Now picture an individual flux tube sitting in a perfectly conducting fluid. Such a tube is, by analogy to a stream-tube in fluid mechanics, just an aggregate of magnetic field lines (Figure 2.4). Since $\mathbf{B}$ is solenoidal ($\nabla \cdot \mathbf{B} = 0$), the flux of $\mathbf{B}$ along the tube, Φ, is constant. (This comes from applying Gauss's divergence theorem to a finite portion of the tube.) Now consider a material curve C_m which at some initial instant encircles the flux tube. The flux enclosed by C_m will remain constant as the flow evolves, and this is true of each and every curve enclosing the tube at $t = 0$. This suggests (but does not

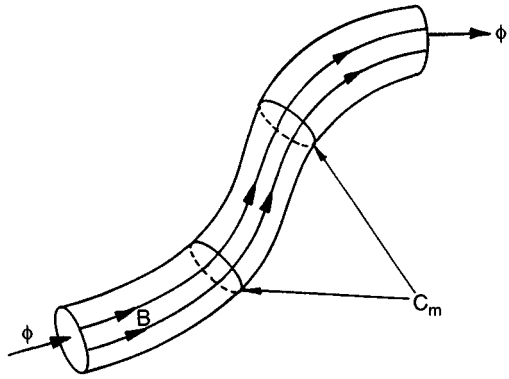

Figure 2.4 A magnetic flux tube.

prove) that the tube itself moves with the fluid, as if frozen into the medium. This, in turn, suggests that every field line moves with the fluid, since we could let the tube have a vanishingly small cross section. We have arrived at Alfvén's theorem (Figure 2.5), which states that:

> magnetic field lines are frozen into a perfectly conducting fluid in the sense that they move with the fluid.

We shall give formal proof of Alfvén's theorem in Chapter 4.

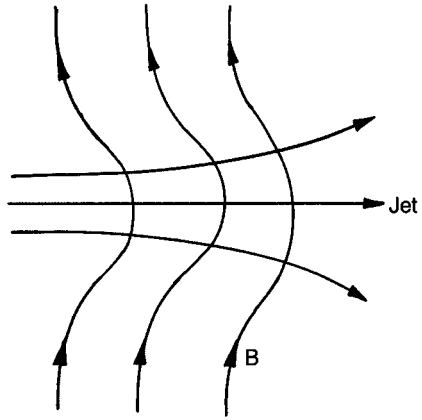

Figure 2.5 An example of Alfvén's theorem. Flow through a magnetic field causes the field lines to bow out.

Suggested Reading

Feynman, Leighton & Sands, *The Feynman lectures on physics, Vol. II, 1964* Addison–Wesley (Chapters 13–18 for an introduction to Maxwell's equations).

P Lorrain & D Corson, *Electromagnetism Principles and Applications*, W H Freeman & Co. (A good all-round text on electricity and magnetism.)

J A Shercliff, *A Textbook of Magnetohydrodynamics, 1965*. Pergamon Press (Chapter 2 for the MHD simplifications of Maxwell's equations).

Examples

2.1 A conducting fluid flows in a uniform magnetic field which is negligibly perturbed by the induced currents. Show that the condition for there to be no net charge distribution in the fluid is that $\mathbf{B} \cdot (\nabla \times \mathbf{u}) = 0$.

2.2 A thin conducting disc of thickness h and diameter d is placed in a uniform alternating magnetic field parallel to the axis of the disc. What is the induced current density as a function of distance from the axis of the disc?

2.3 Show that a coil carrying a steady current, I, tends to orientate itself in a magnetic field in such a way that the total magnetic field linking the coil is a maximum. Also, show that the torque exerted on the coil is $\mathbf{m} \times \mathbf{B}$, where $\mathbf{m}$ is the dipole momentum of the coil. What do you think will happen to a small current loop in a highly conducting fluid which is permeated by a large-scale magnetic field?

2.4 A fluid of small but finite conductivity flows through a tube constructed of insulating material. The velocity is very nearly uniform and equal to u. To measure the velocity of the fluid, a part of the tube is subjected to a uniform transverse magnetic field, B. Two small electrodes which are in contact with the fluid are installed through the tube walls. A voltmeter detects an induced e.m.f. of V. What is the velocity of the fluid?

2.5 Show that it is impossible to construct a generator of electromotive force constant in time operating on the principle of electromagnetic induction.

3

The Governing Equations of Fluid Mechanics

In his 1964 lectures on physics, R P Feynman noted that:

> The efforts of a child trying to dam a small stream flowing in the street, and his surprise at the strange way the water works its way out, has its analog in our attempts over the years to understand the flow of fluids. We have tried to dam the water by getting the laws and equations... but the water has broken through the dam and escaped our attempt to understand it.

In this chapter we build the dam and write down the equations. Later, particularly in Chapter 7 where we discuss turbulence, we shall see how the dam bursts open.

Part 1: Fluid Flow in the Absence of Lorentz Forces

In the first seven sections of this chapter we leave aside MHD and focus on fluid mechanics in the absence of the Lorentz force. We return to MHD in Section 3.8. Readers who have studied fluid mechanics before may be familiar with much of the material in Sections 3.1 to 3.7, and may wish to proceed directly to Section 3.8. The first seven sections provide a self-contained introduction to the subject, with particular emphasis on vortex dynamics, which is so important in the study of MHD.

3.1 Elementary Concepts

3.1.1 Different categories of fluid flow

The beginner in fluid mechanics is often bewildered by the many diverse categories of fluid flow which appear in the text books. There are entire books dedicated to such subjects as potential flow, boundary layers, turbulence, vortex dynamics and so on. Yet the relationship between these different types of flow, and their relationship to 'real' flows, is often unclear. You might ask, if I want to understand natural convection in a room do I want a text on boundary layers, turbulence or vortex

dynamics? The answer, probably, is all three. These subjects rarely exist in isolation, but rather interact in some complex way. For example, a turbulent wake is usually created when the turbulent fluid within one or more thin boundary layers is ejected from the boundaries into the main flow. The purpose of this section is to give some indication as to what expressions such as boundary layers, turbulence and vorticity mean, how these subjects interact, and when they are likely to be important in practice. The discussion is essentially qualitative, and anticipates some of the results proved in the subsequent sections. So the reader will have to take certain facts at face value. Nevertheless, the intention is to provide a broad framework into which the many detailed calculations of the subsequent sections fit.

We shall describe why, for good physical reasons, fluid mechanics and fluid flows are often divided into different regimes. In particular, there are three very broad sub-divisions in the subject. The first relates to the issue of when a fluid may be treated as inviscid, and when the finite viscosity possessed by all fluids (water, air, liquid metals) must be taken into account. Here we shall see that, typically, viscosity and shear stresses are of great importance close to solid surfaces (within so-called boundary layers) but often less important at a large distance from a surface. Next there is the sub-division between laminar (organised) flow and turbulent (chaotic) flow. In general, low speed or very viscous flows are stable to small perturbations and so remain laminar, while high speed or almost inviscid flows are unstable to the slightest perturbation and rapidly develop a chaotic component of motion. The final, rather broad, subdivision which occurs in fluid mechanics is between irrotational (sometimes called potential) flow and rotational flow. (By irrotational flow we mean flows in which $\nabla \times \mathbf{u} = 0$.) Turbulent flows and boundary layers are always rotational. Sometimes, however, under very particular conditions, an external flow may be approximately irrotational, and indeed this kind of flow dominated the early literature in aerodynamics. In reality, though, such flows are extremely rare in nature, and the large space given over to potential flow theory in traditional texts probably owes more to the ease with which such flows are amenable to mathematical description than to their usefulness in interpreting real events.

Let us now explore in a little more detail these three sub-divisions. We need two elementary ideas as a starting point. We need to be able to quantify shear stress and inertia in a fluid.

Let us start with inertia. Suppose, for the sake of argument, that we have a steady flow. That is to say, the velocity field $\mathbf{u}$, which we normally

write as $\mathbf{u}(\mathbf{x},t)$, is a function of $\mathbf{x}$ but not of t. It follows that the speed of the fluid at any one point in space is steady, the flow pattern does not change with time, and the streamlines (the analogue of **B**-lines) represent particle trajectories for individual fluid 'lumps'. Now consider a particular streamline, C, as shown in Figure 3.1, and focus attention on a particular fluid blob as it moves along the streamline. Let s be a curvilinear coordinate measured along C, and $V(s)$ be the speed $|\mathbf{u}|$. Since the streamline represents a particle trajectory, we can apply the usual rules of mechanics and write

$$(\text{acceleration of lump}) = V\frac{dV}{ds}\hat{\mathbf{e}}_t - \frac{V^2}{R}\hat{\mathbf{e}}_n$$

where R is the radius of curvature of the streamline, and $\hat{\mathbf{e}}_t$, $\hat{\mathbf{e}}_n$ represent unit vectors tangential and normal to the streamline. In general, then, the acceleration of a typical fluid element is of order $|\mathbf{u}|^2/l$, where l is a characteristic length scale of the flow pattern.

Next we turn to shear stress in a fluid. In most fluids this is quantified using an empirical law known as Newton's law of viscosity. This is most simply understood in a one-dimensional flow, $u_x(y)$, as shown in Figure 3.2. Here fluid layers slide over each other due to the fact that u_x is a function of y. One measure of this rate of sliding is the angular distortion rate, $d\gamma/dt$, of an initially rectangular element. (See Figure 3.2 for the definition of γ.) Newton's law of viscosity says that a shear stress, τ, is required to cause the relative sliding of the fluid layers. Moreover it states that τ is directly proportional to $d\gamma/dt$: $\tau = \mu(d\gamma/dt)$. The coefficient of proportionality is termed the absolute viscosity. However, it is clear from the diagram that $d\gamma/dt = \partial u/\partial y$, and so this expression is usually rewritten as

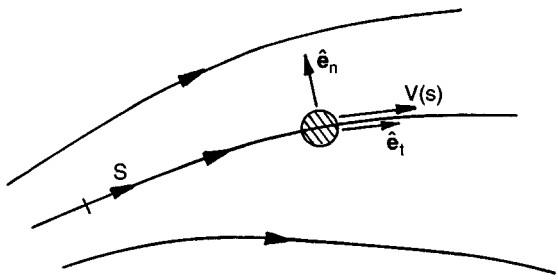

Figure 3.1 Acceleration of a fluid element in a steady flow.

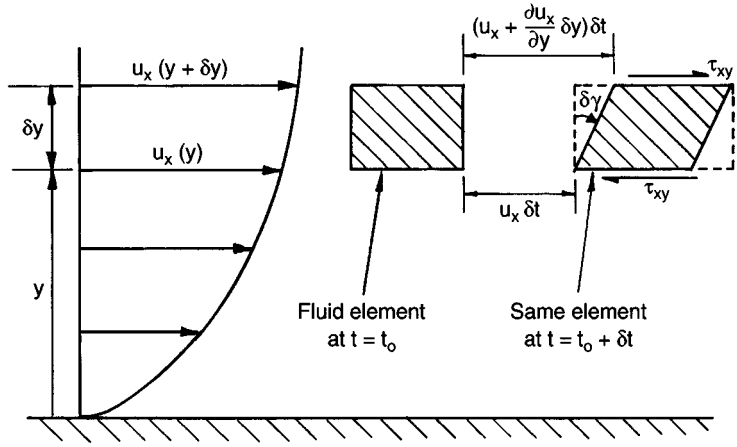

Figure 3.2 Distortion of a fluid element in a parallel flow.

$$\tau = \rho\nu\frac{\partial u_x}{\partial y}, \qquad \nu = \mu/\rho$$

where ν is called the kinematic viscosity. (The choice of kinematic viscosity rather than absolute viscosity is arbitrary, but has the benefit of avoiding confusion between permeability and viscosity.)

In a more general two-dimensional flow, $\mathbf{u}(x, y) = (u_x, u_y, 0)$, it turns out that γ, and hence $d\gamma/dt$, has two components, one arising from the rotation of vertical material lines, as shown above, and one arising from the rotation of horizontal material lines. A glance at Figure 3.9 will confirm that the additional contribution to $d\gamma/dt$ is $\partial u_y/\partial x$. Thus, in two dimensions, Newton's law of viscosity becomes

$$\tau_{xy} = \rho\nu\left(\frac{\partial u_x}{\partial y} + \frac{\partial u_y}{\partial x}\right)$$

This generalises in an obvious way to three dimensions (see Chapter 3, Section 1.2). Now shear stresses are important not just because they cause fluid elements to distort, but because an imbalance in shear stress can give rise to a net force on individual fluid elements. For example, in Figure 3.2 a net horizontal force will be exerted on the element if τ_{xy} at the top of the element is different to τ_{xy} at the bottom of the element. In fact, in this simple example it is readily confirmed that the net horizontal shear force per unit volume is $f_x = \partial\tau_{xy}/\partial y = \rho\nu\partial^2 u_x/\partial y^2$.

We are now in a position to estimate the relative sizes of inertial and viscous forces in a three-dimensional flow. The viscous forces per unit

volume are of the form of gradients in shear stress, such as $\partial\tau_{xy}/\partial y$, and have a size: $f_v \sim \rho\nu|\mathbf{u}|/l_\perp^2$, where $l_\perp$ is a characteristic length scale normal to the streamlines. The inertial forces per unit volume, on the other hand, are of the order of $f_{in} \sim \rho \times$ (acceleration) $\sim \rho u^2/l$ where l is a typical geometric length scale. The ratio of the two is of order

$$\mathrm{Re} = \frac{ul}{\nu}$$

This is the Reynolds number. When Re is small, viscous forces outweigh inertial forces, and when Re is large viscous forces are relatively small. Now we come to the key point. When Re is calculated using some characteristic geometric length scale, it is almost always very large. This reflects the fact that the viscosity of nearly all common fluids, including liquid metal, is minute, of the order of $10^{-6}\,\mathrm{m}^2/\mathrm{s}$. Because of the large size of Re, it is tempting to dispense with viscosity altogether. However, this is extremely dangerous. For example, inviscid theory predicts that a sphere sitting in a uniform cross-flow experiences no drag (d'Alembert's paradox) and this is clearly not the case, even for 'thin' fluids like air.

Something seems to have gone wrong. The problem is that, no matter how small ν might be, there are always regions near surfaces where the shear stresses are significant, i.e. of the order of the inertial forces. These *boundary layers* give rise to the drag on, say, an aerofoil. Consider the flow over an aerofoil shown in Figure 3.3. Here we use a frame of reference moving with the foil. The value of Re for such a flow, based on the width of the aerofoil, will be very large, perhaps around 10^8. Consequently, away from the surface of the aerofoil, the fluid behaves as if it is inviscid. Close to the aerofoil, however, something else happens, and this is a direct result of a boundary condition called the *no-slip condition*. The no-slip condition says that all fluids are 'sticky', in the sense that there can be no relative motion between a fluid and a surface

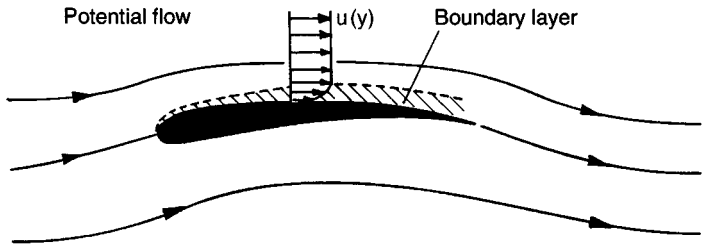

Figure 3.3 Boundary layer on an aerofoil.

with which it comes into contact. The fluid 'sticks' to the surface. In the case of the aerofoil, this means that there must be some transition region near the surface where the fluid velocity drops down from its *free-stream* value (the value it would have if the fluid were inviscid) to zero on the surface. This is the boundary layer. Boundary layers are usually very thin. We can estimate their thickness as follows. Within the boundary layer there must be some force acting on the fluid which pulls the velocity down from the free-stream value to zero at the surface. The force which does this is the viscous force, and so within the boundary layer the inertial and viscous forces must be of similar order. Let δ be the boundary layer thickness and l be the span of the aerofoil. The inertial forces are of order $\rho u^2/l$ and the viscous forces are of order $\rho\nu u/\delta^2$. Equating the two gives

$$\delta/l \sim (ul/\nu)^{-1/2} \ll 1$$

Thus we see that, no matter how small we make ν, there is always some (thin) boundary layer in which shear stresses are important. This is why an aerofoil experiences drag even when ν is very small.

We have reached the first of our three general sub-divisions in fluid mechanics. That is to say, often (but not always) a high-Re flow may be divided into an external, inviscid flow plus one or more boundary layers. Viscous effects are then confined to the boundary layer. This idea was introduced by Prandtl in 1904 and works well for external flow over bodies, particularly streamlined bodies, but can lead to problems in confined flows. (It is true that boundary layers form at the boundaries in confined flows, and that shear stresses are usually large within the boundary layers and weak outside the boundary layers. However, the small but finite shear in the bulk of a confined fluid can, over long periods of time, have a profound influence on the overall flow pattern (see Chapter 3, Section 5.))

Boundary layers have another important characteristic, called *separation*. Suppose that, instead of an aerofoil, we consider flow over a sphere. If the fluid were inviscid (which no real fluid is!) we would get a symmetric flow pattern as shown in Figure 3.4(a). The pressure at the stagnation points A and C in front of and behind the sphere would be equal (by symmetry), and from Bernoulli's equation the pressure at these points would be high, $P_A = P_\infty + \frac{1}{2}\rho V_\infty^2$, with P_∞ and V_∞ being the upstream pressure and velocity, respectively. The real flow looks something like that shown in Figure 3.4(b). A boundary layer forms at the leading stagnation point and this remains thin as the fluid moves to the edges

of the sphere. However, towards the rear of the sphere something unexpected happens. The boundary layer separates. That is to say, the fluid in the boundary layer is ejected into the external flow and a turbulent wake forms. This separation is caused by pressure forces. Outside the boundary layer the fluid, which tries to follow the inviscid flow pattern, starts to slow down as it passes over the outer edges of the sphere (points B and D) and heads towards the rear stagnation point. This deceleration is caused by pressure forces which oppose the external flow. These same pressure forces are experienced by the fluid within the boundary layer and so this fluid also begins to decelerate (Figure 3.4(c)). However, the fluid in the boundary layer has less momentum than the corresponding external flow and very quickly it comes to a halt, reverses direction, and moves off into the external flow, thus forming a wake. Thus we see that the flow over a body at high Re can generally be divided into three regions: an inviscid external flow, boundary layers, and a turbulent wake.

Now the fact that Re is invariably large has a second important consequence: most flows in nature are *turbulent*. This leads to a second classification in fluid mechanics. It is an empirical observation that at low values of Re flows are laminar, while at high values of Re they are turbulent (chaotic). This was first demonstrated in 1883 by Reynolds, who studied flow in a pipe. In the case of a pipe the transition from laminar to turbulent flow is rather sudden, and occurs at around $\mathrm{Re} \sim 2000$, which usually constitutes a rather slow flow rate.

A turbulent flow is characterised by the fact that, superimposed on the mean (time-averaged) flow pattern, there is a random, chaotic motion. The velocity field is often decomposed into its time-averaged component and random fluctuations about that mean: $\mathbf{u} = \bar{\mathbf{u}} + \mathbf{u}'$. The transition from laminar to turbulent flow occurs because, at a certain value of Re, instabilities develop in the laminar flow, usually driven by the inertial

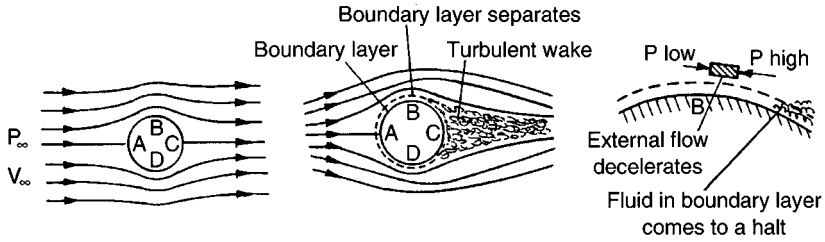

Figure 3.4 Flow over a sphere: (a) inviscid flow; (b) real flow at high Re; (c) pressure forces which cause separation.

forces. At low values of Re these potential instabilities are damped out by viscosity, while at high values of Re the damping is inadequate.

There is a superficial analogy between turbulence and the kinetic theory of gases. The steady laminar flow of a gas has, at the macroscopic level, only a steady component of motion. However, at the molecular level, individual atoms not only possess the mean velocity of the flow, but also some random component of velocity which is related to their thermal energy. It is this random fluctuation in velocity which gives rise to the exchange of momentum between molecules and thus to the macroscopic property of viscosity. There is an analogy between individual atoms in a laminar flow and macroscopic blobs of fluid in a turbulent flow. Indeed, this (rather imperfect) analogy formed the basis of most early attempts to characterise turbulent flow. In particular, it was proposed that one should replace ν in Newton's law of viscosity, which for a gas arises from thermal agitation of the molecules, by an 'eddy viscosity' ν_t, which arises from macroscopic fluctuations.

The transition from laminar to turbulent flow is rarely clear cut. For example, often some parts of a flow field are laminar while, at the same time, other parts are turbulent. The simplest example of this is the boundary layer on a flat plate (Figure 3.5). If the front of the plate is streamlined, and the turbulence level in the external flow is low, the boundary layer usually starts off as laminar. Of course, eventually it becomes unstable and turns turbulent.

Often periodic (non-turbulent) fluctuations in the laminar flow precede the onset of turbulence. This is illustrated in Figure 3.6, which shows flow over a cylinder at different values of Re. At low values of Re we get a

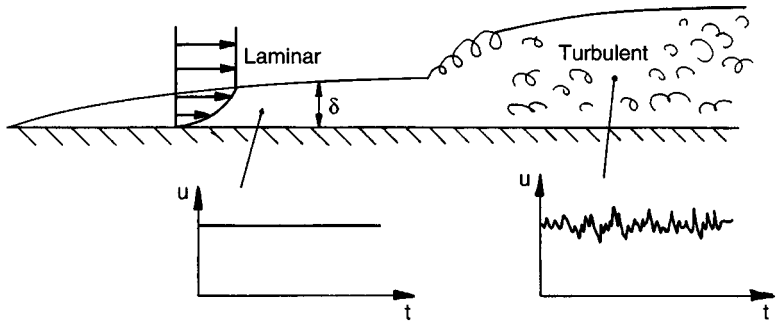

Figure 3.5 Development of a boundary layer on a flat plate.

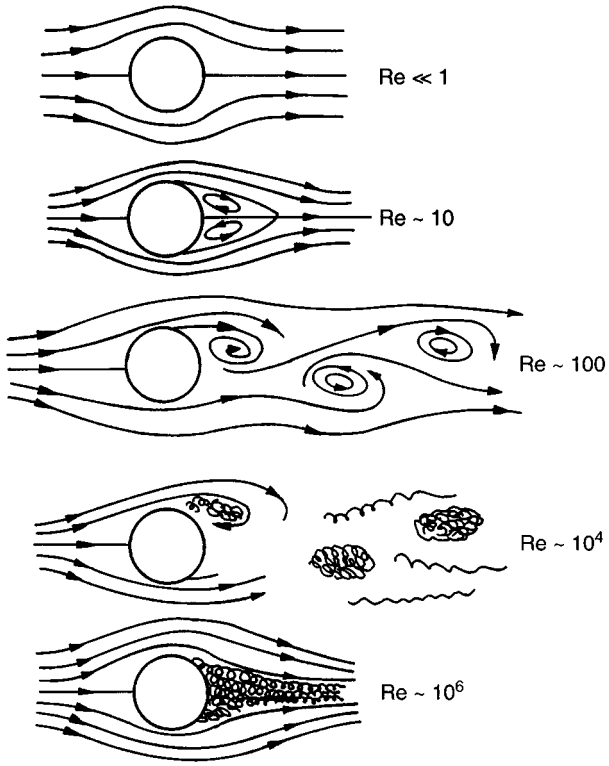

Figure 3.6 Flow behind a cylinder at various values of Re.

symmetric flow pattern. This is called creeping flow. As Re rises above unity, steady vortices appear at the rear of the cylinder. By the time Re has reached ~ 100 these vortices start to peel off from the rear of the cylinder in a regular, periodic manner (at this point the flow is still laminar). This is called Karman's vortex street. At yet higher values of Re the shed vortices become turbulent, but we still have a discernible vortex street. Finally, at a value of Re $\sim 10^5$, the flow at the rear of the cylinder loses its periodic structure and becomes a turbulent wake. Notice that upstream of the cylinder fluid blobs possess linear momentum but no angular momentum. In the Karman street, however, certain fluid elements (those in the vortices) possess both linear and angular momentum. Moreover, the angular momentum seems to have come from the boundary layer on the cylinder. This leads us to our third and final sub-division in fluid mechanics. In some flows (potential flows) the fluid elements possess only linear momentum. In others (vortical flows) they possess

both angular and linear momentum. In order to pursue this idea a little further we need some measure of the rotation of individual fluid elements. This is called vorticity.

So far we have discussed flow fields in terms of the velocity field $\mathbf{u}$. However, there is a closely related quantity, the vorticity, which is defined as $\boldsymbol{\omega} = \nabla \times \mathbf{u}$. From Stokes' theorem we have, for a small disc-like element of fluid (with surface area $d\mathbf{S}$),

$$\boldsymbol{\omega} \cdot d\mathbf{S} = \oint_C \mathbf{u} \cdot d\mathbf{l}$$

We might anticipate, therefore, that $\boldsymbol{\omega}$ is a measure of the angular velocity of a fluid element, and this turns out to be true. In fact, the angular velocity, $\boldsymbol{\Omega}$, of a fluid blob which is passing through point $\mathbf{x}_0$ at time t_0 is just $\boldsymbol{\omega}(\mathbf{x}_0, t_0)/2$. Thus, while $\mathbf{u}$ is related to the linear momentum of fluid elements, $\boldsymbol{\omega}$ is related to the angular momentum of blobs of fluid. Now $\boldsymbol{\omega}$ is a useful quantity because it turns out that, partially as a result of conservation of angular momentum, it cannot be created or destroyed within the interior of a fluid. (At least that is the case in the absence of external forces such as buoyancy or the Lorentz force.)

That is not to say that the vorticity of a fluid particle is constant. Consider the vortices within a Karman vortex street. It turns out that, as they are swept downstream, they grow in size in much the same way that a packet of hot fluid spreads heat by diffusion. Like heat, vorticity can diffuse. In particular, it diffuses between adjacent fluid particles as they sweep through the flow field. However, as with heat, this diffusion does not change the global amount of vorticity (heat) present in an isolated patch of fluid. Thus, as the vortices in the Karman street spread, the intensity of ω in each vortex falls, and it falls in such a way that $\int \omega dA$ is conserved for each vortex.

There is a second way in which the vorticity in a given lump of fluid can change. Consider the ice-skater who spins faster by pulling his or her arms inward. What is true for ice-skaters is true for blobs of fluid. If a spinning fluid blob is stretched by the flow, say from a sphere to cigar shape, it will spin faster, and the corresponding component of $\boldsymbol{\omega}$ increases.

In summary, then, vorticity cannot be created within the interior of a fluid unless there are body forces present, but like heat it spreads by diffusion and can be intensified by the stretching of fluid elements. The way in which we quantify the diffusion and intensification of vorticity will be discussed in the next section. However, for the moment, the important

point to grasp is that, like heat, vorticity cannot be created in the interior of a fluid.

So where does the vorticity evident in Figure 3.6 come from? Here the analogy to heat is useful. We shall see that, in the absence of stretching of fluid elements, the governing equation for ω is identical to that for heat. It is transported by the mean flow (we say it is *advected*) and diffuses outward from regions of intense vorticity. Also, just like heat, it is the boundaries which act as sources of vorticity. In fact, boundary layers are filled with the vorticity which has diffused out from the adjacent surface. (In a pseudo-one-dimensional boundary layer, with velocity $u_x(y)$, the vorticity is $|\omega_z| = \partial u_x/\partial y \sim u/\delta$.) This gives us a new way of thinking about boundary layers: they are diffusion layers for the vorticity generated on a surface. Again there is an analogy to heat. Thermal boundary layers are diffusion layers for the heat which seeps into the fluid from a surface. In both cases the thickness of the boundary layer is fixed by the ratio of: (i) the rate at which heat or vorticity diffuses across the streamlines from the surface, and (ii) the rate at which heat or vorticity is swept downstream by the mean flow. Usually when Re is large, the cross-stream diffusion is slow by comparison with the stream-wise transport of vorticity, and this is why boundary layers are so thin.

We are now in a position to introduce our third and final classification in fluid mechanics. This is the distinction between potential (vorticity free) flows and vortical flows. Consider Figure 3.7(a). This represents classical aerodynamics. There is a boundary layer, which is filled with vorticity, and an external flow. The flow upstream of the aerofoil is (in classical aerodynamics) assumed to be irrotational (free of vorticity), and since the vorticity generated on the surface of the foil is confined to the boundary layer, the entire external flow is irrotational. (This kind of external flow is called a potential flow.)

The problem of computing the external motion is now reduced to solving two kinematic equations: $\nabla \cdot \mathbf{u} = 0$ (conservation of mass) and $\nabla \times \mathbf{u} = 0$. In effect, aerodynamics becomes aerokinematics. However, potential flows (irrotational flows) are extremely rare in nature. In fact, flow over streamlined bodies (plus certain types of water waves) represent the only common examples. Almost all real flows are laden with vorticity: vorticity which has been generated somewhere in a boundary layer and then released into the bulk flow (see Figures 3.6 and 3.7(b)). The rustling of leaves, the blood in our veins, the air in our lungs, the wind blowing down the street, natural convection in a room, and the flows in the oceans and atmosphere are all examples of flows laden with

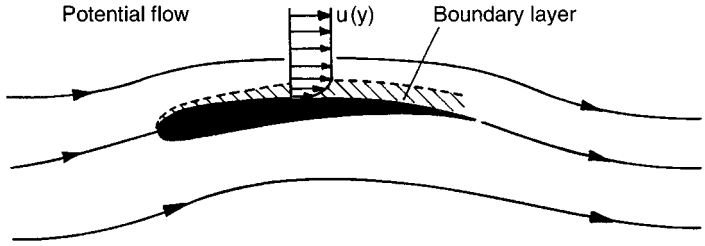

Figure 3.7 (a) Classical aerodynamics (potential flow).

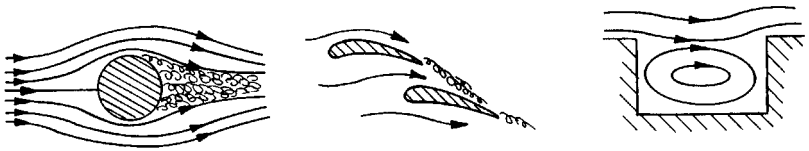

(a) The turbulent wake is full of vorticity

(b) In a turbine the vorticity created by one blade spills out into the next blade

(c) In confined flows the vorticity created at the boundaries slowly seeps into the entire flow, eventually dominating the flow

Figure 3.7 (b) Most real flows are laden with vorticity.

vorticity. So we have two types of flow: potential flows, which are easy to compute but infrequent in nature, and vortical flows, which are very common but much more difficult to understand. The art of quantifying this second category of flow is to track the progress of the vorticity from the boundaries into the bulk of the fluid. Often this arises from wakes or from boundary-layer separation. Sometimes, as in the case of confined flows, it is due to a slow but finite diffusion of vorticity from the boundary into the interior of the flow. In either case, it is the boundaries which generate the vorticity.

To these two classes of flow, potential flow and unforced vortical flow, we should add a third: that of MHD. Here the Lorentz force generates vorticity in the interior of the fluid. On the one hand this makes MHD more difficult to understand, but on the other it makes it more attractive. In MHD we have the opportunity to grab hold of the interior of a fluid and manipulate the flow.

With this brief, qualitative overview of fluid mechanics we now set about quantifying the motion of a fluid. Our starting point is the equation of motion of a fluid blob.

3.1.2 The Navier–Stokes equation

The Navier–Stokes equation is a statement about the changes in linear momentum of a small element of fluid as it progresses through a flow field. Let p be the pressure, τ_{ij} the viscous stresses acting on the fluid, and ν the kinematic viscosity. Then Newton's second law applied to a small blob of fluid of volume δV yields[1]

$$(\rho \delta V)\frac{D\mathbf{u}}{Dt} = -(\nabla p)\delta V + [\partial \tau_{ij}/\partial x_j]\delta V \tag{3.1}$$

That is to say, the mass of the element, $\rho \delta V$, times its acceleration, $D\mathbf{u}/Dt$, equals the net pressure force acting on the surface of the fluid blob,

$$\oint (-p)d\mathbf{S} = \int (-\nabla p)dV = -(\nabla p)\delta V$$

plus the net force arising from the viscous stress, τ_{ij}. The last term in (3.1) may be established by considering the forces acting on a small rectangular element $dxdydz$, as indicated in Figure 3.8.

We shall take the fluid to be incompressible so that the conservation of mass, expressed as $\nabla \cdot (\rho \mathbf{u}) = -\partial \rho/\partial t$, reduces to the so-called continuity equation

$$\nabla \cdot \mathbf{u} = 0 \tag{3.2}$$

We also take the fluid to be Newtonian, so that the viscous stresses are given by the constitutive law

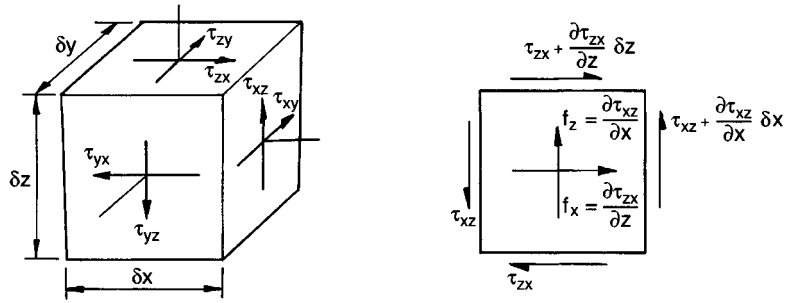

(a) Sign convention for stresses (note that $\tau_{ij} = \tau_{ji}$)

(b) Net effective body force, per unit volume, caused by an inbalance in stresses. Only components in th xz plane are shown

Figure 3.8 Stresses acting on a cube of fluid.

[1] Those unfamiliar with tensor notation will find a brief summary in Section 7.1.

$$\tau_{ij} = \rho\nu\left(\frac{\partial u_i}{\partial x_j} + \frac{\partial u_j}{\partial x_i}\right) \tag{3.3}$$

where ν is the kinematic viscosity of the fluid. Substituting for τ_{ij} in (3.1) and dividing through by $\rho\delta V$ yields the conventional form of the Navier–Stokes equation

$$\boxed{\frac{D\mathbf{u}}{Dt} = -\nabla(p/\rho) + \nu\nabla^2\mathbf{u}} \tag{3.4}$$

The boundary condition on $\mathbf{u}$ corresponding to (3.4) is that $\mathbf{u} = 0$ on any stationary, solid surface, i.e. the fluid 'sticks' to any solid surface. This is the 'no-slip' condition.

The expression $D(\cdot)/Dt$ represents the convective derivative. It is the rate of change of a quantity associated with a given element of fluid. This should not be confused with $\partial(\cdot)/\partial t$, which is, of course, the rate of change of a quantity at a fixed point in space. For example, DT/Dt is the rate of change of temperature of a fluid lump as it moves around, whereas $\partial T/\partial t$ is the rate of change of temperature at a fixed point (through which a succession of fluid particles will move). It follows that $D\mathbf{u}/Dt$ is the acceleration of a fluid element, which is why it appears on the left of (3.4).

An expression for $D\mathbf{u}/Dt$ may be obtained as follows. Consider a scalar function of position and time, $f(\mathbf{x},t)$. We have $\delta f = (\partial f/\partial t)\delta t + (\partial f/\partial x)\delta x + \ldots$ If we are interested in the change in f following a fluid particle, then $\delta x = u_x\delta t$ etc. and so

$$\frac{D}{Dt}(f) = \frac{\partial}{\partial t}(f) + (\mathbf{u}\cdot\nabla)(f) = \frac{\partial}{\partial t}(f) + u_x\frac{\partial}{\partial x}(f) + \ldots$$

The same expression may be applied to each of the components of the vector field, say $\mathbf{a}$. We write this symbolically as

$$\frac{D}{Dt}(\mathbf{a}) = \frac{\partial}{\partial t}(\mathbf{a}) + (\mathbf{u}\cdot\nabla)(\mathbf{a})$$

which represents three scalar equations, each of the form given above. We now set $\mathbf{a} = \mathbf{u}$, which allows us to rewrite (3.4) in the form

$$\frac{\partial\mathbf{u}}{\partial t} + (\mathbf{u}\cdot\nabla)\mathbf{u} = -\nabla(p/\rho) + \nu\nabla^2\mathbf{u} \tag{3.5}$$

Note that, in steady flows (i.e. flows in which $\partial\mathbf{u}/\partial t = 0$), the streamlines represent particle trajectories and the acceleration of a fluid element is $\mathbf{u}\cdot\nabla\mathbf{u}$. The physical origin of this expression becomes clearer when we

rewrite $(\mathbf{u} \cdot \nabla)\mathbf{u}$ in terms of curvilinear coordinates attached to a streamline. As noted earlier,

$$(\mathbf{u} \cdot \nabla)\mathbf{u} = V\frac{\partial V}{\partial s}\hat{\mathbf{e}}_t - \frac{V^2}{R}\hat{\mathbf{e}}_n \tag{3.6}$$

(see Chapter 3, Section 1.1). Here $V = |\mathbf{u}|$, $\hat{\mathbf{e}}_t$ and $\hat{\mathbf{e}}_n$ are unit vectors in the tangential and principle normal directions, s is a streamwise coordinate, and R is the local radius of curvature of the streamline. The first expression on the right is the rate of change of speed, $\frac{DV}{Dt}$, while the second is the centripetal acceleration, which is directed toward the centre of curvature of the streamline and is associated with the change in direction of the velocity of a particle.

3.2 Vorticity, Angular Momentum and the Biot–Savart Law

So far we have concentrated on the velocity field, $\mathbf{u}$. However, in common with many other branches of fluid mechanics, in MHD it is often more fruitful to work with the vorticity field defined by

$$\boldsymbol{\omega} = \nabla \times \mathbf{u} \tag{3.7}$$

The reason is two-fold. First, the rules governing the evolution of $\boldsymbol{\omega}$ are somewhat simpler than those governing $\mathbf{u}$. For example, pressure gradients appear as a source of linear momentum in (3.5), yet the pressure itself depends on the instantaneous (global) distribution of $\mathbf{u}$. By focusing on vorticity, on the other hand, we may dispense with the pressure field entirely. (The reasons for this will become evident shortly.) The second reason for studying vorticity is that many flows are characterised by localised regions of intense rotation (i.e. vorticity). Smoke rings, dust whirls in the street, trailing vortices on aircraft wings, whirlpools, tidal vortices, tornadoes, hurricanes and the great red spot of Jupiter represent just a few examples!

Let us start by trying to endow $\boldsymbol{\omega}$ with some physical meaning. Consider a small element of fluid in a two-dimensional flow $\mathbf{u}(x, y) = (u_x, u_y, 0)$, $\boldsymbol{\omega} = (0, 0, \omega_z)$. Suppose that, at some instant, the element is circular (a disk) with radius r. Let $\mathbf{u}_0$ be the linear velocity of the centre of the element and Ω be its mean angular velocity, defined as the average rate of rotation of two mutually perpendicular material lines embedded in the element. From Stoke's theorem, or else from the definition of the curl as a line integral per unit area, we have

$$\omega_z \pi r^2 = \int (\nabla \times \mathbf{u}) \cdot d\mathbf{S} = \oint \mathbf{u} \cdot d\mathbf{l} \tag{3.8}$$

We might anticipate that the line integral on the right has a value of $(\Omega r)2\pi r$. If this were the case, then

$$\omega_z = 2\Omega \tag{3.9}$$

In fact exact analysis confirms that this is so: the anti-clockwise rotation rate of a short line element, dx, orientated parallel to the x-axis is $\partial u_y/\partial x$, while the rotation rate of a line element, dy, parallel to the y-axis is $-\partial u_x/\partial y$, giving $\Omega = (\partial u_y/\partial x - \partial u_x/\partial y)/2 = \omega_z/2$ (Figure 3.9). This confirms equation (3.9). It appears, therefore, that ω_z is twice the angular velocity of the fluid element. This result extends to three dimensions. The vorticity at a particular location is twice the average angular velocity of a blob of fluid passing through that point. In short, $\boldsymbol{\omega}$ is a measure of the local rotation, or spin, of a fluid element.

It should be emphasised, however, that $\boldsymbol{\omega}$ has nothing at all to do with the global rotation of a fluid. Rectilinear flows may possess vorticity, while flows with circular streamlines need not. Consider, for example, the rectilinear shear flow $\mathbf{u}(y) = (\gamma y, 0, 0)$, γ = constant. The streamlines are straight and parallel yet the fluid elements rotate at a rate $\omega/2 = -\gamma/2$. This is because vertical line elements, dy, move faster at the top of the element than at the bottom, so they continually rotate towards the horizontal.

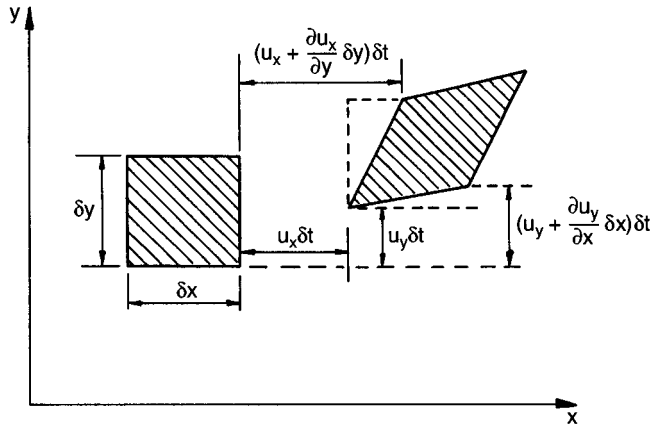

Figure 3.9 Rotation of a fluid element.

Conversely, we can have global rotation of a flow without local rotation of the fluid elements. One example is the so-called free vortex $\mathbf{u}(r) = (0, k/r, 0)$ in (r, θ, z) coordinates. Here k is a constant. It is readily confirmed that $\boldsymbol{\omega} = 0$ in such a vortex.

So far we have been concerned only with kinematics. We now introduce some dynamics. Since we are interested in rotation, it is natural to focus on angular momentum rather than linear momentum. Consider the angular momentum, $\mathbf{H}$, of a small material element that is *instantaneously* spherical. Then

$$\mathbf{H} = \frac{1}{2} I\boldsymbol{\omega}$$

where I is the moment of inertia of the blob. This angular momentum will change at a rate determined by the tangential surface stresses alone. The pressure has no influence on $\mathbf{H}$ at the instant at which the element is spherical since the pressure forces all point radially inward. Therefore, at one particular instant in time, we have

$$\frac{D\mathbf{H}}{Dt} = \nu\mathbf{T}$$

where $\nu\mathbf{T}$ denotes the viscous torque acting on the sphere. Now the convective derivative satisfies the usual rules of differentiation and so we have

$$I\frac{D\boldsymbol{\omega}}{Dt} = -\boldsymbol{\omega}\frac{DI}{Dt} + 2\nu\mathbf{T} \tag{3.10}$$

Evidently, the terms on the right arise from the change in the moment of inertia of a fluid element and the viscous torque, respectively. In cases where viscous stresses are negligible (i.e. outside boundary layers) this simplifies to

$$\frac{D}{Dt}(I\boldsymbol{\omega}) = 0 \tag{3.11}$$

Now (3.10) and (3.11) are not very useful (or even very meaningful) as they stand, since they apply only at the initial instant during which the fluid element is spherical. However, they suggest several results, all of which we shall confirm by rigorous arguments in the next section. First, there is no reference to pressure in (3.10) and (3.11), so that we might anticipate that $\boldsymbol{\omega}$ evolves independently of p. Second, if $\boldsymbol{\omega}$ is initially zero, and the flow is inviscid, then $\boldsymbol{\omega}$ should remain zero in each fluid particle as it is swept around the flow field. This is the basis of potential flow theory in which we set $\boldsymbol{\omega} = 0$ in the upstream fluid, and so we can assume

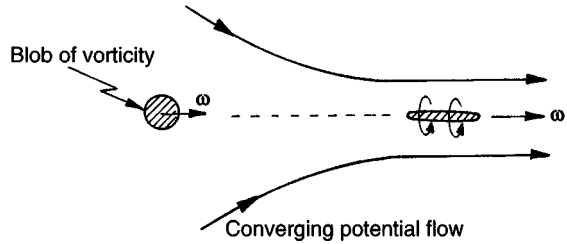

Figure 3.10 Stretching of fluid elements can intensify the vorticity.

that ω is zero at all points. Third, if I decreases in a fluid element (and $\nu = 0$), then the vorticity of that element should increase. For example, consider a blob of vorticity embedded in an otherwise potential flow field consisting of converging streamlines, as shown in Figure 3.10.

An initially spherical element will be stretched into an ellipsoid by the converging flow. The moment of inertia of the element about an axis parallel to ω decreases, and consequently ω must rise to conserve $\mathbf{H}$. It is possible, therefore, to intensify vorticity by stretching fluid blobs. Intense rotation can result from this process, the familiar bath-tub vortex being just one example. We shall see that something very similar happens to magnetic fields. They, too, can be intensified by stretching.

Finally we note that there is an analogy between the differential form of Ampère's law, $\nabla \times \mathbf{B} = \mu\mathbf{J}$, and the definition of vorticity, $\nabla \times \mathbf{u} = \boldsymbol{\omega}$. We can therefore hijack the Biot–Savart law from electromagnetic theory to invert the relationship $\boldsymbol{\omega} = \nabla \times \mathbf{u}$. That is to say, in infinite domains,

$$\mathbf{u} = \frac{1}{4\pi}\int \frac{\boldsymbol{\omega}(\mathbf{x}') \times \mathbf{r}}{r^3} d^3\mathbf{x}', \qquad \mathbf{r} = \mathbf{x} - \mathbf{x}' \tag{3.12}$$

Also, note that, like $\mathbf{u}$ and $\mathbf{B}$, the vorticity field is solenoidal, $\nabla \cdot \boldsymbol{\omega} = 0$, since it is the curl of another vector. Consequently, we may invoke the idea of vortex tubes, which are analogous to magnetic flux tubes or streamtubes.

3.3 Advection and Diffusion of Vorticity

3.3.1 The vorticity equation

We now formally derive the laws governing the evolution of vorticity. We start by writing (3.5) in the form

$$\frac{\partial \mathbf{u}}{\partial t} = \mathbf{u} \times \boldsymbol{\omega} - \nabla(P/\rho + u^2/2) + \nu \nabla^2 \mathbf{u} \tag{3.13}$$

which follows from the identity

$$\nabla(u^2/2) = (\mathbf{u} \cdot \nabla)\mathbf{u} + \mathbf{u} \times \nabla \times \mathbf{u} = (\mathbf{u} \cdot \nabla)\mathbf{u} + \mathbf{u} \times \boldsymbol{\omega}$$

Note, in passing, that steady, inviscid flows have the property that $\mathbf{u} \cdot \nabla(P/\rho + u^2/2) = 0$, so that $C = P/\rho + u^2/2$ is constant along a streamline. This is Bernoulli's theorem, C being Bernoulli's function.

We now take the curl of (3.13), noting that the gradient term disappears:

$$\boxed{\frac{\partial \boldsymbol{\omega}}{\partial t} = \nabla \times [\mathbf{u} \times \boldsymbol{\omega}] + \nu \nabla^2 \boldsymbol{\omega}} \tag{3.14}$$

Compare this with (2.24). It appears that $\boldsymbol{\omega}$ and $\mathbf{B}$ obey precisely the same evolution equation! We shall exploit this analogy repeatedly in subsequent chapters. Now since $\mathbf{u}$ and $\boldsymbol{\omega}$ are both solenoidal, we have the vector relationship

$$\nabla \times (\mathbf{u} \times \boldsymbol{\omega}) = (\boldsymbol{\omega} \cdot \nabla)\mathbf{u} - (\mathbf{u} \cdot \nabla)\boldsymbol{\omega}$$

and so (3.14) may be rewritten as

$$\boxed{\frac{D\boldsymbol{\omega}}{Dt} = (\boldsymbol{\omega} \cdot \nabla)\mathbf{u} + \nu \nabla^2 \boldsymbol{\omega}} \tag{3.15}$$

Compare this with our angular momentum equation for a blob which is instantaneously spherical:

$$I \frac{D\boldsymbol{\omega}}{Dt} = -\boldsymbol{\omega} \frac{DI}{Dt} + 2\nu \mathbf{T}$$

We might anticipate that the terms on the right of (3.15) represent: (a) the change in the moment of inertia of a fluid element due to stretching of that element; (b) the viscous torque on the element. In other words, the rate of rotation of a fluid blob may increase or decrease due to changes in its moment of inertia, or change because it is spun up or slowed down by viscous stresses.

3.3.2 *Advection and diffusion of vorticity: temperature as a prototype*

There is another way of looking at (3.15). It may be interpreted as an *advection–diffusion equation* for vorticity. The idea of an advection–diffusion equation is so fundamental to MHD that it is worth dwelling on its significance. Perhaps this is most readily understood in the context of two-dimensional flows, in which $\mathbf{u}(x, y) = (u_x, u_y, 0)$ and $\boldsymbol{\omega}(x, y) = (0, 0, \omega_z)$. The first term on the right of (3.15) now vanishes to yield

$$\frac{D\omega_z}{Dt} = \nu\nabla^2\omega_z \tag{3.16}$$

Compare this with the equation governing the temperature, T, in a fluid,

$$\frac{DT}{Dt} = \alpha\nabla^2 T \tag{3.17}$$

where α is the thermal diffusivity. This is the advection–diffusion equation for heat. In some ways (3.17) represents the prototype advection–diffusion equation and we shall take a moment to review its properties. When $\mathbf{u}$ is zero, we have, in effect, a solid: the temperature field evolves according to

$$\frac{\partial T}{\partial t} = \alpha\nabla^2 T$$

Heat soaks through material purely by virtue of thermal diffusion (conduction). At the other extreme, if $\mathbf{u}$ is non-zero but the fluid is thermally insulating ($\alpha = 0$), we have

$$\frac{DT}{Dt} = 0$$

As each fluid lump moves around it conserves its heat, and hence temperature. This is referred to as the advection of heat, i.e. the transport of heat by virtue of material movement. In general, though, we have both advection and diffusion of heat. To illustrate the combined effect of these processes, consider the unsteady, two-dimensional distribution of temperature in a uniform cross flow, $(u_x, 0, 0)$. From (3.17) we have

$$\frac{\partial T}{\partial t} + u_x\frac{\partial T}{\partial x} = \alpha\nabla^2 T$$

Suppose that heat is injected into the fluid from a hot wire. When the velocity is low and the conductivity high the isotherms around the wire will be almost circular. When the conductivity is low, however, each fluid

element will tend to conserve its heat as it moves. The isotherms will then become elongated, as shown in Figure 3.11.

The relative size of the advection to the diffusion term is given by the Peclet number $P = ul/\alpha$. (Here l is a characteristic length scale.) If the Peclet number is small, then the transfer of heat is diffusion-dominated. When it is large, advection dominates.

Now consider the case of a wire which is being pulsed with electric current to produce a sequence of hot fluid packets. These are swept downstream and grow by diffusion. In Figure 3.12, heat is restricted to the dotted volumes of fluid. Outside these volumes $T = 0$ (or equal to some reference temperature). Note that advection and diffusion represent processes in which heat is redistributed. However, heat cannot be created or destroyed by advection or diffusion. That is, the total amount of heat is conserved. This is most easily seen by integrating (3.17) over a fixed volume in space and then using Gauss's theorem:

$$\frac{d}{dt}\int T dV + \oint (\mathbf{u}T)\cdot d\mathbf{S} = \alpha \oint \nabla T \cdot d\mathbf{S}$$

Now heat per unit mass is directly proportional to T, and so this states that the net rate of change of heat within a fixed volume decreases if heat is advected across the bounding surface but increases if heat is conducted (diffuses) into the volume from the surrounding fluid. We now apply this equation to a volume which encloses one of the dotted volumes shown in Figure 3.12 (where T is zero at the boundary). We obtain

$$\frac{d}{dt}\int T dV = 0$$

Heat is conserved within each of the dotted volumes as it is swept downstream.

From (3.16) we see that the vorticity in a two-dimensional flow is advected and diffused just like heat. The analogue of the diffusion coefficient is ν and the Reynolds number, ul/ν, now plays the rôle of the Peclet

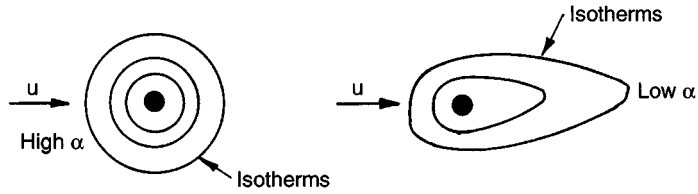

Figure 3.11 Advection and diffusion of heat from a hot wire.

Figure 3.12 Advection and diffusion of heat from a pulsed wire.

number. In other words, vorticity is advected by **u** and diffused by the viscous stresses. Moreover, just like heat, vorticity cannot be created or destroyed within the interior of the flow. The net vorticity within a volume V can change only if vorticity is advected in or out of the volume, or else diffused across the boundary. In the absence of surface effects, global vorticity is conserved. A simple example of this (analogous to the blobs of heat above) are the vortices in the Karman vortex street behind a cylinder (Figure 3.13). The vortices are advected by the velocity and spread by diffusion, but the total vorticity within each eddy remains constant as it moves downstream.

A simple illustration of the diffusion of vorticity is given by the following example (Figure 3.14). Suppose that a plate of infinite length is immersed in a still fluid. At time $t = 0$ it suddenly acquires a constant velocity V in its own plane. We want to find the subsequent motion, $\mathbf{u}(y,t)$. Now, by the no-slip condition, the fluid adjacent to the plate sticks to it, and so moving the plate creates a gradient in velocity, which gives rise to vorticity. The plate becomes a source of vorticity, which subsequently diffuses into the fluid. Since u_x is not a function of x, the continuity equation gives $\partial u_y/\partial y = 0$, and since u_y is zero at the plate, $u_y = 0$ everywhere. The vorticity equation (3.16) then becomes

$$\frac{\partial \omega_z}{\partial t} = \nu \frac{\partial^2 \omega_z}{\partial y^2}, \qquad \omega_z = -\frac{\partial u_x}{\partial y} \tag{3.18}$$

This is identical to the equation describing the diffusion of heat from an infinite, heated plate whose surface temperature is suddenly raised from

Figure 3.13 Karman vortices behind a cylinder.

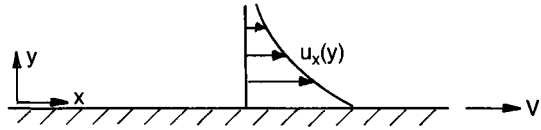

Figure 3.14 Diffusion of vorticity from a plate.

$T = 0$ to $T = T_0$. This sort of diffusion equation can be solved by looking for a similarity solution. To illustrate this, consider first the analogous thermal problem.

We know that heat diffuses a distance $(2\alpha t)^{1/2}$ away from the plate in a time t, and that the temperature distribution has the form

$$T = T_0 f(y/l), \qquad l = (2\alpha t)^{1/2}$$

The quantity l is called the diffusion length. The equation above states that the dimensionless temperature profile, T/T_0, depends only on the dimensionless coordinate y/l. When y is scaled by l in this way, the temperature distribution appears always to have a universal form.

The analogy to heat suggests that we look for a solution of our vorticity equation of the form

$$\omega = \frac{V}{l} f(y/l), \qquad l = (2\nu t)^{1/2}$$

Substituting this into (3.18) reduces our partial differential equation to

$$f'(\eta) + \eta f(\eta) = 0, \qquad \eta = y/l$$

This may be integrated to give

$$\omega_z = \frac{C_1 V}{l} \exp[-\eta^2/2]$$

To fix the constant of integration, C_1, we need to integrate to find u_x on the surface of the plate. From this we find $C_1^2 = 2/\pi$, and so the vorticity distribution is

$$\omega_z = \frac{V}{(\pi\nu t)^{1/2}} \exp[-y^2/(4\nu t)]$$

This may now be integrated once more to give the velocity field. However, the details of this solution are perhaps less important than the overall picture. That is, vorticity is created at the surface of the plate by the shear stresses acting on that surface. This vorticity then diffuses into the interior of the fluid in exactly the same way as heat

diffuses in from a heated surface. There is no vorticity generation within the interior of the flow. The vorticity is merely redistributed (spread) by virtue of diffusion.

3.3.3 *Vortex line stretching*

Let us now return to our general vorticity equation (3.15)

$$\frac{D\boldsymbol{\omega}}{Dt} = (\boldsymbol{\omega} \cdot \nabla)\mathbf{u} + \nu\nabla^2\boldsymbol{\omega}$$

In three-dimensional flows the first term on the right is non-zero, and it is this additional effect which distinguishes three-dimensional flows from two-dimensional ones. It appears that the vorticity no longer behaves like a temperature field. We have already suggested, by comparing this with our angular momentum equation, that $(\boldsymbol{\omega} \cdot \nabla)\mathbf{u}$ represents intensification of vorticity by the stretching fluid elements. We shall now confirm that this is indeed the case.

Consider, by way of example, an axisymmetric flow consisting of converging streamlines (in the r–z plane) as well as a swirling component of velocity, u_θ. By writing $\nabla \times \mathbf{u}$ in terms of cylindrical coordinates, we find that, near the axis, the axial component of vorticity is

$$\omega_z = \frac{1}{r}\frac{\partial}{\partial r}(ru_\theta)$$

Now consider the axial component of the vorticity equation (3.15) applied near $r = 0$. In addition to the usual advection and diffusion terms we have the expression

$$(\boldsymbol{\omega} \cdot \nabla)\mathbf{u} \sim \omega_z \frac{\partial u_z}{\partial z}$$

This appears on the right of (3.15) and so acts like a source of axial vorticity. In particular, the vorticity, ω_z, intensifies if $\partial u_z/\partial z$ is positive, i.e. the streamlines converge. This is because fluid elements are stretched and elongated on the axis, as shown in Figure 3.15. This leads to a reduction in the axial moment of inertia of the element and so, by conservation of angular momentum, to an increase in ω_z.

More generally, consider a thin tube of vorticity, as shown in Figure 3.16. Let $u_{//}$ be the component of velocity parallel to the vortex tube and s be a coordinate measured along the tube. Then

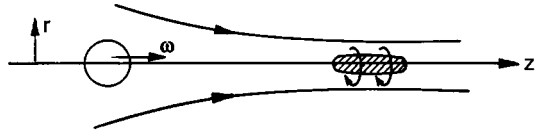

Figure 3.15 Stretching of a material element.

$$|\omega| \frac{du_{//}}{ds} = (\omega \cdot \nabla) u_{//}$$

Now the vortex line is being stretched if the velocity $u_{//}$ at point B is greater than $u_{//}$ at A. That is, the length of the material element AB increases if $du_{//}/ds > 0$. Thus the term $(\omega \cdot \nabla)\mathbf{u}$ represents stretching of the vortex lines. This leads to an intensification of vorticity through conservation of angular momentum, confirming our interpretation of $(\omega \cdot \nabla)\mathbf{u}$ in (3.15).

3.4 Kelvin's Theorem, Helmholtz's Laws and Helicity

We now do something dangerous. We set aside viscosity so that we can discuss the great advances made in inviscid fluid mechanics by the nineteenth century physicists and mathematicians. This is dangerous because, as we shall see, a fluid with no viscosity behaves very differently to a fluid with a small but finite viscosity. To emphasise this, John von Neumann refers to inviscid fluid mechanics as the study of *dry water*!

3.4.1 Kelvin's Theorem and Helmholtz's Laws

We now summarise the classical theorems of inviscid vortex dynamics. We start with the idea of a vortex tube. This is an aggregate of vortex lines, rather like a magnetic flux tube is composed of magnetic field lines. Since $\nabla \cdot \omega = 0$ we have

$$\oint \omega \cdot d\mathbf{S} = 0$$

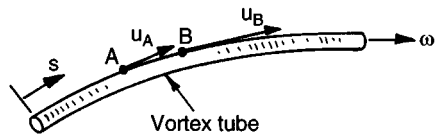

Figure 3.16 Stretching of a tube of vorticity.

It follows that the flux of vorticity, $\Phi = \int \boldsymbol{\omega} \cdot d\mathbf{S}$, is constant along the length of a vortex tube since no flux crosses the side of the tube. A closely related quantity is the circulation, Γ. This is defined as the closed line integral of $\mathbf{u}$:

$$\Gamma = \oint_C \mathbf{u} \cdot d\mathbf{l} \tag{3.19}$$

If the path C is taken as lying on the surface of a vortex tube, and passing once around it (Figure 3.17), Stoke's theorem tells us that $\Gamma = \Phi$. Γ is sometimes called the strength of the vortex tube.

Kelvin's (1869) theorem is couched in terms of circulation. It says that, if $C_m(t)$ is a closed curve that always consists of the same fluid particles (a material curve), then the circulation

$$\Gamma = \oint_{C_m(t)} \mathbf{u} \cdot d\mathbf{l}$$

is independent of time. Note that this theorem does not hold true if C is fixed in space; C_m must be a material curve moving with the fluid. Nor does it apply if the fluid is subject to a rotational body force, $\mathbf{F}$, such as $\mathbf{J} \times \mathbf{B}$, or for that matter if viscous forces are significant at any point on C_m.

The proof of Kelvin's theorem follows directly from the kinematic equation (2.25).

$$\frac{d}{dt} \int_{S_m} \mathbf{G} \cdot d\mathbf{S} = \int_{S_m} \left[\frac{\partial \mathbf{G}}{\partial t} - \nabla \times (\mathbf{u} \times \mathbf{G}) \right] \cdot d\mathbf{S}$$

If we take $\mathbf{G} = \boldsymbol{\omega}$, invoke the vorticity equation (3.14), and use Stokes' theorem, we have

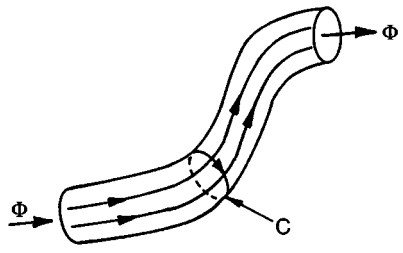

Figure 3.17 A vortex tube.

$$\frac{d\Gamma}{dt} = \frac{d}{dt}\int_{S_m} \boldsymbol{\omega} \cdot d\mathbf{S} = \nu \int_{S_m} \nabla^2 \boldsymbol{\omega} \cdot d\mathbf{S} = 0$$

and Kelvin's theorem is proved.

Helmholtz's laws are closely related to Kelvin's theorem. They were published in 1858 and, like Kelvin's theorem, apply only to inviscid flows. They state that:

(i) the fluid elements that lie on a vortex line at some initial instant continue to lie on that vortex line for all time, i.e. the vortex lines are frozen into the fluid;

(ii) the flux of vorticity

$$\Phi = \int \boldsymbol{\omega} \cdot d\mathbf{S}$$

is the same at all cross sections of a vortex tube and is independent of time.

Consider Helmholtz's first law. In two-dimensional flows it is a trivial consequence of $D\omega_z/Dt = 0$. In three-dimensions, for which

$$\frac{D\boldsymbol{\omega}}{Dt} = (\boldsymbol{\omega} \cdot \nabla)\mathbf{u} \tag{3.20}$$

more work is required. First we need the following result. Let $d\mathbf{l}$ be a short line drawn in the fluid at some instant, and suppose $d\mathbf{l}$ subsequently moves with the fluid. Then the rate of change of $d\mathbf{l}$ is $\mathbf{u}(\mathbf{x} + d\mathbf{l}) - \mathbf{u}(\mathbf{x})$, and so

$$\frac{D}{Dt}(d\mathbf{l}) = \mathbf{u}(\mathbf{x} + d\mathbf{l}) - \mathbf{u}(\mathbf{x})$$

where $\mathbf{x}$ and $\mathbf{x} + d\mathbf{l}$ are the position vectors at the two ends of $d\mathbf{l}$. It follows that

$$\frac{D}{Dt}(d\mathbf{l}) = (d\mathbf{l} \cdot \nabla)\mathbf{u} \tag{3.21}$$

Compare this with (3.20). Evidently, $\boldsymbol{\omega}$ and $d\mathbf{l}$ obey the same equation. Now suppose that at $t = 0$ we have $\boldsymbol{\omega} = \lambda d\mathbf{l}$ then from (3.20) and (3.21) we have $D\lambda/Dt = 0$ at $t = 0$ and so $\boldsymbol{\omega} = \lambda d\mathbf{l}$ for all subsequent times. That is to say, $\boldsymbol{\omega}$ and $d\mathbf{l}$ evolve in identical ways under the influence of $\mathbf{u}$ and so the vortex lines are frozen into the fluid.

Helmholtz's second law is now a trivial consequence of Kelvin's theorem and of $\nabla \cdot \boldsymbol{\omega} = 0$. The fact that the vorticity flux, Φ, is constant along a flux tube follows from the solenoidal nature of $\boldsymbol{\omega}$, and the temporal

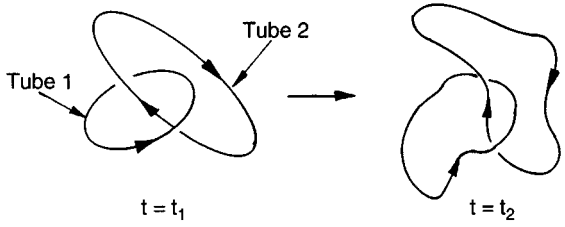

Figure 3.18 Interlinked vortex tubes preserve their topology as they are swept around.

invariance of Φ comes from the fact that a flux tube moves with the fluid and so, from Kelvin's theorem, $\Gamma = \Phi =$ constant. (Here the curve C for Γ lies on the surface of the flux tube.)

Helmholtz's first law, which states that vortex tubes are frozen into an inviscid fluid, has profound consequences for inviscid vortex dynamics. For example, if there exist two interlinked vortex tubes, as shown in Figure 3.18, then as those tubes are swept around they remain linked in the same manner, and the strength of each tube remains constant. Thus the tubes appear to be indestructible and their relative topology is preserved forever. This state of permanence so impressed Kelvin that, in 1867, he developed an atomic theory of matter based on vortices. This rather bizarre theory of the vortex atom has not stood the test of time. However, when, in 1903, the Wright brothers first mastered powered flight, an entirely new incentive for studying vortex dynamics was born. Kelvin's theorem, in particular, plays a central rôle in aerodynamics[2].

3.4.2 Helicity

The conservation of vortex-line topology implied by Helmholtz's laws is captured by an integral invariant called the helicity. This is defined as

$$h = \int_{V_\omega} \mathbf{u} \cdot \boldsymbol{\omega} dV \tag{3.22}$$

where V_ω is a material volume (a volume composed always of the same fluid elements) for which $\boldsymbol{\omega} \cdot d\mathbf{S} = 0$. For example, the surface of V_ω may

[2] Ironically, Kelvin was not a great believer in powered flight. In 1890, on being invited to join the British Aeronautical Society, he is reputed to have said '*I have not the smallest molecule of faith in aerial navigation other than ballooning... so you will understand that I would not care to be a member of the society.*'

be composed of vortex lines. A blob of fluid has helicity if its velocity and vorticity are (at least partially) aligned, as indicated in Figure 3.19.

We may confirm that h is an invariant as follows. First we have

$$\frac{D}{Dt}(\mathbf{u}\cdot\boldsymbol{\omega}) = \frac{D\mathbf{u}}{Dt}\cdot\boldsymbol{\omega} + \frac{D\boldsymbol{\omega}}{Dt}\cdot\mathbf{u} = -\nabla(p/\rho)\cdot\boldsymbol{\omega} + (\boldsymbol{\omega}\cdot\nabla\mathbf{u})\cdot\mathbf{u}$$

Since $\boldsymbol{\omega}$ is solenoidal, this may be written as

$$\frac{D}{Dt}(\mathbf{u}\cdot\boldsymbol{\omega}) = \nabla\cdot\left[(u^2/2 - p/\rho)\boldsymbol{\omega}\right]$$

Now consider an element of fluid of volume δV. The fluid is incompressible and so $D(\delta V)Dt = 0$. It follows that

$$\frac{D}{Dt}[(\mathbf{u}\cdot\boldsymbol{\omega})\delta V] = \nabla\cdot\left[(u^2/2 - p/\rho)\boldsymbol{\omega}\right]\delta V$$

from which

$$\frac{d}{dt}\int_{V_\omega}(\mathbf{u}\cdot\boldsymbol{\omega})dV = \oint_{S_\omega}\left[(u^2/2 - p/\rho)\boldsymbol{\omega}\right]\cdot d\mathbf{S} = 0$$

Thus the helicity, h, is indeed conserved. The connection to Helmholtz's laws and vortex-line topology may be established using the following simple example. Suppose that $\boldsymbol{\omega}$ is confined to two thin interlinked vortex tubes, as shown in Figure 3.18, and that V_ω is taken as all space. Then h has two contributions, one from vortex tube 1, which has volume V_1 and flux Φ_1, and another from vortex tube 2. Let these be denoted by h_1 and h_2. Then

$$h_1 = \int_{V_1}(\mathbf{u}\cdot\boldsymbol{\omega})dV = \oint_{C_1}\mathbf{u}\cdot(\Phi_1 d\mathbf{l}) = \Phi_1\oint_{C_1}\mathbf{u}\cdot d\mathbf{l}$$

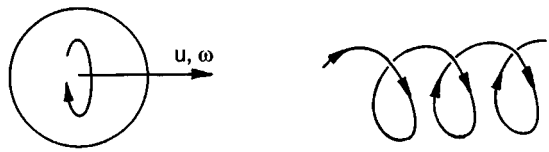

(a) Alignment of velocity and vorticity gives helicity

(b) Particle trajectories

Figure 3.19 A blob of fluid with helicity.

since $\omega dV = \Phi_1 d\mathbf{l}$ (Figure 3.20). Here C_1 is the closed curve representing tube 1. However, $\oint_{C_1} \mathbf{u} \cdot d\mathbf{l}$ is, from Stoke's theorem, equal to Φ_2. A similar calculation may be made for h_2, and we find that

$$h = h_1 + h_2 = \Phi_1 \oint_{C_1} \mathbf{u} \cdot d\mathbf{l} + \Phi_2 \oint_{C_2} \mathbf{u} \cdot d\mathbf{l} = 2\Phi_1\Phi_2$$

Note that if the sense of direction of ω in either tube were reversed, h would change sign. Moreover, if the tubes were not linked, then h would be zero. Thus the invariance of h in this simple example stems directly from the conservation of the vortex line topology. More elaborate examples, illustrating the same fact, are readily constructed.

Finally, we note in passing that minimising kinetic energy subject to conservation of global helicity leads to a Beltrami field satisfying $\nabla \times \mathbf{u} = \alpha\mathbf{u}$, α being constant. We shall not pause to prove this result, but we shall make reference to it later.

This ends our discussion of inviscid vortex dynamics. From a mathematical perspective, inviscid fluid mechanics is attractive. The rules of the game are simple and straightforward. Unfortunately, the conclusions are often at odds with reality and so great care must be exercised in using such a theory. The dangers are nicely summarised by Rayleigh:

> The general equations of (inviscid) fluid motion were laid down in quite early days by Euler and Lagrange ... (unfortunately) some of the general propositions so arrived at were found to be in flagrant contradiction with observations, even in cases where at first sight it would not seem that viscosity was likely to be important. Thus a solid body, submerged to a sufficient depth, should experience no resistance to its motion through water. On this principle the screw of a submerged boat would be useless, but, on the other hand, its services would not be needed. It is little wonder that practical men should declare

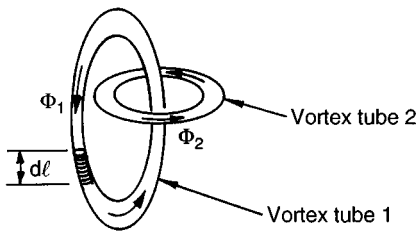

Figure 3.20 The physical interpretation of helicity in terms of flux.

> that theoretical hydrodynamics has nothing at all to do with real fluids.
>
> *Rayleigh (1914)*

Rayleigh was, of course, referring to d'Alembert's paradox. With this warning, we now return to 'real' fluid dynamics.

There are three topics in particular which will be important in our exploration of MHD. The first is the Prandtl–Batchelor theory which says, in effect, that a slow cross-stream diffusion of vorticity can be important even at high Re. The second is the concept of Reynolds' stresses in turbulent motion, and the third is the phenomenon of Ekman pumping, which is a weak secondary flow induced by differential rotation between a viscous fluid and an adjacent solid surface. The Prandtl–Batchelor theorem is important because it has its analogue in MHD (called flux expulsion), Reynolds' stresses and turbulent motion are important because virtually all 'real' MHD is turbulent MHD (Re is invariably very large), and Ekman pumping is important because it dominates the process of magnetic stirring and possibly contributes to the maintenance of the geodynamo.

3.5 The Prandtl–Batchelor Theorem

We now return to viscous flows. We start with the Prandtl–Batchelor theorem which, as we have said, has its analogue in MHD. This theorem is one of the more beautiful results in the theory of two-dimensional viscous flows. It has far-reaching consequences for internal flows. In effect, it states that a laminar motion with high Reynolds number and closed streamlines must have uniform vorticity.

Consider a two-dimensional flow which is steady and has a high Reynolds number. Suppose also that the streamlines are closed. We introduce the streamfunction ψ. The velocity and vorticity are, in terms of ψ,

$$\mathbf{u} = \left(\frac{\partial \psi}{\partial y}, -\frac{\partial \psi}{\partial x}\right), \qquad \omega = -\nabla^2 \psi$$

In two-dimensions, the steady vorticity equation becomes

$$(\mathbf{u} \cdot \nabla)\omega = \nu \nabla^2 \omega$$

If we now take the limit $\nu \to 0$ we obtain

$$(\mathbf{u} \cdot \nabla)\omega = 0$$

The vorticity is therefore constant along the streamlines and so is a function only of ψ, $\omega = \omega(\psi)$. This is all the information which we may obtain from the inviscid equation of motion. Unfortunately, the problem appears to be underdetermined. There are an infinite number of solutions to the equation

$$\nabla^2\psi = -\omega(\psi), \qquad \psi = 0 \text{ on the boundary}$$

each solution corresponding to a different distribution of ω. (Note that $\mathbf{u} \cdot d\mathbf{S} = 0$ at the boundary requires $\psi =$ constant at the boundary and it is usual to take that constant as zero.) So what distribution of ω does nature select? We appear to be missing some information. In cases where the streamlines are open the problem is readily resolved. We must specify the upstream distribution of ω and then track it downstream (Figure 3.21). However, when the streamlines are closed, such as in the cavity in Figure 3.21(b), we have no 'upstream point' at which we can specify $\omega(\psi)$.

Let us go back to the steady, viscous vorticity equation. If we integrate this over the area bounded by some closed streamline then we find, with the help of Gauss's theorem,

$$\nu \int \nabla^2\omega dV = \nu \oint \nabla\omega \cdot d\mathbf{S} = 0$$

This integral constraint must be satisfied for all finite values of ν, no matter how small ν may be. Now if Re is large, then $\omega = \omega(\psi)$ plus some small correction due to the finite value of ν. Consequently

$$\nabla\omega = \omega'(\psi)\nabla\psi + (\text{small correction})$$

where $\omega'(\psi)$ is proportional to the cross-stream gradient of vorticity. Next we substitute back into our integral equation to give

$$\nu\left\{\omega'(\psi) \oint \nabla\psi \cdot d\mathbf{S} + (\text{small correction})\right\} = 0$$

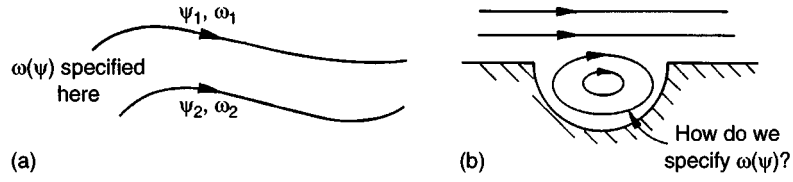

Figure 3.21 The specification of $\omega(\psi)$.

(Note that $\omega'(\psi)$ is constant along a streamline and so may be taken outside the integral.) We now assume ν is very small (Re is large) and throw away the small correction. Invoking Gauss's theorem once again, this time in reverse, we end up with

$$\nu\omega'(\psi)\int \nabla^2\psi dV = -\nu\omega'(\psi)\int \omega dA = 0$$

This expression must be satisfied for all flows with a small but finite value of ν. From Stokes' theorem this can be rewritten in the form

$$\nu\omega'(\psi)\oint_C \mathbf{u}\cdot d\mathbf{l} = 0$$

where C is a streamline. Since ν is finite, the only possibility is that $\omega'(\psi) = 0$. In other words, there is no cross-stream gradient in ω, and so ω is uniform throughout the flow.

We have proved the Prandtl–Batchelor theorem. It states that, for high Reynolds number flows with closed streamlines, the vorticity is uniform throughout the flow, $\omega = \omega_0$, except in the boundary layers (Figure 3.22). (We must exclude the boundary layers since our proof assumed that viscous effects are small and this is clearly not the case in the boundary layers.) In the cavity flow shown below, ω will be constant within the region of closed streamlines (excluding the thin boundary layers). Of all possible vorticity distributions, $\omega(\psi)$, the Prandtl–Batchelor theorem tells us that nature will select the one where vorticity is not only constant along the streamlines, but is also constant *across* the streamlines.

Armed with the Prandtl–Batchelor theorem, it is relatively straightforward to compute flow fields of the type sketched below. One simply solves the equation

$$\nabla^2\psi = -\omega_0, \qquad \psi = 0 \text{ on the boundary}$$

where ω_0 is the (unknown but constant) vorticity in the flow. This yields $\mathbf{u}$ at all points (except in the boundary layer). There is, however, still the

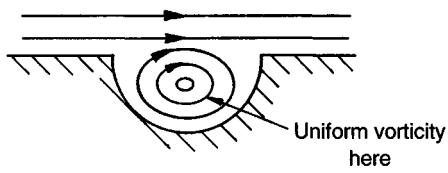

Figure 3.22 Example of the Prandtl–Batchelor theorem.

unknown constant ω_0 to determine. This is usually fixed by solving the boundary layer equations.

Of course, if the Reynolds' number is high enough then the flow will become unsteady and eventually turbulent. The Prandtl–Batchelor theory does not then apply. However, there are many cases where Re is low enough for the motion to be steady and laminar, yet high enough for the Prandtl–Batchelor theorem to work well. One example is the two attached eddies which form in the wake of a cylinder at intermediate Reynolds number. Curiously, even when the flow becomes turbulent, the Prandtl–Batchelor theorem often works surprisingly well when applied to the time-averaged flow. Presumably, this is because the arguments above can be repeated, but with ν now representing an 'eddy viscosity'.

The physical interpretation of the Prandtl–Batchelor theorem is straightforward. Suppose a flow is initiated at, say, $t = 0$. Then, over a short timescale of the order of the eddy turnover-time, the flow adopts a high Reynolds number form: i.e. $\omega = \omega(\psi)$. (Depending on how the flow is initiated, different distributions of $\omega(\psi)$ may appear.) There then begins a slow cross-stream diffusion of vorticity which continues until all the internal gradients in vorticity have been eliminated (except in the boundary layers). This takes a long time, but the flow does not become truly steady until the process is complete.

Examples

1. Starting with the energy equation

$$\frac{DT}{Dt} = \alpha \nabla^2 T$$

show that for laminar, high-Peclet number, closed-streamline flows, the temperature outside the boundary layer is constant. This is the thermal equivalent of the Prandtl–Batchelor theorem. Give a physical interpretation of your result.

2. In two-dimensional MHD flows which have the form $\mathbf{u} = (u_x, u_y, 0)$ and $\mathbf{B} = (B_x, B_y, 0) = \nabla \times (A_z \hat{\mathbf{e}}_z)$, the induction equation (2.24) reduces to

$$\frac{DA_z}{Dt} = \lambda \nabla^2 A_z$$

Where do you think the Prandtl–Batchelor arguments lead here?

3.6 Boundary Layers, Reynolds Stresses and Turbulence Models

3.6.1 Boundary layers

> During the last few years much work has been done in connection with artificial flight. We may hope that before long this may be coordinated and brought into closer relationship with theoretical hydrodynamics. In the meantime one can hardly deny that much of the latter science is out of touch with reality.
>
> *Rayleigh, 1916.*

We have already mentioned boundary layers without really defining what we mean by this term, and so it seems appropriate to review briefly the key aspects of laminar boundary layers. (We leave turbulence to Section 3.6.2.)

The concept of a boundary layer, and of boundary layer separation, was first conceived by the engineer L Prandtl and it revolutionised fluid mechanics. It formed a bridge between the classical 19th century mathematical studies of inviscid fluids and the subject of experimental fluid mechanics, and in doing so it resolved many traditional dilemmas such as d'Alembert's paradox. Prandtl first presented his ideas in 1904 in a short paper crammed with physical insight. Curiously though, it took many years for the full significance of his ideas to be generally appreciated.

Consider a high-Reynolds' number flow over, say, an aerofoil (Figure 3.23). By high Reynolds' number we mean that uL/ν is large where L is a characteristic geometric length scale, say the span of the aerofoil. Since Re is large we might be tempted to solve the inviscid equations of motion,

$$(\mathbf{u} \cdot \nabla)\mathbf{u} = -\nabla(p/\rho)$$

subject to the inviscid boundary condition $\mathbf{u} \cdot d\mathbf{S} = 0$ on all solid surfaces. This determines the so-called *external problem.*

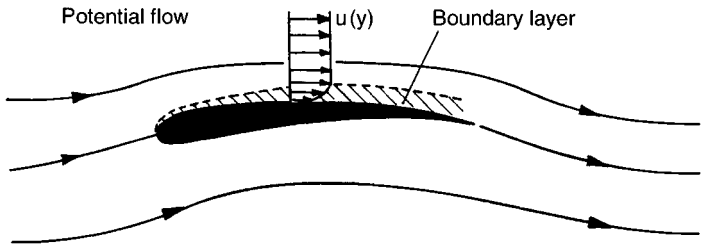

Figure 3.23 Boundary layer near a surface.

Now in reality the fluid satisfies a no-slip boundary condition $\mathbf{u} = 0$ on $d\mathbf{S}$. (We take a frame of reference moving with the aerofoil.) Thus there must exist a region surrounding the aerofoil where the velocity given by the external problem adjusts to zero (Figure 3.23). This region is called the boundary layer, and it is easy to see that such a layer must be thin. The point is that the only mechanical forces available to cause a drop in velocity are viscous shear stresses. Thus the viscous term in the Navier–Stokes equation must be of the same order as the other terms within the boundary layer,

$$\nu\nabla^2\mathbf{u} \sim (\mathbf{u}\cdot\nabla)\mathbf{u}$$

This requires that the transverse length scale, δ, which appears in the Laplacian, is of order

$$\delta \sim (\nu L/u)^{1/2} \sim \mathrm{Re}^{-1/2}$$

which fixes the boundary layer thickness. Since Re is large this implies that

$$\delta \ll L$$

Note that, because the boundary layer is so thin, the pressure within a boundary layer is virtually the same as the pressure immediately outside the layer. (There can be no significant gradient in pressure across a boundary layer since this would imply a significant normal acceleration, which is not possible since the velocity is essentially parallel to the surface.)

Boundary layers occur in other branches of physics; it is not a phenomenon peculiar to velocity fields. In fact, it occurs whenever a small parameter, in this case ν, multiplies a term containing derivatives which are of higher order than the other derivatives appearing in the equation. In the case above, when we throw out $\nu\nabla^2\mathbf{u}$ on the basis that ν is small, our equation drops from second order to first order. There is a corresponding drop in the number of boundary conditions we can meet ($\mathbf{u}\cdot d\mathbf{S} = 0$ rather than $\mathbf{u} = 0$) and so solving the external problem leaves one boundary condition unsatisfied. This is corrected for in a thin transition region (in this case the velocity boundary layer) where the term we had thrown out, i.e. $\nu\nabla^2\mathbf{u}$, is now significant because of the thinness of the transition region. However, we can have other types of boundary layers, such as thermal boundary layers and magnetic boundary layers. In the case of thermal boundary layers the small parameter is α and it multiplies $\nabla^2 T$.

Note that the thickness of a boundary layer is not always $\sim \mathrm{Re}^{-1/2}L$. For example, we shall see later that the force balance within MHD boundary layers is more complicated than that indicated above, and so the estimate $\delta \sim \mathrm{Re}^{-1/2}L$ often needs modifying.

We conclude with one comment. As noted in Section 3.1.1, boundary layers exhibit a phenomenon known as *separation*. That is, when the flow external to the boundary layer decelerates, the pressure gradient causing that deceleration is also imposed on the fluid in the boundary layer. However, this fluid has less kinetic energy than the external flow and so it rapidly comes to a halt and starts to move backward. The fluid within the boundary layer is then ejected into the external flow and a wake is formed, such as the wake at the rear of a cylinder. It is this wake which gives rise to the asymmetric flow over bluff bodies which inviscid theory fails to predict, and which so discredited theoretical hydrodynamics.

3.6.2 Reynolds stresses and turbulence models

We now consider the more elementary aspects of turbulent flow. A more detailed discussion is given in Chapter 7, where we consider the nature of turbulence itself. Here we restrict ourselves to the much simpler problem of characterising the influence of turbulence on the mean flow.

It is an empirical observation that if Re is made large enough (viscosity made small enough) a flow invariably becomes unstable and then turbulent (Figure 3.24). Suppose we have a turbulent flow in which $\boldsymbol{u}$ and p consist of a time-averaged component plus a fluctuating part:

$$\mathbf{u} = \bar{\mathbf{u}} + \mathbf{u}', \qquad p = \bar{p} + p'$$

When we time-average the Navier–Stokes equation, new terms arise from the fluctuations in velocity. For example, the x-component of the time-averaged equation of motion is

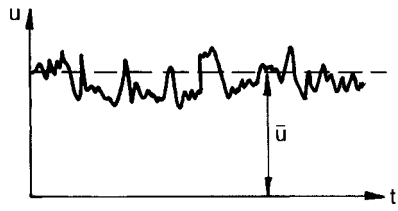

Figure 3.24 Velocity component in a turbulent flow.

$$(\bar{\mathbf{u}}\cdot\nabla)\bar{u}_x = -\frac{\partial}{\partial x}\left(\frac{p}{\rho}\right)+\frac{\partial}{\partial x}\left[2\nu\frac{\partial\bar{u}_x}{\partial x}\right]+\frac{\partial}{\partial y}\left[\nu\left(\frac{\partial\bar{u}_x}{\partial y}+\frac{\partial\bar{u}_y}{\partial x}\right)\right]$$
$$+\frac{\partial}{\partial z}\left[\nu\left(\frac{\partial\bar{u}_x}{\partial z}+\frac{\partial\bar{u}_z}{\partial x}\right)\right]+\frac{\partial}{\partial x}\left[-\overline{u_x'u_x'}\right]+\frac{\partial}{\partial y}\left[-\overline{u_x'u_y'}\right]+\frac{\partial}{\partial z}\left[-\overline{u_x'u_z'}\right]$$

Here the overbar represents time-averaging. Now the laminar stresses, from Newton's law of viscosity, are given by

$$\sigma_x = 2\rho\nu\frac{\partial u_x}{\partial x}$$
$$\tau_{xy} = \rho\nu\left[\frac{\partial u_x}{\partial y}+\frac{\partial u_y}{\partial x}\right]$$
$$\tau_{xz} = \rho\nu\left[\frac{\partial u_x}{\partial z}+\frac{\partial u_z}{\partial x}\right]$$

The turbulence seems to have produced additional stresses. These are called Reynolds stresses in honour of Osborne Reynolds' pioneering work on turbulence ($\sim$1883). The stresses are

$$\sigma_x = -\rho\overline{u_x'u_x'}$$
$$\tau_{xy} = -\rho\overline{u_x'u_y'}$$
$$\tau_{xz} = -\rho\overline{u_x'u_z'}$$

We can rewrite the x-component of the time-averaged equation in a more compact way:

$$(\bar{\mathbf{u}}\cdot\nabla)\bar{u}_x = -\frac{\partial}{\partial x}\left[\frac{p}{\rho}\right]+\nu\nabla^2\bar{u}_x+\frac{\partial}{\partial x_i}\left[-\overline{\rho u_x'u_i'}\right]$$

Here the index, i, is summed over x, y and z. Similar expressions may be written for the y and z components. If we wish to make predictions from this equation we need to be able to relate the Reynolds stresses, $-\rho\overline{u_x'u_i'}$, to some quantity which we know about, such as mean velocity gradients of the type $\partial\bar{u}_x/\partial y$. This is the purpose of *turbulence modelling*. Its aim is to recast the time-averaged equations in a form which may be solved, just like the Navier–Stokes equations. In effect, a *turbulence model* provides a means of estimating the Reynolds stresses.

However, it should be emphasised from the outset that 'Reynolds stress modellers' live dangerously. The quest to find a *universal* turbulence model, which may be defended on theoretical grounds, is doomed to failure from the outset. There is no such thing as a universal turbulence model! The best that we can do is construct semi-empirical models, based

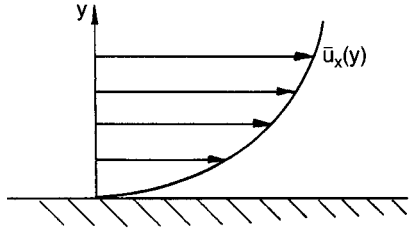

Figure 3.25 Time-averaged velocity in a turbulent flow.

on laboratory tests, and try to apply these models to flows not too different from the laboratory tests on which they were based. For example, Reynolds stress models developed from boundary layer experiments need not work well when applied to rapidly rotating flows.

The reason for this difficulty is the so-called 'closure problem' of turbulence. We can, in principle, derive rigorous equations for $\overline{u_x' u_y'}$ etc. (see Chapter 7). However, this involves quantities of the form $\overline{u_x' u_y' u_z'}$. When an equation for these new quantities is derived, we find that it involves yet more functions such as $\overline{u_x' u_x' u_y' u_z'}$, and so on. There are always more unknowns than equations, and it is impossible to close the set in a rigorous way. This is the price we pay in moving from the instantaneous equations of motion to a statistical (time-averaged) one[3].

This is all bad news since much of fluid mechanics centres around turbulent flows, and quantitative predictions of such flows require a turbulence model. Fortunately, some of the simpler, empirical turbulence models work reasonably well if applied to the appropriate classes of flow.

Historically, the first serious attempt at a theoretical study of turbulent flows was made by Boussinesq around 1877 (6 years before Reynolds' famous pipe experiment). He proposed that the shear-stress strain-rate relationship for time-averaged flows of a one-dimensional nature (Figure 3.25) was of the form

$$\tau_{xy} = (\mu + \mu_t)\frac{\partial \bar{u}_x}{\partial y}$$

(Here μ is the dynamic viscosity, $\mu = \rho\nu$ and should not be confused with the permeability of free space.) Boussinesq termed μ_t an *eddy viscosity*. While μ is a property of the fluid, μ_t will be a property of the *turbulence*. The first attempt to estimate μ_t was due to Prandtl in 1925. He invoked the idea of a *mixing length*, as we shall see shortly.

[3] This is not to say that we cannot make rigorous and useful statements about turbulence. We can! (see Chapter 7.) We cannot, however, produce a rigorous Reynolds stress model.

The idea of an eddy viscosity is not restricted to simple shear flows of the type above, i.e. $\bar{u}_x(y)$. It is common to introduce eddy viscosities into flows of arbitrary complexity. Then,

$$\tau_{xy} = (\mu + \mu_t)\left[\frac{\partial \bar{u}_x}{\partial y} + \frac{\partial \bar{u}_y}{\partial x}\right]$$

$$\tau_{xz} = (\mu + \mu_t)\left[\frac{\partial \bar{u}_x}{\partial z} + \frac{\partial \bar{u}_z}{\partial x}\right]$$

etc. We have, in effect, accounted for the Reynolds stresses by replacing μ in Newton's law of viscosity by $\mu + \mu_t$. Now in virtually all turbulent flows the eddy viscosity is much greater than μ, so the viscous stresses may be dropped, giving

$$\tau_{xy} = -\rho\overline{u_x' u_y'} = \mu_t\left[\frac{\partial \bar{u}_x}{\partial y} + \frac{\partial \bar{u}_y}{\partial x}\right]$$

$$\tau_{xz} = -\rho\overline{u_x' u_z'} = \mu_t\left[\frac{\partial \bar{u}_x}{\partial z} + \frac{\partial \bar{u}_z}{\partial x}\right]$$

We shall refer to these as Boussinesq's equations. The question now is, what is μ_t? Prandtl was struck by the success of the kinetic theory of gases in predicting the properties of ordinary viscosity in which the 'mean free path length' plays a rôle. In fact, the simple kinetic theory of gases leads to the prediction

$$\mu = \frac{1}{3}\rho l V$$

where V is the molecular velocity and l is the mean free path length. Could the same thing be done for the eddy viscosity? In fact, there is an analogy between Newton's law of viscosity and Reynolds stresses. In a laminar flow, layers of fluid which slide over each other experience a mutual shear stress, or drag, because thermally agitated molecules bounce around between the layers exchanging energy and momentum as they do so (Figure 3.26).

For example, a molecule in the slow moving layer at A may move up to B, slowing down the fast moving layer. Conversely, a molecule in the fast moving layer may drop down from C to D, speeding up the lower layer. This is the basic idea which lies behind the expression $\mu = \rho l V/3$. However, just the same sort of thing happens in a turbulent flow, albeit at the macroscopic, rather than molecular, level. Balls of fluid are

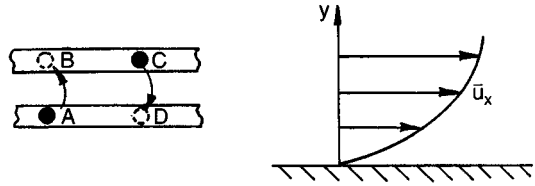

Figure 3.26 Exchange of momentum due to thermal motion of the molecules.

exchanged between the layers due to turbulent fluctuations, and this causes a mixing of momentum across the layers.

This analogy between the transfer of momentum by molecules on the one hand and balls of fluid on the other led Prandtl to propose the relationship

$$\mu_t = \rho l_m V_T$$

where l_m is called the mixing length. (Actually Boussinesq proposed something similar in 1870.) l_m is a measure of the size of the large eddies in the flow. V_T is a measure of u', and indicates the intensity of the turbulence. The more intense the fluctuations, the larger the cross-stream transfer of momentum, and so the larger the eddy viscosity.

To a large extent the equation above is simply a dimensional necessity, since μ_t/ρ has the dimensions of m^2/s. Boussinesq's equations, however, are a little more worrying. At one level we may regard them as simply defining μ_t, and so transferring the problem of estimating τ to one of estimating μ_t, but there is an important assumption here. We are assuming that the eddy viscosity in the xy plane is the same as the eddy viscosity in the xz plane, and so on. This, in turn, requires that the turbulence is statistically isotropic. Still, let us see how far we can get with an eddy viscosity model. We now need to find a way of estimating l_m and V_T. For the particular case of simple shear flows (one-dimensional flows), Prandtl found a way of estimating V_T. This is known as Prandtl's *mixing length theory* (Figure 3.27).

Consider a mean flow, $\bar{u}_x$, which is purely a function of y. Suppose also that the turbulence has components u'_x, u'_y, u'_z.

$$\bar{\mathbf{u}} = (\bar{u}_x, 0, 0)$$

$$\mathbf{u}' = (u'_x, u'_y, u'_z)$$

Then Prandtl's theory says that, in effect, the fluid at y, with mean velocity $\bar{u}_x(y)$, will, on average, have come from levels $y \pm l$, where l is the

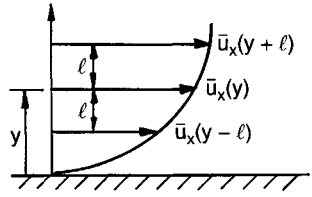

Figure 3.27 Prandtl's mixing length theory.

mixing length. Suppose that, as a fluid lump is thrown from $y + l$ (or $y - l$) to y, it retains its forward momentum, which on average will be $\bar{u}_x(y \pm l)$. Then the mean velocities $\bar{u}_x(y \pm l)$ represent the spread of instantaneous velocities at position y. We can represent this spread by $\bar{u}_x \pm \sqrt{\overline{(u_x')^2}}$. If l is small (unfortunately it is not!), then we have

$$\bar{u}_x(y \pm l) \approx \bar{u}_x(y) \pm l \frac{\partial \bar{u}_x}{\partial y}$$

It follows that

$$\overline{[u_x']^2} \approx l^2 \left[\frac{\partial \bar{u}_x}{\partial y}\right]^2$$

Next we note that there is a strong negative correlation between u_x' and u_y', since a positive u_x' is consistent with fluid coming from $y + l$, requiring a negative u_y'. (If $\partial \bar{u}_x / \partial y$ is negative we expect a positive correlation.) Thus,

$$\overline{u_x' u_y'} = -c_1 \sqrt{\overline{(u_x')^2}} \sqrt{\overline{(u_y')^2}}$$

where c_1 is some constant of order unity (called a correlation coefficient). If u_x' and u_y' are of similar orders of magnitude, we now have

$$\overline{u_x' u_y'} \sim \pm \overline{(u_x')^2} = -c_2 l^2 \left|\frac{\partial \bar{u}_x}{\partial y}\right| \frac{\partial \bar{u}_x}{\partial y}$$

where c_2 is a second constant of order unity. Note the inclusion of the modulus on one of the $\partial \bar{u}_x / \partial y$ terms. This is needed to ensure that the correlation is negative when $\partial \bar{u}_x / \partial y > 0$ and positive when $\partial \bar{u}_x / \partial y < 0$.

We now redefine our mixing length to absorb the unknown constant c_2. We set $l_m^2 = c_2 l^2$, and the end result is

$$\tau_{xy} = -\rho \overline{u_x' u_y'} = \rho l_m^2 \left|\frac{\partial \bar{u}_x}{\partial y}\right| \frac{\partial \bar{u}_x}{\partial y}$$

Compare this with Boussinesq's equation

$$\tau_{xy} = \mu_t \frac{\partial \bar{u}_x}{\partial y} = \rho l_m V_T \frac{\partial \bar{u}_x}{\partial y}$$

Evidently, for this particular sub-class of one-dimensional shear flows, the turbulent velocity scale is

$$V_T = l_m \left| \frac{\partial \bar{u}_x}{\partial y} \right|$$

The eddy viscosity is therefore

$$\mu_t = \rho l_m^2 \left| \frac{\partial \bar{u}_x}{\partial y} \right|$$

This represents what is known as the 'mixing length model' of Prandtl. Conceptually this is a tricky argument which ultimately cannot be justified in any formal way. Besides which, we still need to decide what l_m is, perhaps guided by experiment. Nevertheless, Prandtl's mixing length model appears to work well for one-dimensional shear flows, provided l_m is chosen appropriately. (By shear flows we mean flows like boundary layers, free shear layers and jets.) For flow over a flat plate, it is found that $l_m = ky$, where $k \approx 0.4$ and is known as Karman's constant.

Example: The α-effect in electrodynamics

The process of averaging chaotic or turbulent equations, in the spirit of Reynolds, is not restricted to the Navier–Stokes equation. For example, the heat equation or induction equation can be averaged in a similar way. Suppose we have a highly conducting, turbulent fluid in which $\mathbf{u} = \mathbf{u}_0 + \mathbf{v}$ and $\mathbf{B} = \mathbf{B}_0 + \mathbf{b}$ where $\mathbf{u}_0$ and $\mathbf{B}_0$ are steady or slowly varying and $\bar{\mathbf{v}} = 0$, $\bar{\mathbf{b}} = 0$. Show that the averaged induction equation is

$$\frac{\partial \mathbf{B}_0}{\partial t} = \nabla \times (\mathbf{u}_0 \times \mathbf{B}_0) + \lambda \nabla^2 \mathbf{B}_0 + \nabla \times \overline{(\mathbf{v} \times \mathbf{b})}$$

The quantity $\overline{\mathbf{v} \times \mathbf{b}}$ is the electromagnetic analogue of the Reynolds stress. In some cases it is found that $\overline{\mathbf{v} \times \mathbf{b}} = \alpha \mathbf{B}_0$, where α is the analogue of Boussinesq's eddy diffusivity. This leads to the 'turbulent' induction equation

$$\frac{\partial \mathbf{B}_0}{\partial t} = \nabla \times (\mathbf{u}_0 \times \mathbf{B}_0) + \alpha \nabla \times \mathbf{B}_0 + \lambda \nabla^2 \mathbf{B}_0$$

In Chapter 6 you will see that the new term, called the α-effect, can give rise to the self-excited generation of a magnetic field.

3.7 Ekman Pumping in Rotating Flows

We now consider the phenomenon of Ekman pumping, which occurs whenever there is differential rotation between a viscous fluid and a solid surface. This turns out to be important in magnetic stirring (see Chapter 8) and in the geo-dynamo (Chapter 6). We start with Karman's solution for laminar flow near the surface of a rotating disk.

Suppose we have an infinite disk rotating in an otherwise still liquid. A boundary layer will develop on the disk due to viscous coupling, and Karman found an exact solution for this boundary layer. Suppose that the disc rotates with angular velocity Ω. Then we might expect a boundary layer thickness to scale as $\delta \sim (\nu/\Omega)^{1/2}$. Karman suggested looking for a solution in polar coordinates in which z (which is normal to the disk) is normalised by δ. Karman's solution is of the form

$$u_r = \Omega r F(\eta), \qquad u_\theta = \Omega r G(\eta), \qquad u_z = \Omega \hat{\delta} H(\eta)$$

Here $\hat{\delta} = (\nu/\Omega)^{1/2}$ and $\eta = z/\hat{\delta}$. If these expressions are substituted into the radial and azimuthal components of the Navier–Stokes equation and the equation of continuity, we obtain three differential equations for three unknown functions F, G and H

$$F^2 + F'H - G^2 = F''$$
$$2FG + HG' = G''$$
$$2F + H' = 0$$

We take z to be measured from the surface of the disk, and so we have the boundary conditions

$$z = 0\text{: } F = 0,\ G = 1,\ H = 0$$
$$z \to \infty\text{: } F = 0,\ G = 0$$

Our three equations can be integrated numerically and the result is shown schematically in Figure 3.28. This represents a flow which is radially outward within a boundary layer of thickness $\delta \sim 4\hat{\delta} = 4(\nu/\Omega)^{1/2}$. The flow pattern in the r–z plane is shown in Figure 3.29. Within the thin boundary layer the fluid is centrifuged radially outward, so that each particle spirals outward to the edge of the disk. Outside the boundary layer u_r and u_θ are both zero, but u_z is non-zero. There is a slow drift of fluid towards the disk, at a rate

$$|u_z| \sim 0.9\Omega\hat{\delta} \sim 0.2\Omega\delta$$

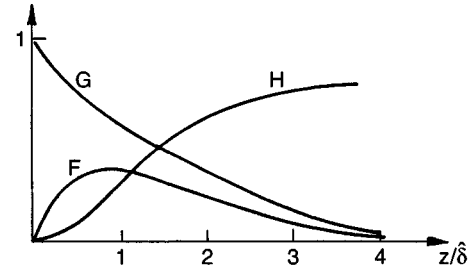

Figure 3.28 Solution of Karman's problem.

Of course, this is required to supply the radial outflow in the boundary layer. We have, in effect, a centrifugal fan.

Suppose now that the disk is stationary but that the fluid rotates like a rigid body ($u_\theta = \Omega r$) in the vicinity of the disk. Near the disk's surface this swirl is attenuated due to viscous drag and so a boundary layer forms. This problem was studied by Bodewadt, who showed that Karman's procedure works as before. It is only necessary to change the boundary conditions. Once again the boundary layer thickness is constant and of the order of $4(\nu/\Omega)^{1/2}$. This time, however, the flow pattern in the r–z plane is reversed (Figure 3.30). Fluid particles spiral radially inward, eventually drifting out of the boundary layer. Outside the boundary layer we have rigid body rotation, $u_\theta = \Omega r$, plus a weak axial flow away from the surface of magnitude

$$u_z \sim 1.4\Omega\hat{\delta} \sim 0.35\Omega\delta$$

The flow in the r–z plane is referred to as a secondary flow, in as much as the primary motion is a swirling flow. The reason for the secondary flow is that, outside the boundary layer, we have the radial force balance

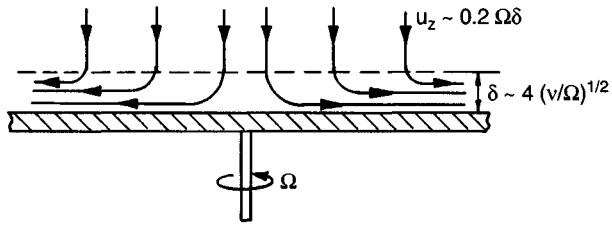

Figure 3.29 Secondary flow in Karman's problem.

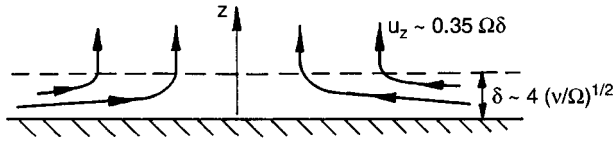

Figure 3.30 Bodewadt's problem (stationary disk, rotating fluid).

$$\frac{\partial p}{\partial r} = \rho \frac{u_\theta^2}{r}$$

That is, the centrifugal force sets up a radial pressure gradient, with a low pressure near the axis. This pressure gradient is imposed throughout the boundary layer on the plate. However, the swirl in this boundary layer is diminished through viscous drag, and so there is a local imbalance between the imposed pressure gradient and the centripetal acceleration. The result is a radial inflow, with the fluid eventually drifting up and out of the boundary layer.

In general then, whenever we have a swirling fluid adjacent to a stationary surface we induce a secondary flow, as sketched in Figure 3.30. This is referred to as Ekman pumping, and the boundary layer is called an Ekman layer.

The axial velocity induced by Ekman pumping is relatively small if the Reynolds number is large:

$$u_z \sim 1.4(\nu\Omega)^{1/2} \ll u_\theta$$

Nevertheless, this weak secondary flow often has profound consequences for the motion as a whole. Consider, for example, the problem of 'spin-down' of a stirred cup of tea. Suppose that, at $t = 0$, the tea is set into a state of (almost) inviscid rotation. Very quickly an Ekman layer will become established on the bottom of the cup, inducing a radial inflow at the base of the vessel. By continuity, this radial flow must eventually drift up and out of the boundary layer, where it is recycled via side layers (called Stewartson layers) on the cylindrical walls of the cup. A secondary flow is established, as shown in Figure 3.31. As each fluid particle passes through the Ekman layer it gives up a significant fraction of its kinetic energy. The tea finally comes to rest when all of the contents of the cup have been flushed through the boundary layer. The existence of the secondary flow is evidenced (in the days before tea-bags!) by the accumulation of tea-leaves at the centre of the cup.

The spin-down time, τ_s, is therefore of the order of the turn-over time of the secondary flow:

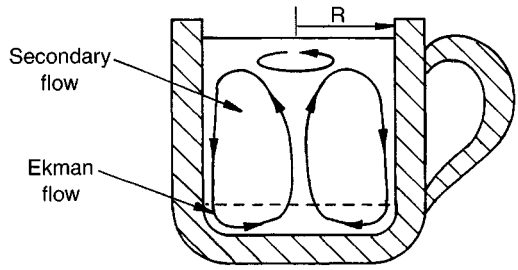

Figure 3.31 Spin-down of a stirred cup of tea.

$$\tau_s \sim R/u_z \sim R/\Omega\delta \sim R/\sqrt{\nu\Omega}$$

If there were no secondary flow, the spin-down time would be controlled by the time taken for the core vorticity to diffuse to the walls:

$$\tau_s^* \sim R^2/\nu$$

Suppose that $R = 3\,\text{cm}$, $\nu = 10^{-6}\,\text{m}^2/\text{s}$ and $\Omega = 1\,\text{s}^{-1}$. Then $\tau_s \sim 30\,\text{s}$, which is about right, whereas $\tau_s^* \sim 15$ min! Evidently, the Ekman layers provide an efficient mechanism for destroying energy.

Now consider a problem more relevant to engineering. Suppose we have a cylindrical vessel in which swirl is induced by rotating the lid (Figure 3.32). If the vessel is much broader than it is deep we might model it as two parallel disks, one rotating and one stationary. If the top disk rotates at a rate Ω, a natural question to ask is: what is the rotation rate in the core flow? It turns out that this is, once again, controlled by the weak secondary flow. The fluid is accelerated by one disk and retarded by the other. Consequently, it will rotate at a rate somewhere between 0 and Ω. It follows that a Bodewadt (or Ekman) layer will form on the lower disk and a Karman layer will form on the upper surface. Fluid will be ejected by the lower boundary layer and then sucked up into the upper layer. The answer to the question of the core rotation rate is now straightforward. The fluid lying outside the two

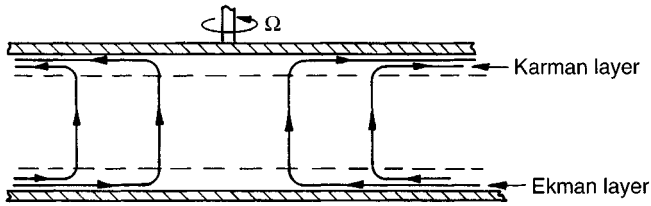

Figure 3.32 Flow between two disks, one of which rotates.

boundary layers will rotate at a rate such that the mass flow out of the Ekman layer balances the mass flow into the Karman layer. If Ω_c is the core rotation rate, then for the fluid leaving the Ekman layer

$$u_z \sim 1.4\Omega_c^{1/2}\nu^{1/2}$$

The fluid entering the Karman layer has velocity

$$u_z \sim 0.9(\Omega - \Omega_c)^{1/2}\nu^{1/2}$$

Equating the two, we find that

$$\Omega_c \sim 0.3\Omega$$

Therefore the bulk of the fluid rotates at approximately one-third of the disk rotation rate. A similar calculation can be performed when an electromagnetic torque induces swirl in a conducting fluid held between two fixed plates (see Chapter 5, Section 5).

Ekman pumping not only dominates confined swirling flows of the type described above, but also plays a key rôle in large-scale geophysical flows. For example, there is some evidence that the solid inner core of the earth rotates at a slightly different rate to the solid outer mantle. Between the two we have liquid iron. If this differential rotation does indeed occur, then we might expect a flow structure such as that shown in Figure 3.33. Ekman layers form on the top and bottom surfaces of the

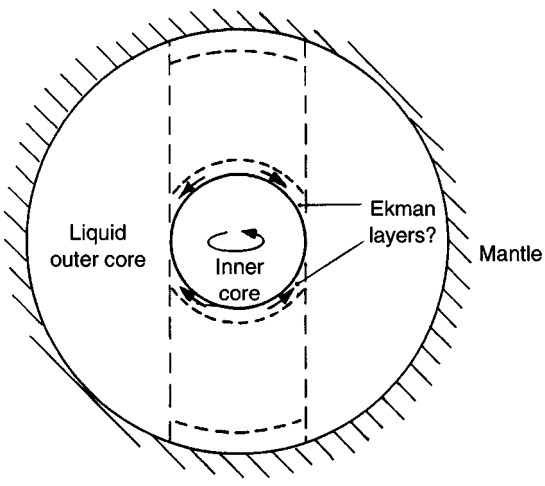

Figure 3.33 Ekman pumping in the core of the earth.

inner core. This kind of differential rotation can cause intense stretching and twisting of magnetic fields and may be a component of the process by which the earth maintains its magnetic field.

Part 2: Incorporating the Lorentz Force

We now incorporate the Lorentz force into the Navier–Stokes equations and consider some of the more elementary and immediate consequences of this.

3.8 The Full Equations of MHD and Key Dimensionless Groups

Let us start by summarising the governing equations of MHD. We have the reduced form of Maxwell's equations

$$\boxed{\nabla \times \mathbf{B} = \mu \mathbf{J}}, \quad \boxed{\nabla \cdot \mathbf{J} = 0} \tag{3.23}$$

$$\boxed{\nabla \times \mathbf{E} = -\frac{\partial \mathbf{B}}{\partial t}}, \quad \boxed{\nabla \cdot \mathbf{B} = 0} \tag{3.24}$$

and the auxiliary expressions

$$\boxed{\mathbf{J} = \sigma(\mathbf{E} + \mathbf{u} \times \mathbf{B})}, \quad \boxed{\mathbf{F} = \mathbf{J} \times \mathbf{B}} \tag{3.25}$$

These combine to give the induction equation

$$\boxed{\frac{\partial \mathbf{B}}{\partial t} = \nabla \times (\mathbf{u} \times \mathbf{B}) + \lambda \nabla^2 \mathbf{B}}, \qquad \lambda = (\mu\sigma)^{-1} \tag{3.26}$$

On the other hand, Newton's second law gives us

$$\boxed{\frac{D\mathbf{u}}{Dt} = -\nabla(p/\rho) + \nu\nabla^2\mathbf{u} + (\mathbf{J}\times\mathbf{B})/\rho} \tag{3.27}$$

from which we obtain the vorticity equation

$$\boxed{\frac{\partial\boldsymbol{\omega}}{\partial t} = \nabla\times(\mathbf{u}\times\boldsymbol{\omega}) + \nu\nabla^2\boldsymbol{\omega} + \nabla\times(\mathbf{J}\times\mathbf{B})/\rho} \tag{3.28}$$

There are four dimensionless groups which regularly appear in the MHD literature. Three of them represent the relative magnitudes of the different force terms in (3.27). The fourth relates to (3.26). The first is the Reynolds number, $\mathrm{Re} = ul/\nu$, where l is a characteristic length scale of the motion and u is a typical velocity. As in conventional fluid mechanics, this is representative of the ratio of inertia, $(\mathbf{u}\cdot\nabla)\mathbf{u}$, to viscous forces, $\nu\nabla^2\mathbf{u}$. The second dimensionless group is the obscurely named interaction parameter,

$$N = \sigma B^2 l/\rho u = l/u\tau \tag{3.29}$$

where τ is the magnetic damping time $(\sigma B^2/\rho)^{-1}$ which was introduced in Chapter 1. This is relevant in situations where $\mathbf{J}$ is primarily driven by $\mathbf{u}\times\mathbf{B}$ in Ohm's law, and so $|\mathbf{J}| \sim \sigma uB$. In such a case, N represents the ratio of the Lorentz force, $\mathbf{J}\times\mathbf{B}/\rho$, to inertia, $(\mathbf{u}\cdot\nabla)\mathbf{u}$.

The third dimensionless group, called the Hartmann number, is a hybrid of Re and N. It is

$$Ha = (N\mathrm{Re})^{1/2} = Bl(\sigma/\rho\nu)^{1/2} \tag{3.30}$$

Evidently $(Ha)^2$ represents the ratio of the Lorentz force to viscous forces. The final dimensionless group has nothing at all to do with forces. Rather, it is indicative of the relative strengths of advection and diffusion in the induction equation (3.26). This is the magnetic Reynolds number

$$R_m = ul/\lambda = \mu\sigma ul \tag{3.31}$$

which was first introduced in Chapter 1. When R_m is large, diffusion is weak. These various groups are listed in Table 3.1.

Note that the characteristic length scale of the flow, l, need not be known in advance, but rather it may emerge from some internal force balance. The obvious example is a boundary layer, where Re based on the boundary layer thickness is always of the order of unity. That is the whole point about boundary layers: viscous and inertia forces are always

Table 3.1. *Dimensionless groups*

Name	Symbol	Definition	Significance
Reynolds number	Re	ul/ν	Ratio of inertia to shear forces
Interaction Parameter	N	$\sigma B^2 l/\rho u$	Ratio of Lorentz forces to inertia
Hartman number	Ha	$Bl(\sigma/\rho\nu)^{1/2}$	Ratio of Lorentz forces to shear forces
Magnetic Reynolds number	R_m	ul/λ	Ratio of advection to diffusion of B

of the same order, no matter how small ν may be. One must always be careful in the choice of length scale when constructing meaningful dimensionless groups. In general, each case must be treated on an individual basis. Nevertheless, dimensionless groups are extremely useful. Often, when they are very large or very small, they allow us to throw out certain terms in the governing equations, thereby greatly simplifying the problem.

3.9 Maxwell Stresses

We conclude this chapter with a discussion of the Lorentz force itself. From Ampère's law we may rewrite the Lorentz force in terms of **B** alone. We start with the vector identity

$$\nabla(\mathbf{B}^2/2) = (\mathbf{B}\cdot\nabla)\mathbf{B} + \mathbf{B}\times\nabla\times\mathbf{B}$$

from which, using $\nabla\times\mathbf{B} = \mu\mathbf{J}$,

$$\mathbf{J}\times\mathbf{B} = (\mathbf{B}\cdot\nabla)(\mathbf{B}/\mu) - \nabla(\mathbf{B}^2/2\mu) \tag{3.32}$$

The second term on the right of (3.32) acts on the fluid in exactly the same way as the pressure force $-\nabla p$. It is irrotational, and so makes no contribution to the vorticity equation. In flows without a free surface its rôle is simply to augment the fluid pressure. (Its absence from the vorticity equation implies that it cannot influence the flow field.) For this reason, $\mathbf{B}^2/2\mu$ is called the magnetic pressure and in many, if not most, problems it is of no dynamical significance. Which brings us to the first term on the right. We can write the ith component of this force as

$$\mathbf{B}\cdot\nabla(B_i/\mu) = \frac{\partial}{\partial x_j}\left[\frac{B_i B_j}{\mu}\right] \tag{3.33}$$

where there is an implied summation over the index j. From this we may show that the effect of the body force in (3.33) is exactly equivalent to a distributed set of fictitious stresses, B_iB_j/μ, acting on the surface of fluid elements. One approach is simply to compare (3.33) with the viscous forces in (3.1), making use of Figure 3.8. Alternatively, this can be established by integrating (3.33) over an arbitrary volume V and invoking Gauss's theorem. Since $\nabla \cdot (B_i\mathbf{B}) = \mathbf{B} \cdot \nabla B_i + B_i \nabla \cdot \mathbf{B} = \mathbf{B} \cdot \nabla B_i$, we find

$$\int [\mathbf{B} \cdot \nabla(B_i/\mu)] dV = \oint (B_i/\mu)\mathbf{B} \cdot d\mathbf{S} \tag{3.34}$$

The surface integral on the right of (3.34) is equal to the cumulative effect of the distributed stress system B_iB_j/μ acting over the surface of V. That is to say, the tangential and normal stresses, B_tB_n/μ and B_n^2/μ, acting on the surface element $d\mathbf{S}$ give rise to a force $\mathbf{B}(\mathbf{B} \cdot d\mathbf{S})/\mu$. However, equation (3.34) tells us that this surface stress distribution is, in turn, equivalent to the integrated effect of the volume force $(\mathbf{B} \cdot \nabla)(\mathbf{B}/\mu)$. Since this is true for any volume V, it follows that the body force $(\mathbf{B} \cdot \nabla)(\mathbf{B}/\mu)$ and the stress system B_iB_j/μ are entirely equivalent in their mechanical action.

In summary then, we may replace the Lorentz force, $\mathbf{J} \times \mathbf{B}$, by an imaginary set of stresses

$$\tau_{ij} = (B_iB_j/\mu) - (\mathbf{B}^2/2\mu)\,\delta_{ij} \tag{3.35}$$

where the second term on the right is the magnetic pressure. (The symbol δ_{ij} means: $\delta_{ij} = 1$ if $i = j$, $\delta_{ij} = 0$ if $i \neq j$.) These are called the Maxwell stresses, and their utility lies in the fact that we can represent the integrated effect of a distributed body force by surface stresses alone.

Now there is another, perhaps more useful, representation of $\mathbf{J} \times \mathbf{B}$. This comes from replacing $\mathbf{u}$ by $\mathbf{B}$ in (3.6):

$$(\mathbf{B} \cdot \nabla)\mathbf{B} = B\frac{\partial B}{\partial s}\hat{\mathbf{e}}_t - \frac{B^2}{R}\hat{\mathbf{e}}_n \tag{3.36}$$

Here s is now a coordinate measured along a magnetic field line, $\hat{\mathbf{e}}_t$ and $\hat{\mathbf{e}}_n$ are unit vectors in the tangential and principal normal direction, respectively, $B = |\mathbf{B}|$, and R is the local radius of curvature of the field line. It follows that the Lorentz force may be written as

$$\boxed{\mathbf{J} \times \mathbf{B} = \frac{\partial}{\partial s}\left[\frac{B^2}{2\mu}\right]\hat{\mathbf{e}}_t - \frac{B^2}{\mu R}\hat{\mathbf{e}}_n - \nabla(B^2/2\mu)} \tag{3.37}$$

We now have two alternative representations of $\mathbf{J} \times \mathbf{B}$. In cases where the magnetic pressure is unimportant, which is usually the case, we are concerned only with $\mathbf{B} \cdot \nabla(\mathbf{B}/\mu)$. In such situations, $\mathbf{J} \times \mathbf{B}$ may be pictured as the result of the stress system $B_t B_n/\mu$, or else it may be written in the form (3.36). To illustrate the difference, consider a flux tube as shown in Figure 3.34. In the first interpretation, $(\mathbf{B} \cdot \nabla)(\mathbf{B}/\mu)$ arises from *tensile stresses* of $\mathbf{B}^2/\mu$ acting on the ends of the tube (there are no stresses on the sides). These are referred to as Faraday tensions, or Maxwell tensions, in the field lines. In the second interpretation there are *force components* $\mu^{-1} B \partial B/\partial S$ and $B^2/\mu R$ tangential and normal, respectively, to the flux tube at each location.

In a qualitative sense then, we may think of field lines as being in tension and exerting a pseudo-elastic stress on the fluid. This lies at the root of many MHD phenomena, particularly the Alfvén wave. We have already seen in Section 2.7 that, when R_m is high, the magnetic field lines tend to be frozen into a fluid (Figure 3.35). Now we see that the field lines also behave as if they are in tension. Consider what happens then if, at $t = 0$, we try to push a region of highly conductive fluid past a magnetic field. The field lines will be swept along with the fluid, and the resulting curvature of the lines will create a back reaction $B^2/\mu R$ on the fluid. The fluid will eventually come to rest and the Faraday tensions will then reverse the flow. Oscillations (Alfvén waves) may even result. This is effectively what happens in the experiment described in Section 1.3.

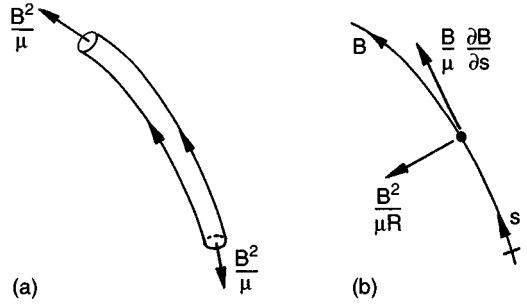

Figure 3.34 The contribution $\mathbf{B} \cdot \nabla(\mathbf{B}/\mu)$ to the Lorentz force may be interpreted either in terms of Faraday tensions, B^2/μ, in the field lines, or else in terms of the forces $(B/\mu)\partial B/\partial S$ and $B^2/\mu R$ acting tangential and normal to the field line, respectively.

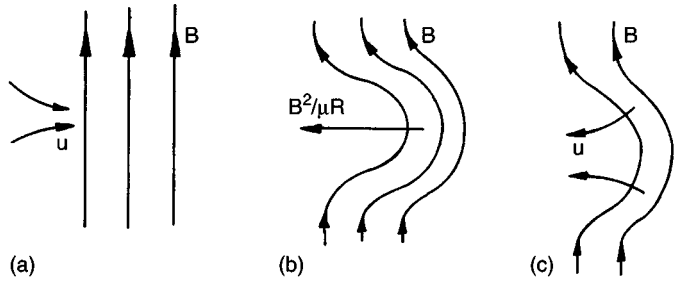

Figure 3.35 Magnetic field lines can behave like elastic bands frozen into the fluid.

Suggested Reading

Feynman, Leighton & Sands, *The Feynman lectures on physics*, vol. II, 1964. Addison–Wesley (Chapters 40, 41 provide an introduction to fluid mechanics).

D J Acheson, *Elementary fluid dynamics*, 1990. Clarendon Press. (Chapter 5 for vortex dynamics, chapter 9 for boundary layers.)

G K Batchelor, *An introduction to fluid mechanics*, 1967. Cambridge University Press. (Chapter 7 for vortex dynamics.)

J A Shercliff, *A textbook of magnetohydrodynamics*, 1965. Pergamon Press. (Chapter 4 for the Lorentz force and Maxwell stresses.)

H Tennekes & J L Lumley, *A first course in turbulence*, 1972. The MIT Press. (Chapter 2 for a discussion of Reynolds stresses.)

Examples

3.1 Show that the circulation is the same around all simple closed circuits enclosing the wing shown in Figure 3.3 (ignore any vorticity in the wake).

3.2 A bathtub vortex forms because random vorticity in the bath becomes aligned with the axis of the vortex by the action of the converging, draining flow. Explain why the vorticity is also intensified by the action of the converging flow.

3.3 A peculiar vortex motion may be observed in rowing. At places where the oar breaks the surface of the water, just previous to being lifted, a pair of small dimples (depressions) appear on the surface. Once the oar is lifted from the water the pair of dimples propagate along the surface. They are the end points of a vortex arc (half of a vortex ring). Explain what is happening.

3.4 Estimate the pressure at the centre of a typical tornado.

3.5 Show that the free surface of a tidal vortex is a hyperbola. You may assume that the velocity distribution is approximately that of a free vortex, $u_\theta \sim \Gamma/r$ where $\Gamma =$ constant (ignore the singularity at the centre of the vortex).

3.6 Use the Biot–Savart law to calculate the velocity at the centre of a thin vortex ring.

4

Kinematics of MHD: Advection and Diffusion of a Magnetic Field

> We adopt the suggestion of Ampère, and use the term 'Kinematics' for the purely geometrical science of motion in the abstract. Keeping in view the properties of language, and following the example of most logical writers, we employ the term 'dynamics' in its true sense as the science which treats the action of force.
>
> *Kelvin (1879), preface to Natural Philosophy*

We now consider one half of the coupling between **B** and **u**. Specifically, we look at the influence of **u** on **B** without worrying about the origin of the velocity field or the back reaction of the Lorentz forces on the fluid. In effect, we take **u** to be prescribed, forget about the Navier–Stokes equation, and focus on the interaction of **u** with Maxwell's equations. This is referred to as the *kinematics of MHD*.

4.1 The Analogy to Vorticity

In Chapter 2 we showed that Maxwell's equations lead to the induction equation

$$\frac{\partial \mathbf{B}}{\partial t} = \nabla \times (\mathbf{u} \times \mathbf{B}) + \lambda \nabla^2 \mathbf{B} \tag{4.1}$$

where $\lambda = (\mu\sigma)^{-1}$. Compare this with the transport equation for vorticity,

$$\frac{\partial \boldsymbol{\omega}}{\partial t} = \nabla \times (\mathbf{u} \times \boldsymbol{\omega}) + \nu \nabla^2 \boldsymbol{\omega} \tag{4.2}$$

There appears to be an exact analogy. In fact, the analogy is not perfect because $\boldsymbol{\omega}$ is functionally related to **u** in a way that **B** is not. Nevertheless, this does not stop us from borrowing many of the theorems of classical vortex dynamics and re-interpreting them in terms of MHD, with **B** playing the rôle of $\boldsymbol{\omega}$. For example, **B** is advected by **u** and diffused by λ, and in the limit $\lambda \to 0$, the counterpart of Helmholtz's first law is that **B** is frozen into the fluid.

4.2 Diffusion of a Magnetic Field

When $\mathbf{u} = 0$ we have

$$\frac{\partial \mathbf{B}}{\partial t} = \lambda \nabla^2 \mathbf{B} \tag{4.3}$$

which may be compared with the diffusion equation for heat,

$$\frac{\partial T}{\partial t} = \alpha \nabla^2 T \tag{4.4}$$

It appears that, like heat, magnetic fields will diffuse through a medium at a finite rate. We cannot suddenly 'impose' a distribution of **B** throughout a conductor. All we can do is specify values at the boundaries and wait for it to diffuse inward. For example, suppose we have a semi-infinite region of conducting material occupying $y > 0$, and at $t = 0$ we apply a magnetic field $B_0 \hat{\mathbf{e}}_x$ at the surface $y = 0$. Then **B** will diffuse into the conductor in precisely the same way as heat or vorticity diffuses. In fact, to find the distribution of **B** at any instant we may simply lift the solution directly from the equivalent thermal problem. Such diffusion problems were discussed in Section 3.3, where we found that T (or ω) diffuses a distance $l \sim \sqrt{\alpha t}$, (or $\sqrt{\nu t}$) in a time t. By implication, **B** diffuses a distance of order $\sqrt{\lambda t}$ in the same time.

Example: Extinction of a magnetic field

Consider a long conducting cylinder which, at $t = 0$, contains a uniform axial magnetic field, B_0. The field outside the cylinder is zero. The axial field inside the cylinder will decay according to the diffusion equation

$$\frac{\partial B}{\partial t} = \lambda \frac{1}{r} \frac{\partial}{\partial r} \left(r \frac{\partial B}{\partial r} \right)$$

subject to $B = 0$ at $r = R$ and $B = B_0$ at $t = 0$. Show that a Fourier–Bessel series of the form

$$B = \sum_{n=1}^{\infty} A_n J_0(\gamma_n r/R) \exp\left(-\gamma_n^2 \lambda t / R^2\right)$$

is a possible solution, where J_0 is the usual Bessel function, γ_n are the zeros of J_0, and A_n represents a set of amplitudes. Deduce that the field decays on a time scale of $R^2/(5.75\lambda)$.

4.3 Advection in Ideal Conductors: Alfvén's Theorem

4.3.1 Alfvén's theorem

We now consider the other extreme, where there is no diffusion ($\lambda = 0$) but $\mathbf{u}$ is finite. This applies to conducting fluids with a very high conductivity (ideal conductors). Consider the similarity between

$$\frac{\partial \mathbf{B}}{\partial t} = \nabla \times (\mathbf{u} \times \mathbf{B}) \tag{4.5}$$

and the vorticity equation for an inviscid fluid,

$$\frac{\partial \boldsymbol{\omega}}{\partial t} = \nabla \times (\mathbf{u} \times \boldsymbol{\omega})$$

We might anticipate, therefore, that Helmholtz's first law and Kelvin's theorem (which is, in effect, Helmholtz's second law) have their analogues in MHD. This turns out to be so. The equivalent theorems are:

Theorem I: (analogue of Helmholtz's first law)	The fluid elements that lie on a magnetic field line at some initial instant continue to lie on that field line for all time, i.e. the field lines are frozen into the fluid.
Theorem II: (analogue of Kelvin's theorem)	The magnetic flux linking any loop moving with the fluid is constant.

These two results are collectively known as Alfvén's theorem. In fact, Theorem II is a direct consequence of the generalised version of Faraday's law, which was introduced in Section 2.7.4. Moreover, the first theorem may be proved in precisely the same manner as Helmholtz's first law, the proof relying on the analogy between (4.5) in the form

$$\frac{D\mathbf{B}}{Dt} = (\mathbf{B} \cdot \nabla)\mathbf{u} \tag{4.6}$$

and equation (3.21) for a material line element

$$\frac{D}{Dt}(d\mathbf{l}) = ((d\mathbf{l}) \cdot \nabla)\mathbf{u}$$

The 'frozen-in' nature of magnetic fields is of crucial importance in astrophysics, where R_m is usually very high. For example, one might ask: why do many stars possess magnetic fields of the order of 10 or 1000 Gauss? The answer, possibly, is that there exists a weak galactic field of $\sim 10^{-6}$ Gauss. As a star starts to form due to the gravitational collapse of an interstellar cloud, the galactic field, which is trapped in the plasma, becomes concentrated by the inward radial movement. A simple estimate of the increase in **B** due to this mechanism can be obtained if we assume the cloud remains spherical, of radius r, during the collapse. Two invariants of the cloud are its mass, $M \propto \rho r^3$, and the flux of the galactic field which traverses the cloud, $\Phi \propto Br^2$. It follows that during the collapse, $B \propto \rho^{2/3}$ which suggest $(B_{\text{star}}/B_{\text{gal}}) \sim (\rho_{\text{star}}/\rho_{\text{gal}})^{2/3}$. Actually, this overestimates B_{star} somewhat, possibly because the collapse is not spherical, and possibly because there is some turbulent diffusion of **B**, despite the high value of R_m.

Now the analogy between **B** and ω can be pushed even further. For example, our experience with vorticity suggests that, in three-dimensions, we can stretch the magnetic field lines (or flux tubes) leading to an intensification of **B**. That is, the left of (4.6) represents the material advection of the magnetic field, so that when $(\mathbf{B} \cdot \nabla)\mathbf{u} = 0$ (as would be the case in certain two-dimensional flows) the magnetic field is passively advected. However, in three-dimensional flows $(\mathbf{B} \cdot \nabla)\mathbf{u}$ need not be zero and, because of the analogy with vortex tubes, we would expect this to lead to a rise in **B** whenever the flux tubes are stretched by the flow (see Section 3.3). In fact, this turns out to be true, as it must because the mathematics in the two cases are formally identical. However, the physical interpretation of this process of intensification is different in the two situations. In vortex dynamics it is a direct consequence of the conservation of angular momentum. In MHD, however, it follows from a combination of the conservation of mass, $\rho\delta V = \rho\delta A dl$, and flux, $\Phi = B\delta A$, applied to an element of a flux tube, as shown in Figure 4.1. If the flux

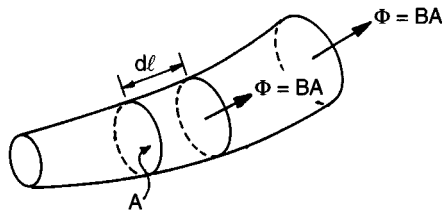

Figure 4.1 Stretching of a flux tube intensifies B.

tube is stretched, δA decreases and so B rises to conserve flux. This is the basis of dynamo theory in MHD, whereby magnetic fields are intensified by continually stretching the flux tubes.

4.3.2 An aside: sunspots

As an illustration of the 'frozen-in' behaviour of magnetic fields, and of flux-tube stretching, we shall describe here the phenomenon of sunspots. We give only a qualitative description, but the interested reader will find more details in the suggested reading list at the end of this chapter.

If you look at the sun through darkened glass it is possible to discern small dark spots on its surface. These come and go, with a typical lifetime of several days. These spots (sunspots) typically appear in pairs and are concentrated around the equatorial plane. The spots have a diameter of $\sim 10^4$ km, which is around the same size as the earth! To understand how they arise, you must first know a little bit about the structure of the sun.

The surface of the sun is not uniformly bright, but rather has a granular appearance. This is because the outer layer of the sun is in a state of convective turbulence. This *convective layer* has a thickness of 2×10^5 km (the radius of the sun is 7×10^5 km) and consists of a continually evolving pattern of convection cells, rather like those seen in Bénard convection (Figure 4.2). The cells nearest the surface are about 10^3 km across. Where hot fluid rises to the surface, the sun appears bright, while the cooler fluid, which falls at the junction of adjacent cells, appears dark. A typical convective velocity is around 1 km/s and estimates of Re and R_m are, $\mathrm{Re} \sim 10^{11}$, $R_m \sim 10^8$, i.e. very large!

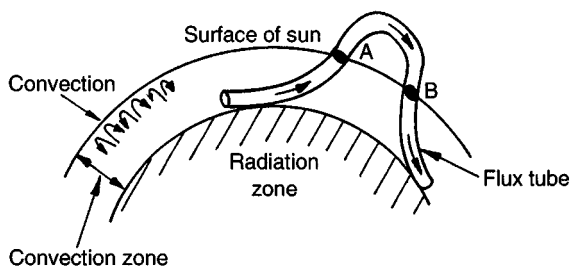

Figure 4.2 Schematic representation of the formation of sunspots. A buoyant flux tube erupts through the surface of the sun. Sunspots form at A and B where the magnetic field suppresses the turbulence, cooling the surface.

Now the sun has an average surface magnetic field of a few Gauss, rather like that of the earth. Because R_m is large, this dipole field tends to be frozen into the fluid in the convective zone. Large-scale differential rotation in this zone stretches and intensifies this field until large field strengths (perhaps 10^3 Gauss) build up in azimuthal flux tubes of varying diameter. The pressure inside these flux tubes is significantly less than the ambient pressure in the convective zone, essentially because the Lorentz forces in a flux tube point radially outward. The density inside the tubes is correspondingly less, and so the tubes experience a buoyancy force which tends to propel them towards the surface. This force is strongest in the thick tubes, parts of which become convectively unstable and drift upwards, with a rise time of perhaps a month. Periodically then, flux tubes of diameter $\sim 10^4$ km burst through the surface into the sun's atmosphere (Figure 4.2). Sunspots are the footpoint areas where the tubes pierce the surface (A and B in Figure 4.2). These footpoints appear dark because the intense magnetic field in the flux tubes ($\sim$3000 Gauss) locally suppresses the fluid motion and convective heat transfer, thus cooling the surface.

This entire phenomenon relies on the magnetic field being (partially) frozen into the fluid. It is this which allows intense fields to form in the first place, and which ensures that the buoyant fluid at the core of a flux tube carries the tube with it as it moves upward. We shall return to this topic in Chapter 6, where we shall see that sun spots are often accompanied by other magnetic phenomena, such as solar flares.

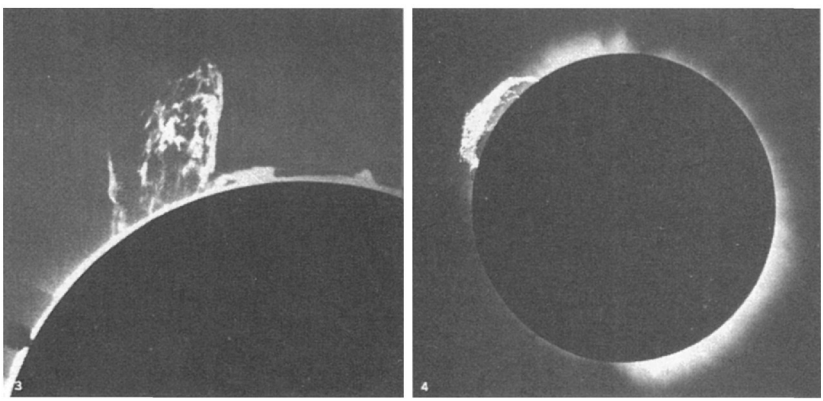

Figure 4.3 Magnetic activity in the solar atmosphere (Encyclopaedia Britannica).

4.4 Magnetic Helicity

We can take the analogy between ω and $\mathbf{B}$ yet further. In Section 3.4 we saw that the helicity

$$h = \int_{V_\omega} \mathbf{u} \cdot \omega dV$$

is conserved in an inviscid flow. Moreover, this is a direct consequence of the conservation of vortex-line topology which is enforced by Helmholtz's laws. We would expect, therefore, that the magnetic helicity

$$h_m = \int_{V_B} \mathbf{A} \cdot \mathbf{B} dV \tag{4.7}$$

will be conserved as a consequence of Alfvén's theorem. ($\mathbf{A}$ is the vector potential defined by (2.19).) This is readily confirmed. First we uncurl (4.5) to give

$$\frac{\partial \mathbf{A}}{\partial t} = \mathbf{u} \times \mathbf{B} + \nabla \phi \tag{4.8}$$

where ϕ is a scalar defined by the divergence of (4.8). From (4.8) and (4.5) we have

$$\frac{\partial}{\partial t}(\mathbf{A} \cdot \mathbf{B}) = \nabla \cdot (\phi \mathbf{B}) + \mathbf{A} \cdot [\nabla \times (\mathbf{u} \times \mathbf{B})]$$

which, with the help of the vector relationship

$$\nabla \cdot [\mathbf{A} \times (\mathbf{B} \times \mathbf{u})] = \nabla \cdot [(\mathbf{A} \cdot \mathbf{u})\mathbf{B} - (\mathbf{A} \cdot \mathbf{B})\mathbf{u}] = \mathbf{A} \cdot \nabla \times [\mathbf{u} \times \mathbf{B}]$$

becomes

$$\frac{D}{Dt}(\mathbf{A} \cdot \mathbf{B}) = \nabla \cdot [(\phi + \mathbf{A} \cdot \mathbf{u})\mathbf{B}] \tag{4.9}$$

We now integrate (4.9) over a material volume V_B which always consists of the same fluid particles (each of volume δV) and for which $\mathbf{B} \cdot d\mathbf{S} = 0$. Remembering that $D(\delta V)Dt = 0$ in an incompressible fluid, we obtain,

$$\frac{d}{dt} \int_{V_B} (\mathbf{A} \cdot \mathbf{B}) dV = 0$$

as required. As with the helicity of a vorticity field, this conservation law is topological in nature. It stems from the fact that interlinked flux tubes

in an ideal conductor remain linked for all time, conserving their relative topology as well as their individual fluxes (see Section 3.4). Finally, we note that minimising magnetic energy subject to the conservation of helicity leads to the field $\nabla \times \mathbf{B} = \alpha \mathbf{B}$ which, as noted in Chapter 2, is called a force-free field.

There is one other topological invariant of ideal (diffusionless) MHD. This is called the cross-helicity, and is defined as

$$\int_{V_B} \mathbf{B} \cdot \mathbf{u} dV$$

Cross-helicity is conserved whenever λ and ν are zero. It represents the degree of linkage of the vortex lines and **B**-lines. We shall not pause here to prove the conservation of cross-helicity, but leave it as an exercise for the reader.

4.5 Advection plus Diffusion

We now consider the combined effects of diffusion and advection. For simplicity we focus on two-dimensional flows in which there is no flux-tube stretching. In such cases it is convenient to work with the vector potential **A**, rather than **B**. Suppose that $\mathbf{u} = (\partial\psi/\partial y, -\partial\psi/\partial x, 0)$ and $\mathbf{B} = (\partial A/\partial y, -\partial A/\partial x, 0)$ where ψ is the streamfunction for **u**, $\mathbf{u} = \nabla \times (\psi \hat{\mathbf{e}}_z)$, and A is the analogous *flux function* for **B**, $\mathbf{B} = \nabla \times (A\hat{\mathbf{e}}_z)$. Then the induction equation (4.1) becomes $\partial \mathbf{A}/\partial t = \mathbf{u} \times \mathbf{B} + \lambda \nabla^2 \mathbf{A}$, from which

$$\frac{DA}{Dt} = \lambda \nabla^2 A \tag{4.10}$$

Note that the contours of constant A represent magnetic field lines. Also, as noted in Section 3.8, $R_m = \mu\sigma ul = ul/\lambda$ is a measure of the relative strengths of advection and diffusion.

4.5.1 Field sweeping

Now A is transported just like heat, c.f. (4.4). Let us start, therefore, with a problem which is analogous to a heated wire in a cross flow, as this example was discussed at some length in Chapter 3, Section 3. The equivalent MHD problem is sketched in Figure 4.4.

We have a thin wire carrying a current I (directed into the page) which sits in a uniform cross flow, **u**. The magnetic field lines surrounding the

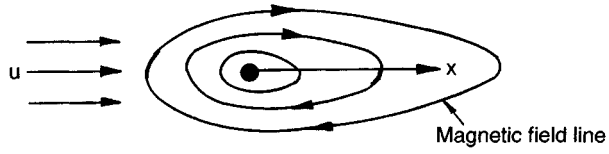

Figure 4.4 Magnetic field induced by a current-carrying wire in a cross flow.

wire are swept downstream by **u**, just like the isotherms in Figure 3.11. In the steady state (4.10) can be written as

$$u\frac{\partial A}{\partial x} = \lambda \nabla^2 A \tag{4.11}$$

Now there is no natural length scale for this problem. (The wire is considered to be vanishingly thin.) The only way of constructing a magnetic Reynolds number is to use $r = (x^2 + y^2)^{1/2}$ as the characteristic length-scale. Thus, $R_m = \mu\sigma ur = ur/\lambda$. Near the wire, therefore, we will have a diffusion-dominated regime ($R_m \ll 1$), while at large distances from the wire ($R_m \gg 1$) advection of **B** will dominate. It turns out that equation (4.11) may be solved by looking for solutions of the form $A = f(x, y)\exp(ux/2\lambda)$. This yields $\nabla^2 f = (u/2\lambda)^2 f$, and the solution for A is thus

$$A = CK_0(ur/2\lambda)\exp(ux/2\lambda)$$

where K_0 is the zero-order Bessel function normally denoted by K. The constant C may be determined by matching this expression to the diffusion-dominated solution $A = (\mu I/2\pi)\ln(r)$ at $r \to 0$. This gives $C = \mu I/2\pi$. The shape of the field lines is as shown in Figure 4.4. They are identical to the isotherms in the analogous thermal problem.

4.5.2 Flux expulsion

We now consider another example of combined advection and diffusion. This is a phenomenon called flux expulsion which, from the mathematical point of view, is nothing more than the Prandtl–Batchelor theorem applied to **A** rather than ω. Suppose that we have a steady flow consisting of a region of closed streamlines of size l, and that $R_m = ul/\lambda$ is large. Then we may show that any magnetic field which lies within that region is gradually expelled (Figure 4.5). The proof is essentially the same as that for the Prandtl–Batchelor theorem. In brief, the argument goes as follows. We have seen that A satisfies an advection

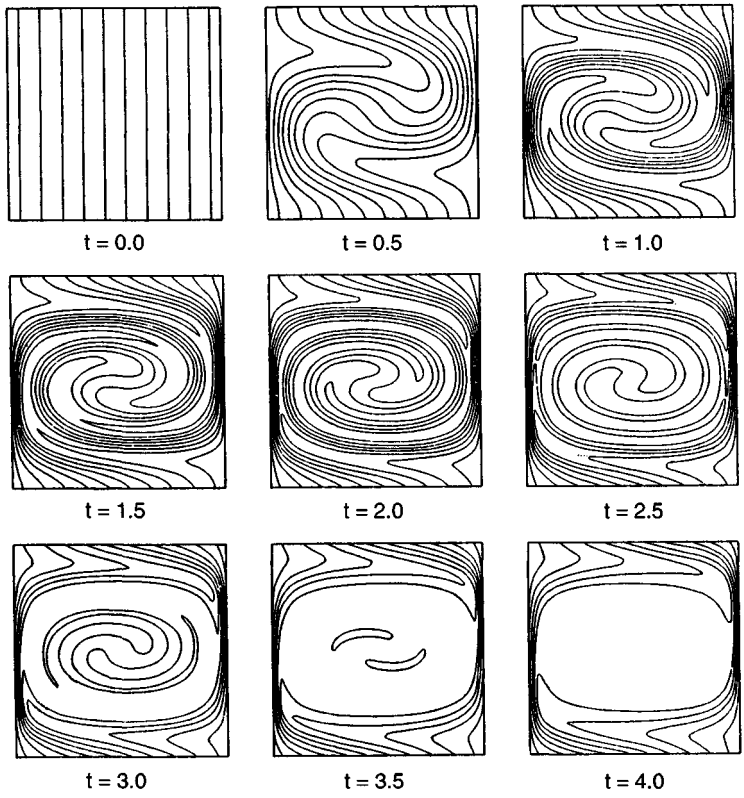

Figure 4.5 An example of flux expulsion in a square at $R_m = 100$ (based on computations by N O Weiss). The figures show the distortion of an initially uniform field by a clockwise eddy. (From H K Moffat, *Magnetic field generation in electrically conducting fluids*. CUP, 1978, with permission.)

diffusion equation, just like vorticity. When R_m is large we find A is almost constant along the streamlines. However, a small but finite diffusion slowly eradicates cross-stream gradients in A until it is perfectly uniform, giving $\mathbf{B} = 0$. We now work through the details, starting with the high R_m equation

$$\frac{DA}{Dt} \approx 0$$

In the steady state this simplifies to $\mathbf{u} \cdot \nabla A = 0$, which in turn implies $A = A(\psi)$. That is, A is constant along the streamlines so that $\mathbf{B}$ and $\mathbf{u}$ are co-linear. Now suppose that λ is small but finite. The steady version of (4.10)

$$\mathbf{u} \cdot \nabla A = \lambda \nabla^2 A$$

yields the integral equation

$$I = \lambda \int_{V_\psi} \nabla^2 A \, dV = 0 \tag{4.12}$$

where V_ψ is the volume enclosed by a closed streamline. Now (4.12) must hold true for any finite value of λ, and in particular it remains valid when λ is very small, so that $A \approx A(\psi)$. Let us now explore the consequences of the integral constraint (4.12) for our high-Rm flow. We have, using Gauss's theorem,

$$I = \lambda \int_{V_\psi} \nabla^2 A \, dV = \lambda \oint_{S_\psi} \nabla A \cdot d\mathbf{S} = \lambda A'(\psi) \oint_{S_\psi} \nabla \psi \cdot d\mathbf{S}$$

where $A'(\psi)$ is the cross-stream gradient of A, which is constant on the surface S_ψ. However, the integral on the right is readily evaluated. We use Gauss's and Stokes' theorems as follows:

$$\oint_{S_\psi} \nabla \psi \cdot d\mathbf{S} = \int_{V_\psi} \nabla^2 \psi dV = - \int_{V_\psi} \omega dV = - \oint_{C_\psi} \mathbf{u} \cdot d\mathbf{l}$$

Here, C_ψ is the streamline which defines S_ψ. It follows that our integral constraint may be rewritten as

$$I = -\lambda A'(\psi) \oint_{C_\psi} \mathbf{u} \cdot dl = 0 \tag{4.13}$$

Again it is emphasised that this holds true no matter how small we make λ. It is only necessary that λ be finite. Now it follows from (4.13) that $A'(\psi) = 0$, since the line integral cannot be zero. We conclude, therefore, that in a region of closed streamlines with a high value of R_m, the flux function is constant. It follows that $\mathbf{B} = 0$. This phenomenon is known as flux expulsion.

An example of this process is shown below. A magnetic field $\mathbf{B} = B_0 \hat{\mathbf{e}}_y$ pervades a conducting fluid, and a region of this fluid, $r < R$, is in a state of rigid body rotation, the remainder being quiescent. This local rotation distorts $\mathbf{B}$ and the distortion is readily calculated. Let Ω be the angular velocity of the fluid. In the steady state, (4.10) gives us

$$\frac{\Omega}{\lambda} \frac{\partial A}{\partial \theta} = \nabla^2 A, \qquad 0 < r < R$$

with $\nabla^2 A = 0$ for $r > R$. It is natural to look for solutions of the form $A = f(r)\exp(j\theta)$, where we extract only the real part of A. This yields

$$\frac{j\Omega}{\lambda} f(r) = \left(\frac{1}{r}\frac{d}{dr} r \frac{d}{dr} - \frac{1}{r^2}\right) f, \qquad 0 < r < R$$

The solution for f is then

$$f = -B_0 r + C/r, \qquad r > R$$
$$f = DJ_1(pr), \qquad 0 < r < R$$

where C and D are constants, J_1 is the usual first-order Bessel function, and $p = (1 - j)(\Omega/2\lambda)^{1/2}$. The unknown constants can be evaluated from the condition that **B** is continuous at $r = R$. In the limit of $R_m \to \infty$, we find that $A = 0$ inside $r = R$ and $A = -B_0(r - R^2/r)\cos\theta$ for $r > R$.

The flux function, A, is then identical to the streamlines of an irrotational flow past a cylinder. The shape of the magnetic field lines for different values of $R_m = \Omega R^2/\lambda$ are shown in Figure 4.6. As R_m increases the distortion of the field becomes greater, and this twisting of the **B**-lines, combined with cross-stream diffusion, gradually eradicates **B** from the rotating fluid. This form of flux expulsion is related to the *skin effect* in electrical engineering. Suppose we change the frame of reference and rotate with the fluid. Then the problem is that of a magnetic field rotating around a stationary conductor. In such a case it is well known that the field will penetrate only a finite distance, $\delta = \sqrt{2\lambda/\Omega}$, into the conductor. This distance is known as the skin depth. As $\Omega \to \infty$ the field is excluded from the interior of the conductor.

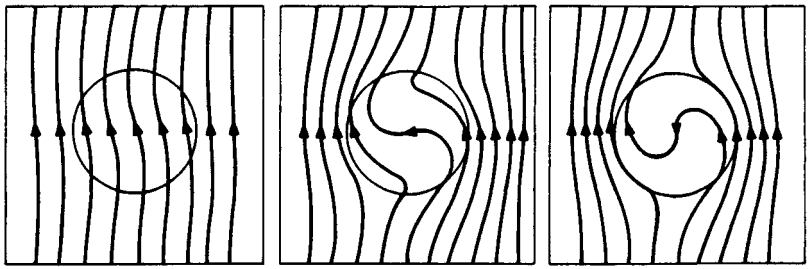

Figure 4.6 Distortion and expulsion of a magnetic field by differential rotation. (From H K Moffatt, *Magnetic field generation in electrically conducting fluids.* CUP, 1978, with permission.)

4.5.3 *Azimuthal field generation by differential rotation*

Our penultimate example of combined advection and diffusion is axisymmetric rather than planar. It is mainly of interest to astrophysics and concerns a rotating fluid permeated by a magnetic field. It turns out that stars do not always rotate as a rigid body. Our own sun, for example, exhibits a variation of rotation with latitude. Consider a non-uniformly rotating star possessing a poloidal magnetic field, i.e. a field of the form $\mathbf{B}_p(r, z) = (B_r, 0, B_z)$ in (r, θ, z) coordinates. Suppose the sun rotates faster at the equator than at its poles, $\mathbf{u} = (0, \Omega(z)r, 0)$, then, by Alfvén's theorem, the poloidal field lines will tend to be advected, as shown in Figure 4.7. The field lines will bow out until such time as the diffusion created by the distortion is large enough to counter the effects of field sweeping. This is readily seen from the azimuthal component of the steady induction equation

$$\frac{\partial \mathbf{B}_\theta}{\partial t} = \nabla \times (\mathbf{u} \times \mathbf{B}_p) + \lambda \nabla^2 \mathbf{B}_\theta = 0$$

where $\mathbf{B}_\mathrm{p}$ is the poloidal magnetic field. The source of the azimuthal field is the term $\nabla \times (\mathbf{u} \times \mathbf{B}_p)$, which may be rewritten as $r(\mathbf{B}_p \cdot \nabla)\Omega$, showing the rôle played by $\Omega(z)$ in generating the azimuthal field. Note that, if λ is very small, then extremely large azimuthal fields may be generated by this mechanism, of order $R_m|\mathbf{B}_p|$. This is a key process in many theories relating to solar MHD, such as the origin of sunspots.

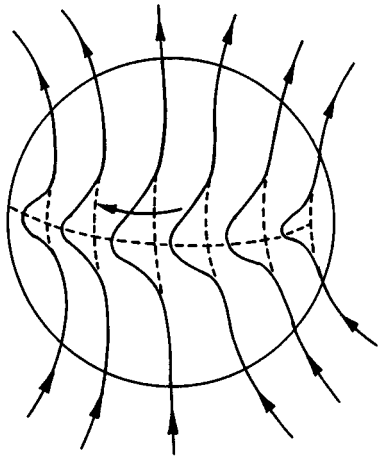

Figure 4.7 Distortion of the magnetic field lines by differential rotation.

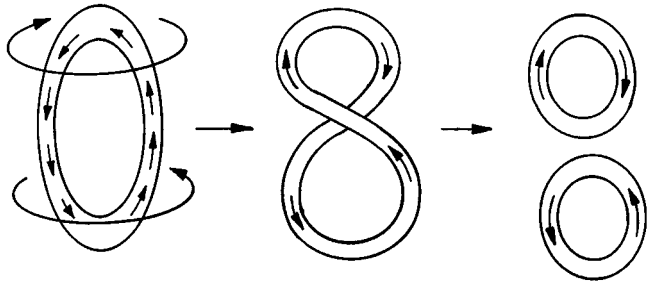

Figure 4.8 Severing of a flux tube.

4.5.4 Magnetic reconnection

Finally, we consider the rôle played by a small but finite diffusivity in the reconnection of magnetic flux tubes. Consider a flux tube in the form of a ring which at $t = 0$ sits in a differentially rotating fluid, as shown in Figure 4.8. When the two branches of the tube come into contact, the field lines locally compress and the gradients in **B** become large. Eventually the gradients become so large that, despite the smallness of λ, significant diffusion sets in. The result is that the magnetic field lines reconnect, forming two smaller flux tubes. This kind of process is very important in solar MHD, particularly the theory of solar flares, where the nominal value of R_m is very large, yet flux-tube reconnections are an important part of the origin of flares.

Suggested Reading

J A Shercliff, *A textbook of magnetohydrodynamics*, 1965, Pergamon Press. (Chapter 3)

R Moreau, *Magnetohydrodynamics*, 1990, Kluwer Acad. Pub. (Chapter 2)

P H Roberts, *An Introduction to magnetohydrodynamics*, 1967, Longmans. (Chapter 2)

H K Moffatt, *Magnetic field generation in electrically conducting fluids*, 1978, Cambridge University Press. (Chapter 3 for kinematics, Chapter 5 for sunspots.)

Examples

4.1 A semi-infinite region of conducting material is subject to mutually perpendicular electric and magnetic fields of frequency ω at, and parallel to, its plane boundary. There are no fields deep inside the

stationary conductor. Derive expressions for the variation of amplitude and phase of the magnetic field as a function of distance from the surface.

4.2 A perfectly conducting fluid undergoes an axisymmetric motion and contains an azimuthal magnetic field $\mathbf{B}_\theta$. Show that B_θ/r is conserved by each fluid element.

4.3 An electromagnetic flow meter consists of a circular pipe under a uniform transverse magnetic field. The voltage induced by the fluid motion between electrodes, placed at the ends of a diameter of the pipe perpendicular to the field, is used to indicate the flow rate. The pipe walls are insulated and the flow axisymmetric. Show that the induced voltage depends only on the total flow rate and not on the velocity profile.

4.4 A perfectly conducting, incompressible fluid is deforming in such a way that the magnetic field lines are being stretched with a rate of strain S. Show that the magnetic energy rises at a rate SB^2/μ per unit volume.

4.5 Fluid flows with uniform velocity past an insulated, thin flat plate containing a steady current sheet orientated perpendicular to the velocity. The intensity of the current sheet varies sinusoidally with the streamwise coordinate, and the electric field in the fluid is zero. Find the form of the magnetic field and show that it is confined to boundary layers when R_m is large.

5

Dynamics at Low Magnetic Reynolds Numbers

> It was perhaps for the advantage of science that Faraday, though thoroughly conscious of the forms of space, time and force, was not a professed mathematician. He was not tempted to enter into the many interesting researches in pure mathematics... and he did not feel called upon either to force his results into a shape acceptable to the mathematical taste of the time, or to express them in a form which the mathematicians might attack. He was thus left to his proper work, to coordinate his ideas with his facts, and to express them in natural, uncomplicated language.
>
> *Maxwell (1873)*

In Chapter 4 we looked at the effect of fluid motion on a magnetic field without worrying about the back reaction of **B** on **u**. We now consider the reverse problem, in which **B** influences **u** (via the Lorentz force), but **u** does not significantly perturb **B**. In short, we look at the effect of a prescribed magnetic field on the flow. To ensure that **B** remains unaffected by **u** we must restrict ourselves to low magnetic Reynolds numbers:

$$R_m = ul/\lambda = \mu\sigma ul \ll 1 \tag{5.1}$$

However, this is not overly restrictive, at least not in the case of liquid-metal MHD. For example, in most laboratory experiments, or industrial processes, $\lambda \sim 1\ \mathrm{m}^2/\mathrm{s}$, $l \sim 0.1$ m and internal friction keeps **u** to a level of around 0.01 m/s $\rightarrow$ 1 m/s. This gives $R_m \sim 0.001 \rightarrow 0.1$. The only exception is dynamo theory, where the large length scales involved result in $R_m \sim 100$. We also note in passing that the viscosity, ν, of liquid metal is similar to that of water, and so the Reynolds numbers of most liquid-metal flows is very high.

Now a magnetic field can alter **u** in three ways. It can suppress bulk motion, excite bulk motion, or alter the structure of the boundary layers in some way. We look at the first of these possibilities in Part 1, where we discuss the damping of flows using a static magnetic field. We tackle the second possibility in Part 2, where the effect of a rotating magnetic field is investigated. Finally, we examine boundary layers (Hartmann layers) in Part 3. We start, however, with the governing equations of low-R_m MHD.

5.1 The Low-R_m Approximation in MHD

The essence of the low-R_m approximation is that the magnetic field associated with induced currents, $\mathbf{J} \sim \sigma \mathbf{u} \times \mathbf{B}$, is negligible by comparison with the imposed magnetic field. There are three distinct cases which commonly arise.

(i) The imposed magnetic field is static, the flow is induced by some external agency, and friction keeps $\mathbf{u}$ to a modest level in the sense that $|\mathbf{u}| \ll \lambda/l$.

(ii) The imposed magnetic field travels or rotates uniformly and slowly such that $\mathbf{u}_{\text{field}} \ll \lambda/l$. This induces a flow $\mathbf{u}$ which, due to friction in the fluid, is somewhat slower than the speed of the field.

(iii) The imposed magnetic field oscillates extremely rapidly, in the sense that the skin-depth $\delta = (2/\mu\sigma\omega)^{1/2}$ is much less than l, ω being the field frequency. The magnetic field is then excluded from the interior of the conductor (see Section 4.5) and inertia or friction in the fluid ensures that $|\mathbf{u}| \ll \omega l$.

Categories (i)–(iii) cover the majority of flows in engineering applications. Typical examples are the magnetic damping of jets, vortices or turbulence (case (i)), magnetic stirring using a rotating magnetic field (case (ii)) and magnetic levitation (case (iii)). We shall leave the discussion of flows of type (iii) until Chapter 12. Here we focus on cases (i) and (ii).

Now if the imposed magnetic field travels or rotates in a uniform manner, then a suitable change of frame of reference will convert problems of type (ii) into those of type (i). Without loss of generality, therefore, we may take $\mathbf{B}$ to be steady.

We now discuss the simplifications which result in the governing equations when R_m is low and the imposed magnetic field is steady. Let $\mathbf{E}_0$, $\mathbf{J}_0$ and $\mathbf{B}_0$ represent the fields which would exist in a given situation if $\mathbf{u} = 0$, and let $\mathbf{e}$, $\mathbf{j}$ and $\mathbf{b}$ be the infinitesimal perturbations in $\mathbf{E}$, $\mathbf{J}$ and $\mathbf{B}$ which occur due to the presence of a vanishingly small velocity field. These quantities are governed by

$$\nabla \times \mathbf{E}_0 = 0, \qquad \mathbf{J}_0 = \sigma \mathbf{E}_0 \tag{5.2a, b}$$

$$\nabla \times \mathbf{e} = -\partial \mathbf{b}/\partial t, \qquad \mathbf{j} = \sigma(\mathbf{e} + \mathbf{u} \times \mathbf{B}_0) \tag{5.3a, b}$$

where we have neglected the second-order term $\mathbf{u} \times \mathbf{b}$ in (5.3b). Now Faraday's equation gives $\mathbf{e} \sim \mathbf{ub}$ and so the perturbation in the electric field may also be neglected in (5.3b). Ohm's law now becomes

$$\mathbf{J} = \mathbf{J}_0 + \mathbf{j} = \sigma(\mathbf{E}_0 + \mathbf{u} \times \mathbf{B}_0)$$

However, $\mathbf{E}_0$ is irrotational and so may be written as $-\nabla V$, where V is an electrostatic potential. Our final version of Ohm's law is therefore

$$\boxed{\mathbf{J} = \sigma(-\nabla V + \mathbf{u} \times \mathbf{B}_0)} \tag{5.4}$$

while the leading-order term in the Lorentz force (per unit volume) is

$$\boxed{\mathbf{F} = \mathbf{J} \times \mathbf{B}_0} \tag{5.5}$$

Equations (5.4) and (5.5) are all that we require to evaluate the Lorentz force in low-R_m MHD. There is no need to calculate $\mathbf{b}$ since it does not appear in the Lorentz force. Moreover, $\mathbf{J}$ is uniquely determined by (5.4) since

$$\nabla \cdot \mathbf{J} = 0, \qquad \nabla \times \mathbf{J} = \sigma \nabla \times (\mathbf{u} \times \mathbf{B}_0) \tag{5.6a, b}$$

and a vector field is unambiguously determined if its divergence and curl are known (and some suitable boundary conditions are specified).

From now on we shall drop the subscript on $\mathbf{B}_0$, on the understanding that $\mathbf{B}$ represents the imposed, steady magnetic field.

Part 1: Suppression of Motion

5.2 Magnetic Damping

There are many industrial and laboratory processes in which an intense, static magnetic field is used to suppress unwanted motion in a liquid metal. For example, in the continuous casting of large steel slabs, an intense DC magnetic field ($\sim 10^4$ Gauss) is commonly used to suppress motion within the mould. Sometimes the motion takes the form of a submerged jet which feeds the mould from above, at others it takes the form of large vortices. In both cases the aim is to keep the free surface of the liquid quiescent, thus avoiding the entrainment of surface debris. Magnetic damping is also used in the laboratory measurements of chemical and thermal diffusivities, particularly where thermal or solutal buoyancy can disrupt the measurement technique. These examples are discussed in more detail in Chapter 9. Here we present just a glimpse of the possibilities offered by magnetic damping. We shall consider the fluid

to be infinite in extent, or else bounded by an electrically insulating surface, S. For simplicity we neglect the viscous forces and take the imposed magnetic field to be uniform.

5.2.1 The destruction of mechanical energy via Joule dissipation

To some extent, the mechanism of magnetic damping is clear. Motion across magnetic field lines induces a current. This leads to Joule dissipation and the resulting rise in thermal energy is accompanied by a corresponding fall in kinetic energy. This is evident from (5.4) and (5.5), which give the rate of working of the Lorentz force as

$$(\mathbf{J} \times \mathbf{B}) \cdot \mathbf{u} = -\mathbf{J} \cdot (\mathbf{u} \times \mathbf{B}) = -(J^2/\sigma) - \nabla \cdot [V\mathbf{J}]$$

while the product of the inviscid equation of motion with $\mathbf{u}$ yields

$$\frac{D}{Dt}\left[\frac{1}{2}\rho \mathbf{u}^2\right] = (\mathbf{J} \times \mathbf{B}) \cdot \mathbf{u} - \nabla \cdot [p\mathbf{u}]$$

Combining the two furnishes the energy equation

$$\frac{d}{dt}\int \frac{1}{2}\rho \mathbf{u}^2 dV = -\frac{1}{\sigma}\int \mathbf{J}^2 dV \tag{5.7}$$

Thus, as anticipated, Joule dissipation leads to a fall in kinetic energy. However, there are other, more subtle effects associated with magnetic damping. Specifically, the action of a magnetic field is anisotropic. It opposes motion normal to the field lines but leaves motion parallel to $\mathbf{B}$ unopposed. Moreover, as we shall see, vorticity and linear momentum tend to propagate along the field lines by a pseudo-diffusion process. These anisotropic effects can be understood in terms of field sweeping and a Maxwell tension in the $\mathbf{B}$-lines, as discussed in Section 3.9.

For example, consider a jet which is directed at right angles to a uniform magnetic field. Motion across the field lines induces a second, weak, magnetic field. The combined field is then bowed slightly in the direction of $\mathbf{u}$ and the resulting curvature gives rise to a Lorentz force $B^2/\mu R$ which opposes the motion. The tension in the field lines then causes the disturbance to spread laterally along the $\mathbf{B}$-lines.

Now all of this is, to say the least, a little heuristic. However, a couple of simple examples will help establish the general ideas. We start with the jet shown in Figure 5.1.

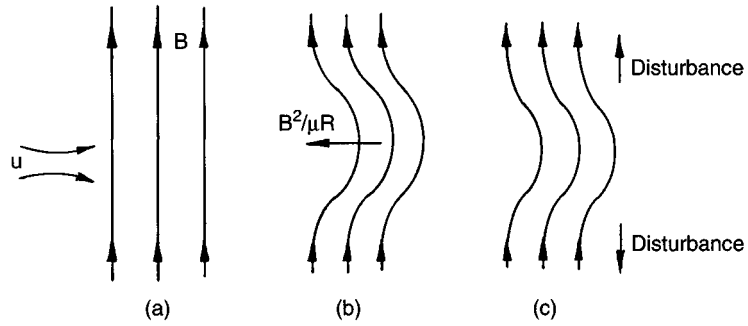

Figure 5.1 Motion across the field lines distorts those lines and the resulting curvature gives rise to a force $B^2/\mu R$ opposing the motion. The disturbance also propagates laterally along the magnetic field lines.

5.2.2 The damping of a two-dimensional jet

The Lorentz force per unit mass acting on the jet shown in Figure 5.1 is, from (5.4),

$$\mathbf{F} = (\mathbf{J} \times \mathbf{B})/\rho = -\mathbf{u}_\perp/\tau - \nabla V \times (\sigma \mathbf{B}/\rho) \tag{5.8}$$

Here $\mathbf{u}_\perp$ represents the velocity components normal to $\mathbf{B}$, and τ is the magnetic damping time, $\tau = (\sigma B^2/\rho)^{-1}$. Note the anisotropic nature of this force. Pressure forces and the effect of V apart, each fluid particle decelerates on a time scale of τ, according to

$$\frac{D\mathbf{u}_\perp}{Dt} \sim -\frac{\mathbf{u}_\perp}{\tau}, \qquad \frac{D\mathbf{u}_{//}}{Dt} \sim 0$$

It is as if each element of fluid which tries to cross a magnetic field line experiences a frictional drag. As a simple example, consider a thin, steady, two-dimensional jet, $\mathbf{u}(x, y) = (u_x, u_y, 0)$, directed along the x-axis and passing through a uniform field imposed in the y-direction. This geometry is particularly easy to handle since both the pressure p and potential V are zero (or constant), as we now show. The divergence of Ohm's law gives

$$\nabla^2 V = \nabla \cdot (\mathbf{u} \times \mathbf{B}) = \mathbf{B} \cdot \boldsymbol{\omega} = 0 \tag{5.9}$$

and so V is zero provided there is no electrostatic field imposed from the boundaries (we exclude such cases). The induced current, $\mathbf{J} = \sigma \mathbf{u} \times \mathbf{B}$, is then directed along the z-axis and the Lorentz force, $\mathbf{J} \times \mathbf{B} = -\sigma u_x B^2 \hat{\mathbf{e}}_x$, acts to retard the flow. Moreover, the fluid surrounding the jet is quiescent and so $\nabla p = 0$ outside the jet. Provided the jet is thin, in the sense that its characteristic thickness, δ, is much less than a characteristic axial

length scale, l, then ∇p is also negligible within the jet. (If the streamlines are virtually straight and parallel then there can be no significant pressure gradients normal to the streamlines.) In this simple example, then, both the pressure forces and $\nabla V \times \mathbf{B}$ are zero. It follows that

$$\mathbf{u} \cdot \nabla u_x = -u_x/\tau \tag{5.10}$$

Equation (5.10) is readily solved. We look for a similarity solution of the form $u_x = u_0(x)f(y/\delta(x))$, where u_0 is the velocity on the axis and $u_0\delta^2$ is constant. Then (5.10) applied to the axis gives $u_0'(x) = -1/\tau$. Next we find u_y using continuity, evaluate $\mathbf{u} \cdot \nabla u_x$, and substitute for this term in (5.10). This yields

$$f^2 - \frac{1}{2}f'(\eta)\int_0^\eta f d\eta = f, \qquad \eta = y/\delta$$

which has solution $f = \operatorname{sech}^2(\eta)$. Thus the velocity distribution in the jet is

$$u_x = [U - x/\tau]\sec h^2(y/\delta) \tag{5.11}$$

where $U = u_x(0, 0)$. The most striking feature of this solution is that the jet is annihilated within a finite distance $L = U\tau$. The situation is as shown below. Note that our solution ceases to be valid as we approach $x = U\tau$ since $\delta/l \sim \delta/U\tau \sim \delta(0)/(U\tau - x)$, which is not small for $x \sim U\tau$.

We shall return to the topic of MHD jets in Chapter 9, where we look at more complex flows. Interestingly, it turns out that Figure 5.2(a) is quite misleading when it comes to three-dimensional jets. In fact, a three-dimensional jet maintains its linear momentum and so cannot come to a halt. It has the shape shown in Figure 5.2(b).

5.2.3 Damping of a vortex

Let us now consider a second example, designed to bring out the tendency for vorticity to diffuse along the magnetic field lines. As before, we take $\mathbf{B}$ to be uniform. This time, however, we consider the initial velocity field to be an axisymmetric, swirling vortex, $\mathbf{u} = (0, \Gamma/r, 0)$ in (r, θ, z) coordinates. $\mathbf{B}$ is taken to be parallel to the z-axis. At $t = 0$ the angular momentum per unit mass, $\Gamma(r, z)$, is assumed to be confined to a sphere of size δ, as shown in Figure 5.3(a).

Now the axial gradients in Γ will, via the centrifugal force, tend to induce a poloidal component of motion, $\mathbf{u}_p = (u_r, 0, u_z)$. That is, if Γ is a function of z then the centripetal force, $(\Gamma^2/r^3)\hat{\mathbf{e}}_r$, is rotational and cannot

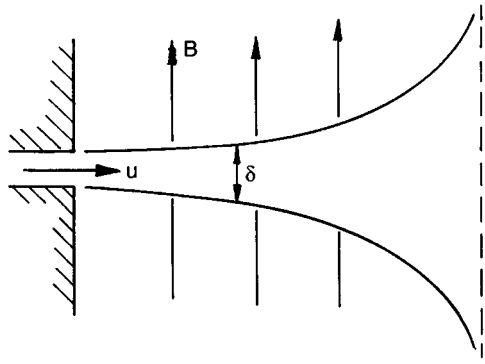

Figure 5.2 (a) A two-dimensional jet is destroyed by a magnetic field in a distance $U\tau$.

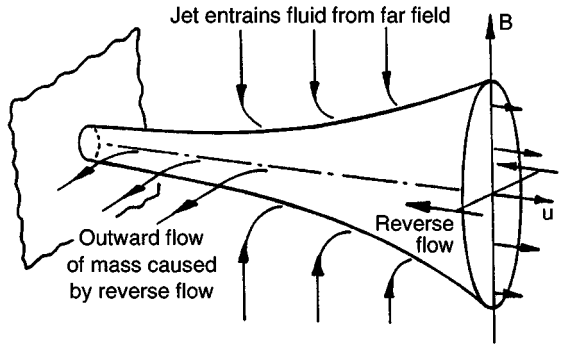

Figure 5.2 (b) A three-dimensional MHD jet.

be balanced by a radial pressure gradient. A secondary, poloidal motion then results which complicates the problem. However, in the interests of simplicity, we shall take $\mathbf{J} \times \mathbf{B} \gg \mathbf{u} \cdot \nabla \mathbf{u}$, which is equivalent to specifying that the magnetic damping time, τ, is much less than the inertial timescale δ/u_0. Since poloidal motion grows on a timescale of δ/u_θ, we may then neglect $\mathbf{u}_p$ for times of order τ.

Let us now determine the induced current, $\mathbf{J}$, and hence the Lorentz force which acts on the (initially) spherical vortex. The term $\mathbf{u} \times \mathbf{B}$ in Ohm's law gives rise to a radial component of current, J_r. However, the current lines must form closed paths and so an electrostatic potential, $V(r, z)$, is established, whose primary function is to ensure that the $\mathbf{J}$-lines close. The distribution of V is in accordance with the first part of (5.9). It

drives an axial component of current, thus allowing **J** to form closed current paths in the r–z plane, as shown in Figure 5.3(a). Since **J** is solenoidal, we can introduce a vector potential defined by

$$\mathbf{J} = \nabla \times [(\phi/r)\hat{\mathbf{e}}_\theta] = \left(-\frac{1}{r}\frac{\partial \phi}{\partial z}, 0, \frac{1}{r}\frac{\partial \phi}{\partial r}\right)$$

In the fluid mechanics literature ϕ would be called the Stokes streamfunction for **J**. For reasons which will become apparent shortly, it is convenient to take the curl of this,

$$\nabla \times \mathbf{J} = -\frac{1}{r}\left(\nabla_*^2 \phi\right)\hat{\mathbf{e}}_\theta$$

where ∇_*^2 is the Laplacian-like operator,

$$\nabla_*^2 \equiv \frac{\partial^2}{\partial z^2} + r\frac{\partial}{\partial r}\left(\frac{1}{r}\frac{\partial}{\partial r}\right)$$

However, Ohm's law (5.6b) gives us $\nabla \times \mathbf{J} = \sigma B \partial \mathbf{u}/\partial z$, and so

$$\nabla_*^2 \phi = -\sigma B \frac{\partial \Gamma}{\partial z} \tag{5.12}$$

We have managed to relate φ, and hence **J**, to the flow field. This allows us to evaluate the Lorentz force per unit mass, $\mathbf{F} = -(J_r B/\rho)\hat{\mathbf{e}}_\theta = F_\theta \hat{\mathbf{e}}_\theta$, in terms of Γ.

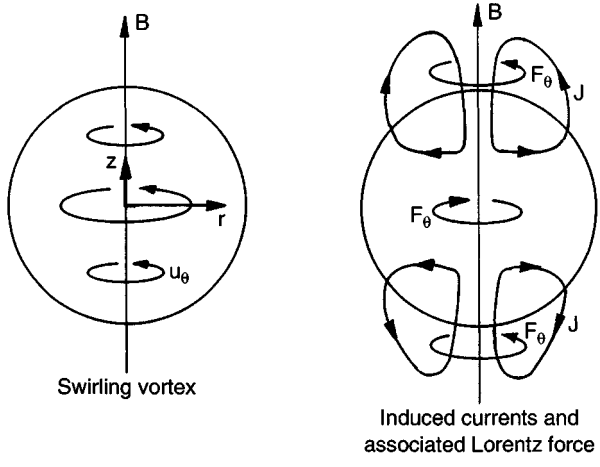

Figure 5.3 (a) An initially spherical vortex is damped by a magnetic field.

$$rF_\theta = \frac{B}{\rho}\frac{\partial \phi}{\partial z} = -\frac{1}{\tau}\frac{\partial^2}{\partial z^2}\left(\nabla_*^{-2}\Gamma\right)$$

Here the inverse operator $f = \nabla_*^{-2}(g)$ is simply a symbolic representation of $\nabla_*^2 f = g$. From Figure 5.3(a) we might anticipate that F_θ is negative in the core of the vortex, decelerating the fluid, and positive above and below the vortex, inducing motion in previously quiesant regions. This, in turn, suggests that Γ spreads along the magnetic field lines. We shall now confirm that this is indeed the case. The azimuthal equation of motion is

$$\frac{D\Gamma}{Dt} = rF_\theta$$

Note that, in the absence of the Lorentz force, angular momentum is materially conserved (i.e. preserved by each fluid particle), there being no azimuthal pressure gradient in an axisymmetric flow. Since we are neglecting the poloidal motion on a timescale of τ, our equation of motion becomes

$$\frac{\partial \Gamma}{\partial t} = \frac{B}{\rho}\frac{\partial \phi}{\partial z} = -\frac{1}{\tau}\frac{\partial^2}{\partial z^2}\left(\nabla_*^{-2}\Gamma\right) \tag{5.13}$$

The first thing to note from (5.13) is that the global angular momentum, H, of the vortex is conserved:

$$\frac{dH}{dt} = \frac{d}{dt}\int \Gamma dV = \frac{B}{\rho}\int \nabla \cdot [\phi \hat{\mathbf{e}}_z] dV = 0$$

Yet energy is continually dissipated in accordance with (5.7),

$$\frac{dE}{dt} = -\frac{1}{\rho\sigma}\int J^2 dV, \qquad E = \frac{1}{2}\int u^2 dV$$

How can the vortex preserve its angular momentum in the face of continual Joule dissipation? We shall see that the answer to this question holds the key to the evolution of the vortex. Let l_r and l_z be characteristic radial and axial length scales, respectively, for the vortex. At $t = 0$ we have $l_r = l_z = \delta$, and we shall suppose that l_r remains of order δ throughout the life of the vortex, there being no reason to suppose otherwise. (We shall confirm this shortly.) Then (5.6b), in the form $\nabla \times \mathbf{J} = \sigma \nabla \times (\mathbf{u} \times \mathbf{B}_0)$, allows us to estimate the magnitude of $\nabla \times \mathbf{J}$, and hence $\mathbf{J}$, from which

$$\frac{dE}{dt} \sim -\frac{1}{\tau}\left(\frac{\delta}{l_z}\right)^2 E, \qquad E \sim \Gamma^2 l_z \tag{5.14}$$

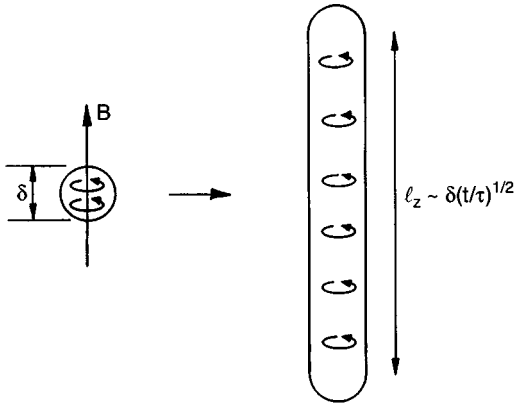

Figure 5.3 (b) Diffusion of angular momentum along the magnetic field lines causes an initially spherical vortex to elongate into a cigar-like shape.

However, we also have

$$H \sim \Gamma \delta^2 l_z = \text{constant} \tag{5.15}$$

It is evident that l_z must increase with time since otherwise E would decay exponentially on a timescale of τ, which contradicts (5.15). In fact the only way of satisfying both (5.14) and (5.15) is when Γ and l_z scale as

$$\Gamma \sim \Gamma_0 (t/\tau)^{-1/2}, \qquad l_z \sim \delta (t/\tau)^{1/2} \tag{5.16}$$

which, in turn, suggests that the kinetic energy of the vortex declines as $(t/\tau)^{-1/2}$. It seems that the vortex evolves from a sphere to an elongated cigar-like shape on a timescale of τ (Figure 5.3(b)). This is the first hint of the pseudo-diffusion process discussed earlier. In fact, we might have anticipated (5.16) from (5.13), written in the form

$$\frac{\partial \Gamma}{\partial t} = -\frac{1}{\tau} \frac{\partial^2}{\partial z^2} \left(\nabla_*^{-2} \Gamma \right) \sim \frac{\delta^2}{\tau} \frac{\partial^2 \Gamma}{\partial z^2} \tag{5.17}$$

suggesting diffusion along the magnetic field lines with a diffusivity of $\alpha_B \sim \delta^2/\tau$. (This argument may be made rigorous by taking Fourier transforms.) Recalling that the diffusion rate in a typical thermal problem is $l \sim \sqrt{\alpha t}$, we have $l_z \sim \delta (t/\tau)^{1/2}$, as in (5.16).

In the spirit of field sweeping and Maxwell tensions, we might picture this diffusion process as a spiralling up of the magnetic field lines, which then slowly unwind, propagating angular momentum along the z-axis. We shall return to this idea in Section 6.1, where we show that this

pseudo-diffusion is the last vestige of Alfvén wave propagation at low R_m. We shall also see, in Chapter 7, that $l_z \sim (t/\tau)^{1/2}$ and $K.E. \sim (t/\tau)^{-1/2}$ characterises MHD turbulence at low R_m, which is perhaps hardly surprising since turbulence just consists of an ensemble of vortices, rather like that shown in Figure 5.3(b).

An exercise for the enthusiastic or the sceptical

The estimates (5.16) may be confirmed by detailed analysis. The most direct method of solving (5.13) is to use Fourier transforms. In axisymmetric problems the three-dimensional Fourier transform reduces to the so-called cosine-Hankel transform, defined by the transform pair

$$F(u_\theta) = U(k_r, k_z) = 4\pi \int_0^\infty \int_0^\infty [u_\theta] J_1(k_r r) \cos(k_z z) r dr dz$$

$$F^{-1}(U) = u_\theta(r, z) = \frac{1}{2\pi^2} \int_0^\infty \int_0^\infty [U] J_1(k_r r) \cos(k_z z) k_r dk_r dk_z$$

This transform has the convenient properties

$$F\left(\partial^2 f/\partial z^2\right) = -k_z^2 F(f), \qquad F(\nabla_*^2 f) = -\left(k_r^2 + k_z^2\right) F(f) = -k^2 F(f)$$

and so the transform of (5.13) is

$$\frac{\partial U}{\partial t} = -\left[\cos^2 \alpha\right] \frac{U}{\tau}, \qquad \cos \alpha = k_z/k$$

Solving for U and performing the inverse transform yields

$$\Gamma = \frac{r}{2\pi^2} \int_0^\infty \int_0^\infty \left[U_0 \exp\left(-\cos^2 \alpha \ (t/\tau)\right)\right] J_1(k_r r) \cos(k_z z) k_r dk_r dk_z$$

where $U_0 = F(u_\theta)$ at $t = 0$. Confirm that for $t \gg \tau$ this integral takes the form

$$\Gamma = (t/\tau)^{-1/2} G(r, z/(t/\tau)^{1/2}) \tag{5.18}$$

where G is determined by the initial condition. Thus confirm that

$$\Gamma \sim (t/\tau)^{-1/2}, \qquad l_z \sim (t/\tau)^{1/2}$$

as suggested earlier on the basis of qualitative arguments. Evidently, the vortex distorts from a sphere to a column, growing axially at a rate $l_z \sim \delta(t/\tau)^{1/2}$. This axial elongation is essential to preserving the angular momentum of the vortex.

5.3 A Glimpse at MHD Turbulence

The last example in Section 5.2 suggests that a turbulent flow evolving in a magnetic field will behave very differently to conventional turbulence, and this is indeed the case. We examine this issue in detail in Chapter 7; here we just give a flavour of some of the underlying ideas. A classic problem in conventional turbulence theory is the so-called free decay of a turbulent flow, and it is worth considering this purely hydrodynamic problem first.

Suppose that the fluid in a large vessel is stirred vigorously and then left to itself. Suppose also that the eddies created by the stirring are randomly orientated and distributed throughout the vessel, so that the initial turbulence is statistically homogeneous and isotropic. Let the vessel have size L and a typical eddy have size l and velocity u. We take $\mathbf{B}$ to be zero and $L \gg l$ so that the boundaries have little influence on the bulk of the motion. The first thing which happens is that some of the eddies which are set up at $t = 0$ break up through inertially driven instabilities, creating a whole spectrum of eddy sizes, from l down to $l_{\min} \sim (ul/\nu)^{-3/4} l$, the latter length scale being the smallest eddy size which may exist in a turbulent flow without being eradicated by viscosity. (Eddies of size $l_{\min}$ are characterised by $\nu\nabla^2\mathbf{u} \sim \mathbf{u} \cdot \nabla\mathbf{u}$ – see Chapter 7.) There then follows a period of decay in which energy is extracted from the turbulence via the destruction of small-scale eddies by viscous stresses, kinetic energy being continually passed down from the large scales to the small scales through the break up of the larger eddies. This 'free decay' process is characterised by the facts that: (i) the turbulence remains approximately homogeneous and isotropic during the decay; (ii) the energy (per unit mass) declines according to Kolmogorov's decay law $E \sim E_0(u_0 t/l_0)^{-10/7}$, or something fairly close to this (u_0 and l_0 are the initial values of u and l). Again, the details are spelled out in Chapter 7.

Now suppose that we repeat this process but in the presence of a uniform magnetic field $\mathbf{B} = B\hat{\mathbf{e}}_z$. For simplicity, we take the fluid to be inviscid and to be housed in a large electrically insulated sphere of radius R, with $R \gg l$ (Figure 5.4(a)). From (5.6b) and (5.7) we have

$$\frac{dE}{dt} = -\frac{1}{\rho\sigma}\int J^2 dV, \qquad E = \frac{1}{2}\int u^2 dV \tag{5.19}$$

$$\nabla \times \mathbf{J} = \sigma B \frac{\partial \mathbf{u}}{\partial z}, \qquad \nabla \cdot \mathbf{J} = 0 \tag{5.20}$$

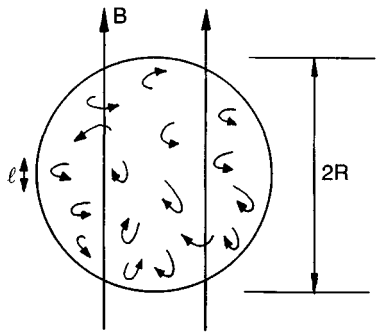

Figure 5.4 (a) Decaying turbulence in a magnetic field.

Clearly the kinetic energy of the flow falls monotonically, and this process ceases if, and only if, **u** is independent of z, i.e. $\mathbf{J} = 0$. However, one component of angular momentum is conserved during this decay. Formally, this may be seen by transforming the expression for the component of torque parallel to **B** as follows:

$$[\mathbf{x} \times (\mathbf{J} \times \mathbf{B})] \cdot \mathbf{B} = [(\mathbf{x} \cdot \mathbf{B})\mathbf{J} - (\mathbf{x} \cdot \mathbf{J})\mathbf{B}] \cdot \mathbf{B} = -(B^2/2)\nabla \cdot [x_\perp^2 \mathbf{J}] \quad (5.21)$$

This integrates to zero over the sphere (remember that $\mathbf{J} \cdot d\mathbf{S} = 0$). Thus the global Lorentz torque parallel to **B** is zero and so, since there are no viscous forces, one component of angular momentum,

$$\mathbf{H}_{//} = \int (\mathbf{x} \times \mathbf{u})_{//} dV$$

is conserved as the flow evolves. (We take the origin of coordinates to lie at the centre of the sphere and use // and $\perp$ to indicate components of a vector parallel and normal to **B**.) The physical interpretation of (5.21) is straightforward. The current density, **J**, may be considered to be composed of many current tubes, and each of these may, in turn, be considered to be the sum of many infinitesimal current loops, as in the proof of Stokes' theorem. However, the torque on each elementary current loop is $d\mathbf{m} \times \mathbf{B}$, where $d\mathbf{m}$ is its dipole moment, and this is perpendicular to **B**. Consequently, the global torque, which is the sum of many such terms, can have no component parallel to **B**. Conservation of $\mathbf{H}_{//}$ then follows.

As we shall see, this conservation law is fundamental to the evolution of a turbulent flow. In fact, we may show that, as in the last example of Section 5.2, the conservation of $\mathbf{H}_{//}$, combined with continual Joule dissipation, leads to an elongation of the eddies. Let us pursue this idea a little further. Since $\mathbf{H}_{//}$ is conserved, the energy of the flow cannot fall to

zero. Yet (5.20) tells us that **J** is non-zero, and the Joule dissipation finite, as long as **u** is a function of z. It follows that, eventually, the flow must settle down to a two-dimensional one, in which **u** exhibits no variation along the field lines. We may determine how quickly this happens as follows. Noting that the ith component of torque may be written as

$$2[\mathbf{x} \times (\mathbf{J} \times \mathbf{B})]_i = [(\mathbf{x} \times \mathbf{J}) \times \mathbf{B}]_i + \nabla \cdot [(\mathbf{x} \times (\mathbf{x} \times \mathbf{B}))_i \mathbf{J}] \tag{5.22}$$

we may rewrite the global Lorentz torque in terms of the dipole moment, **m**, of **J**,

$$\mathbf{T} = \int \mathbf{x} \times (\mathbf{J} \times \mathbf{B}) dV = \frac{1}{2} \left\{ \int \mathbf{x} \times \mathbf{J} dV \right\} \times \mathbf{B} = \mathbf{m} \times \mathbf{B}$$

Also, from Ohm's law (5.4), we have

$$(\mathbf{x} \times \mathbf{J}) = \sigma[\mathbf{x} \times (\mathbf{u} \times \mathbf{B}) + \nabla \times (\mathbf{x} V)]$$

(Here V now stands for the electrostatic potential rather than volume.) On integrating this expression over the spherical volume, the second term on the right converts to a surface integral which is zero since $\mathbf{x} \times d\mathbf{S} = 0$. The first contribution on the right may be rewritten (using a version of (5.22) in which **u** replaces **J**) as $\frac{1}{2}(\mathbf{x} \times \mathbf{u}) \times \mathbf{B}$ plus a divergence, which also integrates to zero. It follows that

$$\mathbf{m} = (\sigma/4)\mathbf{H} \times \mathbf{B}$$

and so the global Lorentz torque becomes

$$\mathbf{T} = -\frac{\sigma B^2}{4} \mathbf{H}_\perp$$

The global angular momentum equation

$$\rho \frac{\partial \mathbf{H}}{\partial t} = \mathbf{T} = -\frac{\sigma B^2}{4} \mathbf{H}_\perp$$

then yields

$$\mathbf{H}_{//} = \text{constant}, \qquad \mathbf{H}_\perp = \mathbf{H}_\perp(0) \exp(-t/4\tau) \tag{5.23a, b}$$

As expected, $\mathbf{H}_{//}$ is conserved while $\mathbf{H}_\perp$ decays exponentially on a time scale of τ. The simplicity of this inviscid result is surprising, partially because of its generality (the initial conditions may be quite random), and partially because the local momentum equation

$$\rho \left(\frac{\partial \mathbf{u}}{\partial t} + \mathbf{u} \cdot \nabla \mathbf{u} \right) = -\nabla p + \mathbf{J} \times \mathbf{B}$$

is quadratic in **u** and so possesses analytical solutions only for the most trivial of flows.

Equations (5.23a, b) are highly suggestive. The preferential destruction of $\mathbf{H}_\perp$ suggests that vortices whose axes are perpendicular to **B** are annihilated, leading to a quasi-two-dimensional flow. We may quantify this as follows. First we need the Schwartz integral inequality. In its simplest form this states that any two functions, f and g, satisfy the inequality

$$\left[\int fg dV\right]^2 \leq \int f^2 dV \int g^2 dV$$

The analogous results for arbitrary vector fields **A** and **B** are

$$\left[\int \mathbf{A} \cdot \mathbf{B} dV\right]^2 \leq \int \mathbf{A}^2 dV \int \mathbf{B}^2 dV$$

and

$$\left[\int \mathbf{A} \times \mathbf{B} dV\right]^2 \leq \int \mathbf{A}^2 dV \int \mathbf{B}^2 dV$$

In the present context, this yields

$$\mathbf{H}_{//}^2 \leq \int \mathbf{x}_\perp^2 dV \int \mathbf{u}_\perp^2 dV$$

which, in turn, furnishes a lower bound on the energy, E,

$$E \geq \mathbf{H}_{//}^2 \left[2 \int \mathbf{x}_\perp^2 dV\right]^{-1} \tag{5.24}$$

Thus, provided $\mathbf{H}_{//}$ is non-zero, the flow cannot come to rest. Yet (5.20) tells us that, as long as there is some variation of velocity along the **B**-lines, the Joule dissipation remains finite, and E falls. Consequently, whatever the initial condition, the flow must evolve to a steady state that is strictly two-dimensional, exhibiting no variation of **u** along the field lines. In short, the flow adopts the form of one or more columnar vortices, each aligned with the **B**-field (Figure 5.4(b)), all other components of angular momentum being destroyed on a time scale of 4τ. The simplicity of this result is surprising, particularly since it is valid for any value of $u\tau/l$, i.e. unlike the example in Section 5.2, this is valid for any ratio of $|\mathbf{J} \times \mathbf{B}|$ to inertia.

It appears, therefore, that magnetic fields tend to induce a strong anisotropy in a turbulent flow, stretching the eddies in the direction of **B**. Of course, any real fluid is viscous and so this stretching of vorticity will be

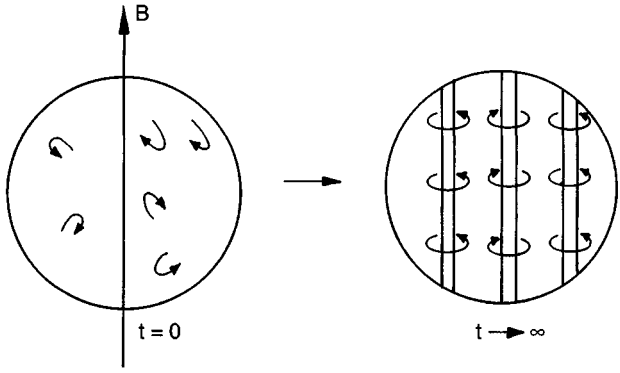

Figure 5.4 (b) MHD turbulences evolve to a two-dimensional state under the influence of pseudo-diffusion.

accompanied by viscous dissipation, just as in conventional turbulence. The eddies become elongated only if they survive for long enough. This, in turn, requires that $\mathbf{J} \times \mathbf{B}$ be at least of order $(\mathbf{u} \cdot \nabla)\mathbf{u}$ and so we would expect strong anisotropy in a real flow only if the interaction parameter $N = l/u\tau$ is greater than unity. We return to this topic in Chapter 7.

5.4 Natural Convection in the Presence of a Magnetic Field

As a final example of the dissipative effect of a static magnetic field we consider the influence of a uniform, imposed field on natural convection. We start with a description of natural convection in the absence of a magnetic field.

5.4.1 Rayleigh–Bénard convection

It is a common experience that a fluid pool heated from below exhibits natural convection. Hot, buoyant, fluid rises from the base of the pool. When this fluid reaches the surface it cools, and sinks back down to the base. Such a flow is characterised by the continual conversion of gravitational energy into kinetic energy, the potential energy being released as light fluid rises and heavy fluid falls. However, this motion is opposed by viscous dissipation, and if the heating is uniform across the base of the pool, and the viscosity high enough, no motion takes place. Rather, the fluid remains in a state of hydrostatic equilibrium and heat diffuses

upwards by conduction alone. The transition between the static, diffusive state and that of natural convection occurs at a critical value of

$$Ra = g\beta\Delta T d^3/\nu\alpha$$

called the Rayleigh number. Here ΔT is the imposed temperature difference between the top and the bottom of the pool, d the depth of the pool, β the expansion coefficient of the fluid (in units of K^{-1}) and α is the thermal diffusivity. The sudden transition from one state to another is called the Rayleigh–Bénard instability, in recognition of Bénard's experimental work in 1900 and the subsequent analytical investigation by Rayleigh in 1916. Rayleigh described Bénard's experiment thus:

> Bénard worked with very thin layers, only about 1 mm deep, standing on a levelled metallic plate which was maintained at a uniform temperature... The layer rapidly resolves itself into a number of 'cells', the motion being an ascension in the middle of a cell and a descension at the common boundary between a cell and its neighbours.

Inspired by these experiments, Rayleigh developed the theory of convective instability for a thin layer of fluid between horizontal planes. He found that the destabilising effect of buoyancy (heavy fluid sitting over light fluid) wins out over the stabilizing influence of viscosity only when Ra exceeds a critical value $(Ra)_c$. For fluid bounded by two solid planes the critical value is 1708, while an open pool with a free upper surface has $(Ra)_c = 1100$. In principle, one can also do the calculation where both the bottom and top surfaces are free (although the physical significance of such a geometry is unclear) and this yields $(Ra)_c = 658$.

Ironically, many years later, it was discovered that the motions observed by Bénard were driven, for the most part, by surface tension, and not by buoyancy. (This is because Bénard used very thin layers.) Nevertheless Rayleigh's analysis of convective instability remains valid. We now extend this analysis to incorporate the stabilising (dissipative) effect of a magnetic field.

5.4.2 The governing equations

When dealing with natural convection in a liquid it is conventional and convenient to use the Boussinesq approximation. In effect, this says that density variations are so small that we may continue to treat the fluid as incompressible and having uniform density, ρ, except to the extent that it introduces a buoyancy force per unit volume, $\delta\rho\mathbf{g}$, into the Navier–Stokes

equation. This buoyancy force is usually rewritten as $-\rho\beta T\mathbf{g}$, where β is the expansion coefficient, $-(\partial\rho/\partial T)/\rho$, and T is the temperature (relative to some datum). The governing equations in the presence of an imposed, vertical field, $\mathbf{B}_0$, are then

$$\frac{D\mathbf{u}}{Dt} = -\nabla\left(\frac{p}{\rho}\right) + \frac{1}{\rho}(\mathbf{J}\times\mathbf{B}_0) + \nu\nabla^2\mathbf{u} - \beta T\mathbf{g}$$

$$\nabla\cdot\mathbf{u} = 0, \qquad \mathbf{J} = \sigma(-\nabla V + \mathbf{u}\times\mathbf{B}_0)$$

$$\frac{DT}{Dt} = \alpha\nabla^2 T$$

Here we have ignored the internal heating due to viscous and Joule dissipation by comparison with the heat transfer from the lower boundary. The stationary configuration whose stability is in question is

$$\mathbf{u}_0 = 0, \qquad T_0 = \Delta T(1 - z/d), \qquad \mathbf{J}_0 = 0$$

Here we take z to point vertically upward, the top and bottom surfaces to lie at $z = 0$ and d, and ΔT is the imposed temperature difference $T(z = 0) - T(z = d)$. Now the formal method of determining the stability of such a base state is straightforward. One looks for slightly perturbed solutions of the form $T = T_0 + \delta T$, $\mathbf{u} = \mathbf{u}_0 + \delta\mathbf{u}$ and $\mathbf{J} = \mathbf{J}_0 + \delta\mathbf{J} = \delta\mathbf{J}$, substitute these into the governing equations, discard terms which are quadratic in the disturbance, and look for separable solutions of the linearised equations in the form $\mathbf{u} = \hat{\mathbf{u}}(\mathbf{x})\exp(jst)$. If all goes well, this results in an eigenvalue problem, the eigenvalues of which determine the growth (or decay) rate of some initial disturbance. This process is long and tedious, resulting in an eighth-order differential system, and we do not intend to do it. Rather, we shall give an heuristic description of the instability which captures the key physics of the process and yields a surprisingly accurate estimate of $(Ra)_c$.

5.4.3 An energy analysis of the Rayleigh–Bénard instability

If we take the product of the Navier–Stokes equation with $\mathbf{u}$, we obtain

$$\frac{\partial}{\partial t}\left(\frac{u^2}{2}\right) = -\nabla\cdot\left[\left(\frac{p}{\rho} + \frac{u^2}{2}\right)\mathbf{u}\right] + \frac{1}{\rho}(\mathbf{J}\times\mathbf{B}_0)\cdot\mathbf{u} - \nu(\mathbf{u}\cdot(\nabla\times\omega)) + g\beta T u_z$$

The rate of working of the Lorentz, viscous and buoyancy forces may be rewritten as

$$\frac{1}{\rho}(\mathbf{J} \times \mathbf{B}_0) \cdot \mathbf{u} = -\frac{1}{\rho}(\mathbf{u} \times \mathbf{B}_0) \cdot \mathbf{J} = -\frac{J^2}{\sigma\rho} - \nabla \cdot (V\mathbf{J}/\rho)$$

$$-\nu[\mathbf{u} \cdot (\nabla \times \boldsymbol{\omega})] = -\nu\lfloor\omega^2 + \nabla \cdot (\boldsymbol{\omega} \times \mathbf{u})\rfloor$$

$$g\beta(Tu_z) = g\beta(\delta Tu_z + \Delta T(1 - z/d)u_z)$$

$$= g\beta\lfloor\delta Tu_z + \nabla \cdot \left((z - z^2/2d)\Delta T\mathbf{u}\right)\rfloor$$

where δT is the (small) departure of T from the static, linear distribution. We now gather all the divergence terms together and rewrite our energy equation as

$$\frac{\partial}{\partial t}\left(\frac{u^2}{2}\right) = \nabla \cdot (*) - \frac{J^2}{\sigma\rho} - \nu\omega^2 + g\beta u_z \delta T$$

Now the divergence term vanishes when this equation is integrated over the entire pool (or a single convection cell) and we obtain

$$\frac{d}{dt}\int\left(\frac{u^2}{2}\right)dV = -\frac{1}{\rho\sigma}\int J^2 dV - \nu\int\omega^2 dV + g\beta\int u_z \delta T dV$$

The dissipative rôles of the viscous and Lorentz forces are now apparent, as is the source of potential energy, $g\beta\delta Tu_z$. We would expect that the equilibrium is unstable wherever the fluid can arrange for

$$g\beta\int u_z \delta T dV \geq \frac{1}{\rho\sigma}\int J^2 dV + \nu\int\omega^2 dV$$

with marginal stability corresponding to the equality sign. Let us now try to estimate the various integrals above. Suppose that the convection cells are two-dimensional, taking the form of rolls, with $\mathbf{u}$ confined to the x–z plane. We might approximate the shape of these by the streamfunction $\psi(\mathbf{x}, t) = \hat{\psi}(t)\sin(\pi z/d)\sin(\pi x/l)$, where $2l$ is the wavelength of the instability. Also, we suppose the onset of the instability to be non-oscillatory, so that $s = 0$ at $Ra = (Ra)_c$. (All of the experimental and analytical evidence suggests that this is the case, except perhaps in certain hot plasmas in which $\nu > \lambda$.) Since the electrostatic potential, V, is zero for two-dimensional flow, (5.4) gives, for one cell,

$$\frac{1}{\rho\sigma}\int J^2 dV = \left(\frac{\sigma B_0^2}{\rho}\right)\int u_x^2 dV = \left(\frac{\sigma B_0^2}{\rho}\right)\left(\frac{\pi}{2d}\right)^2 \hat{\psi}^2 ld$$

The viscous dissipation, on the other hand, takes the form

$$\nu \int \omega^2 dV = (\nu/4)\left[(\pi/l)^2 + (\pi/d)^2\right]^2 \hat{\psi}^2 ld$$

Finally, the buoyancy integral can be estimated with the aid of $(\mathbf{u} \cdot \nabla)T_0 = \alpha \nabla^2(\delta T)$, which yields

$$\delta T = \alpha^{-1}\nabla^{-2}(\mathbf{u} \cdot \nabla T_0) = \alpha^{-1}\left[(\pi/l)^2 + (\pi/d)^2\right]^{-1} u_z(\Delta T/d)$$

where $f = \nabla^{-2}g$ is a symbolic representation of $g = \nabla^2 f$. This gives the estimate

$$g\beta \int \delta T u_z dV = g\beta\alpha^{-1}\left[(\pi/l)^2 + (\pi/d)^2\right]^{-1}(\Delta T/d)(\pi/2l)^2 \hat{\psi}^2 ld$$

Thus the transition to instability occurs when

$$\underbrace{\left[\frac{g\beta\Delta T d^3}{\alpha}\right]\frac{(\pi/l)^2}{\left[(\pi/l)^2 + (\pi/d)^2\right]}}_{\text{(driving force)}} = \underbrace{\pi^2\left[\frac{\sigma B_0^2 d^2}{\rho}\right]}_{\text{(Joule dissipation)}} + \underbrace{\nu\left[\pi^2 + \left(\frac{\pi d}{l}\right)^2\right]^2}_{\text{(viscous dissipation)}}$$

Introducing the cell aspect ratio, $a = (\pi d/l)$, this simplifies to

$$(Ra)_c = a^{-2}(a^2 + \pi^2)\left\{(\pi^2 + a^2)^2 + \pi^2(Ha)^2\right\}$$

where $Ha = (\sigma B_0^2 d^2/\rho\nu)^{1/2}$ is the Hartmann number introduced in Chapter 3. It remains to estimate a. We now suppose that the cell shape is chosen so as to maximise the rate of working of the buoyancy force and minimise the dissipation. That is to say, we choose l/d such that $(Ra)_c$ is a minimum. This yields

$$(2a^2 - \pi^2)(a^2 + \pi^2)^2 = \pi^4(Ha)^2$$

from which we find

$$Ha \to 0: \qquad a = 2.22, \qquad (Ra)_c = 675$$

$$Ha \to \infty: \qquad a = (\pi^4/2)^{1/6}(Ha)^{1/3}, \qquad (Ra)_c = \pi^2(Ha)^2$$

Note that, for $Ha = 0$, the convection rolls are predicted to have an aspect ratio d/l of the order of unity, while the cells are narrow and deep at high Ha. We have made many assumptions in deriving these criteria, and so we must now turn to the exact analysis to see how our guesses have faired. Fortuitously it turns out that our estimate of $(Ra)_c$ at large Ha is exactly correct! Our estimate of $(Ra)_c = 675$ at $Ha = 0$ is less good though. Depending on the boundary conditions at $z = 0$ and d, an

exact analysis gives $(Ra)_c = 658$ (two free surfaces), 1100 (one free, one solid) and 1708 (two solid surfaces). Still, our energy analysis seems to have caught the essence of the process, and it is satisfying that its predictions are exact at high Ha. (The errors at low Ha are due to the assumed distribution of ψ.) It would seem that the cell size automatically adjusts to give the best possibility of an instability, minimising dissipation while maximising the rate of working of the buoyancy flow.

5.4.4 Natural convection in other configurations

The Rayleigh–Bénard configuration represents a singular geometry in the sense that it admits a static solution of the governing equations (uniform conduction, $\mathbf{u} = 0$). Convection appears only because this solution is unstable at high values of ΔT or low values of ν. In most geometries (for example a heated plate whose flat faces are vertical) motion develops irrespective of the size of ν and ΔT. There is no static solution of the governing equations. In such cases the smallest temperature difference will drive motion. The influence of an imposed magnetic field is then different. It does not delay the onset of convection, as in the Rayleigh–Bénard geometry, but rather moderates the motion which inevitably occurs.

Consider the case of a vertical plate held at a temperature ΔT above the ambient fluid temperature. Here the motion is confined to a thermal boundary layer, δ, which grows from the base of the plate as the fluid passes upwards. When there is no imposed field we can estimate u and δ from the equations

$$u(\partial u/\partial z) \sim g\beta\Delta T \qquad \text{(vertical equation of motion)}$$

$$u(\partial T/\partial z) \sim \alpha T/\delta^2 \qquad \text{(heat balance)}$$

This yields

$$u \sim (g\beta\Delta T z)^{1/2}$$

$$\delta \sim (g\beta\Delta T/\alpha^2)^{-1/4} z^{1/4}$$

where z is measured from the base of the plate. (Actually, these estimates are accurate only for low Prandtl number fluids, $\nu/\alpha \ll 1$, such as liquid metals. When the Prandtl number is of order unity, or greater, the viscous term $\nu u/\delta^2$ must be included in the vertical force balance, leading to a modification in the estimate of δ. However, we shall stay with liquid metals for the moment.) Let us see how magnetic damping alters the

situation. The imposition of a horizontal magnetic field, B, modifies the first of these equations to

$$u(\partial u/\partial z) \sim g\beta\Delta T - u/\tau, \qquad \tau^{-1} = \sigma B^2/\rho$$

Evidently, the fluid ceases to accelerate when u reaches a value of u^* given by

$$u^* \sim (g\beta\Delta T)\tau$$

For a plate of length l, the ratio of $u_{\max}$ with and without a magnetic field is therefore

$$\frac{u^*}{u} \sim \frac{(g\beta\Delta Tl)^{1/2}}{\sigma B^2 l/\rho} \sim \frac{(Ra)^{1/2}(\alpha/\nu)^{1/2}}{Ha^2}$$

so that the damping effect goes as $\sim B^2$. (The expression above assumes τ is small enough, or l large enough, for u to saturate before it leaves the plate.) For efficient damping, therefore, we require

$$Ha^2 \geq (Ra)^{1/2}(\alpha/\nu)^{1/2}$$

The use of magnetic fields to curtail unwanted natural convection is quite common. For example, in the casting of aluminium, the natural convection currents in a partially solidified ingot are significant (a few cm/s), and are thought to be detrimental to the ingot structure, causing a non-uniformity of the alloying elements through the transport of crystal fragments. Static magnetic fields have been used to minimise this natural convection. In the laboratory, on the other hand, the standard method of measuring the thermal diffusivity of liquid metals relies on injecting heat into the metal and measuring the rate of spread of heat by conduction. However, natural convection disrupts this procedure, and since it is difficult to design an apparatus free from convection, magnetic damping is employed to minimise the flow. Convection in a magnetic field is also important in geophysics and astrophysics. The terrestrial magnetic field is maintained by motion in the liquid core of the earth and this is driven, in part, by solutal and thermal convection. However, this convection is damped by the terrestrial field (see Chapter 6). Finally, in the outer layers of the sun, heat is transferred from the interior to the surface by natural convection, and in the case of sunspots this happens in the presence of a significant magnetic field. There are many other applications of magnetoconvection and it is not surprising, therefore, that this subject is receiving much attention at the present time.

Part 2: Generation of Motion

5.5 Rotating Fields and Swirling Motions

5.5.1 Stirring of a long column of metal

Let us now consider a problem which frequently arises in engineering. This illustrates the capacity for magnetic fields to induce motion as well as suppress it. Suppose that fluid is held in a long cylinder of radius R and that a uniform magnetic field rotates about the cylinder with angular velocity Ω as shown in Figure 5.5. In effect, we have a simple induction motor, with the fluid playing the rôle of rotor. The rotating magnetic field therefore induces an azimuthal velocity, $u_\theta(r)$, in the fluid, stirring the contents of the cylinder.

The use of magnetic stirring is very common in the continuous casting of steel. Here, alloying elements tend to segregate out of the host metal during solidification, giving rise to inhomogeneity in the final ingot. Moreover, small cavities can form in the ingot either because of trapped gas or because of the shrinkage of the metal during freezing. All of these defects can be alleviated by stirring the liquid pool.

We now try to estimate the magnitude of the induced velocity. Let us start by evaluating the Lorentz force. For simplicity, we suppose that the field rotation rate is low (in the sense that $\Omega R \ll \lambda/R$). Next we change frames of reference so that the field is stationary. The fluid then appears to rotate in a clockwise direction at a rate $\hat{u} = (\Omega r - u_\theta)$. We now satisfy the low-R_m conditions of Section 5.1 and so

$$\mathbf{J} = \sigma(-\nabla V + \hat{\mathbf{u}} \times \mathbf{B}), \qquad \mathbf{F} = \mathbf{J} \times \mathbf{B} \tag{5.25a, b}$$

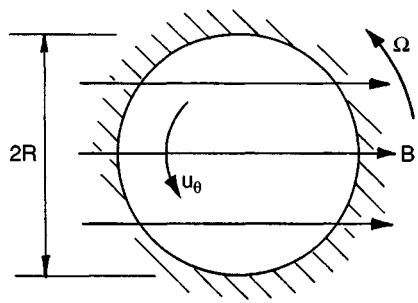

Figure 5.5 Magnetic stirring using a rotating magnetic field.

Now the divergence of (5.25a) gives us $\nabla^2 V = 0$, and so we may take $V = 0$ provided that no electrostatic field is applied at the boundaries. It follows that

$$\mathbf{F} = \mathbf{J} \times \mathbf{B} = \sigma(\hat{\mathbf{u}} \times \mathbf{B}) \times \mathbf{B} = -\sigma B^2 \hat{\mathbf{u}}_\perp \tag{5.26}$$

In (r, θ) coordinates this becomes

$$\mathbf{F} = \sigma B^2(\Omega r - u_\theta)\cos\theta(\sin\theta, \cos\theta)$$

which may be conveniently split into two parts:

$$\mathbf{F} = \frac{1}{2}\sigma B^2(\Omega r - u_\theta)\hat{\mathbf{e}}_\theta + \frac{1}{4}\sigma B^2(\Omega - u_\theta/r)\nabla(r^2 \sin 2\theta) \tag{5.27}$$

Now, although we have assumed that $\Omega R \ll \lambda/R$ (i.e. $\mu\sigma\Omega R^2 \ll 1$), it may be shown that expression (5.27) is a good approximation up to values of $\mu\sigma\Omega R^2 \sim 1$, with a maximum error of $\sim$4%. (There is some hint of this in Figure 4.6, which shows very little field distortion at $R_m = 1$.) It turns out that this is useful since most engineering applications are characterised by the double inequality

$$u_\theta \ll \Omega R \leq \lambda/R$$

and so, for most practical purposes, we may take

$$\mathbf{F} = \frac{1}{2}\sigma B^2 \Omega r \hat{\mathbf{e}}_\theta + \nabla\phi, \qquad \phi = \frac{1}{4}\sigma B^2 \Omega r^2 \sin 2\theta$$

The second term may now be dropped since ϕ simply augments the pressure distribution in the fluid and plays no rôle in the dynamics of the flow. Finally we end up with

$$\mathbf{F} = \frac{1}{2}\sigma B^2 \Omega r \hat{\mathbf{e}}_\theta$$

We now consider the equations of motion for the fluid. The radial component of the Navier–Stokes equation simply expresses the balance between $\partial p/\partial r$ and the centripetal acceleration. The azimuthal component gives, in the steady state,

$$\tau_{r\theta} r^2 = -\int_0^r r^2 F_\theta dr$$

This represents the torque balance on a cylinder of radius r (Figure 5.6). Substituting for $\tau_{r\theta}$ using Newton's law of viscosity yields

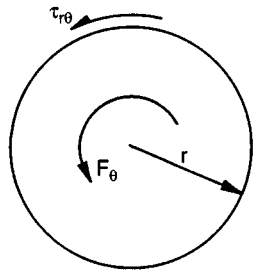

Figure 5.6 Torque balance between the Lorentz force and viscous stresses

$$\tau_{r\theta} = \rho\nu r \frac{d}{dr}\left(\frac{u_\theta}{r}\right) = -\frac{1}{8}\sigma B^2 \Omega r^2 \tag{5.28}$$

which may be integrated to give

$$u_\theta / r = \frac{\sigma B^2 \Omega}{16\rho\nu}\left(R^2 - r^2\right) \tag{5.29}$$

Unfortunately (5.29) is of little practical value since very few flows of this type are laminar. The viscosity, ν, of most liquid metals is similar to that of water, and so the Reynolds' number in practical applications is invariably high, implying a turbulent motion. In such cases we must return to (5.28) and replace the laminar shear stress by the turbulent *Reynolds stress* which appears in the time-averaged equations of motion for a turbulent flow (see Section 3.6). This gives

$$\tau_{r\theta} = -\overline{\rho v_r v_\theta} = -\frac{1}{8}\sigma B^2 \Omega r^2 \tag{5.30}$$

where v represents the fluctuating component of velocity and the overbar denotes a time average. We now need some means of estimating the Reynolds stress. As noted in Section 3.6, a commonly used, although ultimately empirical, model for turbulent shear flows is Prandtl's *mixing length* model. The essence of this model is that we approximate the Reynolds' stress in a planar flow adjacent to a wall by

$$\tau_{xy} = \rho l_m^2 \left|\frac{\partial \bar{u}_x}{\partial y}\right| \frac{\partial \bar{u}_x}{\partial y}, \qquad l_m = \kappa y$$

where $\bar{u}_x$ is the time-averaged velocity, l_m is called the mixing length, and y is the distance from the wall. The empirical constant κ is usually taken to be 0.4. The rotational equivalent of this is,

$$\tau_{r\theta} = \rho l_m^2 r^2 \left|\frac{\partial}{\partial r}\left(\frac{\bar{u}_\theta}{r}\right)\right| \frac{\partial}{\partial r}\left(\frac{\bar{u}_\theta}{r}\right), \qquad l_m = \kappa(R - r)$$

Substituting into (5.30) and integrating yields (see example 5.4)

$$(\bar{u}_\theta/r)_{r=0} = \Omega_f \left\{ \frac{1}{2\sqrt{2}\kappa} \ln\left(\frac{\Omega_f R^2}{\nu}\right) + 1.0 \right\} \tag{5.31}$$

where $\Omega_f^2 = \sigma\Omega B^2/\rho$. Note that in a turbulent flow u_θ scales linearly with B (with a logarithmic correction), whereas in a laminar flow u_θ scales as B^2.

Equation (5.31) gives values of $\bar{u}_\theta$ which compare favourably with estimates obtained using more complicated turbulence models. However, its main limitation is the fact that few engineering applications are strictly one-dimensional. The problem is immediately obvious if we refer back to Figure 3.31 showing spin-down of a stirred cup of tea. In a confined domain, rotation invariably induces a secondary flow via Ekman pumping. The inertial forces in the bulk of the fluid are then no longer zero and, in fact, at high values of Re, these forces greatly exceed the shear stresses, even the Reynolds stress. However, (5.31) is based entirely on a balance between $\mathbf{J} \times \mathbf{B}$ and shear, the inertia associated with secondary flow being ignored. Evidently, such a balance is rarely satisfied in practice, and so estimate (5.31) must be regarded with caution.

We shall examine the practical consequences of Ekman pumping in some detail in Chapter 8, where we shall see that (5.31) is often quite misleading. In the meantime, we can gain some hint as to the difficulties involved by considering a second, related example.

5.5.2 Swirling flow induced between two parallel plates

We can gain some insight into the rôle of Ekman pumping by considering a second model problem. This is the MHD analogue of the classical flow shown in Figure 3.32. Suppose we have two infinite, parallel disks located at $z = 0$ and $z = 2w$, and that the gap is filled with liquid metal. The body force $F_\theta = \frac{1}{2}\sigma\Omega B^2 r$ is applied to the fluid inducing a steady, laminar swirling flow. We choose F_θ so that Re is high and look for a steady solution of the Karman type:

$$u_r = \Omega_c r F(z/l)$$
$$u_\theta = \Omega_c r G(z/l)$$
$$u_z = \Omega_c l H(z/l)$$
$$p = \frac{1}{2}\rho\Omega_c^2 r^2 + \rho\Omega_c^2 l^2 P(z/l)$$

Here l is some characteristic length scale, yet to be determined, and Ω_c is a characteristic rotation rate in the core of the flow. We might anticipate that the flow divides into thin Bodewadt layers on the disk surfaces between which lies an inviscid core (Figure 8.4). In fact, this is precisely what happens, as we now show.

Consider the lower half of the flow $0 \leq z \leq w$. Away from the disc we take $l = l_c = w$ (the subscript on l denotes the core flow). In the boundary layer, on the other hand, we try the scaling $l = l_b = (\nu/\Omega_c)^{1/2}$, which is Bodewadt boundary layer scaling. The ratio of these length scales is a sort of inverse Reynolds number,

$$\varepsilon = (\nu/\Omega_c w^2)^{1/2} = l_b/l_c$$

We shall take ε to be vanishingly small and try to match the velocity profiles in the two regions using the method of *matched asymptotic expansions*. Substituting our proposed velocity functions in the Navier–Stokes and continuity equations yields, for both the core and the boundary layer,

$$F^2 + HF' - G^2 + 1 = (\nu/\Omega_c l^2)F'' \qquad \text{(radial equation)}$$

$$2FG + G'H = (\nu/\Omega_c l^2)G'' + \frac{1}{2}\Omega_f^2/\Omega_c^2 \qquad (\theta \text{ equation})$$

$$H' + 2F = 0 \qquad \text{(continuity)}$$

where the prime represents differentiation with respect to z/l and, as before, Ω_f is defined by $\Omega_f^2 = \sigma\Omega B^2/\rho$. In the core of the flow, where $l = l_c = w$, these equations yield (for $\varepsilon \to 0$)

$$F_c^2 + H_c F_c' - G_c^2 = -1$$

$$2F_c G_c + G_c' H_c = \frac{1}{2}\Omega_f^2/\Omega_c^2$$

$$H_c' + 2F_c = 0$$

where again the prime represents differentiation with respect to z/l_c. The boundary conditions for F_c, G_c and H_c arise from the fact that the flow must be symmetric about $z = w$ and that u_z in the core and boundary layer must match at the interface in the sense that

$$\lim_{z/l_c \to 0}[u_z] = \lim_{z/l_b \to \infty}[u_z]$$

This gives

$z/l_c = 1$: $H_c = 0,\ F_c' = 0,\ G_c' = 0$ (symmetry)

$z/l_c \to 0$: $l_c H_c = l_b H_b(\infty)$, or $H_c = \varepsilon H_b(\infty)$ (matching condition)

$z/l_c \to 0$: $G_c = 1$ (definition of Ω_c)

Here $H_b(\infty)$ is the value of H furnished by the boundary-layer solution, while the condition $G_c = 1$ effectively defines Ω_c. Formally

$$H_b(\infty) = \lim_{z/l_b \to \infty} H_b(z/l_b)$$

We now expand F_c, G_c and H_c in polynomials of ε and substitute these into the governing core equations. To leading order in ε we find

$$F_c = \frac{1}{2}\varepsilon H_b(\infty)$$

$$G_c = 1$$

$$H_c = \varepsilon H_b(\infty)[1 - z/w]$$

So the core velocity distribution is

$$\mathbf{u}_c = \left(\frac{1}{2}\varepsilon H_b(\infty)\Omega_c r,\ \Omega_c r,\ \varepsilon H_b(\infty)\Omega_c[w - z]\right)$$

Note that we have rigid-body rotation in the core and that u_r and u_z are of order $\sim \varepsilon u_\theta$. It appears that, for small ε, the core velocity is determined by only three parameters: ε, Ω_c and $H_b(\infty)$. The second of these, Ω_c, is fixed by the azimuthal component of the core equation of motion, which may be rearranged to give

$$\Omega_c = \Omega_f\left[\Omega_f w^2/\nu\right]^{1/3}[2H_b(\infty)]^{-2/3}$$

It now remains to find $H_b(\infty)$, and this is furnished by the boundary-layer equations. Immediately adjacent to the disk, the azimuthal equation of motion becomes

$$2F_b G_b + G_b' H_b = G_b'' + \frac{1}{2}\Omega_f^2/\Omega_c^2$$

where the prime now represents differentiation with respect to z/l_b. However, we have already shown that the last term on the right of this equation is of order ε. Consequently, magnetic forcing is negligible in the boundary layer (by comparison with viscous and inertial forces) and the equations locally reduce to those for a conventional Bodewadt layer, for which $H_b(\infty) = 1.349$. It follows that the core rotation rate is

$$\Omega_c = 0.516\Omega_f\left[\Omega_f w^2/\nu\right]^{1/3}$$

Compare this with our one-dimensional equation for swirl-only flow,

$$\frac{u_\theta}{r} = \frac{\Omega_f}{16}\left[\frac{\Omega_f R^2}{\nu}\right]\left[1 - \left(\frac{r}{R}\right)^2\right]$$

The dependence of u_θ on B is entirely different in the two cases, reflecting the different force balances. In the swirl-only flow, $\mathbf{J} \times \mathbf{B}$ is balanced by shear. In this second problem the primary balance in the core of the flow is between $\mathbf{J} \times \mathbf{B}$ and Coriolis forces. (This may be confirmed by tracing the origin of the terms in the azimuthal equation of motion.)

So this simple swirling flow is more complex than you might think! There are subtle and unexpected effects introduced by Ekman pumping. We shall return to this issue in Chapter 8, where we show that the balance between $\mathbf{J} \times \mathbf{B}$ and Coriolis forces is, in fact, typical of most flows encountered in practice.

5.6 Motion Driven by Current Injection

There is a second way of driving motion in a conducting fluid. So far we have considered only currents which are induced in the fluid by rotation of the magnetic field. However, we can also inject current directly into a fluid, and the resulting Lorentz force will, in general, produce motion. The simplest example of this is the electromagnetic pump, which was described in Chapter 1. Such a device consists of a duct in which mutually perpendicular magnetic and electric fields are arranged normal to the axis of the duct. The resulting Lorentz force, $\mathbf{J} \times \mathbf{B}$, is directed along the axis of the duct and this can be used to pump a conducting fluid. For example, sodium coolant is pumped around fast breeder nuclear reactors by this method. It turns out, however, that an understanding of this flow comes down to a careful consideration of the boundary layers, and so we shall postpone any discussion of this problem until the next section. Here we consider a configuration related to electric welding. The discussion is brief, but we shall return to this problem in Chapter 10.

5.6.1 A model problem

A useful model problem is the following. Suppose we have a liquid-metal pool which is hemispherical in shape, of radius R. The boundaries are

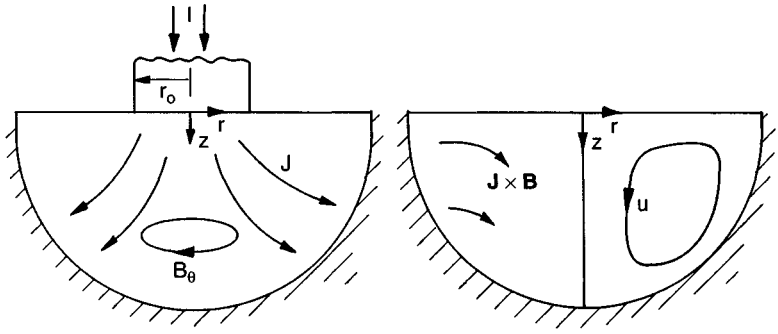

Figure 5.7 Geometry of the model problem.

assumed to be conducting and a current, I, is introduced into the pool by an electrode of radius r_0, which touches the surface. The entire geometry is axisymmetric and we use cylindrical polar coordinates (r, θ, z) with the origin at the pool's surface, as shown in Figure 5.7. The poloidal current gives rise to an azimuthal field, B_θ, and the two are related by Ampère's law, according to which

$$2\pi r B_\theta = \mu \int_0^r (2\pi r J_z) dr$$

The interaction of $\mathbf{J}$ with B_θ gives rise to a Lorentz force, and it is readily confirmed that

$$\mathbf{F} = \mathbf{J} \times \mathbf{B}/\rho = -\nabla(B_\theta^2/2\rho\mu) - \lfloor B_\theta^2/(\rho\mu r) \rfloor \hat{\mathbf{e}}_r$$

Of course, the magnetic pressure merely augments the fluid pressure and does not influence the motion in the pool. We therefore write

$$\mathbf{F} = -\frac{B_\theta^2}{\rho\mu r}\hat{\mathbf{e}}_r$$

on the understanding that p is augmented by $B_\theta^2/(2\mu)$. Clearly, this Lorentz force will drive a recirculating flow which converges at the surface (where B_θ is largest) and diverges near the base of the pool. The question is: can we estimate the magnitude of the induced flow?

5.6.2 A useful energy equation

We now describe a useful trick which we shall employ repeatedly in the subsequent chapters. Whenever we wish to estimate the recirculating flow

induced by a prescribed Lorentz force, it is useful to integrate the Navier–Stokes equation

$$\frac{\partial \mathbf{u}}{\partial t} = \mathbf{u} \times \boldsymbol{\omega} - \nabla\left[\frac{p}{\rho} + \frac{u^2}{2}\right] + \nu\nabla^2\mathbf{u} + \mathbf{F}$$

once around a closed streamline, C. In the steady state this yields

$$\oint_C \mathbf{F} \cdot d\mathbf{l} = -\nu \oint_C \nabla^2\mathbf{u} \cdot d\mathbf{l}$$

since $(\mathbf{u} \times \boldsymbol{\omega}) \cdot d\mathbf{l} = 0$ and the gradient of Bernoulli's function integrates to zero. Evidently there must be a global balance between the Lorentz force and the shear stresses. Physically, this arises because the work done by $\mathbf{F}$ on a fluid particle as it passes once around the streamline must be balanced by the (dissipative) work performed by the shear stresses acting on the same particle. If the two did not match, then the kinetic energy of the fluid particle would not be the same at the beginning and end of the integration, which is clearly not the case in a steady flow. We may use this integral equation to estimate $|\mathbf{u}|$.

Let us see where this leads in our model problem. We take C to be the bounding streamline, comprising the surface, the axis and the curved boundary. Starting with the left-hand integral we have

$$\oint \mathbf{F} \cdot d\mathbf{l} = \left[\int_0^R (B_\theta^2/\rho\mu r)dr\right]_{z=0} - \left[\int_0^R (B_\theta^2/\rho\mu r)dr\right]_{r^2+z^2=R^2}$$

The first of these integrals is readily evaluated since, from Ampère's law, $2\pi r B_\theta = \mu I(r/r_0)^2$ for $r < r_0$ and $2\pi r B_\theta = \mu I$ for $r > r_0$. This yields

$$\left[\int_0^R (B_\theta^2/\rho\mu r)dr\right]_{z=0} = \frac{\mu I^2}{4\pi^2\rho r_0^2}\left[1 - (r_0^2/2R^2)\right]$$

The second integral is more difficult. However, if $r_0 \ll R$ then the field in the vicinity of the boundary is that due to a point source of current, and the corresponding field is readily shown to be

$$2\pi r B_\theta = \mu I\left[1 - z\Big/\left(r^2 + z^2\right)^{1/2}\right], \qquad (r_0 \ll R)$$

This yields

$$\left[\int_0^R (B_\theta^2/\rho\mu r)dr\right]_{r^2+z^2=R^2} = \frac{\mu I^2}{4\pi^2\rho R^2}[\ln 2 - 1/2]$$

Combining these expressions gives us

$$\oint \mathbf{F} \cdot d\mathbf{l} = \frac{\mu I^2}{4\pi^2 \rho}\left[\frac{1}{r_0^2} - \frac{\ln 2}{R^2}\right] = -\nu \oint \nabla^2 \mathbf{u} \cdot d\mathbf{l}$$

For cases where r_0 does not satisfy $r_0 \ll R$ the factor of $\ln 2$ above will need modification. However, the details do not matter. The main point is that

$$\frac{\mu I^2}{4\pi^2 \rho r_0^2} \sim -\nu \oint \nabla^2 \mathbf{u} \cdot d\mathbf{l}$$

Although we have performed the integration only for the bounding streamline, a similar relationship must hold for all streamlines which pass close to the electrode. For streamlines remote from the electrode we would expect

$$\frac{\mu I^2}{4\pi^2 \rho R^2} \sim -\nu \oint \nabla^2 \mathbf{u} \cdot d\mathbf{l}$$

since r_0 ceases to be a relevant dimension in such cases. We can use these equations to estimate $|\mathbf{u}|$.

5.6.3 Estimates of the induced velocity

Suppose that the Reynolds number is not too high, say somewhat less than 100. Then there are no significant boundary layers on the outer wall. (Such layers usually start to form when $\mathrm{Re} > \sim 100$.) The only region where high velocity gradients will form is near the electrode where the characteristic gradient in $\mathbf{F}$ is $|\mathbf{F}|/r_0$, and so we would expect local gradients in $\mathbf{u}$ to be of the order of $|\mathbf{u}|/r_0$. Elsewhere we would expect $\nabla^2\mathbf{u}$ to scale as $|\mathbf{u}|/R^2$. If these statements are true, then our integral equations suggest that

$$u \sim \frac{\mu I^2}{4\pi^2 \rho \nu r_0} \qquad \text{(near electrode)}$$

$$u \sim \frac{\mu I^2}{4\pi^2 \rho \nu R} \qquad \text{(elsewhere)}$$

Somewhat surprisingly these scalings turn out to be valid (provided Re is not too large), as we shall see in Chapter 10.

We end this section by considering the highly idealised case where the outer boundary is removed and $r_0 \to 0$, so that we have a point electrode located on the surface of a semi-infinite fluid. Of course, this is of little practical significance, but it has been the subject of considerable attention

in the literature because it turns out that there is an exact, self-similar, solution for this flow. This solution is of the form

$$u \sim \frac{\mu I^2}{4\pi^2 \rho \nu (r^2 + z^2)^{1/2}} g(\phi, \mathrm{Re})$$

(see suggested reading at the end of this chapter), where ϕ is the angle between the z-axis and the position vector, $\mathbf{x}$, and g is a function of ϕ and of $\mathrm{Re} = u|\mathbf{x}|/\nu$. The similarity to our estimates above is reassuring. However, it would be wrong to place too much emphasis on this exact solution since, in many respects, it is atypical. It turns out that the absence of an outer boundary at large $|\mathbf{x}|$ means that the streamlines in this self-similar flow do not close on themselves, but merely converge towards the axis. The flow is therefore free from integral constraints of the form

$$\oint \mathbf{F} \cdot d\mathbf{l} = -\nu \oint \nabla^2 \mathbf{u} \cdot d\mathbf{l}$$

We might anticipate, therefore, that there is a fundamental difference between this self-similar flow and those in which R is large but finite, and we shall confirm this in Chapter 10.

5.6.4 A paradox

We close this section with an apparent paradox. Of course, there are no real paradoxes in science, only confusion in our muddled attempts to understand nature. We shall describe the paradox here and leave the explanation to Chapter 10.

The integral constraint

$$\oint \mathbf{F} \cdot d\mathbf{l} = -\nu \oint \nabla^2 \mathbf{u} \cdot d\mathbf{l}$$

is a very powerful one. It must be satisfied by *every* closed streamline in a steady flow. Now suppose that we make Re large so that boundary layers form on the boundary of the pool. Inside the boundary layers the viscous dissipation is intense, while outside it is small. The boundary layer thickness usually scales as $\delta \sim (\mathrm{Re})^{-1/2} l$, where l is a typical length-scale for the flow, say R. If this is true here, then the integral equation applied to a streamline lying close to the boundary gives

$$|\mathbf{F}| l \sim (\nu |\mathbf{u}| l)/\delta^2 \sim u^2$$

For a streamline away from the boundary, on the other hand,

$$|\mathbf{F}|l \sim (\nu|\mathbf{u}|l)/l^2 \sim \nu|\mathbf{u}|/l$$

Thus the flow in the boundary layer appears to scale as $u \sim (|\mathbf{F}|l)^{1/2}$, while that in the core scales according to $u \sim |\mathbf{F}|l^2/\nu$, which is much greater than $(|\mathbf{F}|l)^{1/2}$ when Re is large. However, this cannot be so, since the velocity scale in the boundary layer is set by the velocity in the core. Clearly, there is a mistake somewhere! (The mistake is not in the estimate of δ.) Physically, this paradox arises because the fluid in the boundary layer appears to receive significant dissipation, while that in the core is almost inviscid and so, according to previous arguments, larger velocities will develop away from the boundaries.

We will return to this issue in Chapters 8 and 10, where it will be seen that the flow does quite bizarre things in order to satisfy the integral equation.

Example: A false scaling for forced, recirculating flow in a confined domain

Suppose we have a steady laminar, two-dimensional flow, driven by a prescribed Lorentz force, and with a high Reynolds number. The flow is confined to the domain V with the no-slip boundary condition $\mathbf{u} = 0$ on the surface of V. Confirm that, for any streamline C,

$$\oint_C (\mathbf{J} \times \mathbf{B}) \cdot d\mathbf{l} + \rho\nu \oint_C \nabla^2\mathbf{u} \cdot dl = 0$$

The implication is that viscous and magnetic forces are of similar magnitudes. Since $\mathrm{Re} \gg 1$, it follows that inertia greatly exceeds both $\mathbf{J} \times \mathbf{B}$ and $\rho\nu\nabla^2\mathbf{u}$, except in the boundary layers. It follows that, outside the boundary layers, the vorticity is governed by $\mathbf{u} \cdot \nabla\omega \approx 0$, or equivalently, $\omega \approx \omega(\psi)$. Show that

$$\nabla^2\mathbf{u} = -\omega'(\psi)\mathbf{u}$$

and hence confirm that for each streamline which avoids the boundary layers

$$\omega'(\psi) = \oint_C (\mathbf{J} \times \mathbf{B}) \cdot d\mathbf{l} \Big/ \left[\rho\nu \int_A \omega dA\right]$$

where A is the area enclosed by the streamline C. The implication is that $\mathbf{u}$ scales as ν^{-1}. Now show that such a scaling is, in fact, impos-

sible! [Hint: show that this scaling implies an order of magnitude balance between the generation and dissipation of mechanical energy in the core of the flow, which is incompatible with highly dissipative boundary layers.] We appear to have a paradox.

In fact, this is the same paradox as that described above. In practice, the fluid circumvents this dilemma by becoming turbulent at rather low Reynolds numbers (of ~ 100), or else by forcing all of the streamlines through the dissipative boundary layers so that $\omega \neq \omega(\psi)$ (see Chapter 8).

Part 3: Boundary Layers

5.7 Hartmann Boundary Layers

5.7.1 The Hartmann layer

So far we have considered the influence of $\mathbf{J} \times \mathbf{B}$ on the interior of a flow only. We have not considered its effect on boundary layers. We close this chapter with a discussion of a phenomenon which received much attention in the early literature on liquid-metal MHD: the Hartmann layer. This is often discussed in the context of duct flows, but is really just a boundary-layer effect. The main point is that a steady magnetic field orientated at right angles to a boundary can completely transform the nature of the boundary layer, changing its characteristic thickness, for example.

Suppose we have rectilinear shear flow $u(y)\hat{\mathbf{e}}_x$ adjacent to a plane, stationary, surface. Far from the wall the flow is uniform and equal to u_∞, but close to the wall the no slip condition ensures some kind of boundary layer (Figure 5.8). There is a uniform, imposed magnetic field $\mathbf{B} = B\hat{\mathbf{e}}_y$. Now $\mathbf{B} \cdot \boldsymbol{\omega} = 0$ and so (5.9) tells us $\nabla^2 V = 0$, implying that the electric field is zero. We shall also assume that there is no imposed electric field, and so $V = 0$. It then follows from (5.4) and (5.5) that

$$\mathbf{F} = \mathbf{J} \times \mathbf{B} = -\sigma B^2 u \hat{\mathbf{e}}_x$$

and so we have the usual damping force. The Navier–Stokes equation is now

$$\rho\nu \frac{\partial^2 u}{\partial y^2} - \sigma B^2 u = \frac{\partial p}{\partial x} \tag{5.32}$$

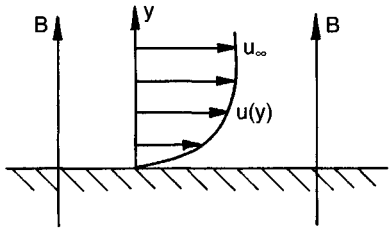

Figure 5.8 A Hartmann flow.

which may be transformed to

$$\frac{\partial^2}{\partial y^2}(u - u_\infty) - \frac{u - u_\infty}{\delta^2} = 0, \qquad \delta = (\rho\nu/\sigma B^2)^{1/2}$$

where u_∞ is the velocity remote from the boundary.

The solution is

$$u = u_\infty[1 - e^{-y/\delta}] \tag{5.33}$$

We see that the velocity increases rapidly over a short distance from the wall (Figure 5.9). This boundary layer, which has thickness $\sim\delta$, is called a Hartmann layer. Note that the thickness of a Hartmann boundary layer is quite different to that of a conventional boundary layer.

5.7.2 Hartmann flow between two planes

We now consider the same flow, but between two stationary parallel plates located at $y = \pm w$. We also allow for the possibility of an imposed electric field, E_0, in the z-direction. Our equation of motion is now

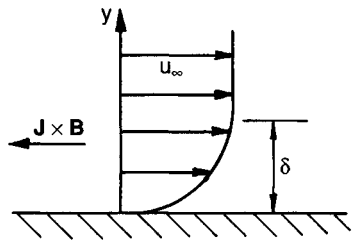

Figure 5.9 The Hartmann boundary layer.

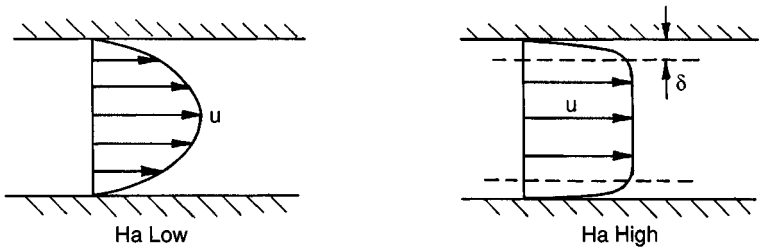

Figure 5.10 Duct flow at low and large Hartmann numbers.

$$\rho\nu\frac{\partial^2 u}{\partial y^2} - \sigma B^2 u = \frac{\partial p}{\partial x} + \sigma B E_0$$

which has the solution,

$$u = u_0\left[1 - \frac{\cosh(y/\delta)}{\cosh(w/\delta)}\right], \qquad \sigma B^2 u_0 = -\frac{\partial p}{\partial x} - \sigma E_0 B$$

It is conventional to introduce the Hartmann number at this point, defined by

$$Ha = w/\delta = Bw(\sigma/\rho\nu)^{1/2}$$

As noted in Section 3.5, $(Ha)^2$ represents the ratio of the Lorentz forces to the viscous forces. Our solution is then

$$u = u_0\left[1 - \frac{\cosh[(Ha)y/w]}{\cosh(Ha)}\right] \tag{5.34}$$

It is instructive to look at the two limits: $Ha \to 0$, $Ha \to \infty$ (Figure 5.10). When Ha is very small we recover the parabolic velocity profile of conventional Poiseuille flow.

$$u = u_0(1 - (y/w)^2)$$

When Ha is very large, on the other hand, we find that exponential Hartmann layers form on both walls, separated by a core of uniform flow. All of the vorticity is pushed to the boundaries.

5.8 Examples of Hartmann and Related Flows

When Ha is large, Hartmann flow is characterised by the three equations

$$u \approx u_0$$

$$J = \sigma(E_0 + u_0 B) \tag{5.35}$$

$$u_0 B = -E_0 - \frac{1}{\sigma B}\frac{\partial p}{\partial x} \tag{5.36}$$

Note that we are free to choose the value of E_0, the external electric field. Depending on how we specify E_0, we obtain quite separate technological devices.

5.8.1 Flow-meters and MHD generators

Suppose we choose $J = 0$, so that $E_0 = -u_0 B$. In this case there is no pressure gradient associated with B, the Lorentz force being zero. Such a device is called an MHD flow-meter since E_0 may be measured to reveal u_0.

Alternatively, if E_0 is zero, or small and positive, we have

$$J \approx \sigma u_0 B, \qquad \left|\frac{\partial p}{\partial x}\right| \approx \sigma B^2 u_0 \tag{5.37}$$

In this case we induce a current, but at the cost of a pressure drop. We are converting mechanical energy into electrical energy plus heat, and such a device is called a generator (Figure 5.11). This is the basis of MHD power generation, where hot ionised gas is propelled down a duct. The technological failure of MHD power generation, which was much publicised in scientific circles, is often attributed to the inability to develop refractory

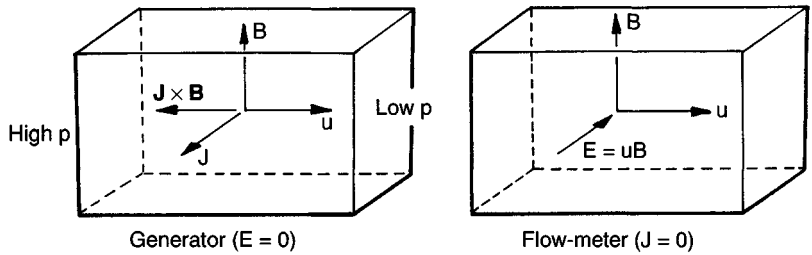

Figure 5.11 Principles of MHD generators and flow-meters.

materials capable of withstanding the high temperatures involved (~3000 K), rather than to any flaw in the MHD principle.

5.8.2 Pumps, propulsion and projectiles

If E_0 is negative, and has a magnitude in excess of $u_0 B$, the direction of J (and hence $\mathbf{J} \times \mathbf{B}$) is reversed. In this case dP/dx is positive and we have a pump. Electrical energy is supplied to the device and this is converted into mechanical energy plus heat.

MHD pumps are in common use, both in the metallurgical and the nuclear industries. Their obvious attraction is that they contain no moving parts and so, in principle, they are mechanically reliable. One can even combine a generator with a pump to produce a so-called MHD flow-coupler. Here two ducts sit side by side, one producing electrical power for the other, which acts as a pump. One application is to transfer mechanical energy from one sodium loop to another in fast breeder reactors.

A variant of the MHD pump is the electromagnetic gun, sometimes called a rail gun or electromagnetic launcher. Here there is no applied magnetic field and so this is not a Hartmann flow. Rather, one relies on the field associated with the flow of current along the electrodes and through the fluid (plasma). It is readily confirmed that the interaction of **J** with its self-field **B** induces a Lorentz force parallel to the electrodes (Figure 5.12). This is used to propel a plasma ahead of which sits a non-conducting projectile. The advantage of such a device is that, as long as current is supplied, the projectile will accelerate. This contrasts with conventional chemical guns where movement of the projectile is

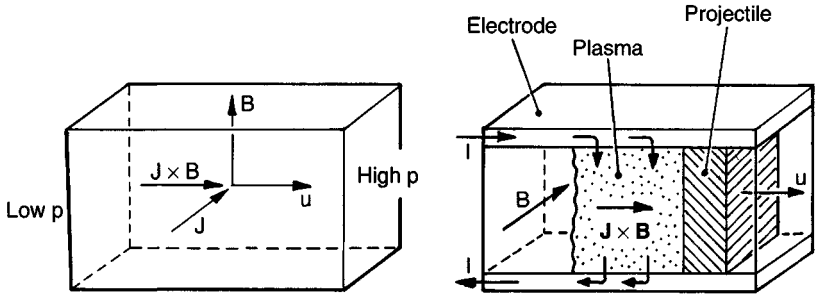

Figure 5.12 Principles of MHD pumps and guns.

associated with an expansion of the gas and hence a loss in pressure. Small masses have been accelerated up to speeds of around 7 km/s in such devices.

Typically the electrodes are connected to a capacitor bank which delivers a current pulse of around $10^5 \rightarrow 10^6$ Amps in a period of a few milliseconds. In the first instance this vaporises a metal foil placed between the electrodes (rails) and so initiates a plasma. Current then enters the top rail, is syphoned off through the plasma and returns via the bottom rail. The resulting force accelerates the plasma along the duct, pushing the projectile ahead of it.

This simple idea is attractive to the extent that it can produce velocities much higher than those achievable by conventional means. It has been suggested that it might be used in fusion research, to create high impact velocities, as a laboratory tool to study high velocity projectiles and, of course, it has military applications. However, in practice it has three major drawbacks. First, the electrical power involved is substantial and this has to be delivered in a very short pulse. Considerable attention must be paid, therefore, to the storage and delivery of the electrical power. Second, the magnetic repulsion forces between the rails is very large, and great care is required in the mechanical design of the gun, otherwise it is prone to self-destruct! Third, the plasma temperatures are very high, $\sim 2.5 \times 10^4$ K, and so there is a severe ablation of material from the inside surface of the duct. As a consequence, the plasma grows rapidly in size and weight, increasing the inertia of the propelled mass and reducing the projectile acceleration.

A variant of the electromagnetic gun, in which the projectile is removed, is the electromagnetic jet thruster. Here the device operates continuously: heating, ionising and propelling a plasma. Typically this has an annular geometry with a central cathode surrounded by a cylindrical anode. The gas is accelerated down the annular gap between the two, producing thrust. This has been proposed as a means of propelling space vehicles, its perceived advantages being its low fuel consumption.

There are many other variants of electromagnetic pumps and thrusters, including the much-publicised, but ill-fated, sea-water thruster for submarines. Some, such as the liquid-metal pump, are in common use. Others, such as the electromagnetic launcher, have yet to find any significant commercial application. In general it seems that the simplest, almost mundane, applications have faired best, while the more exotic suggestions have not been realised.

5.9 Conclusion

We have seen that, because of Joule dissipation, an imposed, static magnetic field tends to dampen out fluid motion, while simultaneously creating a form of anisotropy, in which the gradients in **u** parallel to **B** are preferentially destroyed. Thus turbulence in the presence of a strong magnetic field becomes quasi-two-dimensional as the eddies elongate in the direction of **B**. Travelling or rotating magnetic fields, on the other hand, tend to induce a motion which reduces the relative speed of the field and fluid. The magnitude of the induced velocity is controlled by friction. Finally we have shown that magnetic fields alter the structure of boundary layers, which are now controlled by the competition between Lorentz forces and shear. All in all, it seems that magnetic fields provide a versatile, non-intrusive, means of controlling liquid-metal flows.

Suggested Reading

J A Shercliff, *A Textbook of Magnetohydrodynamics*, 1965, Pergamon Press (Chapter 6).

R Moreau, *Magnetohydrodynamics*, 1990, Kluwer Acad. Pub. (Chapter 4 for Hartmann layers, Chapter 5 for damping of jets, Chapter 6 for rotating flow and for the point electrode problem.)

S Chandrasekhar, *Hydrodynamic Stability*, 1981, Dover. (Chapters 2 and 4 for Bénard convection.)

Examples

5.1 Consider the MHD jet shown in Figure 5.2(b). The imposed magnetic field is weak, in the sense that axial gradients in u are much smaller than the transverse gradient. Sketch the induced current distribution at any one cross section of the jet and estimate, qualitatively, the distribution of $\mathbf{J} \times \mathbf{B}$. Explain why the jet elongates in the direction of **B** and also explain why a reverse flow is induced.

5.2 Consider the vortex shown in Figure 5.3(b). Sketch the induced current distribution (which is poloidal) and estimate, qualitatively, the distribution of $\mathbf{J} \times \mathbf{B}$. Show that this force induces a counter rotation in an annulus which surrounds the primary vortex.

5.3 Consider the inviscid flow shown in Figure 5.4(a). Show that the result $\mathbf{H}_{//} =$ constant is not restricted to low values of N. (Hint, the interaction of **J** with its self-magnetic field can give rise to no net torque on the fluid.)

5.4 The integration of (5.30) using the mixing length model of turbulence yields

$$u_\theta/r\Omega_f = \left(2\sqrt{2}\kappa\right)\ln(R-r) + \text{constant}$$

The constant of integration is determined by the fact that, near the wall, the velocity profile must blend smoothly into the universal law of the wall:

$$\bar{u}/u^* = \kappa^{-1}\ln(u^* y/\nu) + 5.5, \qquad y = R - r$$

where $u^* = (\tau_w/\rho)^{1/2}$ is the shear velocity. This yields (5.31). When the surface is rough, however, the universal law of the wall changes to

$$\bar{u}/u^* = \kappa^{-1}\ln(y/k^*)$$

where k^* is the roughness height. Under these circumstances, show that (5.31) must be modified to

$$(\bar{u}_\theta/r)_0 = \Omega_f\left(2\sqrt{2}\kappa\right)^{-1}\ln(R/k^*)$$

5.5 When liquid metal is stirred in a hemispherical container by an azimuthal Lorentz force, Ekman layers are set up on the boundaries. Sketch the secondary flow induced by Ekman pumping.

6

Dynamics at Moderate to High Magnetic Reynolds' Number

> ... and to those philosophers who pursue the inquiry (of induction) zealously yet continuously, combining experiment with analogy, suspicious of their preconceived notions, paying more respect to the fact than a theory, not too hasty to generalise, and above all things, willing at every step to cross-examine their own opinions, both by reasoning and experiment, no branch of knowledge can afford so fine and ready a field for discovery as this.
>
> *Faraday (1837)*

When R_m is high there is a strong influence of $\mathbf{u}$ on $\mathbf{B}$, and so we obtain a two-way coupling between the velocity and magnetic fields. The tendency for $\mathbf{B}$ to be advected by $\mathbf{u}$, which follows directly from Faraday's law of induction, results in a completely new phenomenon, the Alfvén wave. It also underpins existing explanations for the origin of the earth's magnetic field and of the solar field. We discuss both of these topics below. First, however, it may be useful to comment on the organisation of this chapter.

The subject of high-R_m MHD is vast, and clearly we cannot begin to give a comprehensive coverage in only one chapter. There are many aspects to this subject, each of which could, and indeed has, filled textbooks and monographs. Our aim here is merely to provide the beginner with a glimpse of some of the issues involved, offering a stepping-stone to more serious study. The subject naturally falls into three or four main categories. There is the ability of magnetic fields to support inertial waves, both Alfvén waves and magnetostrophic waves. (The latter involves Coriolis forces, the former does not.) This topic is reasonably clear-cut. Then there is geodynamo theory, which attempts to explain the maintenance of the earth's magnetic field in terms of a self-excited fluid dynamo. This is anything but clear-cut! Geodynamo theory is complex and difficult and there exist many unresolved issues. Next there is plasma containment, motivated for the most part by fusion applications. Here much of the interest lies in the stability of magnetic equilibria, and this is now reasonably well understood, or at least as far as linear (small ampli-

tude) stability is concerned. Finally, there is astrophysical MHD, particularly topics such as star formation and magnetic phenomena in the sun: field oscillations, sunspots, solar flares and so on. Like geodynamo theory, the picture here is far from complete.

The layout of the chapter is as follows. We start with the simplest topic, that of wave theory. We then move to the geodynamo. This divides naturally into two parts. There is the simpler and largely understood kinematic aspect, and the altogether more difficult topic of dynamical theories. We restrict ourselves here to the kinematics of geodynamo theory, where perhaps there is less controversy. Next we give a brief and entirely qualitative tour of one or two aspects of solar MHD. There is no pretence here of a mathematical dissection of the issues involved. The discussion is purely descriptive. We end with a discussion of MHD equilibria. Although the motivation here is plasma MHD, we (artificially) restrict ourselves to incompressible fluids. The reason for this is simple: the algebra involved in developing stability theorems for even incompressible fluids is lengthy and somewhat tedious, and so it seems inappropriate in such a brief discussion to embrace all the additional complexities of compressibility.

Finally, perhaps it is worthwhile to comment on the notation employed in this chapter. Throughout this text we employ only cylindrical polar coordinates (r, θ, z). We make no use of spherical polar coordinates (r', θ', ϕ). When dealing with axisymmetric fields in cylindrical polar coordinates it is natural to divide a vector field, say $\mathbf{B}$, into *azimuthal* $(0, B_\theta, 0)$ and *poloidal* $(B_r, 0, B_z)$ components. For example, the dipole-like external field of the earth is (more or less) poloidal. The field induced by a long straight wire is azimuthal. In the geophysical and astrophysical literature it is normal to use a different terminology. The field is divided into *toroidal* and *poloidal* components. When the field is axisymmetric, toroidal is equivalent to azimuthal. Occasionally the term meridional is substituted for poloidal. We shall not employ the terms toroidal or meridional.

6.1 Alfvén Waves and Magnetostrophic Waves

6.1.1 Alfvén waves

One of the remarkable properties of magnetic fields in MHD is that they can transmit transverse inertial waves, just like a plucked string. We have already discussed the physical origin of this phenomenon. It relies on the

fact that the **B**-field and fluid are virtually frozen together when σ is high. To give an illustration, suppose that a portion of a field line is swept sideways by the lateral movement of the fluid (Figure 6.1). The resulting curvature of the field line gives rise to a restoring force, $B^2/\mu R$, as discussed in §3.9. (R is the radius of curvature of the field line.) As the curvature increases, the restoring force rises and eventually the inertia of the fluid is overcome and the lateral movement is stopped. However, the Lorentz force is still present, and so the flow now reverses, carrying the field lines back with it. Eventually, the field lines return to their equilibrium position, only now the inertia of the fluid carries the field lines past the neutral point and the whole process starts in reverse. Oscillations then develop, and this is called an Alfvén wave.

We now place our physical intuition on a formal mathematical basis. Suppose we have a uniform, steady magnetic field $\mathbf{B}_0$ which is perturbed by an infinitesimally small velocity field $\mathbf{u}$. Let $\mathbf{j}$ and $\mathbf{b}$ be the resulting perturbations in current density and $\mathbf{B}$. Then the leading order terms in the induction equation are

$$\frac{\partial \mathbf{b}}{\partial t} = \nabla \times (\mathbf{u} \times \mathbf{B}_0) + \lambda \nabla^2 \mathbf{b}, \qquad \nabla \times \mathbf{b} = \mu \mathbf{j}$$

which yields

$$\frac{\partial \mathbf{j}}{\partial t} = \frac{1}{\mu}(\mathbf{B}_0 \cdot \nabla)\boldsymbol{\omega} + \lambda \nabla^2 \mathbf{j} \tag{6.1}$$

We now consider the momentum of the fluid. Since $(\mathbf{u} \cdot \nabla)\mathbf{u}$ is quadratic in the small quantity $\mathbf{u}$ it may be neglected in the Navier–Stokes equation and so we have, to leading order in the amplitude of the perturbation,

$$\rho \frac{\partial \mathbf{u}}{\partial t} = \mathbf{j} \times \mathbf{B}_0 - \nabla p + \rho \nu \nabla^2 \mathbf{u}$$

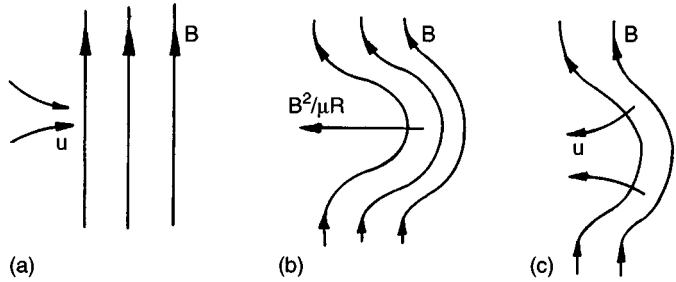

Figure 6.1 Formation of an Alfvén wave.

The equivalent vorticity equation is

$$\frac{\partial \boldsymbol{\omega}}{\partial t} = \frac{1}{\rho}(\mathbf{B}_0 \cdot \nabla)\mathbf{j} + \nu \nabla^2 \boldsymbol{\omega} \tag{6.2}$$

We now eliminate $\mathbf{j}$ from (6.2) by taking the time derivative and then substitute for $\partial \mathbf{j}/\partial t$ using (6.1). After a little algebra, we find

$$\frac{\partial^2 \boldsymbol{\omega}}{\partial t^2} = \frac{1}{\rho\mu}(\mathbf{B}_0 \cdot \nabla)^2 \boldsymbol{\omega} + (\nu + \lambda)\nabla^2\left(\frac{\partial \boldsymbol{\omega}}{\partial t}\right) - \lambda\nu\nabla^4 \boldsymbol{\omega} \tag{6.3}$$

Next we look for plane-wave solutions of the form

$$\boldsymbol{\omega} \sim \boldsymbol{\omega}_0 \exp[i(\mathbf{k} \cdot \mathbf{x} - 2\pi f t)] \tag{6.4}$$

where $\mathbf{k}$ is the wavenumber. Substituting (6.4) into our wave equation (6.3) gives the dispersion relationship

$$2\pi f = -\left[(\nu + \lambda)k^2/2\right]i \pm \left[B_0^2 k_{//}^2/(\rho\mu) - (\nu - \lambda)^2 k^4/4\right]^{1/2}$$

Here $k_{//}$ is the component of $\mathbf{k}$ parallel to $\mathbf{B}_0$. There are three special cases of interest. When $\lambda = \nu = 0$ (a perfect fluid) we obtain $2\pi f = \pm v_a k_{//}$ where v_a is the Alfvén velocity $B_0/(\rho\mu)^{1/2}$. This represents the propagation of transverse inertial waves, with phase velocity v_a. When $\nu = 0$ and λ is small but finite, which is a good approximation in stars, and for liquid-metal flows at high R_m, we find

$$2\pi f = -(\lambda k^2/2)i \pm v_a k_{//}$$

This represents a plane wave propagating with phase velocity v_a and damped by Ohmic dissipation. Finally, we consider the low-R_m case of $\nu = 0$, $\lambda \to \infty$, which characterises most of liquid-metal MHD. Here we find that

$$2\pi f = -i\lambda k^2, \qquad 2\pi f = -i\tau^{-1} k_{//}^2/k^2$$

where τ is the magnetic damping time $\left(\sigma B^2/\rho\right)^{-1}$. The first of these solutions represents a disturbance which is rapidly eradicated by Ohmic dissipation. This is of little interest. However, the second solution represents a non-oscillatory disturbance which decays rather more slowly, on a time scale of τ (Figure 6.2). This is the origin of the pseudo-diffusion phenomenon discussed in Chapter 5.

Alfvén waves are of little importance in liquid-metal MHD since R_m is usually rather modest in such cases. However, they are of considerable importance in astrophysical MHD, where they provide an effective mechanism for propagating energy and momentum. For example, it

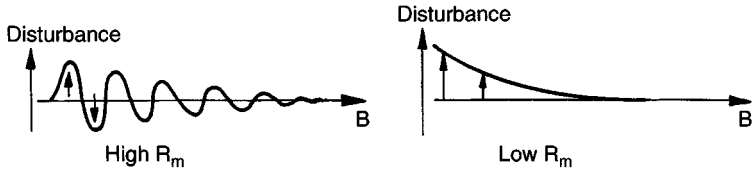

Figure 6.2 Damped Alfvén waves at low and high R_m. Note the low R_m wave is non-oscillatory.

has been suggested that they are responsible for transporting angular momentum away from the core of an interstellar cloud which is collapsing to form a star under the influence of self-gravitation.

Example: Finite-amplitude Alfvén waves

Show that finite-amplitude solutions of the ideal induction equation and Euler's equation exist in the form

$$\mathbf{u} = \mathbf{f}(\mathbf{x} - \mathbf{h}_0 t), \qquad \mathbf{h} = \mathbf{h}_0 - \mathbf{f}(\mathbf{x} - \mathbf{h}_0 t)$$

or

$$\mathbf{u} = \mathbf{g}(\mathbf{x} + \mathbf{h}_0 t), \qquad \mathbf{h} = \mathbf{h}_0 + \mathbf{g}(\mathbf{x} + \mathbf{h}_0 t)$$

where $\mathbf{h} = \mathbf{B}/(\rho\mu)^{1/2}$, $\mathbf{h}_0$ = constant, and $\mathbf{f}$ and $\mathbf{g}$ are arbitrary solenoidal vector fields.

6.1.2 Magnetostrophic waves

There is a second type of inertial wave motion which magnetic fields can sustain. These are called magnetostrophic waves, indicating that they involve both magnetic and rotational effects. Suppose that we repeat the calculation of §6.1.1. This time, however, we let the fluid rotate and take the quiescent base state to be in a rotating frame of reference, rotating at $\boldsymbol{\Omega}$. The effect of moving into a rotating frame of reference is to introduce a centripetal acceleration, which is irrotational and so merely augments the fluid pressure, and a Coriolis force $2\mathbf{u} \times \boldsymbol{\Omega}$. Neglecting dissipative effects, our governing equations are now

$$\frac{\partial \mathbf{b}}{\partial t} = \nabla \times (\mathbf{u} \times \mathbf{B}_0)$$

$$\rho \frac{\partial \mathbf{u}}{\partial t} = 2\rho \mathbf{u} \times \boldsymbol{\Omega} + \mathbf{j} \times \mathbf{B}_0 - \nabla p$$

so that (6.1) and (6.2) become

$$\frac{\partial \mathbf{j}}{\partial t} = \frac{1}{\mu}(\mathbf{B}_0 \cdot \nabla)\boldsymbol{\omega}$$

$$\frac{\partial \boldsymbol{\omega}}{\partial t} = 2(\boldsymbol{\Omega} \cdot \nabla)\mathbf{u} + \frac{1}{\rho}(\mathbf{B}_0 \cdot \nabla)\mathbf{j}$$

We now proceed as before and eliminate $\mathbf{j}$ to give

$$\frac{\partial^2 \boldsymbol{\omega}}{\partial t^2} = 2(\boldsymbol{\Omega} \cdot \nabla)\frac{\partial \mathbf{u}}{\partial t} + \frac{1}{\rho\mu}(\mathbf{B}_0 \cdot \nabla)^2 \boldsymbol{\omega}$$

There are three special cases of interest. First, if $\boldsymbol{\Omega} = 0$ we arrive back at (6.3), representing undamped Alfvén waves. Second, if $\mathbf{B}_0 = 0$, then we find

$$\frac{\partial^2}{\partial t^2}(\nabla^2 \mathbf{u}) + 4(\boldsymbol{\Omega} \cdot \nabla)^2 \mathbf{u} = 0$$

This represents conventional *inertial waves* – waves which propagate in rotating fluids (Figure 6.3). For disturbances of the form $\hat{\mathbf{u}} \exp[j(\mathbf{k} \cdot \mathbf{x} - 2\pi f t)]$ this yields the dispersion relationship

$$2\pi f = \pm 2(\boldsymbol{\Omega} \cdot \mathbf{k})/|\mathbf{k}|$$

and a group velocity (the velocity at which wave energy propagates) of

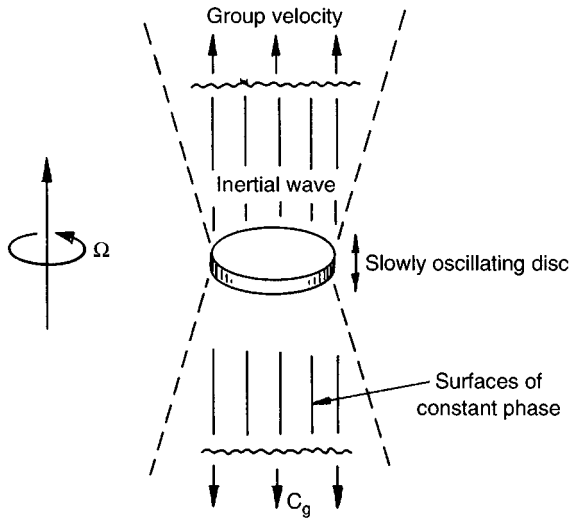

Figure 6.3 An inertial wave.

$$\mathbf{c}_g = \pm 2(k^2\boldsymbol{\Omega} - \mathbf{k}(\mathbf{k}\cdot\boldsymbol{\Omega}))k^{-3}$$

Note that the group velocity is perpendicular to $\mathbf{k}$, so that the phase velocity and group velocity are mutually perpendicular. Thus a wave appearing to travel in one direction, according to the surfaces of constant phase, is actually propagating energy in a perpendicular direction.

Evidently, slow disturbances ($f \ll |\boldsymbol{\Omega}|$) correspond to $\boldsymbol{\Omega}\cdot\mathbf{k} \approx 0$ and $\mathbf{c}_g \approx \pm 2\boldsymbol{\Omega}/|\mathbf{k}|$. Such disturbances propagate as wave packets in the $+\boldsymbol{\Omega}$ and $-\boldsymbol{\Omega}$ directions, and the net effect is that the disturbance appears to elongate along the rotational axis, leading to columnar structures called Taylor columns (Figure 6.4). More generally, the frequency of inertial waves varies from zero, when the group velocity is aligned with $\boldsymbol{\Omega}$, to $2|\boldsymbol{\Omega}|$, when the group velocity is normal to $\boldsymbol{\Omega}$.

The third case of interest is when both $\mathbf{B}_0$ and $\boldsymbol{\Omega}$ are finite but $f \ll |\boldsymbol{\Omega}|$ – slow waves. In this case

$$2(\boldsymbol{\Omega}\cdot\nabla)\frac{\partial \mathbf{u}}{\partial t} + \frac{1}{\rho\mu}(\mathbf{B}_0\cdot\nabla)^2\boldsymbol{\omega} = 0$$

which, on application of the operator $(\boldsymbol{\Omega}\cdot\nabla)\frac{\partial}{\partial t}$, yields

$$4(\boldsymbol{\Omega}\cdot\nabla)^2\frac{\partial^2 \mathbf{u}}{\partial t^2} + \left[\frac{1}{\rho\mu}(\mathbf{B}_0\cdot\nabla)^2\right]^2\nabla^2\mathbf{u} = 0$$

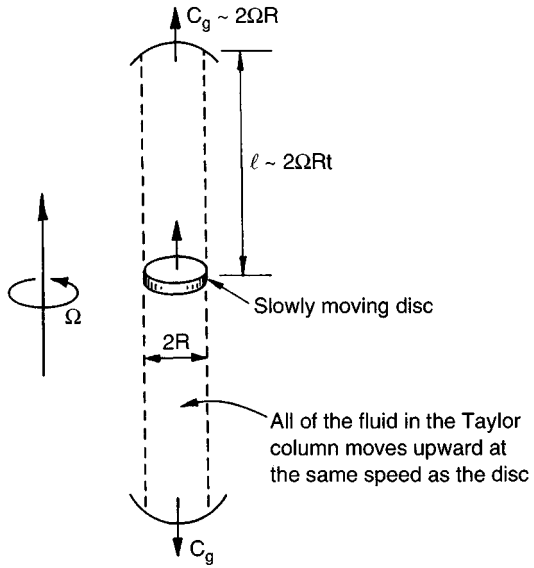

Figure 6.4 Formation of Taylor columns by inertial waves.

This is the governing equation for magnetostrophic waves. The corresponding dispersion equation is

$$2\pi f = \pm\frac{1}{\rho\mu}(\mathbf{B}_0 \cdot \mathbf{k})^2 k/[2(\boldsymbol{\Omega} \cdot \mathbf{k})]$$

Since we require $f \ll |\boldsymbol{\Omega}|$, such waves can exist only if

$$(\boldsymbol{\Omega} \cdot \mathbf{k})^2 \gg (\mathbf{B}_0 \cdot \mathbf{k})^2 k^2/\rho\mu$$

so in some sense we are considering cases where the Coriolis effect is dominant. Magnetostrophic waves are significant in solar and geophysical MHD since both the sun and the earth are rapidly rotating and the Coriolis force is dominant.

6.2 Elements of Geo-Dynamo Theory

> Where does the earth's magnetic field come from? Nobody really knows – there have only been some good guesses.
>
> *R P Feynman (1964) Lectures on Physics*

6.2.1 Why do we need a dynamo theory for the earth?

Dynamo theory is the name given to the process of magnetic field generation by the inductive action of a conducting fluid, i.e. the conversion of mechanical energy to magnetic energy through the stretching and twisting of the magnetic field lines. It is generally agreed that this is the source of the earth's magnetic field, since the temperature of the earth's interior is well above the Curie point at which ferro-magnetic material loses its permanent magnetism. Moreover, the earth's magnetic field cannot be the relic of some primordial field trapped within the interior of the earth. Such a field would long ago have decayed. To see why this is so, suppose that there is negligible motion in the earth's core. The product of **B** with Faraday's law yields the energy equation

$$\frac{\partial}{\partial t}\left(\frac{B^2}{2\mu}\right) = -\nabla \cdot [(\mathbf{E} \times \mathbf{B})/\mu] - \mathbf{J}^2/\sigma \tag{6.5}$$

(Here we have used the fact that $\mathbf{B} \cdot (\nabla \times \mathbf{E}) = (\nabla \times \mathbf{B}) \cdot \mathbf{E} + \nabla \cdot [\mathbf{E} \times \mathbf{B}]$.) We now integrate over all space and note that there is no flux of the Poynting vector, $\mathbf{E} \times \mathbf{B}$, out of a sphere of infinite radius. The result is

$$\frac{dE_B}{dt} = -\int (\mathbf{J}^2/\sigma) dV \tag{6.6}$$

where E_B is the energy of the magnetic field and the integral on the right is confined to $r < R_c$, R_c being the outer radius of the earth's conducting core. As we might have anticipated, E_B falls due to Ohmic dissipation. Now the rate of decline of E_B may be found by a normal mode analysis in which the diffusion equation defines an eigenvalue problem for **B**. It turns out that this yields a decay time of $t_d \sim R_c^2/(\lambda\pi^2)$. For the earth, we have $R_c \sim 3500\,\text{km}$ and $\lambda \sim 2\,\text{m}^2/\text{s}$, which gives $t_d \sim 10^4$ years[1]. However, the earth's magnetic field has been around for at least 10^8 years, and so there must be some additional mechanism maintaining E_B despite the Ohmic losses. Just such a mechanism was discussed in § 4.3: the stretching of flux tubes by an imposed velocity field. In fact, it is not just the earth's magnetic field which is thought to arise from dynamo action. Virtually all of the planets as well as the sun have magnetic fields, many of which are likely to be maintained by a self-excited, fluid dynamo.

Historically there have been many attempts to explain the origins of the earth's magnetic field, other than MHD. Now all abandoned, these included a magnetic mantle, the Hall effect, thermoelectric effects, rotating electrostatic charges, and even, as a last act of desperation, a proposed modification to Maxwell's equations. The electrostatic argument arises from the fact that the earth's surface is negatively charged. In fact, this charge is so great that near the earth's surface there exists an atmospheric electric field of $\sim 100\,\text{V/m}$, directed, on average, radially inward. This surface charge is maintained by lightning storms that are charging the earth, relative to the upper atmosphere, with an average current of 1800 Amperes!

One by one these theories have been abandoned, often because they failed on an order of magnitude basis. Kelvin was on the right track when, in 1867, he noted:

> We may imagine, as Gilbert did, the Earth to be wholly or in part a magnet, such as a magnet of steel, or we may conceive it to be an electromagnet, with or without a core susceptible of induced magnetism. In the present state of our knowledge this second hypothesis seems to be the more probable and indeed we now have reasons for believing in terrestrial currents.... The question which occurs now is this:- Can the magnetic phenomena at the earth's surface, and above it, be produced by an internal distribution of closed currents occupying a certain limited space below the surface.

[1] This calculation was first performed by H Lamb in 1889.

The problem, of course, is what maintains the currents. It was Larmor who, in 1919, first suggested a self-excited fluid dynamo (in the solar context) in his paper: 'How could a rotating body like the sun become a magnet?' When, in 1926, Jeffreys discovered the liquid core of the earth, Larmor's idea suddenly became very relevant to the geo-dynamo.

The general idea behind geo-dynamo theory is that fluid motion in the earth's core stretches and twists the magnetic field lines, thus intensifying the magnetic field. This relies on the advection term in the induction equation being dominant, which in turn requires that R_m is large. However, this seems quite likely. The earth has a liquid iron annulus of inner radius $\sim 10^3$ km and outer radius $\sim 3 \times 10^3$ km (see Figure 6.7). Typical scales for $\mathbf{u}$ and l are estimated to be $u \sim 2 \times 10^{-4}$ m/s and $l \sim 10^3$ km, giving $R_m \sim 100$: not massive, but large.

Mechanical analogues of a self-excited dynamo are readily constructed. A simple, and common, example is the homopolar disk dynamo, shown in Figure 6.5. Here a solid metal disk rotates with a steady angular velocity $\boldsymbol{\Omega}$ and a current path between its rim and its axis is provided by a wire twisted as shown. It is readily confirmed that, provided $\boldsymbol{\Omega}$ is large enough, any small magnetic field which exists at $t = 0$ will grow exponentially in time. First we note that rotation of the disk results in an e.m.f. of $\Omega\Phi/2\pi$ between the axis and the edge of the disk, Φ being the magnetic flux which links the disk. (This may be confirmed by the use of Faraday's law (2.28), or else by a consideration of Ohm's law.) This e.m.f. drives a current, I, which evolves according to

$$L\frac{dI}{dt} + RI = \text{e.m.f.} = \Omega MI/2\pi$$

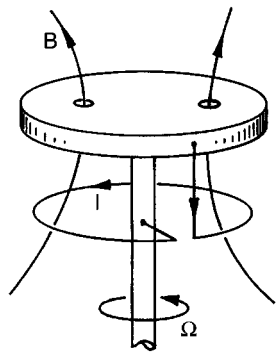

Figure 6.5 Homopolar disk dynamo.

Here M is the mutual inductance of the current loop and the rim of the disk, and L and R are the self-inductance and resistance, respectively, of the total circuit. Evidently I, and hence $\mathbf{B}$, grow exponentially whenever $\boldsymbol{\Omega}$ exceeds $2\pi R/M$. This increase in magnetic energy is accompanied by a corresponding rise in the torque, T, required to drive the disk, the source of the magnetic energy being the mechanical power, $T\boldsymbol{\Omega}$. In any real situation, however, this exponential rise in T cannot be maintained for long, and eventually the applied torque will fall below that needed to maintain a constant $\boldsymbol{\Omega}$. At this point the disk will slow down, eventually reaching the critical level of $\Omega = 2\pi R/M$. T, $\boldsymbol{\Omega}$ and $\mathbf{B}$ then remain steady.

Now this kind of mechanical device differs greatly from a fluid dynamo because the current is directed along a carefully constructed path. Nevertheless a highly conducting fluid can stretch and twist a magnetic field so as to intensify E_B (see Figure 6.6, for example). The central questions in dynamo theory are therefore: (i) can we construct a steady (or steady-on-average) velocity field which leads to dynamo action?; (ii) can such a velocity field be maintained by, say, Coriolis or buoyancy forces in the face of the Lorentz force which, presumably, tends to slow the fluid down? It is now generally agreed that the answers to these questions are 'yes' and 'probably', respectively. However, it should

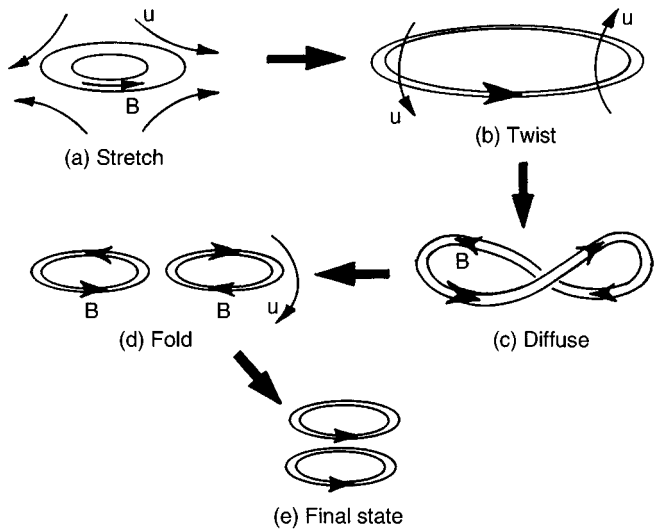

Figure 6.6 A magnetic field can be intensified by a sequence of operations: stretch + twist + diffuse + fold.

be said from the outset that there is, as yet, no self-consistent model of the geo-dynamo. In fact, the entire subject is shrouded in controversy!

In the following subsections we sketch out some of the more elementary ideas and results in geo-dynamo theory. The key points are:

(i) R_m must be large for dynamo action;
(ii) an axisymmetric geo-dynamo is not possible;
(iii) differential rotation in the earth's core can (if it exists) spiral out an azimuthal magnetic field from the familiar dipole one, and in fact this azimuthal field could well be the dominant field in the interior of the earth;
(iv) small-scale turbulence tends to tease out a (small-scale) magnetic field from the large-scale azimuthal field;
(v) this small-scale, random magnetic field is thought (by some) to organise itself in such a way as to reinforce the large-scale dipole field.

In short, one candidate for a geo-dynamo is: dipole field plus differential rotation → azimuthal field; azimuthal field plus turbulence → small-scale, chaotic field; re-organisation of small-scale field → dipole field. However, this model (called the α–$\boldsymbol{\Omega}$ model) is somewhat speculative and, as we shall see, alternatives have been proposed.

The central rôle played by the azimuthal field here is, at first sight, somewhat surprising. After all, measurements made at the surface of the earth indicate only a dipole field. However, it should be remembered that the azimuthal field is supported by poloidal currents which are confined to the core of the earth (Figure 6.7) and that Ampère's law

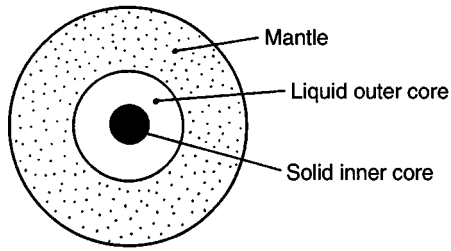

Figure 6.7 The core of the earth. The earth has solid inner core of iron/nickel alloy (radius $\sim 10^3$ km), a liquid outer core of iron plus some lighter elements (radius $\sim 3 \times 10^3$ km), and an outer mantle of ferro-magnesium silicates (radius $\sim 6 \times 10^3$ km).

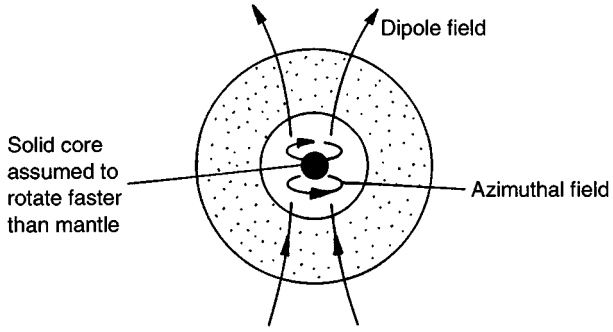

Figure 6.8 Generation of an azimuthal field by differential rotation in the core of the earth.

tells us that such a field cannot extend beyond the core–mantle boundary (see Figure 6.10). The likely source of the azimuthal field is differential rotation between the inner regions of the core and the remainder of the earth (Figure 6.8). This sweeps out B_θ from the dipole field, $\mathbf{B}_p$, and order of magnitude analysis suggests, $B_\theta \sim R_m B_p$ (see Chapter 4 Section 5.3).[2]

6.2.2 A large magnetic Reynolds number is needed

Now it is clear that dynamo action will occur only if R_m is large enough, since the intensification of E_B by flux tube stretching has to outweigh, or at least match, the decay of E_B through Ohmic losses. This may be quantified as follows. Starting with Faraday's equation, $\partial \mathbf{B}/\partial t = -\nabla \times \mathbf{E}$, we may show that,

$$\frac{\partial}{\partial t}\left(\frac{B^2}{2\mu}\right) = -\mathbf{J} \cdot \mathbf{E} - \nabla \cdot [(\mathbf{E} \times \mathbf{B})/\mu]$$

We now integrate over all space, noting that the Poynting flux integrates to zero. This yields

$$\frac{dE_B}{dt} = -\int \mathbf{J} \cdot \mathbf{E} dV$$

[2] The sense of the earth's magnetic field regularly reverses. For simplicity we shall take the field to point from south to north.

Next we assume that **J** and **u** are confined to a sphere $r < R$, and that **u** vanishes at $r = R$. Using Ohm's law to rewrite $\mathbf{J} \cdot \mathbf{E}$ as

$$\mathbf{J} \cdot \mathbf{E} = (\mathbf{J}^2/\sigma) - [\mathbf{B} \times (\nabla \times \mathbf{B})] \cdot (\mathbf{u}/\mu)$$

we have

$$\frac{dE_B}{dt} = \frac{1}{\mu}\int \mathbf{u} \cdot [\mathbf{B} \times (\nabla \times \mathbf{B})]dV - \frac{1}{\sigma}\int \mathbf{J}^2 dV = P - D \tag{6.7}$$

The first term on the right is (minus) the rate of working of the Lorentz force, while the second is, of course, the Joule dissipation. To maintain a magnetic field the first integral must be positive. The next step is to place bounds on D, the dissipation integral, and P, the (so-called) production integral. Starting with P we have

$$\mu^2 P^2 \leq u_{\max}^2 \left[\int \mathbf{B} \times (\nabla \times \mathbf{B})dV\right]^2 \leq u_{\max}^2 \int \mathbf{B}^2 dV \int (\nabla \times \mathbf{B})^2 dV$$

where $u_{\max}$ is the maximum value of $|\mathbf{u}|$ and the second inequality comes from the Schwartz inequality introduce in § 5.3. It follows that

$$|P| \leq (2/\lambda)^{1/2} u_{\max} E_B^{1/2} D^{1/2}$$

Also, by standard methods of the calculus of variations, it may be shown that

$$D \geq 2\pi^2 (\lambda/R^2) E_B$$

(The idea here is that $\int (\nabla \times \mathbf{B})^2 dV$ has a minimum value of $\sim \int \mathbf{B}^2 dV / L_{\max}^2$ where $L_{\max}$ is the maximum relevant length scale. In this case it so happens that $L_{\max}$ is R/π.) Combining the two inequalities yields

$$\frac{dE_B}{dt} \leq (2E_B D/\lambda)^{1/2} [u_{\max} - \pi\lambda/R]$$

Evidently, a necessary (though not sufficient) condition for dynamo action is

$$R_m = (u_{\max} R/\lambda) > \pi \tag{6.8}$$

Below this value of R_m the stretching of the field lines cannot compete with the Ohmic losses.

So how much larger than π must R_m be to get a dynamo, 2π or 200π? The answer is: not much larger, perhaps 5π. The simplest known dynamo is that of Ponomarenko and was developed in the 1970s. It consists of helical pipe flow of the form $\mathbf{u} = (0, \Omega r, V)$, in (r, θ, z) coordinates. Here

Ω and V are constants. For such a flow the induction equation admits separable solutions of the type $\mathbf{B} \sim \exp[j(m\theta + kz + \omega t)]$ and the resulting eigenvalue problem yields growing solutions when $R_m = R(V^2 + \Omega^2 R^2)^{1/2}/\lambda$ exceeds 17.72 (here R is the pipe radius). These growing fields are asymmetric, despite the symmetry of the base flow, with $m = 1$, $V \sim 1.31\Omega R$, and $kR \sim -0.388$.

Later, in the 1980s, generalisations of the Ponomarenko dynamo were developed, in which Ω and V are functions of r and $\Omega = V = 0$ at $r = R$. This avoids the singular behaviour at the pipe wall, inherent in Ponomarenko's dynamo. Yet another variant was developed which has a finite length, a return path being provided for the fluid. In fact, this latter model was put to the test in a laboratory in Riga, but insufficiently high values of R_m were achieved to get a self-sustaining dynamo. Undaunted, the Latvian scientists plan a second attempt at creating a fluid dynamo at the laboratory scale (albeit in a very large laboratory!). A similar experiment was undertaken in Karlsruhe, Germany with successful results, and so the next few years should prove very interesting to dynamo enthusiasts.

Note that the Ponomarenko dynamo has helicity $h = \mathbf{u} \cdot \boldsymbol{\omega}$. This is no accident. Almost all working dynamo models involve helicity. Note also that the dynamo is not symmetric. Again, as we shall see, this is no accident.

Example: Rate of change of dipole moment

It may be shown that, if currents are contained within a spherical volume, V, then the dipole moment, $\mathbf{m}$, of the current distribution is related to its associated magnetic field by

$$\mathbf{m} = \frac{1}{2}\int_V \mathbf{x} \times \mathbf{J} dV = \frac{3}{2\mu}\int_V \mathbf{B} dV$$

Use Faraday's equation and Ohm's law to show that

$$\frac{2\mu}{3}\frac{d\mathbf{m}}{dt} = \int_S \mathbf{u}(\mathbf{B} \cdot d\mathbf{S}) + \lambda \int_S (\mu\mathbf{J}) \times d\mathbf{S}$$

If $\lambda = 0$, show that a motion which tends to sweep the field lines towards the polar regions will increase $\mathbf{m}$. (This dynamo mechanism is limited though, and ceases to operate when all of the flux lines crossing S are concentrated at the poles.) Note that if $\mathbf{u}$ is zero on S then a finite diffusivity is required to increase $\mathbf{m}$.

6.2.3 An axisymmetric dynamo is not possible

The idea of a competition between flux-tube stretching and Ohmic dissipation allows us to rule out the possibility of a steady, axisymmetric dynamo. This is important because the earth's external magnetic field is essentially a dipole, field and so it is natural to look for a steady, axisymmetric, dynamo in which **B** is poloidal, $(B_r, 0, B_z)$ in (r, θ, z) coordinates, **J** is azimuthal $(0, J_\theta, 0)$ and $\mathbf{u}_p$ is also poloidal. However, a result known as Cowling's neutral-point theorem says that such a dynamo cannot exist. The proof is as follows.

Let us suppose that an axisymmetric dynamo can indeed be realised. In the steady state, Ohm's law gives $\mathbf{J} = \sigma(-\nabla V + \mathbf{u} \times \mathbf{B})$: however, $\nabla^2 V = \mathbf{B} \cdot \boldsymbol{\omega} - \mu \mathbf{u} \cdot \mathbf{J} = 0$ since $\boldsymbol{\omega}$ is azimuthal. It follows that $V = 0$ and so $\mathbf{J} = \sigma(\mathbf{u} \times \mathbf{B})$. Now in an axisymmetric, poloidal field there is always at least one so-called neutral ring, N, where **B** vanishes and the **B**-lines are closed in the neighbourhood of the ring (Figure 6.9). It is clear from Ampère's circuital law applied to a **B**-line in the vicinity of N that **J** is non-zero at N. However $\mathbf{J} = \sigma(\mathbf{u} \times \mathbf{B})$ and so we cannot have a finite current where there is no magnetic field. Such a configuration is therefore impossible. This is Cowling's neutral-point theorem.

It seems, therefore, that the earth's dynamo must involve a fairly complex flow field, and in fact the nature of this field is still a matter of considerable debate.

Now there is an alternative, less elegant, but more informative, way of establishing Cowling's theorem. In fact this second proof goes further, showing that a poloidal field cannot be intensified by flux-tube stretching whenever **u** and **B** are both axisymmetric. This includes cases where **u** comprises both poloidal and azimuthal components. The

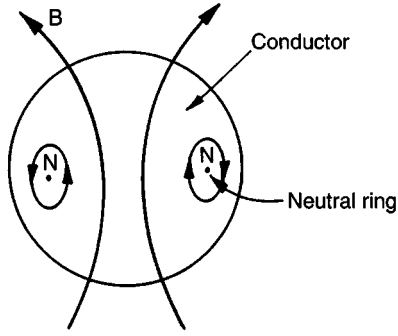

Figure 6.9 All axisymmetric, poloidal fields have a neutral ring, N.

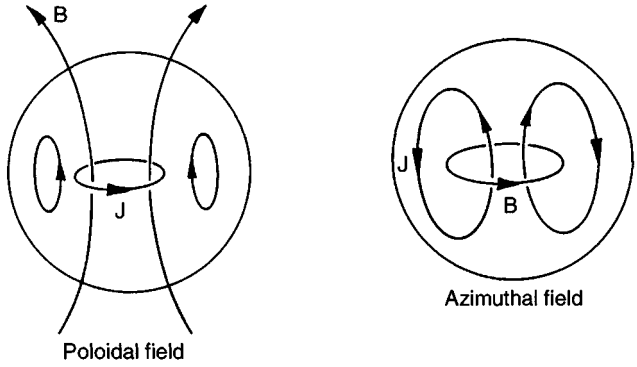

Figure 6.10 Azimuthal and poloidal magnetic fields.

first step is to decompose both **B** and **u** into poloidal and azimuthal parts:

$$\mathbf{B}(r, z) = \mathbf{B}_p + \mathbf{B}_\theta, \qquad \mathbf{u}(r, z) = \mathbf{u}_p + \mathbf{u}_\theta$$

Note that a poloidal magnetic field requires azimuthal currents to support it, while an azimuthal field requires poloidal currents (Figure 6.10). Note also that $\mathbf{B}_\theta$ is restricted to the domain in which the currents flow, which is a direct consequence of Ampère's law.

We now introduce a vector potential for the poloidal field,

$$\mathbf{B}_p = \nabla \times [(\chi/r)\hat{\mathbf{e}}_\theta] = \nabla \times (\mathbf{A}_\theta)$$

which is allowable because $\mathbf{B}_p$ is solenoidal. The parameter χ is called the flux function. It is the magnetic equivalent of the Stokes stream function, the $\mathbf{B}_p$-lines being contours of constant χ. Now it is readily confirmed that the curl of a poloidal field is azimuthal, while the curl of an azimuthal field is poloidal. It follows that the induction equation may also be divided into poloidal and azimuthal components, according to

$$\frac{\partial \mathbf{B}_p}{\partial t} = \nabla \times (\mathbf{u}_p \times \mathbf{B}_p) + \lambda \nabla^2 \mathbf{B}_p \tag{6.9}$$

$$\frac{\partial \mathbf{B}_\theta}{\partial t} = \nabla \times (\mathbf{u}_p \times \mathbf{B}_\theta) + \nabla \times (\mathbf{u}_\theta \times \mathbf{B}_p) + \lambda \nabla^2 \mathbf{B}_\theta \tag{6.10}$$

Uncurling the first of these gives

$$\frac{\partial \mathbf{A}_\theta}{\partial t} = \mathbf{u}_p \times \mathbf{B}_p + \lambda \nabla^2 \mathbf{A}_\theta$$

which yields

$$\frac{D\chi}{Dt} = \lambda \nabla^{*2} \chi \tag{6.11}$$

Here D/Dt is the convective derivative, $\partial/\partial t + (\mathbf{u}_p \cdot \nabla)$, and ∇^{*2} is the Laplacian-like operator defined by

$$\nabla^{*2} = \frac{\partial^2}{\partial z^2} + r \frac{\partial}{\partial r} \frac{1}{r} \frac{\partial}{\partial r} \tag{6.12}$$

The second component of the induction equation may be manipulated into the form

$$\frac{D}{Dt}\left(\frac{B_\theta}{r}\right) = \mathbf{B}_p \cdot \nabla\left(\frac{u_\theta}{r}\right) + \lambda\left[r^{-2}\nabla^{*2}(rB_\theta)\right] \tag{6.13}$$

(This is left as an exercise for the reader.) The important point, as far as Cowling's theorem is concerned, is that (6.11) contains no source term. The flux function is passively advected by $\mathbf{u}_p$, subject only to (a form of) diffusion. There is no term in (6.11) which might lead to an intensification of χ, and hence of $\mathbf{B}_p$. On the contrary, we may use (6.11) to show that $\mathbf{B}_p$ must always decline in accordance with

$$\frac{d}{dt}\int (\chi^2/2\lambda) dV = -\int (\nabla\chi)^2 dV$$

By contrast, (6.13) does contain a source term. Any gradient of swirl along a $\mathbf{B}_p$-line results in the generation of an azimuthal field B_θ. This is readily understood in terms of field sweeping, (see Figure 6.11a).

We might note in passing that (6.13) suggests that, at high R_m, B_θ exceeds $|\mathbf{B}_p|$ in the core of the earth, scaling as $B_\theta \sim R_m|\mathbf{B}_p|$. The point

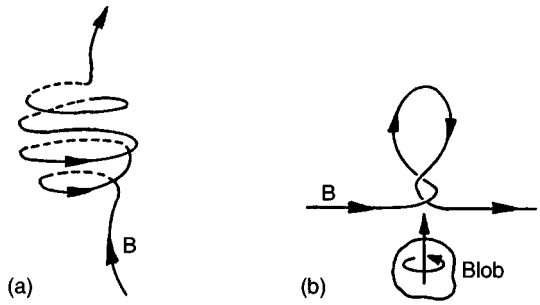

Figure 6.11 An azimuthal magnetic field can be generated by differential rotation in the core of the earth, while turbulence, such as that generated by rising spinning blobs, can tease out a poloidal field from the azimuthal magnetic field. (a) The omega effect. (b) The alpha effect.

is that the left of (6.13) integrates to zero over any volume enclosed (in the r–z plane) by a poloidal stream-line. The two terms on the right must therefore balance (in a global sense), giving $B_\theta \sim (u_\theta l/\lambda)|\mathbf{B}_p|$. Physically, differential rotation causes $\mathbf{B}_\theta$ to build up and, at first, there is nothing to oppose this. (Advection of B_θ/r merely redistributes the azimuthal field.) This process continues until B_θ is so large that diffusion of B_θ is capable of offsetting the generation of an azimuthal field by differential rotation. This happens when $B_\theta \sim (u_\theta l/\lambda)|\mathbf{B}_p|$.

In summary, we conclude that an axisymmetric velocity field cannot intensify a poloidal magnetic field, such as that of the earth, but it can sweep out a (possibly strong) azimuthal field by differential rotation. This is one of the main stumbling blocks to a self-consistent, kinematic, dynamo theory. To complete the dynamo cycle we must find a mechanism of generating a poloidal field from an azimuthal one, i.e.$\mathbf{B}_p \rightarrow \mathbf{B}_\theta \rightarrow \mathbf{B}_p$. Clearly, this last step cannot be axisymmetric.

6.2.4 The influence of small-scale turbulence: the α-effect

This impasse has been circumvented by the suggestion of a two-scale approach to the problem. On the one hand, we might envisage axisymmetric, large-scale behaviour in which $\mathbf{B}_\theta$ is swept out from $\mathbf{B}_p$ through differential rotation between the solid inner core (and its adjacent fluid) and the rest of the liquid annulus. On the other hand, we might postulate small-scale (non-axisymmetric) turbulence which teases out a poloidal field from $\mathbf{B}_\theta$. This would complete the cycle $\mathbf{B}_p \rightarrow \mathbf{B}_\theta \rightarrow \mathbf{B}_p$. This small-scale turbulence might, for example, be generated by natural convection, by shear layers (Ekman layers), by wave motion, or by buoyant, spinning blobs, randomly stretching and twisting the $\mathbf{B}_\theta$-lines as they rise up through the liquid core (Figure 6.11). Such blobs are thought to be released near the inner solid core where relatively pure iron solidifies, leaving liquid rich in an admixture of lighter elements. Whatever the source of the small-scale motion, the general idea is that a random repetition of helical, small-scale events (turbulence, waves or blobs) might lead to the systematic generation of a poloidal field from an azimuthal one. This is known as the 'alpha effect' – a rather obscure name.

Mathematically, the alpha effect may be quantified as follows. Suppose we divide $\mathbf{B}$ and $\mathbf{u}$ into mean and turbulent parts, just as we did when averaging the Navier–Stokes equation in a turbulent flow:

$$\mathbf{B}(\mathbf{x}, t) = \mathbf{B}_0(\mathbf{x}, t) + \mathbf{b}(\mathbf{x}, t)$$

$$\mathbf{u}(\mathbf{x}, t) = \mathbf{u}_0(\mathbf{x}, t) + \mathbf{v}(\mathbf{x}, t)$$

Here $\mathbf{b}$ and $\mathbf{v}$ are the turbulent components which vary rapidly in space and time, whereas $\mathbf{B}_0(\mathbf{x}, t)$ and $\mathbf{u}_0(\mathbf{x}, t)$ vary slowly in space and in time. The means, $\mathbf{B}_0$ and $\mathbf{u}_0$, might for example be defined as spatial averages over a sphere of radius much smaller than R_c (the outer core radius), yet much larger than the scale of the turbulent motion (the blob size in Figure 6.11). The induction equation may also be separated into mean and fluctuating parts:

$$\partial \mathbf{B}_0/\partial t = \nabla \times (\mathbf{u}_0 \times \mathbf{B}_0) + \nabla \times \overline{(\mathbf{v} \times \mathbf{b})} + \lambda \nabla^2 \mathbf{B}_0$$

$$\partial \mathbf{b}/\partial t = \nabla \times (\mathbf{u}_0 \times \mathbf{b}) + \nabla \times (\mathbf{v} \times \mathbf{B}_0) + \nabla \times \left(\mathbf{v} \times \mathbf{b} - \overline{\mathbf{v} \times \mathbf{b}}\right) + \lambda \nabla^2 \mathbf{b}$$

The first of these is reminiscent of the time-averaged Navier–Stokes equation, in which the small-scale turbulence has introduced a new term, $\overline{\mathbf{v} \times \mathbf{b}}$, just as Reynolds stresses appear in the averaged momentum equation. The second of these equations is linear in $\mathbf{b}$ with $\nabla \times (\mathbf{v} \times \mathbf{B}_0)$ acting as a source of $\mathbf{b}$. Now suppose that $\mathbf{b} = 0$ at some initial instant. Then the linearity of this equation ensures that $\mathbf{b}$ and $\mathbf{B}_0$ are linearly related. It follows that $\overline{\mathbf{v} \times \mathbf{b}}$ is also linearly related to $\mathbf{B}_0$, and since the spatial scale for $\mathbf{B}_0$ is assumed to be much larger than that of $\mathbf{b}$, we might expect $\overline{\mathbf{v} \times \mathbf{b}}$ to depend mainly on the local value of $\mathbf{B}_0$. This suggests that $\left(\overline{\mathbf{v} \times \mathbf{b}}\right)_i = \alpha_{ij} B_{0j}$, where α_{ij} is some unknown tensor, analogous to an eddy viscosity in turbulence theory. If the turbulence is assumed to be statistically homogeneous and isotropic (something which is unlikely to be true in practice), then $\alpha_{ij} = \alpha \delta_{ij}$ and the mean part of the induction equation becomes

$$\boxed{\partial \mathbf{B}_0/\partial t = \nabla \times (\mathbf{u}_0 \times \mathbf{B}_0) + \alpha \nabla \times \mathbf{B}_0 + \lambda \nabla^2 \mathbf{B}_0} \qquad (6.14)$$

The turbulence has introduced a new term into the mean component of the induction equation. This is the *α-effect*. In effect, the e.m.f. $\overline{\mathbf{v} \times \mathbf{b}}$ has introduced a mean current density $\mathbf{J}$ which we model as $\mathbf{J} = \sigma \alpha \mathbf{B}_0$.

At first sight, the idea of the α-effect may seem a little implausible. Why should small-scale activity give rise to a large-scale magnetic field? One way to think about it is to consider the small-scale e.m.f, $\overline{\mathbf{v} \times \mathbf{b}}$, as like a battery, driving current through the core. If many such e.m.f's are all aligned, then we would expect a large-scale current to emerge from the

cumulative influence of many small-scale eddies. Presumably the partial alignment of the small-scale eddies (which is a dynamic effect) arises from the combined presence of rotation and of the ambient large-scale field. (This is vaguely reminiscent of the alignment of molecular dipoles in ferromagnetic material under the influence of a mean field, thus enhancing the mean field.) Actually, we have already seen this kind of 'small to large-scale' process at work. Recall the example given in § 5.3, in which low R_m turbulence is confined to a sphere of radius R. The fluid is subject to an imposed field B_0 and maintained in (turbulent) motion by some external agency. We showed that, whatever the motion, there is an induced dipole moment, **m**, whenever the global angular momentum, **H**, of the turbulence is non-zero:

$$\mathbf{m} = (\sigma/4)\mathbf{H} \times \mathbf{B}_0$$

This is illustrated in Figure 6.12. Now it is a standard result in magnetostatics that whenever electrical currents are confined to a sphere, then the spatial average (over the sphere) of the field associated with those currents is proportional to **m**:

$$\int_{V_R} \mathbf{b}dV = (2\mu/3)\mathbf{m}$$

It follows that

$$\int_{V_R} \mathbf{b}dV = (\mathbf{H} \times \mathbf{B}_0)/(6\lambda)$$

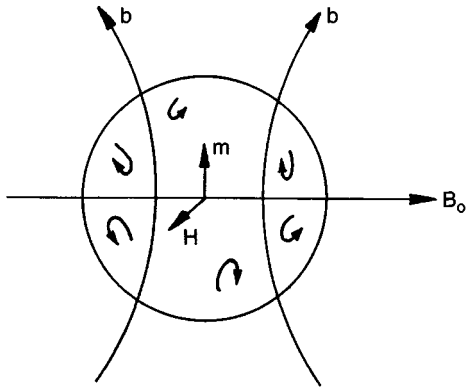

Figure 6.12 Example of small-scale turbulence generating a large-scale field.

Thus we have obtained a (weak) large-scale magnetic field from small-scale turbulence. (Actually, this is not really an α-effect but it does demonstrate the potential for small-scale motion to interact with a mean field to generate a second, large-scale field.)

The α-effect is important in the dynamo context because the poloidal field, $\mathbf{B}_p$, is governed by

$$\frac{\partial \mathbf{B}_p}{\partial t} = \nabla \times (\mathbf{u}_p \times \mathbf{B}_p) + \lambda \nabla^2 \mathbf{B}_p + \alpha \nabla \times \mathbf{B}_\theta$$

or equivalently by

$$\frac{D\chi}{Dt} = \lambda \nabla^{*2} \chi + \alpha r B_\theta$$

The α-effect allows a poloidal field to emerge from an azimuthal one through the action of turbulence. This completes the regenerative cycle $\mathbf{B}_p \rightarrow \mathbf{B}_\theta \rightarrow \mathbf{B}_p$.

The coefficient α, like Boussinesq's eddy viscosity, is a property of the turbulence. We might ask: what properties of the turbulence promote an α-effect, and can we estimate the size of α? In this respect, the most important thing to note is that α is a pseudo-scalar: that is, α changes sign under a coordinate transformation (inversion) of the form $\mathbf{x} \rightarrow -\mathbf{x}$ What do we mean by this? Consider the definition of α: $\overline{\mathbf{v} \times \mathbf{b}} = \alpha \mathbf{B}_0$. Here $\mathbf{v}$ is a polar (true) vector, in the sense that $\mathbf{v}$ always points in the same physical direction, whatever coordinate system is used to describe it. Force is another example of such a vector. However, $\mathbf{b}$ and $\mathbf{B}_0$ are examples of what are called pseudo-vectors, a strange type of vector that reverses physical direction, although it retains the same numerical values of its components, under a coordinate transformation in the form of a reflection through the origin $\mathbf{x} \rightarrow -\mathbf{x}$ (see Chapter 2). Note that such a coordinate inversion involves a change from a right-handed to a left-handed frame of reference. (To confirm that $\mathbf{B}$ is a pseudo-vector, consider its definition, $\mathbf{F} = q\mathbf{u} \times \mathbf{B}$. On inverting the coordinates the numerical values of the components of $\mathbf{F}$ and $\mathbf{u}$ reverse sign, so those of $\mathbf{B}$ cannot.)

Now under the inversion $\mathbf{x}' = -\mathbf{x}$, $\mathbf{b}$ and $\mathbf{B}_0$ retain the same component values, i.e. they reverse direction, while $\mathbf{v}$ retains the same physical direction but reverses its component values. It follows from the definition of α, $\overline{\mathbf{v} \times \mathbf{b}} = \alpha \mathbf{B}_0$, that α must change sign under a coordinate transformation of the form $\mathbf{x} \rightarrow -\mathbf{x}$, and this is what we mean by a pseudo-scalar. It is a strange kind of scalar, not at all like, say, temperature whose value cannot possibly depend on the coordinate system used to describe

space. Another example of a pseudo-scalar is helicity, $\mathbf{v} \cdot (\nabla \times \mathbf{v})$, $\nabla \times \mathbf{v}$ being a pseudo-vector.

This may all sound a little abstract, but it turns out to be important. For example, α is a statistical property of the turbulence which creates it. Thus, if α is to be non-zero, the statistical properties of the turbulence must also change sign under a reflection of the coordinates $\mathbf{x}' = -\mathbf{x}$. We say that the turbulence must lack *reflectional symmetry*, otherwise α will be zero.

The next question might be: can we estimate the size of α? We might expect α to depend on only $|\mathbf{v}|$, λ and l, where $|\mathbf{v}|$ is a measure of the eddy velocity and l is the size of the turbulent eddies or blobs. If this is so then, on dimensional grounds, $\alpha/|\mathbf{v}| = f(|\mathbf{v}|l/\lambda)$, $\alpha/|\mathbf{v}|$ and $|\mathbf{v}|l/\lambda$ being the only two dimensionless groups which we can create from these variables. Two important special cases are $R_m \gg 1$ and $R_m \ll 1$. In cases where R_m is large (on the scale of l) we might expect α not to depend on the diffusivity, λ. That is to say, diffusion should not be an important physical process in the α-effect, except at scales much smaller than l where flux tube reconnections occur. In such a case, we might expect $\alpha \sim |\mathbf{v}|$. However, this cannot be true, since α is a pseudo-scalar while $|\mathbf{v}|$, the r.m.s. turbulence velocity, is not. Given that α is independent of λ, and of order $|\mathbf{v}|$, yet reverses sign in a coordinate inversion, the simplest estimate of α one can come up with is

$$\alpha \sim -\lfloor \overline{\mathbf{v} \cdot (\nabla \times \mathbf{v})} \rfloor l/|\mathbf{v}|, \qquad (R_m \gg 1)$$

Such estimates are, in fact, commonly used. Note the minus sign. This arises because a positive helicity tends to induce **b**-loops whose associated current density, with which we associate $\sigma\alpha\mathbf{B}_0$, is anti-parallel to $\mathbf{B}_0$ (Figure 6.13). This kind of argument implies (but does not prove) that helicity is a key component of the α-effect at high R_m.

For low R_m turbulence we would expect α to depend on λ as well as on l and $|\mathbf{v}|$. In fact, the induction equation tells us $|\mathbf{b}| \sim (|\mathbf{v}|l/\lambda)|\mathbf{B}_0|$, and so

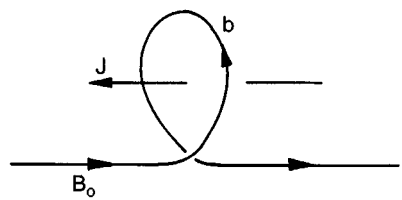

Figure 6.13 (a) Turbulent eddies with positive helicity tend to induce a current density anti-parallel to $\mathbf{B}_0$.

we might expect $\alpha \sim \mathbf{v}^2 l/\lambda$. However, as in the case above, this cannot be true since α is a pseudo-scalar while $\mathbf{v}^2 l/\lambda$ is not. We might anticipate that

$$\alpha \sim -l^2[\overline{\mathbf{v} \cdot \nabla \times \mathbf{v}}]/\lambda, \qquad (R_m \ll 1)$$

which suggests helicity is important whatever the value of R_m, as implied in Figure 6.11.

In fact, when R_m is small, we can evaluate α exactly. We require only that the turbulence be statistically homogeneous. That is, the ensemble average of any turbulent quantity, which we denote $\langle\sim\rangle$, is independent of position. Our starting point is the identity

$$\nabla(\mathbf{a} \cdot \mathbf{b}) - \mathbf{a} \cdot \nabla\mathbf{b} - \mathbf{b} \cdot \nabla\mathbf{a} = \mathbf{a} \times (\nabla \times \mathbf{b}) + \mathbf{b} \times (\nabla \times \mathbf{a})$$

where $\mathbf{a}$ is the vector potential for $\mathbf{v}$: $\mathbf{v} = \nabla \times \mathbf{a}$, $\nabla \cdot \mathbf{a} = 0$. We now substitute for $\nabla \times \mathbf{b}$ using (5.4), the low-R_m form of Ohm's law. This gives

$$\mathbf{v} \times \mathbf{b} = \lambda^{-1}[\mathbf{a} \times (\mathbf{v} \times \mathbf{B}) - \mathbf{a} \times \nabla V] - \nabla(\mathbf{a} \cdot \mathbf{b}) + \nabla \cdot (\sim)$$

Rearranging the term involving the electrostatic potential, V, yields

$$\mathbf{v} \times \mathbf{b} = \lambda^{-1}[\mathbf{a} \times (\mathbf{v} \times \mathbf{B}) - V(\nabla \times \mathbf{a})] - \nabla(\mathbf{a} \cdot \mathbf{b}) + \nabla \cdot (\sim) + \nabla \times (\lambda^{-1} V\mathbf{a})$$

We now express V in terms of $\mathbf{a}$ and $\mathbf{B}$ by taking the divergence of (5.4):

$$\nabla^2 V = \mathbf{B} \cdot \boldsymbol{\omega} = -\nabla^2(\mathbf{B} \cdot \mathbf{a})$$

Thus, to within an arbitrary harmonic function, we have $V = -\mathbf{B} \cdot \mathbf{a}$, and so our expression for $\mathbf{v} \times \mathbf{b}$ simplifies to

$$\mathbf{v} \times \mathbf{b} = \lambda^{-1}[2(\mathbf{a} \cdot \mathbf{B})\mathbf{v} - (\mathbf{a} \cdot \mathbf{v})\mathbf{B}] - \nabla(\sim) + \nabla \cdot (\sim) + \nabla \times (\sim)$$

The final step is to take ensemble averages, at which point the terms involving *grad, div* and *curl* vanish by virtue of our assumption of homogeneity. The end result is

$$\langle \mathbf{v} \times \mathbf{b} \rangle = -\lambda^{-1}\langle(\mathbf{a} \cdot \mathbf{v})\mathbf{B} - 2(\mathbf{a} \cdot \mathbf{B})\mathbf{v}\rangle$$

In terms of α_{ij} this yields

$$\boxed{\alpha_{ij} = -\lambda^{-1}\langle(\mathbf{a} \cdot \mathbf{v})\delta_{ij} - (\mathrm{a}_j \mathrm{v}_i + \mathrm{a}_i \mathrm{v}_j)\rangle} \qquad (R_m \ll 1)$$

If we define $\alpha = \alpha_{ii}/3$, which is consistent with $\alpha_{ij} = \alpha\delta_{ij}$ in the isotropic situation, then

$$\boxed{\alpha = -\langle \mathbf{a} \cdot \mathbf{v} \rangle / (3\lambda)}$$

Compare this with our previous estimate,

$$\alpha \sim -l^2 \left[\overline{\mathbf{v} \cdot \nabla \times \mathbf{v}} \right] / \lambda, \qquad (R_m \ll 1)$$

It seems that the helicity-like pseudo-scalar, $\mathbf{a} \cdot \mathbf{v}$, plays a key role in the low-R_m α-effect.

In summary then, helical turbulence can give rise to an α-effect, and when combined with differential rotation we have the possibility of a self-sustaining dynamo. Actually, integration of the induction equation, incorporating differential rotation and the α-effect, does indeed lead to a self-sustaining dynamo for sufficiently high *dynamo number*, $(\alpha l/\lambda)(u_\theta l/\lambda)$. Typically, in such integrations, α is chosen to be skew-symmetric about the equator, reflecting the supposed structure of the core turbulence. These integrations often yield oscillatory dynamos when the solid inner core is ignored, and non-oscillatory dynamos when the electrical inertia of the inner core is included.

One candidate, then, for a geo-dynamo is the generation of an azimuthal field through differential rotation in the liquid core (the omega effect), supplemented by random, small-scale helical disturbances which convert the azimuthal field back into a poloidal one (the alpha effect). It has to be said, however, that this is a highly simplified picture. For example, we have not addressed the issue of why the turbulence should be dynamically pre-disposed to create an α-effect. Nor have we identified the source of this turbulence.

Example 1: The α-effect induced by helical waves

Suppose that, in Cartesian coordinates, a small amplitude, helical wave of the form

$$\mathbf{v}(\mathbf{x}, t) = Re[\mathbf{v}_0 \exp(i(\mathbf{k} \cdot \mathbf{x} - \omega t))]$$

where $\mathbf{v}_0 = v_0(-i, 1, 0)$ and $\mathbf{k} = (0, 0, k)$, travels through a uniform magnetic field $\mathbf{B}_0$. Confirm that $\mathbf{v}$ is a Beltrami field, in the sense that $\nabla \times \mathbf{v} = k\mathbf{v}$, and that the helicity density is $\mathbf{v} \cdot (\nabla \times \mathbf{v}) = k\mathbf{v}_0^2$. Now use the linearised induction equation to show that the induced magnetic field, $\mathbf{b}$, is

$$\mathbf{b} = \frac{\mathbf{B}_0 \cdot \mathbf{k}}{\omega^2 + \lambda^2 k^4} \left(\lambda k^2 \mathbf{v}^* - \omega \mathbf{v} \right)$$

where $\mathbf{v}^* = \mathrm{Re}[i\mathbf{v}_0 \exp(i(\mathbf{k}\cdot\mathbf{x} - \omega t))]$. Hence show that

$$\overline{\mathbf{v}\times\mathbf{b}} = -\frac{\lambda \mathbf{v}_0^2 k^2 (\mathbf{B}_0\cdot\mathbf{k})}{\omega^2 + \lambda^2 k^4}(0,0,1)$$

In the low R_m limit, $\lambda k^2 \gg \omega$, confirm that α_{ij} is given by

$$\alpha_{ij} = \alpha\delta_{iz}\delta_{jz}, \qquad \alpha = -\mathbf{v}_0^2/(\lambda k) = -\mathbf{v}\cdot(\nabla\times\mathbf{v})/(\lambda k^2)$$

Example 2: A dynamo wave

A two-dimensional analogue of the α-Ω equations can be constructed as follows. Suppose that $\mathbf{B}$ depends only on y and t, $B_y = 0$, and that $\mathbf{u} = \Omega x\hat{\mathbf{e}}_z$. Then

$$\frac{\partial B_z}{\partial t} = \lambda\frac{\partial^2 B_z}{\partial y^2} + \Omega B_x, \qquad \frac{\partial B_x}{\partial t} = \lambda\frac{\partial^2 B_x}{\partial y^2}$$

We might equate B_z to $\mathbf{B}_\theta$ and B_x to $\mathbf{B}_p$. Suppose now that we introduce the α-effect into the equation for B_x, while neglecting it in the B_z equation. Our governing equations now become

$$\frac{\partial B_z}{\partial t} = \lambda\frac{\partial^2 B_z}{\partial y^2} + \Omega B_x, \qquad \frac{\partial B_x}{\partial t} = \lambda\frac{\partial^2 B_x}{\partial y^2} + \alpha\frac{\partial B_z}{\partial y}$$

Show that these equations support solutions of the form $\mathbf{B} \sim \exp(iky + \omega t)$ and that these represent growing, oscillatory waves provided that a suitably defined dynamo number exceeds some threshold. What is the critical value of the dynamo number? (This is known as a dynamo wave.)

Example 3. The dependence of the α-effect on magnetic helicity

Show that, for statistically homogeneous turbulence at low R_m, $\alpha = -\lambda\overline{(\mathbf{b}\cdot\nabla\times\mathbf{b})}/\mathbf{B}_0^2$. Hint, first show that, to within a divergence, which integrates to zero, $\mathbf{b}\cdot\nabla\times\mathbf{b} = \lambda^{-1}\mathbf{b}\cdot(\mathbf{v}\times\mathbf{B}_0)$.

Example 4. Another anti-dynamo theorem

Starting with the induction equation, show that

$$\frac{D}{Dt}(\mathbf{x}\cdot\mathbf{B}) = \mathbf{B}\cdot\nabla(\mathbf{x}\cdot\mathbf{u}) + \lambda\nabla^2(\mathbf{x}\cdot\mathbf{B})$$

Now show that $(\mathbf{x}\cdot\mathbf{u})$ must be non-zero for sustained dynamo action.

6.2.5 Some elementary dynamical considerations

6.2.5.1 Preamble

So far we have restricted ourselves to kinematic aspects of dynamo theory. Of course, this is the simpler part of the problem, in the sense that we give ourselves great latitude in the choice of **u**. That is, we are free to prescribe the velocity field without any concern as to how such a motion might be sustained. Thus, in kinematic dynamo theory we ask only: 'can we find a velocity field, *any* velocity field, which will maintain **B** in the face of Joule dissipation?' It would seem that the answer to this question is 'yes', but this is a long way from providing a coherent explanation for the maintenance of the Earth's magnetic field. We must also determine which of these velocity fields is likely to arise naturally in the interior of the planets, or indeed in the sun. In short, to provide a plausible explanation for the observed planetary magnetic fields, and in particular that of the Earth, we must (somehow) obtain a self-consistent solution of both the induction equation and the momentum equation. This is a tall order and, despite great advances, dynamo enthusiasts are not yet there. Analytical theories tend to be complex and based on rather tentative foundations, while the numerical simulations cannot yet span the wide range of length and time scales inherent in a typical planetary dynamo.

The complexity of the analytical theories lies in stark contrast with the apparently ubiquitous nature of dynamo action. Consider the list of planets, and their magnetic fields, in Table 6.1.

The Earth, Jupiter, Saturn, Uranus and Neptune all have strong dipole moments, Mercury has a rather modest dipole moment, while Venus and Mars exhibit extremely weak (possibly zero) magnetic fields (Venus is probably non-magnetic). It is thought that many of these planetary magnetic fields are self-sustaining dynamos. Yet the constitution, size and rotation rate of the planets vary considerably. The magnetic planets have rotation periods, T, ranging from 0.4 to 59 days, radii which span the range 2400 to 71 000 km and dipole moments from 10^{19} to 10^{27} amps/m^2.

The magnitudes of the planetary fields also vary considerably. It is possible to estimate the mean magnetic field in the planets using the relationship

$$\int_{V_R} \mathbf{B} dV = (2\mu/3)\mathbf{m}$$

Table 6.1. *Properties of the planets*

Planet	Material & density of core (10^3 kg/m^3)	Rotation period, T (days)	Equatorial radius (10^3 km)	Core radius (10^3 km)	Dipole moment (10^{22} amp m^2)	Mean B_z in core (Gauss)	Mean B_z in planet (Gauss)	$(B_x)_p T$ (Gauss-days)
Mercury	Iron, 7.6	59	2.44	1.84	0.005	0.016	0.007	0.60
Venus	Iron, 10.6	243	6.05	3.15	0?	0?	0?	0?
Earth	Iron, 10.6	1	6.38	3.49	7.9	3.7	0.60	0.60
Mars	Iron, 7.5	1.03	3.40	1.50	< 0.002	?	?	?
Jupiter	Liquid hydrogen, 1.3	0.41	71.4	55	150 000	18	8.2	3.4
Saturn	Liquid hydrogen, 0.7	0.43	60.3	28	4700	4.3	0.42	0.18
Uranus	?	0.72	25.6	?	390	?	0.46	0.34
Neptune	?	0.66	24.8	?	200	?	0.26	0.16

where $\mathbf{m}$ is the dipole moment and V_R is any spherical volume which encloses the core currents. This suggests that the mean axial field in the core is of order

$$\bar{B}_z \sim \mu|\mathbf{m}|/(2\pi R_c^3)$$

Estimates of B_z are given in Table 6.1, based on both the core and equatorial radii. Evidently, the mean axial field in the magnetic planets varies from $\sim 10^{-2}$ to ~ 10 Gauss. We might note in passing that, by and large, those planets with the highest rotation rates exhibit the largest magnetic fields, as indicated by the final column in Table 6.1. The main point, though, is that the magnetic planets are all rather different. If it is true that planetary dynamos are so common, yet manifest themselves in such varied circumstances, then one might have hoped that an explanation of dynamo action would be both simple and robust. Not a bit of it! Dynamo theories are complex and, as yet, incomplete.

We shall now outline some of the more elementary dynamical issues. Of course, we have one eye on whether or not the α–Ω dynamo survives scrutiny. In particular, the α–Ω model relies on significant and sustained differential rotation in the core, and requires a separation of scales in the core motion, with a significant amount of kinetic energy at the small scales. We shall see that, while (weak) differential rotation probably does exist, there is little support for a formal separation of scales.

6.2.5.2 Typical time scales in the core

Let us suppose that we have both large-scale motion, for which $L \sim 2000$ km, and small-scale eddies, of size no greater than, say, 2 km. (It may turn out that the small scale-scale motion is both weak and transitory – too weak to contribute to an α-effect. However, we should at least make some provision for such a motion since it is a key ingredient of the α–Ω model.) A common estimate of $|\mathbf{u}|$, based on variations of the surface magnetic field, is 0.2 mm/s. Thus the large-scale motion, which might include differential rotation, buoyant up-wellings and magnetostrophic waves, has a large magnetic Reynolds number, $R_m = uL/\lambda \sim 200$. The small-scale motion, which might be associated with turbulence generated in shear layers, or perhaps small, buoyant plumes, has a relatively low value of R_m, say $R_m = vl/\lambda \sim 0.2$. (We shall take the large-scale

[3] Some caution must be exercised when making the low-R_m approximation. For example, we have seen that Alfvén waves occur when R_m based on the Alfvén speed, v_a, exceeds $\sim \pi$. Typically this wave speed is somewhat greater than v, and so we can have high-R_m phenomena (waves), even though vl/λ is small.

motion, u, and the small-scale velocity, v, to be of similar magnitudes.) A natural starting point, therefore, is to characterise the large-scale phenomena, such as the Ω-effect, as high-R_m, while the small-scale dynamics might be treated as low-R_m.[3]

Let us also allow for differential rotation in the core, as required by the α–Ω model. The probable origin of this relative rotation is discussed more fully in Section 6.2.5.3. We merely note here that differential rotation is observed in certain numerical simulations and in some seismic studies (although the interpretation of the seismic data is not always clear cut). Both the numerical and experimental evidence suggests that the inner core has a rotation rate which is around one degree per year faster than that of the mantle.[4] This differential rotation is thought to be maintained by the secular cooling of the earth, and resisted by viscous coupling of the core and the mantle. That is, cooling causes the solid inner core to grow by solidification, precipitating the release of latent heat and solute-rich, buoyant fluid at the inner-core boundary. The resulting thermal and compositional buoyancy drives a large-scale motion, convecting angular momentum across the core in a systematic manner. The end result is a slight difference in rotation between the inner core and the mantle.

The most important consequence of differential rotation is the inevitable shearing of the dipole field, which sweeps out an azimuthal field of magnitude $B_\theta \sim (u_\theta L/\lambda)B_z$. Thus the dominant field in this picture is azimuthal. Given that $B_z \sim 4$ Gauss in the core, and that $(u_\theta L/\lambda) \sim 200$ we might anticipate that $B_\theta \sim 800$ Gauss in regions of intense differential rotation, i.e. near the inner core. Of course, B_θ does not penetrate beyond the core-mantle boundary, so we have no way of verifying this. We must fall back on the (imperfect) numerical simulations. These suggest that 800 Gauss is an overestimate, and that ~ 50 Gauss is more realistic near the inner core, where the differential rotation is strongest, while B_θ is somewhat weaker in the rest of the core, say, 20 Gauss.

Thus our picture of the large-scale field is one dominated by B_θ. We might further suppose that non-axisymmetric, large-scale convection exists which advects the azimuthal field, forcing low-wavenumber oscillations (magnetostrophic waves) in the large–scale field. This is also a high-R_m process, operating on the scale L. Thus, in this picture, the large-scale field is weakly non-axisymmetric and predominantly azimuthal, as shown in Figure 6.13(b). If we arbitrarily take the internal dipole field to point

[4] A differential rotation of 1 degree per year translates to a velocity of 0.6 mm/s, which is consistent with the estimate of u above.

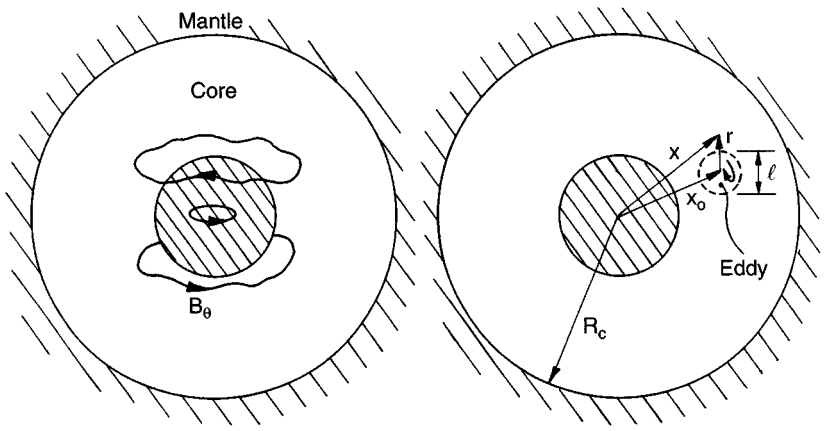

Figure 6.13 (b) (1) The dominant large-scale field is assumed to be azimuthal, produced by differential rotation. It contains a non-axisymmetric, low-wavenumber oscillation caused by large-scale convective motions. Both the differential rotation and the large-scale convective motions occur at large R_m. (2) A small eddy of size l teases out a small-scale field, **b**. This occurs at low R_m.

north (at present it points south), then enhanced rotation of the core relative to the mantle implies that B_θ is positive in the southern hemisphere and negative in the north, as shown.

In addition to these large-scale structures we shall suppose that we have a range of small-scale eddies of size $\sim l$. For lack of a better phrase we might call these small eddies 'turbulence'. In the α–$\boldsymbol{\Omega}$ model, the role of these small eddies is to tease out a small-scale field, **b**, from B_θ, thus regenerating the dipole field $\mathbf{B}_p$.

Let us now try to estimate the characteristic times associated with the large and small-scale structures. To focus thoughts we shall (somewhat arbitrarily) take: $u \sim v \sim 0.2\,\text{mm/s}$, $L \sim 2000\,\text{km}$, $l \sim 2\,\text{km}$, $\lambda \sim 2\,\text{m}^2/\text{s}$, $\nu \sim 3 \times 10^{-6}\,\text{m}^2/\text{s}$, $\rho \sim 10^4\,\text{kg/m}^3$, $|\mathbf{B}_p| \sim 4$ Gauss, $B_\theta \sim 50$ Gauss (near the inner core), and $B_\theta \sim 20$ Gauss (elsewhere).

Table 6.2. *Approximate time scales for large-scale phenomena in the core*

Decay/diffusion time for **B**, $t_d \sim R_c^2/\lambda\pi^2$	10^4 years
Period of magnetostrophic waves ,T	10^4 years
Convective time scale, L/u	300 years

Table 6.3. *Approximate time scales for small-scale phenomena in the core*

Eddy turn-over time, l/v	100 days
Time required to form a Taylor column, $t_\Omega = L/(2\Omega l)$	80 days
Damping time for an Alfvén wave, $l^2/(2\lambda\pi^2)$	1 day
Low-R_m magnetic damping time away from the inner core, $4\tau = 4(\sigma B^2/\rho)^{-1}$	8 hours
Low-R_m magnetic damping time near the inner core, $4\tau = 4(\sigma B^2/\rho)^{-1}$	1 hour

Consider first the large-scale phenomena. There are at least three time scales of interest here: (i) the convective time scale L/u; (ii) the period, T, of the magnetostrophic waves which propagate along the B_θ-lines (see section 6.1.2); (iii) the large-scale diffusion/decay time for **B**, $t_d \sim R_c^2/\lambda\pi^2$. Estimates of these are given in Table 6.2.

The key point is that all of these time scale are relatively large. For example, it takes 10^4 years for a fluctuation in **B** to diffuse through the core!

Now consider the time scales associated with a small-scale eddy. If we can categorise its behaviour as low-R_m (and it is not clear that this is always valid – see footnote at the beginning of this sub-section), then there are three time scales of interest. These are: (i) the eddy turn-over time, l/v; (ii) the time required for an inertial wave to propagate across the core and thus form a Taylor column, $t_\Omega = L/(2\Omega)l$ (iii) the low-R_m damping time, $4\tau = 4(\sigma B^2/\rho)^{-1}$. (Here Ω is the angular velocity of the Earth.) For cases where $v_a l/\alpha >\sim \pi$, v_a being the Alfvén speed, we must add a fourth time scale – that of the damping time for Alfvén waves, $l^2(2\lambda\pi^2)$. (For $v_a l/\alpha <\sim \pi$ these waves do not exist.) Thus the key time scales are as given in Table 6.3.

Of course, we do not really know what B_θ or u are in the core, and so these estimates must be regarded with extreme caution. Nevertheless, if these are at all indicative of the real time scales then they give considerable food for thought. For example, the small-scale processes seem to be extremely rapid by comparison with the large-scale phenomena. Thus, if a buoyant plume left the inner core on the day that Newton first picked up his pen to write *Principia*, it would only just be arriving at the mantle now! Yet small-scale inertial waves can traverse the core in a month or so, while small, neutrally buoyant eddies located near the inner core are

annihilated in a matter of hours! This separation of time scales suggests that we might picture the small-scale eddies as evolving in a pseudo-static, large-scale environment.

We might also note that the turn-over time of a small eddy is large by comparison with the magnetic damping time. This implies that the inertial forces associated with a small eddy are negligible by comparison with the Lorentz forces. The immediate implication is that there is little small-scale turbulence (in the conventional meaning of the word) since the non-linear inertial forces, which are responsible for the turbulent cascade, are absent.

It seems probable, therefore, that the dominant forces acting on a small eddy are the Lorentz, Coriolis and buoyancy forces. The ratio of the Lorentz to Coriolis forces, or equivalently the ratio of the inertial wave period to the magnetic damping time, is represented by the *Elsasser number*, $A = \sigma B^2/(2\rho\Omega)$. If $B_\theta \sim 50$ Gauss, as it might be near the inner core, then $A \sim 7$, and if $B_\theta \sim 20$ Gauss, then $A \sim 1$. Thus, if our estimates of B_θ are reasonable, it would seem that the Coriolis and Lorentz forces are of similar magnitudes in the core. In regions where the Coriolis force wins out we might anticipate quasi-two-dimensional structures, two-dimensionality being enforced by the rapid propagation of inertial waves across the core (see Figure 6.4). In regions where the Lorentz force is dominant, on the other hand, we might expect heavily damped Alfvén waves (if $v_a l/\alpha >\sim \pi$) or else non-oscillatory, low-R_m damping of the type discussed in Section 5.2 (when $v_a l/\alpha <\sim \pi$). In either case, eddies are smeared out along the B_θ-lines while undergoing intense dissipation. The low-R_m damping of eddies is discussed at length in Chapter 9. However, for the present purposes it is sufficient to note that, in the absence of buoyancy, the kinetic energy of an eddy declines as $(t/\tau)^{-1/2}$, where $\tau = (\sigma B^2/\rho)^{-1}$.

The broad picture which emerges, then, is that there is a wide range of time scales. Small eddies are either damped by B_θ or else extruded into Taylor columns by inertial wave propagation. Both processes take place in a matter of days. The convective transport of momentum or magnetic flux is much slower, taking several hundred years to traverse the core. Finally, the large-scale magnetic phenomena (diffusion, magnetostrophic waves) occur on vast time scales, of the order of 10^4 years. There are two important implications of this. First, full numerical simulations are difficult to realise because a wide range of scales have to be resolved. Second, the efficiency with which the particularly small eddies are damped (by Joule dissipation) raises some doubt as to the likely-hood of an energetic small-

scale motion, as required by the α–$\boldsymbol{\Omega}$ model. We shall return to this second issue in Section 6.2.5.4. First, however, we consider the large scales.

6.2.5.3 The large-scale dynamics

The discussion above raises at least two questions relating to the large-scale motion. First, why should compositional or thermal buoyancy give rise to differential rotation? Second, if the inertial forces are so small, is it possible to achieve a quasi-static balance between Coriolis, Lorentz and buoyancy forces? This second question leads to something known as *Taylor's constraint*. Let us start, however, with the issue of differential rotation.

Perhaps the simplest way to picture how differential rotation might arise is to consider an axisymmetric motion, consisting of an up-welling of buoyant fluid rising vertically upward from the inner core. Let us suppose that inertial and viscous forces are negligible (we shall justify this shortly). Moreover, for simplicity, we shall ignore the Lorentz force. (This is completely unjustified. However, the Lorentz force, while modifying the motion, plays no part in the mechanism we are about to describe.) In a frame of reference rotating with the Earth, we have

$$2\mathbf{u} \times \boldsymbol{\Omega} - \nabla(p/\rho) + (\delta\rho/\rho)\mathbf{g} = \text{inertial forces} \approx 0$$

where $\delta\rho$ is the perturbation in density which drives the convection, $\boldsymbol{\Omega}$ is the angular velocity of the Earth, and $\mathbf{g}$ is the gravitational vector which points inwards. Taking the curl of this force balance yields

$$2\Omega \frac{\partial u_\theta}{\partial z} = -\frac{\partial}{\partial z}\left(\frac{\delta\rho}{\rho}\right)g_r + \frac{\partial}{\partial r}\left(\frac{\delta\rho}{\rho}\right)g_z$$

(Remember that we using cylindrical polar coordinates.) Now it is observed in some numerical simulations that the regions above and below the inner core tend to consist of relatively light, buoyant fluid and that, consequently, $\delta\rho$ rises as r increases. The implication is that $\partial u_\theta/\partial z$ is negative in the north and positive in the south.The fluid near the inner core then rotates faster than the mantle, and magnetic coupling, via the dipole field, causes the inner core to rotate at a speed close to that of the surrounding fluid. (The inner core has a relatively small moment of inertia and so reacts almost passively to the magnetic forces which couple it to the surrounding fluid.) The net effect, therefore, is a difference in rotation between the inner core and the mantle.

Thus it appears that there are plausible grounds for believing in differential rotation. Indeed, recent seismic evidence has tended to confirm that the inner core has a prograde rotation relative to the mantle of between 0.3 and 3 degrees per year (although the interpretation of this evidence has been disputed). The energy which maintains this differential rotation (in the face of viscous coupling) comes from the slow growth of the inner core. That is to say, as relatively pure iron solidifies on the inner core, latent heat and solute-rich buoyant fluid are released. The resulting thermal and compositional convection drives the differential rotation, compositional convection probably being the more important of the two.

Let us now turn to the broader issue of how, in the absence of inertial and viscous forces, the Lorentz, buoyancy and Coriolis forces all balance. We have already seen that $\mathbf{u} \cdot \nabla \mathbf{u}$ is negligible by comparison with the Lorentz and Coriolis forces. For example, the ratio of the inertial to Coriolis terms is, $u/2\Omega L \sim 10^{-6}$. The viscous stresses are also small (outside the boundary layers) since $\mathrm{Re} = uL/\nu \sim 10^8$, while the so-called *Ekman number*, $E = \nu/(2\Omega L^2)$, is of the order of 10^{-14}. (The Ekman number represents the ratio of viscous to Coriolis forces.) It appears, therefore, that the viscous and inertial forces are negligible outside the boundary layers.

Now, we have already seen (in Section 3.7) that differential rotation between a fluid and an adjacent solid surface sets up an Ekman boundary layer of thickness $(\nu/\Omega)^{1/2}$ provided, of course, that the flow is laminar. Such layers might be expected to form on the inner core and on the mantle. Indeed, it is the viscous coupling between the core and the mantle which moderates the differential rotation. However, the Ekman layers in the core cannot be laminar since the estimate $\delta \sim (\nu\Omega)^{1/2}$ leads to the bizarre conclusion that $\delta \sim 20$ cms, yet all other relevant length scales are measured in kilometres. For example, the surface of the inner core is thought to consist of a 'forest' of dendritic crystals, about 1 km deep. It seems probable, therefore, that the Ekman thickness is controlled by surface roughness and by turbulence. Some authors allow for this by replacing ν by an eddy viscosity, ν_t. It should be noted, however, that an effective Ekman number based on ν_t is not expected to exceed $\sim 10^{-9}$, so that turbulent stresses are negligible outside the Ekman layers.

The neglect of inertial and viscous forces has profound implications for the large-scale motion. Consider a control-volume, V, confined to the core and bounded by the cylindrical surface $r = r_0$ and by the mantle. In the absence of the non-linear inertial term we have

$$\frac{\partial \mathbf{u}}{\partial t} = 2\mathbf{u} \times \boldsymbol{\Omega} - \nabla(p/\rho) + (\delta\rho/\rho)\mathbf{g} + \rho^{-1}\mathbf{J} \times \mathbf{B} + \nu\nabla^2\mathbf{u}$$

which yields the angular momentum equation

$$\frac{\partial(\mathbf{x} \times \mathbf{u})}{\partial t} = 2\mathbf{x} \times (\mathbf{u} \times \boldsymbol{\Omega}) + \nabla \times (p\mathbf{x}/\rho) + \rho^{-1}\mathbf{x} \times (\mathbf{J} \times \mathbf{B}) + \nu\mathbf{x} \times (\nabla^2\mathbf{u})$$

If we now integrate the z-component of this equation over the volume V, then the pressure torque integrates to zero while the Coriolis term, which can be expanded as a vector triple product, also vanishes, i.e.

$$\int_V 2(\mathbf{x} \times (\mathbf{u} \times \boldsymbol{\Omega}))_z dV = 2\Omega \int_V (zu_z - \mathbf{x} \cdot \mathbf{u}) dV = \Omega \int_V \nabla \cdot \left((z^2 - \mathbf{x}^2)\mathbf{u}\right) dV$$

$$= -r_0^2 \Omega \oint \mathbf{u} \cdot d\mathbf{S} = 0$$

Thus we are left with,

$$\frac{d}{dt}\int (\mathbf{x} \times \mathbf{u})_z dV = \rho^{-1} \int (\mathbf{x} \times (\mathbf{J} \times \mathbf{B}))_z dV + (\text{viscous torque on mantle})$$

It is conventional to reformulate this so that it applies to a thin annulus at $r = r_0$. The end result is

$$\frac{d}{dt}\int u_\theta dA = \rho^{-1} \int (\mathbf{J} \times \mathbf{B})_\theta dA + (\text{viscous torque})$$

Here dA is an element of the surface $r = r_0$. Now the viscous contribution to this equation is of order $\nu_t(u_\theta/\delta)$. Thus the ratio of the Lorentz to the viscous torques is $\sim AE_t^{-1/2}$, where A is the Elsasser number and E_t is the effective Ekman number based on a turbulent eddy viscosity. Since $A \sim 1$, we have

$$\frac{d}{dt}\int u_\theta dA = \rho^{-1} \int (\mathbf{J} \times \mathbf{B})_\theta dA + 0(E_t^{1/2})$$

Thus, in the steady state, the Lorentz torque must satisfy

$$T(r_0) = \rho^{-1} \int (\mathbf{J} \times \mathbf{B})_\theta dA = 0(E_t^{1/2}) \approx 0$$

This is known as Taylor's constraint. In short, the annulus cannot support a sizeable Lorentz torque since there are no significant forces (inertial or viscous) to balance such a torque. If, at some initial instant, this

constraint is broken, torsional oscillations are thought to ensue between adjacent annuli, these annuli being coupled by the B_r field. Damping of the oscillations then causes the flow to evolve towards an equilibrium state, called a *Taylor state*.

There are several ways in which the Taylor constraint can be satisfied. It turns out that one of these is to ensure that B_r is suitably small in the core. That is, in terms of Maxwell stresses,

$$\int (r_0 B_r B_\theta / \mu) dA = \int (\mathbf{x} \times (\mathbf{J} \times \mathbf{B}))_z dV$$

(There is no contribution to the integral on the left from the core–mantle boundary since B_θ is zero there.) Thus the Taylor constraint is satisfied if B_r is suitably small in the core, i.e. the poloidal field lines are almost axial in the core. (This idea has led to a clutch of models known collectively as *Model z*.)

The limitations imposed by the Taylor constraint are quite profound, and in fact this has dominated much of the recent literature on the geodynamo. It might be noted, however, that the net toque arising from a closed system of currents interacting with its 'self field' is necessarily zero. Thus, in a global sense, the Taylor constraint is always satisfied (if we ignore any currents in the mantle).

6.2.5.4 The small-scale dynamics

We now turn to the small-scale motion in the core. The main issue here is whether or not the small-scale structures, which are so important in the α–$\boldsymbol{\Omega}$ model, can survive the relatively intense Joule dissipation and so contribute, via the α-effect, to the global dipole field.

We have already seen that, at scales of $1 \sim 2$ km the magnetic Reynolds number is less than unity. This suggests that many of the small-scale eddies are subject to low-R_m damping of the type discussed in Chapters 5 and 9. Such eddies will decay rather rapidly unless they are maintained by some external force, such as buoyancy. For example, it is shown in Chapter 9 that, in the absence of buoyancy, the kinetic energy of a low-R_m eddy evolving in a uniform magnetic field declines as $(t/\tau)^{-1/2}$, where τ is the Joule damping time $(\sigma B^2/\rho)^{-1}$. Moreover, in the absence of Coriolis and buoyancy forces, an eddy whose axis of rotation is parallel to $\mathbf{B}$ conserves its angular momentum, while one whose axis is normal to $\mathbf{B}$ loses its angular momentum at a rate $\mathbf{H}_\perp \sim \mathbf{H}_{\perp 0} \exp(-t/4\tau)$. In the former case, the eddy evolves into an elongated, cigar-like structure

whose main axis is aligned with **B** (see Figure 5.3b), while in the latter case the eddy loses its angular momentum by disintegrating into a network of plate-like structures whose planes are orientated parallel to **B** (see Figure 9.12). In both cases the eddy elongates in the direction of **B** at a rate $(t/\tau)^{1/2}$.

The situation is more complicated when both Lorentz and Corlios forces act on a small eddy. Some hint as to how Coriolis forces might influence the decay of a low-R_m eddy is furnished by the following simple model problem.

Suppose we have a small, localised, low-R_m eddy sitting in a locally uniform field $\mathbf{B} = B\mathbf{e}_x$. It has finite angular momentum and is subject to Coriolis and Lorentz forces (with $\boldsymbol{\Omega} = \Omega\mathbf{e}_z$). However, viscous, gravitational and non-linear inertial forces are neglected. Thus the momentum equation simplifies to

$$\frac{\partial \mathbf{u}}{\partial t} = 2\mathbf{u} \times \boldsymbol{\Omega} - \nabla(p/\rho) + \rho^{-1}\mathbf{J} \times \mathbf{B}$$

from which we have

$$\frac{\partial(\mathbf{x} \times \mathbf{u})}{\partial t} = 2\mathbf{x} \times (\mathbf{u} \times \boldsymbol{\Omega}) + \nabla \times (p\mathbf{x}/\rho) + \rho^{-1}\mathbf{x} \times (\mathbf{J} \times \mathbf{B})$$

Using (5.22) to rearrange the Lorentz force, and a variant of (5.22) to recast the Coriolis force, we find that

$$\frac{\partial(\mathbf{x} \times \mathbf{u})}{\partial t} = (\mathbf{x} \times \mathbf{u}) \times \boldsymbol{\Omega} + \nabla \times (p\mathbf{x}/\rho) + (2\rho)^{-1}(\mathbf{x} \times \mathbf{J}) \times \mathbf{B} + \nabla \cdot (\sim \mathbf{u}) + \nabla \cdot (\sim \mathbf{J})$$

Next we integrate over a large spherical volume, and insist that $\mathbf{u}.d\mathbf{S}$ and $\mathbf{J}.d\mathbf{S}$ are zero on some remote boundary. This yields

$$\frac{d\mathbf{H}}{dt} = \mathbf{H} \times \boldsymbol{\Omega} + \mathbf{m} \times \mathbf{B}/\rho$$

where **m** is the dipole moment induced by the interaction of the eddy with **B**. Finally, following the arguments leading up to (5.23), and on the assumption (which is not always valid in the core) that the low-R_m form of Ohm's law applies, we recast **m** in terms of **H** to give

$$\frac{d\mathbf{H}}{dt} = \mathbf{H} \times \boldsymbol{\Omega} - \frac{\mathbf{H}_\perp}{4\tau}, \qquad \mathbf{H}_\perp = (0, H_y, H_z)$$

It appears that H_z declines exponentially. H_y and H_x, on the other hand, decay in a sinusoidal fashion if $A = \sigma B^2/(2\rho\Omega)$ is less than 4, and decay

exponentially if A exceeds 4. In either case the characteristic decay time is 4τ. Now it is readily confirmed that the Coriolis force does not change the rate of decline of energy and so the energy of the eddy falls as $(t/\tau)^{-1/2}$. An algebraic decline in energy, yet exponential decline in angular momentum, requires that the eddy adopts a spatial structure in which the angular momentum alternates in sign and integrates to zero. So we might anticipate that, whatever the value of A, plate-like structures will emerge, as shown in Figure 9.12. Moreover, when A is small, an eddy presumably undergoes a substantial elongation before being destroyed, the Coriolis force extruding the eddy into a Taylor column. Thus the eddy shown on the left of Figure 9.12 will grow at a rate $(t/\tau)^{1/2}$ parallel to $\mathbf{B}$ and at a rate Ωt parallel to $\boldsymbol{\Omega}$, forming a set of platelets of alternating vorticity which, when added together, have zero net angular momentum.

So what does all this mean in the context of the Earth's core? For $B_\theta \sim$ 20 Gauss we have a dissipation time scale of $4\tau \sim 1$ day. This is very rapid by comparison with the other relevant time scales, and so it is by no means clear that these eddies can be replenished as fast as they are destroyed.

At present, the prevailing view is that, as far as planetary dynamos are concerned, the α-effect is, at best, a pedagogical idealisation.

6.2.6 Competing kinematic theories for the geo-dynamo

Two-scale α–$\boldsymbol{\Omega}$ models have been around for some time now. They represented a significant breakthrough in dynamo theory because they circumvented the fundamental limitations imposed by Cowling's theorem while providing a theoretical framework for constructing possible dynamo mechanisms. Their weaknesses, however, are three-fold. First, the α-effect is essentially a kinematic theory. Why should the turbulence in the earth's core be dynamically predisposed to reconstruct a large-scale dipole field from a random small-scale field? Second, they rely on significant differential rotation in the core, which requires the inner core and the mantle to rotate at different rates. As noted above, there is some indication that this is indeed the case. However, the evidence is not yet conclusive. Third, they presuppose a two-scale structure for $\mathbf{u}$ and $\mathbf{B}$, with significant energy in the small-scale turbulence. There is no real evidence that this is the case and, as we have seen, there are arguments to the contrary.

Many other dynamo mechanisms have been proposed. For example, if we accept the notion of a two-scale approach, but reject the idea of strong differential rotation, then we can still get a dynamo through the α-effect. That is, B_θ can be generated from $|\mathbf{B}_p|$ by an α-effect, which is then converted back into a poloidal field, again by the α-effect. This is called an α^2-dynamo (see example below). Alternatively, we might abandon the two-scale picture altogether and consider large-scale convective motions driven by buoyancy and Coriolis forces. Indeed, there have been many computer simulations of that type. However, despite all of this research, there is still no self-consistent theory which explains the observations.

In any event, it looks like the search for an entirely self-consistent model of the geo-dynamo will continue for some time. Great advances have been made, yet there is still some resonance in Maxwell's comment:

> ... we are not yet fully acquainted with one of the most powerful agents in nature, the scene of whose activity lies in those inner depths of the earth, to the knowledge of which we have so few means of access.
>
> *(1873)*

Example: An α^2-dynamo

Consider the averaged induction equation in cases where $\alpha =$ constant and $\mathbf{u}_0 = 0$:

$$\frac{\partial \mathbf{B}_0}{\partial t} = \alpha \nabla \times \mathbf{B}_0 + \lambda \nabla^2 \mathbf{B}_0$$

Consider solutions of this equation of the form $\mathbf{B}_0 = \hat{\mathbf{B}}(\mathbf{x})e^{pt}$where $\hat{\mathbf{B}}(\mathbf{x})$is a so-called 'force-free' field satisfying,

$$\nabla \times \hat{\mathbf{B}} = k\hat{\mathbf{B}}$$

Show that, for suitable initial conditions, this is a solution of the averaged induction equation, and that

$$p = \alpha k - \lambda k^2$$

Deduce the criterion for a self-sustaining α^2-dynamo.

6.3 A Qualitative Discussion of Solar MHD

One lot cogitates on the way of religion, Another ponders on the path of mystical certainty; But I fear one day the cry will go up, 'Oh you fools, neither this nor that is the way!'

Omar Khayyam

The capricious behaviour of sunspots has been the source of speculation since the first observations in ancient China. Considered debate in the West probably dates back to the early 17th century and to the development of the telescope by Galileo. Indeed it was Galileo's *Letters on Solar Spots*, published in Rome in 1613, which precipitated the clash between Galileo and the church. Thus the battle between science and religion began; a skirmish which had still not abated by 1860 when Huxley and Bishop Wilberforce debated Darwin's *Origin of the Species.*

Records of sunspot appearances have been kept more or less continuously since Galileo's time. By 1843 it was realised that the appearance of spots followed an eleven-year cycle (although there was a curious dearth of sunspots during the reign of the Roi Soleil in France!). The reason for the eleven-year cycle remained a mystery for some time, but it was clear by the end of the 19th century that there was an electromagnetic aspect to the problem. As Maxwell noted in 1873, when discussing terrestrial magnetic storms: '*It has been found that there is an epoch of maximum disturbance every eleven years, and that this coincides with the epoch of maximum number of sunspots in*

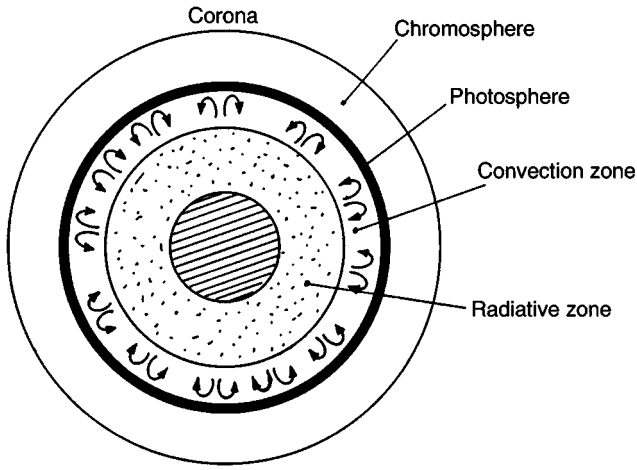

Figure 6.14 (a) The structure of the sun.

the sun.' Maxwell was on the right track, but it was not until the development of MHD that we have begun to understand some of the observations.

The following paragraphs give a brief qualitative introduction to solar MHD. The focus is on sunspots and solar flares. The discussion is purely descriptive, intended only to give a glimpse of some of the more intriguing phenomena involved. To date, many problems concerned with the solar dynamo have not been solved, and models which have been proposed require for their understanding mathematics beyond the level of this book. Some reading suggestions are given at the end of the chapter which fearless readers may consult.

6.3.1 The structure of the sun

The sun's interior is conventionally divided into three zones (Figure 6.14(a). The central core of radius $\sim 2 \times 10^5$ km is the seat of thermonuclear fusion. This is surrounded by the so-called radiative zone which extends up to a radius of $\sim 5 \times 10^5$ km Here heat is transported diffusively by radiation and conditions are hydrodynamically stable. The outer region is called the convection zone. It is approximately 2×10^5 km deep, convectively unstable and so in a state of constant motion. Heat is carried to the surface via convection.

The solar atmosphere is also divided into three regions. The 'surface' of the sun is called the photosphere. This is a thin transparent layer of relatively dense material about 500 km deep. Above this lies the hotter, lighter chromosphere which is around 2500 km deep. The outermost layer is the corona, which has no clear upper boundary and extends in the form of the solar wind out to the planets. There is a dramatic rise in temperature in passing from the chromosphere to the corona.

The existence of the solar convection zone is evident in the granular appearance of the photosphere. In photographs it looks like a gravel path and is reminiscent of multi-cellular Bénard convection. The granules (convection cells), which are continually evolving on a time-scale of minutes, have a typical diameter of $\sim 10^3$ km and are bright at the centre, where hot plasma is rising to the surface, and darker at the cell boundaries where cooler plasma falls. Because they are influenced by surface radiation, these granules are not necessarily representative of the scale of the internal motion deep within the convection zone.

As was mentioned in Chapter 4, the sun does not rotate as a rigid body. The average surface rotation is faster at the equator than it is near the poles but the radiative zone rotates more or less like a rigid body at a rate somewhere between the equatorial and polar surface rates. This differential rotation is crucial to much of solar MHD.

6.3.2 Is there a solar dynamo?

The natural decay time for a magnetic dipole field in the sun is around 10^9 years, which is about the age of the solar system itself. This is not inconsistent with the notion that the field is the relic of some galactic field which was trapped in the solar gas at the time of the sun's formation. However, the sun's magnetism is constantly varying in a manner that cannot be explained by some frozen-in primordial field. Sunspot activity could be attributable to transient, small-scale processes, but the periodic (22-year) variation of the sun's global field suggests that theories based on a frozen-in relic are incorrect. It seems likely, therefore, that the explanation of solar magnetism lies in dynamo action within the convective zone. Note that while dynamo theory is invoked to explain the unexpected persistence of the earth's magnetic field, it is invoked in the solar context to explain the rapid evolution of the sun's field.

The dynamo theories which have been developed in the context of the earth and the sun are, however, very different. In the core of the earth, velocities are measured in fractions of a millimetre per second, and as a result R_m is rather modest, $R_m \leq 100$. In the convective zone of the sun, on the other hand, velocity fluctuations are around 1 km/s, giving $R_m \sim 10^7$. While concerns in geodynamo theory often centre around finding turbulent motions which have an R_m high enough to induce significant field stretching, in the solar dynamo the problem is of the opposite nature. R_m is so high that molecular diffusivity becomes very weak, and so extremely large gradients in the magnetic field must develop in order to allow the flux tube reconnections needed to explain the observed behaviour.

6.3.3 Sunspots and the solar cycle

We have already discussed sunspots in Chapter 4. They are a manifestation of unstable, buoyant flux tubes which float up through the convective zone and erupt into the solar atmosphere (see Figure 4.2). These dark

spots appear in pairs and are the foot-points of the flux tube in the solar surface, where the intense local magnetic field (~ 3000 G) suppresses fluid motion and cools the surface. The spots are typically 10^4 km in diameter (much larger than a granule) and they appear mainly near the equatorial plane. Often they occur in groups (an 'active region') and this gives rise to an increased brightness, called photospheric faculae.

The intensity of sunspot activity fluctuates on a regular 11-year cycle. At the sunspot minimum there may be no sunspots, while at the maximum there are typically around a hundred. After their rapid initial formation, sunspot pairs may survive for some time, disintegrating over a period of days or weeks, the so-called 'following spot' vanishing first. The fragments of the flux tube which caused the spot are then convected around by the photospheric flows accumulating along granular boundaries.

The area of the photosphere covered by sunspots varies during the 11-year cycle. At the minimum point new spots appear first at latitudes of $\sim \pm 30°$. The number of active zones then increases, gathering towards the equator, until finally the sunspot activity dies away. The magnetic field in an active region is predominantly azimuthal (field lines which circle the solar axis), so that the sunspot pairs are aligned (almost) with a line of latitude. They rotate with the surface of the sun, the leading spot being slightly closer to the equator than the following spot. Leading and following spots are observed to have opposite orientations of **B**, as you would expect. However, all pairs in one hemisphere have the same orientation (e.g. **B** directed outward in the leading spot and **B** directed inward in the following spot) and this orientation reverses as we move from one hemisphere to the other. This suggests that the sub-surface azimuthal field is unidirectional in each hemisphere and antisymmetric about the equator: a picture which is consistent with an azimuthal field being swept out from a dipole field by differential rotation (see §4.5.3). Crucially, however, the field orientation in the sunspot pairs reverses from one 11-year cycle to the next, suggesting a periodic variation of the subsurface azimuthal field every 22 years. If this azimuthal field is generated from a dipole field by differential rotation, then this, in turn, suggests a periodicity in the dipole field, or else a periodic reversal in the differential rotation which sweeps out the azimuthal field. If the latter were true there would be no need for a solar dynamo to explain the 22-year cycle. However, observation suggests that it is the first explanation which is correct. The sun's poloidal (dipole) field appears to reverse at the sunspot maximum, strongly sug-

gesting (but not proving) that the solar magnetic field is maintained by dynamo action in the convective zone.

6.3.4 The location of the solar dynamo

It might be thought that the entire convective zone contributes equally to dynamo action, and indeed this was once taken to be the case. However, recently it has been suggested that much of the dynamo action occurs in a relatively thin layer at the interface of the radiative and convection zones. In part, this change in view arose from measurements of rotation in the sun which suggest that differential rotation is concentrated at this interface and so this thin layer is likely to be the location of intense azimuthal field generation.

Mathematical models of the solar dynamo have been proposed based on this idea, including, for example, an α–Ω model. In this picture, strong azimuthal fields build up at the base of the convective zone due to differential rotation (the Ω-effect). These fields support low-frequency magnetostrophic waves (see Section 6.1) which, when combined with buoyancy-driven motion, regenerate a dipole field from the azimuthal one (the α-effect). However, such a model is, perhaps, a little idealistic, representing a convenient conceptual framework which captures key physical mechanisms, but not really providing a truly predictive model of the solar dynamo. As with the geo-dynamo, much remains to be done.

6.3.5 Solar flares

The solar atmosphere is anything but passive. It is threaded with vast magnetic flux tubes which arch up from the photosphere into the corona and which are constantly evolving, being jostled by the convective motions in the photosphere (see Figure 4.3). Some of these flux tubes are associated with sunspots, others are associated with so-called *prominences*. Prominences extend from the chromosphere up into the corona, appearing as arch-like, tubular structures of length $\sim 10^5$ km and thickness $\sim 10^4$ km. They contain cold, chromospheric gas, perhaps 300 times colder than the surrounding coronal gas. This relatively cold plasma is threaded by a magnetic field of ~ 10 Gauss, which is much weaker than that in a sunspot, but larger than the mean surface field of ~ 1 Gauss. A prominence is itself immersed in, and surrounded by,

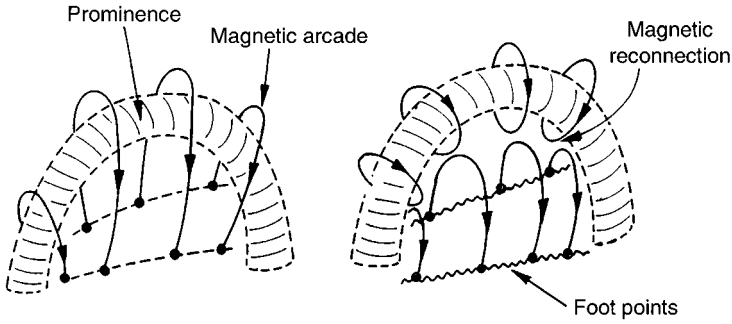

Figure 6.14 (b) A cartoon of a two-ribbon solar flare.

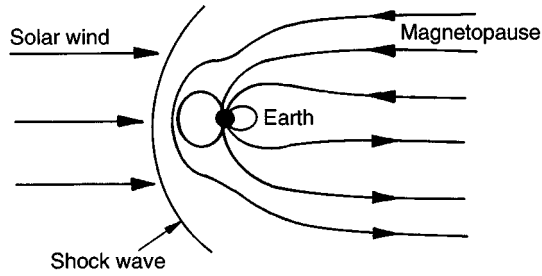

Figure 6.14 (c) The solar wind.

thinner flux tubes which arch up from the photosphere, criss-crossing the prominence. Some flux tubes lie below the prominence, providing a magnetic cushion. Others lie above, pushing down on the prominence. The flux tubes which overlie the prominences are sometimes referred to as a *magnetic arcade*.

Quiescent prominences are stable, long-lived structures which survive for many weeks, while *explosively eruptive prominences* give rise to spectacular releases of mass and energy in relatively short periods of time (hours). The mass which is propelled from the sun in this way is called a coronal mass ejection (CME), and the sudden release of energy is called a *solar flare*.

As yet, there is no self-consistent model for solar flares, although all current theories agree that the power source is stored magnetic energy whose release is triggered by magnetic reconnection. The largest flares

are called *two-ribbon-flares* and they are thought to arise as follows. Consider a prominence which is supported by a magnetic cushion and has a magnetic arcade overlying it. Now suppose that the prominence starts to rise, perhaps because of a build-up of magnetic pressure in the magnetic cushion (which itself might arise from the photospheric jostling of the flux tube roots). The field lines in the overlying arcade, which also have their roots in the photosphere, will become increasingly stretched. Eventually, large gradients in **B** will build up, allowing magnetic reconnections to occur. This, in turn, allows the arcade flux tubes to 'pinch off', releasing magnetic energy, as shown in Figure 6.14(b). When this occurs the downward force associated with the overlying flux tubes is suddenly removed and so the prominence is propelled explosively upward by the magnetic pressure in the underlying magnetic cushion. Some of this energy is also propagated down the arcade field lines to their foot points in the chromosphere and photosphere. The footprints of these field lines then appear as two highly energetic 'ribbons' in the chromosphere – hence the name.

It has to be said, however, that this picture is rather simplistic. Recent measurements suggest that there is not a one-to-one correspondence between coronal mass ejection and solar flares. Often CMEs occur without flares while flares need not be accompanied by a CME. Clearly, the entire process is much more complicated than that suggested above.

Whatever the true explanation of solar flares, it cannot be denied that they are spectacular events. They are vast in scale, extending over $\sim 10^5$ km, and release prodigious amounts of energy, of the order of $\sim 10^{25}$ J. This sudden release of mass and energy enhances the solar wind which, even in quiescent times, spirals radially outward from the sun. At times of vigorous solar activity (at sunspot maximum) the concentration of particles in the solar wind can increase from $\sim 5 \times 10^6\ \mathrm{m}^{-3}$ to $\sim 10^7\ \mathrm{m}^{-3}$, and their velocity rises from around 400 km/s to 900 km/s. The mass released by these solar flares sweeps through the solar system and one or two days after a large flare is observed the earth is buffeted by magnetic storms.

Such storms can cause significant damage, as one Canadian power company discovered to its embarrassment in 1989. Around the 11th of March 1989 a large solar flare burst from the surface of the sun, and as dawn broke on the 13th of March six million Canadians found themselves without power!

6.4 Energy-Based Stability Theorems for Ideal MHD

One of the major successes of high-R_m MHD lies in the area of stability theory. This has its roots, not in liquid-metal MHD, but rather in plasma physics. A question which is often asked in fluid mechanics is: 'Is a given equilibrium or steady motion stable to small disturbances?' That is to say, if a steady flow is disturbed, will it evolve into a radically different form or will it remain close (in some sense) to its initial distribution. The method used most often to answer this question is so-called normal mode analysis. This proceeds by looking for small amplitude disturbances which are of the separable form $\delta\mathbf{u}(\mathbf{x}, t) = \mathbf{u}_0(\mathbf{x})e^{pt}$. When quadratic terms in the small disturbance are neglected the governing equations of motion become linear in $\delta\mathbf{u}$, and this defines an eigenvalue problem for the amplitude of the disturbance, $\mathbf{u}_0(\mathbf{x})$. The eigenvalues of this equation determine p, and the motion is deemed to be unstable if any p can be found which has a real positive part. This works well when the geometry of the base flow is particularly simple, possessing a high degree of symmetry, e.g. one-dimensional flow. However, if there is any significant complexity to the base flow (it is two- or three-dimensional) this procedure rapidly becomes very messy, requiring numerical methods to determine the eigenvalues.

In MHD an alternative method has been developed, which relies on the conservation of energy. This has the advantage that it may be applied to equilibria of arbitrary complexity, but it has two major short-comings. First, it applies only to non-dissipative systems ($\lambda = \nu = 0$), which we might call *ideal MHD*. Second, it usually provides sufficient, but not necessary, conditions for stability. Thus often an equilibrium may be proved stable, but it cannot be shown to be unstable. We shall describe this energy method here. First, however, we shall discuss the motivation for developing special stability methods in MHD.

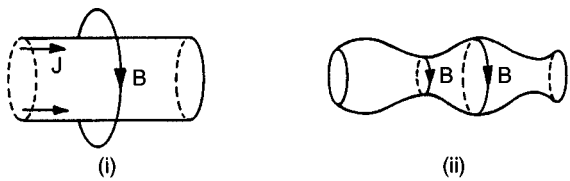

Figure 6.15 The linear pinch. (i) The confinement principle. (ii) Instability of the pinch.

6.4.1 The need for stability theorems in ideal MHD: plasma containment

In the 1950s the quest for controlled thermonuclear fusion began in earnest. This required that the (very) hot plasma be confined away from material surfaces, and since these plasmas are good conductors, magnetic pressure seemed the obvious confinement mechanism. A simple confinement system is shown in Figure 6.15. An axial current is induced in the surface of the plasma, which is in the form of a cylinder, and the resulting azimuthal field creates a radial Lorentz force which is directed inward. (To form a more compact confinement system, the cylinder could be deformed into a torus.) This configuration is known as the linear pinch. Regrettably, it is unstable. Let I be the total current passing along the column. Then the surface field is $B_\theta = \mu I/2\pi R$ where R is the radius of the column. If R locally decreases for some reason, then B_θ rises by an amount $\delta B_\theta = B_\theta \delta R/R$. A 'sausage-mode' instability then develops because there is a rise in magnetic pressure, $\delta p_m = B_\theta \delta B_\theta/\mu$, at precisely those points where the radius reduces.

This sausage-mode instability may be stabilised by trapping a longitudinal magnetic field, B_L, within the plasma. The idea is the following. If λ is very small then this longitudinal field is frozen into the plasma, so if R reduces locally to $R - \delta R$, the longitudinal magnetic field will increase by an amount $\delta B_L = 2B_L \delta R/R$, the total longitudinal flux remaining constant. The magnetic pressure due to B_L therefore increases by $\delta p_m = B_L \delta B_L/\mu = 2B_L^2 \delta R/\mu R$ and this tends to counterbalance the rise in 'pinch pressure' $\delta p_m = B_\theta^2 \delta R/\mu R$. The column is then stable to axisymmetric disturbances provided that $B_L^2 > B_\theta^2/2$.

Unfortunately, this is not the end of the story. The column is unstable to non-axisymmetric disturbances even in the presence of a longitudinal field. This is known as the *kink instability*. Suppose that the column is bent slightly, as shown in Figure 6.16. The field lines are pressed together on the concave side, and spaced out on the other side. Thus the magnetic field, and hence the magnetic pressure, is increased on the concave side of

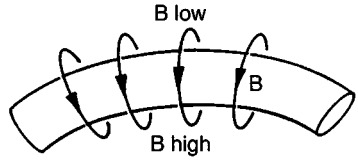

Figure 6.16 The kink instability.

the column and reduced on the convex side. This produces a net sideways force which accentuates the initial disturbance.

In fact, confining plasmas using magnetic fields turns out to be altogether rather tricky. It is not just the linear pinch which is unstable. In the late 1950s, plasma physicists were faced with the problem of deciding which confinement schemes were unstable. Conventional, normal-mode techniques seemed cumbersome and so a new stability theory was developed (primarily at Princeton), first for magnetostatic equilibria, such as that shown in Figure 6.15, and shortly afterwards for any steady solution of the equations of ideal MHD, static or otherwise. This new method is based on the conservation of energy, and in fact it is more in line with our intuitive notions of stability than conventional normal-mode analysis. For example, it predicts that a magnetostatic equilibrium is stable if its magnetic energy is a minimum at equilibrium. Unfortunately, though, the proof of these new stability theorems requires a great deal of vector manipulation. Consequently, the proofs which follow are not for the impatient or the faint-hearted. The end result, though, is rewarding.

6.4.2 The energy method for magnetostatic equilibria

To get an idea of how conservation of energy may be used in a stability analysis, we first consider the simpler problem of the magnetostatic equilibrium of an ideal, incompressible fluid. The fluid and magnetic field are both assumed to be contained in a volume, V, with a solid surface, S, and the equilibrium is governed by

$$\mathbf{J}_0 \times \mathbf{B}_0 = \nabla P_0, \qquad \mathbf{B}_0 \cdot d\mathbf{S} = 0$$

Here the subscript 0 indicates a steady, base configuration whose stability is in question, and $d\mathbf{S}$ is an element of the boundary, S. Now suppose that this equilibrium is slightly disturbed, and that during the initial disturbance the magnetic field is frozen into the fluid. Let $\boldsymbol{\zeta}(\mathbf{x}, t)$ be the displacement of a particle, p, from its equilibrium position $\mathbf{x}$,

$$\boldsymbol{\zeta}(\mathbf{x}, t) = \mathbf{x}_p(t) - \mathbf{x}_p(0), \qquad \mathbf{x}_p(0) = \mathbf{x}$$

Following the initial disturbance some motion will ensue, perhaps in the form of an oscillation, e.g. Alfvén waves, or perhaps something rather more drastic. In any event, $\mathbf{B}$ will be frozen into the fluid and the resulting velocity field, $\mathbf{u}(\mathbf{x},t)$, is related to the instantaneous particle displacement, $\boldsymbol{\zeta}$, by

$$\frac{\partial \boldsymbol{\zeta}}{\partial t} = \mathbf{u}(\mathbf{x} + \boldsymbol{\zeta}, t) = \mathbf{u}(\mathbf{x}) + \boldsymbol{\zeta} \cdot \nabla \mathbf{u} + \ldots \tag{6.15}$$

Let us now evaluate the change in magnetic energy, E_B, which results from the particle displacement, $\boldsymbol{\zeta}$. We first expand E_B in a series

$$E_B(\boldsymbol{\zeta}, t) = \int (\mathbf{B}^2/2\mu) dV = E_{B0} + \delta^1 E_B + \delta^2 E_B + \ldots$$

Here $\delta^1 E_B$ and $\delta^2 E_B$ are the first- and second-order changes in E_B, $\boldsymbol{\zeta}$ being assumed small at all times. We shall see shortly that $\delta^1 E_B = 0$, while the stability of the magnetostatic equilibrium is determined by the sign of $\delta^2 E_B$. Specifically, if $\delta^2 E_B$ is positive, so that E_B is a minimum at equilibrium, the magnetic field is stable. The question, then, is how to evaluate $\delta^1 E_B$ and $\delta^2 E_B$. We now employ a trick. E_B depends only on the instantaneous position of the fluid particles and not their previous histories. That is, E_B is completely determined by the instantaneous spatial distribution of $\mathbf{B}$. There are infinitely many ways in which each particle could get from $\mathbf{x}$ to $\mathbf{x} + \boldsymbol{\zeta}$, but, since E_B does not care about the history of the particles, we shall consider the simplest. Suppose that we apply an imaginary, steady velocity field, $\mathbf{v}(\mathbf{x})$, to the fluid for a short time τ. We choose $\mathbf{v}(\mathbf{x})$ such that it shifts the fluid from its equilibrium configuration to $\mathbf{x} + \boldsymbol{\zeta}$. Since the fluid is incompressible, $\mathbf{v}(\mathbf{x})$ must be solenoidal. We shall call $\mathbf{v}(\mathbf{x})$ a *virtual velocity field* (Figure 6.17). Since $\mathbf{B}$ is frozen into the fluid during the application of $\mathbf{v}$ we have

$$\frac{\partial \mathbf{B}}{\partial t} = \nabla \times (\mathbf{v} \times \mathbf{B}), \qquad 0 < t < \tau \tag{6.16}$$

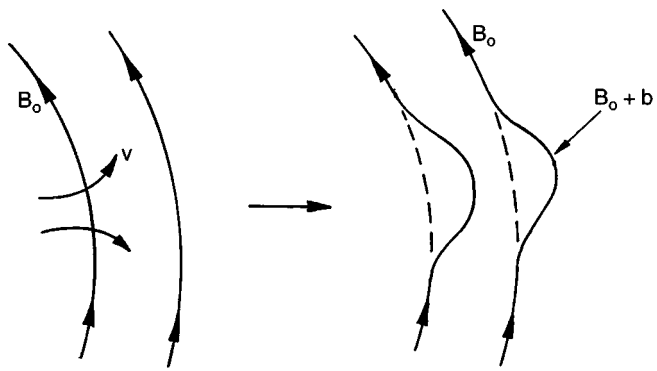

Figure 6.17 Perturbation of $\mathbf{B}_0$ by a virtual velocity field.

It follows that the first- and second-order changes in **B** are

$$\delta^1\mathbf{B} = \nabla \times (\boldsymbol{\eta} \times \mathbf{B}_0) \tag{6.17a}$$

$$\delta^2\mathbf{B} = \frac{1}{2}\nabla \times (\boldsymbol{\eta} \times \delta^1\mathbf{B}) \tag{6.17b}$$

where $\boldsymbol{\eta} = \mathbf{v}\tau$. This new fields satisfies

$$\nabla \cdot \boldsymbol{\eta} = 0, \qquad \boldsymbol{\eta} \cdot d\mathbf{S} = 0 \tag{6.18}$$

We shall call $\boldsymbol{\eta}$ the *virtual displacement field* in order to distinguish it from the Lagrangian particle displacement $\boldsymbol{\zeta}$. Note that $\boldsymbol{\eta}$ and $\boldsymbol{\zeta}$ are not identical. During the application of our imaginary velocity field, $\mathbf{v}(\mathbf{x})$, we have, from (6.15),

$$\frac{\partial \boldsymbol{\zeta}}{\partial t} = \mathbf{v}(\mathbf{x} + \boldsymbol{\zeta}) = \mathbf{v}(\mathbf{x}) + \boldsymbol{\zeta} \cdot \nabla \mathbf{v} + \ldots$$

It follows that

$$\boldsymbol{\zeta} = \boldsymbol{\eta} + \frac{1}{2}\boldsymbol{\eta} \cdot \nabla \boldsymbol{\eta} + \ldots \tag{6.19a}$$

$$\boldsymbol{\eta} = \boldsymbol{\zeta} - \frac{1}{2}\boldsymbol{\zeta} \cdot \nabla \boldsymbol{\zeta} + \ldots \tag{6.19b}$$

Thus, the particle displacement and the virtual displacement are equal only at first order. Let us now use (6.17) to evaluate the changes in E_B which result from the application of $\boldsymbol{\eta}$. The first-order change is

$$\delta^1 E_B = \frac{1}{\mu}\int (\mathbf{B}_0 \cdot \delta^1\mathbf{B}) dV = \frac{1}{\mu}\int \mathbf{B}_0 \cdot \nabla \times [\boldsymbol{\eta} \times \mathbf{B}_0] dV$$

which we might anticipate is zero. To show that this is indeed the case, we note that the integrand may be rewritten as

$$\mathbf{B}_0 \cdot \nabla \times [\boldsymbol{\eta} \times \mathbf{B}_0] = (\boldsymbol{\eta} \times \mathbf{B}_0) \cdot (\nabla \times \mathbf{B}_0) + \nabla \cdot [(\boldsymbol{\eta} \times \mathbf{B}_0) \times \mathbf{B}_0]$$

Rearranging the scalar triple product and expanding the vector triple product yields

$$\mathbf{B}_0 \cdot \nabla \times [\boldsymbol{\eta} \times \mathbf{B}_0] = -\mu(\mathbf{J}_0 \times \mathbf{B}_0) \cdot \boldsymbol{\eta} + \nabla \cdot \left[(\mathbf{B}_0 \cdot \boldsymbol{\eta})\mathbf{B}_0 - \mathbf{B}_0^2 \boldsymbol{\eta}\right]$$

The divergence integrates to zero and so

$$\delta^1 E_B = -\int \boldsymbol{\eta} \cdot (\nabla P_0) dV = -\int \nabla \cdot [P_0 \boldsymbol{\eta}] dV = 0$$

The first-order change in energy is evidently zero, as stated above. The second-order change is

$$\delta^2 E_B = \frac{1}{\mu}\int\left[\frac{1}{2}\left(\delta^1\mathbf{B}\right)^2 + \mathbf{B}_0 \cdot \delta^2\mathbf{B}\right]dV$$

from which,

$$\boxed{\delta^2 E_B = \frac{1}{2\mu}\int\left[\mathbf{b}^2 + \mathbf{B}_0 \cdot \nabla \times [\boldsymbol{\eta} \times \mathbf{b}]\right]dV, \qquad \mathbf{b} = \nabla \times [\boldsymbol{\eta} \times \mathbf{B}_0]} \quad (6.20a)$$

Now $\boldsymbol{\eta}$ is an imaginary displacement resulting from our virtual velocity field. However, we have $\boldsymbol{\eta} = \boldsymbol{\zeta} - \frac{1}{2}\boldsymbol{\zeta} \cdot \nabla\boldsymbol{\zeta} + \text{H.O.T.}$ and so when we substitute for $\boldsymbol{\eta}$ and discard cubic and higher-order terms we find that

$$\boxed{\delta^2 E_B = \frac{1}{2\mu}\int\left[\mathbf{b}^2 + \mathbf{B}_0 \cdot \nabla \times [\boldsymbol{\zeta} \times \mathbf{b}]\right]dV, \qquad \mathbf{b} = \nabla(\boldsymbol{\zeta} \times \mathbf{B}_0)} \quad (6.20b)$$

This gives us the instantaneous perturbations in magnetic energy and magnetic field (to leading order) at any instant in terms of the Lagrangian particle displacement field, $\boldsymbol{\zeta}(x, t)$. Now we expect the equilibrium to be stable if E_B is a minimum at equilibrium, i.e. $\delta^2 E_B > 0$. We now show that this is indeed the case. First we note that the total energy is conserved in ideal MHD, that is, the momentum equation gives us

$$\frac{D}{Dt}\left(\frac{1}{2}\rho\mathbf{u}^2\right) = -\nabla \cdot (P\mathbf{u}) + (\mathbf{J} \times \mathbf{B}) \cdot \mathbf{u}$$

while the dot product of $\mathbf{B}$ with the induction equation yields, after a little work,

$$\frac{\partial}{\partial t}\left(\mathbf{B}^2/(2\mu)\right) = (\mathbf{u} \times \mathbf{B}) \cdot \mathbf{J} + \nabla \cdot [(\mathbf{u} \times \mathbf{B}) \times (\mathbf{B}/\mu)]$$

Rearranging the scalar triple product and combining the two we have

$$\frac{\partial}{\partial t}\left[\frac{B^2}{2\mu} + \frac{\rho\mathbf{u}^2}{2}\right] = -\nabla \cdot \left[\left(p + \frac{1}{2}\rho\mathbf{u}^2\right)\mathbf{u} + (\mathbf{u} \times \mathbf{B}) \times (\mathbf{B}/\mu)\right]$$

If we take $\mathbf{B} \cdot d\mathbf{S} = \mathbf{u} \cdot d\mathbf{S} = 0$ at the boundary (we are assuming $\mathbf{B}$ is contained within V), then this gives us conservation of energy in the form

$$E = E_u + E_B = \frac{1}{2}\int\left[\rho\mathbf{u}^2 + \mathbf{B}^2/\mu\right]dV = \text{constant} \quad (6.21)$$

It follows that, for our perturbed magnetostatic equilibrium,

$$E - E_0 = \frac{1}{2}\int [\rho \mathbf{u}^2] dV + \delta^2 E_B = \text{constant}$$

(cubic and higher-order terms have been neglected here). We also have, to leading order in ζ, $\mathbf{u}(\mathbf{x}, t) = \dot{\zeta}(\mathbf{x}, t)$. Conservation of energy therefore gives us

$$\boxed{\int \left[\frac{1}{2}\rho \dot{\zeta}^2\right] dV + \delta^2 E_B = \text{constant} = \Delta E} \tag{6.22}$$

where $\dot{\zeta}$ indicates a partial derivative with respect to time. We can now, at last, discuss stability. We take as our definition of stability the condition that the kinetic energy of the disturbance is always bounded from above by the initial energy of the disturbance, ΔE. In effect, this limits the size of the resulting velocity field. It follows that an equilibrium is stable if $\delta^2 E_B$ is positive for all possible shapes of disturbances. That is to say, stability is ensured if $\delta^2 E_B > 0$ for all possible ζ (or η). Thus, to show that a magnetostatic equilibrium is stable we merely need to demonstrate that (6.20) is positive for any choice of η. We have, in effect, a form of stability test.

All of this is in accord with our intuitive notions of stability. We may think of E_B as potential energy, in the sense that it is the conserved energy of a force acting on the fluid. Like a ball sitting on a hillside, the fluid (or ball) is in equilibrium if the potential energy is stationary, $\delta^1 E_B = 0$, and it is stable if the potential (i.e. magnetic) energy is a minimum (Figure 6.18).

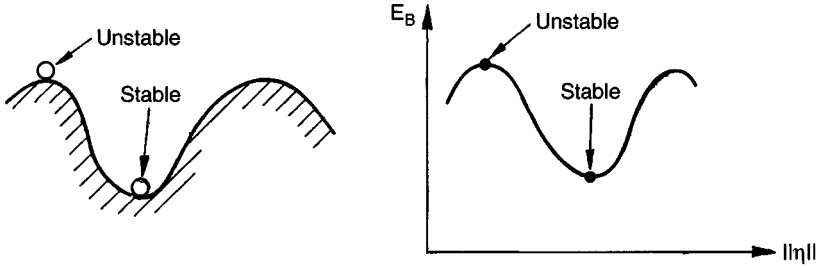

Figure 6.18 Analogy between magnetostatic and mechanical equilibria.

6.4.3 An alternative method for magnetostatic equilibrium

Now there is a different, though ultimately equivalent, route to establishing this stability criterion. This alternative method proves more useful when working with non-static equilibria, and so we shall describe it in some detail. The idea is to develop a dynamic equation for the disturbance. This time we work, not with the virtual displacement field, $\boldsymbol{\eta}$, but rather with the particle displacement, $\boldsymbol{\zeta}$. Of course, to leading order in the amplitude of the disturbance, $\boldsymbol{\zeta}$ and $\boldsymbol{\eta}$ are equal. We also work only with first-order quantities, such as $\mathbf{b} = \delta^1\mathbf{B}$, and discard all higher-order terms. The induction and momentum equations then give us the disturbance equations

$$\frac{\partial \mathbf{b}}{\partial t} = \nabla \times (\mathbf{u} \times \mathbf{B}_0)$$

$$\rho \frac{\partial \mathbf{u}}{\partial t} = \mathbf{j} \times \mathbf{B}_0 + \mathbf{J}_0 \times \mathbf{b} - \nabla p$$

Here lower-case letters represent perturbed quantities, e.g. $\mathbf{J} = \mathbf{J}_0 + \mathbf{j}$, and quadratic terms in the disturbance, such as $\mathbf{u} \cdot \nabla \mathbf{u}$ or $\mathbf{j} \times \mathbf{b}$, are neglected. We also have, to leading order,

$$\dot{\boldsymbol{\zeta}}(\mathbf{x}, t) = \mathbf{u}(\mathbf{x}, t), \qquad \nabla \cdot \boldsymbol{\zeta} = 0, \qquad \boldsymbol{\zeta} \cdot d\mathbf{S} = 0$$

The perturbation equations then give us

$$\mathbf{b} = \nabla \times (\boldsymbol{\zeta} \times \mathbf{B}_0) \tag{6.23}$$

$$(\rho\mu)\ddot{\boldsymbol{\zeta}} = (\nabla \times \mathbf{b}) \times \mathbf{B}_0 + (\nabla \times \mathbf{B}_0) \times \mathbf{b} - \nabla p \tag{6.24}$$

The first of these is a restatement of (6.17a), since $\boldsymbol{\zeta} = \boldsymbol{\eta}$ to leading order. The second equation may be rewritten as

$$(\rho\mu)\ddot{\boldsymbol{\zeta}} = \mathbf{F}(\boldsymbol{\zeta}) + \nabla(\cdot) \tag{6.25}$$

where $\nabla(\cdot)$ denotes the gradient of some scalar function whose value does not concern us, and

$$\mathbf{F}(\boldsymbol{\zeta}) = (\nabla \times \mathbf{b}) \times \mathbf{B}_0 + (\nabla \times \mathbf{B}_0) \times \mathbf{b}, \qquad \mathbf{b} = \nabla \times (\boldsymbol{\zeta} \times \mathbf{B}_0) \tag{6.26}$$

It is straightforward, but tedious, to show that the linear force operator $\mathbf{F}(\boldsymbol{\zeta})$ is self-adjoint, in the sense that

$$\int \boldsymbol{\zeta}_1 \cdot \mathbf{F}(\boldsymbol{\zeta}_2) dV = \int \boldsymbol{\zeta}_2 \cdot \mathbf{F}(\boldsymbol{\zeta}_1) dV \tag{6.27}$$

We now multiply (6.25) by $\dot{\zeta}$, and invoke (6.27) in the form, $\zeta_1 = \zeta$, $\zeta_2 = \dot{\zeta}$ The result is an energy-like equation

$$\frac{d}{dt}\int\left(\frac{1}{2}\rho\dot{\zeta}^2\right)dV = \frac{d}{dt}\left[\frac{1}{2\mu}\int \mathbf{F}(\zeta)\cdot\zeta dV\right] \tag{6.28}$$

The next step is to evaluate the integral on the right. In fact, it may be shown that

$$W(\zeta) = -\frac{1}{2\mu}\int \mathbf{F}(\zeta)\cdot\zeta dV = \delta^2 E_B \tag{6.29}$$

which, when combined with (6.28), gets us back to the energy stability criterion (6.22). The proof of (6.29) is a little involved and so we give here a schematic outline only.

Schematic proof of (6.29)

First we need a vector identity based on the equilibrium equation $\mathbf{J}_0 \times \mathbf{B}_0 = \nabla P_0$

$$\mathbf{J}_0 \times [\nabla \times (\mathbf{q} \times \mathbf{B}_0)] + [\nabla \times (\mathbf{q} \times \mathbf{J}_0)] \times \mathbf{B}_0 = -\nabla(\mathbf{q}\cdot\nabla P_0) \tag{6.30}$$

where $\mathbf{q}$ is any solenoidal field. (We shall not pause to prove (6.30).) Next we take $\mathbf{q} = \zeta$ and rewrite (6.26) as

$$\mathbf{F}(\zeta) = \nabla \times [\nabla \times (\zeta \times \mathbf{B}_0) - \zeta \times (\nabla \times \mathbf{B}_0)] \times \mathbf{B}_0 + \nabla(\cdot)$$

from which

$$\mathbf{F}(\zeta)\cdot\zeta = -(\zeta \times \mathbf{B}_0)\cdot\nabla \times [\nabla \times (\zeta \times \mathbf{B}_0) - \zeta \times (\nabla \times \mathbf{B}_0)] + \zeta\cdot\nabla(\cdot)$$

After a little algebra we find

$$\int \mathbf{F}(\zeta)\cdot\zeta dV = -\int [\mathbf{b}^2 + \mathbf{B}_0\cdot\nabla \times [\zeta \times \mathbf{b}]]dV \tag{6.31}$$

It is evident from (6.20b) that the right-hand integral is equal to $-2\mu\delta^2 E_B$ and so

$$W(\zeta) = -\frac{1}{2\mu}\int \mathbf{F}(\zeta)\cdot\zeta dV = \delta^2 E_B$$

as required.

It follows from (6.29) and our energy-like equation (6.28) that the sum of the kinetic energy of the disturbance, plus $\delta^2 E_B$, is conserved in the linear approximation, i.e.

$$\int \frac{1}{2}\rho\dot{\zeta}^2 dV + \delta^2 E_B = \text{constant} \tag{6.32}$$

Of course, this is identical to (6.22). Once again we conclude that the magnetostatic equilibrium is stable if $\delta^2 E_B$ is positive for all possible $\boldsymbol{\zeta}$ (or equivalently, all possible $\boldsymbol{\eta}$). This is known as *Bernstein's stability criterion.*

6.4.4 Proof that the energy method provides both necessary and sufficient conditions for stability

This second proof of (6.32) is less elegant than the first. However, it does set the scene for our more general stability analysis ($\mathbf{u}_0 \neq 0$). In fact, we can push this second method a little further. It can be used to establish both necessary and sufficient conditions for stability. That is to say, a magnetostatic equilibrium is stable if and only if E_B is a minimum. The proof of the necessity of $\delta^2 E_B > 0$ is as follows: suppose that $W(\boldsymbol{\zeta}) < 0$ for some $\boldsymbol{\zeta} = \boldsymbol{\zeta}^*$. Then we introduce a constant, γ, defined by

$$W(\boldsymbol{\zeta}^*) = -\gamma^2 \int \left[\frac{1}{2}\rho \boldsymbol{\zeta}^{*2}\right] dV$$

Next we note that (6.24) is second order in t, and so $\boldsymbol{\zeta}$ and $\dot{\boldsymbol{\zeta}}$ may be specified separately at $t = 0$. We choose $\boldsymbol{\zeta}(0) = \boldsymbol{\zeta}^*$ and $\dot{\boldsymbol{\zeta}}(0) = \gamma \boldsymbol{\zeta}^*$ The total disturbance energy is then zero and so, for all t,

$$\frac{1}{2}\int \rho \dot{\boldsymbol{\zeta}}^2 dV = -W(\boldsymbol{\zeta}) \tag{6.33}$$

We now return to (6.25) which, on multiplication by $\boldsymbol{\zeta}$ and integration over V, yields

$$\frac{1}{2}\ddot{I} = \frac{1}{2}\int \rho \dot{\boldsymbol{\zeta}}^2 dV - W(\boldsymbol{\zeta})$$

where $I = \frac{1}{2}\rho \int \boldsymbol{\zeta}^2 dV$. Combining this with (6.33) gives us

$$\frac{1}{2}\ddot{I} = \int \rho \dot{\boldsymbol{\zeta}}^2 dV \tag{6.34}$$

Now the Schwartz inequality tells us that

$$\dot{I}^2 \leq 2I \int \rho \dot{\boldsymbol{\zeta}}^2 dV$$

and so (6.34) may be rewritten as, $I\ddot{I} \geq \dot{I}^2$. This, in turn, ensures the exponential growth of any disturbance at a rate, $I \geq I(0)\exp[2\gamma t]$. [The proof of this last statement can be verified by making the substitution $y = \ln(I/I(0))$, which yields $\ddot{y} \geq 0$. Integrating this equation subject to $\dot{y}(0) = 2\gamma$ and $y(0) = 0$ gives $y \geq 2\gamma t$.] Thus a magnetostatic equilibrium

is stable if and only if E_B is a minimum. Unfortunately, when we extend the energy method to the stability of non-static equilibria ($\mathbf{u}_0 \neq 0$), we obtain only sufficient conditions for stability. That is to say, we can prove that a given flow is stable, but not that it is unstable.

6.4.5 The stability of non-static equilibria

We now repeat these arguments, but for equilibria in which $\mathbf{u}_0$ is non-zero. Our aim is to use conservation of energy to provide a sufficient condition for stability. To avoid carrying the constants ρ and μ all the way through the analysis, we take $\rho = \mu = 1$. (In effect, we rescale $\mathbf{B}$ as $\mathbf{B}/(\rho\mu)^{1/2}$.) Also, in the interests of simplicity, we shall take $\mathbf{B}$ to be confined to the fluid domain, V. Now the development of a more general stability criterion turns out to be no more difficult than the magnetostatic case, at least at a conceptual level. However, the algebra is long and tedious. We shall therefore give a schematic proof only. We start with

$$\frac{\partial \mathbf{u}}{\partial t} = \mathbf{u} \times \boldsymbol{\Omega} - \mathbf{B} \times \mathbf{J} - \nabla C, \qquad \mathbf{u} \cdot d\mathbf{S} = 0$$

$$\frac{\partial \mathbf{B}}{\partial t} = \nabla \times (\mathbf{u} \times \mathbf{B}), \qquad \mathbf{B} \cdot d\mathbf{S} = 0$$

which are the governing equations of ideal MHD. Here C is Bernoulli's function and $\boldsymbol{\Omega}$ is the vorticity. It is readily confirmed that these are consistent with the conservation of energy $E = \frac{1}{2}\int (\mathbf{u}^2 + \mathbf{B}^2) dV$ (see (6.21)). Steady flows are governed by

$$\mathbf{u}_0 \times \mathbf{B}_0 = \nabla D \tag{6.35}$$

$$\mathbf{u}_0 \times \boldsymbol{\Omega}_0 - \mathbf{B}_0 \times \mathbf{J}_0 = \nabla C_0 \tag{6.36}$$

and it is the stability of equilibria governed by these equations which concern us here. At this point it is convenient to introduce two vector identities, analogous to (6.30), which stem directly from the equilibrium equations. If $\mathbf{q}$ is any solenoidal field, then it may be shown that

$$\mathbf{u}_0 \times [\nabla \times (\mathbf{q} \times \mathbf{B}_0)] + [\nabla \times (\mathbf{q} \times \mathbf{u}_0)] \times \mathbf{B}_0 = -\nabla(\mathbf{q} \cdot \nabla D) \tag{6.37}$$

$$\mathbf{u}_0 \times [\nabla \times (\mathbf{q} \times \boldsymbol{\Omega}_0)] + [\nabla \times (\mathbf{q} \times \mathbf{u}_0)] \times \boldsymbol{\Omega}_0 + \mathbf{J}_0 \times [\nabla \times (\mathbf{q} \times \mathbf{B}_0)] + [\nabla \times (\mathbf{q} \times \mathbf{J}_0)] \times \mathbf{B}_0 = -\nabla(\mathbf{q} \cdot \nabla C_0) \tag{6.38}$$

We shall not pause to prove these uninspiring-looking relationships, but they will be used in the analysis which follows.

We now consider small-amplitude perturbations in $\mathbf{u}_0$ and $\mathbf{B}_0$, in which $\mathbf{B} = \mathbf{B}_0 + \mathbf{b}$, $(\mathbf{b} \cdot d\mathbf{S} = 0)$ and $\mathbf{u} = \mathbf{u}_0 + \delta\mathbf{u}$, $(\delta\mathbf{u} \cdot d\mathbf{S} = 0)$. Related quantities are $\mathbf{j} = \nabla \times \mathbf{b}$ and $\omega = \nabla \times (\delta\mathbf{u})$. In the analysis which follows we shall ignore all quantities which are quadratic, or of higher order, in the amplitude of the disturbance. As with the magnetostatic stability analysis, our first step is to introduce the particle displacement field $\zeta(\mathbf{x}, t)$, defined by

$$\zeta(\mathbf{x}, t) = \mathbf{x}_p(t) - \mathbf{x}_{p0}(t)$$

where $\mathbf{x}_{p0}$ is the position vector of particle p in the base flow and $\mathbf{x}_p$ is the position of the same particle in the perturbed flow. The generalisation of (6.15) is then

$$\frac{D\zeta}{Dt} = \mathbf{u}(\mathbf{x} + \zeta, t) - \mathbf{u}_0(\mathbf{x})$$

In the linear (small-amplitude) approximation, this becomes

$$\frac{\partial \zeta}{\partial t} + \mathbf{u}_0 \cdot \nabla\zeta = \delta\mathbf{u}(\mathbf{x}, t) + \mathbf{u}_0(\mathbf{x} + \zeta) - \mathbf{u}_0(\mathbf{x})$$

which, using the approximation $\mathbf{u}_0(\mathbf{x} + \zeta) - \mathbf{u}_0(\mathbf{x}) = \zeta \cdot \nabla\mathbf{u}_0$, simplifies to

$$\frac{\partial \zeta}{\partial t} = \delta\mathbf{u}(\mathbf{x}, t) - \nabla \times (\zeta \times \mathbf{u}_0) \tag{6.39}$$

Note that, in the small-amplitude approximation, ζ is solenoidal. Also, since $\mathbf{u} \cdot d\mathbf{S} = 0$, we have $\zeta \cdot d\mathbf{S} = 0$. We now turn to the perturbation equations $\mathbf{b}$ and $\delta\mathbf{u}$. When we discard quadratic and higher-order terms in the perturbation, we find

$$\frac{\partial \mathbf{b}}{\partial t} = \nabla \times [\delta\mathbf{u} \times \mathbf{B}_0 + \mathbf{u}_0 \times \mathbf{b}] \tag{6.40}$$

$$\frac{\partial(\delta\mathbf{u})}{\partial t} = \delta\mathbf{u} \times \boldsymbol{\Omega}_0 + \mathbf{u}_0 \times \omega - \mathbf{b} \times \mathbf{J}_0 - \mathbf{B}_0 \times \mathbf{j} - \nabla c \tag{6.41}$$

We concentrate first on the induction equation. Introducing, $\Delta\mathbf{B} = \mathbf{b} - \nabla \times (\zeta \times \mathbf{B}_0)$, this may be rewritten as

$$\frac{\partial}{\partial t}(\Delta\mathbf{B}) = \nabla \times [\mathbf{u}_0 \times \Delta\mathbf{B} + \mathbf{u}_0 \times (\zeta \times \mathbf{B}_0) + \nabla \times (\zeta \times \mathbf{u}_0) \times \mathbf{B}_0]$$

which, by virtue of (6.37), simplifies to

$$\frac{\partial}{\partial t}(\Delta\mathbf{B}) = \nabla \times [\mathbf{u}_0 \times \Delta\mathbf{B}] \tag{6.42}$$

Evidently, if we set $\Delta\mathbf{B} = 0$ at some initial instant, then $\Delta\mathbf{B}$ remains zero for all time. Let us assume that this is so. We then have

$$\mathbf{b} = \nabla \times (\boldsymbol{\zeta} \times \mathbf{B}_0) \tag{6.43}$$

which is identical to (6.23). Setting $\Delta\mathbf{B} = 0$ in the initial condition is therefore equivalent to assuming that $\mathbf{B}$ is frozen into the fluid during the initial disturbance. Such a disturbance might be triggered by, say, a pressure pulse travelling through the fluid. In the analysis which follows, therefore, we shall assume that $\Delta\mathbf{B} = 0$ at $t = 0$ so that (6.43) holds at all times.

We now turn to the momentum equation (6.41). Substituting for $\mathbf{b}$ and $\delta\mathbf{u}$ using (6.39) and (6.43) we find, after a little algebra, that

$$\boxed{\ddot{\boldsymbol{\zeta}} + 2\mathbf{u}_0 \cdot \nabla(\dot{\boldsymbol{\zeta}}) = \mathbf{F}(\boldsymbol{\zeta}) + \nabla(\cdot)} \tag{6.44}$$

Here $\mathbf{F}$ is given by

$$\boxed{\mathbf{F}(\boldsymbol{\zeta}) = (\nabla \times \mathbf{b}) \times \mathbf{B}_0 + (\nabla \times \mathbf{B}_0) \times \mathbf{b} - (\nabla \times \hat{\mathbf{u}}) \times \mathbf{u}_0 - (\nabla \times \mathbf{u}_0) \times \hat{\mathbf{u}}} \tag{6.45}$$

and $\mathbf{b}$ and $\hat{\mathbf{u}}$ are defined by

$$\boxed{\mathbf{b} = \nabla \times (\boldsymbol{\zeta} \times \mathbf{B}_0); \qquad \hat{\mathbf{u}} = \nabla \times (\boldsymbol{\zeta} \times \mathbf{u}_0)} \tag{6.46}$$

It should be noted that, while $\mathbf{b}$ represents the perturbation in $\mathbf{B}$, $\hat{\mathbf{u}}$ does not represent the perturbation in $\mathbf{u}$. Rather, $\hat{\mathbf{u}}$ is the difference between $\delta\mathbf{u}$ and $\dot{\boldsymbol{\zeta}}$: $\hat{\mathbf{u}} = \delta\mathbf{u} - \dot{\boldsymbol{\zeta}}$.

Now compare (6.44) and (6.45) with (6.25) and (6.26). It is clear that we have extended the dynamical equation for $\boldsymbol{\zeta}$ from equilibria in which $\mathbf{u}_0$ is zero to those where it is not. Note that (6.44) and (6.45) reduce to the magnetostatic perturbation equations (6.25) and (6.26) when $\mathbf{u}_0 = 0$, as they should. Note also the skew-symmetric rôles played by $\mathbf{B}_0$ and $\mathbf{u}_0$ in (6.45). It is now a small step to obtain a sufficient condition for stability. In effect, we simply repeat the arguments used in the magnetostatic case. As before, $\mathbf{F}$ is self-adjoint:

$$\int \mathbf{F}(\boldsymbol{\zeta}_1) \cdot \boldsymbol{\zeta}_2 dV = \int \mathbf{F}(\boldsymbol{\zeta}_2) \cdot \boldsymbol{\zeta}_1 dV \tag{6.47}$$

and so (6.44), multiplied by $\dot{\boldsymbol{\zeta}}$, yields

$$\frac{d}{dt}\int \frac{1}{2}\dot{\zeta}^2 dV = \frac{d}{dt}\left[\frac{1}{2}\int \mathbf{F}(\zeta)\cdot\zeta dV\right] \tag{6.48}$$

Also, using (6.37) and (6.38), we can determine the analogue of (6.29). After a little work we find

$$\boxed{W(\zeta) = -\frac{1}{2}\int \mathbf{F}(\zeta)\cdot\zeta dV = \delta^2 E_B - \frac{1}{2}\int\left[(\hat{\mathbf{u}})^2 + \mathbf{u}_0\cdot\nabla\times[\zeta\times\hat{\mathbf{u}}]\right]dV} \tag{6.49}$$

which leads to the conservation equation

$$\boxed{\frac{1}{2}\int\dot{\zeta}^2 dV + \delta^2 E_B - \frac{1}{2}\int\left[(\hat{\mathbf{u}})^2 + \mathbf{u}_0\cdot\nabla\times(\zeta\times\hat{\mathbf{u}})\right]dV = \text{constant}} \tag{6.50}$$

or

$$\boxed{\frac{1}{2}\int\dot{\zeta}^2 dV + W(\zeta) = e = \text{constant}} \tag{6.51}$$

If we take $\int\dot{\zeta}^2 dV$ as a measure of our disturbance, then the equilibrium flow $(\mathbf{u}_0, \mathbf{B}_0)$ is stable whenever $W(\zeta)$ is positive for all possible choices of ζ. This is, in effect, a generalisation of Bernstein's criterion and was developed in the 1960s by researchers working at Princeton on plasma containment.

Unfortunately, we cannot extend the argument to give a necessary condition for stability. The term involving $\mathbf{u}_0$ on the right of (6.44) prevents us from repeating the arguments used for the magnetostatic case. In fact, it is not difficult to construct flows which are stable yet admit negative values of $W(\zeta)$. Consider the axisymmetric flow $\mathbf{u}_0 = \Omega r\hat{\mathbf{e}}_\theta$, $\mathbf{B}_0 = \alpha\mathbf{u}_0$ (for some constants α, Ω) which is confined to $r < R$. If the two-dimensional stability of this flow is examined then (6.44) leads (eventually) to the dynamic equation,

$$\left[\frac{\partial}{\partial t} + \Omega(1+\alpha)\frac{\partial}{\partial\theta}\right]\left[\frac{\partial}{\partial t} + \Omega(1-\alpha)\frac{\partial}{\partial\theta}\right]\nabla^2(r\zeta_r) = 0$$

The resulting solutions are stable Alfvén waves travelling (clockwise or anti-clockwise) along the $\mathbf{B}_0$-lines and riding on the back of the base flow.

$$\zeta_r = \zeta_r(\theta - \Omega(1 \pm \alpha)t)$$

However, it is readily confirmed that $W(\zeta)$ is negative whenever $|\alpha| < 1$, and so this is an example of a flow which violates our stability criterion, yet is perfectly stable.

In summary then, equilibrium solutions of the ideal MHD equations are stable to small disturbances provided that $W(\zeta)$, defined by

$$\boxed{W(\zeta) = \frac{1}{2}\int [\mathbf{b}^2 + \mathbf{B}_0 \cdot \nabla \times (\zeta \times \mathbf{b})]\, dV - \frac{1}{2}\int [\hat{\mathbf{u}}^2 + \mathbf{u}_0 \cdot \nabla \times (\zeta \times \hat{\mathbf{u}})]\, dV} \tag{6.52}$$

$$(\mathbf{b} = \nabla \times (\zeta \times \mathbf{B}_0), \qquad \hat{\mathbf{u}} = \nabla \times (\zeta \times \mathbf{u}_0))$$

is positive for all possible choices of ζ. This is a remarkably general result which has been rediscovered many times by alternative means. It covers magnetostatics, ideal MHD, and inviscid flows in the absence of a magnetic field. Unfortunately, there are relatively few three-dimensional flows for which $W(\zeta)$ can be shown to be positive. However, there are many two-dimensional flows which may be shown to be stable by this method.

It turns out that a simpler derivation of (6.51) and (6.52) may be formulated by appealing directly to Lagrange's equation, and this is described in Appendix 2.

6.5 Conclusion

This concludes our brief exploration of high-R_m dynamics. The subject is an attractive one, rich in physical phenomena and full of unresolved problems. For example, we have discussed stability criteria only in the context of incompressible flows. Yet ideal MHD only really holds in plasma MHD, not liquid-metal MHD, and so actually we want stability criteria for compressible fluids. Then there is dynamo theory. While kinematic aspects of the subject seem well understood, there are many unanswered questions concerning the dynamics of the geo-dynamo and solar dynamo. The interested reader is urged to consult the references given below.

Suggested Reading

H K Moffatt, *Magnetic field generation in electrically conducting fluids*, 1978. Cambridge University Press. (Chapters 6–12 for a very detailed discussion of dynamo theory.)

P H Roberts, *An introduction to magnetohydrodynamics,* 1967, Longmans. (Chapter 3 for dynamo theory (without the α-effect), Chapter 5 for Alfvén waves, Chapters 8 and 9 for stability theory.)

M R E Proctor & A D Gilbert, *Lectures on solar and planetary dynamos*, 1994. Cambridge University Press. (Chapter 1, by P H Roberts, for an introduction to geo-dynamo theory, Chapter 2, by N O Weiss, for solar MHD.)

D Biskamp, *Nonlinear magnetohydrodynamics*, 1993. Cambridge University Press. (Chapter 4 for stability theory.)

Examples

6.1 In an ideal fluid ($\lambda = \nu = 0$) there exist a velocity field $\mathbf{u}$ and a scaled magnetic field $\mathbf{h} = \mathbf{B}/(\rho\mu)^{1/2}$. Now consider the alternative fields, $\mathbf{v}_1 = \mathbf{u} + \mathbf{h}$ and $\mathbf{v}_2 = \mathbf{u} - \mathbf{h}$. Show that these fields are governed by

$$\partial \mathbf{v}_1/\partial t + (\mathbf{v}_2 \cdot \nabla)\mathbf{v}_1 = -\nabla(p/\rho)$$

$$\partial \mathbf{v}_2/\partial t + (\mathbf{v}_1 \cdot \nabla)\mathbf{v}_2 = -\nabla(p/\rho)$$

where p is the sum of the fluid pressure and the magnetic pressure ($\mathbf{v}_1$ and $\mathbf{v}_2$ are known as Elsasser variables).

6.2 Suppose that a uniform magnetic field permeates an (almost) inviscid, (almost) perfectly conducting fluid and is orientated at right angles to a plane solid surface which forms the boundary of the semi-infinite fluid domain. A constant current sheet, J, is suddenly applied in the stationary wall giving rise to a tangential field, $\mathbf{B}_{//}$, at the wall. Show that jumps in $\mathbf{u}_{//}$ and $\mathbf{B}_{//}$ across the Hartmann-vortex sheet at the wall are related by

$$|\Delta \mathbf{B}_{//}|/(\rho\mu)^{1/2} = |\Delta \mathbf{u}_{//}|(\nu/\lambda)^{1/2}$$

Determine the subsequent motion and field distribution for the case where $\nu \ll \lambda$.

6.3 Show that W in (6.52) is always sign-indefinite for three-dimensional equilibria in which $\mathbf{B}$ and $\mathbf{u}$ are not aligned. (The inference is that such equilibria are usually unstable.)

6.4 Consider a two-dimensional magnetic field which is in equilibrium and sits in a steady, two-dimensional velocity field. Show that W in (6.52) is always sign-indefinite if $B^2 < \rho\mu u^2$ at any point. (Restrict the analysis to two-dimensional stability.)

7

MHD Turbulence at Low and High Magnetic Reynolds Number

> You asked, 'What is this transient pattern?'
> If we tell the truth of it, it will be a long story;
> It is a pattern that came up out of an ocean
> And in a moment returned to that ocean's depth
>
> *(Omar Khayyam)*

Turbulence is not an easy subject. Our understanding of it is limited, and those bits we do understand are arrived at through detailed and difficult calculation. G K Batchelor gave some hint of the difficulties when, in 1953, he wrote:

> It seems that the surge of progress which began immediately after the war has now largely spent itself, and there are signs of a temporary dearth of new ideas.... we have got down to the bedrock difficulty of solving non-linear partial differential equations.

Little has changed since 1953. Nevertheless, it is hard to avoid the subject of turbulence in MHD, since the Reynolds number, even in metallurgical MHD, is invariably very high. So at some point we simply have to bite the bullet and do what we can. This chapter is intended as an introduction to the subject, providing a springboard for those who wish to take it up seriously. In order not to demotivate the novice, we have tried to keep the mathematical difficulties to a minimum. Consequently, only schematic outlines are given of certain standard derivations and proofs. For example, deriving the standard form for second- and third-order velocity correlation tensors in isotropic turbulence can be hard work. Such derivations are well documented elsewhere and so there seems little point in giving a blow-by-blow description here. We have concentrated rather on trying to get the main physical ideas across.

Now the sceptic might say: 'if the theory of turbulence is so hard, why bother with it at all? After all we now have powerful computers available to us, which can compute both the mean flow and the motion of every turbulent eddy.' The experimentalist Corrsin had one answer to this.

Having estimated the computing resources required to simulate even the most modest of turbulent flows, and shown them to be well beyond the capacity of the time, he made the following whimsical comment:

> The foregoing estimate (of computing power) is enough to suggest the use of analog instead of digital computation; in particular, how about an analog consisting of a tank of water?

Corrsin said this in 1961, but actually it is still pertinent today. Despite the great advances which have occurred in computational fluid dynamics, forty years later our capacity to simulate accurately turbulent flows by computation is still rather poor, restricted to simple geometries and low Reynolds numbers (around 500). The problem, as you will see shortly, is that turbulent flows contain, at any instant, eddies (vortical structures) which have a wide range of sizes from the large to the minute, and it is difficult to capture this full spectrum of eddies in a numerical simulation.

7.1 A Survey of Conventional Turbulence

As a prelude to discussing MHD turbulence it seems prudent to summarise first the simpler features of conventional turbulence. Of course, turbulence is a vast subject, filling many erudite if forbidding texts. We have time to touch on only a few issues here. We start with a short historical introduction.

7.1.1 A historical interlude

> At times water twists to the northern side, eating away the base of the bank; at times it overthrows the bank opposite on the south; at times it leaps up swirling and bubbling to the sky; at times revolving in a circle it confounds its course.... Thus without any rest it is ever removing and consuming whatever borders upon it. Going thus with fury it is **turbulent** and destructive.
>
> *Leonardo da Vinci*

So began man's study of turbulent fluid motion.

We start this section with a brief historical survey of turbulence, a survey which begins with Newton and the ideas of viscosity and eddy viscosity (Table 7.1). The relationship between shear stress and gradients in mean velocity has been a recurring theme in turbulence theory. In the laminar context this was established in 1687 by Newton who, in *Principia*, hypothesised that the resistance to relative movement in parts of a fluid

Table 7.1. *Comparison of the history of theories of turbulence with those of magnetism*

Theory of turbulence			Electricity and magnetism
		11th century	Compass
1500s	Leonardo's first observations	1269	Peregrinus: magnetic poles
		1600	Gilbert: geomagnetism
		1750s	Coulomb: action at a distance
		1820s	Ampère: forces on currents
		1831	Faraday: electromagnetic induction, concept of fields
1850s	Boussinesq: eddy viscosity		
		1860s	Maxwell's equations
1880s	Reynolds: two types of flow, turbulent stresses		
1904	Prandtl: boundary layers	1889	Hertz: emission of electromagnetic waves
1920s	Prandtl: mixing-length theory		
1930s	Taylor, von Kármán: statistical theory of turbulence		
1940s	Kolmogorov: modern theory of turbulence		
1942 beginning of MHD – Alfvén's waves discovered			

are *'proportional to the velocity with which the parts of fluid are separated from one another'*, i.e. the relative rate of sliding of layers in the fluid. The constant of proportionality is, of course, the coefficient of viscosity. Newton's idea of internal friction was somewhat overlooked by the 18th century mathematicians and it languished until 1823 when Navier, and a little later Stokes, introduced viscous forces into the equations of hydrodynamics.

Shortly after the introduction of Newton's law of viscosity, questions were raised as to the uniformity of ν. For example, in 1851 Saint-Venant speculates that*:

> If Newton's assumption, ..., which consists in taking interior friction proportional to the speed of the fluid elements sliding against one another, can be applied approximately to the set of points of a given fluid section, all the known facts lead us to

* Translation by U. Frisch, 1995.

> infer that the coefficient of this proportionality should increase with the size of transverse sections; this may be explained up to a point by noticing that the fluid elements are not progressing parallel to each other with regularly graded velocities, and that ruptures, eddies and other complex and oblique motions, which must strongly effect the magnitude of frictions, are formed.

There is clearly some embryonic notion of turbulence and of *eddy viscosity* here, albeit confused with molecular action. This was pursued by both Reynolds and Boussinesq, the latter being Saint-Venant's student. Boussinesq came first, noting that turbulence must greatly increase the (eddy) viscosity because: '*the (turbulent) friction experienced, being caused by finite sliding between adjacent layers, will be much larger than would be the case should velocities vary in a continuous way*' (1870). Shortly after, Reynolds' classic paper on pipe flow appeared (1883). This clearly differentiates between laminar and turbulent flow, and identifies the key role played by ul/ν in determining which state prevails. Later, Reynolds reaffirmed the idea of an eddy viscosity while introducing the notion that the fluid velocity might be decomposed into a mean and fluctuating component, the latter giving rise to the fictitious, time-averaged shear stresses which now bear Reynolds' name. Reynolds used the term *sinuous* to describe the appearance of turbulence.

By 1925 Prandtl clearly recognised the analogy between the turbulent transport of momentum (through turbulent eddies) and the laminar shear stress caused by molecular motion, as predicted by the kinetic theory of gases. He introduced the mixing length model of turbulence described in Chapter 3, which had some notable successes at the time (e.g. the log-law of the wall) but is now regarded as flawed. (The problem is that there is no real separation of length scales between the turbulent fluctuations and gradients in mean velocity as required by a mixing length theory. In fact, any result deduced by mixing length can also be deduced by purely dimensional arguments.)

The great breakthrough in turbulence theory came with the pioneering work of G I Taylor in the early 1930s, who for the first time fully embraced the need for a statistical approach to the subject. He introduced the idea of the velocity correlation function $Q_{ij}(\mathbf{r}) = \overline{u_i'(\mathbf{x})u_j'(\mathbf{x}+\mathbf{r})}$, a generalisation of the Reynolds stress, which is now the common currency of turbulence theory. The quantity Q_{ij} tells us about the degree to which the fluctuating component of motion, $\mathbf{u}'$, is statistically correlated at two points separated by a distance $|\mathbf{r}|$. A strong correlation implies that there

are eddies which span the gap $|\mathbf{r}|$. Conversely, if Q_{ij} is very small, then $\mathbf{x}$ and $\mathbf{x}+\mathbf{r}$ are statistically independent. Thus Q_{ij} contains information about the structure of the turbulence. Taylor also promoted the useful idealisation of statistically homogeneous and isotropic turbulence. This initiative was pursued by the engineer von Kármán, who showed that, with the help of the symmetry implied by isotropy, Q_{ij} could be expressed in terms of a single scalar function, $f(|\mathbf{r}|)$, and that the Navier–Stokes equation could be manipulated into the form $\partial f/\partial t = (\ldots)$. At last there was the possibility of making rigorous, quantitative predictions about turbulence. Unfortunately the right-hand side of this equation includes new terms such as triple velocity correlations of the form $\overline{u_i(\mathbf{x})u_j(\mathbf{x})u_k(\mathbf{x}+\mathbf{r})}$. Consequently, it is not always possible to predict the evolution of f. Nevertheless, in certain circumstances the triple correlations can be finessed away, and so Karman's equation, now called the Karman–Howarth equation, can provide useful information.

The statistical theory of turbulence was greatly developed in the (then) USSR in the 1940s, particularly by Kolmogorov and Obukhov. These researchers realised that a vast range of scales (eddy sizes) exist in a turbulent flow, and that viscosity influences only the smallest eddies. They quantified the idea of the energy cascade, in which eddies continually break up into smaller and smaller vortices, until viscosity destroys the motion. This allowed them to predict how the energy of a turbulent flow is distributed between the various eddy sizes. Great strides were made, and by 1950 a physical and mathematical picture of homogeneous turbulence had emerged which is little different today. However, this picture is not completely deductive, but relies rather on certain (plausible) physical assumptions based on empirical evidence.

Turbulence plays a key part in MHD. Virtually all laboratory and industrial flows are turbulent. Moreover, turbulence is an essential ingredient of geo-dynamo theory, and it is needed in astrophysical MHD to explain the flux tube reconnections which are so hard to account for in terms of the vanishingly small molecular diffusivity. Comparing the development of turbulence and the laws of electromagnetism, we see that turbulence was rather a late developer, reflecting the formidable difficulties inherent in tackling a non-linear, random process. Even today there is no universal 'theory of turbulence'. We have a few theoretical results relating to various idealised configurations, and a great deal of experimental data. Sometimes, but not always, the two coincide. Of course, it is when theory and experiment differ, and we try to reconcile those differences, that we learn the most. As with all fluid mechanics, our

understanding of turbulence has developed through a careful assessment of the experimental evidence; which brings us back to Leonardo da Vinci's observations.

One cannot help but be struck by the similarities between Reynolds' idea of two motions, a mean forward motion and a turbulent vortical motion, and his observation of the sinuous nature of turbulence in a pipe, and Leonardo da Vinci's note in 1513:

> Observe the motion of the surface of water, which resembles the behaviour of hair, which has two motions, of which one depends on the weight of the strands, the other on the line of its revolving; thus water makes revolving eddies, one part of which depends upon the impetus of the principle current, and the other depends on the incident and reflected motions.

[Note accompanying Leonardo's well-known sketches of water flow around obstacles.]

7.1.2 A note on tensor notation

It is difficult to make much progress in turbulence without the use of tensor notation, something which we have managed to avoid so far. This sub-section is for those who have not met tensors before, or who have studiously avoided them.

Tensor notation is compact and efficient, but it can be off-putting to those who are unfamiliar with it. Luckily, to get through this chapter, there is only one thing you need to know about tensors, and that is the *implied summation convention*. A couple of examples will get the general idea across.

Consider the convective derivative $(\mathbf{u} \cdot \nabla)f$, where f is some scalar function:

$$(\mathbf{u} \cdot \nabla)f = u_x \frac{\partial f}{\partial x} + u_y \frac{\partial f}{\partial y} + u_z \frac{\partial f}{\partial z}$$

In tensor notation we write this as simply $u_i(\partial f / \partial x_i)$. The rule is: if a suffix is repeated then there is an implied summation over that index. Thus, in the example above,

$$u_i \frac{\partial f}{\partial x_i} = u_x \frac{\partial f}{\partial x} + u_y \frac{\partial f}{\partial y} + u_z \frac{\partial f}{\partial z}$$

Sometimes there is more than one suffix. For example, $(\mathbf{u} \cdot \nabla)\mathbf{u}$ is a symbolic representation of the vector having the three components $(\mathbf{u} \cdot \nabla)u_x$,

$(\mathbf{u}\cdot\nabla)u_y$ and $(\mathbf{u}\cdot\nabla)u_z$. In tensor notation, we would write $(\mathbf{u}\cdot\nabla)\mathbf{u}$ as $u_i(\partial u_j/\partial x_i)$, implying an automatic summation over the repeated suffix i (but no summation over j). Put another way, $u_i(\partial u_j/\partial x_i)$ is the jth component of $(\mathbf{u}\cdot\nabla)\mathbf{u}$. Sometimes we have two repeated indices, in which case there are two implied summations. For example, $[(\mathbf{u}\cdot\nabla)\mathbf{u}]\cdot\mathbf{B}$ is written as $[u_i(\partial u_j/\partial x_i)]B_j$. That is, we take the jth component of $(\mathbf{u}\cdot\nabla)\mathbf{u}$, multiply it by the jth component of B, repeat the operation for $j = x$, y and z, and sum the terms.

The Navier–Stokes equation

$$\rho\left[\frac{\partial\mathbf{u}}{\partial t}+(\mathbf{u}\cdot\nabla)\mathbf{u}\right]=-\nabla p+\rho\nu\nabla^2\mathbf{u}$$

is, in tensor notation,

$$\rho\left[\frac{\partial u_j}{\partial t}+u_i\frac{\partial u_j}{\partial x_i}\right]=-\frac{\partial p}{\partial x_j}+\rho\nu\frac{\partial^2 u_j}{\partial x_i^2} \tag{7.1}$$

This represents the jth component of the Navier–Stokes equation and the summation convention has appeared twice, once in the convective derivative, $u_i[\partial(\cdot)/\partial x_i]$, and once in the Laplacian, $\partial^2/\partial x_i^2 = \partial^2/\partial x^2 + \partial^2/\partial y^2 + \partial^2/\partial z^2$. The continuity equation is, in tensor form,

$$\frac{\partial u_i}{\partial x_i}=0 \tag{7.2}$$

Some quantities, such as the stress tensor, τ_{ij}, depend themselves on two indices. In the case of the stress tensor, τ_{ij} represents the component of stress pointing in the jth direction and evaluated on the surface whose normal points in the ith direction. This is illustrated in Figure 7.1.

The Navier–Stokes equation written in terms of the viscous stress tensor is

$$\rho\left[\frac{\partial u_j}{\partial t}+u_i\frac{\partial u_j}{\partial x_i}\right]=-\frac{\partial p}{\partial x_j}+\frac{\partial\tau_{ij}}{\partial x_i} \tag{7.3}$$

where Newton's law of viscosity stipulates that

$$\tau_{ij}=\rho\nu\left(\frac{\partial u_i}{\partial x_j}+\frac{\partial u_j}{\partial x_i}\right)=2\rho\nu S_{ij} \tag{7.4}$$

Here S_{ij} is called the strain-rate tensor. (The reader might wish to check that substituting (7.4) into (7.3), and using (7.2), we arrive back at (7.1).) The term $\partial\tau_{ij}/\partial x_i$ in (7.3) arises from the fact that the net viscous force per unit volume acting on the cube shown in Figure 7.1 is

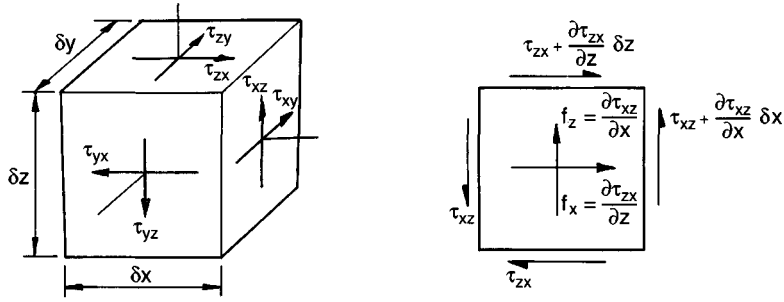

(a) Sign convention for stresses (note that $\tau_{ij} = \tau_{ji}$)

(b) Net effective body force, per unit volume, caused by an inbalance in stresses. Only components in th xz plane are shown

Figure 7.1 The stress tensor.

$$f_x = \frac{\partial \tau_{xx}}{\partial x} + \frac{\partial \tau_{yx}}{\partial y} + \frac{\partial \tau_{zx}}{\partial z}$$

in the x-direction, with analogous expressions for f_y and f_z.

Finally we introduce the symbol δ_{ij}, which has the usual meaning of $\delta_{ij} = 1$ if $i = j$ and $\delta_{ij} = 0$ if $i \neq j$. Armed with this brief introduction to tensor notation, we now start our survey of conventional (non-MHD) turbulence.

7.1.3 The structure of turbulent flows: the Kolmogorov picture of turbulence

Let us start with a traditional question in turbulence theory. Suppose we have a (statistically) steady flow, say flow in a pipe. Then the turbulent eddies are continually subject to viscous dissipation yet the energy of the turbulence does not, on average, change. Where does the turbulence energy come from? Of course, in some sense it comes from the mean flow. The traditional way of quantifying this relies on the idea of dividing the flow into two distinct parts, a mean component and a turbulent motion, and then examining the exchange of energy between the two: which brings us back to the idea of a Reynolds stress.

You are already familiar with the concept of the Reynolds stress, τ_{ij}^R. In Chapter 3 we showed that, when we time-average the Navier–Stokes equation in a turbulent flow, the presence of the turbulence gives rise to additional stresses, $\tau_{ij}^R = -\rho \overline{u_i' u_j'}$, which act on the mean flow. Here

the prime on $\mathbf{u}'$ indicates that this is a fluctuating component of velocity, $\mathbf{u}' = \mathbf{u} - \bar{\mathbf{u}}$, and the overbar signifies a time average. Now these Reynolds stresses give rise to a net force acting on the mean flow, $f_i = \partial \tau_{ij}^R / \partial x_j$, and if the rate of working of this force, $f_i \bar{u}_i$, is negative, then the mean flow must lose mechanical energy to the agent which supplies the force, i.e. the turbulence. We say that energy, usually kinetic, is transferred from the mean flow to the turbulence. This is why the turbulence in a pipe, say, does not die away. The viscous dissipation of turbulent eddies is matched by the rate of working of f_i.

Of course, this is all a little artificial, in the sense that we have just one fluid and one flow. All we are saying is that when we decompose $\mathbf{u}$ into $\bar{\mathbf{u}}$ and $\mathbf{u}'$ then the total kinetic energy, which is conserved in the absence of viscosity, is like-wise divided between $\frac{1}{2}\bar{\mathbf{u}}^2$ and $\frac{1}{2}\overline{\mathbf{u}'^2}$. When $f_i \bar{u}_i$ is negative, energy is transferred from $\bar{\mathbf{u}}$ to $\mathbf{u}'$. Physically this corresponds to the creation of turbulent eddies through some form of instability in the mean flow. Now we can write $f_i \bar{u}_i$ as

$$f_i \bar{u}_i = \frac{\partial}{\partial x_j}\left[\bar{u}_i \tau_{ij}^R\right] - \tau_{ij}^R S_{ij}, \qquad S_{ij} = \frac{1}{2}\left[\frac{\partial \bar{u}_i}{\partial x_j} + \frac{\partial \bar{u}_j}{\partial x_i}\right] \tag{7.5}$$

Here S_{ij} is the strain-rate tensor introduced in Chapter 7, Section 1.2. The first term on the right of (7.5) is just the divergence of $\bar{u}_i \tau_{ij}^R$. In a finite, closed domain, in which $\bar{u}_j$ is zero on the boundary, or else in a statistically homogeneous turbulent flow, this term integrates to zero. Thus the net rate of transfer of mechanical energy to the turbulence is just the volume integral of $\tau_{ij}^R S_{ij}$, which is sometimes called the *deformation work*. Usually $\tau_{ij}^R S_{ij}$ is a positive quantity, reflecting the tendency for parts of the mean flow to disintegrate into eddies due to inertially driven instabilities. Thus a finite strain-rate in the mean flow tends to keep the turbulence alive. Note that there are no viscous effects involved in this transfer of energy (if Re is large): it is a non-dissipative process. The next question, therefore, is where does this turbulent energy go to?

If we have a steady-on-average flow in a pipe, say, then there is a continual energy transfer from the mean flow, via $\tau_{ij}^R S_{ij}$, to the turbulence. However, the turbulence in such a situation will be statistically steady and so this energy must be dissipated somehow. Ultimately, of course, it is viscosity which destroys the mechanical energy of the eddies. However, when Re is large, the viscous stresses acting on the large eddies are negligible, so there must be some rather subtle process at work. This leads to the idea of the energy cascade, a concept first proposed by the British meteorologist L F Richardson in the 1920s.

It is an empirical observation that any turbulent flow comprises 'eddies' which have a wide range of sizes. That is to say, there is always a wide spectrum of length scales, velocity gradients etc. Richardson's idea is that the largest eddies, which are created by instabilities in the mean flow, are themselves subject to inertial instabilities and rapidly break up into yet smaller vortices. These smaller eddies then, in turn, become unstable and break up into even smaller vortices and so on. There is a continual *cascade* of energy from the large scale down to the small (Figure 7.2).

It should be emphasised, however, that viscosity plays no part in this cascade. That is, when Re is large (based on $\mathbf{u}'$ and a typical eddy size), then the viscous stresses acting on the larger eddies are negligible. The whole thing is essentially driven by inertia. The cascade is halted, however, when the eddies become so small that the Reynolds number based on the small-scale eddy size is of the order of unity. That is, the very smallest eddies are dissipated by viscous forces, and for the viscous forces to be significant we need a Reynolds number of order unity. We may think of viscosity as providing a dustbin for energy at the very end of the cascade. In this sense the viscous forces are passive in nature, mopping up whatever energy is fed down from above. This process of a progressive energy cascade from large to small eddies was nicely summed up by Richardson in his parody of Swift's 'Fleas Sonnet': '*Big whirls have little whirls, which feed on their velocity, and little whirls have lesser whirls and so to viscosity.*'

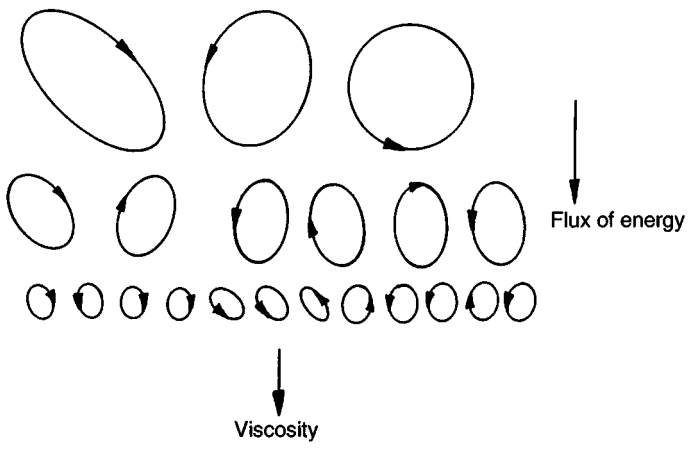

Figure 7.2 A schematic representation of the energy cascade.

Let us try to quantify this process. Let l and u' be typical length and velocity scales for the larger eddies. We might, for example, define u' through $(u')^2 = \overline{(u_x')^2}$ or $\overline{(u_y')^2}$. Also, let ε be the rate of dissipation of mechanical energy (per unit mass) due to viscosity acting on the small-scale eddies. In statistically steady turbulence ε must also equal the rate at which energy is fed to the turbulence from the mean flow, $\tau_{ij}^R S_{ij}$. If it did not, the turbulence would either gain or lose energy. In fact, if we are to avoid a build-up of eddies of a particular size, ε must equal the rate at which energy is past down the cascade at any point within that cascade. Let G be the rate at which energy (per unit mass) is passed down the cascade. Symbolically, we have $G = \varepsilon$.

If we plot the energy contained in the eddies of a particular size against eddy size we might get something that looks like Figure 7.3. Remember, there is dissipation only at the smallest scales, and so G has to be the same at all points between A and B, i.e. $G_A = G_B$, where $G_A = \tau_{ij}^R S_{ij}/\rho$. Now it is an empirical observation that the rate of extraction of energy (per unit mass) from the large eddies to the energy cascade is of the order of

$$G_A \sim (u')^3/l$$

This is not a trivial result. As we shall see, it turns out to be very useful. Physically, it states that the largest eddies break up on a time scale of l/u', their turn-over time.

We now try to determine the size of the smallest eddies. Let v and η be the velocity and length scales, respectively, of the smallest structures in

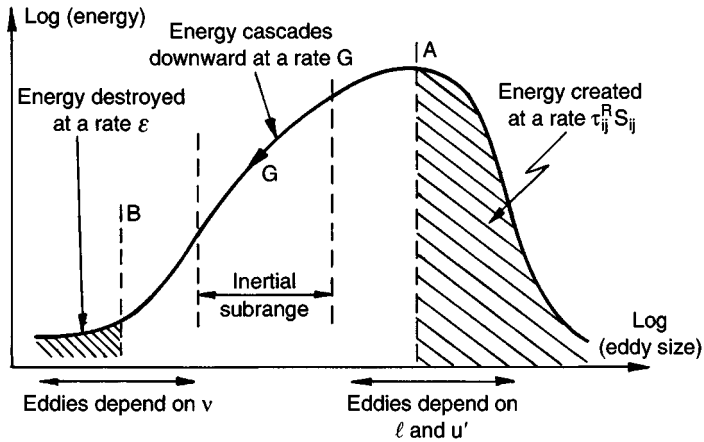

Figure 7.3 The energy cascade.

the flow. There are two things we can say about these eddies. First, $v\eta/\nu \sim 1$. That is, rather like a boundary layer, the size of the small eddies automatically adjusts to make the viscous forces an order-one quantity. Second, the energy dissipation rate per unit mass, which in a laminar flow is $-\nu(\nabla^2\mathbf{u}) \cdot \mathbf{u}$, must be of order $\varepsilon \sim \nu v^2/\eta^2$. Let us now summarise everything we know about the energy cascade.

1. The process is inviscid except at the smallest scales and so, in statistically steady turbulence,
$$\varepsilon = G, \qquad G_A = G_B \tag{7.6a, b}$$
2. Empirically it is observed that energy is extracted from the large scales, through eddy break-up, at a rate
$$G_A \sim (u')^3/l \tag{7.7}$$
3. The smallest scales must satisfy
$$v\eta/\nu \sim 1, \qquad \varepsilon \sim \nu v^2/\eta^2 \tag{7.8a, b}$$

We may eliminate either η or v from (7.8a) and (7.8b), and then use the fact of $\varepsilon \sim (u')^3/l$ to express η or v in terms of the large-scale parameters. Following this procedure we find that

$$\eta/l \sim (u'l/\nu)^{-3/4} = (\mathrm{Re})^{-3/4} \tag{7.9}$$

$$v/u' \sim (u'l/\nu)^{-1/4} = (\mathrm{Re})^{-1/4} \tag{7.10}$$

Here the Reynolds number is based on the large-scale velocity and length scales. Suppose, for example, that $\mathrm{Re} \sim 10^4$ and $l \sim 1\,\mathrm{cm}$, which is not untypical in a wind tunnel. Then $\eta \sim 0.01\,\mathrm{mm}$, which is very small! There is, therefore, a large spectrum of eddy sizes in a typical turbulent flow, and it is this which makes them so difficult to simulate numerically.

The quantities v and η are known as the *Kolmogorov microscales* of velocity and length, respectively, whereas l, the size of the large eddies, is known as the *integral scale* of the turbulence. (It is possible to give a rigorous definition of l, which we do later.)

There is something else of interest to be extracted from these simple estimates. Eliminating v from (7.8a) and (7.8b), and then equating ε to G_B, we find that the rate at which energy cascades downward at the tail end of the energy cascade is

$$G_B \sim \frac{v^3}{\eta} \tag{7.11}$$

Table 7.2. *Time and velocity scales for small eddies*

Dimension	Ratio of Kolmogorov scale to large scale
Length	$\eta/l = \mathrm{Re}^{-3/4}$
Velocity	$\mathbf{v}/u' = \mathrm{Re}^{-1/4}$
Time	$u'\tau/l = \mathrm{Re}^{-1/2}$

Compare this with (7.7). The implication is that the small eddies, just like the largest ones, break up on a timescale of their turn-over time, $\tau = \eta/v$. Moreover, (7.9) and (7.10) give $\tau \sim (\mathrm{Re})^{-1/2} l/u' \ll l/u'$. So the characteristic timescale for the break up of the small eddies is very much faster than the turn-over time of the large eddies. Things happen very rapidly at the small scales. The relationship between the smallest and largest scales is given in Table 7.2.

Let us now try to predict the shape of the energy curve shown in Figure 7.3. We focus attention on the central region, well removed from the largest scales and the Kolmogorov microscale. For convenience we shall assume that this part of the eddy spectrum is statistically isotropic and homogeneous, an approximation which becomes increasingly sound as we move away from region A. We need to introduce some notation. Let r be the size of some intermediate eddy in the cascade, $\eta < r < l$. Next, we introduce the so-called *velocity increment*, Δv, defined by $[\Delta v(r)]^2 = [u'_x(\mathbf{x}) - u'_x(\mathbf{x} + r\hat{\mathbf{e}}_x)]^2$, or else defined using the equivalent expression involving y or z. Only eddies of size r or smaller contribute to Δv, and so $(\Delta v)^2$ is an indication of the energy per unit mass contained in eddies of size r and less.

We now try to predict Δv at points well removed from regions A and B, the so-called *inertial subrange*. If we are well away from A, then the eddies which concern us have a complicated heritage. They are the offspring of larger eddies which, in turn, come from yet bigger eddies, and so on. We would expect, therefore, that Δv in the inertial subrange is independent of the structure of the very largest scales, and hence of l and u'. Moreover, since we are well removed from region B, Δv will not depend on ν. Thus, provided $\eta \ll r \ll l$, Δv will be a function of $G = \varepsilon$ and r alone, there being no other relevant physical parameter. Symbolically, $\Delta v = \Delta v(\varepsilon, r)$. Now Δv has dimensions of ms^{-1}, ε has dimensions of $m^2 s^{-3}$ and r has dimensions of m. The only dimensionless group which can be constructed from Δv, ε and r is $(\Delta v)/\varepsilon^{1/3} r^{1/3}$. It follows that $(\Delta v)/\varepsilon^{1/3} r^{1/3}$ is a pure number, presumably of the order of unity, and so

$$(\Delta v)^2 \sim \varepsilon^{2/3} r^{2/3} \tag{7.12}$$

This is known as *Kolmogorov and Obukhov's two-thirds law* and it is an excellent fit to the experimental data!

Sometimes (7.12) is expressed in a slightly different way. Many researchers work in Fourier space and introduce an *energy spectrum*, $E(k)$, where k is a wave number, $k \sim 1/r$. $E(k)$ is defined by the requirement that $E(k)dk$ gives all the energy contained in eddies whose size lies in the range $k \to k + dk$. Since

$$(\Delta v)^2 \sim \int_k^\infty E(k)dk \sim (\text{energy in eddies of size smaller than } k^{-1})$$

we find

$$E(k) \sim \varepsilon^{2/3} k^{-5/3} \tag{7.13}$$

In this form it is known as Kolmogorov's five-thirds law.

Now the arguments above are all rather qualitative and more than a little heuristic. What, for example, do we mean by an eddy? It would be a mistake, however, to dismiss them lightly. The Kolmogorov–Richardson picture of turbulence gives an excellent qualitative description of conventional turbulence. Still, there is a need to introduce a more formal descriptive framework, and we start with the idea of velocity correlation functions.

7.1.4 Velocity correlation functions and the Karman–Howarth equation

In order to simplify matters we now restrict ourselves to a form of idealised turbulence. We consider flows which are statistically homogeneous and isotropic, i.e. their statistical properties do not depend on position or direction. Also, we shall take the mean velocity to be zero. Since, in the absence of a mean shear, there is no mechanism for injecting energy into the turbulence, such a flow will always decay in the course of time. We might picture this as a fluid which is subjected to vigorous stirring and then left to itself. The properties of the turbulence are now time-dependent and so we need to introduce a different means of performing averages. We rely on ensemble averages, i.e. an average over many realisations of the flow. This is represented by $\langle \cdot \rangle$. In homogeneous turbulence, such an average can be shown to be equivalent to a spatial average, while in statistically steady turbulence, ensemble averages are equivalent to time averages, $\langle \cdot \rangle = \overline{(\cdot)}$.

From a practical point of view, the easiest way of generating homogeneous turbulence is to pass air uniformly through a wire mesh in a wind tunnel and adopt a frame of reference moving with the mean flow. (Actually, such a turbulence is not strictly homogeneous because of the boundaries and because it decays as we move downstream, but it is not a bad approximation.) The workhorse of turbulence theory is the *velocity correlation tensor*, sometimes called the velocity correlation function (Figure 7.4). This plays the same rôle in turbulence theory as velocity or momentum does in laminar flow. The *second-order velocity correlation tensor* is defined as

$$Q_{ij}(\mathbf{r}) = \langle u_i(\mathbf{x}) u_j(\mathbf{x}+\mathbf{r}) \rangle \tag{7.14}$$

(Actually Q_{ij} also depends on t, so strictly this should be written as $Q_{ij}(\mathbf{r}, t)$.) Note that, because the turbulence is homogeneous, Q_{ij} does not depend on $\mathbf{x}$. Also, since the mean velocity is zero, there is no need to use a prime to indicate a fluctuating velocity component. This correlation function has the geometric property $Q_{ij}(\mathbf{r}) = Q_{ji}(-\mathbf{r})$ and is related to the kinetic energy per unit mass by $\frac{1}{2}\langle \mathbf{u}^2 \rangle = \frac{1}{2} Q_{ii}(0)$.

So what does $Q_{ij}(\mathbf{r})$ represent? Conceptually it is easier to think in terms of time averages rather than ensemble averages, and so we temporarily move back to thinking about steady-on-average flows and write

$$Q_{ij}(\mathbf{r}) = \overline{u_i(\mathbf{x}) u_j(\mathbf{x}+\mathbf{r})}$$

The first thing to note about Q_{ij} is that, when $\mathbf{r} = 0$, it is proportional to the Reynolds stress, $\tau_{ij}^R = -\rho Q_{ij}(0)$. Yet what if $\mathbf{r} \neq 0$? In this case Q_{ij} simply tells us if two scalar quantities, $f = u_i(\mathbf{x})$ and $h = u_j(\mathbf{x}+\mathbf{r})$, are statistically correlated. We say that f and h are correlated if $\overline{fh} \neq 0$ and uncorrelated if $\overline{fh} = 0$. Often a *correlation coefficient*, c, is introduced, defined by

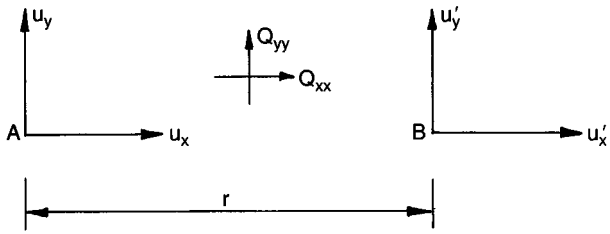

Figure 7.4 (a) Definition of velocity correlation functions.

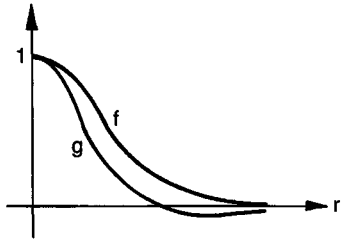

Figure 7.4 (b) Shape of the velocity correlation functions.

$$c^2 = \frac{(\overline{fh})^2}{\overline{f^2}\,\overline{h^2}}$$

If $c = \pm 1$, the correlation is said to be perfect. (Any variable is, of course, perfectly correlated to itself.) If $\overline{fh} = 0$ then it means that both f and h fluctuate in time in a manner quite independent of each other.

We now go back to ensemble averages. Consider two points, A and B, separated by $\mathbf{r} = r\hat{\mathbf{e}}_x$ (Figure 7.4(a)). The correlation function $Q_{xx}(r\hat{\mathbf{e}}_x)$ represents the degree to which the horizontal velocities at A and B (at some particular instant) are correlated when averaged over many realisations. If the velocity fluctuations at A and B were statistically independent then $Q_{xx}(r)$ would be zero. On the other hand, if precisely the same thing is happening at A and B (the two points are perfectly correlated) then $Q_{xx} = \langle u_x^2 \rangle$. We expect that $Q_{xx} \to \langle u_x^2 \rangle$ as $r \to 0$ and $Q_{xx} \to 0$ as $r \to \infty$, remote points in a turbulent flow being uncorrelated. We now introduce some additional notation. Let u be a characteristic turbulence velocity, defined by

$$u^2 = \langle u_x^2 \rangle = \langle u_y^2 \rangle = \langle u_z^2 \rangle \tag{7.15}$$

and write $Q_{xx}(r)$ and $Q_{yy}(r)$ in the form

$$Q_{xx}(r\hat{\mathbf{e}}_x) = u^2 f(r) \tag{7.16}$$

$$Q_{yy}(r\hat{\mathbf{e}}_x) = u^2 g(r) \tag{7.17}$$

The functions f and g are known as the longitudinal and lateral velocity correlation functions (or coefficients), respectively. They are dimensionless, satisfy $f(0) = g(0) = 1$, and have the shape shown in Figure 7.4(b). The integral scale, l, of the turbulence is often defined as

$$l = \int_0^\infty f(r)dr$$

This provides a convenient measure of the extent of the region within which velocities are appreciably correlated, i.e. the size of the large eddies. In fact, f and g are not independent functions. It may be shown that the continuity equation demands

$$g = f + \frac{1}{2} r f'$$

Moreover, symmetry and continuity arguments allow us to express $Q_{ij}(\mathbf{r})$ purely in terms of $f(r)$ and $\mathbf{r}$. The details are long and tedious and we merely state the end result. For isotropic turbulence it may be shown that

$$Q_{ij}(\mathbf{r}) = \frac{u^2}{2r}\left[\frac{d}{dr}(r^2 f)\delta_{ij} - f' r_i r_j\right] \tag{7.18}$$

(see suggested reading at end of the chapter).

The *third-order (or triple) velocity correlation function (or tensor)* is defined as

$$S_{ijl}(\mathbf{r}) = \langle u_i(\mathbf{x}) u_j(\mathbf{x}) u_l(\mathbf{x}+\mathbf{r})\rangle$$

It too can be written in terms of a single scalar function, $k(r)$, defined by

$$u^3 k(r) = \langle u_x^2(\mathbf{x}) u_x(\mathbf{x} + r\hat{\mathbf{e}}_x)\rangle$$

Again, symmetry and continuity arguments may be used to show that, in homogeneous, isotropic, turbulence

$$S_{ijl} = u^3\left[\left(\frac{k - rk'}{2r^3}\right) r_i r_j r_l + \left(\frac{2k + rk'}{4r}\right)(r_i \delta_{jl} + r_j \delta_{il}) - \frac{k}{2r} r_l \delta_{ij}\right] \tag{7.19}$$

The function k is known as the longitudinal triple-velocity correlation function.

So far we have made lots of definitions and exploited certain kinematic relationships. However, this has not really got us very far. To make progress we need to introduce some dynamics in the form of the Navier–Stokes equation. Let $\mathbf{x}' = \mathbf{x} + \mathbf{r}$ and $\mathbf{u}' = \mathbf{u}(\mathbf{x}')$. (From now on, a prime will indicate a quantity at position $\mathbf{x}'$ and has nothing to do with a fluctuating, as distinct from mean, variable.) Then we have

$$\frac{\partial u_i}{\partial t} = -\frac{\partial}{\partial x_k}(u_i u_k) - \frac{\partial}{\partial x_i}(p/\rho) + \nu \nabla_x^2 u_i \tag{7.20}$$

$$\frac{\partial u_j'}{\partial t} = -\frac{\partial}{\partial x_k'}(u_j' u_k') - \frac{\partial}{\partial x_j'}(p'/\rho) + \nu \nabla_{x'}^2 u_j' \tag{7.21}$$

On multiplying the first of these by u_j', and the second by u_i, adding the two and averaging, we obtain

$$\frac{\partial}{\partial t}\langle u_i u_j' \rangle = -\left\langle u_i \frac{\partial u_j' u_k'}{\partial x_k'} + u_j' \frac{\partial u_i u_k}{\partial x_k} \right\rangle - \frac{1}{\rho}\left\langle u_i \frac{\partial p'}{\partial x_j'} + u_j' \frac{\partial p}{\partial x_i} \right\rangle + \nu\langle u_i \nabla_{x'}^2 u_j' + u_j' \nabla_x^2 u_i \rangle \tag{7.22}$$

This looks a bit of a mess! However, it may be tidied up considerably. We note that, (i) operations of taking averages and differentiation permute, (ii) $\partial/\partial x_i$ and $\partial/\partial x_j'$ operating on averages may be replaced by $-\partial/\partial r_i$ and $\partial/\partial r_j$, respectively, and (iii) u_i is independent of $\mathbf{x}'$ while u_j' is independent of $\mathbf{x}$. (7.22) then simplifies to something a lot neater:

$$\frac{\partial Q_{ij}}{\partial t} = \frac{\partial}{\partial r_k}\left[S_{ikj} + S_{jki}\right] + 2\nu\nabla^2 Q_{ij} \tag{7.23}$$

(Consult one of the suggested texts at the end of the chapter for the details.) We have dropped the terms involving pressure since it may be shown that $\langle pu_j' \rangle = 0$ in isotropic turbulence.

We have managed to relate the rate of change of the second-order velocity correlation tensor to the third-order one. We might now go on to obtain an equation for the rate of change of S_{ijk}. Unfortunately, however, this contains terms involving fourth-order correlations, which in turn depend on fifth-order correlations and so on. We have come up against the *closure problem* of turbulence. So let us stick with (7.23) and see where it leads. Substituting for Q_{ij} and S_{ijk} in terms of the scalar functions $f(r)$ and $k(r)$ yields, after a considerable amount of algebra,

$$\boxed{\frac{\partial}{\partial t}\left[u^2 r^4 f(r)\right] = u^3 \frac{\partial}{\partial r}\left[r^4 k(r)\right] + 2\nu u^2 \frac{\partial}{\partial r}\left[r^4 f'(r)\right]} \tag{7.24}$$

This is known as the Karman–Howarth equation and it constitutes one of the central results in the theory of isotropic turbulence. We shall see in the next section that it can be used to estimate the rate of decay of freely evolving turbulence.

We close this section with a brief discussion of a different type of velocity correlation function, sometimes called a second-order structure function. It is defined by

$$B_{ik} = \langle (u_i' - u_i)(u_k' - u_k) \rangle \tag{7.25}$$

For example, $B_{ii} = \left\langle (\mathbf{u} - \mathbf{u}')^2 \right\rangle$. This is closely related to the velocity increment, $\Delta \mathbf{v}$, introduced in the last section. It is easy to show that the second-order correlation tensors Q_{ij} and B_{ij} are related by

$$B_{ij} = \frac{2}{3}\langle \mathbf{u}^2 \rangle \delta_{ij} - 2Q_{ij} \tag{7.26}$$

and so B_{ij} may be expressed in terms of f, just like Q_{ij}. However, the tensor B_{ij} has an advantage over Q_{ij}. Only eddies of size less than or equal to $|\mathbf{r}|$ can contribute to $B_{ij}(\mathbf{r})$. Consequently, by making $|\mathbf{r}|$ progressively smaller, we can move down the energy cascade, focusing on smaller and smaller eddies.

7.1.5 Decaying turbulence: Kolmogorov's law, Loitsyansky's integral, Landau's angular momentum and Batchelor's pressure forces

It is natural to suppose that well-separated points in a turbulent flow are statistically uncorrelated, and so we expect $f(r)$ and $k(r)$ to decrease rapidly with distance. In fact, prior to 1956 it was assumed that f and k decay exponentially at large r. *If* this is the case, then the Karman–Howarth equation may be integrated to yield

$$I = u^2 \int_0^\infty r^4 f(r) dr = \text{constant} \tag{7.27}$$

This is known as Loitsyansky's integral. A N Kolmogorov took advantage of the (supposed) invariance of I to predict the rate of decay of energy in freely evolving, isotropic turbulence. The argument goes as follows. The integral scale, l, is defined as $\int_0^\infty f dr$. We would expect, therefore, that in freely evolving (decaying) turbulence

$$I \sim u^2 l^5 = \text{constant} \tag{7.28}$$

We also know that the large eddies tend to break up on a timescale of their turn-over time, so that the large scales lose energy at a rate

$$\frac{du^2}{dt} \sim -\frac{u^3}{l} \tag{7.29}$$

and this energy is not replenished. Combining (7.28) and (7.29) yields *Kolmogorov's decay laws* for isotropic turbulence:

$$u^2 = u_0^2 [1 + (7/10)(u_0 t / l_0)]^{-10/7} \tag{7.30}$$

$$l \sim l_0 [1 + (7/10)(u_0 t / l_0)]^{2/7} \tag{7.31}$$

Here u_0 and l_0 are initial values of u and l. In fact, these predictions are reasonably in line with the experimental data, which typically give $l \sim t^{0.35}$ and $u \sim t^{-1.26} \rightarrow t^{-1.34}$, depending on the Reynolds number.

The supposed invariance of I has another consequence. It can be shown that for many, if not most, types of turbulence the energy spectrum at small k has the form $E \sim (I/3\pi)k^4$ (plus higher order terms in k). We would expect, therefore, that the conservation of I should lead to the energy spectrum at small k being invariant during the decay, and this is indeed observed. This phenomenon is termed the *permanence of the large eddies* (since E at small k represents the energy of the largest eddies). All-in-all, it would seem that the experiments support (7.27).

There remain two problems, however. First, if we are to trust (7.27), then we would really like some *physical* explanation for the invariance of I. Second, we need some evidence that f and k decay exponentially, rather than algebraically, at large r. The physicist L D Landau resolved the first of these issues. He showed that, provided f and k decay exponentially, as assumed by Loitsyansky and Kolmogorov, then the invariance of I is a direct consequence of the conservation of angular momentum. He argued as follows.

In general, a patch of turbulence will contain a finite amount of angular momentum. Consider, for example, turbulence which has been created in a wind tunnel by passing air through a wire grid. The turbulence is created because vortices are randomly shed from the wires, just like Karman vortices are shed from a cylinder. This ensemble of coherent vortices interact as the fluid is swept downstream until eventually a full field of turbulence emerges. Now each time a vortex is shed from a wire a finite amount of angular momentum is injected into the flow. (An eddy contains angular momentum.) This is evident from the shuddering of a loosely suspended grid, which is a manifestation of the back reaction (torque) exerted by the fluid on the grid. Thus, in grid-produced turbulence, we inject angular momentum into the fluid in the form of a sequence of randomly orientated vortices.

Now this angular momentum is important since, as the fluid moves downstream, its energy decays according to

$$\frac{du^2}{dt} \sim -\frac{u^3}{l}$$

yet this decay is subject to the constraint that the angular momentum of a given mass of turbulent fluid is conserved. (We ignore the viscous torque

exerted by the boundaries.) Landau's great achievement was to show that the conservation of I is simply a manifestation of the conservation of angular momentum.

There are two hurdles to overcome, however, in establishing this fact. First, $I =$ constant is a statistical statement about the turbulence, in the sense that it says something about the local, quadratic quantity $\langle \mathbf{u} \cdot \mathbf{u}' \rangle$. However, the angular momentum

$$\mathbf{H} = \int \mathbf{x} \times \mathbf{u} dV$$

is a global, linear measure of the velocity field, which is clearly not a statistical quantity. We must find someway of relating $\mathbf{H}$ to $\langle \mathbf{u} \cdot \mathbf{u}' \rangle$. The second problem is that as our field of turbulence becomes infinite ($V \to \infty$) we would expect the angular momentum per unit volume, $\mathbf{H}/V$, associated with a field of randomly orientated vortices to tend to zero. How can an infinitesimally small quantity influence the dynamical behaviour of the turbulence?

The trick is to consider a large but finite volume of turbulent fluid which has been stirred up and then left to itself. In this finite volume there will, in general, be an imperfect cancellation of the angular momentum associated with the vortices. In fact, as we shall see shortly, $\mathbf{H}/V$ does tend to zero as V tends to infinity, but at finite rate: $V^{-1/2}$. Thus a finite volume contains a finite global angular momentum of order $V^{1/2}$. (The relationship $\langle \mathbf{H}^2 \rangle \sim V$ follows from the central limit theorem. This states that, if $\mathbf{x} \times \mathbf{u}$ at each location, $\mathbf{x}$, can be considered as an independent random variable, which might be the case at $t = 0$, then the variance of the volumetric average of $\mathbf{x} \times \mathbf{u}$ over some large volume V will tend to zero at the rate V^{-1} as $V \to \infty$. It follows that, if we take $\langle \cdot \rangle$ to be a volume average, $\langle \mathbf{H}^2 \rangle \sim V$.)

We are still left with the problem of how to convert the conservation of $\mathbf{H}$ into a statistical statement. To this end it is useful to take $\langle \cdot \rangle$ as an ensemble average and to consider a large number of realisations of the turbulence in our large but finite volume. That is, we stir the fluid up N times and examine the subsequent decay for each realisation. Now if the size of V is very much larger than the eddy size, l, then the turbulence should behave in a way which does not depend on the boundaries. We may then ignore the torque associated with the shear stresses exerted on the fluid by the boundaries. In each realisation, then, $\mathbf{H}^2/V$ will be independent of t. It follows that, when we average over all of the realisations, $\langle \mathbf{H}^2 \rangle / \mathrm{V}$ will be independent of time and of the size of the domain. It is the

invariance of $\langle \mathbf{H}^2 \rangle / V$, rather than $\mathbf{H}$, which leads to (7.27). The exact relationship between $\langle \mathbf{H}^2 \rangle / V$ and I may be established as follows.

Suppose the turbulent flow evolves in a large, closed sphere, whose radius R greatly exceeds l (Figure 7.5). The global angular momentum of the turbulence is then

$$\mathbf{H} = \int_V \mathbf{x} \times \mathbf{u} dV$$

(We will not bother carrying the density ρ through the calculation.) The square of $\mathbf{H}$

$$\mathbf{H}^2 = \int_V \mathbf{x} \times \mathbf{u} dV \cdot \int_V \mathbf{x}' \times \mathbf{u}' dV'$$

can, with a little effort, be rearranged into the form

$$\mathbf{H}^2 = -\int_V \int_{V'} (\mathbf{x}' - \mathbf{x})^2 \mathbf{u} \cdot \mathbf{u}' dV dV'$$

We now ensemble average over each pair of points separated by a fixed distance $\mathbf{r} = \mathbf{x}' - \mathbf{x}$ to give

$$\langle \mathbf{H}^2 \rangle = -\int \int \mathbf{r}^2 \langle \mathbf{u} \cdot \mathbf{u}' \rangle d^3\mathbf{r} dV$$

Next, Landau assumed that $\langle \mathbf{u} \cdot \mathbf{u}' \rangle$ decays rapidly with $\mathbf{r}$ so that far-field contributions to the integral

$$\int r^2 \langle \mathbf{u} \cdot \mathbf{u}' \rangle d^3\mathbf{r}$$

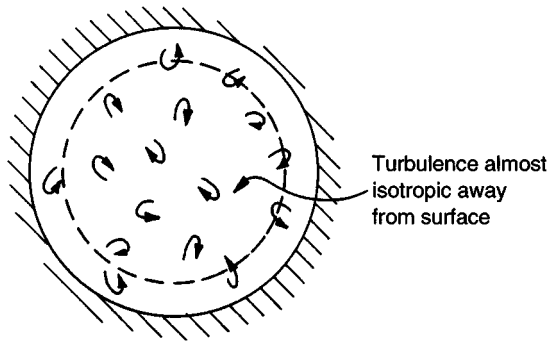

Figure 7.5 Landau's thought experiment.

are small. In such a situation only those velocity correlations taken close to the surface R are aware of the presence of the boundary, and in this sense the turbulence is approximately homogeneous and isotropic. To leading order in l/R we then have

$$\boxed{\langle H^2\rangle/V = -\int \mathbf{r}^2\langle \mathbf{u}\cdot\mathbf{u}'\rangle d^2\mathbf{r}} \tag{7.32}$$

However, (7.18) allows us to evaluate the integral on the left, which turns out to be $8\pi I$. The invariance of I then follows from conservation of angular momentum, the viscous stresses on the boundary having negligible effect as $R/l \to \infty$. So, according to L D Landau, Kolmogorov's decay law is a direct consequence of the conservation of angular momentum. Given that the predictions of (7.30) and (7.31) are reasonably in line with the experimental data, and that there is a firm physical basis for the conservation of I, there was, for some time, a general feeling of satisfaction with the $t^{-10/7}$ decay law.

However, in 1956, G K Batchelor opened a can of worms when he showed that, at least in *anisotropic* turbulence, $k \sim r^{-4}$ as $r \to \infty$. *If* this is also true of isotropic turbulence, then the Karman–Howarth equation gives

$$\frac{dI}{dt} = [u^3 r^4 k]_\infty \neq 0 \tag{7.33}$$

and Loitsyansky's integral becomes time-dependent. The reason for the relatively slow decline in k (algebraic rather than exponential) is interesting and subtle. It arises from the action of long-range pressure forces. A fluctuation in $\mathbf{u}$ at one point in a flow sends out pressure waves, which travel infinitely fast in an incompressible fluid, and these produce pressure forces, and hence accelerations, which fall off algebraically with distance from the source. Thus, because of pressure, a fluctuation in $\mathbf{u}$ at one point is felt everywhere within the fluid. Now Batchelor argued that turbulence in, say, a wind-tunnel would behave as if it had emerged from initial conditions in which remote points were statistically independent. However, because of the long-range pressure forces such a situation cannot persist, and long-range (algebraic) velocity correlations, $\langle \mathbf{u}\cdot\mathbf{u}'\rangle$, inevitably develop. At least this is the case in anisotropic turbulence (Figure 7.6).

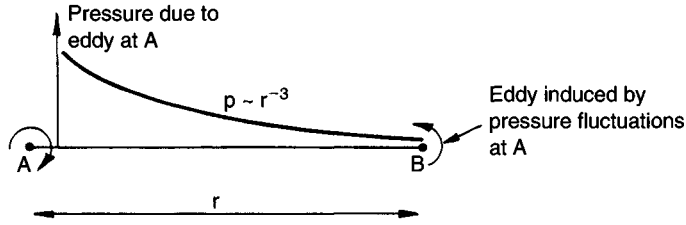

Figure 7.6 A schematic representation of Batchelor's long-range effects.

For *isotropic* turbulence, however, there is a high degree of symmetry in the statistics, and this symmetry is sufficiently strong to cause the direct effect of the long-range pressure forces on $\langle \mathbf{u} \cdot \mathbf{u}' \rangle$ to cancel. (This is why the pressure terms disappeared as we moved from (7.22) to (7.23).) Nevertheless, the pressure forces can still influence the triple correlations in isotropic turbulence and these, in turn, can influence the double correlations. In particular, it may be shown that,[1]

$$\frac{d}{dt}[u^3 r^4 k]_\infty = 3 \int r^2 \langle ss' \rangle dr$$

where $s = u_x^2 - u_y^2$. Combining this with (7.33) yields

$$\frac{d^2 I}{dt^2} = \frac{d}{dt}[u^3 r^4 k]_\infty = 3 \int r^2 \langle ss' \rangle dr = J$$

Thus, in general, we would expect I to be time dependent. This is a direct result of the pressure forces which induce a $k_\infty \sim r^{-4}$ algebraic tail in the triple correlations and thus an r^{-6} tail in f_∞. (Remember that such algebraic tails invalidate both Landau's and Loitsyansky's arguments.) Crucially, however, we have failed to determine the magnitude of J. Now, over the years, J has been estimated using a variety of *closure hypotheses*, such as the so-called quasi-normal approximation. However, these closure hypotheses are unreliable. In fact, the safest thing to do is to examine the experimental evidence. Interestingly, this suggests that J is rather small. There are no direct measurements of J, but there is some indirect evidence. This comes in three parts.

[1] This equation only holds if the so-called cummulants of the fourth-order velocity correlations are negligible for well-separated points. Such a situation occurs when fourth-order velocity correlations are statistically independent for well-separated points. There is some experimental evidence to support this assertion.

- First, there is the predicted invariance of $E(k)$ at small k (permanence of the large eddies) which comes from $E \sim (I/3\pi)k^4$. Is this in accordance with observation?
- Second, there have been measurements of $u^2(t)$. How do these compare with Kolmogorov's decay law?
- Third, there exist measurements of Q_{ij} in the so-called final period of decay (when the turbulence is weak and viscosity is important). Do these show exponential or algebraic behaviour at large r?

It seems that, by and large, the experiments support Landau, Loitsyansky and Kolmogorov to the extent that they suggest that, once the turbulence is fully developed, J is negligible. The permanence of the large eddies is indeed observed, and the form of Q_{ij} at large r is exponential in the final period of decay. Moreover, the measured decay rate of isotropic turbulence is not too far out of line with Kolmogorov's law. In 1960, Corrsin found $u^2 \sim t^{-n}$ where n lies in the range $1.2 \rightarrow 1.4$ with an average value of 1.26. Later, Lumley, in 1978, found $u^2 \sim t^{-1.34}$ and $l \sim t^{0.35}$. (Kolmogorov's law predicts $u^2 \sim t^{-1.43}$ and $l \sim t^{0.29}$) The observed exponential decay of Q_{ij} in particular seemed to have surprised Batchelor who, having just established the existence of these long-range pressure forces and the associated long-range correlations in anisotropic turbulence, noted that: '*it is disconcerting that the present more extensive analysis cannot do as well as the old*'.

Interestingly, some authors suggest that Loitsyansky's integral is strongly time-dependant, or else does not exist (i.e. diverges). There are two reasons for this. First, a turbulence closure model which was popular in the 1960s, the quasi-normal (QN) model, predicts that I varies as

$$\frac{d^2I}{dt^2} \propto \int \frac{E^2}{k^2} dk \neq 0$$

where $E(k)$ is the energy spectrum. (This was shown by Proudman and Reid in 1954.) However, the quasi-normal model has no real physical basis and is known to produce anomalous effects, such as a negative energy spectrum. A variant of this, called the EDQNM model, avoids some of the worst excesses of the QN model, while still predicting a (slight) time-dependance for I. However, the EDQNM model automatically assumes $k_\infty \sim r^{-4}$ and so builds in long-range effects from the outset. In short, it prejudges the issue.

The second reason often given for doubting the approximate conservation of I is the discovery by Saffman in 1967 that, *for suitable initial*

conditions, long-range correlations can exist in a turbulent motion which are even stronger than those of Batchelor. This leads to an energy spectrum at small k of the form $E \sim k^2$, unlike the usual assumption of $E \sim k^4$. In such a situation Loitsyansky's integral diverges. However, these particularly potent long-range correlations are too strong to have emerged from Batchelor's pressure forces, and so if they are to exist they must be imbedded in the initial conditions. Saffman himself argued that such initial conditions are unlikely to be met in, say, wind-tunnel turbulence, and so we would expect 'conventional' turbulence to have a Batchelor spectrum, $E \sim k^4$. Certainly, this is in accord with measurements of the decline of u^2 in the final period of decay, which clearly shows results compatible with $E \sim k^4$ and incompatible with Saffman's spectrum.

All-in-all, it would seem likely that the Landau–Loitsyansky equation

$$\langle \mathbf{H}^2 \rangle / V = 8\pi I = \text{constant} \tag{7.34}$$

is approximately valid in isotropic turbulence provided the initial conditions are of the form assumed by Batchelor (i.e. those where remote points are statistically independent). Moreover, such initial conditions are probably typical of, say, wind-tunnel turbulence.

7.1.6 On the difficulties of direct numerical simulations (DNS)

For some time now people have been computing the evolution of turbulent flows in a cubic domain in which the boundaries have very special properties; they are periodic. That is to say, whatever is happening at one face of the cube happens on the opposite face. Such domains are called periodic cubes and they lend themselves to particularly efficient numerical algorithms for solving the Navier–Stokes equations. So far these simulations have been restricted to Reynolds numbers of around $ul/\nu \sim 100 \rightarrow 500$. Higher values of Re are difficult to achieve because of the computational cost of computing all of the turbulent scales down to the Kolmogorov microscale. (As Re increases so the range of scales increases.) Still, many people believe that turbulence at, say, $\mathrm{Re} = 500$ might capture some of the features of high-Re turbulence, and so considerable attention has been given to these simulations.

It might be thought, therefore, that issues such as the rate of dissipation of energy, or the invariance (or otherwise) of Loitsyansky's integral could be settled by computer simulations in a periodic cube. After all, such simulations are now routinely performed and it is usually assumed,

either implicitly or else explicitly, that turbulence in a periodic cube is representative of homogeneous, isotropic turbulence in an infinite domain. Unfortunately, such an assumption is somewhat misleading. In fact, turbulence in a periodic cube represents a rather special dynamical system, the large scales of which are somewhat different from real-life turbulence. It is this which makes it difficult to investigate the behaviour of $u^2(t)$ or of I.

There are two important points to note. First, turbulence in a periodic cube is anisotropic at the large scales. To see that this is so, simply consider $Q_{ij}(\mathbf{r})$. Suppose that $r = L_{\text{box}}$ and choose $\boldsymbol{x}$ and $\boldsymbol{x}'$ to lie at the bottom corners of one of the vertical faces of the cube. Then $Q_{ii}(\mathbf{r}) = 3u^2$ since the two points are perfectly correlated. Now rotate $\mathbf{r}$ by some angle, say, 45°. One point lies at the corner of the box and the other in the interior. $Q_{ii}(\mathbf{r})$ is now less than $3u^2$ since there is no longer a perfect correlation. It follows that the turbulence is anisotopic, at least at the large scales. Worse still, strong, long-range correlations, which are quite unphysical, are built into the periodic cube at the scale of the box.

Still, it seems plausible that if L_{box} is, say, two orders of magnitude greater than the integral scale, l, then there may be some sub-domain within the box in which the influence of the boundaries are not felt. The bulk of the turbulence might then be homogeneous and isotropic. It seems likely, therefore, that the requirements for a simulation to be representative of real-life turbulence are

(i) $\text{Re} \gg 1$
(ii) $l \ll L_{\text{box}}$

Unfortunately, because of limitations in computer power, it is difficult to satisfy both of these criteria. In order to obtain $\text{Re} \sim 500$, it is normally required to have $l \sim L_{\text{box}}/3$. Conversely, if we require a value of $l \sim L_{\text{box}}/100$, then it is difficult to get Re much larger than ~ 20. In short, turbulence in a periodic cube usually knows it is in a periodic cube and the large scales behave accordingly. At least, that is the story to date.

This concludes our introduction to turbulence. We have omitted a great deal in our brief survey, including many of the details of the derivations of (7.18), (7.19) and the Karman–Howarth equation, as well as the proof of

$$\langle \mathbf{H}^2 \rangle / V = 8\pi I$$

However, the interested reader can readily fill the gaps using one or more of the many excellent texts which exist on turbulence.

We now turn to MHD turbulence, which is our main interest. We shall see that Landau's ideas prove particularly fruitful, but that G K Batchelor's warnings of long-range statistical correlations continue to haunt the subject.

7.2 MHD Turbulence

We now examine the influence of a uniform, imposed magnetic field on the decay of (initially isotropic) freely evolving turbulence. We start by returning to the model problem discussed in §5.3, extending it, with the help of Landau's ideas, to a formal statistical theory (Figure 7.7).

7.2.1 The growth of anisotropy at low and high R_m

Suppose that a conducting fluid is held in an insulated sphere of radius R. The sphere sits in a uniform, imposed field $\mathbf{B}_0$, so that the total magnetic field is $\mathbf{B} = \mathbf{B}_0 + \mathbf{b}$, $\mathbf{b}$ being associated with the currents induced by $\mathbf{u}$ within the sphere. For simplicity, we take the fluid to be inviscid (we shall put viscosity back in later). However, we place no restriction on R_m, nor on the interaction parameter which we define here to be $N = \sigma B_0^2 l/\rho u$, l being the integral scale of the turbulence. When R_m is small we have $|\mathbf{b}| \ll |\mathbf{B}_0|$, but in general $|\mathbf{b}|$ may be as large as, or possibly even larger than, $|\mathbf{B}_0|$. At $t = 0$ the fluid is vigorously stirred and then left to itself. The questions of interest are: (i) can we characterise the anisotropy introduced into the turbulence by $\mathbf{B}_0$; (ii) how does the energy decay?

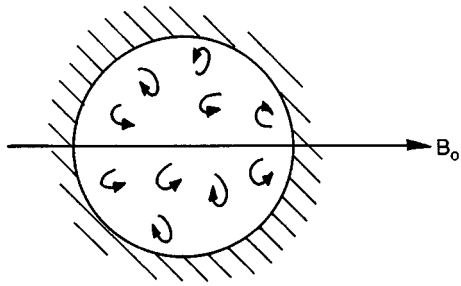

Figure 7.7 MHD turbulence evolving in a sphere.

We shall attack the problem in precisely the same way as in § 5.3. We start by noting that the global torque exerted on the fluid by the Lorentz force is

$$\mathbf{T} = \int \mathbf{x} \times (\mathbf{J} \times \mathbf{B}_0) dV + \int \mathbf{x} \times (\mathbf{J} \times \mathbf{b}) dV \tag{7.35}$$

However, a closed system of currents produces zero net torque when they interact with their self-field, **b**. (This follows from conservation of angular momentum.) It follows that the second integral on the right is zero. We now transform the first integral using the identity

$$2\mathbf{x} \times [\mathbf{G} \times \mathbf{B}_0] = [\mathbf{x} \times \mathbf{G}] \times \mathbf{B}_0 + \nabla \cdot [(\mathbf{x} \times (\mathbf{x} \times \mathbf{B}_0))\mathbf{G}] \tag{7.36}$$

(Here **G** is any solenoidal vector field.) Setting $\mathbf{G} = \mathbf{J}$ we find

$$\mathbf{T} = \left\{ \frac{1}{2} \int (\mathbf{x} \times \mathbf{J}) dV \right\} \times \mathbf{B}_0 = \mathbf{m} \times \mathbf{B}_0 \tag{7.37}$$

and consequently the global angular momentum evolves according to

$$\rho \frac{d\mathbf{H}}{dt} = \mathbf{T} = \mathbf{m} \times \mathbf{B}_0, \qquad \mathbf{H} = \int (\mathbf{x} \times \mathbf{u}) dV \tag{7.38}$$

By implication, $\mathbf{H}_{//}$ is conserved. This, in turn, gives a lower bound on the total energy of the system,

$$E = E_{\mathbf{b}} + E_{\mathbf{u}} > \mathbf{H}_{//}^2 \left(2 \int \mathbf{x}_\perp^2 dV \right)^{-1} \tag{7.39}$$

(Expression (7.39) follows from the Schwarz inequality in the form $\mathbf{H}_{//}^2 \geq \int \mathbf{u}_\perp^2 dV \int \mathbf{x}_\perp^2 dV$. See Chapter 5, Section 3.) However, the total energy declines due to Joule dissipation and so we also have

$$\frac{dE}{dt} = \frac{d}{dt} \int_{V_R} \frac{\rho \mathbf{u}^2}{2} dV + \frac{d}{dt} \int_{V_\infty} \frac{b^2}{2\mu} dV = -\frac{1}{\sigma} \int_{V_R} \mathbf{J}^2 dV \tag{7.40}$$

We have the makings of a paradox. One component of angular momentum is conserved, requiring that E is non-zero, yet energy is dissipated as long as **J** is finite. The only way out of this paradox is for the turbulence to evolve to a state in which $\mathbf{J} = 0$, yet $E_{\mathbf{u}}$ is non-zero (to satisfy (7.39)). However, if $\mathbf{J} = 0$ then Ohm's law requires $\mathbf{E} = -\mathbf{u} \times \mathbf{B}_0$, while Faraday's law requires that $\nabla \times \mathbf{E} = 0$. It follows that, at large times, $\nabla \times (\mathbf{u} \times \mathbf{B}_0) = (\mathbf{B}_0 \cdot \nabla)\mathbf{u} = 0$, and so **u** becomes independent of $\mathbf{x}_{//}$ as $t \to \infty$. The final state is therefore strictly two-dimensional, of the form $\mathbf{u}_\perp = \mathbf{u}_\perp(\mathbf{x}_\perp)$, $\mathbf{u}_{//} = 0$. In short, the turbulence ultimately reaches a state which consists of one or more columnar eddies, each aligned

with $\mathbf{B}_0$. Note that all of the components of $\mathbf{H}$, other than $\mathbf{H}_{//}$ are destroyed during this evolution.

At low R_m this transition will occur on the timescale of $\tau = (\sigma B_0^2/\rho)^{-1}$, the magnetic damping time. This was demonstrated in § 5.3 and the argument is straightforward. A low R_m, the current density is governed by

$$\mathbf{J} = \sigma(-\nabla V + \mathbf{u} \times \mathbf{B}_0) \tag{7.41}$$

and so the global dipole moment, $\mathbf{m}$, is

$$\mathbf{m} = \frac{1}{2}\int \mathbf{x} \times \mathbf{J} dV = (\sigma/2)\int \mathbf{x} \times (\mathbf{u} \times \mathbf{B}_0) dV - (\sigma/2)\oint (V\mathbf{x}) \times d\mathbf{S}$$

The surface integral vanishes while the volume integral transforms, with the aid of (7.36), to give

$$\mathbf{m} = (\sigma/4)\mathbf{H} \times \mathbf{B}_0$$

Substituting into (7.38) we obtain

$$\frac{d\mathbf{H}}{dt} = -\frac{\mathbf{H}_\perp}{4\tau}, \qquad \tau^{-1} = \sigma B_0^2/\rho \tag{7.42}$$

and so $\mathbf{H}_{//}$ is conserved (as expected) while $\mathbf{H}_\perp$ declines exponentially on a timescale of τ.

In summary then, whatever the initial condition, and for any Rm or N, the flow evolves towards the anisotropic state (Figure 7.8)

$$\mathbf{u}_\perp = \mathbf{u}_\perp(\mathbf{x}_\perp), \qquad \mathbf{H}_{//} = \mathbf{H}_{//}(0), \qquad \mathbf{H}_\perp = \mathbf{u}_{//} = \mathbf{b} = \mathbf{J} = \mathbf{0} \tag{7.43}$$

From the point of view of turbulence theory, the two most important points are: (i) $\mathbf{B}_0$ introduces severe anisotropy into the turbulence, and (ii)

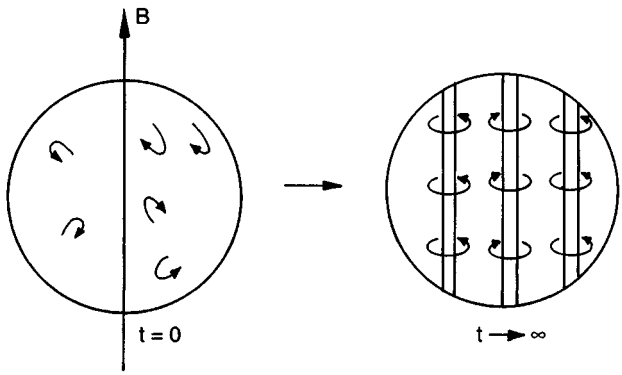

Figure 7.8 Growth of anistropy in MHD turbulence.

$\mathbf{H}_{//}$ is conserved during the decay. Following Landau's arguments, the latter point implies that

$$\langle \mathbf{H}_{//}^2 \rangle = -\int\int \mathbf{r}_\perp^2 \langle \mathbf{u}_\perp \cdot \mathbf{u}'_\perp \rangle d^3\mathbf{r}\, d^3\mathbf{x} = \text{constant} \tag{7.44}$$

where $\mathbf{r} = \mathbf{x}' - \mathbf{x}$. If (and it is a significant if) we can ignore Batchelor's long-range statistical correlations, then, for as long as $R \gg l$, we have the invariant

$$\langle \mathbf{H}_{//}^2 \rangle / V = -\int \mathbf{r}_\perp^2 \langle \mathbf{u}_\perp \cdot \mathbf{u}'_\perp \rangle d^3\mathbf{r} = \text{constant} \tag{7.45}$$

This is Loitsyansky's integral for MHD turbulence. (When $\mathbf{B}_0 = 0$ and the turbulence is isotropic, we can replace (7.45) by (7.34).)

Of course, in these arguments we have ignored ν and hence the process of energy removal via the energy cascade. In reality, for a finite ν, the predicted growth of anisotropy will occur only if the turbulence lives for long enough and this, in turn, requires $\mathbf{J} \times \mathbf{B} \geq\sim \rho(\mathbf{u} \cdot \nabla)\mathbf{u}$, i.e. $N \geq\sim 1$. Note, however, that (7.45) is valid for any N provided that the long-range statistical correlations are weak.

7.2.2 Decay laws at low R_m

We now restrict ourselves to low values of R_m, and reintroduce viscosity. We would like to develop the MHD equivalent of Kolmogorov's decay laws (7.30) and (7.31)

$$u^2 \sim u_0^2[1 + (7/10)(u_0 t/l_0)]^{-10/7}$$

$$l \sim l_0[1 + (7/10)(u_0 t/l_0)]^{2/7}$$

Recall that these were based on the estimates

$$\frac{du^2}{dt} \sim -\frac{u^3}{l}, \qquad \int \mathbf{r}^2 \langle \mathbf{u} \cdot \mathbf{u}' \rangle d^3\mathbf{r} \sim u^2 l^5 = \text{constant} \tag{7.46a, b}$$

We require MHD analogues of these equations.

In MHD turbulence the total energy, which at low R_m is dominated by kinetic energy ($\mathbf{b}$ being vanishingly small), declines due to both Joule dissipation and viscosity:

$$\frac{dE}{dt} = -\frac{1}{\sigma}\int \mathbf{J}^2 dV - \rho\nu \int \omega^2 dV \tag{7.47}$$

(Here we have used the fact that the viscous dissipation is minus the rate of working of the viscous force, $-\nu(\nabla^2\mathbf{u}) \cdot \mathbf{u}$, and this is related to the

vorticity by $-(\nabla^2\mathbf{u})\cdot\mathbf{u} = \omega^2 + \nabla\cdot(\omega\times\mathbf{u})$, the latter term integrating to zero.) Now let us suppose that the energy cascade proceeds as usual,[2] on a timescale of l/u. Then the MHD analogue of (7.46a) is

$$\frac{du^2}{dt} \sim -\frac{u^3}{l_\perp} - \left(\frac{l_\perp}{l_{//}}\right)^2 \frac{u^2}{\tau} \tag{7.48}$$

Here $l_\perp$ and $l_{//}$ represent suitably defined transverse and longitudinal integral scales for the turbulence. The new term in (7.47) represents the Joule dissipation $\langle \mathbf{J}^2\rangle/\rho\sigma$, $\langle \mathbf{J}^2\rangle$ having been estimated from the curl of the low-R_m form of Ohm's law, $\nabla\times\mathbf{J} = \sigma(\mathbf{B}_0\cdot\nabla)\mathbf{u}$. We now need the analogue of (7.46b). This is provided by our conservation law (7.45), which, in the absence of long-range statistical correlations, yields the estimate

$$u^2 l_{//} l_\perp^4 = \text{constant} \tag{7.49}$$

Expressions (7.48) and (7.49) are the analogues of Kolmogorov's equations (7.46a, b). However, because of the anisotropy of MHD turbulence, we have three, rather than two, unknowns: u, $l_{//}$, $l_\perp$. We need a third relationship if we are to predict the rate of decay of energy. This comes from the fact that $l_{//}/l_\perp = 1$ if N is small, and obeys (5.16) if N is large. For example, in the high-N examples given in Chapter 5, Section 2, where isolated vortices evolve in a uniform magnetic field, $l_{//}$ increases due to $\mathbf{B}_0$ but $l_\perp$ is unaffected by the field. The end result is $l_{//}/l_\perp \sim (t/\tau)^{1/2}$. Both limits (low and high N) are captured by the heuristic expression

$$\frac{d}{dt}\left(\frac{l_{//}}{l_\perp}\right)^2 \sim \frac{2}{\tau} \tag{7.50}$$

Expressions (7.48) → (7.50) represent a closed system for u, $l_{//}$ and $l_\perp$. They contain two timescales, τ and $l_\perp/u$, the ratio of which is N, and they predict very different kinds of behaviour depending on the initial value of N. For example, whenever inertia is negligible by comparison with $\mathbf{J}\times\mathbf{B}_0$, (7.48) → (7.50) reduce to

$$\frac{du^2}{dt} \sim -\left(\frac{l_\perp}{l_{//}}\right)^2 \frac{u^2}{\tau}$$

$$u^2 l_{//} l_\perp^4 = \text{constant}$$

$$\frac{d}{dt}\left(\frac{l_{//}}{l_\perp}\right)^2 = \frac{2}{\tau}$$

[2] This is plausible since the Lorentz force is felt only by the largest eddies, the turnover time of the bulk of the eddies being much shorter than τ. See Appendix 4.

These are readily integrated to yield $u^2 \sim (t/\tau)^{-1/2}$, $l_{//} \sim (t/\tau)^{1/2}$, results which coincide with our study of isolated vortices at high N (see Section 5.2). In fact, these turbulence scalings may be verified by exact analysis through integration of the linearised (inertia-less) Navier–Stokes equation. However, the procedure is complicated, involving three-dimensional Fourier transforms, and so we shall not reproduce the results here.

When N is small, on the other hand, (7.48) → (7.50) yield Kolmogorov's law, $u^2 \sim t^{-10/7}$, with a small correction due to Joule dissipation. For intermediate values of N, however, the situation is rather different. In general there is no power law decay behaviour, although for the particular case $N(t=0) = 7/15$ we find $u^2 \sim (t/\tau)^{-11/7}$, $l_{//} \sim (t/\tau)^{5/7}$and $l_\perp \sim (t/\tau)^{3/14}$. This compares favourably with laboratory experiments performed at $N \sim 1$.[3]

So the general theme here is that the eddies tend to elongate in the direction of B_0, causing $l_{//}$ to grow faster than $l_\perp$, as anticipated in Chapter 7, Section 2.1. There are three distinct but related explanations for the growth of $l_{//}$ given in the literature. One is the argument presented in the preceding section, the essence of which is that the conservation of $\mathbf{H}_{//}$, in the face of continual Joule dissipation, is possible only if $l_{//}$ grows. That is to say, at high N

$$\frac{du^2}{dt} \sim -\left(\frac{l_\perp}{l_{//}}\right)^2 \frac{u^2}{\tau}$$

which implies that u^2 declines according to

$$u^2 \sim u_0^2 \exp\left[-\frac{1}{\tau}\int_0^t (l_\perp/l_{//})^2 dt\right] \tag{7.51}$$

If $l_\perp/l_{//}$ were to remain of order unity, then u^2 would decline exponentially, in direct contradiction to

$$u^2 l_{//} l_\perp^4 = \text{constant}$$

It is inevitable, therefore, that $l_{//}/l_\perp$ grows, thus introducing anisotropy into the turbulence.

An alternative argument relies on the fact that the curl of the Lorentz force (per unit mass) may be written in the form

$$\nabla \times \mathbf{F} = \nabla \times [\mathbf{J} \times \mathbf{B}_0/\rho] = -\tau^{-1}\nabla^{-2}\left[\partial^2 \omega / x_{//}^2\right] \tag{7.52}$$

which looks a bit like

[3] See Appendix 4.

$$\nabla \times [\mathbf{F}] \sim (l_\perp^2/\tau)\partial^2\omega/\partial x_{//}^2 \tag{7.53}$$

(When $l_{//} \gg l_\perp$, this may be made rigorous by Fourier transforming the vorticity equation in the transverse plane, so that (7.52) transforms to $(k_\perp^2\tau)^{-1}\partial^2\omega/\partial x_{//}^2$, $k_\perp$ being a wavenumber in the transverse plane). The implication is that, provided inertia is small, so that $\nabla \times (\mathbf{u} \times \omega)$ is much weaker than (7.52), the vorticity will diffuse along the $\mathbf{B}_0$-lines with a diffusion coefficient of $l_\perp^2/\tau$. This pseudo-diffusion is the last vestige of Alfvén wave propagation, as discussed in Chapter 6, Section 1.

A third, more mechanistic, argument is the following. Suppose we have a vortex, as shown in Figure 7.9, in which ω is aligned with $\mathbf{B}_0$. (We use local cylindrical polar coordinates as shown.) Then the vortex will spread along the **B**-line. The mechanism for this elongation is as follows. The term $\mathbf{u}_\theta \times \mathbf{B}$ tends to drive a current, J_r, in accordance with Ohm's law. Near the centre of the vortex, where axial gradients in u_θ are small, this is counter-balanced by an electrostatic potential, ∇V, and so no current flows. However, near the top and bottom of the vortex, the current can return through regions of small or zero swirl, as shown. The resulting inward flow of current above and below the vortex gives rise to an azimuthal torque which, in turn, creates swirl in previously stagnant regions. In this way vorticity diffuses out along the **B**-lines. (We will return to this issue in Chapter 9, where we look at vortices of arbitrary orientation.)

We close this section on a note of caution. Because of anisotropy, great care must be taken in the definition of N. A nominal definition might be

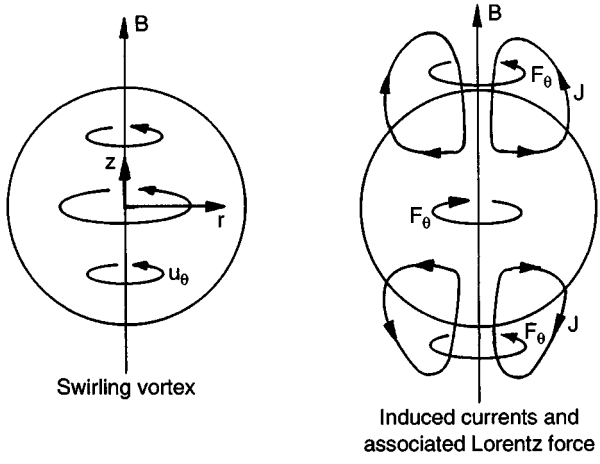

Figure 7.9 Mechanism for the elongation of vortices in a magnetic field.

$$N_{\perp} = \sigma B_0^2 l_{\perp}/\rho u \tag{7.54a}$$

or perhaps

$$N_{//} = \sigma B_0^2 l_{//}/\rho u \tag{7.54b}$$

However, it is readily demonstrated that the true ratio of $\mathbf{J} \times \mathbf{B}_0$ to inertia is

$$N_{\text{true}} = N_{//}(l_{\perp}/l_{//})^3 \tag{7.54c}$$

In practice, the difference between $N_{//}$ and N_{true} can be large. Suppose, for example, that $l_{//} \sim 3l_{\perp}$ and $N_{//} \sim 10$ (which is not untypical in the laboratory). It might be thought, naively, that $\mathbf{J} \times \mathbf{B}_0$ is the dominant force. In fact N_{true} in this case is less than unity, so that inertia is dominant! Such misconceptions occur commonly in the literature.

Interestingly, whatever the initial value of N, N_{true} always evolves towards unity, representing a balance between $\mathbf{J} \times \mathbf{B}_0$ and inertia. For example, if N is initially very large, then $u^2 \sim t^{-1/2}$, $l_{//} \sim t^{1/2}$ and $l_{\perp} = \text{constant}$. As a result $N_{\text{true}} = N_{\perp}(l_{\perp}/l_{//})^2 \sim N_0(t/\tau)^{-3/4}$, N_0 being the initial value of N (the initial conditions are assumed to be isotropic). Thus, N_{true} will fall as the eddies elongate, essentially because $\mathbf{J} \times \mathbf{B}_0$ declines due to a fall in $\mathbf{J}$. Conversely, if N is initially very small, so the turbulence remains (almost) isotropic, then $u^2 \sim t^{-10/7}$, $l \sim t^{2/7}$ and $N_{\text{true}} \sim N_0(u_0 t/l_0)$. In this case N_{true} rises as the inertia of the eddies becomes weaker. In either case, for large or small N_0, $N_{\text{true}} \to \sim 1$ as $t \to \infty$.

7.2.3 *The spontaneous growth of a magnetic field at high R_m*

We now turn to high-R_m turbulence and consider the case where the imposed field, $\mathbf{B}_0$, is zero. We are interested in whether or not a small 'seed' field, present in the fluid at $t = 0$, will grow or decay in statistically steady turbulence. An intriguing argument, proposed by G K Batchelor, suggests a seed field will grow if $\lambda < \nu$ and decay if $\lambda > \nu$.

Batchelor noted that the fate of the seed field is determined by the balance between the random stretching of the flux tubes by $\mathbf{u}$, which will tend to increase $\langle B^2 \rangle$, and Ohmic dissipation, which operates mainly on the small-scale flux tubes (which have large spatial gradients in $\mathbf{B}$). He also noted the analogy between $\boldsymbol{\omega}$ and $\mathbf{B}$ in the sense that they are governed by similar equations:

$$\frac{\partial \boldsymbol{\omega}}{\partial t} = \nabla \times (\mathbf{u} \times \boldsymbol{\omega}) + \nu \nabla^2 \boldsymbol{\omega}$$

$$\frac{\partial \mathbf{B}}{\partial t} = \nabla \times (\mathbf{u} \times \mathbf{B}) + \lambda \nabla^2 \mathbf{B}$$

If $\lambda = \nu$, there exists a solution for the seed field of the form $\mathbf{B} = \text{constant} \times \boldsymbol{\omega}$. Thus, since $\langle \omega^2 \rangle$ is steady, so is $\langle \mathbf{B}^2 \rangle$. It follows that, if $\lambda = \nu$, flux-tube stretching and Ohmic dissipation have equal but opposite influences on $\langle \mathbf{B}^2 \rangle$. If λ exceeds ν, however, we would expect enhanced Ohmic dissipation and a decline in $\langle \mathbf{B}^2 \rangle$, while $\lambda < \nu$ should lead to spontaneous growth in the seed field, a growth which is curtailed only when $\mathbf{J} \times \mathbf{B}$ is large enough to suppress the turbulence significantly. (Note that the threshold $\lambda = \nu$ is a very stringent condition. In most liquid metals, for example, $\nu/\lambda \sim 10^{-6}$. Since σ and ν increase with the mean free path lengths of the charge and mass carriers, respectively, the condition $\lambda < \nu$ is likely to be met only in the astrophysical context, perhaps in the solar corona or the interstellar gas.)

These arguments are intriguing but imperfect. The problems are twofold. First, the analogy between $\mathbf{B}$ and $\boldsymbol{\omega}$ is not exact: $\boldsymbol{\omega}$ is functionally related to $\mathbf{u}$ in a way in which $\mathbf{B}$ is not. Second, if the turbulence is to be statistically steady, then a forcing term must appear in the vorticity equation representing some kind of mechanical stirring (which is required to keep the turbulence alive). Since the corresponding term is absent in the induction equation, the analogy between $\mathbf{B}$ and $\boldsymbol{\omega}$ is again broken. One might try to circumvent this objection by considering freely decaying turbulence. Unfortunately, this also leads to problems, since the turbulence will die on a timescale of l/u, and if $R_m = u_0 l_0/\lambda$ is large, this implies we can get a growth in $\langle B^2 \rangle$ only for times much less than the Ohmic timescale, l^2/λ. However, in the dynamo context, such transient growths are of little interest. Thus the conditions under which $\langle \mathbf{B}^2 \rangle$ will spontaneously grow are still unclear.

If we accept the argument that a seed field is amplified for sufficiently small λ, it is natural to ask what the spatial structure of this field might be. Will it have a very fine-scale structure due to flux tube stretching, or a large-scale structure due to flux-tube mergers? In this context it is interesting to note that arguments have been put forward to suggest that there is an *inverse cascade* of the magnetic field in freely evolving, high-R_m turbulence. That is to say, the integral scale for $\mathbf{B}$ grows as the flow evolves because small-scale flux tubes merge to produce a large-scale field. The arguments are rather tentative, and rest on the approximate

conservation of magnetic helicity which, in turn, relies on the three equations:

$$\frac{D}{Dt}\left(\frac{\rho \mathbf{u}^2}{2}\right) = -\nabla \cdot [p\mathbf{u}] - \rho\nu[\omega^2 + \nabla \cdot (\omega \times \mathbf{u})] + [\mathbf{J} \cdot \mathbf{E} - \mathbf{J}^2/\sigma]$$

$$\frac{\partial}{\partial t}\left(\frac{B^2}{2\mu}\right) = -\mathbf{J} \cdot \mathbf{E} - \nabla \cdot [(\mathbf{E} \times \mathbf{B})/\mu]$$

$$\frac{D}{Dt}(\mathbf{A} \cdot \mathbf{B}) = \nabla \cdot [(\mathbf{u} \cdot \mathbf{A})\mathbf{B}] - \sigma^{-1}[2\mathbf{J} \cdot \mathbf{B} + \nabla \cdot (\mathbf{J} \times \mathbf{A})]$$

The first of these equations comes from taking the product of $\mathbf{u}$ with the Navier–Stokes equation, noting that the rate of working of the Lorentz force is $(\mathbf{J} \times \mathbf{B}) \cdot \mathbf{u} = -(\mathbf{u} \times \mathbf{B}) \cdot \mathbf{J}$, and then using Ohm's law to write $\mathbf{u} \times \mathbf{B}$ in terms of $\mathbf{E}$ and $\mathbf{J}$. The second arises from the product of $\mathbf{B}$ with Faraday's law, and noting that

$$\mathbf{B} \cdot \nabla \times \mathbf{E} = \mathbf{E} \cdot \nabla \times \mathbf{B} + \nabla \cdot (\mathbf{E} \times \mathbf{B}) = \mathbf{E} \cdot (\mu\mathbf{J}) + \nabla \cdot (\mathbf{E} \times \mathbf{B})$$

The third relates to magnetic helicity which, as we saw in Chapter 4, Section 4, is globally conserved when $\lambda = 0$. We now take averages, and assume that the turbulence is statistically homogeneous so that the divergences of averaged quantities disappear. Adding the first two equations to eliminate $\langle \mathbf{J} \cdot \mathbf{E} \rangle$ yields

$$\frac{d}{dt}\left[\frac{1}{2}\rho\langle \mathbf{u}^2 \rangle + \langle B^2 \rangle/2\mu\right] = -\rho\nu\langle \omega^2 \rangle - \langle J^2 \rangle/\sigma$$

$$\frac{d}{dt}[\langle \mathbf{A} \cdot \mathbf{B} \rangle] = -2\langle \mathbf{J} \cdot \mathbf{B} \rangle/\sigma$$

We recognise the first of these as representing the decline of energy through viscous and Ohmic dissipation. Let us write these symbolically as

$$\frac{dE}{dt} = -\rho\nu\langle \omega^2 \rangle - \langle J^2 \rangle/\sigma$$

$$\frac{dH_B}{dt} = -2\langle \mathbf{J} \cdot \mathbf{B} \rangle/\sigma$$

The next step is to show that, as $\sigma \to \infty$, dE/dt remains finite while dH_B/dt tends to zero. We proceed as follows. The Schwarz inequality (see Chapter 5, Section 3) tells us

$$\left\{\int \mathbf{J}\cdot\mathbf{B}dV\right\}^2 \leq \int J^2 dV \int B^2 dV$$

This may be rewritten as

$$|\langle \mathbf{J}\cdot\mathbf{B}\rangle|/\sigma \leq (2\mu/\sigma)^{1/2}\left[|\dot{E}|E\right]^{1/2}$$

and so we can place an upper bound on the rate of destruction of magnetic helicity:

$$|\dot{H}_B|/\mu \leq (8\lambda)^{1/2}|\dot{E}|^{1/2}E^{1/2}$$

We now let $\sigma \to \infty$. In the process, however, we assume that $\dot{E}$ remains finite. We might try to justify this as follows. We expect that, as $\sigma \to \infty$ more and more of the Joule dissipation is concentrated into thin current sheets. However, by analogy with viscous dissipation at small ν, we might expect that $\langle J^2\rangle/\sigma$ remains finite in the limiting process. (This is, however, an assumption.) If this is true, it follows that, in the limit $\lambda \to 0$, H_B is conserved. Thus, for small λ, we have the destruction of energy subject to the conservation of magnetic helicity. In finite domains this presents us with a well-defined variational problem. Minimising E subject to the conservation of H_B in a bounded domain gives us (see Chapter 4, Section 4)

$$\nabla\times\mathbf{B} = \alpha\mathbf{B}, \qquad \mathbf{u} = 0$$

where α is an eigenvalue of the variational problem. The implication is that **B** ends up with a large length scale, comparable with the domain size.

In summary then, the assumption that E remains finite as $\sigma \to \infty$ leads to the conservation of helicity, and minimising energy subject to the invariance of H_B gives, for a finite domain, a large-scale static magnetic field with **J** and **B** aligned. However, this picture of high-R_m turbulence raises as many questions as it answers. What, for example, is the physical mechanism for the inverse cascade of **B**?

This completes our survey of MHD turbulence. We have left a great deal out. For example, we have not discussed the growth of anisotropy in high-R_m turbulence, where two-dimensionality is thought to be related to the propagation of Alfvén waves. However, the reader will find many useful references at the end of the chapter. We now turn to one of the extreme consequences of an intense magnetic field – two-dimensional turbulence.

7.3 Two-Dimensional Turbulence

Everything should be made as simple as possible, but not simpler.

A Einstein

Probably the most common statement made about two-dimensional turbulence is that it does not exist. While factually correct, it rather misses the point. There are many flows whose large-scale behaviour is, in some sense, two-dimensional. Large-scale atmospheric and oceanic flows fall into this category, if only because of the thinness of the atmosphere and oceans in comparison with their lateral dimensions. Moreover, both rapid rotation and strong stratification tend to promote two-dimensional flows through the propagation of internal waves, and, of course, strong magnetic fields promote two-dimensionality. While no flow will ever be truly two-dimensional, it seems worthwhile to examine the dynamics of strictly two-dimensional motion in the hope that it sheds light on certain aspects of real, 'almost' two-dimensional phenomena.

In moving from three- to two-dimensions we greatly simplify the equations. Most importantly, we throw out vortex stretching. One might expect, therefore, that two-dimensional turbulence should be much simpler than isotropic turbulence. Mathematically, this is correct, as it must be. Curiously though, the physical characteristics of two-dimensional turbulence are, in many ways, more counter-intuitive than conventional turbulence. At least, this is the case for one brought up in the tradition of Richardson and Kolmogorov. For example, in two dimensions, there is an *inverse cascade* of energy, from the small to the large, as small vortices merge to form larger ones!

7.3.1 *Batchelor's self-similar spectrum and the inverse energy cascade*

When a number of vortices having the same sense of rotation exist in proximity to one another, they tend to approach one another, and to amalgamate into one intense vortex.

(Aryton, 1919)

We shall restrict ourselves to strictly two-dimensional turbulence, $\mathbf{u}(x, y) = (u_x, u_y, 0)$, $\boldsymbol{\omega} = (0, 0, \omega)$, and to turbulence which is homogeneous and isotropic (in a two-dimensional sense). We shall ignore all body forces, such as Lorentz forces or the Coriolis force, and address the problem of freely evolving turbulence. As before, we define the characteristic velocity u through $u^2 = \langle u_x^2 \rangle = \langle u_y^2 \rangle$.

All existing phenomenological theories are based on the two equations

$$\frac{d}{dt}\left[\frac{1}{2}\langle \mathbf{u}^2\rangle\right] = -\nu\langle\omega^2\rangle \tag{7.55}$$

$$\frac{d}{dt}\left[\frac{1}{2}\langle \omega^2\rangle\right] = -\nu\langle(\nabla\omega)^2\rangle \tag{7.56}$$

These state that the kinetic energy density, $\frac{1}{2}\langle\mathbf{u}^2\rangle$, and the so-called enstrophy, $\langle\omega^2\rangle$, both decline monotonically in freely evolving two-dimensional turbulence. The first of these relationships comes from taking the product of $\mathbf{u}$ with

$$\frac{D\mathbf{u}}{Dt} = -\nabla\left(\frac{p}{\rho}\right) - \nu\nabla\times\boldsymbol{\omega}$$

which yields

$$\frac{D}{Dt}\left[\frac{\mathbf{u}^2}{2}\right] = -\nabla\cdot\left[\frac{p\mathbf{u}}{\rho}\right] - \nu\{\omega^2 - \nabla\cdot(\mathbf{u}\times\boldsymbol{\omega})\}$$

We now average this equation, noting that an ensemble average is equivalent to a spatial average, and that statistical homogeneity of the turbulence ensures that all divergences integrate to zero. The end result is (7.55). Similarly, starting with

$$\frac{D\omega}{Dt} = \nu\nabla^2\omega$$

from which

$$\frac{D}{Dt}\left(\frac{\omega^2}{2}\right) = -\nu\{(\nabla\omega)^2 - \nabla\cdot(\omega\nabla\omega)\}$$

we obtain, on forming a spatial average, (7.56).

Now the key point about (7.55) and (7.56) is that, as $\mathrm{Re}\to\infty$, u^2 is conserved, since the enstrophy remains finite and bounded by its initial value. This is in stark contrast to three-dimensional turbulence, where a decline in ν is accompanied by a rise in $\langle\omega^2\rangle$ in such a way that the dissipation of kinetic energy remains finite (of order u^3/l) as $\mathrm{Re}\to\infty$. This conservation of energy in two-dimensional turbulence implies a long-lived evolution for these flows.

In the limit $\mathrm{Re}\to\infty$ diffusion becomes small (except at the smaller scales) and so the isovortical lines become material lines, and are continually teased out as the flow evolves so that the vorticity field rapidly adopts the structure of thin, sinuous sheets, like cream stirred into coffee.

This filamentation of vorticity feeds an enstrophy cascade (lumps of vorticity are teased out to smaller and smaller scales) which is halted at the small scales only when the transverse dimensions of the sheets are small enough for viscosity to act, destroying the enstrophy and diffusing the vorticity. As in three dimensions, viscosity plays a passive rôle, mopping up the enstrophy (energy in three dimensions) which has cascaded down from above. The dynamics are controlled by the large scales, and even as $\nu \to 0$ the destruction of enstrophy remains finite.

This passive rôle of viscosity led G K Batchelor to propose a self-similar distribution of energy for the large and intermediate scales. In terms of the velocity increment, Δv, which represents the r.m.s. difference in velocity between two points separated by a distance r (see Chapter 7, Section 1.3), this self-similar energy spectrum takes the form

$$[\Delta v(r)]^2 = u^2 g(r/ut) \tag{7.57}$$

The argument behind (7.57) is essentially a dimensional one. If the turbulence has evolved long enough for the influence of the initial conditions to be erased, and viscosity controls only the smallest scales, then all that the large scales remember is u. It follows that u, r and t are the only parameters determining $\Delta v(r)$, and (7.57) is then inevitable. In this model then, the integral scale grows as $l \sim ut$. That is, if we divide Δv by u and r by $l = ut$, we obtain a self-similar energy spectrum valid throughout the evolution of the flow (Figure 7.10) and so the size of the most energetic eddies must grow as ut.

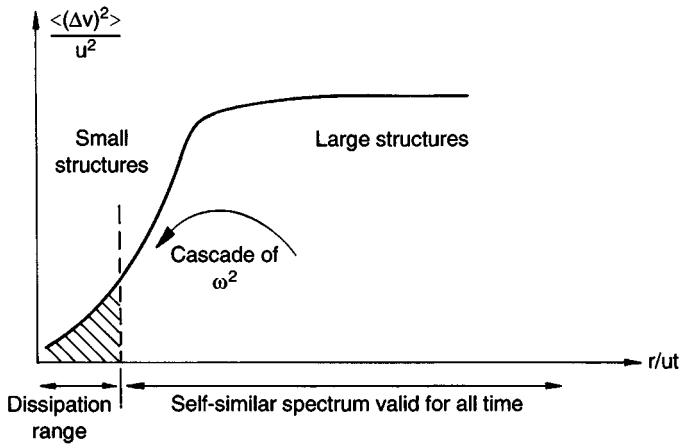

Figure 7.10 Batchelor's universal energy spectrum for two-dimensional turbulence.

For almost thirty years, dating from its introduction in 1969, Batchelor's self-similar energy spectrum, and associated theories by Kraichnan, dominated the literature on two-dimensional turbulence. Note, however, that this dimensional argument hinges on the flow remembering nothing other than u. It might, for example, also remember $\langle H^2 \rangle$, but this is a whole new story to which we shall return later.

In the Batchelor–Kraichnan picture we have two cascades: a direct cascade of enstrophy from the large scale to the small, going hand-in-hand with an *inverse cascade* of energy (as anticipated by Ayrton in 1919) as more and more energy moves to larger scales, the total energy being conserved. Physically, we can picture this in terms of the filamentation of vorticity, as shown in Figure 7.11. A (red) blob of vorticity, such as that shown in Figure 7.11(a), will be teased out into a strip of thickness δ by eddies whose dimensions are comparable with the blob size, R. Area is conserved by the vortex patch and so δ falls as the characteristic integral dimension, l, increases. The strip is then further teased and twisted by the flow ((b) → (c)), and in the process l continues to grow at a rate $l \sim ut$ while δ declines. The process ceases, for this particular vortex patch, when δ becomes so small that diffusion sets in, and the red spaghetti of Figure 7.11(c) becomes the pink cloud of (d). The direct cascade of enstropy is associated with the reduction in δ, while the inverse cascade of energy is associated with the growth of l, which characterises the eddy size associated with the vortex patch.

7.3.2 Coherent vortices

In Batchelor's theory the vorticity is treated essentially like a passive tracer in the flow. However, following the rapid development of compu-

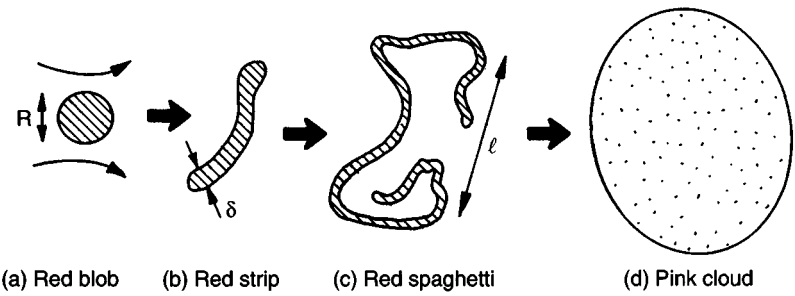

Figure 7.11 Destruction of a lump of vorticity in two-dimensional turbulence.

tational fluid dynamics in the 1980s, and its application to two-dimensional turbulence, it soon became clear that this was not the whole story. While filamentation of vorticity does indeed occur, numerical experiments suggested that intense patches of vorticity, embedded in the initial conditions, survive the filamentation process (process (a) → (b) in Figure 7.11), forming long-lived *coherent vortices*. These coherent vortices obey a different set of dynamical rules, interacting with each other, sometimes merging and sometimes being destroyed by a stronger vortex. The picture is now one of two sets of dynamical processes coexisting in the same vorticity field. Weak vorticity is continually filamented, feeding the enstrophy cascade in the manner suggested by Batchelor. However, within this sea of quasi-passive vorticity filaments, bullets of coherent vorticity fly around, rather like point vortices, increasing in size and decreasing in number through a sequence of mergers.

The emergence of coherent vortices is generally attributed to the equation

$$\frac{D^2}{Dt^2}[\nabla\omega] + \frac{1}{4}[\omega^2 - S_1^2 - S_2^2]\nabla\omega = \text{terms of order}\left(\frac{\mathrm{DS}_{1,2}}{\mathrm{Dt}}\nabla\omega\right) \qquad (7.58)$$

where S_1 and S_2 represent the strain fields $2\partial u_x/\partial x$ and $(\partial u_x/\partial y + \partial u_y/\partial x)$, respectively. ((7.58) follows from $D\omega/Dt = 0$). If the rate of change of S_1 and S_2 (following a material particle) is much less than the corresponding rate of change of $\nabla\omega$, then the right-hand side of (7.58) may be neglected. It then follows that vorticity gradients will grow exponentially in regions where the strain field dominates, or else oscillate in regions where the vorticity dominates. The latter regime leads to coherent vortices, or at least that is the idea. It should be stressed, however, that there is no real justification for neglecting the terms on the right of (7.58) and so this is an imperfect explanation. Nevertheless, we have the empirical observation that the peaks in vorticity, say $\hat{\omega}$, survive the filamentation and so are remembered by the flow. This leads to the idea that Batchelor's energy spectrum should be generalised to

$$[\Delta v(r)]^2 = u^2 g(r/ut, \hat{\omega}t) \qquad (7.59)$$

7.3.3 The governing equations of two-dimensional turbulence

The arguments above are essentially heuristic, although the evidence of the numerical experiments suggest that they are reasonably sound. However, it seems natural to go further and establish the governing

equations for two-dimensional turbulence to see if they tell us anything more.

The two-dimensional analogues of (7.18) and (7.19) are

$$Q_{ij}(\mathbf{r}) = u^2\left\{\frac{d}{dr}(rf)\delta_{ij} - \frac{r_i r_j}{r}f'(r)\right\} \tag{7.60a}$$

$$S_{ijl} = u^3\left\{\frac{1}{2r}\frac{d}{dr}(rk)(r_i\delta_{jl} + r_j\delta_{il}) - \frac{r_i r_j r_l}{r}\frac{d}{dr}\left(\frac{k}{r}\right) - \frac{r_l\delta_{ij}k}{r}\right\} \tag{7.60b}$$

where f and k are the usual longitudinal velocity correlation functions. Substituting these into the dynamic equation

$$\frac{\partial Q_{ij}}{\partial t} = \frac{\partial}{\partial r_k}\left[S_{ikj} + S_{jki}\right] + 2\nu\nabla^2 Q_{ij} \tag{7.61}$$

yields the two-dimensional analogue of the Karman–Howarth equation:

$$\boxed{\frac{\partial}{\partial t}\left[u^2 r^3 f\right] = u^3\frac{\partial}{\partial r}\left[r^3 k\right] + 2\nu u^2\frac{\partial}{\partial r}\left[r^3\frac{\partial f}{\partial r}\right]} \tag{7.62}$$

(Compare this with (7.24).) Next we integrate over all space. This furnishes a result reminiscent of Loitsyansky's integral equation

$$\frac{d}{dt}\left\{u^2\int_0^\infty r^3 f dr\right\} = u^3\left[r^3 k\right]_{r\to\infty} + 2\nu u^2\left[r^3 f'(r)\right]_{r\to\infty} \tag{7.63}$$

Now, if we follow Batchelor's argument and look at the long-range pressure forces in order to determine the form of k_∞, then it can be shown that $k_\infty \sim r^{-3}$, or less. This is the analogue of the three-dimensional result, $k_\infty \sim r^{-4}$ (or less) (see Chapter 7, Section 1.4). It follows from (7.62) that, at most, $f_\infty \sim r^{-5}$, and so our integral equation simplifies to

$$\frac{d}{dt}\left\{u^2\int_0^\infty r^3 f dr\right\} = u^3\left[r^3 k\right]_{r\to\infty} \tag{7.64}$$

Owing to the similarity between (7.64) and Loitsyansky's integral (7.27) it seems natural to investigate the angular momentum of two-dimensional turbulence. (Remember, Loitsyansky's integral is a measure of angular momentum.) In two dimensions, the global angular momentum of a flow is $H = \int_V (\mathbf{x}\times\mathbf{u})_z dV = 2\int_V \psi dV$, where ψ is the streamfunction. This, in turn, suggests that we introduce the correlation function $\langle\psi\psi'\rangle$, which is related to Q_{ii} by

$$Q_{ii} = -\nabla^2\left[\langle\psi\psi'\rangle\right] \tag{7.65}$$

(see references at the end of this chapter). Substituting for Q_{ii} using (7.60a) we find

$$\langle \psi\psi' \rangle = \langle \psi^2 \rangle - u^2 \int_0^r r f dr \tag{7.66}$$

We now introduce the two-dimensional analogue of Loitsyansky's integral

$$I = u^2 \int_0^\infty r^3 f dr = (4\pi)^{-1} \left\{ 4 \int \langle \psi\psi' \rangle d^2\mathbf{r} \right\} \tag{7.67}$$

where the second equality comes from (7.66). In terms of I, (7.64) becomes

$$\frac{dI}{dt} = u^3 [r^3 k]_{r\to\infty} \tag{7.68}$$

So far we have made no assumption about k_∞, other than noting that it decreases no more slowly than $k_\infty \sim r^{-3}$. Now it turns out that, just like in three-dimensional turbulence, Batchelor's long-range pressure forces cannot directly influence $\langle \mathbf{u} \cdot \mathbf{u}' \rangle$, although they can create an algebraic tail in the triple correlations. This, in turn, can produce an algebraic tail in $\langle \mathbf{u} \cdot \mathbf{u}' \rangle$. In fact it may be shown that

$$\frac{d}{dt} [u^3 r^3 k]_\infty = \int r \langle ss' \rangle dr$$

where $s = u_x^2 - u_y^2$, from which,

$$\frac{d^2 I}{dt^2} = \frac{d}{dt} [u^3 r^3 k]_\infty = \int r \langle ss' \rangle dr$$

Thus a $k_\infty \sim r^{-3} (f_\infty \sim r^{-5})$ tail is kinematically feasible. Of course, this would invalidate a Loitsyansky-type argument for the invariance of I. However, there is some slight evidence that, for *certain initial conditions* (i.e. those where the long-range correlations are absent), the long-range pressure forces remain weak as the flow evolves. This leads to precisely the conditions assumed by Loitsyansky and Kolmogorov prior to Batchelor's discovery of long-range, pressure-induced forces. Under these conditions Landau's angular momentum argument of Chapter 7, Section 1.4, adapted to two-dimensions, yields

$$\langle H^2 \rangle / V = 4 \int \langle \psi\psi' \rangle d^2\mathbf{r} = \text{constant} \tag{7.69}$$

This is consistent with (7.68) which, for $k_\infty < 0(r^{-3})$, becomes

$$4\pi I = 4 \int \langle \psi\psi' \rangle d^2\mathbf{r} = \text{constant} \tag{7.70}$$

Combining these we obtain the Landau–Loitsyansky equation for two-dimensional turbulence

$$\boxed{I = u^2 \int_0^\infty r^3 f dr = \langle H^2 \rangle / (4\pi V) = \text{constant}} \tag{7.71}$$

[conservation of angular momentum]

Of course, we also have conservation of energy (at high Re) and so

$$\boxed{u^2 = \text{constant}} \tag{7.72}$$

[conservation of energy]

These conservation laws provide powerful constraints on the evolution of freely decaying turbulence. If valid, they invalidate Batchelor's self-similar energy spectrum which relies on the existence of only one invariant, u^2. However, it is believed by many that the long-range effects can be significant in two-dimensional turbulence, in which case (7.71) is incorrect and the most that we can say is

$$\boxed{u^2 = \text{constant}, \qquad \frac{d}{dt} \int_0^\infty r^3 f dr = u[r^3 k]_{r \to \infty}} \tag{7.73}$$

(long-range effects significant)

The whole issue of freely evolving two-dimensional turbulence is still a matter of considerable debate and, as of now, it does not seem possible to progress much beyond this point.

7.3.4 Variational principles for predicting the final state in confined domains

We now turn to freely decaying turbulences in confined domains (at high Re). Unlike three-dimensional turbulence, the conservation of u^2, and the continual growth of l, means that two-dimensional turbulence in a finite domain will evolve to a quasi-steady state, containing (almost) the same energy as the initial conditions, but with an integral scale comparable with the domain size. In short, a two-dimensional turbulent flow will

eventually evolve into just one or two eddies which fill the domain. Although contrary to intuition, this is precisely what is observed in the numerical simulations. Once this quasi-steady state has been reached, which takes a time $t \sim R/u$, R being the domain size, the flow then settles down to a laminar motion which decays slowly due to friction on the boundary (Figure 7.12).

Heuristic theories have been developed which, given the initial conditions, purport to identify the quasi-steady state reached at the end of the cascade-enhanced destruction of enstrophy. These theories are essentially all variational principles and we shall discuss them in the context of circular domains, where H is (almost) conserved.

The simplest model for predicting the quasi-steady state (state (c) in Figure 7.12) is the so-called *minimum enstrophy theory*. The idea is that the enstrophy falls monotonically during the cascade-enhanced evolution and this occurs on the fast (inertial) timescale of the eddy turn-over time. Once a quasi-steady state is reached, the enstrophy, as well as the energy and angular momentum, evolve on the much slower diffusive timescale, R^2/ν. It is plausible, therefore, that the quasi-steady state corresponds to a minimum in $\langle\omega^2\rangle$ subject to the conservation of u^2 and of H. In practice, though, this (and all other similar variational principles) suffer from three major drawbacks. First, while seeming plausible, they are all ultimately heuristic. Second, the transition from a cascade-enhanced evolution to a slow diffusive evolution is not always clear-cut. Third, at finite Re, H and u^2 will not be exactly conserved. Nevertheless, let us see where the minimum enstrophy theory leads.

Minimising enstrophy subject to the conservation of u^2 and $H = 2\int \psi dV$ is equivalent to minimising the functional

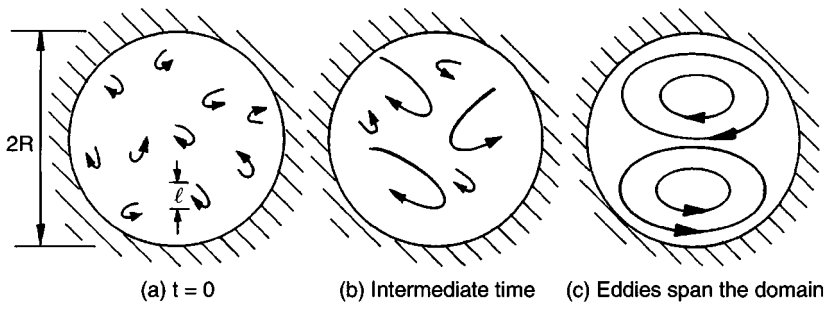

Figure 7.12 Two-dimensional turbulence in a confined domain.

$$F = \int \left[R^2\omega^2 - \lambda^2(\nabla\psi)^2 + 2\lambda^2\Omega\psi\right]dV$$

where λ and Ω are constants (Lagrange multipliers) which we shall determine from the initial condition. The use of the calculus of variations shows that the minimum value of F, compatible with no-slip boundary conditions on $r = R$, is obtained when ω is given by

$$\frac{\omega}{\Omega} = 1 - \frac{\lambda J_0(\lambda r/R)}{2J_1(\lambda)} \tag{7.74}$$

Here J_0, J_1, etc are the usual Bessel functions denoted by these symbols. The Lagrange multipliers are now fixed by the initial values of H and u^2. On integration of (7.74) we find

$$H = -(\pi/4)\Omega R^4 J_3(\lambda)/J_1(\lambda) \tag{7.75}$$

$$\left[\pi R^3 u/H\right]^2 = \left[2J_2^2(\lambda) - 3J_1(\lambda)J_3(\lambda)\right]/J_3^2(\lambda) \tag{7.76}$$

The second of these equations fixes λ in terms of u^2 and H, so that the first determines Ω. The vorticity distribution (and by implication the velocity distribution) of the quasi-steady state is now uniquely determined by the initial conditions through (7.74)–(7.76). Somewhat surprisingly, (7.74) compares well with numerical experiments of two-dimensional turbulence (provided H is not too small), so that, at least for this simple geometry, the minimum enstrophy-theory works well.

There are other variational principles designed to do the same as minimum enstrophy. One has the impressive name: *maximum entropy*. In effect, this defines some measure of mixing and then assumes that the turbulence maximises this mixing (rather than minimising enstrophy) subject to the conservation of u^2 and H. The maximum entropy theory seems, at first sight, appealing because there are analogues in statistical physics. In practice, however, it is a heuristic model and has all the same advantages and disadvantages of the minimum entrophy theory. In fact, as often as not, maximum entropy and minimum enstrophy give virtually identical predictions.

Suggested Reading

L D Landau & E M Lifshitz, *Course of theoretical physics, vol. 6, Fluid mechanics*. 1st Edition, 1959. Butterworth–Heinemann Ltd. (Chapter 3, §38 for a discussion of angular momentum in turbulence.)

L D Landau & E M Lifshitz, *Course of theoretical physics, vol. 6, Fluid mechanics.* 2nd Edition, 1987. Butterworth–Heinemann Ltd. (Chapter 3, §33 for a discussion of the general structure of turbulence.)
H Tennekes & J L Lumley, *A first course in turbulence,* 1972, The MIT Press. (Chapters 1–3 for the general structure of turbulence.)
J O Hinze, *Turbulence*, 1959. McGraw-Hill Co. (Chapter 1 for the properties of velocity correlation functions, Chapter 3 for isotropic turbulence.)
G K Batchelor, *The theory of homogeneous turbulence*, 1953. Cambridge University Press. (Chapter 3 for velocity correlation functions, Chapter 5 for the dynamics of decaying turbulence.)
M Lesieur, *Turbulence in Fluids*, 1990. Kluwer Acad. Pub. (Chapter 9 for two-dimensional turbulence.)
R Moreau, *Magnetohydrodynamics*, 1990. Kluwer Acad. Pub. (Chapter 7 for MHD turbulence at low R_m, particularly the experimental evidence.)
D Biskamp, *Nonlinear magnetohydrodynamics*, 1993. Cambridge University Press. (Chapter 7 for MHD turbulence at high R_m.)

Selected Journal References

Section 7.1.5

Batchelor G K & Proudman I 1956, Phil. Trans. R. Soc. Lon., 248(A).
Saffman P G 1967, J. Fluid Mech., 27.
Proudman I & Reid W H 1954, Phil. Trans. R. Soc. Lon., 247(A).
Compte-Bellot G & Corrsin S 1966, J. Fluid Mech., 25(4).
Warhaft Z & Lumley J L 1978, J. Fluid Mech., 88.

Section 7.2

Davidson P A 1997, J. Fluid. Mech., 336.

Section 7.3

Batchelor G K 1969, Phys. Fluids Suppl. II,12.
McWilliams J C 1984, J. Fluid Mech., 146.

Examples

7.1 Derive Kolmogorov's five-thirds law by dimensional analysis.

7.2 Show that $\langle pu_i' \rangle = 0$ is homogeneous, isotropic turbulence.

7.3 Sketch the shape of the second-order structure function $B_{xx}(r\hat{\mathbf{e}}_x)$.

7.4 Show that the idea of a self-similar energy spectrum, $E(k/l)$, in freely decaying isotropic turbulence is incompatible with conservation of Loitsyansky's integral.

7.5 Show that low-R_m MHD turbulence in a large spherical domain (of radius much greater than the integral scale) which is subject to a uniform magnetic field, $\mathbf{B}_0$, and has angular momentum $\mathbf{H}$, satisfies

$$\langle (\mathbf{H} \cdot \mathbf{B}_0)^2 \rangle = -\int\int \mathbf{r}_\perp^2 \langle \mathbf{u}_\perp \cdot \mathbf{u}'_\perp \rangle d^3\mathbf{r} d^3\mathbf{x} B_0^2$$

7.6 Show that low-R_m turbulence always tends to a state where $N_{\text{true}} \sim 1$.

7.7 Give a physical explanation for the growth of the integral scale, $l \sim ut$, in Batchelor's self-similar spectrum for 2D turbulence.

Part B:

Applications in Engineering and Metallurgy

Introduction: An Overview of Metallurgical Applications

1 The History of Electrometallurgy

> When Faraday first made public his remarkable discovery that a magnetic flux produces an emf, he was asked, 'What use is it?'. His answer was: 'What use is a new-born baby?' Yet think of the tremendous practical applications his discovery has led to... Modern electrical technology began with Faraday's discoveries. The useless baby developed into a prodigy and changed the face of the earth in ways its proud father could never have imagined.
>
> *R P Feynman (1964)*

There were two revolutions in the application of electricity to industrial metallurgy. The first, which occurred towards the end of the nineteenth century, was a direct consequence of Faraday's discoveries. The second took place around eighty years later. We start with Faraday.

The discovery of electromagnetic induction revolutionised almost all of 19th century industry, and none more so than the metallurgical industries. Until 1854, aluminium could be produced from alumina only in small batches by various chemical means. The arrival of the dynamo transformed everything, sweeping aside those inefficient, chemical processes. At last it was possible to produce aluminium continuously by electrolysis. Robert Bunsen (he of the 'burner' fame)[1] was the first to experiment with this method in 1854. By the 1880s the technique had been refined into a process which is little changed today (Figure I.1).

In the steel industry, electric furnaces for melting and alloying iron began to appear around 1900. There were two types: arc-furnaces and induction furnaces (Figure I.2). Industrial-scale arc furnaces made an appearance as early as 1903. (The first small-scale furnaces were designed by von Siemens in 1878.) These used an electric arc, which was made to play on the molten metal surface, as a means of heating the metal. Modern vacuum-arc remelting furnaces are a direct descendant of this

[1] Actually, it was Faraday who invented the burner!

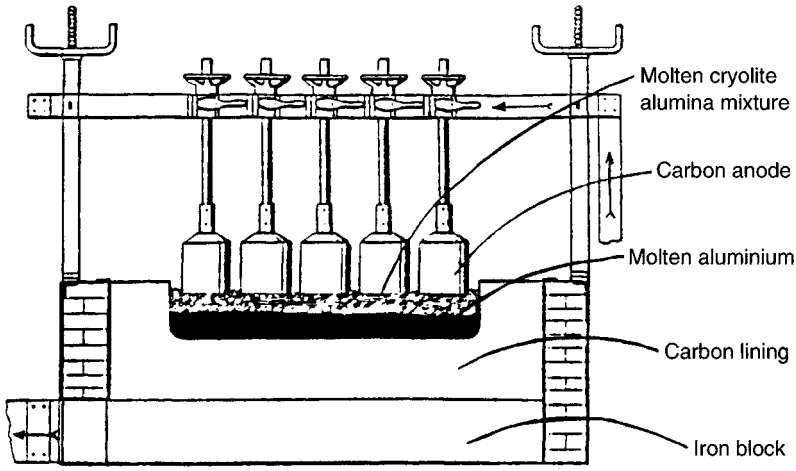

Figure I.1 Turn-of-the-century aluminium reduction cell.

technology (see Figure I.6). The first induction furnace, which used an AC magnetic field (rather than an arc) to heat the steel, was designed by Ferranti in 1887. Shortly thereafter, commercial induction furnaces became operational in the USA. Thus, by the turn of the century, electromagnetic fields were already an integral part of industrial metallurgy. However, their use was restricted essentially to heating and to electro-

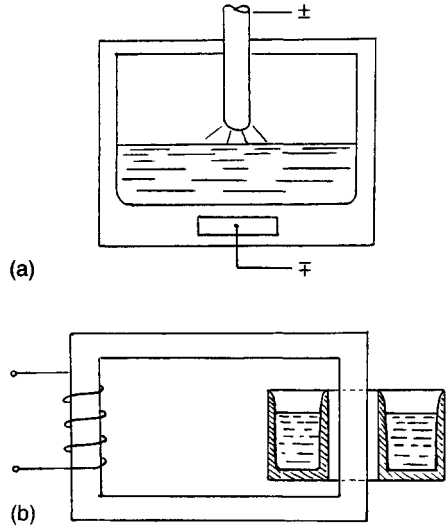

Figure I.2 (a) An early arc-furnace. (b) An early induction furnace.

lysis. The next big step, which was the application of electromagnetic fields to casting, was not to come for another eighty years or so.

The great flurry of activity and innovation in electrometallurgy which began at the end of the nineteenth century gave way to a process of consolidation throughout much of the twentieth. Things began to change, however, in the 1970s and 1980s. The steel industry was revolutionised by the concept of continuous casting, which displaced traditional batch-casting methods. Around the same time, the oil crisis focused attention on the cost of energy, while the worldwide growth in steelmaking, particularly in the East, increased international competition. Once again, the time was ripe for innovative technologies. It is no coincidence that around this time 'near-net-shape' casting began to make an appearance (Figure I.3a). Instead of casting large steel ingots, letting them cool, and then expending large amounts of energy reheating the ingots and rolling them into sheets, why not continuously cast sheet metal in the first place?

There was another reason for change. The aerospace industry was making increasing demands on quality. A single, microscopic, non-metallic particle trapped in, say, a turbine blade can lead to a fatigue crack and perhaps ultimately to the catastrophic failure of an aircraft engine. New techniques were needed to control and monitor the level of non-metallic inclusions in castings.

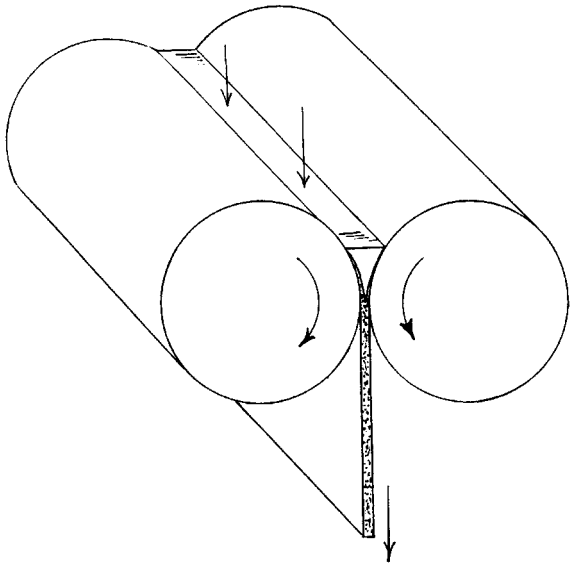

Figure I.3 (a) Twin-roll casting of steel.

Metallurgists set about rethinking and redesigning traditional casting and melting processes, but increasing demands on cost, purity and control meant that traditional methods and materials were no longer adequate. However, just like their predecessors a century earlier, they found an unexpected ally in the electromagnetic field, and a myriad of electromagnetic technologies evolved. Metallurgical MHD, which had been sitting in the wings since the turn of the century, suddenly found itself centre-stage.

Magnetic fields provide a versatile, non-intrusive, means of controlling the motion of liquid metals. They can repel liquid-metal surfaces, dampen unwanted motion and excite motion in otherwise still liquid. In the 1970s, metallurgists began to recognise the versatility of the Lorentz force, and magnetic fields are now routinely used to heat, pump, stir, stabilise, repel and levitate liquid metals.

Metallurgical applications of MHD represent a union of two very different technologies – industrial metallurgy and electrical engineering – and it is intriguing to note that Faraday was a major contributor to both. It will come as no surprise to learn that, on Christmas day 1821,

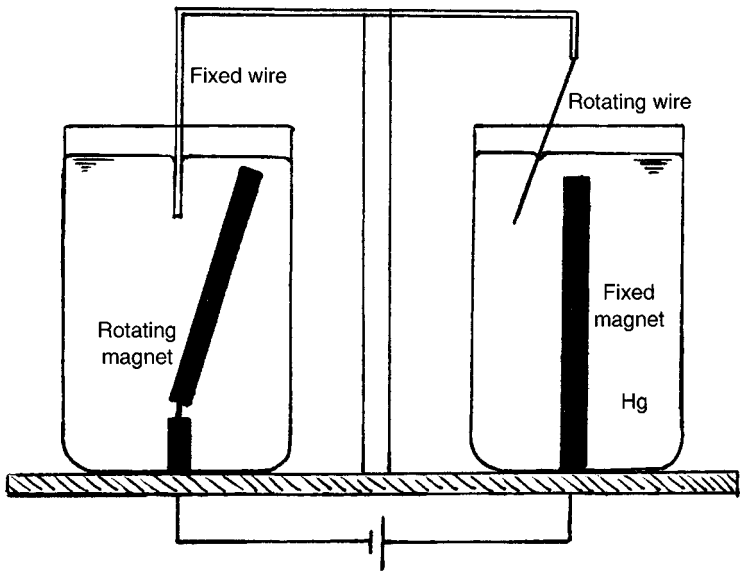

Figure I.3 (b) The first electric motor as devised by Faraday in 1921. A wire carrying a current can be made to rotate about a stationary magnet, and a magnet to rotate about a stationary wire.

Faraday built the first primitive electric motor (Figure I.3b) and of course his discovery of electromagnetic induction (in 1831) marked the beginning of modern electrical technology. However, Faraday's contributions to metallurgy are, perhaps, less well known. Not only did his researches into electrolysis help pave the way for modern aluminium production, but his work on alloy steels, which began in 1819, was well ahead of his time. In fact, as far back as 1820, he was making razors from a non-rusting platinum steel as gifts for his friends. As noted by Robert Hadfield: '*Faraday was undoubtedly the pioneer of research on special alloy steel; and had he not been so much in advance of his time in regard to general metallurgical knowledge and industrial requirements his work would almost certainly have led immediately to practical development*'. It is interesting to speculate how Faraday would have regarded the fusion of two of his favourite subjects – chemistry and electromagnetism – in a single endeavour.

In any event, that unlikely union of sciences has indeed occurred, and the application of magnetic fields to materials processing has acquired not one but two names! The term *electromagnetic processing of materials* (or EPM for short) has found favour in France and Japan. Elsewhere, the more traditional label of *metallurgical MHD* still holds sway: we shall stay with the latter. The phrase *metallurgical MHD* was coined at an IUTAM conference held in Cambridge in 1982 (Moffatt, 1984). In the years immediately preceding this conference, magnetic fields were beginning to make their mark in casting, but those applications which did exist seemed rather disparate. This conference forged a science from these diverse, embryonic technologies, and almost two decades later we have a reasonably complete picture of these complex processes. From both a technological and a scientific perspective, the subject has come of age.

Unfortunately, much of this research has yet to find its way into text books and monographs, but rather is scattered across various conference proceedings and journal papers. The purpose of Part B, therefore, is to give some sense of the breadth of the industrial developments and of our attempts to understand and quantify these complex flows.

2 The Scope of Part B

The content and style of Part B is quite different to that of Part A. It is not of an introductory nature, but rather provides a contemporary account of recent developments in metallurgical MHD.

We shall look at five applications of MHD. These are:

(i) *magnetic stirring* induced by a rotating magnetic field (Chapter 8);
(ii) *the magnetic damping* of jets, vortices and natural convection (Chapter 9);
(iii) motion arising from the *injection of current* into a liquid-metal pool (Chapter 10);
(iv) *interfacial instabilities* which arise when a current is passed between two conducting fluids (Chapter 11);
(v) *magnetic levitation and heating* induced by high-frequency magnetic fields (Chapter 12).

The hallmark of all these processes is that R_m is invariably very small. Consequently, Part B of this text rests heavily on the material of Chapter 5.

Although these five processes may be unfamiliar in the metallurgical context, they all have simple mechanical analogues, each of which would have been familiar to Faraday.

- *Magnetic stirring* (the first topic) is nothing more than a form of induction motor where the liquid metal takes the place of the rotor.
- *Magnetic damping* takes advantage of the fact that the relative motion between a conductor and a magnetic field tends to induce a current in the conductor whose Lorentz force opposes the relative motion. (As far back as the 1860s, designers were placing conducting circuits around magnets in order to dampen their vibration.) This is the second of our topics.
- *Current injected* into a conducting bar causes the bar to pinch in on itself (parallel currents attract each other), and the same is true if current passes through a liquid-metal pool. Sometimes the pinch forces caused by the injection of current can be balanced by fluid pressure; at other times it induces motion in the pool (topic (iii)).
- The *magnetic levitation* of small metallic objects is also quite familiar. It relies on the fact that an induction coil carrying a high-frequency current will tend to induce opposing currents in any adjacent conductor. Opposite currents repel each other and so the conductor is repelled by the induction coil. What is true of solids is also true of liquids. Thus a 'basket' composed of a high-frequency induction coil can be used to levitate liquid-metal droplets (topic (v)).

Let us now re-examine each of these processes in a little more detail, placing them in a metallurgical context. Magnetic stirring is the name given to the generation of swirling flows by a rotating magnetic field (Figure I.4). This is routinely used in casting operations to homogenise the liquid zone of a partially solidified ingot. In effect, the liquid metal acts as the rotor of an induction motor, and the resulting motion has a profound influence on the metallurgical structure of the ingot, producing a fine-grained product with little or no porosity. From the perspective of a fluid dynamicist, this turns out to be a study in Ekman pumping. That is, Ekman layers form on the boundaries, and the resulting Ekman pumping (a secondary, poloidal motion which is superimposed on the primary swirling flow) is the primary mechanism by which heat, chemical species and angular momentum are redistributed within the pool. Magnetic stirring is discussed in Chapter 8.

In contrast, magnetic fields are used in other casting operations to suppress unwanted motion. Here we take advantage of the ability of a static magnetic field to convert kinetic energy into heat via Joule dissipation. This is commonly used, for example, to suppress the motion of submerged jets which feed casting moulds. If unchecked, these jets can disrupt the free surface of the liquid, leading to the entrainment of oxides or other contaminants from the surface (Figure I.5). It turns out, however, that although the Lorentz force associated with a static magnetic field destroys kinetic energy, it cannot create or destroy linear or angular momentum. A study of magnetic damping, therefore, often comes down to the question: how does a flow manage to dissipate kinetic energy while preserving its linear and angular momentum? The answer to this question

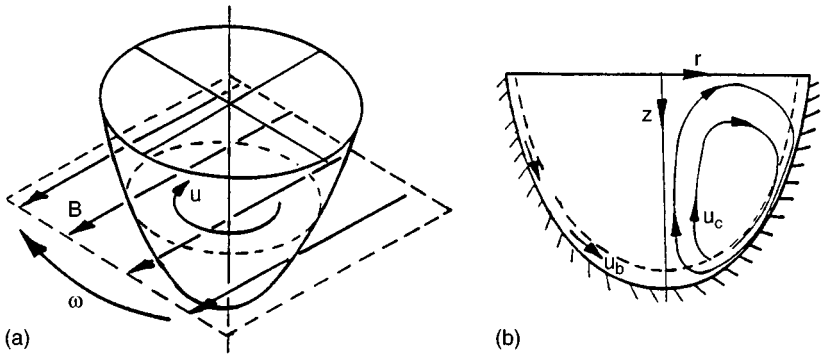

Figure I.4 (a) Electromagnetic stirring. (b) Ekman pumping.

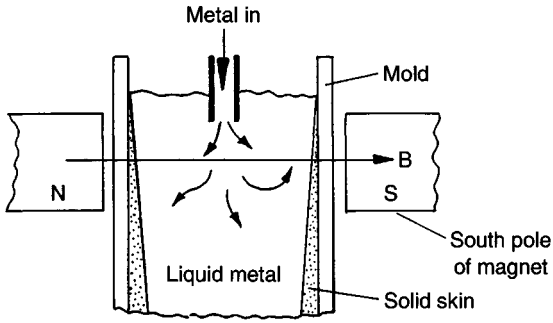

Figure I.5 Magnetic damping.

furnishes a great deal of useful information, and we look at the damping of jets and vortices in Chapter 9.

In yet other metallurgical processes, an intense DC current is used to fuse metal. An obvious (small-scale) example of this is electric welding. At a larger scale, intense currents are used to melt entire ingots! Here the intention is to improve the quality of the ingot by burning off impurities and eliminating porosity. This takes place in a large vacuum chamber and so is referred to as vacuum-arc remelting (VAR). In effect, VAR resembles a form of electric-arc welding, where an arc is struck between an electrode and an adjacent metal surface. The primary difference is one of scale. In VAR the electrode, which consists of the ingot which is to be melted and purified, is $\sim$ 1 m in diameter. As in electric welding, a liquid pool builds up beneath the electrode as it melts, and this pool eventually solidifies to form a new, cleaner, ingot (Figure I.6(a)).

However, vigorous stirring is generated in the pool by buoyancy forces and by the interaction of the electric current with its self-magnetic field. This motion, which has a significant influence on the metallurgical structure of the recast material, is still poorly understood. It appears that there is delicate balance between the Lorentz forces, which tend to drive a poloidal flow which converges at the surface, and the buoyancy forces associated with the relatively hot upper surface. (The buoyancy-driven motion is opposite in direction to the Lorentz-driven flow.) Modest changes in current can transform the motion from a buoyancy-dominated flow to a Lorentz-dominated motion. This change in flow regime is accompanied by a dramatic change in temperature distribution and of ingot structure (Figure I.6(b)). This is discussed in Chapter 10.

Next, in Chapter 11, we give a brief account of an intriguing and unusual form of instability which has bedevilled the aluminium industry

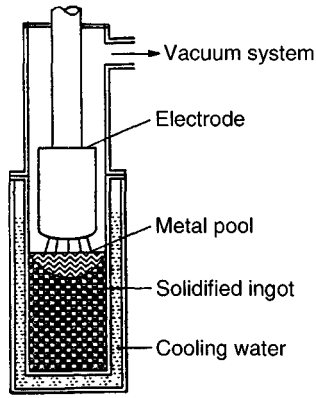

Figure I.6 (a) Vacuum-arc remelting.

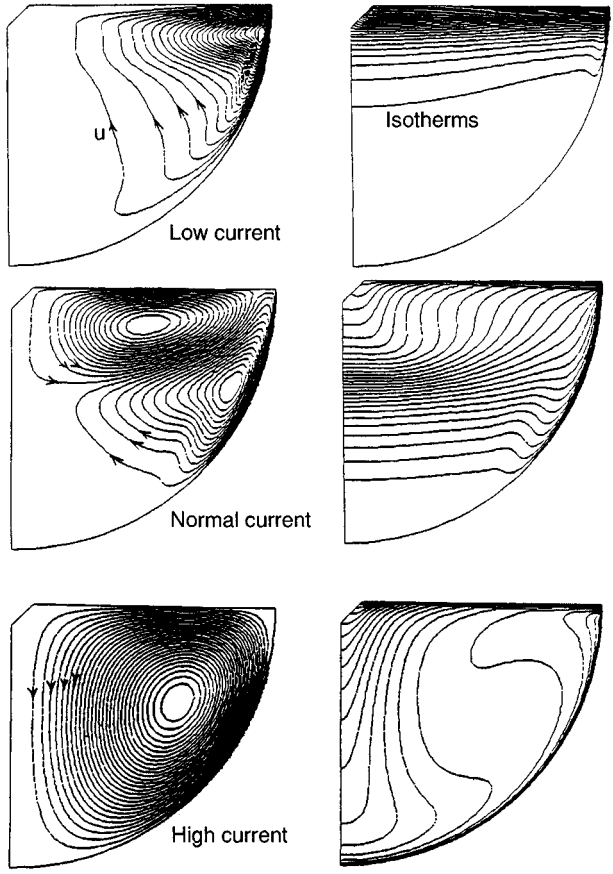

Figure I.6 (b) Changes in flow pattern and temperature field with current in VAR.

for several decades. As we shall see, the solution to this problem is finally in sight and the potential for savings is enormous.

The instability arises in electrolysis cells which are used to reduce alumina to aluminium. These cells consist of broad, but shallow, layers of electrolyte and liquid aluminium, with the electrolyte lying on top. A large current (perhaps 300 k Amps) passes vertically downward through the two layers, continually reducing the oxide to metal (Figure I.7). The process is highly energy-intensive, largely because of the high electrical resistance of the electrolyte. For example, in the USA, around 2% of all generated electricity is used for aluminium production. It has long been known that stray magnetic fields can destabilise the aluminium–electrolyte interface, in effect, by amplifying interfacial gravity waves. In order to avoid this instability, the electrolyte layer must be maintained at a thickness above some critical threshold, and this carries with it a severe energy penalty.

This instability has been the subject of intense research for over two decades. In the last few years, however, the underlying mechanisms have finally been identified and, of course, with hindsight they turn out to be simple. The instability depends on the fact that the interface can support interfacial gravity waves. A tilting of the interface causes a perturbation in current, **j**, as shown in Figure I.8. Excess current is drawn from the anode at points where the highly resistive layer of electrolyte thins, and less current is drawn where the layer thickens. The resulting perturbation in current shorts through the highly conducting aluminium layer, leading to a large horizontal current in the aluminium. This, in turn, interacts with the vertical component of the background magnetic field to produce a Lorentz force which is directed into the page. It is readily confirmed

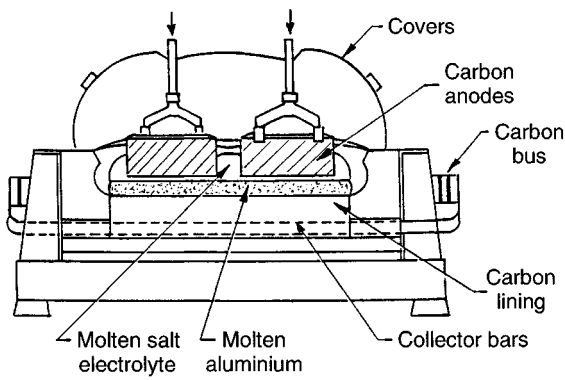

Figure I.7 A modern aluminium reduction cell.

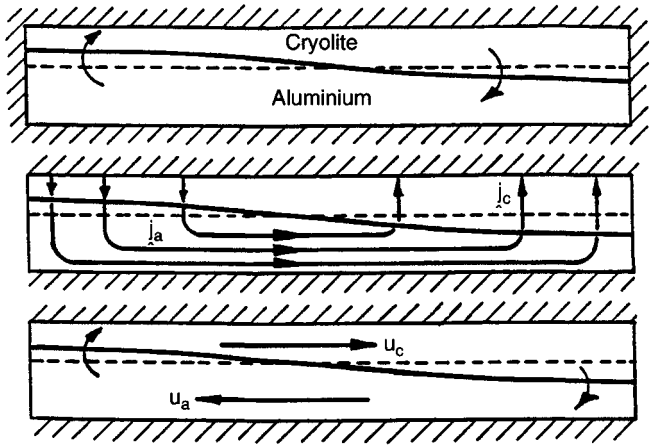

Figure I.8 Unstable waves in a reduction cell.

that two such sloshing motions, which are mutually perpendicular, can feed on each other, the Lorentz force from one driving the motion of the other. The result is an instability. This is discussed in Chapter 11.

A quite different application of MHD in metallurgy is magnetic levitation. This relies on the fact that a high-frequency induction coil will repel any adjacent conducting material by inducing opposing currents in the adjacent conductor (opposite currents repel each other). Thus a 'basket' formed from a high-frequency induction coil can be used to levitate and melt highly reactive metals (Figure I.9), or a high-frequency solenoid can be used to form a magnetic valve which modulates the flow of a liquid-metal jet (Figure I.10).

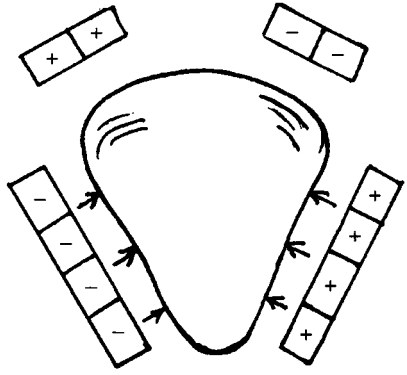

Figure I.9 Magnetic levitation.

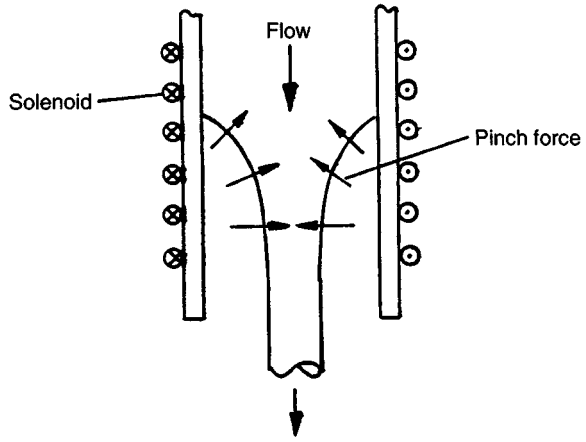

Figure I.10 An electromagnetic valve.

The use of high-frequency fields to support liquid-metal surfaces is now commonplace in industry. For example, in order to improve the surface quality of large aluminium ingots, some manufacturers have dispensed with the traditional, water-cooled mould and replaced it with a high-frequency induction coil. Thus ingots are cast by pouring the molten metal through free space, the sides of the ingot being supported by magnetic pressure (Figure I.11). Such applications are discussed in Chapter 12.

This concludes our brief overview of Part B of this textbook.

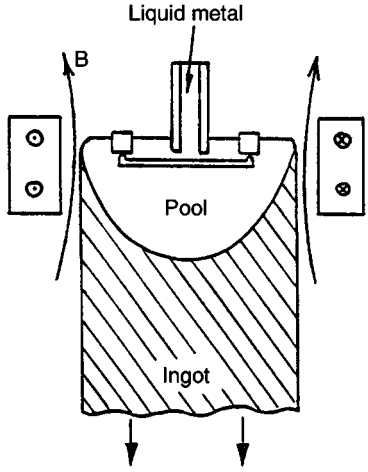

Figure I.11 Electromagnetic casting of aluminium.

8

Magnetic Stirring Using Rotating Fields

Liquid metals freeze in much the same way as water. First, snowflake-like crystals form, and as these multiply and grow a solid emerges. However, this solid can be far from homogeneous. Just as a chef preparing ice-cream has to beat and stir the partially solidified cream to break up the crystals and release any trapped gas, so many steelmakers have to stir partially solidified ingots to ensure a fine-grained, homogeneous product. The preferred method of stirring is electromagnetic, and has been dubbed the 'electromagnetic teaspoon'. We shall describe this process shortly. First, however, it is necessary to say a little about commercial casting processes.

8.1 Casting, Stirring and Metallurgy

> It will emerge from dark and gloomy caverns, casting all human races into great anxiety, peril and death. It will take away the lives of many; with this men will torment each other with many artifices, traductions and treasons. O monstrous creature, how much better it would be if you were to return to hell
>
> *(Leonardo da Vinci on the extraction and casting of metals)*

Man has been casting metals for quite some time. Iron blades, perhaps 5000 years old, have been found in Egyptian pyramids, and by 1000 BC we find Homer mentioning the working and hardening of steel blades. Until relatively recently, all metal was cast by a batch process involving pouring the melt into closed moulds. However, today the bulk of aluminium and steel is cast in a continuous fashion, as indicated in Figure 8.1. In brief, a solid ingot is slowly withdrawn from a liquid-metal pool, the pool being continuously replenished from above. In the case of steel, which has a low thermal diffusivity, the pool is long and deep, resembling a long liquid-metal column. For aluminium, however, the pool is roughly hemispherical in shape, perhaps 0.5 m in diameter. Casting speeds are of the order of a few mm/s.

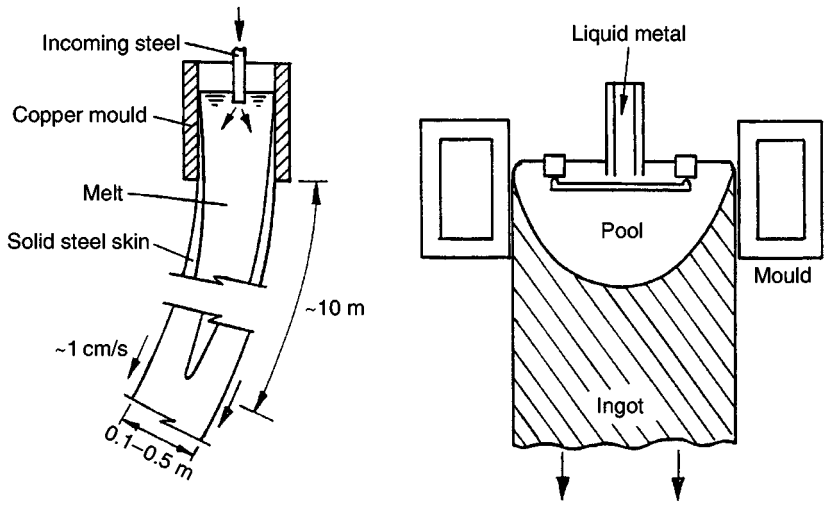

Figure 8.1 (a) Casting of steel; (b) casting of aluminium.

Unfortunately, ingots cast in this manner are far from homogeneous. For example, during solidification alloying elements tend to segregate out of the host material, giving rise to inhomogeneities in the final structure. This is referred to as *macro-segregation*[1]. Moreover, small cavities can form on the ingot surface or near the centre-line. Surface cavities are referred to as blow holes or pin holes, and arise from the formation of gas bubbles (CO or N_2 in the case of steel). Centre-line porosity, on the other hand, is associated with shrinkage of the metal during freezing.

All of these defects can be alleviated, to some degree, by stirring the liquid pool (Birat & Chone, 1983; Takeuchi et al., 1992). This is most readily achieved using a rotating magnetic field, as shown in Figure 8.2. The stirring has the added benefit of promoting the nucleation and growth of *equi-axed crystals* (crystals like snowflakes) at the expense of *dendritic crystals* (those like fir-trees) which are large, anisotropic and generally undesirable. In addition to these metallurgical benefits, it has been found that stirring has a number of incidental operational advantages, such as allowing higher casting temperatures and faster casting rates (Marr, 1984).

[1] Macro-segregation was a recognized problem in casting as far back as 1540, when Biringuccio described macro-segregation problems in the production of gun barrels.

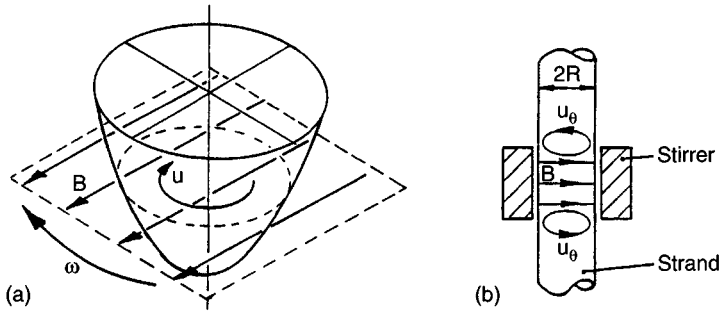

Figure 8.2 (a) Magnetic stirring of aluminium; (b) stirring of steel.

The perceived advantages of magnetic stirring led to a widespread implementation of this technology in the 1980s, particularly in the steel industry. In fact, by 1985, some 20% of slab casters (casters producing large steel ingots) and 50% of bloom casters (casters producing medium-sized steel ingots) had incorporated magnetic stirring.

However, this was not the end of the story. While some manufacturers reported significant benefits, others encountered problems. For example, in steel-making excessive stirring can lead to the entrainment of debris from the free surface and to a thinning of the solid steel shell at the base of the mould. This latter phenomenon is particularly dangerous as it can lead to a rupturing of the solid skin. Different problems were encountered in the aluminium industry. Here it was found that, in certain alloys, macrosegregation was aggravated (rather than reduced) by stirring, possibly because centrifugal forces tend to separate out crystal fragments of different composition.

By the mid-1980s it was clear that there was a need to rationalise the effects of magnetic stirring and this, in turn, required that metallurgists and equipment manufacturers develop a quantitative picture of the induced velocity field. The first, simple models began to appear in the early 1980s, usually based on computer simulations. However, these were somewhat naive and the results rather misleading. The difficulty arose because early researchers (quite naturally) tried to simplify the problem, and an obvious starting point was to consider a two-dimensional idealisation of the process. Unfortunately, it turns out that the key dynamical processes are all three-dimensional, and so two-dimensional idealisations of magnetic stirring are hopelessly inadequate. We shall describe both the early two-dimensional models and their more realistic three-dimensional counterparts in the subsequent sections.

There are many ways of inducing motion in a liquid-metal pool. The most common means of stirring is to use a rotating, horizontal magnetic field, an idea which dates back to 1932. The field acts rather like an induction motor, with the liquid taking the place of the rotor (Figure 8.3a). In practice, a rotating magnetic field may be generated in a variety of ways, each producing a slightly different spatial structure for **B**. (The

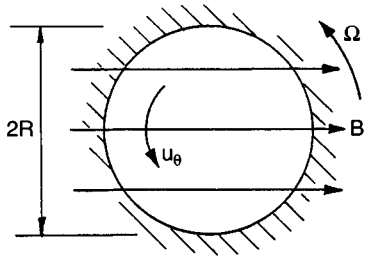

Figure 8.3 (a) A one-dimensional model of stirring.

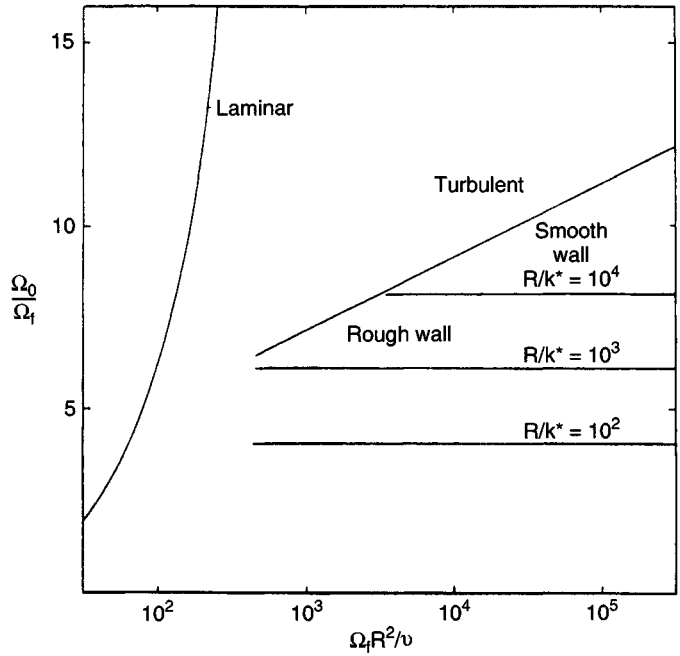

Figure 8.3 (b) Core angular velocity versus Ω_f for one-dimensional flow.

field is never perfectly uniform nor purely horizontal.) However, the details do not matter. The key point is that a rotating magnetic field, which is predominantly horizontal, induces a time-averaged Lorentz force which is a prescribed function of position, is independent of the velocity of the metal, and whose dominant component is azimuthal: $(0, F_\theta, 0)$ in (r, θ, z) coordinates. The important questions are: (i) How does the induced velocity scale with the Lorentz force? (ii) Does the induced swirl $(0, u_\theta, 0)$ have a spatial structure which mimics the spatial variations of the applied Lorentz force (i.e. strong swirl in regions where F_θ is intense and weak swirl where F_θ is low)? (iii) Are there significant secondary flows $(u_r, 0, u_z)$? To cut a long story short, the answers turn out to be:

(i) $u_\theta \sim B$
(ii) u_θ does *not* mimic the spatial variations in the Lorentz force;
(iii) the secondary flows are intense and dominate the dynamics of the liquid metal.

It is the subtle, yet critical, rôle played by the secondary flows which invalidates the results of the early, two-dimensional models and which makes this problem more interesting than it might otherwise be.

8.2 Early Models of Stirring

The first step in predicting the spatial structure of $\mathbf{u}$ is to determine the Lorentz force. Fortuitously, the magnitude and distribution of the time-averaged Lorentz force is readily calculated. There are two reasons for this. First, the magnetic field associated with the current induced in the liquid metal is almost always negligible by comparison with the imposed field, $\mathbf{B}$ (see, for example, Davidson & Hunt, 1987.) Faraday's law then gives the electric field as

$$\nabla \times \mathbf{E} = -\partial \mathbf{B}_0 / \partial t \tag{8.1}$$

where $\mathbf{B}_0$ is the known, imposed magnetic field. Second, the induced velocities are generally so low (by comparison with the rate of rotation of the $\mathbf{B}$-field) that Ohm's law reduces to

$$\mathbf{J} = \sigma \mathbf{E} \tag{8.2}$$

Consequently, **E** (and hence **J**) may be found directly by uncurling (8.1) and the Lorentz force follows. In fact, we have already seen an example of just such a calculation in Chapter 5, Section 5.1. Here we evaluated the time-averaged Lorentz force generated by a uniform magnetic field rotating about an infinitely long, liquid-metal column. The force is

$$\mathbf{F} = \frac{1}{2}\sigma B^2 \Omega r \hat{\mathbf{e}}_\theta \tag{8.3}$$

where Ω is the field rotation rate and r is the radial coordinate. The restrictions on this expression are

$$u_\theta \ll \Omega R \leq \lambda/R, \qquad \lambda = (\mu\sigma)^{-1} \tag{8.4}$$

where R is the radius of the column. However, these conditions are almost always satisfied in practice. The first inequality, $u_\theta \ll \Omega R$, is precisely the condition required to ignore $\mathbf{u} \times \mathbf{B}$ in Ohm's law, while the second, $\Omega R \leq \lambda/R$, is equivalent to saying that R_m (based on ΩR) is small, so that the induced magnetic field is negligible.

Of course, for more complicated distributions of **B** we cannot use (8.3). Nevertheless, for almost any rotating field the Lorentz force is predominantly azimuthal, and on dimensional grounds it must be of order $\sigma B^2 \Omega R$ (provided that (8.4) is satisfied). Moreover, for fields which are symmetric about a plane through the origin, the Lorentz force must vanish on the axis. It follows that rotating, symmetric magnetic fields which satisfy (8.4) will induce a force of the form

$$\mathbf{F} = \left[\frac{1}{2}\sigma \Omega B_0^2 r\right] f(\mathbf{x}/R)\hat{\mathbf{e}}_\theta \tag{8.5}$$

Here B_0 is some characteristic field strength, and f is a function of order unity whose spatial distribution depends on that of **B** and whose exact form can be determined by uncurling (8.1). When **B** is uniform, $f = 1$.

We now consider the dynamical consequences of this force. The earliest attempts to quantify magnetic stirring consisted of taking a transverse slice through the problem. That is, the axial variations in **F** were neglected, the sides of the pool were considered to be vertical, and end effects were ignored. In effect, this represents uniform stirring of a long, deep column of radius R. Although this is a natural first step, it turns out that this idealisation is quite misleading, as we shall now show.

These z-independent models are characterised by the fact that **F** drives a one-dimensional swirl flow $u_\theta(r)$. There are no inertial forces and so rings of fluid simply slide over each other like onion rings, driven by F_θ

and resisted by shear stresses (Figure 8.3a). The Reynolds-averaged Navier–Stokes equation reduces to a balance between the applied Lorentz force and shear:

$$\tau_{r\theta} = \rho\nu r \frac{d}{dr}\left(\frac{u_\theta}{r}\right) - \rho\overline{v_r v_\theta} = -r^{-2}\int_0^r F_\theta r^2 dr \tag{8.6}$$

Here ν is the viscosity, v represents the fluctuating component of velocity and the overbar denotes a time average. In fact we have already met this problem. We used a simple mixing length model to estimate $\overline{v_r v_\theta}$ in Chapter 5, Section 5.1. Integration of (8.6) is then straightforward. The results are best expressed in terms of a quantity Ω_f defined by

$$\Omega_f^2 = \sigma\Omega B^2/\rho \tag{8.7}$$

When **B** is uniform and $f = 1$, equation (8.6) yields

$$(u_\theta/r)_{r=0} = \Omega_f\{\Omega_f R^2/16\nu\} \tag{8.8}$$

(Laminar flow)

$$(u_\theta/r)_{r=0} = \Omega_f\left\{\frac{1}{2\sqrt{2}\kappa}\ln\left(\frac{\Omega_f R^2}{\nu}\right) + 1.0\right\} \tag{8.9}$$

(Turbulent flow)

These correspond to (5.29) and (5.31). Note that $\kappa = 0.4$ is Karman's constant. When the surface at $r = R$ is rough and dendritic, rather than smooth, the mixing length estimate of $\overline{v_r v_\theta}$ must be modified slightly. The required modification is well known in hydraulics and it turns out that, if k^* is the typical roughness height, then (8.9) becomes

$$(u_\theta/r)_{r=0} = \Omega_f\left\{\frac{1}{2\sqrt{2}\kappa}\ln\left(\frac{R}{k^*}\right)\right\} \tag{8.10}$$

(Turbulent flow, rough wall)

Note that in a turbulent flow u_θ scales linearly with $|\mathbf{B}|$ (with a possible logarithmic correction), whereas in a laminar flow u_θ scales linearly as $\mathbf{B}^2$. These results are summarised in Figure 8.3(b).

Expressions (8.9) and (8.10) were first given by Davidson & Hunt (1987). However, there were many earlier 'numerical experiments'. (Computerised integrations of the Navier–Stokes equation for particular values of B, R, Ω, σ, etc.) For example, Tacke & Schwerdtfeger (1979) integrated the time-averaged Navier–Stokes equations and used a popu-

lar, if rather complex, two-parameter turbulence model to estimate the Reynolds stresses. (They used a variant of the popular k–ε model.) However, their results are very similar to the mixing length predictions above.

There were many other numerical experiments, but unfortunately *all* predictions based on integrating (8.6) are substantially out of line with the experimental data, no matter what turbulence model is used![2] The key point is that the force balance (8.6) relies on the time-averaged inertial forces being exactly zero. However, in practice, there are always significant secondary flows $(u_r, 0, u_z)$ induced, for example, by Ekman pumping on the base of the pool (see Chapter 3, Section 7 for a discussion of Ekman pumping). This secondary motion ensures that the inertial forces are finite. Indeed, when Re is large, as it always is, we would expect the inertial forces to greatly exceed the shear stresses, except near the boundaries. Consequently, in the core of the flow, the local force balance should be between F_θ and inertia, not between F_θ and shear. To obtain realistic predictions of $\mathbf{u}$ we must embrace the three-dimensional nature of the problem, seek out the sources of secondary motion, and incorporate these into the analysis.

Some hint as to the rôle of secondary motion appears in the example discussed in Chapter 5, Section 5.2. Here we looked at the laminar flow of a liquid held between two flat, parallel plates and subject to the force (8.3). It was found that Ekman-like layers form on the top and bottom surfaces, and that these layers induce a secondary, poloidal flow as shown

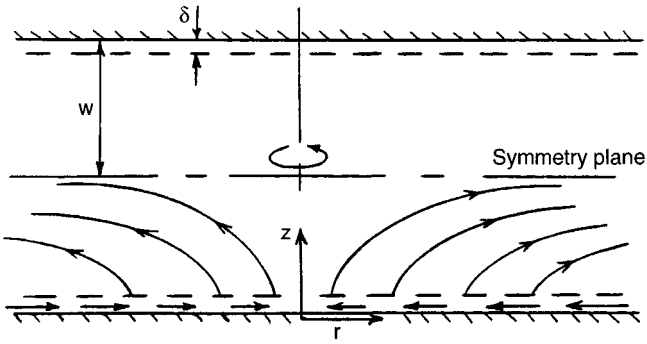

Figure 8.4 Swirling flow between two discs driven by the force $F_\theta = \frac{1}{2}\sigma\Omega B^2 r$.

[2] See Davidson & Hunt, 1987, and Davidson, 1992.

in Figure 8.4. We showed that, outside the Ekman (or Bodewadt) layers, the viscous stresses are negligible and the fluid rotates as a rigid body, the rotation rate being quite different to that predicted by (8.8). In fact, the core rotation is

$$\Omega_c = 0.516\Omega_f\left[\Omega_f w^2/\nu\right]^{1/3} \tag{8.11}$$

where $2w$ is the distance between the plates. Moreover, we saw that the Ekman layers are unaffected by the presence of the forcing (the Lorentz force is negligible by comparison with the viscous forces) and so they look like conventional Bodewadt layers. For example, the thickness of the boundary layer is of the order of $\delta \sim 4(\nu/\Omega)^{1/2}$.

This simple model problem is discussed at some length in Davidson (1992), where the key features are shown to be:

(i) the flow may be divided into a forced, inviscid core, and two viscous boundary layers in which the Lorentz force is negligible;
(ii) all of the streamlines pass through both regions, collecting energy in one region and losing it in the other;
(iii) the applied Lorentz force in the core is exactly balanced by the Coriolis force.

We shall see shortly that all of these features are characteristic of stirring an aluminium ingot. The main point, however, is (iii). When a secondary flow is present, the Lorentz force is balanced locally by inertia, not shear, and this is why (8.8) and (8.11) look so different. An important question is, therefore: what kinds of secondary flow occur during the stirring of an ingot?

From an industrial perspective there are two distinct cases of particular interest. The first is where the pool is as deep as it is broad, which is typical of aluminium casting. Here the source of secondary motion is Ekman pumping, as in the model problem above. The second case is where we have a long column of liquid, but with the stirring force F_θ applied over a short portion of that column. This is relevant to the casting of steel, and in this case the secondary motion arises from differential rotation along the length of the column. We shall consider each of these in turn, starting with pools which are roughly hemi-spherical or parabolic in shape.

8.3 The Dominance of Ekman Pumping in the Stirring of Confined Liquids

Suppose that the pool has an aspect ratio of the order of unity, as indicated in Figure 8.2(a). We make no particular assumptions about the shape of the boundary, although we have in mind profiles which are roughly parabolic. It turns out that this is a long-standing and much studied problem, and not just in the case of aluminium casting. For example, Zibold et al. (1986) looked at magnetically forced swirl in a cylindrical cavity in the context of single crystal pulling. Bojarevics & Millere (1982) studied the equivalent problem in a hemisphere, motivated by problems in electric-arc welding, while Vlasyuk & Sharamkin (1987) and Muizhnieks & Yakovich (1988) looked at forced swirl in paraboloids and cylinders, motivated this time by vacuum-arc remelting of ingots. All of these studies were, in effect, numerical experiments. (Integrations of Navier–Stokes equation for particular values of B, Ω, R, σ, ν, etc.) However, as we shall see, it is possible to develop a single unified model which encapsulates all of these studies.

The key to establishing the distribution of swirl lies in the simple, text-book problem of 'spin-down' of a stirred cup of tea (Figure 8.5). (This is discussed in Chapter 3, Section 7.) In this well-known example, the main body of the fluid is predominantly in a state of inviscid rotation. The associated centrifugal force is balanced by a radial pressure gradient, and this pressure gradient is also imposed throughout the boundary layer on the base of the cup. Of course, the swirl in this boundary layer (the Ekman layer) is diminished through viscous drag, and so there is a local imbalance between the radial pressure force and u_θ^2/r. The result is a radial inflow along the bottom of the cup, with the fluid eventually drifting up and out of the boundary layer. In short, we

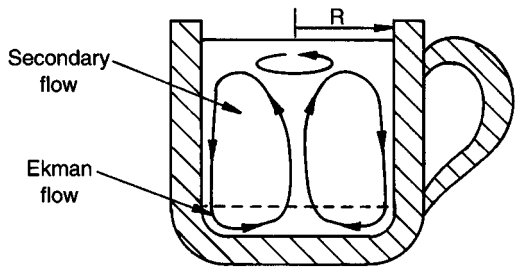

Figure 8.5 Spin-down of a stirred cup of tea.

have a kind of Bodewadt layer. Of course, continuity then requires that the boundary layer is replenished via the side walls and the end result is a form of Ekman pumping, as shown above. As each fluid particle passes through the Ekman boundary layer, it gives up a significant fraction of its kinetic energy and the tea finally comes to rest when all the contents of the cup have been flushed through the Ekman layer. The spin-down time, therefore, is of the order of the turn-over time of the secondary flow.

It is useful to consider a variant of this problem. Suppose now that the tea is continuously stirred. Then it will reach an equilibrium rotation rate in which the work done by the tea-spoon exactly balances the dissipation in the Ekman layers. This provides the clue to analysing magnetic stirring, and we now return to this problem.

Suppose we integrate the time-averaged Navier–Stokes equations around a streamline which is closed in the r–z plane. For a steady flow, we obtain

$$\oint \mathbf{F} \cdot d\mathbf{x} + \nu_t \oint \nabla^2 \mathbf{u} \cdot d\mathbf{x} = 0 \tag{8.12}$$

Here ν_t is an eddy viscosity which for simplicity we treat as constant, and $\mathbf{F}$ is the Lorentz force per unit mass. This is an energy balance: it states that all of the energy imparted to a fluid particle by the Lorentz force must be destroyed or diffused away by shear before it returns to its original position. However, the shear stresses are significant only in the boundary layers. By implication, *all* streamlines must pass through a boundary layer. Of course, Ekman pumping provides the necessary entrainment mechanism. Note also that Ekman layers can and will

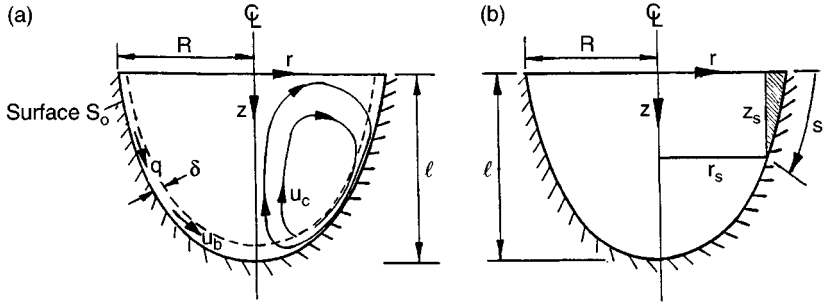

Figure 8.6 (a) Secondary (poloidal) flow induced by swirl in a cavity. (b) Coordinate system.

form on all surfaces non-parallel to the axis of rotation. The structure of the flow, therefore, is as shown in Figure 8.6(a) (Davidson, 1992). It consists of an interior body of (nearly) inviscid swirl surrounded by Ekman wall jets on the inclined surfaces. Each fluid particle is continually swept first through the core, where it collects energy and angular momentum, and then through the Ekman layers, where it deposits its energy. The motion is helical, spiralling upwards through the core, and downwards through the boundary layers.

The fact that all streamlines pass through the Ekman layers has profound implications for the axial distribution of swirl. Let u_b and u_c be characteristic values of the poloidal recirculation $(u_r, 0, u_z)$ in the boundary layer and in the core. Also, let δ be the boundary layer thickness, R be a characteristic linear dimension of the pool, and $\Gamma = u_\theta r$ be the angular momentum. Now u_b and u_θ are of similar magnitudes (one drives the other) and so continuity requires that

$$u_c \sim u_b(\delta/\mathrm{R}) \sim \mathrm{u}_\theta(\delta/\mathrm{R}) \tag{8.13}$$

That is, the core recirculation is weak. However, the core recirculation is related to the core angular momentum, Γ_c, by the inviscid vorticity equation

$$\mathbf{u} \cdot \nabla(\omega_\theta/r) = \frac{\partial}{\partial z}\left(\frac{\Gamma_c^2}{r^4}\right) \tag{8.14}$$

Combining (8.13) and (8.14) we have (Davidson, 1992)

$$\Gamma_c = \Gamma_c(r)\left[1 + O(\delta/R)^2\right] \tag{8.15}$$

It is extraordinary that, no matter what the spatial distribution of the Lorentz force, the induced swirl is independent of height to second order in (δ/R). This prediction has been confirmed in the experiments of Davidson, Short & Kinnear (1995), where highly localised distributions of F_θ were used.

Since the flow has a simple, clear structure, it is possible to piece together an approximate, quantitative model of the process. We give only a schematic outline here, but more details may be found in Davidson (1992). In the inviscid core the applied Lorentz force is balanced by inertia: $(\mathbf{u} \cdot \nabla)\Gamma_c = rF_\theta$. Since Γ_c is a function only of r, the left-hand side reduces to $u_r\Gamma_c'(r)$, the Coriolis force. Thus,

$$u_r = rF_\theta/\Gamma_c'(\mathrm{r}) \tag{8.16}$$

Now all the fluid which moves radially outward is recycled via the boundary layer and so (8.16) may be used to calculate the mass flux in the Ekman layer. In particular, if we apply the continuity equation to the shaded area in Figure 8.6(b) we obtain an estimate of the mass flux in the boundary layer:

$$\dot{q} = 2\pi r_s \int_0^{\delta} u_b dn = 2\pi r_s \int_0^{z_s} u_r dz = \frac{1}{\Gamma_c'(r_s)} \frac{dT}{dr_s} \tag{8.17a}$$

where

$$T = \int_0^{r_s} \int_0^{z_s} 2\pi r^2 F_\theta dr dz \tag{8.17b}$$

Here T is the total magnetic torque applied to the fluid between $r = 0$ and $r = r_s$, where (r_s, z_s) represents the coordinates of the boundary (Figure 8.6(b)). Also, n is a coordinate measured from the boundary into the fluid, and $u_b(n)$ is the velocity profile in the boundary layer.

Next, we turn our attention to the boundary layer. Equation (8.16) tells us that the ratio of the Lorentz force to inertia in the boundary layer is $rF_\theta/(\mathbf{u} \cdot \nabla\Gamma) \sim (u_c\Gamma_c/R)/(u_b\Gamma_c/R) \sim \delta/R$. Since ($\delta \ll R$ we may neglect F_θ in the boundary layer and the azimuthal equation of motion reduces to

$$(\mathbf{u} \cdot \nabla)\Gamma = \text{viscous terms}$$

In integral form this becomes

$$\oint_S \Gamma \mathbf{u} \cdot d\mathbf{S} \sim \oint_S (\text{viscous stresses}) d\mathbf{S}$$

where S is any closed surface. This states that the net flux of angular momentum out of some closed surface is proportional to the viscous torque acting on that surface. Frequently, in boundary layer analysis, it is useful to apply an integral equation of this form to a short portion of the boundary layer. (This is equivalent to integrating the equation of motion across the boundary layer.) The result is referred to as a momentum integral equation, and in this case the azimuthal integral equation takes the form (see Davidson, 1992)

$$\frac{\dot{q}}{\pi} \frac{d\Gamma_c}{ds} - \frac{d}{ds}\left\{\chi\Gamma_c\left[\frac{\dot{q}}{\pi}\right]\right\} = -c_f\Gamma_c^2 \tag{8.18}$$

Here c_f is the dimensionless skin-friction coefficient, $\tau_\theta/(\frac{1}{2}\rho u_\theta^2)$, χ is a shape factor related to the velocity profile in the Ekman wall jet (usually

taken as 1/6), and s is a curvilinear coordinate measured along the boundary from the surface. (Typically, $c_f = 0.052(\Gamma_c/\nu)^{-1/5}$). Eliminating $\dot{q}$ from (8.17a) and (8.18) furnishes

$$\frac{dT}{ds} - \frac{d}{ds}\left\{\chi \frac{\Gamma_c}{\Gamma_c'(s)} \frac{dT}{ds}\right\} = -\pi c_f \Gamma_c^2 \tag{8.19}$$

This simple o.d.e. allows the distribution of the core swirl, $\Gamma_c(r)$, to be calculated whenever the applied Lorentz torque, T, is known. It applies to any shape of cavity and any distribution of F_θ, and so provides a unified model of forced swirl in a cavity. For example, in hemispheres with $f = 1$ it predicts a maximum value of Γ_c of $0.42\Omega_f R^2 c_f^{-1/2}$, so that Γ scales as $F_\theta^{5/9}$. The predictions of (8.19) have been tested against experiments performed in cones, hemispheres and cylinders, and there is a reasonable correspondence between theory and experiment. (Davidson et al. 1995.) However, perhaps the most important results are (i) the existence of the Ekman wall jets, which sweep down the solidification front carrying crystal fragments with them, and (ii) equation (8.15), which shows that the fluid is quite insensitive to the detailed distribution of the applied Lorentz force. It cares only about the globally averaged torque. This model has been generalised to unsteady flows by Ungarish (1997).

8.4 The Stirring of Steel

The simplest idealisation of the magnetic stirring of steel is that shown in Figure 8.2(b). That is, the fluid occupies a long cylindrical column, while the Lorentz force, F_θ, is applied over a relatively short portion of that column. Evidently, there is no Ekman pumping and we must seek a different way of satisfying (8.12). Once again, the secondary flows turn out to be crucial. This time the secondary (poloidal) motion is generated by differential rotation between the forced and unforced regions of the column. The relatively low pressure on the axis of the more rapidly rotating fluid causes the magnetic stirrer to act like a centrifugal pump (Figure 8.7). Fluid is drawn in from the far field, moving along the axis towards the magnetic field. It enters the forced region, is spun up by the Lorentz force and is then thrown to the walls. Finally, the fluid spirals down the solidification front where, eventually, it loses its excess energy and angular momentum through wall shear. In the steady state the fluid cannot return until its excess energy is lost (c.f. (8.12)), and it takes a long time for the boundary layers on the outer cylindrical walls to

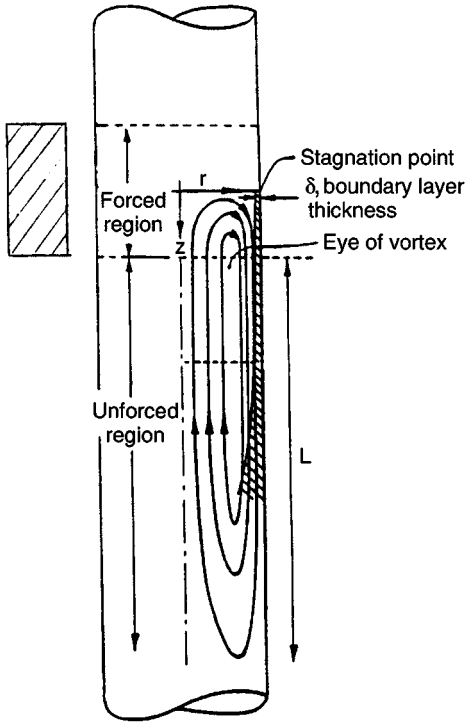

Figure 8.7 Secondary flow in the stirring of steel.

dissipate this energy, essentially because the cross-stream diffusion of energy to the wall is a slow process. Consequently, this centrifugal pumping ensures that a very long portion of the liquid metal column is eventually set into rotation (of order $l \sim u_\theta R^2/\nu_t$), even though F_θ is restricted to a relatively short part of the column. The picture, therefore, is one of fluid being continuously cycled first through the forced region, where it is spun up, then through the side-wall boundary layers, where energy is lost. Note that the local force balance is between inertia ($\mathbf{u} \cdot \nabla \Gamma$) and the applied torque, rather than between F_θ and shear. As a consequence, one-dimensional models of the form discussed in Section 8.2 over-estimate the induced swirl by a factor of around five! (Davidson & Hunt, 1987.) An approximate analytical model of this flow has been proposed by Davidson Hunt, which predicts that the maximum swirl occurs, not where F_θ is largest, but rather at the upper and lower edges of the forced region, where F_θ falls to zero. This has

been confirmed by experiment. Yet again, we see that the spatial distribution of swirl does not mimic that of F_θ, and that secondary (poloidal) flows play a key rôle in the overall dynamics.

From a practical point of view perhaps the most important point to note is that the swirl generated by a stirrer will penetrate many diameters above and below the stirrer. This gives the designer some latitude in his choice of location of the device.

Examples

8.1 Estimate the magnitude of swirl, u_θ, in terms of the force, F_θ, induced by the localised stirring of a long steel strand. (Hint: first estimate the relationship between $\mathbf{u}_p$ and u_θ.)

8.2 Show that the depth of stirring induced in a long steel column by a localised Lorentz force is of order $l \sim u_\theta R^2/\nu_t$. Use two different methods: (1) perform an overall torque balance on the column; and (2) estimate the rate of growth of the boundary layer on the wall $r = R$.

8.3 Derive the momentum equation (8.18) by integrating the azimuthal equation of motion across the boundary layer.

8.4 By considering the appropriate overall torque balance, explain why one-dimensional models of stirring will always overestimate the localised stirring in a long steel strand by an order of magnitude.

9

Magnetic Damping Using Static Fields

> Science is nothing without generalisations. Detached and ill-assorted facts are only raw material, and in the absence of a theoretical solvent, have little nutritive value. At the present time and in some departments, the accumulation of material is so rapid that there is a danger of indigestion.
>
> *Rayleigh (1884)*

We have seen that the relative movement of a conducting body and a magnetic field can lead to the dissipation of energy. This has been used by engineers for over a century to dampen unwanted motion. Indeed, as far back as 1873 we find Maxwell noting: '*A metallic circuit, called a damper, is sometimes placed near a magnet for the express purpose of damping or deadening its vibrations.*' Maxwell was talking about a magnetic field moving through a stationary conductor. We are interested in a moving conductor in a stationary field, but of course, this is really the same thing. We have already touched upon magnetic damping in Chapter 5, and we discussed some of its consequences in Chapter 6. In particular, we saw that the intense magnetic field in a sunspot locally deadens the convective motions in the outer layer of the sun, thus cooling the spot and giving it a dark appearance. Here we make the jump from sunspots to steelmaking, and describe how magnetic fields are used in certain casting operations to suppress unwanted motion.

There has been a myriad of papers on this topic and at times one is reminded of Rayleigh's *indigestion*. Here we focus on the unifying themes. We shall see that the hallmark of magnetic damping is that the dissipation of energy is subject to the constraint of *conservation of momentum*, and that this constraint is a powerful one.

9.1 Metallurgical Applications

We have already seen that a static magnetic field can suppress motion of an electrically conducting liquid. The mechanism is straightforward: the motion of a liquid across the magnetic field lines induces a current. This leads to Joule dissipation and the resulting rise in

thermal energy is accompanied by a fall in magnetic and/or kinetic energy. We are concerned here only with cases where the magnetic Reynolds number is small, so that changes to the applied magnetic field are negligible. In such cases, the rise in Joule dissipation is matched by a fall in kinetic energy. Thus, for example, in an electrically insulated pool, (5.7) gives

$$\frac{d}{dt}\int\left(\frac{1}{2}\rho\mathbf{u}^2\right)dV = -\frac{1}{\sigma}\int\mathbf{J}^2 dV + \text{viscous dissipation}$$

In the last decade this phenomenon has been exploited in a range of metallurgical processes. For example, in the continuous casting of large steel slabs, an intense, static magnetic field (of around 0.5 Tesla) is commonly used to suppress motion within the mould (Figure 9.1). Sometimes the motion takes the form of a submerged jet which feeds the mould from above; at others it takes the form of large eddies or vortices. In both cases the objective is to keep the free surface of the liquid quiescent, thus avoiding the entrainment of surface debris (see Iron & Steel Institute of Japan, 1994.) In other solidification processes, such as the Bridgeman technique for growing semi-conductor crystals or the continuous casting of aluminium, it is widely believed that natural convection has a detrimental effect on the metallurgical structure of the solid. Again, the imposition of a static magnetic field is seen as one means of suppressing these unwanted motions (Muller, Neumann & Weber, 1984). This is discussed in Section 5 of this chapter. Finally, magnetic damping is used in the laboratory measurements of chemical and thermal diffusivities, particu-

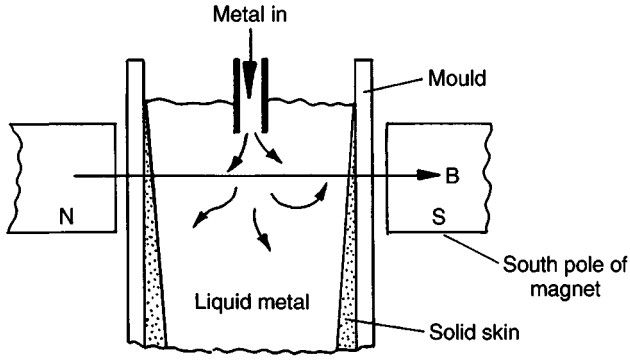

Figure 9.1 Magnetic damping is used to suppress motion in the continuous casting of steel slabs.

larly where solutal or thermal buoyancy can disrupt the measurement technique (Nakamura et al., 1990). For example, in the 'hot-wire' technique for measuring the thermal conductivity of liquid metals, the conductivity is determined by monitoring the rate at which heat diffuses into the liquid from a long, thin, vertical wire. This technique relies on conduction being dominant over convection. Yet natural convection is always present to some degree in the form of a buoyant plume. The simplest way of suppressing the unwanted motion is magnetic damping (Figure 9.2(a)).

In this chapter we examine the magnetic damping of jets, vortices and natural convection. Our aim is to present a unified theoretical framework from which the many disparate published studies may be viewed. We shall see that the hallmark of magnetic damping is that mechanical energy is destroyed while momentum is conserved. It is this need to conserve momentum, despite the dissipation of energy, which gives magnetic damping its special character.

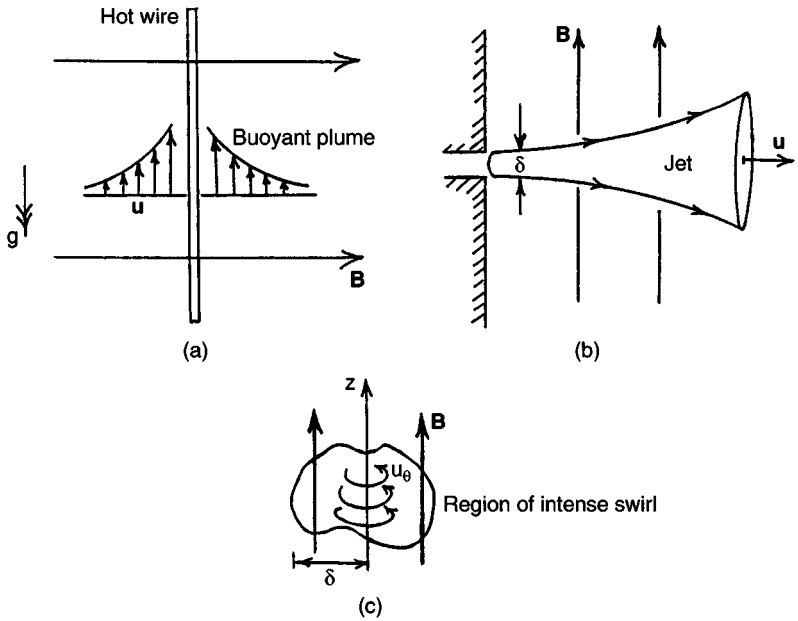

Figure 9.2 Examples of magnetic damping of liquid-metal flows. (a) A buoyant plume is generated by a hot wire and suppressed by an imposed field. (b) A jet is created by side-wall injection at the boundary. (c) A magnetic field dissipates an isolated vortex.

9.2 Conservation of Momentum, Destruction of Energy and the Growth of Anisotropy

We consider flows in which the Reynolds number is large and the magnetic field induced by currents flowing in the liquid is much smaller than the externally imposed field. This covers most laboratory and industrial applications. In view of the large Reynolds number, we may treat the motion as inviscid, except of course when it comes to the small-scale components of turbulence. In the interests of simplicity we take **B** to be uniform, imposed in the z-direction, and consider domains which are infinite in extent or else bounded by an electrically insulated surface.

Since **B** is fixed and uniform, Faraday's equation demands that $\nabla \times \mathbf{E} = 0$. Ohm's law then takes the form

$$\mathbf{J} = \sigma(-\nabla\Phi + \mathbf{u} \times \mathbf{B}) \tag{9.1a}$$

where Φ is the electrostatic potential and **B** is the uniform, imposed magnetic field. Now we also know, from Ampère's law, that **J** is solenoidal and so we have

$$\nabla \cdot \mathbf{J} = 0, \qquad \nabla \times \mathbf{J} = \sigma \mathbf{B} \cdot \nabla \mathbf{u} \tag{9.1b}$$

Equations (9.1b) uniquely determine **J**. (Recall that a vector field is uniquely determined if its divergence and curl are specified.) The key point is that **J** is zero if and only if **u** is independent of z. Now the Lorentz force per unit mass, $\mathbf{J} \times \mathbf{B}/\rho$, is readily obtained from (9.1a):

$$\mathbf{F} = -\frac{\mathbf{u}_\perp}{\tau} + \frac{\sigma(\mathbf{B} \times \nabla\Phi)}{\rho}, \qquad \tau = \rho/\sigma B^2 \tag{9.2}$$

Here $\mathbf{u}_\perp = (u_x, u_y, 0)$ and τ is the Joule damping term. Note that the first term in (9.2) looks like a linear friction term. However, this expression for **F** is awkward as it contains the unknown potential Φ. This potential is given by the divergence of Ohm's law (9.1a), which yields $\Phi = \nabla^{-2}(\mathbf{B} \cdot \boldsymbol{\omega})$ (here $\boldsymbol{\omega}$ is the vorticity field.) Clearly, when **B** and $\boldsymbol{\omega}$ are mutually perpendicular, the Lorentz force simplifies to $-\mathbf{u}_\perp/\tau$, and so (pressure forces apart) $\mathbf{u}_\perp$ declines on a time scale of τ. This is the phenomenological basis of magnetic damping. Loosely speaking, we may think of rotational motion being damped out provided that its axis of rotation is perpendicular to **B**. The ratio of the damping time, τ, to the characteristic advection time, l/u, gives the interaction parameter

$$N = \sigma B^2 l/\rho u$$

Typically, N is indicative of the relative sizes of the Lorentz and inertial forces.

We now consider the rôle of Joule dissipation. This provides an alternative way of quantifying magnetic damping. The inviscid equation of motion

$$\frac{D\mathbf{u}}{Dt} = -\nabla\left(\frac{p}{\rho}\right) + \mathbf{F}, \qquad \mathbf{F} = \mathbf{J} \times \mathbf{B}/\rho$$

yields the energy equation

$$\frac{dE}{dt} = -\frac{1}{\rho\sigma}\int \mathbf{J}^2 dV = -D \tag{9.3}$$

where D is the Joule dissipation rate and E is the global kinetic energy. Clearly, E declines until $\mathbf{J}$ is zero, which happens only when $\mathbf{u}$ is independent of z. We can use (9.3) to estimate the rate of decline of energy. Let $l_{//}$ and $l_{\min}$ be two characteristic length scales for the flow, the first being parallel to $\mathbf{B}$. Then $\nabla \times \mathbf{J}$, and hence $|\mathbf{J}| \sim l_{\min}\nabla \times \mathbf{J}$, may be estimated from (9.1b), and this yields

$$\frac{dE}{dt} = -D \sim -\left(\frac{l_{\min}}{l_{//}}\right)^2 \frac{E}{\tau} \tag{9.4a}$$

from which

$$E \sim E_0 \exp\left[-\tau^{-1}\int_0^t \left(l_{\min}/l_{//}\right)^2 dt\right] \tag{9.4b}$$

The implication is that, provided $l_{\min}$ and $l_{//}$ remain of the same order, the flow will be destroyed on a time scale of τ. Indeed, this might have been anticipated from (9.2). However, this is not the end of the story. The dissipation is subject to some powerful integral constraints. The key point is that $\mathbf{F}$ cannot create or destroy linear momentum, nor (one component of) angular momentum. For example, since $\mathbf{J}$ is solenoidal,

$$\rho\int \mathbf{F} dV = -\mathbf{B} \times \int \mathbf{J} dV = 0 \tag{9.5}$$

Thus the Lorentz force cannot itself alter the global linear momentum of the fluid. Similarly, following Davidson (1995), we have

$$(\mathbf{x} \times \mathbf{F}) \cdot \mathbf{B} = \rho^{-1}[(\mathbf{x} \cdot \mathbf{B})\mathbf{J} - (\mathbf{x} \cdot \mathbf{J})\mathbf{B}] \cdot \mathbf{B} = -\left(B^2/2\rho\right)\nabla \cdot \left[\mathbf{x}_\perp^2 \mathbf{J}\right] \tag{9.6}$$

which integrates to zero over the domain (see also the discussion in Chapter 5, Section 3). Evidently, the Lorentz force has zero net torque parallel to $\mathbf{B}$, and so cannot create or destroy the corresponding compo-

nent of angular momentum. The physical interpretation of (9.6) is that **J** may be considered to be composed of many current tubes, and that each of these tubes may, in turn, be considered to be the sum of many infinitesimal current loops, as in the proof of Stokes' theorem. However, the torque on each elementary current loop is $(d\mathbf{m}) \times \mathbf{B}$, where $d\mathbf{m}$ is its dipole moment. Consequently, the global torque, which is the sum of many such terms, can have no component parallel to **B**.[1]

Now the fact that **F** cannot create or destroy linear momentum, nor one component of angular momentum, would not be important if the mechanical forces themselves changed these momenta. However, in certain flows, such as submerged jets, the mechanical (pressure) forces cannot alter the linear momentum of the fluid. In others, such as flow in an axisymmetric container, the pressure cannot alter the axial component of angular momentum. In such cases there is always some component of momentum which is conserved, despite the Joule dissipation. This implies that the flow cannot be destroyed on a time scale of τ, and from (9.4) we may infer that $l_{//}/l_{\min}$ must increase with time. We might anticipate, therefore, that these flows will exhibit a pronounced anisotropy, with $l_{//}$ increasing as the flow evolves, and indeed, this is exactly what happens. These results are summarised in Table 9.1.

Of course, it has been known for a long time that a strong magnetic field promotes two-dimensional turbulence. However, the traditional explanation is rather different from that given above, and so is worth repeating here. If $\nabla \times \mathbf{F}$ is evaluated from (9.2) and substituted into the vorticity equation, we obtain

$$\frac{D\boldsymbol{\omega}}{Dt} = \boldsymbol{\omega} \cdot \nabla \mathbf{u} - \frac{1}{\tau} \nabla^{-2} \left[\partial^2 \boldsymbol{\omega} / \partial z^2 \right] \tag{9.7}$$

(Roberts, 1967). Phenomenologically, we might consider ∇^{-2} to be replaced by $-l_{\min}^2$, in which case the Lorentz term promotes a unidirectional diffusion of vorticity along the **B**-lines, with a diffusivity of $l_{\min}^2/\tau$. For cases where $l_{//} \gg l_{\min}$, this may be made rigorous by taking the two-dimensional Fourier transform of (9.7) in the x–y plane. This argument is a powerful one when N is large, so that the non-linear inertial terms are negligible. However, when N is small or moderate, the vortex lines stretch and twist on a time scale of l/u, which is smaller than, or of the order of, τ. In such cases it is difficult to infer much from (9.7) and there is an advantage in returning to the integral arguments given above.

[1] Private communication, S. Davidson, 1993.

Table 9.1. *The 'rules' of magnetic damping*

Quantity	Equation	Implication
Energy	$\frac{dE}{dt} = -\frac{1}{\rho\sigma}\int \mathbf{J}^2 dV \sim -\left(\frac{l_{\min}}{l_{//}}\right)^2 \frac{E}{\tau}$	If E is to remain finite then $l_{//}$ must grow relative to $l_{\min}$. Some form of anisotropy then develops
Global Lorentz force	$\int \mathbf{J} \times \mathbf{B}_0 dV = 0$	Linear momentum is neither created nor destroyed by the Lorentz force
Global Lorentz torque	$\int [\mathbf{x} \times (\mathbf{J} \times \mathbf{B}_0)]_{//} dV = 0$	The parallel component of angular momentum is neither created nor destroyed by the Lorentz force

9.3 Magnetic Damping of Submerged Jets

We are interested here in the dissipation of submerged jets such as that shown in Figure 9.2(b). However, we start with the slightly artificial problem of a long, uniform jet which is dissipated by the sudden application of a magnetic field. This provides a useful stepping stone to the more important problem of a submerged jet which evolves in space, rather than in time.

Suppose that we have a unidirectional jet, $\mathbf{u} = u(x, z, t)\hat{\mathbf{e}}_y$, which is initially axisymmetric (Figure 9.3a). At $t = 0$ we impose a uniform magnetic field in the z-direction. Current will be induced as shown in Figure 9.3(b), driven parallel to x by $\mathbf{u} \times \mathbf{B}$, but forced to recirculate back through regions of weak or zero flow by the electrostatic potential. Since the current is two-dimensional, we may introduce a streamfunction, ψ, for $\mathbf{J}$ which is related to $\mathbf{u}$ by Ohm's law.

$$\mathbf{J} = \nabla \times [\psi \hat{\mathbf{e}}_y], \qquad \nabla^2 \psi = -\sigma B \frac{\partial u}{\partial z} \tag{9.8}$$

Our equation of motion is then

$$\frac{\partial u}{\partial t} = \frac{B}{\rho}\frac{\partial \psi}{\partial z} = -\frac{1}{\tau}\nabla^{-2}\left[\frac{\partial^2 u}{\partial z^2}\right] \tag{9.9}$$

Evidently, linear momentum is conserved, since $\partial\psi/\partial z$ integrates to zero. Now let δ be the thickness of the jet in the x-direction and $l_{//}$ be the characteristic lengthscale for u parallel to $\mathbf{B}$.

Then, from conservation of momentum, in conjunction with energy equation (9.4a), we have

$$\frac{dE}{dt} = -\left(\frac{\delta}{l_{//}}\right)^2 \frac{E}{\tau}, \qquad E = u^2 l_{//}\delta, \qquad u l_{//}\delta = \text{constant} \tag{9.10}$$

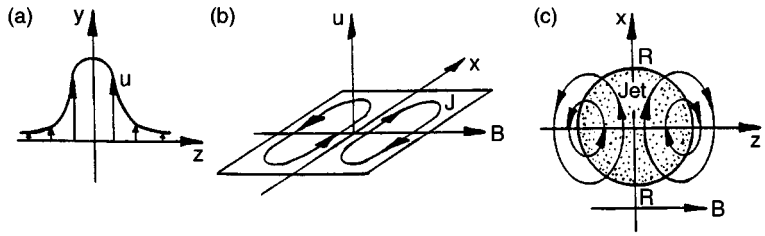

Figure 9.3 Magnetic damping of a jet: (a) initial axisymmetric velocity profile; (b) the induced current; (c) cross-section through the jet. A reverse flow forms at points marked R.

Clearly, $l_{//}/\delta$ must increase with time. If it did not, then E would decline exponentially, which is forbidden by conservation of momentum. For fixed δ the only possible solutions to (9.10) are (Davidson, 1995)

$$l_{//} \sim \delta(t/\tau)^{1/2}, \qquad u \sim u_0(t/\tau)^{-1/2} \tag{9.11}$$

Thus the flow spreads laterally along the field lines, evolving from a jet into a sheet. The mechanism for this lateral spreading is evident from Figure 9.3. The induced currents within the jet give rise to a braking force, as expected. However, the current which is recycled either side of the jet actually accelerates previously stagnant fluid at large $|z|$. Hence the growth in $l_{//}$. Notice also, that at points marked R a counterflow will be generated since **F** points in the negative y-direction and u is initially zero.

The existence of a counterflow, as well as the scaling laws (9.11), are readily confirmed by exact analysis. For example, taking the Fourier transform of (9.9) leads to an exact solution in terms of hypergeometric functions, as we now show. Let U be the cosine transform of u. Then

$$U(k_x, k_z) = 4\int_0^\infty \int_0^\infty u(x, z)\cos(xk_x)\cos(zk_z)dxdz$$

Our equation of motion (9.9) transforms to

$$\frac{\partial U}{\partial t} + \cos^2\phi\frac{U}{\tau} = 0, \qquad \cos\phi = k_z/k$$

where $k^2 = k_x^2 + k_z^2$. Solving for U and taking the inverse transform yields

$$u(\mathbf{x}, t) = \pi^{-2}\int_0^\infty \int_0^{\pi/2} e^{-(\cos^2\phi)\hat{t}}\cos(xk_x)\cos(zk_z)U_0(k)kdkd\phi$$

Here $\hat{t}$ is the scaled time, t/τ and $U_0(k)$ is the transform of the initial axisymmetric velocity profile, $u_0(r)$. For large t this can be simplified using the relationship

$$\int_0^\infty e^{-p^2}\cos(\lambda p)dp = (\sqrt{\pi}/2)e^{-\lambda^2/4}$$

to give

$$u(\mathbf{x}, t) = \frac{1}{2\pi\sqrt{\pi\hat{t}}}\int_0^\infty e^{-k^2z^2/4\hat{t}}\cos(xk)U_0(k)kdk$$

(This is left as an exercise for the reader.) It is clear from this integral that, for large t, u must be of the form

$$u(\mathbf{x}, t) \sim \hat{t}^{-1/2} F(z/\hat{t}^{1/2}, x)$$

which confirms the scaling laws (9.11). Of course, the form of F depends on the initial conditions. For example, if we take $u_0(r) = V \exp(-r^2/\delta^2)$, $r^2 = x^2 + z^2$, then the integral above yields

$$u(\mathbf{x}, t) = \frac{V}{\sqrt{\pi \hat{t}}} \frac{G(\zeta)}{[1 + z^2/(\delta^2 \hat{t})]}, \qquad \zeta = \frac{x^2}{\delta^2 + z^2/\hat{t}}$$

where $G(\zeta)$ is Kummer's hypergeometric function, $G(\zeta) = M(1, \frac{1}{2}, -\zeta)$. An examination of the shape of $G(\zeta)$ confirms that a reverse flow develops, as anticipated in Figure 9.3.

Consider now a submerged, steady jet evolving in space, rather than in time. This is illustrated in Figure 9.4. It is generated by injecting fluid through a circular aperture in a side wall and into a uniform magnetic field. We consider the case where **B** is weak (N is small) so that the jet inertia is much larger than the Lorentz force. This configuration is particularly relevant to the magnetic damping of jets in castings.

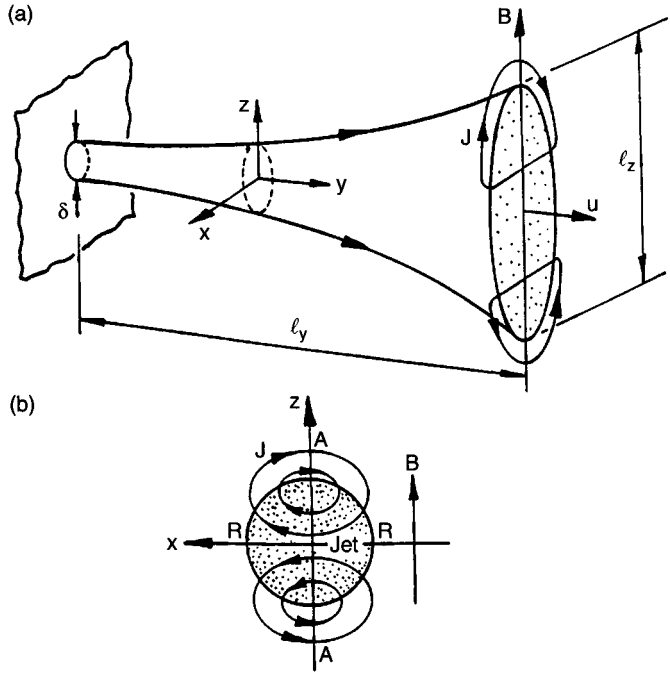

Figure 9.4 MHD jet produced by side-wall injection: (a) spatial evolution of jet; (b) the current paths. A reverse flow occurs at points marked R.

Since N is small, the magnetic field influences the jet only slowly. As a result, the characteristic axial length scale of the jet, l_y, is much greater than l_x and l_z. Now the current must form closed paths. However, each cross section of the jet looks very much like its neighbouring cross sections, and so the current must close in the (x,z)-plane, just as it did in the previous example. Figure 9.4 illustrates the situation. As before, the induced current recirculates through regions of weak or zero flow. It follows that a reverse flow will form at points marked R, and momentum will diffuse out along the z-axis by precisely the same mechanism as before. Thus the jet cross section becomes long and elongated. Now if the jet is to spread laterally along the **B**-lines, then continuity of mass requires that there is some entrainment of the surrounding fluid. (We shall confirm this shortly.) We would expect, therefore, that the jet draws in fluid from the far field, predominantly at large $|z|$. Conversely, regions of reverse flow on the x-axis will produce an outward flow of mass near the wall (Figure 9.5). This complex three-dimensional flow pattern was proposed independently by Davidson (1995), based on theoretical considerations, and by Harada et al. (1994), based on experimental observations.

We now confirm this picture using the Euler equation. The equation of motion for the jet is very similar to (9.9). In terms of the streamfunction ψ, we have

$$\frac{Du_y}{Dt} = \mathbf{u} \cdot \nabla u_y = \frac{B}{\rho}\frac{\partial \psi}{\partial z} = -\frac{1}{\tau}\nabla^{-2}\left[\frac{\partial^2 u_y}{\partial z^2}\right] \tag{9.12}$$

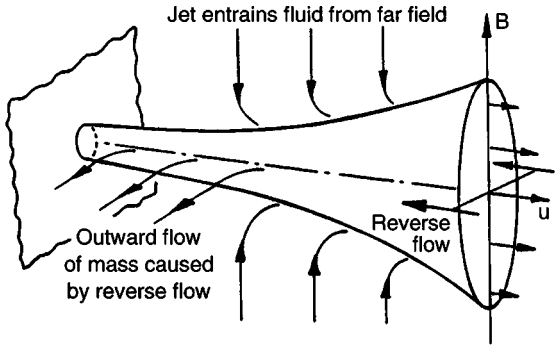

Figure 9.5 MHD jet produced by side-wall injection. The jet draws in fluid from the far field and the reverse flow produces on outward flow of mass near the wall.

Unlike (9.9), this is non-linear, and so exact solutions are unlikely to be found. However, we may still use conservation of momentum in conjunction with an energy dissipation equation. Let M be the momentum flux in the jet, $M = \int u_y^2 dA$. From (9.12) this is conserved. Also from (9.12) we can construct an energy equation reminiscent of (9.4a).

$$\frac{d}{dy}\int\left(\frac{1}{2}u_y^3\right)dA = -\frac{1}{\rho\sigma}\int \mathbf{J}^2 dA$$

It follows that u_y and $l_{//}$ scale as (Davidson, 1995)

$$u_y \sim \left[\frac{\tau M^2}{\delta^4 y}\right]^{1/3}, \qquad l_{//} \sim \left[\frac{\delta^5 y^2}{\tau^2 M}\right]^{1/3} \tag{9.13}$$

(It is readily confirmed that these are the only scalings which satisfy $M =$ constant as well as the energy equation above.) Note that mass flux in the jet increases with y, as shown in Figure 9.5.

It is interesting to compare (9.13) and Figure 9.5 with the two-dimensional jet analysed in Chapter 5, Section 2.2. Evidently a two-dimensional jet, where the current paths do not close in the fluid, behaves quite differently from a three-dimensional jet. Of course, it is the three-dimensional jet which is the more important in practice.

9.4 Magnetic Damping of Vortices

9.4.1 General considerations

So far we have considered only cases where the conservation of linear momentum provides the key integral constraint. We now consider examples where conservation of angular momentum is important, i.e. vortices. The discussion is restricted to inviscid fluids. Suppose we have one or more vortices, of arbitrary orientation, held in a spherical domain. Then, as we saw in Chapter 5, Section 3, the global magnetic torque is given by

$$\mathbf{T} = \frac{1}{\rho}\int \mathbf{x} \times (\mathbf{J} \times \mathbf{B}) d\mathrm{V} = -\frac{1}{4\tau}\int (\mathbf{x} \times \mathbf{u})_\perp d\mathrm{V} \tag{9.14}$$

(This holds for any distribution of $\mathbf{u}$.) If $\mathbf{H}$ is the global angular momentum of the fluid, then (9.14) gives the inviscid equation of motion

$$\frac{\partial \mathbf{H}}{\partial t} = -\frac{\mathbf{H}_\perp}{4\tau}$$

It follows that $\mathbf{H}_{//}$ is conserved while $\mathbf{H}_{\perp}$ declines exponentially (Davidson, 1995):

$$\mathbf{H}_{//} = \text{constant}; \qquad \mathbf{H}_{\perp}(t) = \mathbf{H}_{\perp}(0)\exp[-t/4\tau] \tag{9.15a, b}$$

The simplicity of this result is rather surprising, particularly as it applies for any value of N, and so is valid even when inertia is dominant and the stretching and twisting of vorticity is more vigorous than the damping. Now the conservation of $H_{//}$ gives us a lower bound on E:

$$E \geq H_{//}^2 \left[2 \int \mathbf{x}_{\perp}^2 dV \right]^{-1} \tag{9.16}$$

This, in conjunction with the energy equation

$$\frac{dE}{dt} = -\frac{1}{\rho\sigma} \int J^2 dV$$

provides a powerful constraint on the way in which these flows evolve. Typically, the energy of the flow decreases through the destruction of $\mathbf{H}_{\perp}$ until only $\mathbf{H}_{//}$ remains. Since there is a lower bound on E, it follows that the flows must eventually evolve to a state in which $\mathbf{u}$ is finite, but $\mathbf{J}$ is everywhere zero. From (9.1b) it is clear that the final motion must be two-dimensional (Figure 9.6), $\mathbf{u} = \mathbf{u}(x, y)$ consisting of one or more columnar vortices which span the sphere and whose axes are parallel to $\mathbf{B}$. A natural question to ask is: how do the vortices evolve into these long columnar structures? We would expect the initial evolution of a small vortex to be independent of the shape of the remote boundaries, and so we now dispense with the spherical boundary and consider vortices in

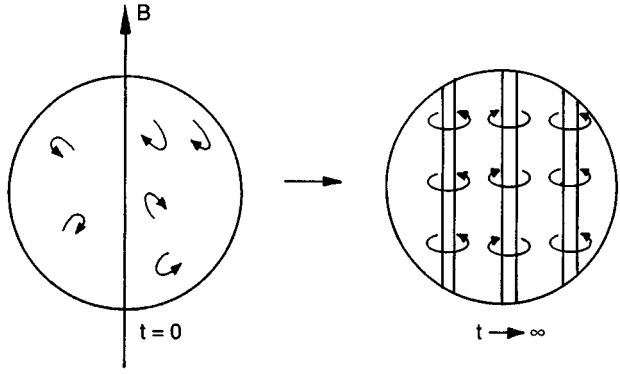

Figure 9.6 Inviscid flow in a sphere which is subject to a uniform field always evolves towards a two-dimensional state.

infinite (or else large, but finite) domains. There are two special cases which deserve particular attention. One is where the vorticity is aligned with **B**, and the other is where **B** and ω are mutually perpendicular. We start with transverse vortices.

9.4.2 Damping of transverse vortices

In the interests of simplicity we shall consider a two-dimensional vortex whose axis is normal to the imposed magnetic field. Suppose our flow is confined to the (x,z)-plane and bounded by the cylindrical surface $x^2 + z^2 = R^2$. We are interested particularly in isolated vortices whose characteristic radius, δ, is much less than R. We shall take the vortex to be initially axisymmetric and subject to a uniform magnetic field, **B**, imposed in the z-direction (see Figure 9.7). Once again, we shall find that global angular momentum provides the key to determining the evolution of the flow.

Since **B** and ω are mutually perpendicular the electrostatic potential is zero (c.f. $\Phi = \nabla^{-2}(\mathbf{B} \cdot \omega)$), and so (9.2) gives the Lorentz force and magnetic torque as

$$\mathbf{F} = -(u_x/\tau)\hat{\mathbf{e}}_x, \qquad T_y = -\tau^{-1} \int z u_x dV = -H_y/2\tau \qquad (9.17, 9.18)$$

Here H_y is the global angular momentum, which may be expressed either in terms of u or else in terms of the two-dimensional streamfunction, ψ:

$$H_y = \int (z u_x - x u_z) dV = 2 \int z u_x dV = 2 \int \psi dV$$

It follows immediately that, even in the low N (non-linear) regime, the angular momentum decays in a remarkably simple manner:

$$H_y(t) = H_y(0) e^{-t/2\tau} \qquad (9.19)$$

This is the two-dimensional counterpart of (9.15). It is tempting to conclude, therefore, that the vortex decays on a time-scale of 2τ. However, this appears to contradict (9.7) which, in the present context, simplifies to

$$\frac{D\omega}{Dt} = -\frac{1}{\tau} \nabla^{-2} [\partial^2 \omega / \partial z^2] \qquad (9.20)$$

We may write this in the form

$$\frac{D\omega}{Dt} \sim \frac{\delta^2}{\tau} \frac{\partial^2 \omega}{\partial z^2}$$

and anticipate (correctly) that there is a continual diffusion of vorticity along the z-axis. In the limit of large N we have the simple diffusion equation

$$\frac{\partial \omega}{\partial t} \sim \frac{\delta^2}{\tau} \frac{\partial^2 \omega}{\partial z^2} \tag{9.21}$$

which suggest that the cross section of the vortex distorts from a circle to a sheet on a time-scale of τ. If this picture is correct, and we shall see that it is, this distortion should proceed in accordance with

$$l_z \sim \delta(t/\tau)^{1/2} \tag{9.22}$$

This elongation of the eddy will cease only when the influence of the boundary is felt. We therefore have two conflicting views. On the one hand, (9.19) suggests that the flow is destroyed on a time-scale of 2τ. On the other, (9.22) suggests a continual evolution of the vortex until such time as the boundary plays an important rôle. This will occur when $l_z \sim R$, which requires a time of the order of $(R/\delta)^2\tau$. We shall now show how these two viewpoints may be reconciled.

We consider the linear case where the magnetic field is relatively intense, so that $N \gg 1$. We further simplify the problem by insisting that the boundaries are remote ($R \gg \delta$) so that we may consider flow in an infinite domain. This greatly simplifies the algebra, but at a cost. In order that all relevant integrals converge, particularly the angular momentum, we require that the integral of ψ converges, and this limits our possible choice of initial conditions. However, this sub-class of flows will suffice to show the general behaviour.

Let us introduce the Fourier transform

$$\Psi(k_x, k_z) = 4 \int_0^\infty \int_0^\infty \psi(x, z) \cos(xk_x) \cos(zk_z) dx dz \tag{9.23}$$

and apply this transform to (9.20), rewritten as

$$\frac{\partial \psi}{\partial t} = -\frac{1}{\tau} \nabla^{-2} \frac{\partial^2 \psi}{\partial z^2} \tag{9.24}$$

Let $\hat{t}$ be the dimensionless time t/τ, k the magnitude of $\boldsymbol{k}$, and Ψ_0 the transform of ψ at $t = 0$. Then the transformed version of (9.24) is readily integrated to give $\Psi = \Psi_0(k) e^{-(\cos^2\phi)\hat{t}}$; $\cos\phi = k_z/k$. However, this is identical to the solution we obtained for a two-dimensional jet in Section 9.3. Thus, without any further work, we may say that at large times

$$\psi(\mathbf{x}, t) = \frac{1}{2\pi(\pi\hat{t})^{1/2}} \int_0^\infty e^{-k^2 z^2/4\hat{t}} \cos(xk_x)\Psi_0(k)k\,dk \tag{9.25}$$

Evidently, for $t \gg \tau$, $\psi(\mathbf{x}, t)$ adopts the form

$$\psi(\mathbf{x}, t) \sim \hat{t}^{-1/2} F(z/\hat{t}^{1/2}, x) \tag{9.26}$$

where F is determined by the initial conditions. It would appear, therefore, that the arguments leading to (9.22) are substantially correct. An initially axisymmetric vortex progressively distorts into a sheet-like structure, with a longitudinal length scale given by (9.22). Note that (9.26) implies that $u_x \ll u_z$ while $u_z \sim \hat{t}^{-1/2}$. It follows that the kinetic energy of the eddy is progressively 'channelled' into the z-component of motion, and that the energy, E, declines as $E \sim (t/\tau)^{-1/2}$.

Let us now consider a specific example. Suppose that the initial eddy structure is described by

$$\psi_0(r) = \Phi_0 e^{-r^2/\delta^2}, \qquad r^2 = x^2 + z^2 \tag{9.27}$$

Then (9.25), which is valid for large t, may be integrated to give

$$\psi(\mathbf{x}, t) = \frac{\Phi_0}{(\pi\hat{t})^{1/2}} \frac{\zeta}{x^2} G(\zeta), \qquad \zeta = \frac{x^2}{\delta^2 + z^2/\hat{t}} \tag{9.28}$$

where G is Kummer's hypergeometric function, $G(\zeta) = M(1, \frac{1}{2}, -\zeta)$. Now expressions (9.26) and (9.28) seem to contradict (9.19), which predicts that the angular momentum decays as $\exp(-t/2\tau)$. However, (9.28) has an interesting property. For $t \gg \tau$, the global angular momentum, H_y, is

$$H_y = \frac{4\Phi_0\delta^2}{\pi^{1/2}} \int_0^\infty (1 + x^2)^{-1/2} \int_0^\infty \zeta^{-1/2} G(\zeta)\,d\zeta\,dx$$

This integrates to zero, since $\int_0^\infty \zeta^{-1/2} G(\zeta)\,d\zeta = 0$. It would appear, then, that the structure of the flow at large times is such that the angular momentum is zero. The reason for this can be seen from Figure 9.7, which shows the flow for $t \gg \tau$ (the structure of the flow at low N is also shown). Regions of reverse flow occur either side of the centre line of the vortex. This reverse flow has a magnitude which is just sufficient to cancel the angular momentum of the primary eddy.

We conclude, therefore, that the structure of the flow for large t is long and streaky, comprising vortex sheets of alternating sign. In short, the vorticity diffuses along the **B**-lines in accordance with (9.22) while simultaneously adopting a layered structure which has zero net angular momentum, thus satisfying (9.19).

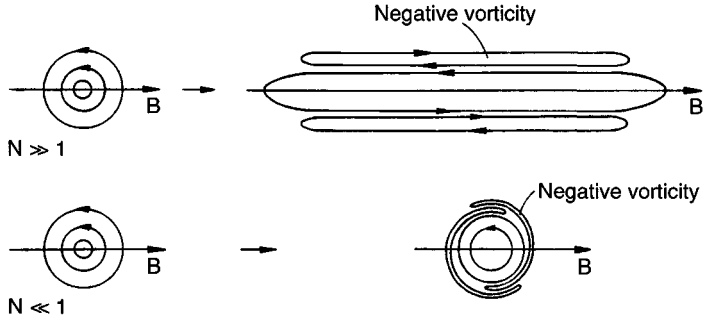

Figure 9.7 Magnetic damping of a transverse vortex at low and high N: a schematic view.

9.4.3 Damping of parallel vortices

We now consider a vortex whose axis is aligned with **B**. For simplicity, we restrict ourselves to axisymmetric vortices, described in terms of cylindrical polars (r, θ, z) with **B** parallel to z. We shall neglect viscosity and assume that initial conditions are such that the integral of the angular momentum converges at $t = 0$. Aspects of this problem have been touched upon in Chapter 5, Section 2.3

Suppose we have an isolated region of intense swirl, of characteristic radius δ, in an otherwise quiescent liquid. We may uniquely define the instantaneous state of the flow using just two scalar functions: Γ, the angular momentum, and Ψ, the Stokes streamfunction. These are defined through the expressions

$$\mathbf{u} = \mathbf{u}_\theta + \mathbf{u}_p = (\Gamma/r)\hat{\mathbf{e}}_\theta + \nabla \times [(\Psi/r)\hat{\mathbf{e}}_\theta] \tag{9.29}$$

$$\nabla_*^2 \Psi = \frac{\partial^2 \Psi}{\partial z^2} + r\frac{\partial}{\partial r}\left(\frac{1}{r}\frac{\partial \Psi}{\partial r}\right) = -r\omega_\theta \tag{9.30}$$

Note that the velocity has been divided into azimuthal and poloidal components. The Lorentz force, which is linear in **u**, may be similarly divided, giving

$$\mathbf{F}_p = -\frac{u_r}{\tau}\hat{\mathbf{e}}_r = \frac{1}{r\tau}\frac{\partial \Psi}{\partial z}\hat{\mathbf{e}}_r, \qquad F_\theta = -\frac{1}{\tau}\frac{J_r}{\sigma B} = \frac{1}{r\tau}\frac{\partial \phi}{\partial z} \tag{9.31, 9.32}$$

Here $\sigma B\phi$ is the Stokes streamfunction for $\mathbf{J}_p$ which, by virtue of Ohm's law, is related to Γ by

$$\nabla_*^2 \phi = -\partial \Gamma / \partial z \tag{9.33}$$

The governing equations for Γ and Ψ are the azimuthal components of the momentum and vorticity equations, respectively (Davidson, 1995):

$$\frac{D\Gamma}{Dt} = \frac{1}{\tau}\frac{\partial \phi}{\partial z} = -\frac{1}{\tau}\frac{\partial^2}{\partial z^2}\left[\nabla_*^{-2}\Gamma\right] \tag{9.34}$$

$$\frac{D}{Dt}\left(\frac{\omega_\theta}{r}\right) = \frac{1}{r^4}\frac{\partial \Gamma^2}{\partial z} - \frac{1}{r^2\tau}\frac{\partial^2}{\partial z^2}\left[\nabla_*^{-2}(r\omega_\theta)\right] \tag{9.35}$$

Note the appearance of the pseudo-diffusion terms. We might anticipate that angular momentum propagates along the magnetic field lines, and we shall see that this is substantially correct.

We shall now draw some general conclusions from (9.34) and (9.35). First, it is apparent from (9.34) that the global angular momentum is conserved:

$$I_\Gamma = \int \Gamma dV = \text{constant}. \tag{9.36}$$

This is a special case of (9.15a) and may be contrasted with the angular momentum of a transverse vortex. Second, for confined domains the kinetic energy of the flow has a lower bound. Specifically, the Schwarz inequality gives

$$E_\theta \geq I_\Gamma^2 \Big/ 2\int r^2 dV \tag{9.37}$$

where E_θ is the energy of the azimuthal component of motion. Third, as noted earlier, any initial condition (in a confined domain) must evolve to a steady state of the form $(0, u_\theta(r), 0)$. In fact, this is true for any value of N, and follows directly the energy equation (9.3). That is, we know that the flow eventually reaches a steady state with non-zero E_θ, at which time the Joule dissipation must vanish. Yet from (9.31) $\rightarrow$ (9.33) we know that $|\mathbf{J}|$, and hence the dissipation disappears only when u_r and $\partial\Gamma/\partial z$ are both zero. This is a special case of the three-dimensional result discussed in Section 4.1 of this chapter.

For infinite domains (9.37) does not apply. However, we can still use conservation of angular momentum to determine the manner in which the flow evolves. From (9.4a) we have

$$\frac{dE}{dt} \sim -\left(\frac{\delta}{l_z}\right)^2 \frac{E}{\tau} \tag{9.38}$$

Thus the total energy declines as

$$E \sim E_0 \exp\left[-\int_0^{\hat{t}} (\delta/l_z)^2 d\hat{t}\right] \tag{9.39}$$

If angular momentum is to be conserved, then there are only two ways in which this decrease in energy can be accommodated. Either l_z increases with time to reduce the dissipation, thus avoiding the exponential decline in energy, or else the angular momentum centrifuges itself radially outward, allowing the energy to decline despite the conservation of I_Γ. We shall see that axial spreading of angular momentum is typical of high-N flows, while the radial spreading of angular momentum is characteristic of low-N flows.

Let us now consider separately the limits of high and low N. When N is large, the azimuthal and poloidal motions are decoupled. Specifically, N is of the order of $l/u\tau$, so that when N is large the kinetic energy exchange between u_θ and $\boldsymbol{u}_p$ (via the centrifugal force) is negligible by comparison with the Joule dissipation. If the energy of the poloidal flow, E_p, is initially small (of the order of $N^{-1}E_\theta$), it remains small. The flow is then governed by the simple linear equation

$$\frac{\partial \Gamma}{\partial t} = -\frac{1}{\tau}\frac{\partial^2}{\partial z^2}\left[\nabla_*^{-2}\Gamma\right] \tag{9.40}$$

We expect, therefore, that any localised region of swirl will diffuse along the magnetic field lines at a rate determined by

$$l_z \sim \delta(t/\tau)^{1/2} \tag{9.41}$$

We may confirm this by taking the Fourier transform of (9.40). Suppose that the flow is unbounded and let U be the first-order Hankel-cosine transform of u_θ.

$$U(k_r, k_z) = 4\pi \int_0^\infty \int_0^\infty \Gamma(r, z) J_1(k_r r) \cos(k_z z) r dr dz \tag{9.42}$$

Then (9.40) shows that U decays as

$$U = U_0 e^{-(\cos^2\phi)\hat{t}}, \qquad \cos\phi = k_z/k \tag{9.43}$$

As before, $\hat{t}$ is the dimensionless time t/τ, U_0 represents the initial condition, and k is the magnitude of $\boldsymbol{k}$. We can now determine Γ by taking the inverse transform. For large times this is (Davidson, 1997)

$$\Gamma(\hat{t} \to \infty) = \frac{r\hat{t}^{-1/2}}{2\pi^2} \int_0^\infty \int_0^\infty [kU_0(k, k_z)] e^{-q^2} J_1(kr) \cos\left(kqz/\hat{t}^{1/2}\right) k dk dq \tag{9.44}$$

This confirms that, for large values of t, the distribution of angular momentum is of the form

$$\Gamma(\mathbf{x}, t) = (t/\tau)^{-1/2} F\big(r, z/(t/\tau)^{1/2}\big) \tag{9.45}$$

Note the similarity between (9.45) and the evolution of ψ for two-dimensional transverse vortices. As expected, the angular momentum propagates along the z-axis at a rate governed by (9.41), but decays according to $u_\theta \sim (t/\tau)^{-1/2}$. The energy of the vortex therefore declines at a rate

$$E \sim (t/\tau)^{-1/2} \tag{9.46}$$

which is exactly the same as for a transverse vortex.

By way of an example, suppose that, at $t = 0$, we have a spherical blob of swirling fluid, so that our initial condition is

$$\Gamma_0(r, z) = \Omega r^2 \exp\big[-\big(r^2 + z^2\big)/\delta^2\big]$$

Then it is readily confirmed that (9.44) gives

$$u_\theta\big(\hat{t} \to \infty\big) = \Omega\delta\hat{t}^{-1/2}\frac{3}{4}\pi^{1/2}\left(\frac{\delta}{r}\right)^4 \zeta^{5/2} H(\zeta), \qquad \zeta = \frac{r^2}{\delta^2 + z^2/\hat{t}} \tag{9.47}$$

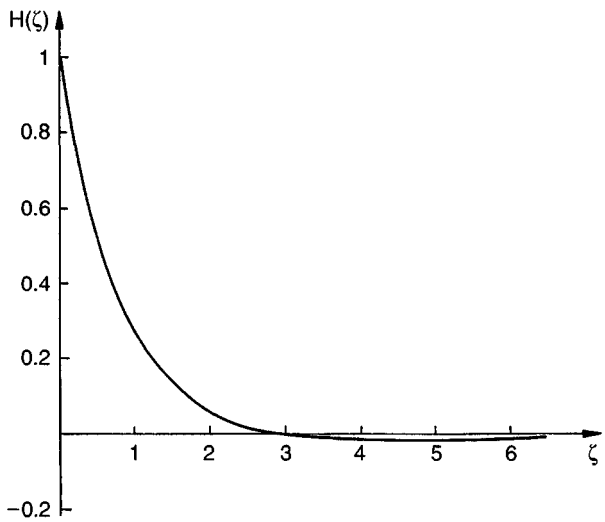

Figure 9.8 Magnetic damping of a parallel vortex at high N. $H(\zeta)$ is the distribution of swirl with radius at large t. Note the reverse rotation at large radii.

Here $H(\zeta)$ is the hypergeometric function $H(\zeta) = M(\frac{5}{2}, 2, -\zeta)$. The shape of $H(\zeta)$ is shown in Figure 9.8. Curiously, at large ζ, the function H becomes negative ($H \sim -\zeta^{-5/2}/2\pi^{1/2}$), so that the primary vortex is surrounded by a region of counter-rotating fluid. This may be attributed to the way in which the induced currents recirculate back through quiescent regions outside the initial vortex (see later). We conclude, therefore, that the asymptotic structure of a vortex aligned with **B** is as shown schematically in Figure 9.9. It is cigar-like in shape, and quite different in structure to the transverse vortex shown in Figure 9.7. Curiously, though, despite the fact that the two classes of vortices adopt very different structures, their energies both decay as $(t/\tau)^{-1/2}$

The mechanism for the propagation of angular momentum is shown in Figure 9.10. The term $\mathbf{u}_\theta \times \mathbf{B}$ tends to drive a radial current, J_r. Near the centre of the vortex, where the axial gradient in Γ is small, this is counter-balanced by an electrostatic potential, Φ, and so almost no current flows. However, near the top and bottom of the vortex, the current can return through regions of small or zero swirl. The resulting inward flow of current above and below the vortex gives rise to a positive azimuthal torque which, in turn, creates positive angular momentum in previously stagnant regions. Notice also that regions of reverse flow form in an annular zone surrounding the initial vortex where F_θ is negative.

We now turn our attention to the case where N is low. Since the Joule dissipation is negligible on time scales of the order of l/u, the flow evolves

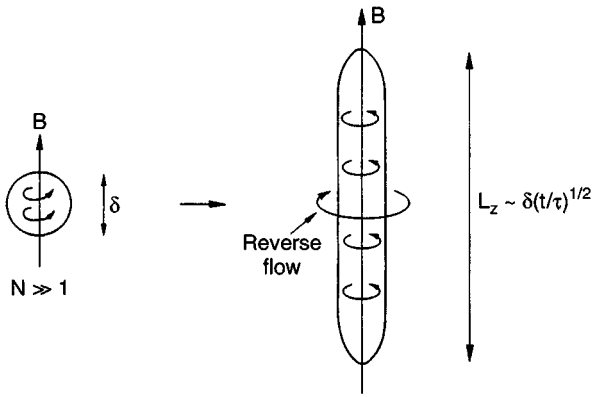

Figure 9.9 Magnetic damping of a parallel vortex at high N. The figure shows schematically the structure of the flow at large t.

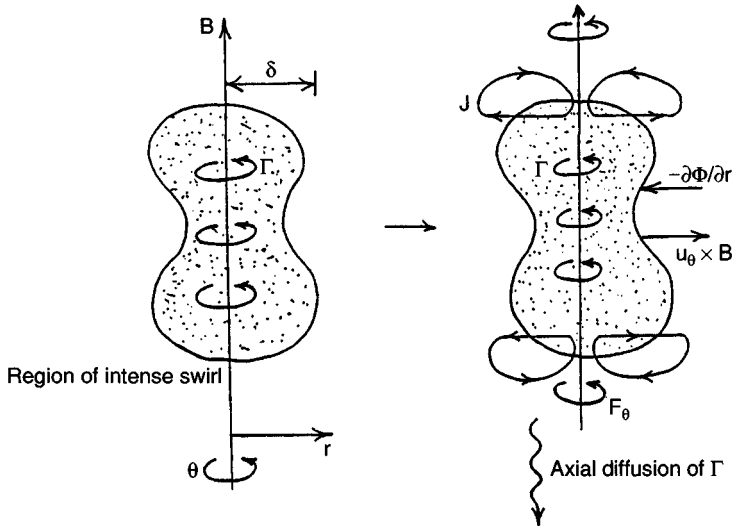

Figure 9.10 Magnetic damping of a region of intense swirl: (a) the initial swirl distribution; (b) the axial diffusion of angular momentum.

in accordance with the undamped Euler equations. Our initial blob of swirling fluid, which is centrifugally unstable, will centrifuge itself radially outward. This occurs through the angular momentum organizing itself into one or more ring-shaped vortices. These propagate radially outward with the characteristic mushroom-like structure of a thermal plume. This is shown schematically in Figure 9.11.

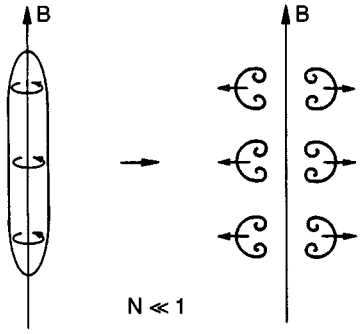

Figure 9.11 Magnetic damping of a parallel vortex at low N. The vortex will disintegrate through hoops of swirling fluid centrifuging themselves radially outward.

9.4.4 Implications for low-R_m turbulence

Consider a homogeneous, low-R_m turbulent flow which is freely evolving in a uniform magnetic field. Suppose that the interaction parameter, $N = \sigma B_0^2 l/\rho u$, is large when based on the integral scale of the turbulence. Then inertia may be neglected as far as the large (energy containing) eddies are concerned and, since $\mathbf{J}$ is linear in $\mathbf{u}$, these eddies are governed by the (linear) equation of motion,

$$\rho \frac{\partial \mathbf{u}}{\partial t} = -\nabla(P) + \mathbf{J} \times \mathbf{B}_0$$

In view of the linearity of this equation, we might regard the turbulence as an ensemble of independent eddies, some of which are initially aligned with the field $\mathbf{B}_0$ and some of which are non-aligned. These eddies will evolve in a manner not unlike those described in the previous sections. Vortices whose rotation axis is aligned with the magnetic field will develop into long, columnar structures. Those which are perpendicular to $\mathbf{B}_0$ will develop into sheet-like structures consisting of thin, interwoven layers of oppositely signed vorticity, the dominant velocity being $\mathbf{u}_{//}$. Both types of vortices will lose their kinetic energy at a rate $E \sim (t/\tau)^{-1/2}$. Thus we might expect two generic types of structures to emerge: columns and sheets (Figure 9.12). Moreover, since $\mathbf{u}_\perp$ is prefer-

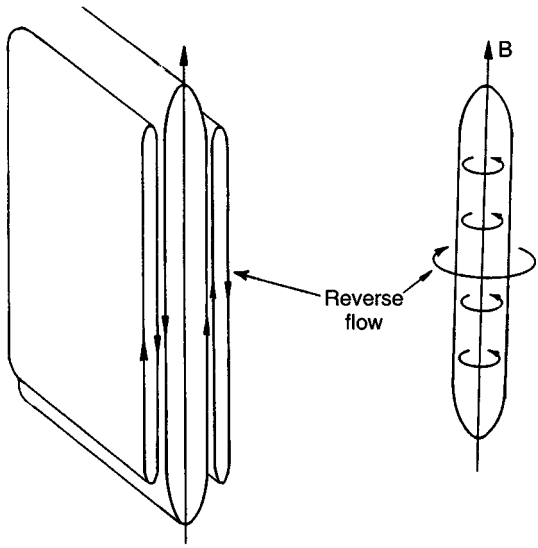

Figure 9.12 Typical flow structure in high-N turbulence.

entially destroyed in the sheets, we might expect $\mathbf{u}_{//}^2/\mathbf{u}_{\perp}^2$ to increase as the flow evolves from some initial isotropic state. In fact, this is precisely what is observed in numerical simulations. The ratio $\mathbf{u}_{//}^2/\mathbf{u}_{\perp}^2$ tends to a value of 2 at large times (as predicted by Moffatt, 1967), as long as N remains large.

9.5 Damping of Natural Convection

We have already discussed the damping of natural convection in the context of Rayleigh–Benard convection. Here we shall consider a different configuration, which is particularly important in the casting of aluminium. We shall examine natural convection in an axisymmetric pool, driven by a difference in temperature between the surface and the sides of the pool. We consider first convection in the absence of a magnetic field, and then examine the influence of an imposed field.

9.5.1 Natural convection in an aluminium ingot

Consider a cavity which is filled with liquid metal and has maximum radius R. Suppose that the walls of the cavity are maintained at a reference temperature, T_M, while the upper surface of the metal is maintained at the higher temperature of $T_M + \Delta T$. Then natural convection will ensure that the liquid metal flows as shown in Figure 9.13, falling at the walls and rising up through the core. The problem just specified is a zero-order model of the casting of aluminium. Figure 9.14 is a simple representation of an aluminium caster. In essence, a solid ingot is slowly withdrawn from a liquid metal pool, the pool being continuously replenished from above. It is well known that buoyancy-driven flow arises during this process, and that this flow has a substantial influence on the metallurgical structure of the solid, affecting both the grain size and the macro-segregation within the ingot. There is considerable motivation then to understand how the magnitude and distribution of the flow field varies with, say, the pool size or superheat ΔT.

The Reynolds number for the flow is assumed to be large, and the flow is taken to be laminar (although in practice it is likely to be turbulent). The Prandtl number is, of course, much less than one. We shall invoke the Boussinesq approximation, in which the velocity field remains solenoidal. The equation of motion for the liquid metal is then

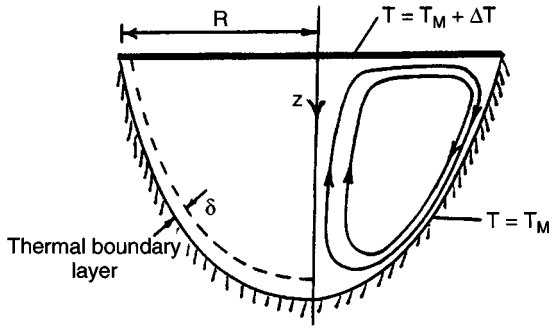

Figure 9.13 Thermally driven flow in a cavity. The upper surface is maintained at temperature $T_M + \Delta T$ and the walls at the lower temperature of T_M. Cold fluid falls near the walls.

$$\frac{D\mathbf{u}}{Dt} = -\nabla\left(\frac{P}{\rho}\right) - g\beta(T - T_M)\hat{\mathbf{k}} + \nu\nabla^2\mathbf{u} \tag{9.48}$$

and the corresponding transport equations for vorticity and heat are, in cylindrical polar coordinates,

$$\frac{D}{Dt}\left(\frac{\omega_\theta}{r}\right) = g\beta\frac{1}{r}\frac{\partial T}{\partial r} + \nu\left\{\nabla^2\left(\frac{\omega_\theta}{r}\right) + \frac{2}{r}\frac{\partial}{\partial r}\left(\frac{\omega_\theta}{r}\right)\right\} \tag{9.49}$$

$$\frac{DT}{Dt} = \alpha\nabla^2 T \tag{9.50}$$

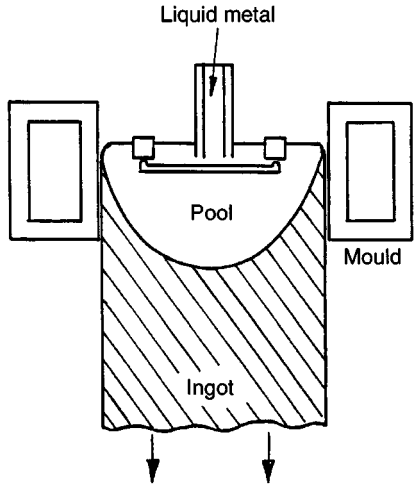

Figure 9.14 Casting of aluminium.

Here α is the thermal diffusivity, β the expansion coefficient and ν the kinematic viscosity.

We shall denote the thickness of the thermal boundary layer on the cavity wall by δ, and use subscripts c and b to indicate parameters inside and outside the thermal boundary layer, respectively. Thus, for example, the temperature field in the core is T_c, while the velocity field in the thermal boundary layer is $\mathbf{u}_b$. We now show that the core of the melt is thermally stratified: that is

$$T_c \approx T_c(z) \tag{9.51}$$

To this end it is useful to integrate (9.48) around any closed streamline to give

$$g\beta \oint (T - T_M)dz = \nu \oint \nabla^2 \mathbf{u} \cdot d\mathbf{l} \tag{9.52}$$

This states that the energy gained by a fluid particle, by virtue of the buoyancy force, must be diffused or dissipated out of the particle by shear. However, in view of the smallness of ν, the second integral would appear to be vanishingly small. Nevertheless, there are three ways in which we could guarantee that all streamlines satisfy (9.52). These are:

(a) $\mathbf{u}$ scales as l/ν;
(b) *all* streamlines pass through a singular region, where the velocity gradients scale as $\nu^{1/2}$;
(c) the core is thermally stratified, in accordance with (9.51).

We may eliminate the first of these possibilities, as it implies very large velocities. We are left, therefore, with options (b) and (c). There are two possible singular regions which are candidates for option (b). One is the viscous boundary layer on the cavity wall, and the other is the region at the bottom of the cavity where the wall jets collide. However, to pass through the dissipative region at the base of the cavity, a streamline must first have entered the wall jet. Consequently, option (b) is equivalent to saying that all streamlines must pass through the thermal boundary layer.

In fact, we may show that *both* (b) and (c) hold true. That is, the core is thermally stratified, and all the streamlines pass through the thermal boundary layer. The argument proceeds by showing that if either one of (b) or (c) holds, then the other must follow. The argument is as follows. Suppose (c) holds true, but (b) does not. Then (9.50) applied to the core requires that

$$u_{zc}T_c'(z) = \alpha T_c''(z) \tag{9.53}$$

This implies that u_{zc} is a function of z only, and hence from continuity, u_{rc} is a linear function of r. This, in turn, implies that all streamlines will pass out of the core and into the boundary layer. Consequently, (b) must hold true after all.

We may also show that the converse is true by using scaling arguments. For convenience, we shall take the datum for temperature to be T_M. Also, let L_T be the axial length-scale in the core. Then (9.48) applied in the boundary layer requires that

$$\frac{u_{zb}^2}{L_T} \sim g\beta T_c$$

In addition, if all the streamlines pass through the thermal boundary layer, continuity requires that

$$u_{zc} \sim \frac{u_{zb}\delta}{R}$$

These estimates show that, in the core,

$$\mathbf{u} \cdot \nabla(\omega_\theta) \sim g\beta \frac{T_c\delta^2}{(RL_T^2)}$$

from which we deduce

$$\frac{\partial T_c}{\partial r} \sim \frac{T_c}{R}\left(\frac{\delta}{L_T}\right)^2$$

Consequently, provided $L_T \gg \delta$ (and we shall see that this is indeed the case), the core is thermally stratified according to

$$T_c = T_c(z)\left\{1 + 0\left(\frac{\delta}{L_T}\right)^2\right\}$$

Thus it appears that the flow satisfies both conditions (b) and (c) (Davidson & Flood, 1994)

We might speculate, then, that the flow field is as shown in Figure 9.15. There is a relatively quiescent, stratified core, bounded by thermal wall jets, within which the temperature adjusts from the core distribution to the wall temperature. The rôle of the wall jets is to carry hot fluid away from the top surface and allow it to cool on the colder, curved boundary. If we now allow for a small inflow, u_0, at the top surface, then some additional (open) streamlines will start at the surface and leave through the cavity wall. Since these additional lines cannot cross the recirculating

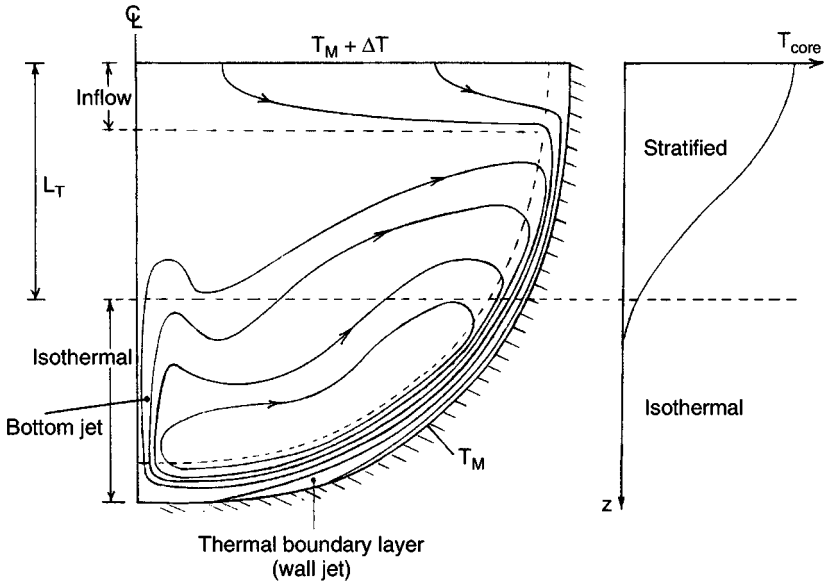

Figure 9.15 General structure of the flow field.

streamlines, they must be diverted into the wall jet and pass down behind the closed streamlines. Eventually, they will leave the flow field in (predominantly) the lower half of the cavity. We shall show later that the axial length-scale for the decay of core temperature, L_T, typically has a value of $\sim R/6$. (This follows from general scaling arguments.) Consequently, the stratified region occupies only the upper part of the pool. Below this, we have an isothermal melt, with $T = T_M$.

Let us now determine the scaling laws for L_T, u_c, u_b and δ. We have four equations to be satisfied. First (9.48) and (9.50) demand that, in the boundary layer,

$$u_b^2/L_T \sim g\beta\Delta T, \qquad u_b/L_T \sim \alpha/\delta^2 \tag{9.54, 9.55}$$

Next, (9.53) and continuity yield

$$u_c \sim \alpha/L_T, \qquad u_c R \sim u_b \delta \tag{9.56, 9.57}$$

If we introduce the dimensionless parameter

$$Gr = \frac{g\beta R^3 \Delta T}{\alpha^2}$$

then (9.54) to (9.57) give us the required scaling laws:

$$L_T \sim (Gr)^{-1/7} R, \qquad \frac{\delta}{R} \sim (Gr)^{-2/7} \tag{9.58, 9.59}$$

$$u_b \sim \frac{\alpha}{R}(Gr)^{3/7}, \qquad u_c \sim \frac{\alpha}{R}(Gr)^{1/7} \tag{9.60, 9.61}$$

In casting, typical parameter values are $Gr = 10^6$, $\alpha = 4 \times 10^{-5}\,\mathrm{m}^2/\mathrm{s}$ and $R = 0.3\,\mathrm{m}$, from which $L_T \sim 0.14R$, $\delta \sim 0.02R$, $u_c \sim 1\,\mathrm{mm/s}$ and $u_b \sim 50\,\mathrm{mm/s}$. The inlet velocity is typically of the order of $u_0 = 1\,\mathrm{mm/s}$, which is similar to u_c but much less than u_b. These scaling laws have been tested against experimental data and numerical simulations and found to be reasonably accurate. A typical numerical simulation, taken from Davidson & Flood (1994), is shown in Figure 9.16.

It is widely believed that this natural convection pattern is detrimental to the ingot structure, causing inhomogeneities in chemical composition. The argument is that small (snow-flake-like) crystals, which nucleate near the boundaries, become caught up in the wall jets and are swept down to the base of the pool. For thermodynamic reasons, the crystals which form near the top of the pool tend to be depleted in the alloying elements, and it is these crystals which get caught up in wall jets and end up at the centre of the ingot. Two radically different solutions to this problem have been proposed. One is magnetic stirring, which was discussed in the previous chapter, and the other is magnetic damping.

9.5.2 Magnetic damping in an aluminium ingot

It is evident that the driving force for natural convection is concentrated near the top of the pool and within the thermal boundary layer. Since the sides of the pool are approximately vertical at this point, it seems natural to use a (predominantly) horizontal magnetic field to suppress the motion. The required magnitude of the imposed field may be determined as follows. If the Lorentz force is to reduce the velocity significantly it must be as large as the buoyancy force, and so

$$u/\tau \sim g\beta\Delta T, \qquad \tau^{-1} = \sigma B^2/\rho$$

This implies that u_b is of the order of $u_b \sim (g\beta\Delta T)\tau$. If the damping is to be effective then u_b should be less than the estimate (9.60), and so we find that the minimum acceptable value of $|\mathbf{B}|$ is given by

$$\sigma B_{\min}^2 R^2/\rho\alpha \sim (Gr)^{4/7} \tag{9.62}$$

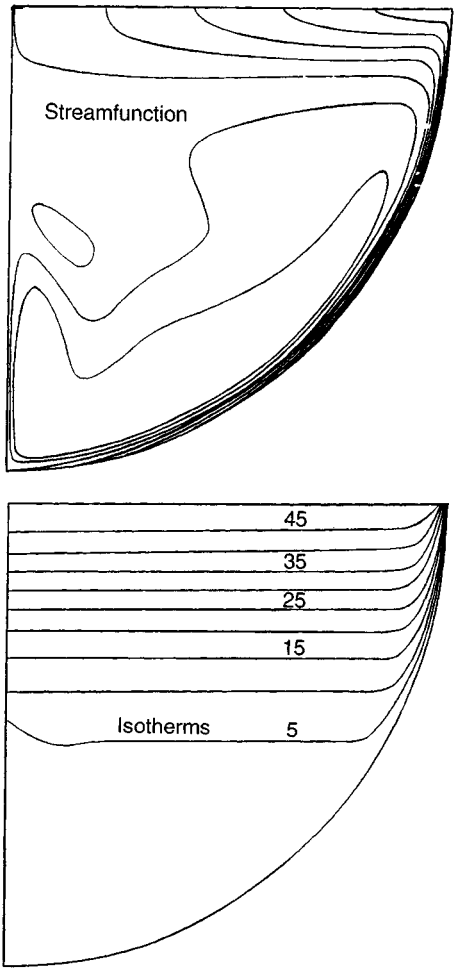

Figure 9.16 Computed isotherms and streamfunction for $\Delta T = 50°C$.

Examples

9.1 Consider the one-dimensional jet shown in Figure 9.3. Suppose that the jet is driven by buoyancy and that $N \gg 1$, $\alpha \to 0$. Show that, at large times,

$$u \sim g\beta\tau\Delta T(t/\tau)^{1/2} F\left(\frac{z}{(t/\tau)^{1/2}}, x\right)$$

where ΔT is a measure of the temperature difference driving the flow.

9.2 Consider the axisymmetric vortex discussed in Section 9.4.3. Show that the energies of the azimuthal and poloidal motions are governed by

$$\frac{dE_\theta}{dt} = -\int \frac{u_\theta^2}{r} u_r dV - \frac{1}{\tau}\int (\nabla\phi)^2 \frac{dV}{r^2}$$

$$\frac{dE_p}{dt} = +\int \frac{u_\theta^2}{r} u_r dV - \frac{1}{\tau}\int u_r^2 dV$$

Now show that these are compatible with the overall energy balance 9.4(a). When N is small, estimate the time taken for the structures shown in Figure 9.11 to emerge.

10

Axisymmetric Flows Driven by the Injection of Current

Matters of elegance should be left to the tailor and to the cobbler.

A. Einstein 1916

When an electric current is made to pass through a liquid-metal pool it causes the metal to pinch in on itself. That is to say, like-signed currents attract one another, and so each part of the pool is attracted to every other part. When the current is perfectly uniform, the only effect is to pressurise the liquid. However, often the current is non-uniform; for example, it may spread radially outwards from a small electrode placed at the surface of the pool. In such cases the radial pinch force will also be non-uniform, being largest at places where the current density is highest (near the electrode). The (irrotational) pressure force, $-\nabla p$, is then unable to balance the (rotational) Lorentz force. Motion results, with the fluid flowing inward in regions of high current density and returning through regions of small current.

Perhaps the first systematic experimental investigation of the 'pinch effect' in current-carrying melts was that of E F Northrup who, in 1907, injected current into pools of mercury held in a variety of different configurations. It should be noted, however, that industrial metallurgists have been routinely passing large currents through liquid metals since 1886, when Hall and Héroult first developed the aluminium reduction cell and von Siemens designed the first electric-arc furnace. One of the many descendants of the electric-arc furnace is vacuum-arc remelting (VAR).

10.1 The VAR Process and a Model Problem

10.1.1 The VAR process

There are occasions when an ingot cast by conventional means is of inadequate quality, either because of excessive porosity in the ingot or else because it contains unacceptably high levels of pollutants (oxides,

refractory material and so on). This is particularly the case in the casting of high-temperature melts, such as titanium or nickel-based alloys, which tend to react with (or erode) the refractory vessel in which they are melted. It also arises when the components fashioned from the ingot are expected to exhibit consistently high levels of strength and ductility. Here, aerospace applications come to mind. In such situations it is normal to improve the ingot quality by remelting it in a partial vacuum, burning off the impurities, and then slowly casting a new ingot. This is achieved by a process known as vacuum-arc remelting.

In effect, VAR resembles a giant version of electric welding (Figure 10.1). The initial ingot, which may be a metre in diameter and several metres long, is used as an electrode. A large current is passed down the ingot (electrode) and an arc is struck between the tip of the ingot and a cooled metal surface. The ingot then starts to melt, and droplets of molten metal fall through the plasma arc to form a pool on the cooled plate. As the electrode is slowly melted, so a new ingot forms beneath it. The entire process takes place in a partial vacuum. The metallurgical structure of the final ingot depends critically on the temperature distribution and fluid motion within the molten pool and this, in turn, depends on the gravitational and Lorentz forces acting on the melt. There is some incentive, therefore, to characterise the flow within the pool and to determine its dependence on such factors as ingot current.

In this regard a useful model problem is the following. Suppose we have a hemispherical pool of radius R. The boundaries of the pool are conducting, and a current, I, is introduced into the pool via an electrode

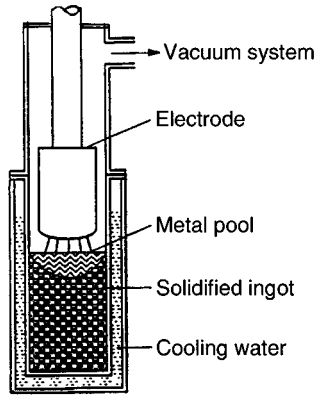

Figure 10.1 Vacuum-arc remelting.

of radius r_0, the current density being uniform in the electrode. We neglect buoyancy forces and try to determine the motion within the pool as a function of I, r_0 and R.

This model problem is relevant, not only to VAR, but also to electro-slag remelting of ingots and electric-arc welding. The flow pattern is as shown in Figure 10.2. Like-signed currents attract each other, and so the current passing through the pool causes the liquid to pinch in on itself. This radially inward force is greatest at the surface, where $|\mathbf{J}|$ is most intense, and weakest at the base of the pool where $|\mathbf{J}|$ is smallest. The net result is a flow which converges at the surface.

This seemingly simple problem has been the subject of a myriad of papers. Indeed, an entire book has been devoted to it (Bojarevics et al., 1989). Yet, arguably, we know less about this problem than about most of the other flows discussed in Part B of this book. One reason is that the apparently simple flow shown in Figure 10.2 turns out to be surprisingly complex. For example, it becomes unsteady (and eventually turbulent) at surprisingly low Reynolds numbers, around $\mathrm{Re} \sim 10$. It is also extremely sensitive to weak, stray magnetic fields, such as those associated with remote inductors or perhaps even the Earth's magnetic field. In particular, a stray magnetic field which is only 1% of the primary field (i.e. that field associated with the passage of the current through the pool) is enough to suppress completely the poloidal flow shown in Figure 10.2 and replace it by an intense swirling motion. It seems that, one way or another, the laminar flow shown in Figure 10.2 is somewhat ephemeral, evolving into something quite different at the slightest provocation. The word 'unstable' appears quite often in the literature.

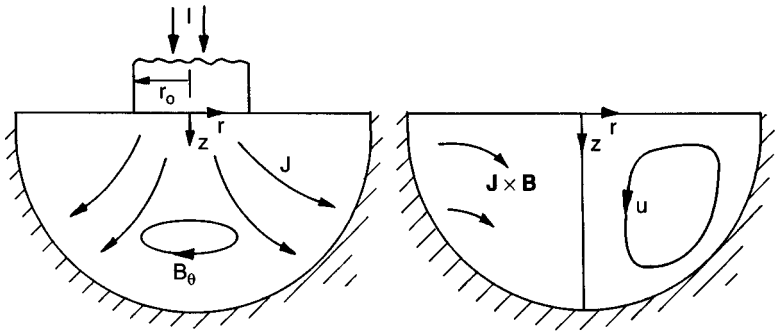

Figure 10.2 A model problem.

However, this is not the only reason that our attempts to understand this flow have been so unsuccessful. It turns out that the special case of a point electrode ($r_0 \to 0$) injecting current into a semi-infinite fluid ($R^{-1} = 0$) has an exact solution for laminar flow. Of course, exact solutions of the Navier–Stokes equations are extremely rare and beautiful things, and so it was natural for those first investigating this problem to focus on the semi-infinite-domain, point-electrode problem. In a sense this exercise has been successful: we now know a lot about this exact solution. Unfortunately, though, it turns out that the point-electrode problem tells us very little about the flow shown in Figure 10.2. That is to say, the special case $r_0 \to 0$, $R^{-1} = 0$ is a singular one, whose characteristics are often quite misleading in the context of real, confined flows. Yet a tradition grew up where a detailed, elegant analysis of some feature of the exact solution was performed, and then inferences were made about real, confined flows such as those observed in the laboratory. Unfortunately, when the experimental data were examined, the 'theory' was often found to be wanting. In short, we had been solving the wrong problem. (Perhaps we should have heeded Einstein's warning!)

There are a number of questions which naturally arise concerning the model problem shown in Figure 10.2.

(i) What is the direction and magnitude of the Lorentz force acting on the pool?

(ii) Why is there such a large difference in behaviour between real, confined flows and the point-electrode, semi-infinite-domain problem? Is there some fundamental physical difference between the two?

(iii) What does the exact solution of the (laminar) point-electrode problem tell us and can we transcribe *any* of its conclusions to real, confined flows?

(iv) Why do real, confined flows become unstable (and then turbulent) at such low Reynolds numbers?

(v) Given that any industrial flows will be turbulent, how does $\mathbf{u}$ scale with I, R and r_0 in a turbulent flow?

(vi) How does buoyancy influence this flow (the surface of the pool is assumed to be hotter than the sides)?

(vii) Why is the flow so sensitive to weak, stray magnetic fields, and does the laminar, point-electrode problem (about which we know so much) give us any hint as to the nature of this sensitivity?

(viii) Can we construct a quantitative theory which predicts the sensitivity of this flow to stray magnetic fields? Will this theory predict the unexpected emergence of swirl?

With the impatient reader in mind, these questions are listed in Table 10.1 along with some hints as to the answers. (Note that we use cylindrical polar coordinates (r, θ, z) throughout this chapter, and that the term 'azimuthal' refers to the θ components of a vector field, while 'poloidal' refers to the r–z components.)

Much of the discussion which follows (in Sections 2 to 7) is based on a variety of energy arguments. It seems appropriate to review first the key energy equations which are relevant to our model problem.

10.1.2 Integral constraints on the flow

The Lorentz force, $\mathbf{J} \times \mathbf{B}$, does work on the fluid. This causes the kinetic energy of the flow to rise until such time as the viscous dissipation matches the rate of working of $\mathbf{J} \times \mathbf{B}$. If, for a given current, we can characterise the relationship between $(\mathbf{J} \times \mathbf{B}) \cdot \mathbf{u}$ and the rate of dissipation of energy, then we should be able to estimate the magnitude of $|\mathbf{u}|$. Thus the key to estimating $|\mathbf{u}|$ lies in determining the mechanism by which the fluid dissipates the energy injected into the flow. For example, is the dissipation confined to boundary layers or are internal shear layers set up, and what happens to those streamlines which manage to avoid all such dissipative layers? There are two energy equations of importance here; both rest on the steady version of the Navier–Stokes equation:

$$0 = \mathbf{u} \times \boldsymbol{\omega} - \nabla\left(p/\rho + u^2/2\right) + \nu \nabla^2 \mathbf{u} + \mathbf{F} \tag{10.1}$$

(Here $\mathbf{F}$ is the Lorentz force per unit mass.) The first equation comes from integrating (10.1) around a closed streamline, which yields

$$\oint \mathbf{F} \cdot d\mathbf{l} + \nu \oint \nabla^2 \mathbf{u} \cdot d\mathbf{l} = 0 \tag{10.2}$$

This represents the balance between the work done by the Lorentz and viscous forces acting on a fluid particle as it passes once around a closed streamline. The second energy equation comes from taking the product of (10.1) with $\mathbf{u}$ and then integrating the result over the entire domain. Noting that terms of the form $\mathbf{u} \cdot \nabla(\sim) = \nabla \cdot (\sim \mathbf{u})$ integrate to zero and that $\left(\nabla^2 \mathbf{u}\right) \cdot \mathbf{u} = \nabla \cdot (\mathbf{u} \times \boldsymbol{\omega}) - \boldsymbol{\omega}^2$, we find

$$\int \mathbf{F} \cdot \mathbf{u} dV = \nu \int \boldsymbol{\omega}^2 dV \tag{10.3}$$

Table 10.1. *Questions concerning the model problem shown in Figure 10.2*

	Question	Answer	Consult
(i)	What is the magnitude and direction of the Lorentz force?	Radial, of magnitude $-B_\theta^2/(\rho\mu r)$	10.2
(ii)	Why are confined and unconfined flows so different?	Two reasons. (a) Unconfined flows are free from intense, boundary-layer-dissipation. Confined flows are dominated by the balance between the work down by $\mathbf{J} \times \mathbf{B}$ and boundary-layer dissipation (b) The streamlines in unconfined flows do not close on themselves, so that we are free to 'impose' conditions in the far field	10.3.1
(iii)	Does the point-electrode, semi-infinite-domain problem tell us anything useful?	Yes, but only about the point-electrode, semi-infinite-domain problem	10.3.2
(iv)	Why do confined flows become unstable at such low values of Reynolds number?	We do not know, but it appears that the boundary layer becomes unstable at relatively low values of Re	10.3.3
(v)	How does $\mathbf{u}$ scale in a turbulent flow?	$\lvert\mathbf{u}\rvert \sim \dfrac{I(\mu/\rho)^{1/2}}{2\pi R}$	10.3.3
(vi)	What is the influence of buoyancy?	It tends to drive motion in the opposite direction	10.4
(vii)	Why is the flow so sensitive to weak, stray magnetic fields?	Stray fields produce an azimuthal torque which tends to induce swirl. It is much easier to spin a fluid in the azimuthal direction than generate the poloidal motion shown in Figure 10.2	10.5 10.7.1
(viii)	Does the point electrode problem help explain this sensitivity to stray fields?	Probably not	10.6
(ix)	Can we construct a quantitative theory which predicts the unexpected emergence of swirl?	Yes. This relies on establishing a balance between the centripetal acceleration and the poloidal Lorentz force	10.7.2, 10.7.3

This represents a global balance between the rate of working of the Lorentz force and the viscous dissipation. Either (10.2) or (10.3) may be used to estimate the magnitude of **u** provided, of course, that **F** is known. Actually, it is not difficult to show that (10.3) is equivalent to evaluating (10.2) for each streamline in the flow and then adding together all such integrals (see Example 1 at the end of the chapter).

In the remainder of this chapter we shall see how (10.2) and (10.3) may be used to determine the flow in our model problem. The discussion is arranged as follows. In Section 2 we determine the Lorentz force associated with the current. Next, in Section 3, we discuss the structure of, and scaling laws for, this flow. Here particular attention is given to the special (if somewhat misleading) case in which $r_0 \to 0$ and R recedes to infinity. As explained above, the reason for the extended discussion for this (singular) case is that, rather surprisingly, it possesses an exact, self-similar solution. Traditionally, a great deal of emphasis has been placed on this exact solution.

Next, in Section 4, we note that in both VAR and arc-welding the upper surface of the pool is hotter than its sides. We therefore consider the influence of buoyancy on the Lorentz-driven flow. Buoyancy forces tend to drive a flow which diverges at the surface of the pool; precisely opposite to the Lorentz-driven flow. Thus there is a direct competition between the buoyancy and Lorentz forces. We determine the conditions under which buoyancy prevails.

We conclude, in Sections 5 to 7, with a discussion of an old, but still controversial, subject. We shall examine the influence of weak, stray magnetic fields on the fluid motion. As mentioned above, these stray fields have a disproportionate influence on the pool dynamics, suppressing the poloidal flow and driving an intense swirling motion. There has been a great deal written about this problem. In Section 5 we review the experimental evidence for the extraordinary sensitivity of the confined, current-carrying fluids to a weak, stray magnetic field. Next, in Section 6, we discuss the traditional, if flawed, explanation of the phenomenon. We conclude, in Section 7, with a modern interpretation.

10.2 The Work Done by the Lorentz Force

If we are to use (10.2) or (10.3) to estimate the magnitude of **u** then the first step is to evaluate the Lorentz force, **F**. Let us assume that the entire geometry is axisymmetric. We shall use cylindrical polar coordinates (r,

θ, z) with the origin at the pool's surface, as shown in Figure 10.3. Evidently, the current is poloidal $(J_r, 0, J_z)$, and this gives rise to an azimuthal magnetic field, $(0, B_\theta, 0)$ (see Figure 10.2). The magnetic field and current density are related via Ampère's circuital law, according to which

$$2\pi r B_\theta = \mu \int_0^r (2\pi r J_z) dr \tag{10.4}$$

An expression for the corresponding Lorentz force per unit mass is given in Chapter 5, Section 6.1:

$$\mathbf{F} = \mathbf{J} \times \mathbf{B}/\rho = -\frac{B_\theta^2}{\rho \mu r} \hat{\mathbf{e}}_r \tag{10.5}$$

This drives a flow which converges at the surface, where B_θ is largest, and diverges near the base of the pool (Figure 10.2).

There are certain cases, such as electric-arc welding, where $r_0 \ll R$. Here we might try to model the electrode as a point source of current. In these situations it is useful to introduce the additional (spherical polar) coordinates, s and ϕ, defined by $s^2 = r^2 + z^2$ and $\cos\phi = r/s$. It is not difficult to show that, for a point source of current,

$$\mathbf{J} = \frac{I}{2\pi s^2}(\cos\phi, 0, \sin\phi), \qquad \mathbf{F} = -\frac{\mu I^2}{4\pi^2 \rho r^3}(1 - \sin\phi)^2 \hat{\mathbf{e}}_r \tag{10.6, 10.7}$$

Let us now return to the more general case of finite r_0. Given the importance of the integral constraint (10.2), it seems appropriate to evaluate the work done by **F**. The simplest case to consider is a fluid particle which follows a streamline lying close to the boundary. Integrating **F** along the surface from point 'a' ($r = R, z = 0$) in Figure 10.3 to point 'b' ($r = 0, z = 0$) gives

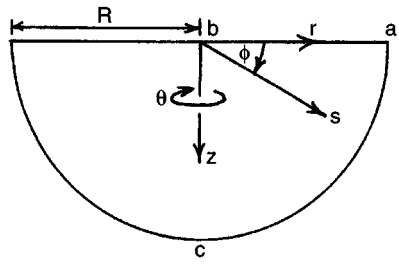

Figure 10.3 Coordinate system.

$$\int_a^b \mathbf{F} \cdot d\mathbf{l} = \frac{\mu I^2}{4\pi^2 \rho r_0^2}\left(1 - \frac{r_0^2}{2R^2}\right) \tag{10.8}$$

The integral of $\mathbf{F}$ along the symmetry axis is zero, since $B_\theta = 0$ on $r = 0$, while the integral along the curved boundary depends on the aspect ratio r_0/R. When $r_0 \ll R$, (10.7) yields

$$\int_c^a \mathbf{F} \cdot d\mathbf{l} = \frac{\mu I^2}{4\pi^2 \rho R^2}\left[\frac{1}{2} - \ln 2\right] \tag{10.9}$$

from which

$$\boxed{\oint \mathbf{F} \cdot d\mathbf{l} = \frac{\mu I^2}{4\pi^2 \rho r_0^2}\left[1 - \frac{r_0^2}{R^2}\ln 2\right]} \tag{10.10}$$

This represents the work done by $\mathbf{F}$ on a fluid particle as it completes one cycle in the r–z plane. It is the balance between this integral and the viscous dissipation which determines the magnitude of the induced velocity. It is interesting to note that $\oint \mathbf{F} \cdot d\mathbf{l}$ tends to infinity as $r_0 \to 0$. This, in turn, suggests that there is something singular about the point electrode problem. We shall return to this issue shortly.

10.3 Structure and Scaling of the Flow

10.3.1 Differences between confined and unconfined flows

Both electric welding and VAR are characterised by the facts that: (i) the electrode has a finite size; (ii) the Reynolds number is high and the flow turbulent; (iii) the presence of the boundary at $s = R$ controls the magnitude of $\mathbf{u}$ since most of the dissipation occurs in the boundary layers. Nevertheless, most studies of this problem have focused on laminar flow driven by a point electrode in a semi-infinite domain! The reason for this concentration on an idealised problem was the discovery by Shercliff (1970) and others that there exists an exact solution of the Navier–Stokes equation for the case of a point electrode on the surface of a semi-infinite domain. Unfortunately, as noted above, these point-electrode, semi-infinite-domain problems can be quite misleading in the context of real, confined flows. There are three key differences. First, the streamlines in the semi-infinite problem converge toward the axis but

do not close on themselves (Figure 10.4). They are therefore free from integral constraints of the form

$$\oint_C \mathbf{F} \cdot d\mathbf{l} + \nu \oint_C \nabla^2 \mathbf{u} \cdot d\mathbf{l} = 0 \tag{10.11}$$

where C is a closed streamline. Integrals such as (10.11) determine the magnitude of $\mathbf{u}$ in closed-streamline problems, yet are irrelevant in cases where the streamlines are open. Thus, for example, any difference between $\int \mathbf{F} \cdot d\mathbf{l}$ and $\nu \int \nabla^2 \mathbf{u} \cdot d\mathbf{l}$ in the semi-infinite problem simply appears as a difference in the energy of the incoming and outgoing fluid.

The second, related, difference lies in the fact that flows in confined domains are subject to (intense) dissipation associated with the boundary layer at $s = R$. This is significant since, as we have seen,

$$\int_V \mathbf{F} \cdot \mathbf{u} dV = \nu \int_V \omega^2 dV \tag{10.12}$$

That is to say, the global rate of working of $\mathbf{F}$ must be balanced by viscous dissipation. For confined domains the right-hand side of (10.12) is dominated by the boundary-layer dissipation and so we might expect the boundary layers to determine the magnitude of $\mathbf{u}$. However, there are no boundary layers in the infinite-domain problem, and so we might expect the characteristic velocity in confined and unconfined problems to be rather different.

The third difference is evident from (10.10). The point-electrode problem represents a singular (and somewhat artificial) problem in which the work done by $\mathbf{F}$ on the fluid becomes infinite:

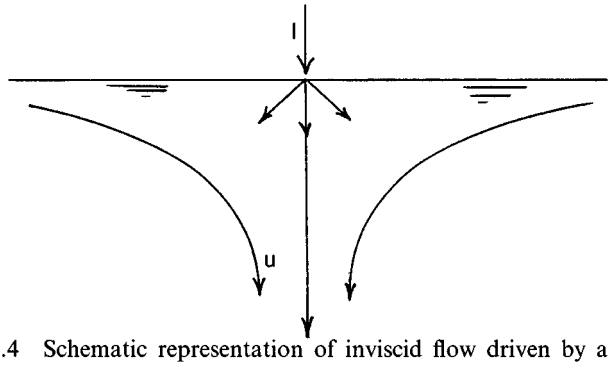

Figure 10.4 Schematic representation of inviscid flow driven by a point electrode.

$$\oint \mathbf{F} \cdot d\mathbf{l} = \frac{\mu I^2}{4\pi^2 \rho r_0^2} \to \infty$$

The implication is that, whenever ν is small, a fluid particle will acquire an infinite amount of kinetic energy as it passes by the electrode. This turns out to be the case, and it is the hallmark of these point-electrode, semi-infinite-domain problems that, as ν becomes small (Re becomes large), a singularity appears in the velocity field. Indeed, it is the combination of a self-similar solution (which makes the algebra clean) plus the intriguing appearance of a singularity in $\mathbf{u}$ which has made this point-electrode problem such a popular subject of study. It should be emphasised, however, that the appearance of a singularity in $\mathbf{u}$ is simply an artefact of the (unphysical) assumption that r_0 is vanishingly small.

All in all, it would seem that confined and unconfined flows represent quite different problems. Our primary concern here is in confined flows, such as those which occur in VAR or electric welding. Nevertheless, since the bulk of the literature addresses the semi-infinite-domain, point-electrode problem, it would seem prudent to review first the key features of such flows.

10.3.2 Shercliff's self-similar solution for unconfined flows

Let us consider a semi-infinite domain and look for a solution of (10.1) in which $\mathbf{F}$ is given by the point electrode distribution (10.7). It is convenient to introduce the Stokes streamfunction defined by

$$\mathbf{u} = \left(-\frac{1}{r}\frac{\partial \psi}{\partial z}, 0, \frac{1}{r}\frac{\partial \psi}{\partial r} \right) \tag{10.13}$$

and to take the curl of (10.1), converting it into a vorticity transport equation:

$$\mathbf{u} \cdot \nabla\left(\frac{\omega_\theta}{r}\right) = \frac{1}{r}\frac{\partial F}{\partial z} + \nu\left[\nabla^2\left(\frac{\omega_\theta}{r}\right) + \frac{2}{r}\frac{\partial}{\partial r}\left(\frac{\omega_\theta}{r}\right)\right] \tag{10.14}$$

We now look for self-similar solutions of (10.14) of the form

$$\psi = -sg(\eta), \qquad \eta = \sin\phi = z/s \tag{10.15}$$

Let us evaluate the various terms in (10.14). After a little algebra we find that

$$\mathbf{u} \cdot \nabla(\omega_\theta/r) = -(g^2)'''/(2s^5), \qquad \frac{1}{r}\frac{\partial F}{\partial z} = \frac{\mu I^2}{4\pi^2 \rho s^5}\left[(1+\eta)^2 \ln(1+\eta)\right]'''$$

$$\nabla^2\left(\frac{\omega_\theta}{r}\right) + \frac{2}{r}\frac{\partial}{\partial r}\left(\frac{\omega_\theta}{r}\right) = \frac{1}{s^5}\left[(1-\eta^2)g' + 2\eta g\right]''' \tag{10.16}$$

where the primes represent differentiation with respect to η. Substituting these into (10.14) and integrating three times we obtain the governing equation for g,

$$g^2 + 2K(1+\eta)^2 \ln(1+\eta) + 2\nu[(1-\eta^2)g' + 2\eta g] = a\eta^2 + b\eta + c \tag{10.17}$$

Here

$$\boxed{K = \frac{\mu I^2}{4\pi^2 \rho}} \tag{10.18}$$

and a, b and c are constants of integration. The simplest case to consider is the inviscid one. The constants a, b and c are then determined (in part) by the requirements that: (i) u_z is zero on $z = 0$; (ii) u_r is zero on $r = 0$. These conditions are equivalent to demanding that $g(0) = g(1) = 0$. Inspection of the inviscid equation yields $c = 0$, $a + b = 8K \ln 2$, from which

$$g^2 = K[a\eta(\eta - 1) + (8 \ln 2)\eta - 2(1+\eta)^2 \ln(1+\eta)] \tag{10.19}$$

This represents a flow of the type shown in Figure 10.4

Of course, the question now is: what determines a? Before answering this question it is instructive to return to (10.8), which gives the integral of $\mathbf{F}$ along the surface from $r = R$ to $r = 0$. If we let R recede to infinity then we obtain

$$\int_{r=\infty}^{r=0} \mathbf{F} \cdot d\mathbf{l} = \frac{\mu I^2}{4\pi^2 \rho r_0^2} = \frac{K}{r_0^2} \tag{10.20}$$

This represents the work done on a fluid particle as it moves along the surface under the influence of the Lorentz force. Recall that r_0 is the radius of the electrode. For a point source of current this integral diverges. Evidently, in the case of a point electrode, an infinite amount of work is done on each fluid particle as it moves radially inward along the surface. This suggests that something is going to go wrong with our inviscid solution, since we have no mechanism for dissipating the energy

created by **F**. In practice, this manifests itself in the following way. We could try to fix 'a' by demanding that u_r is finite on the surface (i.e. the incoming flow has finite energy). In such cases we find that u_z is infinite on the axis (i.e. the outgoing flow has infinite energy), which is an inevitable consequence of (10.20). The details are simple to check. The requirement that u_r is finite on $z = 0$ demands that, $a = 8 \ln 2 - 2$, from which

$$g^2 = K[(8 \ln 2 - 2)\eta^2 + 2\eta - 2(1 + \eta)^2 \ln(1 + \eta)] \tag{10.21}$$

Near the axis, however, this leads to an axial velocity of

$$u_z = -\frac{K^{1/2}(3 - 4 \ln 2)^{1/2}}{r}$$

Evidently, u_z diverges as r tends to zero.

If we now reinstate viscosity into our analysis, then it seems plausible that a regular solution of (10.18) will emerge, provided, of course, that the viscous stresses are large enough to combat the tendency for **F** to generate an infinite kinetic energy. In practice, this is exactly what occurs. When the (Reynolds-like) parameter $K^{1/2}/\nu$ is less than ~ 7, regular solutions of (10.18) exist without any singularity in **u**. For higher values of $K^{1/2}/\nu$, u_z becomes singular on the axis (Bojarevics et al., 1989). Of course, this does not imply that anything special, such as an instability, occurs at the critical value of $K^{1/2}/\nu$. It merely means that our attempt to find a self-similar solution of the form $\psi \sim sg(\eta)$ has failed. Notice that $K^{1/2}/\nu = 7$ corresponds to a relatively low current, of around 1 Amp, which is several orders of magnitude smaller than the currents used in industrial applications.

10.3.3 Confined flows

Let us now return to flows which are confined to the hemisphere $s < R$ and in which the electrode has a finite radius, r_0, of order R. In VAR and electric welding the Reynolds number is invariably high. It is natural, therefore, to ask two questions:

(i) what is the structure of the laminar flow when Re is large?
(ii) what is the magnitude of **u** when the flow becomes turbulent?

The answer to the first of these questions is surprising: it is likely that there are no stable, laminar flows at moderate-to-high values of Re! The reasons for this are discussed in detail in Kinnear & Davidson (1998) and

we will give here only a brief summary of the arguments. Suppose that we have a steady, laminar flow and that $r_0 \sim R$, then the key equation is (10.2)

$$\oint \mathbf{F} \cdot d\mathbf{l} + \nu \oint \nabla^2 \mathbf{u} \cdot d\mathbf{l} = 0 \tag{10.22}$$

This integral constraint is powerful. It must be satisfied by *every* closed streamline. When Re is of the order unity (or less) it tells us that $u \sim FR^2/\nu$, where F is a characteristic value of $|\mathbf{F}|$. Now suppose that Re is large so that boundary layers form on the wall $s = R$. Inside the boundary layer the viscous dissipation is intense, while outside it is small. The boundary thickness, δ, is determined by the force balance $(\mathbf{u} \cdot \nabla)\mathbf{u} \sim \nu \nabla^2 \mathbf{u}$, which gives $\delta \sim (Re)^{-1/2} R$. Thus our integral equation applied to a streamline lying close the boundary yields

$$FR \sim (\nu u R)/\delta^2 \sim u^2$$

For a streamline away from the boundary, however, $\nabla^2 \sim R^{-2}$, and so

$$FR \sim (\nu u R)/R^2 \sim \nu u/R$$

The implication is that the flow in the boundary layer scales as $u_b \sim (FR)^{1/2}$, while that in the core scales according to $u_c \sim FR^2/\nu$, which is much larger than u_b. However, this cannot be so, since the velocity scale in the boundary layer is set by the core velocity. Clearly, something has gone wrong!

The numerical experiments discussed in Kinnear & Davidson (1998) suggest that nature resolves this dilemma in an unexpected way. At surprisingly low Reynolds numbers, of the order of 10, the flow becomes unstable and starts to oscillate. The integral equation (10.22) is then irrelevant. The oscillation consists of a periodic 'bursting' motion in the boundary layer which gives rise to a continual exchange of fluid between the dissipative boundary layer and the less dissipative core. If we now increase Re a little further, the flow becomes turbulent, which brings us to our second question.

We wish to determine how $|\mathbf{u}|$ scales with I and R in a turbulent flow. Let us apply (10.22) to the time-averaged streamlines of a turbulent flow, with Reynolds stresses replacing the laminar shear stress. Noting that, for a streamline close to the boundary, (10.8) yields

$$\oint \mathbf{F} \cdot d\mathbf{l} \sim K/2R^2$$

(assuming $r_0 \sim R$), we obtain

$$\frac{K}{2R^2} \sim \frac{\pi R}{2}\frac{\tau_w}{\rho\delta_w} \tag{10.23a}$$

Here τ_w and δ_w are the wall shear stress and the characteristic length scale for gradients in τ near the wall. Now $\tau_w/\rho \sim (u')^2$ and so (10.23a) can be used to estimate the turbulence level in the pool:

$$\frac{K}{2R^2} \sim \frac{\pi R}{2}\frac{(u')^2}{\delta_w} \tag{10.23b}$$

We now take $u' \sim u/3.5$ and $\delta_w \sim R/10$, where u is a typical mean velocity. (These estimates are typical of a confined, turbulent flow, as observed in induction furnaces.) In this case (10.23b) yields

$$\boxed{u \sim 0.6\frac{K^{1/2}}{R} \sim 0.6\frac{(\mu/\rho)^{1/2}I}{2\pi R}} \tag{10.24}$$

Velocities compatible with (10.24) are indeed observed.

10.4 The Influence of Buoyancy

So far we have neglected the buoyancy forces acting on the pool. In VAR these can be significant. Indeed, in some cases, they are the dominant forces acting on the liquid. It is useful to start by considering two extremes: one in which buoyancy may be neglected by comparison with $\mathbf{J} \times \mathbf{B}$, and the other in which buoyancy greatly outweighs the Lorentz force. These two extremes are shown in Figure 10.5. Notice that the Lorentz and gravitational forces tend to drive motion in opposite directions.

In Chapter 9, Section 5 we discussed natural convection in an axisymmetric cavity driven by a difference in temperature, ΔT, between the surface and the boundary. We showed that the maximum velocity in the pool is of the order of

$$\hat{u} \sim \frac{\alpha}{R}\left(\frac{g\beta R^3 \Delta T}{\alpha^2}\right)^{3/7} = \frac{\alpha}{R}(Gr)^{3/7} \tag{10.25}$$

where α is the thermal diffusivity and β the expansion coefficient. Actually, it turns out that (Davidson & Flood, 1994),

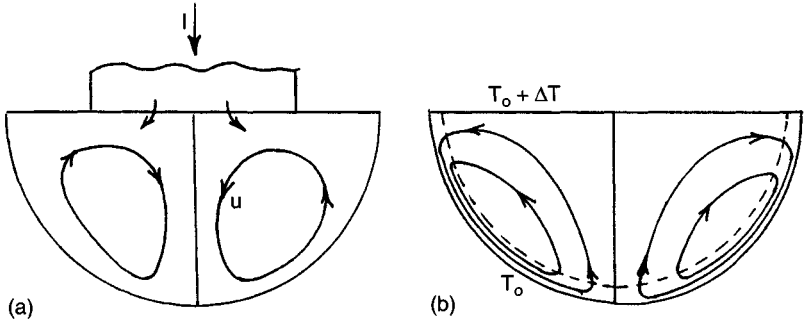

Figure 10.5 Two extremes in vacuum-arc remelting: (a) buoyancy forces are neglected; (b) the Lorentz forces are neglected.

$$\hat{u} = 1.3\frac{\alpha}{R}\left(\frac{g\beta R^3 \Delta T}{\alpha^2}\right)^{3/7} = 1.3\frac{\alpha}{R}(Gr)^{3/7} \tag{10.26}$$

Compare this with the other extreme where buoyancy is neglected and the flow is driven by $\mathbf{J} \times \mathbf{B}$:

$$\hat{u} \sim 0.6\frac{(\mu/\rho)^{1/2} I}{2\pi R} = 0.6\frac{K^{1/2}}{R} \tag{10.27}$$

In the case where the gravitational forces are dominant the fluid diverges at the surface and falls at the outer boundary. When the Lorentz forces dominate we have the opposite pattern, with the fluid converging at the surface. We might estimate the point of transition between these two flows by equating (10.26) and (10.27):

$$(Gr)^{3/7} \sim \frac{K^{1/2}}{\alpha} \tag{10.28}$$

Thus, the transition from buoyancy to Lorentz-driven flow should occur when the dimensionless parameter

$$\chi = K^{1/2}(Gr)^{-3/7}/\alpha \tag{10.29}$$

exceeds a number of order unity. In practice, it is found that the motion resembles a classical buoyancy-driven flow (of the type discussed in Chapter 9, Section 5.1) when χ is less than ~ 0.4. In such cases the Lorentz forces may be neglected when calculating **u**. Conversely, when χ exceeds ~ 1.4 the buoyancy forces are unimportant. For intermediate values, $0.4 < \chi < 1.4$, the flow may have a complex, multi-cellular structure. This is illustrated in Figure I.6(b) (see introduction to Part B), where

the three figures correspond to $\chi = 0.5$, 1.2, 1.5. Apparently, modest changes in current can transform the motion from a buoyancy-dominated flow to a Lorentz force-dominated one. This change in flow regime is accompanied by a dramatic change in temperature distribution and of ingot structure. Interestingly, many commercial VAR units operate at just the verge of this transition.

10.5 Stability of the Flow and the Apparent Growth of Swirl

There are several industrial processes where current is injected into a liquid-metal pool, via its surface, but where the pool is also subject to a weak, stray magnetic field, perhaps associated with remote inductors. In such cases, the weak, stray magnetic field can have an astonishing influence on the motion in the pool, often to the detriment of the process. There is some incentive, therefore, to understand why stray magnetic fields have such a disproportionate influence on the pool motion. It is this question which occupies the remainder of this chapter.

10.5.1 An extraordinary experiment

Bojarevics et al. (1989) reported an intriguing experiment which exhibits a curious phenomenon, often called 'spontaneous swirl'. In this experiment, current is passed radially downward through an axisymmetric pool of liquid metal, as indicated in Figure 10.6. As we have seen, the interaction of the current density, $\mathbf{J}$, with its associated magnetic field, B_θ gives rise to a Lorentz force, $\mathbf{F} = \mathbf{J} \times \mathbf{B}/\rho$, which is poloidal. Of course, the resulting motion is also poloidal; at least this is the case at low levels

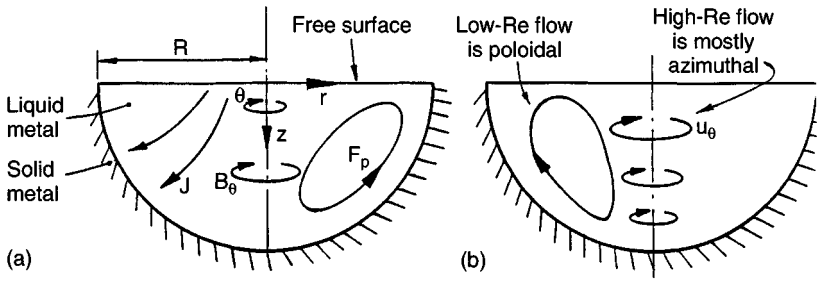

Figure 10.6 Experiment of Bojarevics et al. (a) Current flows down through the pool producing a poloidal force $\mathbf{F}_p = \mathbf{J}_p \times \mathbf{B}_\theta$. (b) At low levels of current the flow is poloidal, while a higher level of current initiates an intense swirling motion.

of forcing. At higher levels of current, though, something rather surprising occurs. The pool is seen to rotate, and this rotation is much more vigorous than the poloidal motion.

The observed rotation must, in some sense, result from a lack of symmetry in **J** or **B**. That is, a finite azimuthal force, F_θ, is required to maintain the swirl and in particular to overcome the frictional torque exerted on the pool by the boundaries. This additional force is thought to arise from the interaction of **J** with a weak, stray magnetic field. (For example, a vertical field B_z gives rise to an azimuthal force $-J_r B_z/\rho$.) Nevertheless, it is surprising that a force composed of a large poloidal component plus a weaker azimuthal contribution can give rise to a flow dominated by swirl, i.e. $u_\theta \gg u_r, u_z$. In the experiment the stray field arises in part from the Earth's magnetic field (Bojarevics et al., 1989). At the lower levels of current used ($\sim$ 15 Amps) the average magnetic field induced by the current on the pool surface is $\sim$ 0.6 Gauss, which is comparable with the Earth's magnetic field. However, at the highest current levels ($\sim$ 1200 Amps) the average surface value of B_θ is around 42 Gauss, which is a factor of $\sim$ 100 greater than the Earth's magnetic field. The key question, therefore, is why do low levels of azimuthal forcing give rise to disproportionately high levels of swirl?

Precisely the same phenomenon is seen at a larger scale in industrial processes such as vacuum-arc remelting of ingots. Here the stray magnetic field arises from inductors which carry current to and from the apparatus. Unless great effort is made to minimize the stray magnetic fields, an intense swirling motion is generated which can adversely affect the final product.

In all of these processes the Reynolds number, Re, is high, perhaps $300 \rightarrow 10^4$ in Bojarevic's experiment, and around 10^5 in industrial applications. It is almost certain, therefore, that these flows are turbulent. Moreover, the phenomenon seems to be particular to high Reynolds numbers, in the sense that there is a value of Re below which disproportionately high levels of swirl are not observed (Bojarevics et al., 1989). There is, however, a second threshold. That is, as we shall see, u_θ dominates the poloidal motion, $\mathbf{u}_p$, only when F_θ exceeds $\sim 0.01|\mathbf{F}_p|$. (We use subscript p to indicate poloidal components of **u** or **F**.) Below this threshold, the poloidal motion remains dominant, no matter what the value of Re. In particular, if $F_\theta \rightarrow 0$ then there is no swirling motion at all.

Let us summarise the experimental evidence. The term 'spontaneous swirl' is commonly used to describe high-Re flows in which the forcing

has both azimuthal and poloidal components, $\mathbf{F} = \mathbf{F}_\theta + \mathbf{F}_p$, but where the swirl dominates the motion despite the relative weakness of $\mathbf{F}_\theta$. That is,

$$u_\theta \gg |\mathbf{u}_p|, \qquad F_\theta \ll |\mathbf{F}_p|, \qquad (\mathrm{Re} \gg 1) \tag{10.30}$$

Note that it is not the appearance of abnormally high values of u_θ which typifies the experiment. Rather, it is the high value of the ratio $u_\theta/|\mathbf{u}_p|$ which is unexpected. This distinction may seem trivial, but it turns out to be important. Traditionally, this phenomenon was regarded as an instability, with the sudden appearance of swirl marking some instability threshold, rather like the sudden eruption of Taylor vortices in unstable Couette flow. Recently, however, it has been shown that this view is incorrect. We shall see that the magnitude of u_θ is simply governed by the (prescribed) magnitude of F_θ, and that there is nothing mysterious about the level of swirl. In fact, it is an unexpected suppression of $|\mathbf{u}_p|$ rather than a growth in u_θ, which typifies the observations.

10.5.2 There is no spontaneous growth of swirl!

We shall see that flows characterised by (10.30) do indeed exist, but that the phrase 'spontaneous swirl' is somewhat of a misnomer. Such flows would be better characterized by the term *poloidal suppression*. That is, the mystery is not that u_θ is unexpectedly large, but that, in the presence of swirl, $|\mathbf{u}_p|$ is disproportionately small. In fact, the magnitude of u_θ can always be estimated from the global torque balance,

$$\rho \int rF_\theta dV = \oint 2\pi r^2 \tau_\theta dl \tag{10.31}$$

Here l is a curvilinear coordinate measured along the pool boundary and τ_θ is the azimuthal surface shear stress. In a turbulent flow $\tau_\theta = c_f(\frac{1}{2}\rho u_\theta^2)$, where the skin friction coefficient c_f is, perhaps, of the order 10^{-2} (Davidson, Short and Kinnear, 1995). If R is a typical pool radius, this yields the estimate

$$u_\theta \sim (RF_\theta/c_f)^{1/2} \sim 10(RF_\theta)^{1/2} \tag{10.32}$$

Similar estimates may be made for laminar flow, but the details are unimportant. The key point is that u_θ is fixed in magnitude by F_θ.

We shall see that flows of type (10.30) arise from the action of the centrifugal force. That is, there are two driving forces for poloidal motion, the poloidal Lorentz force, $\mathbf{F}_p$, and the centrifugal force $-(u_\theta^2/r)\hat{\mathbf{e}}_r$, and it turns out that these conspire to eliminate each other.

Specifically, provided $\mathrm{Re} \gg 1$ and $F_\theta/|\mathbf{F}_p| >\sim 0.01$, the angular momentum of the fluid always distributes itself in such a way that these two forces almost exactly cancel (to within the gradient of a scalar), and that consequently, the poloidal motion is extremely weak. It is this balance between $\mathbf{F}_p$ and u_θ^2/r which underpins the experimental observations.

10.6 Flaws in the Traditional Explanation for the Emergence of Swirl

Traditionally, great significance has been attached to the fact that there appears to be a threshold value of Re above which swirl is dominant. This has led some researchers to conclude that the underlying poloidal motion is unstable and that the appearance of swirl is simply a manifestation of this instability. Consequently, it has been popular to study the breakdown of the self-similar poloidal flow associated with the injection of current from a point source located on the surface of a semi-infinite domain. As we have seen, these flows are characterised by the fact that the self-similar solution breaks down at a low value of Re. However, it turns out that a self-similar solution may be re-established above the critical value of Re if (somehow) just the right amount of angular momentum is injected into the flow at infinity. One of the deductions of this type of analysis is that flows which converge at the surface are potentially unstable, whereas those which diverge are stable. (Self-similar diverging flows may be realized using a slightly more complex, but still singular, arrangement of current injection.)

Perhaps the most thorough study of this type is that of Shtern & Barrero (1995). Like many before, they examined the breakdown of the self-similar flow, attributed this breakdown to an instability, and then suggested that these stability characteristics extend to confined domains, thus explaining the experimental observations. However, such a model problem differs from confined flows in two crucial respects. First, there is no outer frictional boundary and so this model problem is free from the integral constraint (10.31). That is, no external torque is required to maintain the swirl. Second, the streamlines in the self-similar solution do not close, but rather converge radially, as shown in Figure 10.7.

Now it happens that at $\mathrm{Re} \sim 7$ the similarity solution breaks down in the sense that the velocity on the axis becomes infinite (see Section 8.3.2). However, if just the right amount of swirl is introduced into the far field then, due to the radially inward convection of angular momentum, the singularity on the axis is alleviated. Thus, in semi-infinite domains there

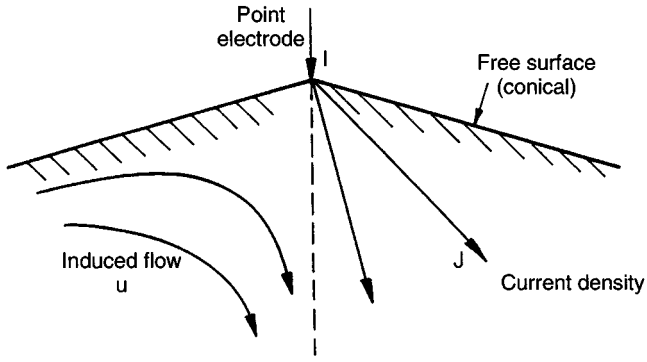

Figure 10.7 Geometry analysed by Shtern & Barrero.

exists the possibility of a bifurcation from a non-swirling to a swirling flow, provided, of course, that (somehow) nature provides just the right amount of angular momentum in the far field. This, according to traditional argument, is the origin of the experimental observations.

However, there are several fundamental objections to making the jump from infinite to confined flows. The first point to note is that the appearance of a singularity in the self-similar solution is simply an artefact of the (idealised) assumption of a point source of current (see (10.20)). Second, flow in a hemisphere bears little resemblance to the self-similar flow in an infinite domain. If R is the pool radius and r_0 the electrode radius, then a self-similar solution may be justified only in the small region $r_0 \ll (r^2 + z^2)^{1/2} \ll R$. In the experiments of Bojarevics et al. no such region exists ($R/r_0 \sim 45$). Third, the evidence for spontaneous swirl (poloidal suppression) is not restricted to point sources of current, but rather exists for many different distributions of current within the pool. An explanation of this behaviour which rests on the breakdown of a very particular class of motion (the self-similar flow) cannot explain the widespread occurrence of this phenomenon. Fourth, the infinite domain model relies on angular momentum being injected into the fluid in the far field. In confined domains, where does this angular momentum come from? If swirl exists in confined flows it must be maintained by an external torque, and the magnitude of this torque fixes the magnitude of the swirl. There can be no sudden 'eruption' of swirl due to an increase in Re. Fifth, according to the semi-infinite domain, point-electrode model, the sudden appearance of swirl occurs only if the flow converges at the surface. In practice, however,

this is not the case. As we shall see, the dominance of swirl ($u_\theta \gg |\mathbf{u}_p|$) occurs just as readily if the flow diverges at the surface. Clearly, we must seek an alternative explanation of the phenomenon.

10.7 The Rôle of Ekman Pumping in Establishing the Dominance of Swirl

10.7.1 A glimpse at the mechanisms

As a prelude to our detailed analysis we provide here a qualitative explanation of the phenomenon. The key point is this: it turns out to be easier to generate swirl in a hemispherical pool than poloidal motion. Suppose, for example, that we apply a force F_θ and measure the resulting swirl. We then remove F_θ and apply a force $\mathbf{F}_p$, again measuring the resulting motion. Then we would find that $u_\theta/F_\theta \gg |\mathbf{u}_p|/|\mathbf{F}_p|$. Thus small azimuthal forces, which result from the stray magnetic field, can give rise to a relatively large swirling motion. However, this is not the end of the story. This swirl, when large enough, arranges itself such that the centripetal acceleration, u_θ^2/r, counterbalances the poloidal Lorentz force (to within the gradient of a scalar). The poloidal flow then virtually disappears.

When we work through the details, it turns out that *Ekman pumping*, which played such an important rôle in Chapter 8, once again rears its head. You will recall that Ekman pumping is an inevitable by-product of confined swirl. Perhaps it is worth digressing for a moment to describe its main features. It is most simply understood in those cases where the Lorentz force is purely azimuthal ($\mathbf{F}_p = 0$), and so we now consider this special case.

Suppose that $\mathbf{F} = (0, F_\theta, 0)$ and the dominant motion is u_θ. Ekman pumping takes the form of a wall jet, as shown on the right of Figure 10.8. That is to say, the swirl induces a secondary poloidal motion consisting of a high-speed wall jet (Ekman jet) which runs downward within the boundary layer (the Ekman layer) and recirculates back up through the (almost) inviscid core flow. The driving force for the wall jet is a radial pressure gradient which is established in the core of the flow in order to maintain the centripetal acceleration of the swirling fluid. (This radial pressure gradient is unbalanced in the boundary layer where u_θ^2/r falls to zero.) It is important to note that Ekman pumping is not an incidental feature of this flow, but rather controls the magnitude of the swirl (see Chapter 8, Section 3). That is, in the steady state, the rate of generation of

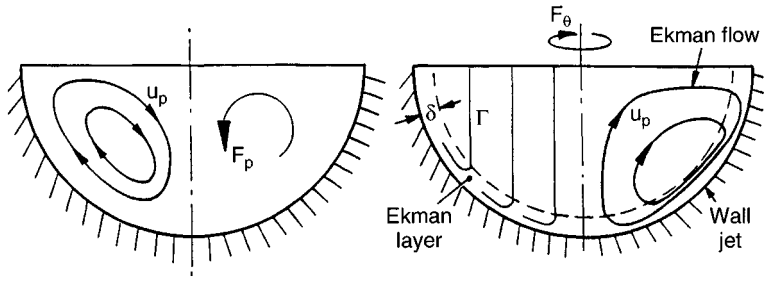

Figure 10.8 Flows driven by poloidal and azimuthal Lorentz forces. (a) Poloidal flow driven by a poloidal force. (b) Angular momentum contours and secondary Ekman flow induced by azimuthal force.

angular momentum and energy by F_θ must be matched by frictional dissipation, and it is this balance between the generation and dissipation of energy which dictates the steady state value of u_θ. However, the dissipation of energy is controlled by the Ekman pumping. It ensures that *all* the fluid particles are periodically flushed through thin, dissipative boundary layers, and this is the mechanism by which (10.2) is satisfied and a steady state is achieved.

We now return to the case in hand, where the dominant Lorentz force is poloidal rather than azimuthal. Suppose we have a pool of liquid metal into which we inject current (Figure 10.6). The current may be injected through a small region near the axis, or else distributed across the top of the pool. It does not matter. The current density in the metal is poloidal and induces an azimuthal magnetic field, $\mathbf{B}_\theta$. Suppose that, in addition, we have a weak, stray magnetic field, B_z. Then $\mathbf{F}$ comprises a strong poloidal component, $\mathbf{J} \times \mathbf{B}_\theta/\rho$, plus a weaker azimuthal contribution $\mathbf{J} \times \mathbf{B}_z/\rho$. Now suppose that, at least initially, B_z is so small that the induced swirl is much weaker than the primary poloidal motion. The distribution of $\mathbf{u}_p$ is then uniquely determined by the poloidal force (u_θ^2/r is negligible). Now consider the swirl. The governing equation for the angular momentum, $\Gamma = ru_\theta$, is

$$\frac{D\Gamma}{Dt} = \frac{\partial \Gamma}{\partial t} + \mathbf{u}_p \cdot \nabla \Gamma = rF_\theta + \nu_t \nabla \cdot \left[r^2 \nabla (\Gamma/r^2)\right] \tag{10.33}$$

Here the subscript on ν_t indicates that we have in mind a turbulent flow which we model rather crudely using a turbulent eddy viscosity. Let the pool be a hemisphere of radius R (the precise shape is not too important), and define an effective Reynolds number by $\mathrm{Re}_t = |\mathbf{u}_p|_{\max} R/\nu_t$. When Re_t

is large (typically it has a value of ~ 100), the shear stresses are dominant only in the boundary layers. Outside these regions (10.33) simplifies to

$$\frac{D\Gamma}{Dt} \approx rF_\theta + 0(Re_t^{-1}) \tag{10.34}$$

Evidently, angular momentum is generated in each fluid particle as a result of the azimuthal force and, provided boundary layers are avoided, this growth in Γ is constrained only by the relatively weak shear stresses in the core. Consequently, large values of swirl can build up, even though F_θ is small. From (10.33) we can estimate u_θ by equating the two terms on the right:

$$u_\theta/u_p \sim (F_\theta R/u_p^2)Re_t \tag{10.35}$$

Now suppose that we increase F_θ with $\mathbf{F}_p$ fixed, up to the point where u_θ and $\mathbf{u}_p$ are of similar magnitudes. (In practice we could do this by increasing the stray field B_z.) We have seen that, for small u_θ, $\mathbf{u}_p$ scales roughly as $|\mathbf{u}_p| \sim (|\mathbf{F}_p|R)^{1/2}$ (see equation (10.24), and so $u_\theta \sim \mathbf{u}_p$ when $F_\theta \sim Re_t^{-1}|\mathbf{F}_p| \sim 0.01|\mathbf{F}_p|$. Thus a small but finite azimuthal force can give rise to a significant (i.e. large) swirling motion. Once u_θ reaches a value of $\sim \mathbf{u}_p$, Γ ceases to play a passive rôle. It can react back on the poloidal motion through the centrifugal force $(-u_\theta^2/r)\hat{\mathbf{e}}_r$. There now exists an intriguing possibility. Suppose that Γ is distributed in such a way that $(-u_\theta^2/r)\hat{\mathbf{e}}_r$ balances $\mathbf{F}_p$ to within the gradient of a scalar:

$$(-u_\theta^2/r)\hat{\mathbf{e}}_r = \mathbf{F}_p + \nabla\phi + 0(Re_t^{-1}) \tag{10.36}$$

The driving force for poloidal motion then disappears (ϕ is absorbed into the pressure) and we are left with a swirling motion plus its associated (weak) Ekman pumping. If this were to occur, then the energy of the poloidal flow, and hence of the flow as a whole, should collapse as F_θ approaches a value of $\sim 0.01|\mathbf{F}_p|$. We shall see that this is precisely what happens, the resulting core flow being governed by

$$\mathbf{u}_p \cdot \nabla\Gamma = rF_\theta + 0(\nu_t), \qquad -\frac{\partial}{\partial z}\left(\frac{\Gamma^2}{r^3}\right) = (\nabla \times \mathbf{F}_p)_\theta + 0(\nu_t) \tag{10.37, 10.38}$$

Note that when the poloidal force is effectively eliminated, the poloidal motion reduces to a weak Ekman pumping. This not only dramatically reduces the energy of the poloidal flow, but also helps keep u_θ at a modest level. That is, if the only poloidal motion is Ekman pumping, all of the streamlines will be flushed through the dissipative Ekman layers where the angular momentum created by F_θ can be efficiently destroyed.

Evidently, if we can find core solutions for $\mathbf{u}_p$ and Γ which satisfy (10.37) and (10.38), then this represents an energetically favourable state. We shall see that these core equations are readily satisfied, and that the flow does indeed adopt this low-energy state. The net result is that when F_θ exceeds the modest threshold of $\sim 0.01|\mathbf{F}_p|$, the flow is dominated by swirl, despite the weakness of the azimuthal force.

10.7.2 A formal analysis

Let us assume that the flow is axisymmetric and the liquid pool occupies a hemisphere of radius R, as shown in Figure 10.6. The current enters the pool at the free surface and spreads radially outward as it passes down through the pool. In addition to the azimuthal field, we shall allow for a weak external magnetic field. For simplicity, we take this to be uniform and vertical. It is convenient to introduce the scaled magnetic field $\mathbf{C} = \mathbf{B}/(\rho\mu)^{1/2}$, which has the dimensions of velocity. Then, from (10.5), the Lorentz force (per unit mass) has components

$$\mathbf{F}_p = -\frac{C_\theta^2}{r}\hat{\mathbf{e}}_r, \qquad F_\theta = C_z\frac{\partial C_\theta}{\partial z} \tag{10.39, 10.40}$$

We shall take the flow to be turbulent and model the Reynolds stresses using a turbulent eddy viscosity, ν_t. The poloidal velocity field, $\mathbf{u}_p$, is uniquely determined by its vorticity, ω_θ. From (10.39), (10.40) and the Navier–Stokes equation, it is easy to show that the governing equations for ω_θ and Γ are

$$\mathbf{u}\cdot\nabla\Gamma = \frac{\partial}{\partial z}[rC_zC_\theta] + \nu_t\nabla\cdot\left[r^2\nabla(\Gamma/r^2)\right] \tag{10.41}$$

$$\mathbf{u}\cdot\nabla(\omega_\theta/r) = \frac{\partial}{\partial z}\left[\frac{\Gamma^2}{r^4} - \frac{C_\theta^2}{r^2}\right] + \nu_t\nabla\cdot\left[r^{-2}\nabla(r\omega_\theta)\right] \tag{10.42}$$

In terms of velocity, equation (10.42) may be uncurled to give the poloidal equation of motion

$$\mathbf{u}_p\cdot\nabla\mathbf{u}_p = -\nabla(p/\rho) + \left[\left(u_\theta^2 - C_\theta^2\right)/r\right]\hat{\mathbf{e}}_r + \nu_t\nabla^2\mathbf{u}_p \tag{10.43}$$

Evidently, whenever $u_\theta^2 - C_\theta^2$ is independent of z, the poloidal motion vanishes. Let us now look for solutions to these equations for the case where $F_\theta \ll |\mathbf{F}_p|$. We start by examining the energy balance in these confined flows. For a steady-on-average turbulent flow, (10.2) becomes

$$\oint \mathbf{F} \cdot d\mathbf{l} + \nu_t \oint \nabla^2 \mathbf{u} \cdot d\mathbf{l} = 0 \tag{10.44}$$

This integral constraint must be satisfied by every streamline in the time-averaged flow. This could be achieved by high levels of internal dissipation. However, when ν_t is small, it is natural to look for solutions in which the dissipation is largely confined to the boundary layers. This, in turn, requires that each streamline passes through a boundary layer. (Every streamline must satisfy (10.44).) If Ekman pumping is to supply the necessary entrainment mechanism, then it is essential that it dominates the poloidal flow, despite the weakness of F_θ. However, inspection of (10.41) and (10.42) shows that such a flow is indeed possible. Let Γ_c be the angular momentum distribution in the core of the flow, and $\Gamma_{cs}(r)$ be the corresponding value of Γ_c just outside the Ekman layer (at the same radius). Now suppose we require Γ_c to satisfy

$$\Gamma_c^2 = r^2 C_\theta^2 + f(r) \tag{10.45}$$

where $f(r)$ is an arbitrary function of radius. Then from (10.42) there is no source of poloidal motion other than Ekman pumping. This guarantees entrainment of all of the streamlines and so provides an effective dissipation mechanism for the flow. We now explore the consequences of this distribution of swirl. We shall see that there is no contradiction between (10.45) and the azimuthal equation of motion.

If (10.45) is satisfied, then the poloidal equations of motion (10.42) and (10.43) tell us nothing more about the core flow, other than the fact that Ekman pumping will occur. It remains to be seen if our assumed distribution of Γ, (10.45), is consistent with the azimuthal equation of motion (10.41). Now suppose that $C_z = -C_0$ where $C_0 > 0$. Since B_θ is a decreasing function of z this ensures that $\Gamma > 0$. Equation (10.41) now becomes, in the core of the flow,

$$\mathbf{u} \cdot \nabla \Gamma_c = -rC_0 \frac{\partial C_\theta}{\partial z} = rC_0 \left| \frac{\partial C_\theta}{\partial z} \right| \tag{10.46}$$

Clearly, as each fluid particle spirals upward through the core its angular momentum increases. We now ask if this is consistent with our assumed distribution of Γ: that is, is $\partial \Gamma_c / \partial z < 0$ compatible with (10.45)? The answer is 'yes'. Note that (10.45) gives

$$\Gamma_c \frac{\partial \Gamma_c}{\partial z} = r^2 C_\theta \frac{\partial C_\theta}{\partial z} < 0 \qquad (\text{since } J_r > 0) \tag{10.47}$$

which is exactly what is required.

Finally, we must check that (10.45) is consistent with the azimuthal equation of motion in the Ekman layer. To this end we use (10.31), the integrated version of this equation:

$$\int rF_\theta dV = \pi \oint c_f \Gamma_{cs}^2 dl \tag{10.48}$$

Typically, c_f is of the order of 10^{-2} in a confined turbulent flow (the precise value depends on Re). Now the left-hand side of (10.48) is of order $C_0 C_\theta R^3$ while the right-hand side is at least of order $c_f C_\theta^2 R^3$. Thus (10.48) requires $C_0 \geq c_f C_\theta$, or equivalently $F_\theta \geq c_f |\mathbf{F}_p| \sim 0.01 |\mathbf{F}_p|$. This estimate was introduced earlier. It places a bound on the value of $F_\theta/|\mathbf{F}_p|$ below which an Ekman-dominated flow cannot be seen. If F_θ is less than this value, then the the induced swirl is too weak to counterbalance $\mathbf{F}_p$.

It appears, therefore, that an Ekman-dominated flow is physically realisable provided that F_θ is not too small. We shall see shortly that this is exactly what happens. When $F_\theta/|\mathbf{F}_p| < 10^{-3}$, $u_\theta \ll |\mathbf{u}_p|$. In the range $10^{-3} < F_\theta/|\mathbf{F}_p| < 10^{-2}$the swirl u_θ grows to be of order $|\mathbf{u}_p|$, and for $F_\theta/|\mathbf{F}_p| > 10^{-2}$the poloidal force is balanced by gradients in u_θ^2/r and we get Ekman pumping, with $u_\theta \gg |\mathbf{u}_p|$. It is remarkable that the velocity field should be dominated by u_θ despite the relative weakness of F_θ.

Finally, we note that, in the arguments above, we have made no assumption about the direction of the poloidal force. We might anticipate, therefore, that the proposed solution works equally well for flows which (in the absence of F_θ) diverge at the surface, and we shall see that this is so in the next section. (Diverging surface flows may be created by a rather more elaborate arrangement of current injection.)

10.7.3 Some numerical experiments

We now describe a sequence of numerical experiments reported in Davidson et al. (1999). These relate to the flow of liquid steel in a hemispherical pool of radius $R = 0.1$ m. The flow was taken to be turbulent $(\mathrm{Re} \sim 10^5)$ and the Reynolds stresses τ_{ij} were estimated using the κ–ε turbulence closure model. The current distribution is controlled by the boundary condition set for $\mathbf{J}$, and the distribution used in the simulations is shown in Figure 10.9(a). The computations also allowed for an axial magnetic field $C_z = -C_0$, where C_0 lies in the range $0 \rightarrow 1$ m/s. The contours of constant F_r and F_θ (for $C_0 = 0.01$) are shown in Figure 10.9(b) and 10.9(c).

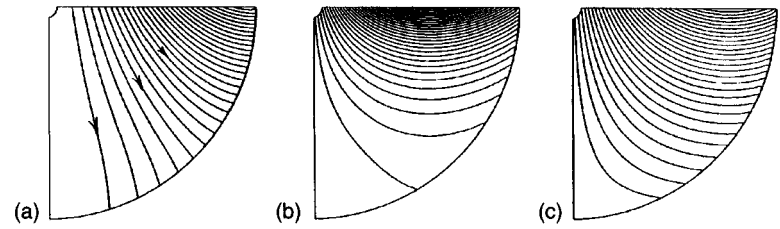

Figure 10.9 Current and forces in the liquid pool: (a) current; (b) contours of F_p, (c) contours of F_θ.

It is convenient to introduce the symbol $\hat{C}$ to represent the maximum value of C_θ. Note that $C_0/\hat{C}$ is a measure of the relative size of $F_\theta/|\mathbf{F}_p|$. With $\hat{C}$ fixed at 1 m/s, the flow was calculated for a range of values of $C_0/\hat{C}$, corresponding to 0, 0.005, 0.01, 0.02, 0.05, 0.1 and 1.0. This represents the full range from $F_\theta = 0$ to $F_\theta \sim |\mathbf{F}_p|$. The resulting variation of the kinetic energies E_θ and E_p (defined as the integrals of $u_\theta^2/2$ and $\mathbf{u}_p^2/2$) are shown in Figure 10.10. Note that, when the azimuthal force reaches a value of $\sim 0.01|\mathbf{F}_p|$, the swirl and poloidal motions have similar intensities. As F_θ is further increased, the energy of the poloidal motion collapses, dropping by a factor of 100. This is exactly the behaviour anticipated in Section 7.3.

The flow patterns for the cases $C_0 = 0$, 0.01 and 0.05 are shown in Figure 10.11. The transition to an Ekman-dominated structure is quite striking. For $F_\theta <\sim 0.01|\mathbf{F}_p|$, there is no Ekman pumping and the poloidal flow is dominated by $\mathbf{F}_p$, the swirl being too weak to react back on $\mathbf{u}_p$. For $F_\theta >\sim 0.01|\mathbf{F}_p|$ the poloidal flow is virtually eliminated through the balance $\mathbf{F}_p \sim -(u_\theta^2/r)\hat{\mathbf{e}}_r + \nabla\phi$. What little poloidal motion there is corresponds to Ekman pumping. Moreover, it is clear from Figure 10.10 that, for low values of F_θ, u_θ scales as $u_\theta \propto F_\theta$, which is what we would expect from (10.35). For large F_θ, on the other hand, we have $u_\theta \propto F_\theta^{5/9}$, which is typical of an Ekman flow (see Chapter 8).

The flows for the cases $C_0 = 0.1$ and 1.0 are shown in Figure 10.12 and compared with the case where the poloidal forcing is removed ($C_0 = 1.0$, $\hat{C} = 0$). Again, the motion is clearly dominated by Ekman pumping. It is remarkable that removing the poloidal forcing altogether makes almost no difference to the flow pattern. It is even more remarkable that, when the azimuthal forcing is only a few per cent of $\mathbf{F}_p$, the motion is dominated by swirl.

Finally, Davidson et al. (1999) considered a different distribution of $\mathbf{J}$, designed to drive a base flow, $\mathbf{u}_p$, which diverges at the surface. The

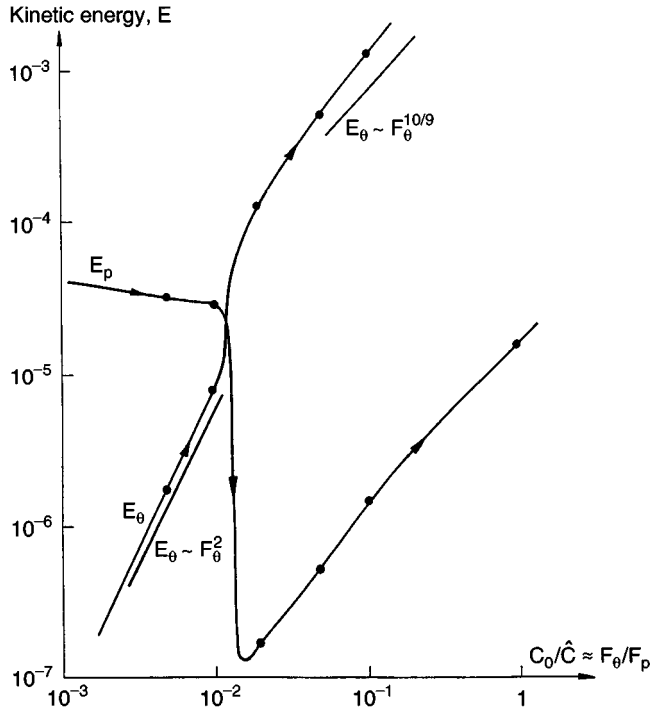

Figure 10.10 Variations of energy of the swirling (E_θ) and poloidal (E_p) components of motion as the ratio $F_\theta/|\mathbf{F}_p|$ is increased.

motivation here is to demonstrate that the phenomenon is quite unrelated to the direction of the poloidal base flow. Current was fed into the pool from the base and withdrawn at the sides. The resulting poloidal flow (in the absence of azimuthal forcing) then diverges at the surface. Nevertheless, they found precisely the same behaviour as before. When F_θ reaches a value of $\sim 0.01|\mathbf{F}_p|$ the energy of the poloidal motion collapses as an Ekman-dominated flow emerges.

These numerical experiments are broadly in line with the predictions of Section 7.1. It seems that the phenomenon of poloidal suppression is quite unrelated to the direction of the poloidal base flow and is not a manifestation of the breakdown of the self-similar solution. Rather, it results from a suppression of the poloidal motion through the balance $u_\theta^2/r \sim \mathbf{F}_p$. This allows the motion in the r–z plane to be dominated by Ekman pumping which, in turn, ensures that every streamline is flushed through the thin, dissipative Ekman layer. The result is a flow of low energy: E_p is virtually eliminated while $\mathbf{E}_\theta$ scales as $F_\theta^{10/9}$, rather than F_θ^2.

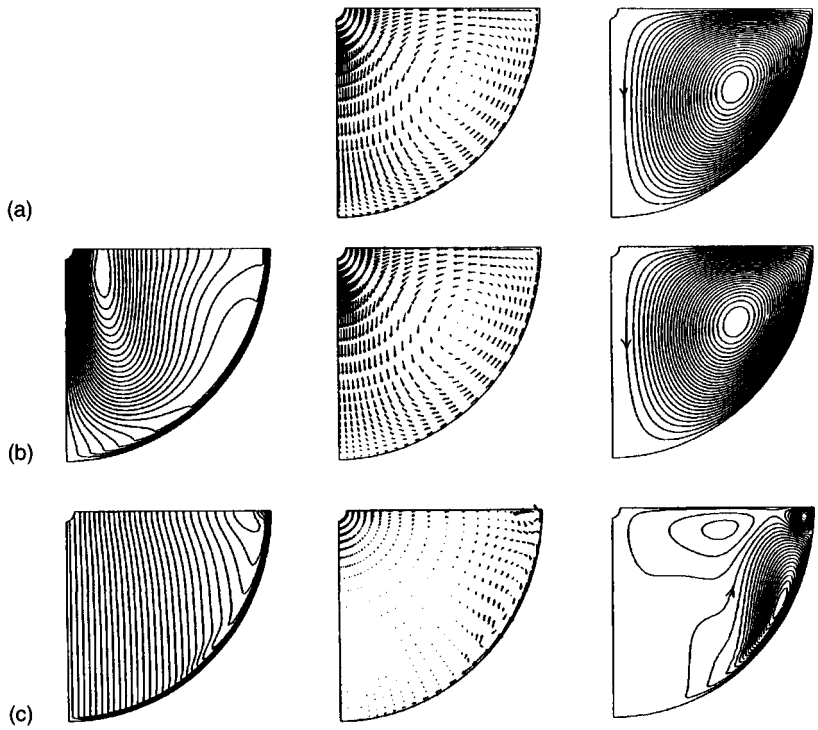

Figure 10.11 Contours of constant u_θ, poloidal velocity vectors and poloidal streamfunction for (a) $C_0 = 0$, (b) $C_0 = 0.01$ and (c) $C_0 = 0.05$.

Examples

10.1 Show that, for 2D flows, the global energy equation (10.3) is equivalent to evaluating the line integral (10.2) for each streamline and then adding all such integrals. Hint: consider a streamtube characterised by a jump in the stream-function $\delta\psi$, and then show that $u\delta A = \delta\psi dl$ where δA is an element of area with streamwise length dl.

10.2 Show that, for a point source of current on the surface of a semi-infinite domain,

$$B_\theta = \frac{\mu I}{2\pi r}(1 - \sin\phi)$$

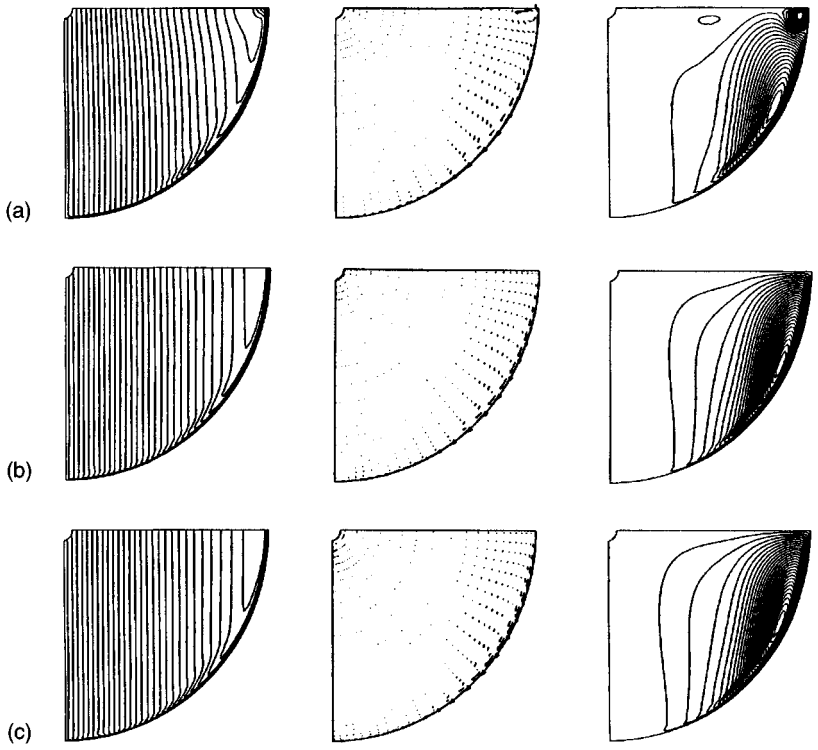

Figure 10.12 Contours of constant u_{θ_λ} poloidal velocity vectors and poloidal streamfunction for (a) $C_0 = 0.1$, $\hat{C} = 1.0$, (b) $C_0 = 1.0$, $\hat{C} = 1.0$ and (c) $C_0 = 1.0$, $\hat{C} = 0$.

10.3 The magnetic field used in the numerical experiments of Section 10.7.3 is

$$C_\theta = \hat{C} J_1(\delta_1 r/R) \cosh(\delta_1(1 - z/R))/[J_1(\delta_1)\cosh(\delta_1)]$$

Show that this corresponds to a current which leaves the cylinder $r < R$, $z < R$ normal to the surfaces $r = R$, $z = R$.

11

MHD Instabilities in Reduction Cells

> It is easier to write ten volumes on theoretical principles than to put one into practice.
>
> *Tolstoy*

The amount of energy required to reduce alumina to aluminium in electrolysis cells is staggering. In North America, for example, around 2% of all generated electricity is used to produce aluminium. Worldwide, around 2×10^{10} kg of aluminium are produced annually, and this requires in excess of 10^{11} kWh p.a. The corresponding electricity bill is around £10^{10} p.a.! Yet much of this energy (around one half) is wasted in the form of I^2R heating of the electrolyte used to dissolve the alumina. Needless to say, strenuous efforts have been made to reduce these losses, mostly centred around minimising the volume of electrolyte. However, the aluminium industry is faced with a fundamental problem. When the volume of electrolyte is reduced below some critical threshold, the reduction cell becomes unstable. It is this instability, which is driven by MHD forces, which is the subject of this chapter.

11.1 Interfacial Waves in Aluminium Reduction Cells

11.1.1 Early attempts to produce aluminium by electrolysis

It is not an easy matter to produce aluminium from mineral deposits. The first serious attempt to isolate elemental aluminium was that of Humphrey Davy, Faraday's mentor at the Royal Institution. (In fact, Davy's preferred spelling – aluminum – is still used today in North America.) In 1809 he passed an electric current through fused compounds of aluminium and into a substrate of iron. Although an alloy of aluminium and iron resulted in place of the pure aluminium he sought, Davy had at least managed to prove that aluminium oxide was indeed reducible.

Oersted, and later Wöhler, set aside electricity and concentrated on chemical means of isolating aluminium. By 1827 Wöhler was able to produce small quantities of aluminium powder by displacing the metal

from its chloride using potassium. Later, in the 1850s, potassium was replaced by sodium, which was cheaper, and aluminium fluoride was substituted for the more volatile chloride. Wöhler's laboratory technique had at last become commercially viable and the industrial production of aluminium began. However, those chemical processes were all swept aside by the revolution in electrical technology initiated by Faraday. In particular, the development of the dynamo made it possible to produce aluminium by electrolysis.

The electrolytic route was first proposed by Robert Bunsen in 1854, but it was not until 1886 that a continuous commercial process was developed. It was a 22-year-old college student from Ohio, Charles Martin Hall, and the Frenchman Paul Héroult who made this breakthrough: the Frenchman as a result of good fortune (which he had the wit to pursue), and the American as a result of systematic enquiry. Hall and Héroult realised that molten cryolite, a mineral composed of fluorine, sodium and aluminium, readily dissolves alumina and that a current passed through the solution will decompose the alumina, leaving the cryolite unchanged. Full commercial production of aluminium began on Thanksgiving Day 1888 in Pittsburgh in a company founded by Hall. An example of an early Hall–Héroult reduction cell is shown in Figure 11.1(a). Remarkably, over a century later, the process is virtually unchanged.

11.1.2 The instability of modern reduction cells

Today almost all aluminium is produced by electrolysis, and the cells which are used look remarkably similar to those envisaged by Hall and Héroult. A schematic of a modern cell is shown in Figure 11.1(b). A large vertical current, perhaps 300 kA, flows downward from the carbon anode, passing first through the electrolytic layer (where it reduces the alumina) and then through a liquid aluminium pool before finally being collected at the carbon cathode at the base of the cell. The liquid layers are broad and shallow, perhaps 4 m × 10 m in plan, yet only a few centimetres deep.

The aluminium is an excellent conductor, the carbon a moderate one and the electrolyte (cryolite) a very poor conductor. Consequently, most of the electrical energy consumed by the cell is lost in Ohmic heating of the cryolite. In fact, these losses are vast, and there is considerable incentive to lower the resistance of the electrolyte layer by reducing its thick-

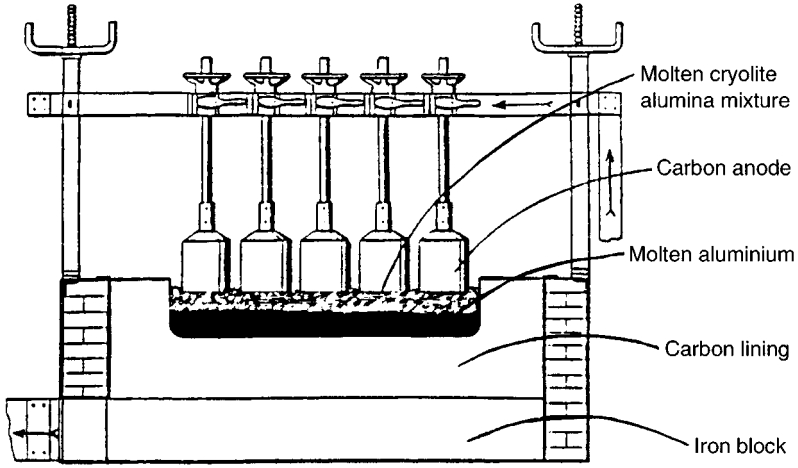

Figure 11.1 (a) A schematic of a 1920s reduction cell.

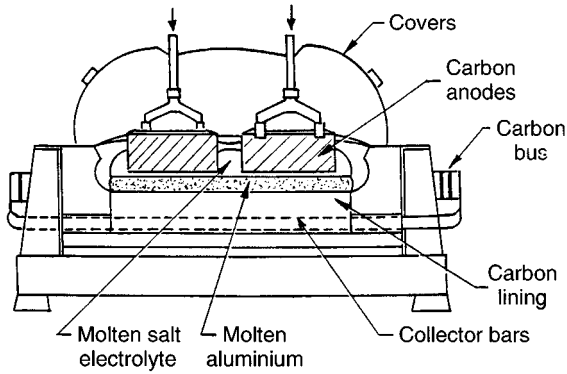

Figure 11.1 (b) A modern reduction cell.

ness. (Note the difference in electrolyte thickness in Figures 11.1(a) and 11.1(b).)

The energy problem aside, this process works reasonably well. However, there is one fundamental problem. It turns out that unwanted disturbances are readily triggered at the electrolyte–aluminium interface (Figure 11.2). In effect, these are long-wave-length, interfacial gravity waves, modified by the intense magnetic and electric fields which pervade the cell. Under certain conditions these disturbances are observed to grow, disrupting the operation of the cell. These instabilities have been

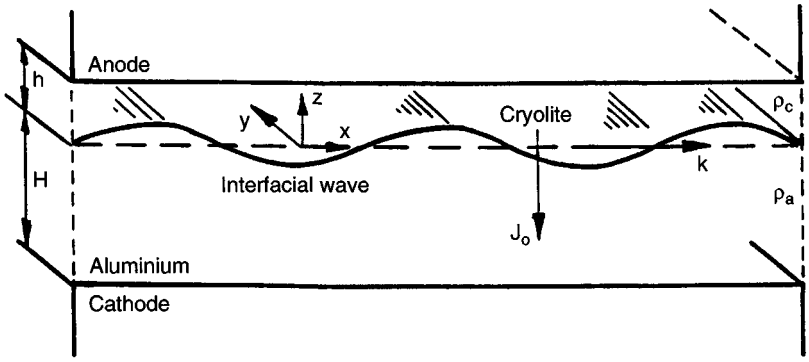

Figure 11.2 Interfacial waves in a reduction cell.

the subject of much research over the last two decades, since they represent the greatest single impediment to increasing the energy efficiency of these cells. In particular, the cryolite depth, h, must be maintained above a certain critical value to ensure stability, and this imposes a large energy penalty. Indeed, one aluminium company has estimated that each millimetre of cryolite costs them \$1 million per year in waste heat!

To some extent, the mechanism of the instability is clear. Tilting the interface causes a perturbation in current, $\mathbf{j}$. Excess current is drawn into the aluminium at those points where the thickness of the highly resistive cryolite is reduced, and less current is drawn at points where the electrolyte depth is increased. Since the carbon cathode is much more resistive than the aluminium, these perturbations in vertical current feed into the aluminium but do not penetrate the cathode. In the long-wavelength approximation ($kh \to 0$, k being the wavenumber) the perturbed current in the electrolyte is purely vertical while that in the aluminium is horizontal (to leading order in kh). This perturbation in current is shown in Figure 11.3 for the simplest of wave shapes.

Now the change in current causes a perturbation in the Lorentz force, $\delta\mathbf{F} = \mathbf{j} \times \mathbf{B}_0 + \mathbf{J}_0 \times \mathbf{b}$. In the long-wavelength limit, the dominant contribution to $\delta\mathbf{F}$ can be shown to be $\mathbf{j} \times \mathbf{B}_z$, where $\mathbf{B}_z$ is the vertical component of the ambient magnetic field in the cell (see Section 3 of this chapter). The key question is, therefore, whether or not this change in Lorentz force amplifies the initial motion.

After many years of research, this issue was finally resolved by Sneyd & Wang (1994) and Bojorevics & Romerio (1994). Subsequently, their analyses were generalised by Davidson & Lindsay (1998). These authors all

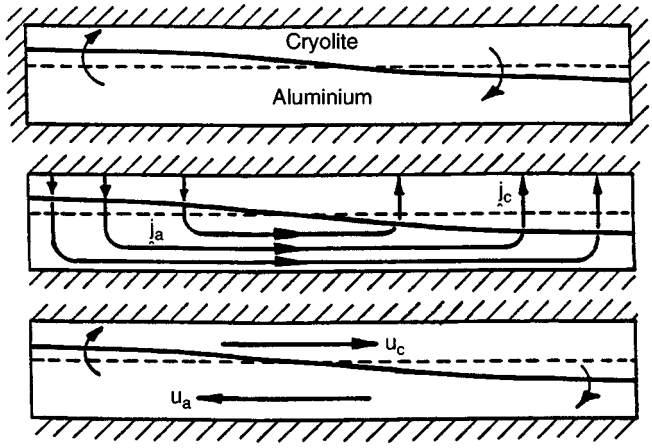

Figure 11.3 Perturbations in current caused by a movement of the interface. In the long-wave-length limit the perturbation current, **j**, is largely vertical in the cryolite and horizontal in the aluminium. The 'sloshing' motion in the two liquids is largely horizontal.

simplify the geometry to that of a closed, rectangular domain (i.e. a shoe-box), as shown in Figure 11.2. Sneyd & Wang start by noting that, in the absence of a magnetic field, the interface may support an infinite number of conventional standing waves. The normal modes associated with these form an orthogonal set of functions, so that one can represent an arbitrary disturbance of the interface as the superposition of many such gravitational modes. When the Lorentz force is absent, these modes are decoupled. However, when the Lorentz force is taken into account, certain gravitational modes are coupled. That is, the redistribution of current caused by one mode gives rise to a Lorentz force which, when Fourier-decomposed, can excite many other modes. This leads to a coupled set of equations of the form

$$\ddot{\mathbf{x}} + \boldsymbol{\Omega}\mathbf{x} = \hat{\varepsilon}\mathbf{K}\mathbf{x}, \qquad \hat{\varepsilon} = J_0 B_z/\rho_a H \tag{11.1}$$

Here **x** is a column vector which represents the amplitudes of the gravitational modes, $\boldsymbol{\Omega}$ is diagonal with elements equal to the square of the conventional gravitational frequencies, H and ρ_a are the depth and density of the aluminium, respectively, and **K** is the interaction matrix which arises from $\mathbf{j} \times \mathbf{B}_z$. Now **K** is skew-symmetric and so complex eigenvalues, and hence instabilities, are guaranteed when $\hat{\varepsilon}$ is large. Unfortunately

however, (11.1) sheds little light on the all-important instability mechanism. Consequently, before going on to describe the instability in detail, we shall discuss a simple mechanical analogue which highlights the basic instability mechanism. This is due to Davidson & Lindsay (1998) and relies on the fact that, in the long-wavelength limit, the motion in the aluminium is purely horizontal (Figure 11.3).

11.2 A Simple Mechanical Analogue for the Instability

Suppose we replace the liquid aluminium by a thin, rigid, aluminium plate attached to the centre of the anode by a light rigid strut. The strut is pivoted at its top and so the plate is free to swing as a compound pendulum about two horizontal axes, x and y (Figure 11.4a). Let the plate have thickness H, lateral dimensions L_x, L_y and density ρ_a. The gap h between the plate and the anode is filled with an electrolyte of negligible inertia and poor electrical conductivity. A uniform current density, J_0, passes vertically downward into the plate and is tapped off at the centre of the plate. Finally, suppose that there is an externally imposed vertical magnetic field B_z.

Evidently, we have replaced one mechanical system (the cell), which has an infinite number of degrees of freedom, with another which has only two degrees of freedom. However, electrically the two geometries are alike. Moreover, the nature of the motion in the two cases is not dissimilar. In both systems we have movement of the aluminium associated with tilting of the electrolyte–aluminium interface. In a cell this takes the form of a 'sloshing' back and forth of the aluminium as the interface tilts first one way and then the other (Figure 11.3).

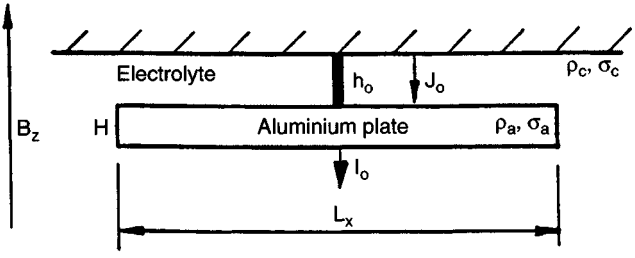

Figure 11.4 (a) The compound pendulum shown here contains all of the essential physics of the reduction cell instability.

Let θ_x and θ_y be the angles of rotation of the plate measured about x and y axes. Then it is not difficult to show that, as a result of these rotations, the perturbation of the current I in the aluminium plate is given by

$$\delta I_x = \frac{J_0 L_y \theta_y}{2h}\left[(L_x/2)^2 - x^2\right]$$

$$\delta I_y = -\frac{J_0 L_x \theta_x}{2h}\left[(L_y/2)^2 - y^2\right]$$

The perturbation in the Lorentz force $\mathbf{j} \times \mathbf{B}_z$ can be calculated from these expressions and the equations of motion for the compound pendulum then follow. They are

$$\ddot{\gamma}_x + \omega_x^2 \gamma_x = -(J_0 B_z/\rho_a H)\gamma_y = -\hat{\varepsilon}\gamma_y \tag{11.2a}$$

$$\ddot{\gamma}_y + \omega_y^2 \gamma_y = +(J_0 B_z/\rho_a H)\gamma_x = \hat{\varepsilon}\gamma_x \tag{11.2b}$$

where $\gamma_x = \theta_x/L_x^2$, $\gamma_y = \theta_y/L_y^2$ and ω_x, ω_y are the conventional gravitational frequencies of the pendulum. Note the similarity to (11.1). If we look for solutions of the form $\gamma \sim \exp(i\omega t)$ we find oscillatory solutions for small values of $\hat{\varepsilon} = J_0 B_z/\rho_a H$ and exponential (unstable) solutions for large $\hat{\varepsilon}$.

Figure 11.4(b) shows the movement of ω^2 in the complex plane as $\hat{\varepsilon}$ is increased. The two natural frequencies ω_x^2 and ω_y^2 move along the real axis until they meet. At this point, they move off into the complex plane and an instability develops. The important points to note are:

1. The tendency for instability depends only on the magnitude of $J_0 B_z/\rho_a H$ and on the natural gravitational frequencies ω_x and ω_y.

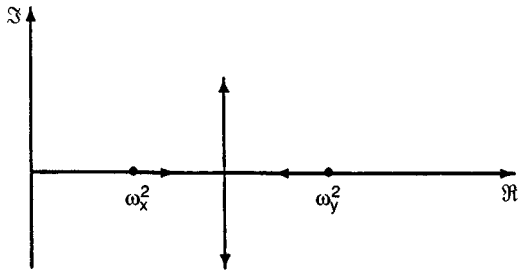

Figure 11.4 (b) Variations of ω^2 with $J_0 B_z$ in the complex plane for the pendulum.

2. To minimise the danger of an instability it is necessary to keep $J_0 B_z/\rho_a H$ low and the gravitational frequencies well apart. The closer the natural frequencies are, the lower the threshold value of $J_0 B_z$ at which an instability appears. (Circular and square plates are unstable for vanishingly small values of $J_0 B_z$.)
3. The system is unstable whenever

$$\frac{J_0 B_z}{\rho_a H} \geq \frac{1}{2}|\omega_x^2 - \omega_y^2|$$

4. When $\hat{\varepsilon}$ is large the unstable normal mode corresponds to a rotating, tilted plate.

Very similar behaviour is seen in reduction cells governed by (11.1). In particular, the sensitivity of reduction cells to the destabilising influence of $J_0 B_z$ depends on the initial separation of the gravitational frequencies. The closer the gravitational frequencies, the lower the stability threshold. Moreover, unstable waves frequently correspond to a rotating, tilted interface.

The physical origin of the instability of the pendulum is now clear. Tilting the plate in one direction, say θ_x, produces a horizontal flow of current in the aluminium which interacts with B_z to produce a horizontal force δF_x, which is perpendicular to the movement of the plate and in phase with θ_x. This tilting also produces a horizontal velocity, u_y, which is $\pi/2$ out of phase with the force δF_x and mutually perpendicular to it. Two such tilting motions in perpendicular directions can reinforce each other, with the force from one doing work on the motion of the other. This is the instability mechanism of the pendulum, and essentially the same thing happens in a reduction cell.

We may think of the Lorentz force as playing two rôles. In the first instance it modifies the gravitational frequencies, pulling them together on the real axis. Once these frequencies coincide, so that the plate oscillates at the same frequency in two directions, the Lorentz force adopts a second rôle in which it supplies energy to the pendulum. Unstable motion then follows.

A simple energy argument shows why, whenever the plate oscillates with a single frequency in two perpendicular directions, an instability is inevitable. From the expressions for δI_x and δI_y we can calculate the Lorentz force $\delta \mathbf{F}$ and hence the rate of work done by the force, $\delta \mathbf{F} \cdot \mathbf{u}$,

$$W = \delta \mathbf{F} \cdot \mathbf{u} = J_0 B_z L_x L_y \left[L_y^2 \theta_x \dot{\theta}_y - L_x^2 \theta_y \dot{\theta}_x\right]/12 \qquad (11.3)$$

Now suppose that θ_x and θ_y both oscillate at frequency ω, but are $\pi/2$ out of phase. Then the time-averaged value of $\dot{W}$ is non-zero, implying unstable motion.

Note that this *instability mechanism* is independent of the action of gravity. That is, provided the plate can oscillate at the same frequency in two directions, it will become unstable. (Circular and square plates are unstable at arbitrarily small values of B_z.) The *stability threshold*, on the other hand, does depend on gravity, in that it is dependent on the initial separation of the gravitational frequencies.

We now return to reduction cells. We shall see that interfacial waves are described by the wave-like differential equation

$$\frac{\partial^2 \mathbf{q}}{\partial t^2} - c^2 \nabla^2 \mathbf{q} = \omega_B^2 [\hat{\mathbf{e}}_z \times \mathbf{q}]_P \tag{11.4}$$

where $\mathbf{q}$ is the horizontal mass flux in the cryolite, $\omega_B^2 = J_0 B_z/(\rho_c H + \rho_a h)$ and $c^2 = (\rho_a - \rho_c)g/((\rho_c/h) + (\rho_a/H))$. The subscript P on the term $\hat{\mathbf{e}}_z \times \mathbf{q}$ implies that we take only the irrotational (i.e. potential) component of $\hat{\mathbf{e}}_z \times \mathbf{q}$. This equation is valid quite generally and makes no assumption regarding the existence or shape of the lateral boundaries. Also, note that all of the electromagnetic effects are captured by the single parameter ω_B^2. There are four special cases of interest.

(i) When $\omega_B = 0$ we recover the standard wave equation for interfacial disturbances,

$$\frac{\partial^2 \mathbf{q}}{\partial t^2} - c^2 \nabla^2 \mathbf{q} = \mathbf{0}$$

(ii) If ω_B is non-zero, and we look for solutions in the channel $0 < x < L$, then we find unstable travelling waves.

(iii) For a closed circular domain, (11.4) yields unstable standing waves for vanishingly small values of ω_B. (Remember, a circular pendulum is unstable for vanishingly small $J_0 B_z$.) Moreover, the unstable normal mode corresponds to a rotating, tilted interface, just like that of the pendulum.

(iv) If we place (11.4) in a rectangular domain we recover the matrix equation of Sneyd & Wang (1994):

$$\ddot{\mathbf{x}} + \boldsymbol{\Omega}\mathbf{x} = \hat{\varepsilon}\mathbf{K}\mathbf{x}, \qquad \hat{\varepsilon} = J_0 B_z/\rho_a H$$

where the coupling matrix, $\mathbf{K}$, is skew-symmetric and Ω is diagonal with elements equal to the square of the gravitational wave frequencies. (Note the similarity to (11.2).) We now set about deriving (11.4).

11.3 Simplifying Assumptions

A model of the cell is shown in Figure 11.2. The undisturbed depths of cryolite and aluminium are h and H, respectively, and the unperturbed current flow is purely vertical and has magnitude J_0. We use a Cartesian coordinate system, (x, y, z), where the positive direction of z is upward and the origin for z lies at the undisturbed interface. On occasion we shall refer to cells which are rectangular in plan view, and these are given dimensions L_x and L_y. However, much of the analysis can be applied to any shape of cell.

We take the characteristic time-scale for the wave motion to be much greater than the diffusion time of the magnetic field. That is, we make the pseudo-static approximation $\mu\sigma uh \ll 1$, where μ is the permeability, σ is the conductivity, and u is a typical velocity. Thus, each time the interface moves, the current immediately relaxes to a new equilibrium distribution. Ohm's law is then

$$\mathbf{J} = \sigma\mathbf{E} = -\sigma\nabla\Phi, \qquad \nabla^2\Phi = 0$$

We are concerned only with linear stability, and so we consider infinitesimal perturbations of the interface of the form $z_s = \eta$, $\eta \ll h, H$. The corresponding distributions of $\mathbf{J}$ and $\mathbf{B}$ are

$$\mathbf{J} = \mathbf{J}_0 + \mathbf{j} = -J_0\hat{\mathbf{e}}_z - \sigma\nabla\phi, \qquad \mathbf{B} = \mathbf{B}_0 + \mathbf{b}$$

and the boundary conditions on $\mathbf{J}$ arise from the ranking of the conductivities. That is,

$$\sigma_a \gg \sigma_{\text{carbon}} \gg \sigma_c \tag{11.5}$$

Here the subscripts 'a' and 'c' refer to the aluminium and cryolite. It is not difficult to show that (11.5) requires $\phi_c = 0$ on $z = h$ and $\partial\phi_a/\partial z = 0$ on $z = -H$. Here ϕ is the perturbation in the electrostatic potential. The first of the boundary conditions states that the anode potential is fixed, while the second ensures that $\mathbf{j}$ does not penetrate into the cathode blocks.

We shall assume that the fluid is inviscid, that surface tension can be ignored, and that there is no background motion in the unperturbed state. The first of these assumptions means that our equations of motion cannot mimic the damping of high-wavenumber perturbations which occur in practice. To compensate for this, we simply ignore those modes whose wavelengths are shorter than a certain (small but arbitrary) value. The last of the three assumptions (i.e. $\mathbf{u}_0 = 0$) greatly simplifies the stability analysis. However, this simplification does severely limit

the allowable distributions of $\mathbf{B}_0$. That is, to ensure that the perturbation occurs about an equilibrium configuration, we must satisfy $\nabla \times (\mathbf{J}_0 \times \mathbf{B}_0) = \mathbf{0}$. Given our assumed distributions of $\mathbf{J}_0$, we require $\mathbf{B}_0$ to be of the form

$$\mathbf{B}_0 = \big(B_x(x, y), B_y(x, y), B_z\big) \tag{11.6}$$

where B_z is spatially uniform. We shall assume that all three components of $\mathbf{B}_0$ are of the same order of magnitude. From Ampere's law, $\nabla \times \mathbf{B} = \mu\mathbf{J}$, which implies that $B_x \sim B_y \sim B_z \sim \mu J_0 L$ where L is a typical lateral dimension.

Our final assumption relates to the aspect ratio of the liquid layers. We shall assume that $kh \ll 1$, where k is a typical wavenumber. In effect, we use the shallow-water approximation. This leads directly to a number of simplifying features. In particular, as a result of the shallow-water approximation, and to leading order in kh, it may be shown that:

(a) $\mathbf{j}$ is vertical in the cryolite;
(b) $\mathbf{j}$ is horizontal in the aluminium and is uniformly distributed across that layer;
(c) the perturbed Lorentz force acting on the cryolite may be neglected;
(d) the velocity in each layer is uniform in z and horizontal;
(e) the dominant contribution to the perturbed Lorentz force in the aluminium is $\mathbf{j} \times (B_z\hat{\mathbf{e}}_z)$.

In fact, it is not difficult to see how these simplifications arise. Consider the situation shown in Figure 11.3, where the disturbance has a long wavelength. Approximations (a) and (b) are purely geometric and are a consequence of the ranking of the conductivities. That is, the dominant resistance to the flow of current is the thin sheet of cryolite, so that the current passes directly downward through this layer (condition (a)). The aluminium, which is a very good conductor, is almost an equipotential surface, so that spatial variations of J_z in the cryolite (due to undulations of the interface) lead to a 'shorting' of the perturbed current through the aluminium. This 'shorted' current is almost purely horizontal (condition (b)). The neglect of the perturbed Lorentz force in the cryolite (condition (c)) stems from the fact that $\mathbf{j}_c \ll \mathbf{j}_a$, which in turn arises from the aspect ratio $kh \ll 1$. The uniformity of the velocity in the two fluid layers (condition (d)) follows from the fact that the Lorentz force in the aluminium is independent of depth.

This leaves only simplification (e) to justify, and here there is some subtlety in the argument. Using subscripts H and V to indicate horizontal

and vertical components of $\mathbf{J}$ and $\mathbf{B}$, it seems reasonable to neglect $\mathbf{j}_H \times \mathbf{B}_H$ and $\mathbf{j}_V \times \mathbf{B}_H$ because the former is vertical and so merely perturbs the vertical pressure gradient, while the latter is much smaller than $\mathbf{j}_H \times \mathbf{B}_V$, by virtue of (b). Finally, the neglect of $\mathbf{b} \times \mathbf{J}_0$ relies on the fact that $|\mathbf{b}|$ is of order $|\mu \mathbf{j}_H H|$, while $|\mathbf{B}_0|$ is of order $\mu J_0 L_x$, so that $|\mathbf{J}_0 \times \mathbf{b}|$ is of order kH smaller than $|\mathbf{j} \times \mathbf{B}_V|$.

11.4 A Shallow-Water Wave Equation and Key Dimensionless Groups

We now derive a dynamic equation for interfacial waves. This equation (11.4) is more general than the 'mode-by-mode' description of (11.1) in that it makes no assumption regarding the existence or shape of lateral boundaries. The derivation is long and somewhat technical, and so the impatient reader may wish to jump directly to the end result, which is equation (11.18).

11.4.1 A shallow-water wave equation

We start with conventional shallow-water theory. It is not difficult to show that, to second order in kH, the pressure in each layer is hydrostatic. As a consequence, we may apply the conventional shallow-water equation to each layer in turn. This is a two-dimensional equation for the horizontal motion:

$$\rho \frac{D\mathbf{u}_H}{Dt} + \rho g \nabla H_a = -\nabla P_0 + \mathbf{F}_H$$

Here $H_a(x, y)$ is the aluminium depth, P_0 is the interfacial pressure, and $\mathbf{F}_H$ is the horizontal body force in each layer. The unfamiliar term on the left arises from the horizontal gradient in pressure. For example, the pressure at the base of the aluminium layer is $P_0 + \rho_a g H_a$, so that the horizontal pressure force at the base of the layer is $-\nabla P_0 - \rho_a g \nabla H_a$. Similarly, the horizontal pressure force at the top of the cryolite layer is $-\nabla P_0 + \rho_c g \nabla H_c = -\nabla P_0 - \rho_c g \nabla H_a$.

Note that, since $\mathbf{F}_H$ is independent of z (to leading order in kH), our shallow-water equation is a strictly two-dimensional equation of motion. We now linearise our equation of motion about a base state of zero background motion. Taking $H_a = H + \eta(x, y, t)$, we obtain

$$\rho \frac{\partial \mathbf{u}_H}{\partial t} + \rho g \nabla \eta = -\nabla P_0 + \mathbf{F}$$

Although $\mathbf{u}_H$ is a two-dimensional velocity field, vertical movement of the interface means that the two-dimensional divergences of $\mathbf{u}_{aH}$ and $\mathbf{u}_{cH}$ are both non-zero. In fact, it is readily confirmed that (figure 11.5)

$$\nabla \cdot (H\mathbf{u}_a) = -\nabla \cdot (h\mathbf{u}_c) = -\frac{\partial \eta}{\partial t}$$

(Here we have dropped the subscript H for convenience.)

Next, we replace $\mathbf{u}_a$ and $\mathbf{u}_c$ by the volume fluxes $\mathbf{q}_a = H\mathbf{u}_a$ and $\mathbf{q}_c = -h\mathbf{u}_c$. Also, by virtue of condition (c) in Section 3 of this chapter, we may take $\mathbf{F}_c = 0$ (to leading order in kH). This is valid because, as we have seen, the current perturbation in the cryolite is an order of magnitude smaller than that in the aluminium. The governing equations become

$$\frac{\rho_c}{h}\frac{\partial \mathbf{q}_c}{\partial t} - \rho_c g \nabla \eta = \nabla P_0 \tag{11.7}$$

$$\frac{\rho_a}{H}\frac{\partial \mathbf{q}_a}{\partial t} + \rho_a g \nabla \eta = -\nabla P_0 + \mathbf{F}_a \tag{11.8}$$

$$\nabla \cdot \mathbf{q}_c = \nabla \cdot \mathbf{q}_a = -\frac{\partial \eta}{\partial t} \tag{11.9}$$

We now perform a so-called Helmholtz decomposition on $\mathbf{q}$: $\mathbf{q} = \mathbf{q}_R + \mathbf{q}_p$. That is, we divide $\mathbf{q}$ into a solenoidal, rotational part and an irrotational component of finite divergence. The boundary conditions on $\mathbf{q}_a$ and $\mathbf{q}_c$ are that $\mathbf{q} \cdot \mathbf{n}$ vanishes at the boundary, S. An appropriate decomposition is therefore

$$\nabla \times \mathbf{q}_p = 0, \qquad \nabla \cdot \mathbf{q}_p = -\frac{\partial \eta}{\partial t}, \qquad \mathbf{q}_p \cdot \mathbf{n} = 0 \qquad \text{on S} \tag{11.10}$$

$$\nabla \times \mathbf{q}_R = \nabla \times \mathbf{q}, \qquad \nabla \cdot \mathbf{q}_R = 0, \qquad \mathbf{q}_R \cdot \mathbf{n} = 0 \qquad \text{on S} \tag{11.11}$$

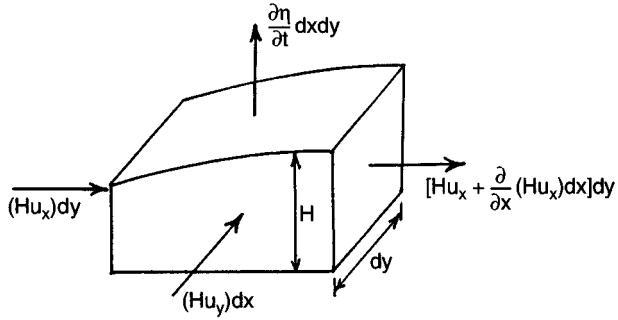

Figure 11.5 The horizontal divergence of u_a.

Evidently, $\mathbf{q}_R$ is zero in the electrolyte, while $\mathbf{q}_P$ is the same in both layers: $\mathbf{q}_c = \mathbf{q}_p$; $\mathbf{q}_a = \mathbf{q}_p + \mathbf{q}_R$. We now rewrite (11.7) and (11.8) in terms of $\mathbf{q}_P$ and $\mathbf{q}_R$, eliminate P_0 by adding the equations, and use (11.10) to express η in terms of $\mathbf{q}_P$. The resulting equation of motion is

$$\bar{\rho}\frac{\partial^2 \mathbf{q}_P}{\partial t^2} - \Delta\rho g \nabla^2 \mathbf{q}_P = \left[\frac{\partial \mathbf{F}_a}{\partial t}\right]_p \tag{11.12}$$

where $\bar{\rho} = \rho_c/h + \rho_a/H$ and $\Delta\rho = \rho_a - \rho_c$. The subscript P on the bracket implies that we take only the irrotational component of the corresponding term. Note that, when the Lorentz force is zero, we recover the conventional equation for interfacial waves in the shallow-water limit:

$$\boxed{\frac{\partial^2 \mathbf{q}_p}{\partial t^2} - c^2 \nabla^2 \mathbf{q}_p = 0, \qquad c^2 = \Delta\rho g/\bar{\rho}} \tag{11.13}$$

We now evaluate $\mathbf{j}_a$, and hence $\mathbf{F}_a$, using the long-wavelength approximation. In the cryolite we have, to leading order in kH, $\partial^2\Phi/\partial z^2 = 0$, from which

$$\Phi_c = \Phi_0 z/(h - \eta) + O(kh)$$
$$\mathbf{J}_c = -(J_0\eta/h)\hat{\mathbf{e}}_z + O(kh)$$

This current passes into the aluminium, and so the boundary conditions on $\mathbf{J}_{za}$ are

$$\mathbf{j}_{za} = -(J_0\eta/h)\hat{\mathbf{e}}_z \qquad \text{on } z = 0$$
$$\mathbf{j}_{za} = 0 \qquad \text{on } z = -H$$

It is readily confirmed that the conditions of zero divergence and zero curl, as well as the boundary conditions given above, are satisfied by

$$\mathbf{j}_a = \mathbf{j}_H(x, y) - (1 + z/H)(J_0\eta/h)\hat{\mathbf{e}}_z \tag{11.14}$$

Here $\mathbf{j}_H$ is the horizontal component of the current density in the aluminium, which satisfies

$$\nabla \times \mathbf{j}_H = 0, \qquad \nabla \cdot \mathbf{j}_H = \frac{J_0\eta}{Hh}, \qquad \mathbf{j}_H \cdot \mathbf{n} = 0 \qquad \text{on S} \tag{11.15}$$

Comparing equation (11.15) with (11.10) we find that

$$\boxed{\frac{\partial \mathbf{j}_H}{\partial t} = -\frac{J_0}{hH}\mathbf{q}_p} \tag{11.16}$$

This is the key relationship which allows us to express the Lorentz force in terms of the fluid motion, and therefore it deserves some special attention. The physical basis for (11.16) is contained in Figure 11.3. When the interface tilts, there is a horizontal flow of current from the high to the low side of the interface. Simultaneously, there is a horizontal rush of the aluminium in the opposite direction. It is this coupling which lies at the heart of the instability, and which is expressed by (11.16).

We now invoke condition (e) of Section 11.3 which states that the leading term in the Lorentz force arises from the background component of B_z. Substituting for $\mathbf{F}_a$ in (11.12) and introducing

$$\boxed{\omega_B^2 = J_0 B_z / \bar{\rho} h H} \tag{11.17}$$

we find, after a little algebra, that

$$\boxed{\frac{\partial^2 \mathbf{q}_p}{\partial t^2} - c^2 \nabla^2 \mathbf{q}_p = \omega_B^2 \left[\hat{\mathbf{e}}_z \times \mathbf{q}_p\right]_p} \tag{11.18}$$

Finally, to obtain the most compact version of our wave equation, it is convenient to introduce potentials for $\mathbf{q}_p$ and $\mathbf{F}_p = \mathbf{F}_a - \mathbf{F}_R$.

$$\mathbf{q}_P = \nabla \phi_P, \qquad \frac{\partial \mathbf{F}_P}{\partial t} = \bar{\rho} \omega_B^2 \nabla \Psi$$

Then (11.18) becomes

$$\boxed{\frac{\partial^2 \phi_p}{\partial t^2} - c^2 \nabla^2 \phi_p = c^2 k_B^2 \Psi, \qquad \nabla^2 \Psi = 0} \tag{11.19}$$

$$\boxed{k_B^2 = \frac{J_0 B_z}{\Delta \rho g h H}} \tag{11.20}$$

where k_B is defined as ω_B/c. The corresponding boundary conditions on ϕ_P and Ψ are

$$\boxed{\nabla\phi_P \cdot \mathbf{n} = 0, \qquad \nabla\Psi \cdot \mathbf{n} = (\nabla\phi_p \times \mathbf{n})_z} \tag{11.21}$$

Note that the boundary condition on Ψ comes directly from (11.16) and from the definition of $\mathbf{F}_P$.

11.4.2 Key dimensionless groups

At last we are in a position to investigate cell stability! Solving (11.19) subject to boundary conditions (11.21) will determine the stability of the interface. Note that (11.19) is valid for any shape of domain, since we have made no assumptions about the lateral boundaries. We shall see that (11.19) can support both standing waves and travelling waves, and that both may go unstable.

Consider now a rectangular domain of size L_x, L_y. We can make (11.19) dimensionless by rescaling t according to $\hat{t} = k_B ct$ and $\mathbf{x}$ according to $\hat{\mathbf{x}} = k_B\mathbf{x}$. In scaled units, (11.19) becomes

$$\ddot{\phi}_P - \nabla^2\phi_P = \Psi, \qquad \nabla^2\Psi = 0$$

Evidently, the behaviour of interfacial waves in a rectangular domain is controlled only by (scaled) boundary shape, i.e. by $\hat{L}_x = k_B L_x$ and $\hat{L}_y = k_B L_y$. It follows that the stability threshold in a rectangular domain is uniquely determined by two dimensionless parameters,

$$\boxed{\varepsilon^* = k_B^2 L_y^2 = \frac{J_0 B_z L_y^2}{\Delta\rho g h H}, \qquad r = L_x/L_y} \tag{11.22a, b}$$

Here ε^* is a dimensionless version of $\hat{\varepsilon}$ introduced in (11.1). Later, when we show some examples of cell instabilities, we shall find it convenient to introduce a slightly different dimensionless measure of $J_0 B_z$.

$$\varepsilon = \left(\frac{2L_y}{\pi}\right)^4 \frac{J_0 B_z}{\Delta\rho g h H L_x L_y} = \left(\frac{2L_y}{\pi}\right)^4 \frac{k_B^2}{L_x L_y} \tag{11.22c}$$

11.5 Travelling Wave and Standing Wave Instabilities

Our shallow-water equation supports both travelling waves and standing waves. We shall show that both may become unstable.

11.5.1 Travelling waves

Consider an infinitely long channel of width L, say $0 < x < L$, as shown in Figure 11.6. The easiest way of identifying travelling waves is to write both Ψ and ϕ_P in the form

$$\phi_P = \hat{\phi}(x)\exp[j(\omega t - k_y y)]$$

and define a second wavenumber, k_x, through the expression $k_x^2 = (\omega^2/c^2) - k_y^2$. Then (11.19) gives the eigenvalue problem

$$\hat{\phi}'' + k_x^2\hat{\phi} = -k_B^2\hat{\Psi}, \qquad \frac{\partial\hat{\phi}}{\partial x} = 0 \qquad \text{on } x = 0, L$$

$$\hat{\Psi}'' - k_y^2\hat{\Psi} = 0, \qquad \frac{\partial\hat{\Psi}}{\partial x} = jk_y\hat{\phi} \qquad \text{on } x = 0, L$$

After a little algebra this yields a dispersion relationship for k_x in the form

$$2(k_BL)^4\left[\cosh q\cos p - 1 + \frac{1}{2}(p/q - q/p)\sinh q\sin p\right] + (p^2 + q^2)^2(p/q)\sinh q\sin p = 0 \tag{11.23}$$

where $p = k_xL$ and $q = k_yL$. When the Lorentz forces are zero ($k_B = 0$), this gives $k_x = m\pi/L$, which represents conventional travelling waves in a channel. For a finite value of k_B, and for an arbitrary wavenumber, k_y, we can always find a solution of (11.23) for which k_x is real. This represents stable travelling waves. However, (11.23) also supports unstable waves. That is, for real values of k_B and k_y, we can find complex values of k_x

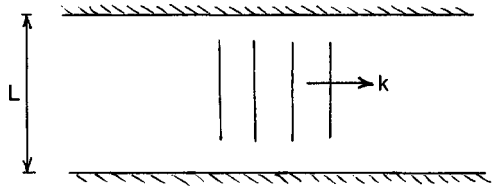

Figure 11.6 Travelling waves in a channel.

which satisfy (11.23). This leads to complex frequencies and therefore to unstable motion. Figure 11.7 shows the neutral stability curve for waves in the range $0 < q < 10$.

11.5.2 Standing waves in circular domains

We now consider waves in a closed, circular domain. This is of interest as it demonstrates the instability in a particularly simple way. Suppose the fluids occupy the domain $0 < r < R$, and consider solutions of the form

$$\phi_P = \hat{\phi}(r)\exp[j(\theta - \omega t)], \qquad \Psi = \hat{\Psi}(r)\exp[j(\theta - \omega t)]$$

It is readily confirmed that (11.19) requires $\hat{\Psi}$ to be linear in r, $\hat{\Psi} = Ar$, and that $\hat{\phi}$ takes the form

$$\hat{\phi}(r) = BJ_1(kr) - (k_B^2/k^2)Ar, \qquad k = \omega/c$$

where J_1 is the usual Bessel function. Boundary conditions (11.21) require

$$\hat{\phi}'(R) = 0, \qquad \hat{\phi}(R) = jRA$$

which yields the dispersion relation

$$k_B^2 J_2(kR) = jk^2 J_1'(kR)$$

This requires that k is complex, and so the waves are unstable for all non-zero k_B. The key point, though, is that the interface near marginal stability is of the form

$$\eta \sim J_1(kr)\sin(\theta - \omega t)$$

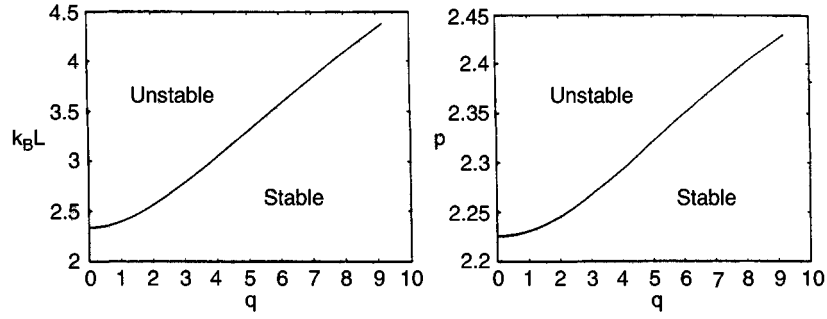

Figure 11.7 Neutral stability curves corresponding to (11.23).

which represents a rotating, tilted interface. This is precisely what is expected from the compound pendulum analogue.

11.5.3 Standing waves in rectangular domains

We now turn to rectangular domains. Here it is convenient to rewrite (11.19) in matrix form. This can be achieved by expanding $\mathbf{q}_P$ in a set of orthogonal cosine functions ψ_i of the form

$$\mathbf{q}_P = \sum \mathbf{q}_i = \sum k_i^{-1} x_i(t) \nabla \psi_i$$

$$\psi_i = \psi_{mn} \sim \cos(m\pi x/L_x) \cos(n\pi y/L_y)$$

$$k_i^2 = k_{mn}^2 = (m\pi/L_x)^2 + (n\pi/L_y)^2$$

Here $x_i(t)$ are the amplitudes of the modes. Of course, ψ_i are just the gravitational modes in the absence of Lorentz forces, and k_i are the corresponding wavenumbers.

We now take the dot-product of (11.18) and $\nabla\psi_i$ and integrate over V. The result is

$$\ddot{x}_i(t) + \omega_{gi}^2 x_i = \omega_B^2 \sum K_{ij} x_j \tag{11.24}$$

where ω_{gi} are the gravitational frequencies and the interaction matrix K_{ij} has elements

$$k_i k_j K_{ij} = \int (\nabla\psi_j \times \nabla\psi_i)_z dV \tag{11.25}$$

We have normalized ψ_i such that

$$\int \psi_i^2 dV = 1 \tag{11.26}$$

Note that K_{ij} is skew-symmetric and has all of its diagonal elements equal to zero:

$$K_{ij} = -K_{ji} \tag{11.27}$$

Finally we truncate x_i at some suitably small wavenumber and rewrite (11.24) in matrix form:

$$\ddot{\mathbf{x}} + \boldsymbol{\Omega}_g \mathbf{x} = \omega_B^2 \mathbf{K} \mathbf{x} \tag{11.28}$$

Let us now consider some of the more general properties of (11.28). Consider the case where ω_B is much greater than the gravitational frequencies of the truncated system. In this case, (11.28) gives

$$\frac{d^4\mathbf{x}}{dt^4} = -\omega_B^4 \mathbf{S}_1 \mathbf{x}, \qquad \mathbf{S}_1 = -\mathbf{K}\mathbf{K} \tag{11.29}$$

The equivalent eigenvalue problem is

$$\mathbf{S}_1\mathbf{x} = -(\omega/\omega_B)^4\mathbf{x} = \lambda\mathbf{x} \tag{11.30}$$

Now $\mathbf{S}_1$ is real, symmetric and has positive diagonal elements. It follows that the eigenvalues, λ_i, are real and at least some of them are positive. We conclude, therefore, that for large ω_B at least some frequencies of our truncated system are complex.

Let us now return to the general eigenvalue problem represented by (11.28):

$$(\boldsymbol{\Omega}_g - \omega_B^2\mathbf{K})\mathbf{x} = \lambda\mathbf{x}, \qquad \lambda = \omega^2 \tag{11.31}$$

Suppose that $\mathbf{x}$ is truncated after N modes and that the diagonal elements of $\boldsymbol{\Omega}_g$ are arranged in order of increasing frequency from ω_{g1}^2 to ω_{gN}^2. Then we may show that in the truncated system the eigenvalues, λ_i, have the following general properties:

(a) $\omega_{g1}^2 \leq \mathrm{Re}(\lambda) \leq \omega_{gN}^2$;
(b) $\sum \lambda_i = \sum \omega_{gi}^2$;
(c) λ_i/ω_B^2 are zero or purely complex if, $\omega_B^2 \gg \omega_{gN}^2$.

These properties are sufficient to define the general behaviour of λ. The first follows from the skew-symmetry of $\mathbf{K}$. That is, if $\bar{x}_i$ is the complex conjugate of x_i, then

$$\sum_i (\omega_{gi}^2 - \lambda)|x_i|^2 = \omega_B^2 \sum_i \sum_j K_{ij} x_j \bar{x}_i$$

If we normalize the eigenvectors to have unit magnitude and take the complex conjugate of the transpose of this equation, we obtain

$$\mathrm{Re}(\lambda) = \sum \omega_{gi}^2 |x_i|^2$$

Condition (a) then follows. Condition (b), on the other hand, arises from the fact that the sum of the eigenvalues equals the trace of $\boldsymbol{\Omega}_g - \omega_B^2\mathbf{K}$, while condition (c) is a standard result for skew-symmetric matrices.

The situation is therefore clear. As ω_B is increased, the eigenvalues move along the real axis but remain within the limits $\omega_{g1}^2 < \lambda < \omega_{gN}^2$. At some critical value of ω_B two or more eigenvalues become complex (an inevitable consequence of condition (c)) and do so in the form of complex conjugate pairs (condition (b)). However, the real part of the

complex eigenvalues remain bounded by the least and largest gravitational frequency of the truncated set of modes (condition (a)).

We now present a simple numerical example which illustrates the phenomenon. We shall show that frequently it is not the pair of modes with the closest gravitational frequencies which go unstable first. Moreover, the modes which go unstable at the lowest value of $J_0 B_z$ need not be the most dangerous. Often the highest growth rates are observed in the pairs of modes which are the second or third to go unstable. Of course, it is the modes with the highest growth rates which are most likely to survive the friction which is inevitably present in any real flow. We start by rewriting (11.31) in dimensionless form. We use $k_1 = \pi/L_y$ as a characteristic (inverse) lengthscale and introduce $\hat{k}_i = k_i/k_1$, $\hat{\lambda} = \omega^2/(ck_1)^2$, and

$$\varepsilon = \left(\frac{2L_y}{\pi}\right)^4 \frac{J_0 B_z}{\Delta\rho g h H L_x L_y} = \left(\frac{2L_y}{\pi}\right)^4 \frac{\omega_B^2}{c^2 L_x L_y}$$

Consider the case $L_y/L_x = 0.3$, which is typical of a real cell. The trajectories of the eigenvalues in the complex plane are shown in Figure 11.8. Three ranges of ε are indicated, corresponding to $\varepsilon < 0.12$, $\varepsilon < 0.15$ and $\varepsilon < 0.20$. Figure 11.8(a) shows that, by $\varepsilon = 0.12$, one pair of eigenvalues has coalesced and moved into the complex plane. In fact, these complex eigenvalues first appear at $\varepsilon = 0.0577$, through the interaction of the (3, 0) and (0, 1) modes. (We classify the eigenvalues in terms of their mode number (m, n) when $\varepsilon = 0$). By $\varepsilon = 0.15$, the complex eigenvalues have returned to the real axis and a new pair of unstable frequencies have appeared. This arises from an interaction of a (2, 0)mode with one of the pair of previously unstable eigenvalues. By $\varepsilon = 0.2$ two additional unstable pairs have appeared. One arises from the interaction of (1, 1) and (2, 1) modes, and the other through the interaction of the (1, 0) mode with the second of the pair of previously unstable modes. The behaviour is summarised in Table 11.1.

Table 11.1. *Formation of unstable frequencies*

Instability	Modes	Comments
First...	(3, 0) + (0, 1)	Restabilises
Second...	(2, 0) + ½[(3, 0) + (0, 1)]	–
Third...	(1, 1) + (2, 1)	Furthest to the right
Fourth...	(1, 0) + ½[(3, 0), (0, 1)]	Furthest to the left

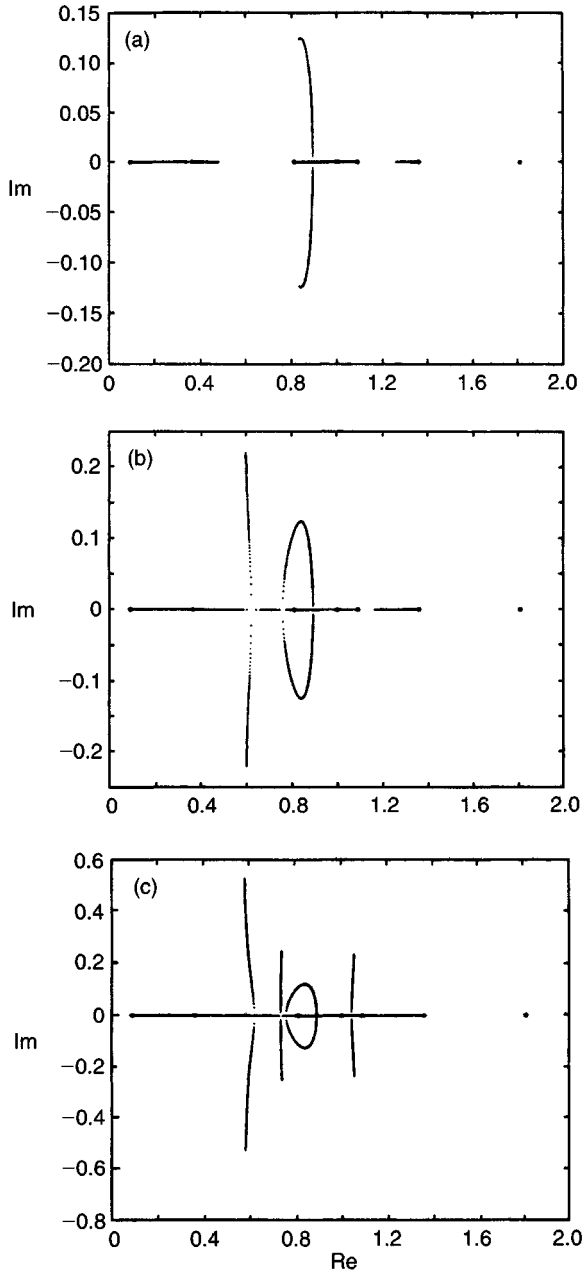

Figure 11.8 Instabilities in a rectangular cell, $L_y/L_x = 0.3$.

This simple example exhibits two interesting features. First, it is not the modes with the closest gravitational frequencies ω_{gi} which go unstable. In fact, the closest gravitational frequencies are the (0, 1) and (1, 1) modes, yet at no time do they combine to produce an instability. Second, by $\varepsilon = 0.2$, the largest growth rate is exhibited not by the first instability, but by the fourth one. Given that any real flow has dissipation, it is this last instability which is the most likely to appear in practice.

Notice that the first instability appears at quite low values of ε, $\varepsilon = 0.0577$ (i.e., $\omega_B L_y/c = 1.08$). The idea is that, while ω_B is still quite small, two adjacent frequencies might interact, converge and move off onto the complex plane. If the initial frequencies are close, this interaction is a local one, in the sense that it does not involve the other modes. This, in turn, leads to the idea that modes with close gravitational frequencies are dangerous. However, it is important to note that **K** is very sparse. Indeed only around one in five mode-pairs are coupled. In general, then, relatively few modes exchange energy. It is not difficult to show that an instability cannot develop from these uncoupled modes, so it is only the separation of the coupled modes which is important. Thus a stability criterion based on keeping all gravitational modes apart is overly conservative. This point is of considerable practical importance.

11.6 Implications for Reduction Cell Design

There are many idealisations embedded in our stability analysis, and so it would be imprudent to consider it as representing an accurate working model of a real cell. Nevertheless, it does capture the key instability mechanism and so the broad conclusions of the model should be valid. It follows that if we wish to avoid instabilities it is sensible to:

(i) choose the cell aspect ratio L_x/L_y to ensure that the natural frequencies of the dominant interfacial waves are well separated;
(ii) minimise the ambient vertical field, B_z;
(iii) carefully control the fluid depths, h and H.

If we wish to eliminate the instability completely then more drastic action is required. One possibility is to introduce baffles into the liquid aluminium, whose function is to break up the long-wavelength sloshing motions. Another is to monitor the interface position continuously, and slowly tilt or move the anode in sympathy with any wave so as to keep the electrolyte thickness roughly uniform. This will prevent the build

up of large current perturbations and so remove the driving force for the instability. However, there are many practical problems associated with these modifications. Perhaps Tolstoy was right when he suggested that it is easier to hypothesise than to act.

Examples

11.1 The depth of the electrolyte in present-day reduction cells is around 5 cm. Estimate the annual savings which would result from reducing this by 1 cm.

11.2 There are at least three simple ways of eliminating the instability. Two are listed above. The third is to use sloping cathode blocks to continuously drain the aluminium and so avoid the build-up of a thick aluminium layer. Why do you think this has not been implemented?

11.3 Find the normal mode shape for the oscillations of the compound pendulum shown in Figure 11.5. Confirm that for large ε the mode consists of a rotating, tilted plate.

11.4 Give a simple physical explanation, based on the compound pendulum, why travelling wave instabilities in a channel are inevitable.

12

High-Frequency Fields: Magnetic Levitation and Induction Heating

> Electricity is of two kinds, positive and negative. The difference is, I presume, that one comes a little more expensive, but is more durable; the other is a cheaper thing, but the moths get in.
>
> *Stephen Leacock*

A high-frequency induction coil can be used to heat, levitate and stir liquid metal. This has given rise to a number of metallurgical processes, some old (such as induction furnaces) and some new. In this chapter, we shall discuss five.

(i) *Induction furnaces.* These have remained virtually unchanged for the best part of a century, yet we are still unable to calculate reliably the stirring velocity within a furnace!

(ii) *Cold crucible melting.* This is an ingenious process which combines the functions of an induction melter and a continuous caster, all in one device.

(iii) *Levitation melting.* This is now routinely used in the laboratory to melt small specimens of highly reactive metals. Unfortunately, if the levitated drop becomes too large, it tends to drip.

(iv) *The electromagnetic valve.* This provides a non-contact means of modulating and shaping a liquid-metal jet. It is a sort of levitation melter in which the metal is allowed to leak out of the bottom.

(v) *Electromagnetic casting.* Some aluminium producers have replaced the casting mould in a continuous caster by a high-frequency induction coil. Thus, the melt pool is supported by magnetic pressure rather than by mechanical means. It is extraordinary that large ingots, which may be a metre wide and ten metres long, can be formed by pouring the liquid metal into free space and soaking it with water jets!

These industrial processes are described in Section 3 of this chapter. First, however, there is some work to do. We need to develop expressions for the levitation force per unit area (magnetic pressure), the heating rate per

unit volume, and the stirring force (the rotational part of $\mathbf{J} \times \mathbf{B}$) induced by a high-frequency magnetic field.

12.1 The Skin Effect

We are concerned here with the ability of high-frequency magnetic fields to heat, levitate and stir liquids. All of these processes are controlled by the so-called *skin effect*: the ability of a conducting medium, solid or liquid, to exclude high-frequency fields. In this section, we describe (in words) the physical origin of this phenomenon. In Section 2, we will quantify the process.

The skin effect is most readily understood in the context of solid, rather than fluid, conductors, and so we start with solids. We have already seen that a magnetic field diffuses through a solid conductor according to

$$\frac{\partial \mathbf{B}}{\partial t} = \lambda \nabla^2 \mathbf{B} \tag{12.1}$$

We cannot suddenly *impose* a magnetic field throughout a conductor. All we can do is apply a field at the boundaries and then let it diffuse inward. In fact, we saw in Chapter 4 that a magnetic field diffuses inwards by a distance of under $(2\lambda t)^{1/2}$ in a time t. There is an analogy here with heat. Heat (temperature) diffuses through a thermally conducting medium according to

$$\frac{\partial T}{\partial t} = \alpha \nabla^2 T \tag{12.2}$$

If the surface temperature of a body is suddenly raised by an amount ΔT, then that temperature difference will diffuse inward into the conducting medium, travelling a distance of order $(2\alpha t)^{1/2}$ in a time t.

Let us stay with the thermal analogy as we consider oscillating, rather than steady, boundary conditions. Suppose that the temperature at the surface of some thermally conducting medium oscillates rapidly according to $T = T_0 + \Delta T \sin(\omega t)$, where T_0 is the initial bulk temperature of the medium. Heat is periodically injected into, and extracted from, the conductor. As successive waves of positive and negative temperature difference diffuse inward from the boundary, there is a tendency for them to overlap and cancel. In the limit of a high angular frequency, ω, the temperature fluctuations are felt only in a thin region adjacent to the surface, of thickness $\delta \sim (2\alpha/\omega)^{1/2}$ (Figure 12.1). (This is readily confirmed by looking for oscillatory solutions of (12.2).) What is true of

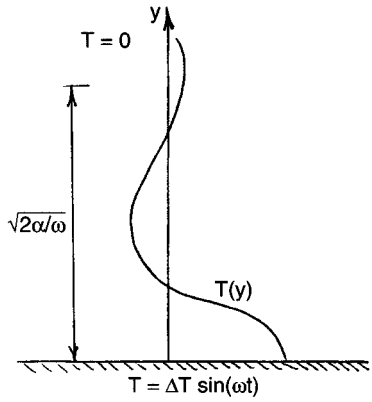

Figure 12.1 Thermal oscillations imposed at a boundary are restricted to thin boundary layers adjacent to that boundary.

T is also true of **B**. If an oscillating magnetic field is applied parallel to the surface of an electrically conducting medium, the field will penetrate only a finite distance, of order $(2\lambda/\omega)^{1/2}$, into the medium. This is illustrated in Figure 12.2.

Now if the magnetic field is excluded from the interior of the medium then there must be currents induced in the surface of the conductor whose direction is, in some average sense, opposite to that of the external currents which generated the field. That is to say, the magnetic field in the interior of the conducting medium is the superposition of two fields: one associated with the external currents and one associated with the induced currents, each calculated in accordance with the Biot–Savart law. If the combined field is to be zero in the interior then the external and induced currents must, in some average sense, oppose each other.

In general, then, a high-frequency magnetic field induces currents in the surface of a conductor whose distribution is such as to shield the interior of the conductor from the imposed field. These currents are restricted to a thin surface layer of thickness $\delta \sim (2\lambda/\omega)^{1/2}$, called the *skin depth*. In fact, we take as our working definition of the term 'high frequency' that δ must be much less than any relevant geometric length scale, say the characteristic size of the body. Now the fact that a magnetic field is shielded from the interior of a conductor is not, in itself, particularly important in metallurgical MHD. However, the existence of a thin surface layer of induced current is useful. Opposite currents repel each other, and so the conductor shown in Figure 12.2 will experience a sideways repulsion

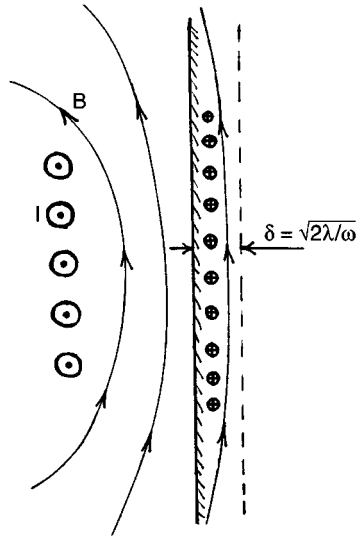

Figure 12.2 A high-frequency magnetic field is shielded from the interior of a conductor by the formation of surface currents which are restricted to a thin layer of thickness $(2\lambda/\omega)^{1/2}$.

force. Moreover, the induced currents will heat the conductor. It is the ability of high-frequency conductors to repel and heat conducting material, liquid or solid, which is the key to many industrial processes.

12.2 Magnetic Pressure, Induction Heating and High-Frequency Stirring

Let us now quantify the arguments of the previous section. We shall derive expressions for:

(i) the levitation force;
(ii) the surface heating rate;
(iii) the stirring force (the rotational part of $\mathbf{J} \times \mathbf{B}$).

Suppose that we have a magnetic field $\mathbf{B} = B_0 \cos(\omega t)\hat{\mathbf{e}}_z$ applied at the surface of a conducting fluid, as shown in Figure 12.3. In the first instance we shall take B_0 to be uniform. Let us assume that the velocity of the fluid is everywhere much less than ωl, where l is the smallest characteristic length scale of the problem. (This is almost always true in practice.) Then, for the purposes of calculating $\mathbf{B}$, we may treat the fluid as a

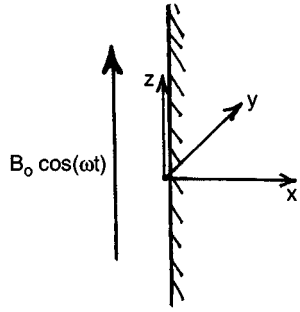

Figure 12.3 A simple model problem.

stationary, solid conductor. The governing equation for **B** simplifies to (12.1), which has the simple solution

$$\mathbf{B} = B_0 \exp(-x/\delta)\cos(\omega t - x/\delta)\hat{\mathbf{e}}_z, \qquad \delta = (2\lambda/\omega)^{1/2}$$

As expected, **B** is confined to a thin layer of thickness $\sim \delta$. The induced current is given by Ampère's law which, for this geometry, simplifies to

$$\mathbf{J} = -\frac{1}{\mu}\frac{\partial B_z}{\partial x}\hat{\mathbf{e}}_y \tag{12.3}$$

Substituting for B_z we find

$$J_y = (B_0/\mu\delta)\exp(-x/\delta)[\cos(\omega t - x/\delta) - \sin(\omega t - x/\delta)] \tag{12.4}$$

The Lorentz force within the skin depth can now be calculated:

$$\mathbf{J} \times \mathbf{B} = J_y B_z \hat{\mathbf{e}}_x = -\frac{\partial}{\partial x}\left[\frac{B_z^2}{2\mu}\right]\hat{\mathbf{e}}_x$$

This contains both a mean and an oscillatory component. However, we are interested only in the time-averaged value of the Lorentz force, since the finite inertia of the fluid means that a high-frequency, oscillatory force induces very little motion in the fluid. The time-averaged force is

$$\overline{\mathbf{J} \times \mathbf{B}} = -\frac{\partial}{\partial x}\left[\frac{B_0^2}{4\mu}\exp(-2x/\delta)\right]\hat{\mathbf{e}}_x \tag{12.5}$$

If we integrate this through the skin depth we find

$$\boxed{\int_0^\infty \overline{\mathbf{J} \times \mathbf{B}}\,dx = \frac{B_0^2}{4\mu}\hat{\mathbf{e}}_x} \tag{12.6}$$

This is the repulsion force anticipated in the previous section. Of course, $B_0^2/4\mu$ is simply the magnetic pressure which is an inevitable consequence of $|\mathbf{B}|$ dropping from B_0 to zero across the skin depth.

It is also of interest to calculate the Joule dissipation, J^2/σ, within the fluid. Integrating J^2/σ across the skin depth gives the net heating rate per unit surface area. It is readily confirmed that

$$\boxed{\dot{q} = \int_0^\infty (J^2/\sigma)dx = (B_0^2/4\mu)\omega\delta} \tag{12.7}$$

Let us now consider some of the consequences of allowing B_0 to vary slowly along the surface, as indicated in Figure 12.2. Let L be a typical geometric length scale, say $B_0/(\partial B_0/\partial z)$. We shall take $L \gg \delta$. (Recall that this is our working definition of 'high-frequency'.) When $L \gg \delta$, expressions (12.6) and (12.7) remain valid (to leading order in δ/L) provided that B_0 is interpreted as the local field strength. However, allowing B_0 to vary slowly within z introduces an additional effect: it induces motion in the fluid.

Consider the simplest case where $\mathbf{B}$ is two-dimensional: $(B_x, 0, B_z)$. The variation of B_z along the surface implies that B_x is non-zero, and in fact $\nabla \cdot \mathbf{B} = 0$ fixes the horizontal field as

$$B_x = \frac{\delta}{2}\frac{\partial B_0}{\partial z}[\cos(\omega t - x/\delta) + \sin(\omega t - x/\delta)]\exp(-x/\delta) \tag{12.8}$$

Since we have a small but finite horizontal field, the Lorentz force takes on a slightly different form. To find this force it is convenient to rewrite $\mathbf{J} \times \mathbf{B}$ as

$$\mu\mathbf{J} \times \mathbf{B} = -\nabla(B^2/2) + (\mathbf{B} \cdot \nabla)\mathbf{B}$$

We now throw out all terms of order $(\delta/L)^2$ and smaller. The result is

$$\mu\mathbf{J} \times \mathbf{B} = -\nabla(B_z^2/2) + \left[B_z\frac{\partial B_z}{\partial z} + B_x\frac{\partial B_z}{\partial x}\right]\hat{\mathbf{e}}_z$$

This can be further simplified. Noting that

$$\partial B_z/\partial x = (B_0/\delta)\exp(-x/\delta)[-\cos(\omega t - x/\delta) + \sin(\omega t - x/\delta)]$$

it is evident that $B_x(\partial B_z/\partial x)$ has zero time average, and so the mean Lorentz force is

$$\overline{\mathbf{J} \times \mathbf{B}} = -\nabla\left[\frac{B_0^2}{4\mu}\exp(-2x/\delta)\right] + \left[\frac{B_0}{2\mu}\frac{\partial B_0}{\partial z}\exp(-2x/\delta)\right]\hat{\mathbf{e}}_z \qquad (12.9)$$

We may regard $\overline{\mathbf{J} \times \mathbf{B}}$ as being composed of two parts. The first is irrotational and for confined fluids this merely supplements the fluid pressure. It is this term which leads to the magnetic pressure, $B_0^2/4\mu$. The second term is rotational and so cannot be balanced by the fluid pressure. It is much smaller than the first and is directed along the surface towards the peak value of B_0. This tangential force drives a fluid motion within the skin depth, pushing fluid from regions of low magnetic pressure to those of high magnetic pressure, as shown in Figure 12.4.

In summary, then, a high-frequency magnetic field, imposed at the boundary of a conducting fluid, has three effects:

(i) it repels the surface with a magnetic pressure of $B_0^2/4\mu$;
(ii) it generates heat at a rate of $(B_0^2/4\mu)\,\omega\delta$ per unit surface area;
(iii) it induces a tangential force $\partial/\partial z(B_0^2/4\mu)\exp(-2x/)\hat{\mathbf{e}}_z$ which drives fluid motion from regions of low magnetic pressure to regions of high pressure.

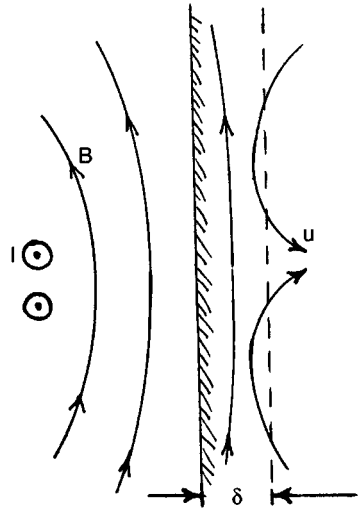

Figure 12.4 Motion induced by a variation in surface field strength.

12.3 Applications in the Casting of Steel, Aluminium and Super-Alloys

12.3.1 The induction furnace

The first induction furnace was designed by Ferranti in 1887. It reached more or less its present form around the turn of the century and has changed very little over the last one hundred years. The so-called 'coreless' induction furnace consists of a cylindrical, refractory vessel, filled with liquid metal, and surrounded by a high-frequency induction coil in the form of a solenoid. The coil generates a magnetic field which is almost parallel to the axis of the vessel, but which is confined to the skin depth of the molten pool. The primary purpose of the magnetic field is to heat the metal, although it has the added effect of stirring the liquid. This stirring turns out to be useful because it provides an effective mechanism for transporting the heat created at the boundaries into the interior of the liquid. However, it has the disadvantage that excessive velocities can lead to the erosion of the vessel wall.

We have already seen that the stirring force is confined to regions where the magnetic field varies along the surface of the melt. That is to say, the rotational component of $\overline{\mathbf{J} \times \mathbf{B}}$ is, from (12.9),

$$\mathbf{F}_r = \frac{\partial}{\partial s}\left(\frac{B_0^2}{4\mu}\right)\exp(-2n/\delta)\hat{\mathbf{e}}_s \tag{12.10}$$

Here the subscript 'r' indicates a rotational force, $B_0(s)$ is the surface field, s is a coordinate measured along the boundary and n is the distance from the surface. An inspection of Figure 12.5 suggests that this stirring force is confined largely to the corner regions of the furnace where the magnetic field enters and leaves the metal. In fact, this is often the case, and so the motion in the fluid is largely determined by the magnetic field distribution in a relatively small part of the furnace. This has two consequences. First, there exists the interesting possibility of controlling the flow by making small local changes to **B**. Second, if the driving force for **u** is rather sensitive to small geometrical features then it may be difficult to formulate simple, reliable estimates of $|\mathbf{u}|$. Still, we might expect the gross flow pattern to be like that shown in Figure 12.5. The rotational Lorentz force will drive fluid along the walls from the corner regions, where the magnetic pressure is low, to the midplane of the furnace where B_0 is high. This flow will then recirculate back through the core of the furnace, giving us an axisymmetric flow pattern consisting of two toroidal vortices. (If the stirring force in one

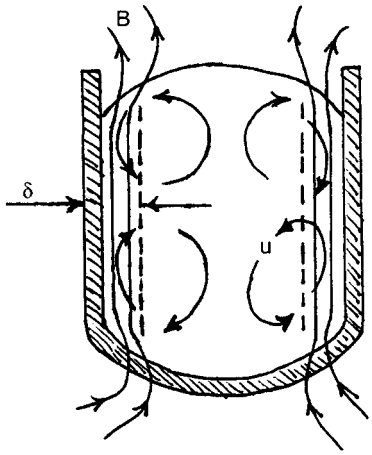

Figure 12.5 An induction furnace.

corner greatly outweighs the force in the other, then one of the toroidal vortices may be suppressed.

We shall now try to estimate the magnitude of $|\mathbf{u}|$. The procedure is somewhat circuitous, in that we first estimate the turbulence level in the furnace and then try to estimate the magnitude of the mean flow which would support such a level of turbulence. The arguments are all a bit rough and ready, but they do furnish estimates which are reasonably in line with experiments.

The starting point is to integrate the time-averaged Navier–Stokes equation around a closed streamline. When conditions are steady on average, this yields

$$\frac{1}{\rho}\oint \mathbf{F}_r \cdot d\mathbf{l} + \oint \frac{\partial}{\partial x_i}\left(\frac{\tau_{ij}}{\rho}\right) dl_j = 0 \tag{12.11}$$

where $\mathbf{u}$ is time-averaged velocity and τ_{ij} is the Reynolds stress. This represents an energy balance. It states that the work done by $\mathbf{F}_r$ on a fluid particle moving once around a closed streamline must be exactly balanced by the (negative) work done by the frictional shear stresses. If the two did not balance then the fluid particle would return to its starting position with a different mean energy, which cannot be the case in a steady-on-average flow. Now τ_{ij} might be estimated as $\tau_{ij} \sim \rho u'^2$ where u' is a measure of the fluctuating velocity. It follows from (12.11) that

$$\oint \mathbf{F}_r \cdot d\mathbf{l} \sim \rho u'^2 l / l_\tau$$

where l is a characteristic geometric length scale and l_τ is a typical length scale for cross-stream gradients in τ_{ij}. Substituting for $\mathbf{F}_r$ yields

$$u' \sim \frac{B_0}{\sqrt{\rho\mu}} \left(\frac{l_\tau}{l}\right)^{1/2}$$

However, we are interested in the mean velocity $\mathbf{u}$, rather than u'. In many forced, confined flows u' is around one-third of the peak mean velocity. If this is true in an induction furnace (and there are measurements to suggest it is), we might anticipate that the peak stirring velocity is of the order of

$$u \sim \frac{3B_0}{(\rho\mu)^{1/2}} \left(\frac{l_\tau}{l}\right)^{1/2} \tag{12.12}$$

The next question is, of course: what is l_τ? Some researchers assume that, since $\mathbf{F}_r$ is concentrated in a thin surface region of thickness δ, the flow near the wall must consist of thin wall jets, of thickness δ, which are driven by $\mathbf{F}_r$. These jets start near the corners of the furnace and direct fluid along the walls towards the mid-plane where opposing jets collide, driving fluid out into the core. If this is all true, then the bulk of the turbulent dissipation will be confined to the wall regions. In such cases l_τ should be taken as δ, and (12.12) yields (Hunt & Maxey, 1980)

$$u \sim \frac{3B_0}{(\rho\mu)^{1/2}} \left(\frac{\delta}{l}\right)^{1/2} \tag{12.13a}$$

An alternative possibility is that jets do not form and so the dissipation is distributed across the whole of the flow, in which case $l_\tau \sim l$ and we have the simpler estimate

$$u \sim \frac{3B_0}{(\rho\mu)^{1/2}} \tag{12.13b}$$

There are many assumptions and approximations built into (12.13a, b). Somewhat surprisingly, the experimental data tend to support (12.13a, b). It is found that u does indeed scale linearly with $B_0/(\rho\mu)^{1/2}$, and typically it is of the order of $B_0/(\rho\mu)^{1/2}$. It is less clear, however, which of these two estimates is the better. In most experiments $(\delta/l)^{1/2}$is around $0.4 \rightarrow 0.8$, and in view of the uncertainty in the multiplying factor of 3 it is not possible to distinguish clearly between (12.13a) and (12.13b) by simply examining the magnitude of u. A better test is to examine the dependence of u on ω, since (12.13a) suggests $u \sim \omega^{-1/4}$ while (12.13b) gives u independent of ω. The experiments indicate a behaviour some-

where between the two (Taberlet & Fautrelle, 1985), suggesting that (12.13a,b) are really too simplistic and that a more detailed analysis is required. So one hundred years after its introduction, we are still unable to estimate the velocity induced in an induction furnace!

12.3.2 The cold crucible

We now consider a device known as the cold crucible. This is designed to both melt and cast a metal in a single operation. The upper part of the crucible acts like an induction furnace, into which solid material is fed. This is inductively melted to form a liquid pool. The lower part acts like a casting mould, in which the liquid metal freezes on contact with the cold walls of the crucible. In steady-state operation solid fragments are continually fed in from above, while an ingot is withdrawn from the bottom. A schematic representation of the process is shown in Figure 12.6.

The name 'cold crucible' derives from the fact that the walls of the vessel are constructed from water-cooled metal segments which cause the molten pool to freeze on contact with the vessel wall. This is quite different from an induction furnace whose insulating, refractory walls are hot, leaving the metal as a liquid. The ingenious part of the cold crucible lies in the construction of the wall. In order to heat the metal it is necessary to find some way of allowing the magnetic field to pass through the conducting wall of the crucible. This is achieved by segmenting the wall, as shown in Figure 12.6. Each segment is electrically insulated and so the eddy currents which are induced in the outer surface of the wall, and which would ordinarily shield the interior from the applied field, are forced to recirculate around each segment. The end result is a smooth distribution of current on the inside surface of the wall, which in turn generates a magnetic field in the interior of the crucible. It is as if the segmented wall is transparent to the magnetic field. The lower part of the vessel acts just like a conventional casting mould, with the liquid freezing on contact with the water-cooled metal wall. As in conventional casting, it is necessary to feed small quantities of casting flux down the gap between the ingot and the crucible wall. This acts as a lubricant and provides a thin thermal barrier between the ingot and the walls.

Cold crucibles are also used to melt material in batches, rather like an induction furnace. In such cases the bottom of the crucible is blanked off using a segmented, water-cooled plate. The bulk of the crucible contents is then liquid, but we retain a thin crust of solid metal (called a skull)

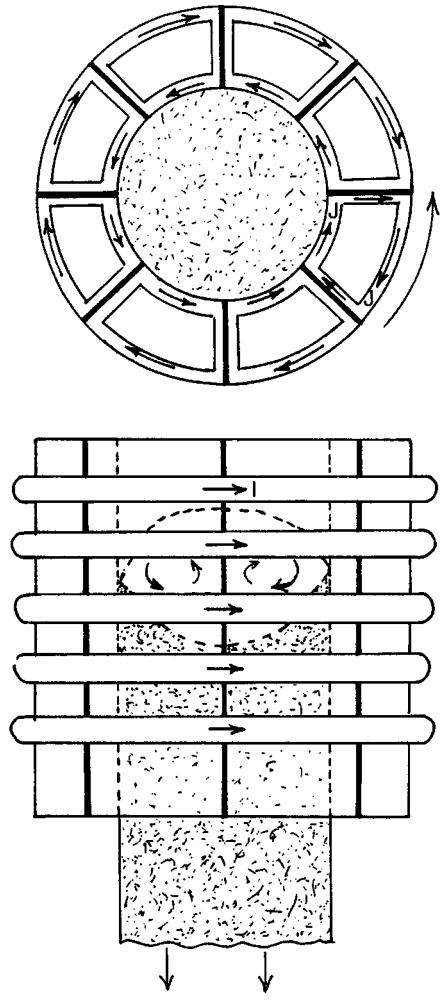

Figure 12.6 A cold crucible consists of water-cooled segments surrounded by a high-frequency induction coil.

adjacent to the walls and base. This is often used to melt highly reactive metals, such as titanium or nickel, which would attack the refractory walls of a conventional furnace.

12.3.3 Levitation melting

We now turn to industrial and laboratory processes where the primary function of the magnetic field is to levitate or repel the liquid metal.

These, of course, rely on the existence of the magnetic pressure, $B_0^2/4\mu$. In this section we focus on levitation melting, a technique which was first suggested in 1923, but had to wait until the 1950s to be tried in the laboratory, and the 1960s to be developed commercially.

Levitation melting is now commonly used in the laboratory as a means of melting small specimens of highly reactive metal. It is also used as a means of measuring the surface tension of liquid metals. The topics we will discuss here are:

(i) the shape of the levitation coils;
(ii) the fact that the process is pseudo-static (the induced velocities are low);
(iii) there is a limit on the drop size which may be levitated;
(iv) a method for calculating the drop shape;
(v) a variational principle associated with the drop shape.

A simple levitation device is shown in Figure 12.7. It consists of a lower toroidal coil, wound into a basket shape, above which sits the metal droplet. A second, smaller, coil is located above the specimen and this carries a current which is 180° out of phase with the lower coil. We shall see shortly that there is a strict limit to the size of specimens which may be levitated in this way: typically the droplet size is no more than one or two centimetres. Since we require $\delta \ll$ (drop size) in order to generate magnetic pressure, this implies that high frequencies are required, of the order of 100 kHz.

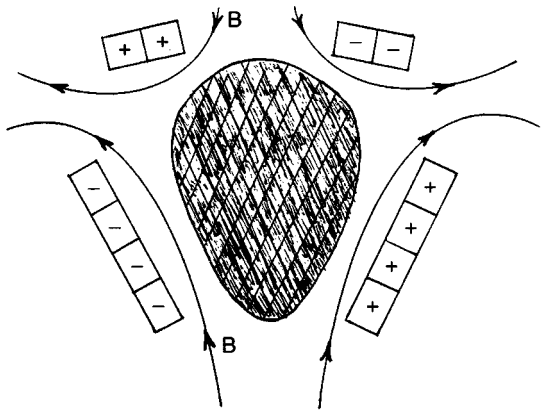

Figure 12.7 Levitation melting of a small metal specimen.

The two coils shown in Figure 12.7 have rather different functions. The lower coil provides support against the weight of the metal. The top coil, on the other hand, is required to provide stability. That is, the introduction of the upper coil creates a field configuration which, in the absence of the specimen, has a null point somewhere on the axis between the two coils. A small test specimen placed at such a point is stable to small lateral movements because any movement of the specimen brings it into a region of higher magnetic field, and the resulting change in magnetic pressure will tend to push the metal back towards the null point. At least that is the theory. In practice, instabilities such as vertical oscillations and rotations often develop.

In order to understand the shape of the levitated droplet, and to predict the maximum mass which can be levitated, it is necessary to consider the balance between magnetic pressure, fluid pressure (which is due to self-weight) and surface tension. Usually this balance may be treated as pseudo-static, in the sense that the effect of motion on the fluid pressure may be ignored. The reason for this simplification is as follows. The rotational component of the Lorentz force, which drives motion in the droplet, is of order $|\mathbf{F}_r| \sim B_0^2/\mu l$ where B_0 is the surface field strength and l is a typical geometric length scale (say the droplet size). This force acts parallel to the surface. Now suppose we integrate this through the (narrow) skin depth and replace the distributed force by an effective shear stress of order $\tau \sim (B_0^2/\mu)(\delta/l)$. Compare this with the magnetic pressure, $p_m = B_0^2/4\mu$. Evidently, since δ is much less than l, we have $\tau \sim p_m(\delta/l) \ll p_m$. However, τ leads to fluid motion, while p_m counterbalances the hydrostatic pressure, and so we would expect $\rho u^2 \ll \rho g l$ in the limit of $\delta \ll l$. Thus, if our sole purpose is to determine the equilibrium shape of the drop, we may ignore $\mathbf{F}_r$ and the associated motion within the liquid. It follows that the surface shape is determined by the pseudo-static force balance

$$\frac{B_0^2}{4\mu} + \rho g z + \gamma K = \text{constant}$$

where K is the surface curvature, z is the vertical position of the surface and γ is the surface tension coefficient. If we take the origin of z to be at the base of the droplet, and note that the Lorentz force is zero at $z = 0$, we obtain

$$\frac{B_0^2}{4\mu} + \rho g z + \gamma K = \gamma K_0 \tag{12.14}$$

where K_0 is the curvature at the base of the drop.

It is now clear that there is a fundamental limitation to this process. In any axisymmetric configuration the induced currents fall to zero on the axis, and so the magnetic pressure is zero at the base and the top of the drop. It follows that the hydrostatic pressure on the axis must be balanced by surface tension alone, and this limits the height of the droplet which can be levitated. We can estimate this critical height, h_c, from (12.14). The maximum value of K_0 will be of order δ^{-1}, since we require the local droplet thickness to be greater than δ in order to maintain some magnetic pressure. If we take K at the top of the drop to be much less than K_0, which seems reasonable, then (12.14) gives $\rho g h_c \sim \gamma/\delta$ and so the critical height is of the order of

$$h_c \sim \gamma/\rho g \delta \tag{12.15}$$

Drops larger than this will tend to drip near the axis.

The process of calculating the drop shape, although pseudo-static, is still non-trivial. This is because the shape depends on the distribution of $\mathbf{B}_0(s)$, the surface field strength. Yet $\mathbf{B}_0(s)$ itself depends on the presence and shape of the drop since the field is excluded from the interior of the drop and so must deform around its surface. In general, it is necessary to adopt an iterative approach to calculate the shape, in which an initial guess of the surface profile leads to a provisional estimate of $\mathbf{B}_0(s)$. (This is obtained by solving $\nabla \cdot \mathbf{B} = 0$ and $\nabla \times \mathbf{B} = 0$ outside the droplet, subject to $\mathbf{B} \cdot \mathbf{n} = 0$ on the drop surface.) From this estimate of $\mathbf{B}_0(s)$ the magnetic pressure can be calculated and compared with that required to hold the droplet in its chosen shape. At points the actual magnetic pressure will be greater than that required by (12.14) and at other positions it will be too small. The surface shape is then changed slightly, moving outward at places where p_m is found to be too small and inward where p_m is excessive. The procedure is now repeated for the new estimate of the drop shape. After a few iterations a solution of (12.14) can be found which is compatible with the external coil geometry.

An alternative iterative procedure for calculating the drop shape can be established using a variational principle. This principle applies only in the limit $\delta \to 0$ and assumes that the electric current in the external coils is fixed and independent of the droplet shape. We proceed as follows. We know that the equilibrium configuration, if stable, must correspond to a minimum value of $E_g + E_\gamma + E_p$ where E_g is the total gravitational potential energy, E_γ is the surface tension energy, and E_p is the potential energy associated with the magnetic pressure. This latter energy is the work done

against p_m by the fluid boundary in establishing the presence of the drop. (Imagine blowing up a balloon which is subject to some external pressure.) The complication is that p_m itself depends on the presence and shape of the drop, and so we need some way of calculating E_p. It turns out that, to within a constant, E_p is (minus) the energy of the external magnetic field.

To see why this is so, consider what happens if the surface S of the droplet deforms slightly. Let δn be the movement of the surface at any point on S, being positive if outward and negative if inward. We now deform the drop, while conserving volume. The work done by the fluid against p_m is

$$\delta W = \oint_S p_m \delta n dS$$

It follows that the increase in E_p caused by this movement is

$$\delta E_p = \oint_S (B_0^2/4\mu)\delta n dS \tag{12.16}$$

Now consider the change in magnetic energy E_B associated with the deformation of the surface. This comes in two parts. First there is the reduction in E_B associated with the fact that the small volume $\delta n dS$ previously contained a magnetic field which had an energy of $(B_0^2/4\mu)(\delta n dS)$. Second, the deformation of the drop changes the eddy currents circulating in its surface, and this leads to a change in the external magnetic field. If V_{ext} is external volume we have

$$\delta E_B = \delta \int_{V_{ext}} (B^2/4\mu) dV - \oint_S (B_0^2/4\mu)\delta n dS \tag{12.17}$$

However, it is easily seen that the first integral is zero. To this end we write $\mathbf{B} = \mathbf{B}_1 + \mathbf{B}_2$, where $\mathbf{B}_1$ is the field due to the coil which would exist in the absence of the drop and $\mathbf{B}_2$ is the field associated with the eddy currents in the surface S. Within the drop $\mathbf{B}_1$ and $\mathbf{B}_2$ are equal and opposite. Outside we have $\delta(\mathbf{B}^2) = 2\mathbf{B} \cdot \delta\mathbf{B} = 2\mathbf{B} \cdot \delta\mathbf{B}_2$ since $\delta\mathbf{B}_1 = 0$, the coil current being fixed. However, $\delta\mathbf{B}_2$ satisfies $\nabla \times \mathbf{B} = 0$ in V_{ext} and so this can be written as $\delta\mathbf{B}_2 = \nabla(\phi)$. This yields $\delta(\mathbf{B}^2) = 2\nabla \cdot (\phi\mathbf{B})$, which integrates to zero in V_{ext} since $\mathbf{B} \to 0$ at infinity and $\mathbf{B} \cdot \mathbf{n} = 0$ on S. It follows that

$$\delta E_B = -\oint_S (B_0^2/4\mu)\delta n dS = -\delta E_p \tag{12.18}$$

It follows that the equilibrium configuration corresponds to a stationary value of $E_g + E_\gamma - E_B$ (Sneyd & Moffatt, 1982). This provides the basis for an alternative iterative procedure for finding the droplet shape, i.e. the boundary is systematically deformed so as to minimise $E_g + E_\gamma - E_B$.

12.3.4 Processes which rely on magnetic repulsion: EM valves and EM casters

Suppose we increase the mass of the droplet shown in Figure 12.7 until the critical height, h_c, is exceeded. The drop will start to drip, and if h is made large enough a small jet will emerge, centred on the axis. If the droplet mass is continually replenished from above we have a rudimentary form of electromagnetic valve. The simplest embodiment of such a device is shown in Figure 12.8. This provides a means of modulating the flow of a liquid-metal jet without the need for any moving mechanical part. By increasing the power in the induction coil, the flow rate through the electromagnetic valve is reduced.

A simple estimate of the reduction in flow rate may be determined by applying Bernoulli's equation from some upstream location, say the surface of the reservoir which feeds the valve, to the point at which the jet separates from the nozzle wall. The pressure in the jet at the separation point is p_m (atmospheric pressure being taken as a datum for pressure). In the absence of friction, Bernoulli's equation yields

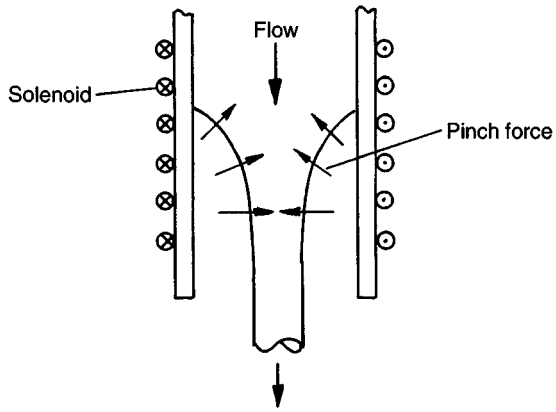

Figure 12.8 A simple electromagnetic valve.

$$\rho g H = \frac{1}{2}\rho u^2 + p_m$$

where H is the head of liquid above the separation point. The mean velocity at the separation point is then

$$u = \left[2gH - B_0^2/(2\rho\mu)\right]^{1/2} \tag{12.19}$$

Of course, this is a rather simplistic estimate, which ignores frictional losses and variations in velocity across the jet. For example, it predicts that the flow is completely shut off at a critical value of magnetic pressure, $p_m = \rho g H$, yet we have already seen that this cannot be true in an axisymmetric configuration. Nevertheless, experiments suggest that (12.19) captures the gross behaviour of the device provided p_m is not too close to the critical value.

A quite different application of magnetic repulsion is illustrated in Figure 12.9. This shows the electromagnetic casting of aluminium, a process which was developed by Getselev in the USSR in 1971 and is now used throughout Europe and North America. In effect, it is identical to the conventional casting of aluminium except that the water-cooled mould which normally surrounds the liquid pool (see Figure 8.1) is replaced by a high-frequency induction coil. However, the mould and coil fulfil similar rôles: they are both required to maintain the pool shape, the former achieving this by mechanical support while the latter uses magnetic pressure. Remarkably, the process turns out to be stable. The primary advantage of electromagnetic casting is that the surface quality of the ingot is improved. This means that the ingot surface does not require machining prior to rolling.

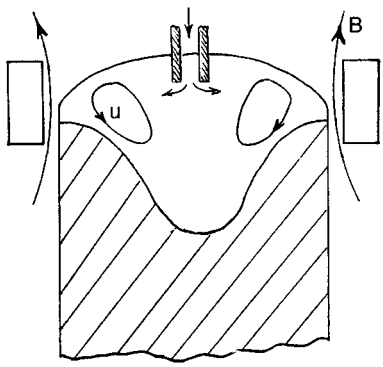

Figure 12.9 Electromagnetic casting of aluminium.

Appendix 1

Vector Identities and Theorems

(1) Grad, div and curl in Cartesian coordinates:

$$\nabla\phi = \frac{\partial\phi}{\partial x}\mathbf{i} + \frac{\partial\phi}{\partial y}\mathbf{j} + \frac{\partial\phi}{\partial z}\mathbf{k}$$

$$\nabla \cdot \mathbf{F} = \frac{\partial F_x}{\partial x} + \frac{\partial F_y}{\partial y} + \frac{\partial F_z}{\partial z}$$

$$\nabla \times \mathbf{F} = \left(\frac{\partial F_z}{\partial y} - \frac{\partial F_y}{\partial z}\right)\mathbf{i} + \left(\frac{\partial F_x}{\partial z} - \frac{\partial F_z}{\partial x}\right)\mathbf{j} + \left(\frac{\partial F_y}{\partial x} - \frac{\partial F_x}{\partial y}\right)\mathbf{k}$$

In cylindrical polar coordinates

$$\nabla\phi = \frac{\partial\phi}{\partial r}\hat{\mathbf{e}}_r + \frac{1}{r}\frac{\partial\phi}{\partial\theta}\hat{\mathbf{e}}_\theta + \frac{\partial\phi}{\partial z}\hat{\mathbf{e}}_z$$

$$\nabla \cdot \mathbf{F} = \frac{1}{r}\frac{\partial}{\partial r}(rF_r) + \frac{1}{r}\frac{\partial F_\theta}{\partial\theta} + \frac{\partial F_z}{\partial z}$$

$$\nabla \times \mathbf{F} = \left(\frac{1}{r}\frac{\partial F_z}{\partial\theta} - \frac{\partial F_\theta}{\partial z}\right)\hat{\mathbf{e}}_r + \left(\frac{\partial F_r}{\partial z} - \frac{\partial F_z}{\partial r}\right)\hat{\mathbf{e}}_\theta + \left(\frac{1}{r}\frac{\partial}{\partial r}(rF_\theta) - \frac{1}{r}\frac{\partial F_r}{\partial\theta}\right)\hat{\mathbf{e}}_z$$

$$\nabla^2\phi = \frac{1}{r}\frac{\partial}{\partial r}\left(r\frac{\partial\phi}{\partial r}\right) + \frac{1}{r^2}\frac{\partial^2\phi}{\partial\theta^2} + \frac{\partial^2\phi}{\partial z^2}$$

(2) Vector identities:

$$\nabla \cdot (\phi \mathbf{u}) = \phi \nabla \cdot \mathbf{u} + \mathbf{u} \cdot \nabla \phi$$
$$\nabla \times (\phi \mathbf{u}) = \phi \nabla \times \mathbf{u} + \nabla \phi \times \mathbf{u}$$
$$\nabla (\mathbf{u} \cdot \mathbf{v}) = \mathbf{u} \times \nabla \times \mathbf{v} + \mathbf{v} \times \nabla \times \mathbf{u} + (\mathbf{u} \cdot \nabla)\mathbf{v} + (\mathbf{v} \cdot \nabla)\mathbf{u}$$
$$\nabla \cdot (\mathbf{u} \times \mathbf{v}) = \mathbf{v} \cdot \nabla \times \mathbf{u} - \mathbf{u} \cdot \nabla \times \mathbf{v}$$
$$\nabla \times (\mathbf{u} \times \mathbf{v}) = \mathbf{u}(\nabla \cdot \mathbf{v}) - \mathbf{v}(\nabla \cdot \mathbf{u}) + (\mathbf{v} \cdot \nabla)\mathbf{u} - (\mathbf{u} \cdot \nabla)\mathbf{v}$$
$$\nabla \times (\nabla \times \mathbf{u}) = \nabla(\nabla \cdot \mathbf{u}) - \nabla^2 \mathbf{u}$$
$$\nabla \times \nabla \phi = 0$$
$$\nabla \cdot \nabla \times \mathbf{u} = 0$$

(3) Integral theorems:

$$\int_V \nabla \cdot \mathbf{F} dV = \oint_S \mathbf{F} \cdot \mathbf{n} da$$
$$\int_V \nabla \phi dV = \oint_S \phi \mathbf{n} da$$
$$\int_V (\nabla \times \mathbf{F}) dV = \oint_S (\mathbf{n} \times \mathbf{F}) da$$
$$\int_S (\nabla \times \mathbf{F}) \cdot \mathbf{n} da = \oint_C \mathbf{F} \cdot d\mathbf{l}$$
$$\int_S (\mathbf{n} \times \nabla \phi) da = \oint_C \phi d\mathbf{l}$$

(4) Navier–Stokes equations in cylindrical polar coordinates:

$$\frac{\partial}{\partial t} u_r + (\mathbf{u} \cdot \nabla) u_r - \frac{u_\theta^2}{r} = -\frac{1}{\rho} \frac{\partial p}{\partial r} + \nu \left(\nabla^2 u_r - \frac{u_r}{r^2} - \frac{2}{r^2} \frac{\partial u_\theta}{\partial \theta} \right)$$
$$\frac{\partial u_\theta}{\partial t} + (\mathbf{u} \cdot \nabla) u_\theta + \frac{u_r u_\theta}{r} = -\frac{1}{\rho r} \frac{\partial p}{\partial \theta} + \nu \left(\nabla^2 u_\theta + \frac{2}{r^2} \frac{\partial u_r}{\partial \theta} - \frac{u_\theta}{r^2} \right)$$
$$\frac{\partial u_z}{\partial t} + (\mathbf{u} \cdot \nabla) u_z = -\frac{1}{\rho} \frac{\partial p}{\partial z} + \nu \nabla^2 u_z$$

Appendix 2

Stability Criteria for Ideal MHD Based on the Hamiltonian

This appendix is a generalisation of the discussion of stability given in §6.4. There are several systematic approaches to developing sufficient conditions for the stability of ideal (conservative) flows. The Kelvin–Arnold[1] variational principle, and the energy–Casimir[2] method are, perhaps, the best known (see Morrison, 1998, or Davidson, 1998, for a review of these). Both methods are, in effect, elaborate procedures for constructing an (energy-like) functional which is (i) quadratic in the disturbance, and (ii) conserved by the linearised dynamics. Provided the resulting integral invariant is non-zero for all possible disturbance shapes, it can be used like a Lyaponov functional to bound the growth of disturbances. That is to say, if $\|\delta\mathbf{u}\|$ is some norm for the disturbance, and $\delta^2 F$ a conserved quadratic function of $\delta\mathbf{u}$ then the flow will be unstable if $\|\delta\mathbf{u}\|$ grows despite the conservation of $\delta^2 F$, and so for instability we require $\|\delta\mathbf{u}\|^2/\delta^2 F \to \infty$. Consequently, if there exist bounds of the form $|\delta^2 F| \geq \lambda\|\delta\mathbf{u}\|^2$for all $\delta\mathbf{u}$, then the flow cannot be unstable. In short, stability is ensured if $\delta^2 F$ is positive or negative definite.

However, as we shall see, there exists a third procedure for creating a conserved, quadratic functional. Like the Kelvin–Arnold and energy–Casimir methods it relies (in some sense) on the conservation of energy. However, unlike these other methods, it is the Lagrangian, L, rather than the energy, E, which plays the central rôle. We shall describe this procedure in a moment, but we might note in passing that it relies on expanding the Lagrangian up to quadratic terms in particle displacement, using Lagrange's equations to discard the first variation in L, and then con-

[1] This principle is often attributed to Arnold, but actually is was first stated (without proof) by Kelvin in 1887 (see Phil. Mag. **23**, 529–539.) Indeed, Kelvin used it to prove what is now known as Rayleigh's inflection point theorem. It was later rediscovered by Arnold in 1966.

[2] A Casimir is any integral invariant other than energy.

structing a conserved Hamiltonian for the truncated system. In order to differentiate this procedure from the Kelvin–Arnold and energy–Casimir methods we briefly summarise these other approaches.

In the Kelvin–Arnold method the appropriate functional is the disturbance energy $\Delta E = E - E_0$, where E_0 is the energy of the base flow. Evidently, ΔE is conserved by the perturbed flow. However, in order to ensure that ΔE is quadratic in the disturbance it is necessary to insist that $\delta^1 E = 0$. It turns out that this can be achieved by restricting the choice of disturbances to those which conserve the topological (frozen-in) invariants of the flow. (Such perturbations are termed isovortical perturbations in the case of Euler flows, or generalised isovortical perturbations for other systems.) In such cases, $\delta^2 E$ provides a conserved, quadratic measure of the disturbance (as far as the linearised dynamics are concerned), and stability to infinitesimal disturbances is then ensured if $\delta^2 E$ is positive or negative definite. The art of applying the Kelvin–Arnold variational principle lies in spotting how to conserve all of the topological (frozen-in) invariants when calculating ΔE, i.e. knowing how to construct the generalised isovortical perturbations. This is readily achieved for Euler flows where it is necessary only to ensure that Ω is frozen-in during the disturbance. However, it becomes quite intricate when it comes to MHD, where it becomes necessary to ensure that **B** is frozen-in as well as to conserve the cross-helicity of **B** and **u**.

In the energy–Casimir method, on the other hand, the appropriate functional is $A = E + C$ where C (the Casimir) is an integral invariant for the flow which reflects, as generally as possible, the frozen-in (topological) invariants such as helicity, cross-helicity etc. If C is constructed in a sufficiently general way, then it is usually possible to choose the precise form of C such that $\delta^1 A = 0$ at equilibrium (i.e. we choose C so that $\delta^1 C = -\delta^1 E$). Linear stability is then ensured if $\delta^2 A$ is positive or negative definite. The Kelvin–Arnold and energy–Casimir methods are, in fact, closely related, with C playing the rôle of a Lagrange multiplier, effectively building in the topological constraints required by the Kelvin–Arnold method (see, e.g. Davidson, 1998)

The use of conserved, quadratic functionals (which are non-zero for all possible disturbance shapes) to bound the growth of perturbations is often referred to as establishing *formal stability*.

We now differentiate our procedure from the Kelvin–Arnold and energy–Casimir methods. A trivial example taken from mechanics will suffice to show the difference. Consider a particle of mass m moving in a circular orbit of radius r_0 under the influence of the radial force

$\mathbf{F} = f(r)\hat{\mathbf{e}}_r$. Suppose that f has potential $V, f = -V'(r)$ and let $\Gamma = r^2\dot{\theta}$ be the angular momentum of the particle. (We restrict ourselves to two-dimensional motion and use polar coordinates r and θ.) We now perturb the trajectory, $r = r_o + \eta$, $\theta = \theta_0 + \zeta/r_0$, and examine the linear stability of the perturbed trajectory. For this simple system a conventional perturbation analysis provides the necessary and sufficient conditions for stability. The trajectory is stable if and only if $[r_0^3 V_0'' + 3r_0^2 V_0'] > 0$.

Let us now see if we can obtain the same information using the energy principles described above. The energy of the particle on the perturbed path is

$$E = T + V = \frac{1}{2}m(\dot{r}^2 + r^2\dot{\theta}^2) + V = E_0 + \delta^1 E + \delta^2 E + \ldots$$

where δ^1 and δ^2 represent terms which are linear and quadratic in the disturbance, respectively. For arbitrary values of η and ζ, $\delta^1 E$ is non-zero. Thus, despite the conservation of E, $\delta^2 E$ does not, in general, provide a conserved, quadratic measure of the disturbance. (Remember, formal stability requires that we can find a conserved, quadratic measure of the disturbance which is positive or negative definite.) In the Kelvin–Arnold procedure we remedy this as follows. We note that the particle conserves not only E but also Γ. We now restrict ourselves to initial perturbations in which $\delta\Gamma = 0$. Since $\delta\Gamma = 0$ at $t = 0$, it must remain zero for all t. Thus we write E as

$$E = \frac{1}{2}m(\dot{r}^2 + \Gamma^2/r^2) + V(r)$$

and treat Γ as a constant, $\Gamma = \Gamma_0$. For this restricted set of disturbances we find $\delta^1 E = 0$ and $\delta^2 E = \frac{1}{2}m\dot{\eta}^2 + \frac{1}{2}\eta^2[V'' + 3V'/r]_0$. In this case conservation of E does indeed ensure that $\delta^2 E$ is conserved by the disturbance (to quadratic order), and so we have formal stability if $\delta^2 E > 0$ for all possible η and $\dot{\eta}$. Thus stability is ensured if $[r^3 V'' + 3r^2 V']_0 > 0$, which coincides with our conventional perturbation analysis. Note that the Kelvin–Arnold method only provides a stability criterion for a restricted set of perturbations (in this case ones where $\delta\Gamma = 0$), although it is readily verified that the value of $\delta\Gamma$ at $t = 0$ does not influence the stability of the perturbed trajectory.

The energy–Casimir method also requires that we spot that Γ is conserved by the particle, although this time there is no need to restrict the form of the initial disturbance. It proceeds as follows. We introduce the generalised invariant, $A = E + C(\Gamma)$ where C is an arbitrary function of Γ (a Casimir). We now choose C such that $\delta^1 A = 0$ for all possible choices

of η and ζ (this requires $C = -m\theta_0\Gamma$). It follows that $\delta^2 A$ is conserved by the motion. It is readily confirmed that

$$\delta^2 A = \frac{1}{2}m(\dot{\eta}^2 + \dot{\zeta}^2) + \frac{1}{2}\eta^2[V_0'' - V_0'/r_0]$$

We have formal stability if $\delta^2 A > 0$ for all (η, ζ) and this requires that $V_0'' - V_0'/r_0 > 0$. This coincides with our perturbation analysis since $V_0'' - V_0'/r_0 > 0$ ensures that $V_0'' + 3V_0'/r_0 > 0$. Thus the energy–Casimir method has provided a sufficient (though not necessary) condition for stability.

The third approach does not require that the Casimir invariants of the system (in this case Γ) be identified, although it still relies on the conservation of energy. We proceed as follows. Let $L = T - V$ and η and ζ be generalised coordinates, q_i. We now evaluate

$$L = L_0 + \delta^1 L + \delta^2 L + \ldots$$

and calculate the generalised momenta, $p_i = \partial L/\partial \dot{q}_i$. The final step is to evaluate the Hamiltonian, H:

$$H = \sum (p_i \dot{q}_i) - L$$

Since L is not an explicit function of time, H is an invariant. It turns out that

$$e = H + L_0 = \frac{1}{2}m(\dot{\eta}^2 + \dot{\zeta}^2) + \frac{1}{2}\eta^2[V_0'' - V_0'/r_0]$$

Once again we have a conserved quadratic measure of the disturbance and the motion is stable provided that e is positive definite.

Now in this simple example the third procedure offers no obvious advantage over the others. However, when it comes to more complex systems, where it is by no means obvious what the Casimir invariants are, it does provide an advantage, as we shall see.

We shall now show that for any conservative system

$$\boxed{e = \frac{1}{2}\int \dot{\boldsymbol{\eta}}^2 dV - d^2 L(\eta) = \text{constant}} \qquad \text{(A2.1)}$$

which is a generalisation of (6.51). (Here $\boldsymbol{\eta}$ is the virtual displacement field introduced in Section 6.4.2.) This furnishes a variety of stability criteria. The proof of (A2.1) relies on expanding the Lagrangian up to second order in the particle displacements, invoking Lagrange's equation to dis-

pense with the first variation in L, and then performing a transformation to create a conserved Hamiltonian, which is quadratic in the disturbance. The first and most important step is to introduce the Lagrangian displacement,

$$\boldsymbol{\zeta}(\mathbf{x}, t) = \mathbf{x}_p(t) - \mathbf{x}_{p0}(t)$$

where $\mathbf{x}_{p0}$ is the position vector of particle p in the base flow and $\mathbf{x}_p$ is the position of the same particle in the perturbed flow. The generalisation of (6.15) is then

$$\frac{\partial \boldsymbol{\zeta}}{\partial t} + \mathbf{u}_0(\mathbf{x}) \cdot \nabla \boldsymbol{\zeta} = \frac{D\boldsymbol{\zeta}}{Dt} = \mathbf{u}(\mathbf{x} + \boldsymbol{\zeta}, t) - \mathbf{u}_0(\mathbf{x}) \tag{A2.2}$$

In the linear (small amplitude) approximation, this becomes

$$\frac{\partial \boldsymbol{\zeta}}{\partial t} + \mathbf{u}_0 \cdot \nabla \boldsymbol{\zeta} = \delta\mathbf{u}(\mathbf{x}, t) + \mathbf{u}_0(\mathbf{x} + \boldsymbol{\zeta}) - \mathbf{u}_0(\mathbf{x}) \tag{A2.3}$$

which, using the approximation $\mathbf{u}_0(\mathbf{x} + \boldsymbol{\zeta}) - \mathbf{u}_0(\mathbf{x}) = \boldsymbol{\zeta} \cdot \nabla \mathbf{u}_0$, simplifies to

$$\delta^1\mathbf{u} = \dot{\boldsymbol{\zeta}} + \nabla \times [\boldsymbol{\zeta} \times \mathbf{u}_0] \tag{A2.4}$$

The key step is now to switch from $\boldsymbol{\zeta}$ to $\boldsymbol{\eta}(\mathbf{x}, t)$, the virtual displacement field. (The two are related by (6.19).) This greatly simplifies the subsequent analysis. Since $\boldsymbol{\eta}$ and $\boldsymbol{\zeta}$ are equal to leading order, (A2.4) yields

$$\delta^1\mathbf{u} = \dot{\boldsymbol{\eta}}(\mathbf{x}, t) + \nabla \times [\boldsymbol{\eta} \times \mathbf{u}_0] \tag{A2.5}$$

Returning to (A2.2), but retaining terms up to second order, we find

$$\delta^2\mathbf{u} = \frac{1}{2}\nabla \times [\boldsymbol{\eta} \times \dot{\boldsymbol{\eta}}] + \frac{1}{2}\nabla \times [\boldsymbol{\eta} \times (\nabla \times (\boldsymbol{\eta} \times \mathbf{u}_0))] \tag{A2.6}$$

We now introduce some notation. We take δ to represent an arbitrary (physically realisable) variation of some field, say $\delta\mathbf{u}$. We take d, on the other hand, to represent a frozen-in variation of any field. In the case of the **B**-field, the two coincide ($\delta\mathbf{B} = d\mathbf{B}$) since (6.42) demands that, if **B** is frozen into the fluid during the initial perturbation, then it is frozen in for all subsequent time. In the case of **u**, however, $d\mathbf{u}$ does not represent a dynamically meaningful perturbation. Nevertheless, we are still free to ask what happens to **u** and T (the kinetic energy) in the event of a variation in which the **u**-lines are frozen in. What we choose to do with that information is another matter. From (6.17) and (6.20) (with **u** replacing **B**) we have, in terms of the virtual displacement field,

$$d^1\mathbf{u} = \nabla \times (\boldsymbol{\eta} \times \mathbf{u}_0), \qquad d^2\mathbf{u} = \frac{1}{2}\nabla \times [\boldsymbol{\eta} \times d^1\mathbf{u}] \tag{A2.7}$$

$$d^1T = \int (\mathbf{u}_0 \cdot d^1\mathbf{u})dV, \qquad d^2T = \frac{1}{2}\int [(d^1\mathbf{u})^2 + 2\mathbf{u}_0 \cdot d^2\mathbf{u}]dV \tag{A2.8}$$

Evidently,

$$\delta^1\mathbf{u} = \dot{\boldsymbol{\eta}} + d^1\mathbf{u}, \qquad \delta^2\mathbf{u} = \frac{1}{2}\nabla \times [\boldsymbol{\eta} \times \dot{\boldsymbol{\eta}}] + d^2\mathbf{u} \tag{A2.9}$$

(The equivalent expressions in terms of ζ are far more complicated.) We shall return to these expressions shortly. In the meantime, let us try to understand the significance of d-perturbation as applied to $\mathbf{u}$. We shall use the term 'd-variation' to mean a perturbation of the equilibrium configuration in which: (i) $\mathbf{u}$ is perturbed according to (A2.7), i.e. the $\mathbf{u}$-lines are frozen in during the perturbations; (ii) any auxiliary field, such as $\mathbf{B}$, is perturbed in a manner compatible with the governing equations, e.g. $\mathbf{B}$ is frozen in. (This requires that the perturbations in $\mathbf{B}$ are given by (6.17).) Also, let us introduce a generalised version of the Euler equation in the form

$$\frac{\partial \mathbf{u}}{\partial t} = \mathbf{u} \times \boldsymbol{\Omega} - \nabla C + \mathbf{f} \tag{A2.10}$$

where $\mathbf{f}$ is any conservative body force, such as $[\mathbf{J} \times \mathbf{B}]/\rho$. Let V be the potential energy associated with $\mathbf{f}$. This could, for example, be magnetic energy, gravitational energy, or some combination of these. From (A2.7) and (A2.8),

$$d^1T = \int [\boldsymbol{\Omega}_0 \cdot (\boldsymbol{\eta} \times \mathbf{u}_0)]d\mathbf{x} = -\int \boldsymbol{\eta} \cdot \mathbf{f}_0 d\mathbf{x} = d^1V \tag{A2.11}$$

It follows that $d^1L = 0$ under this type of variation, which is the first hint that there is, in fact, some significance to our d-variation. Actually, in two dimensions, the physical significance of $d\mathbf{u}$ is that, by advecting the $\mathbf{u}$-lines, we create a new set of particle trajectories with the special property that the time of flight between two fixed points is preserved. This is precisely the sort of perturbation demanded by Hamilton's principle and $d^1L = 0$ is, in fact, a direct consequence of Hamilton's principle (see Davidson, 1998.) In three dimensions we must do a little more work to explain the significance of $d^1L = 0$. Once again it rests on the fact that the time of flight of a fluid particle is preserved by the d-variation. To see that this is so, consider the time of flight equation

$$t_B - t_A = \int_A^B \frac{d\mathbf{l}}{|\mathbf{u}|} = \frac{1}{\Phi}\int_A^B dV \tag{A2.12}$$

Here Φ is the volume flux down a stream-tube which surrounds a path-line linking A and B, and $\int dV$ is the volume of the stream-tube (of rectangular cross section) which may be constructed from pairs of intersecting stream surfaces which, in turn, might be locally represented by Clebsch variables. Such stream surfaces are frozen into the fluid during a d-perturbation and so, as in two dimensions, the time of flight of fluid particles is preserved. This ensures that the first variation of the action integral is zero, and it is this which lies behind (A2.11).

So the idea of a *d-variation* has some physical basis. We now examine second variations, and this will lead to our stability criterion (A2.1). The first step is to calculate $\Delta T = T - T_0$ and $\Delta L = L - L_0$ for an arbitrary (physically realisable) δ-variation of the equilibrium state. We have

$$\delta^1 T = \int \mathbf{u}_0 \cdot \delta^1 \mathbf{u} dV, \qquad \delta^2 T = \frac{1}{2}\int \left[\left(\delta^1 \mathbf{u}\right)^2 + 2\mathbf{u}_0 \cdot \delta^2 \mathbf{u} \right] dV$$

Next, using (A2.9) to substitute for $\delta^1 \mathbf{u}$ and $\delta^2 \mathbf{u}$, we find

$$\delta^1 T = d^1 T(\boldsymbol{\eta}) + \int \mathbf{u}_0 \cdot \dot{\boldsymbol{\eta}} dV \tag{A2.13}$$

$$\delta^2 T = d^2 T(\boldsymbol{\eta}) + \frac{1}{2}\int \dot{\boldsymbol{\eta}}^2 dV + \hat{I}(\boldsymbol{\eta}, \dot{\boldsymbol{\eta}}) \tag{A2.14}$$

where $\hat{I}$ is bi-linear in $\boldsymbol{\eta}$ and $\dot{\boldsymbol{\eta}}$ and is given by

$$\hat{I} = \frac{1}{2}\int \dot{\boldsymbol{\eta}} \cdot \left[2d^1 \mathbf{u} + \boldsymbol{\Omega}_0 \times \boldsymbol{\eta} \right] dV \tag{A2.15}$$

Now if $\mathbf{f}$ is conservative, then the potential energy, V, will depend only on the instantaneous configuration of the flow and not on its history. Thus,

$$\Delta V = V - V_0 = \delta^1 V(\boldsymbol{\eta}) + \delta^2 V(\boldsymbol{\eta}) + \text{H.O.T.}$$

This gives us an expression for ΔL in terms of $\boldsymbol{\eta}$ and $\dot{\boldsymbol{\eta}}$:

$$\Delta L = \frac{1}{2}\int \dot{\boldsymbol{\eta}}^2 dV + \left[d^1 T(\boldsymbol{\eta}) - \delta^1 V(\boldsymbol{\eta}) \right] + \left[d^2 T(\boldsymbol{\eta}) - \delta^2 V(\boldsymbol{\eta}) \right] + I(\boldsymbol{\eta}, \dot{\boldsymbol{\eta}}) + \text{H.O.T}$$

where $I(\boldsymbol{\eta}, \dot{\boldsymbol{\eta}}) = \hat{I} + \int \mathbf{u}_0 \cdot \dot{\boldsymbol{\eta}} dV$. Now recall that we defined our *d-variation* such that $\mathbf{u}$ is perturbed according to (A2.7), but the auxiliary fields, such as $\mathbf{B}$ and ρ, are varied in a physically realisable manner. (This requires that $\mathbf{B}$ is frozen in.) It follows that, as a matter of notation, we can write $\delta^1 V = d^1 V$ and $\delta^2 V = d^2 V$. Our expression for the Lagrangian becomes

$$\Delta L = \frac{1}{2}\int \dot{\eta}^2 dV + [d^1 T(\eta) - d^1 V(\eta)] + [d^2 T(\eta) - d^2 V(\eta)] + I(\eta, \dot{\eta})$$

We now use η as a set of generalised coordinates describing the instantaneous state of the system. Note that ΔL is a function only of η and $\dot{\eta}$. It is not an explicit function of time. Now for a system with a finite number of degrees of freedom, η_i, we have

$$\frac{d}{dt}\left(\frac{\partial L}{\partial \dot{\eta}_i}\right) - \frac{\partial L}{\partial \eta_i} = 0 \tag{A2.16}$$

so that steady solutions are represented by $\partial L/\partial \eta_i = 0$. Also if $L = L(\eta_i, \dot{\eta}_i)$ is not an explicit function of time, the system possesses a conserved Hamiltonian:

$$e = \dot{\eta}_i \frac{\partial L}{\partial \dot{\eta}_i} - L = \text{constant}$$

The equivalent results for our continuous system are that $d^1 L = 0$ for an equilibrium solution and

$$e = \left[\int \dot{\eta}^2 dV + I(\eta, \dot{\eta})\right] - \Delta L = \text{constant}$$

The fact that $d^1 L = 0$ follows directly from Lagrange's equations is reassuring since (for two-dimensional flows) we have already noted that this may be deduced from Hamilton's principle. Next, substituting for ΔL yields, at last, our conserved, quadratic functional:

$$\boxed{e = \frac{1}{2}\int \dot{\eta}^2 dV - d^2 L(\eta) = \text{constant}, \qquad d^1 L(\eta) = 0} \tag{A2.17}$$

$$\boxed{d^2 L(\eta) = \frac{1}{2}\int \left[(d^1 \mathbf{u})^2 + \mathbf{u}_0 \cdot \nabla \times (\eta \times d^1 \mathbf{u})\right] dV - \delta^2 V(\eta)} \tag{A2.18}$$

This is the key result. Since e is a conserved quadratic measure of the disturbance, many stability criteria may be established on the back of (A2.17). We might refer to (A2.17) as a principle of maximum action.

The following two theorems follow directly from (A2.17) and (A2.18).

Theorem 1

The equilibrium of any conservative, incompressible flow possesses (formal) stability provided that

$$d^2L(\boldsymbol{\eta}) = \frac{1}{2}\int\left[\left(d^1\mathbf{u}\right)^2 + \mathbf{u}_0 \cdot \nabla \times \left(\boldsymbol{\eta} \times d^1\mathbf{u}\right)\right]dV - \delta^2 V(\boldsymbol{\eta}),$$

$$d^1\mathbf{u} = \nabla \times (\boldsymbol{\eta} \times \mathbf{u}_0)$$

is negative definite for all possible $\boldsymbol{\eta}$.

Theorem 2

The equilibrium of any conservative, incompressible flow posses (formal) stability provided that

$$e = \frac{1}{2}\int \dot{\boldsymbol{\eta}}^2 dV - d^2L(\boldsymbol{\eta}), \qquad \dot{\boldsymbol{\eta}} = \delta^1\mathbf{u} - \nabla \times (\boldsymbol{\eta} \times \mathbf{u}_0)$$

is positive or negative definite for all possible perturbations of the equilibrium.

It is easy to show that special cases of Theorem 1 are Rayleigh's circulation criterion, the Rayleigh–Taylor criterion for stratified fluids, Bernstein's (1958) principle for magnetostatics (c.f.(6.32)), and Friedlander & Vishik's (1990) and Frieman & Rottenberg's (1960) stability tests for ideal MHD equilibria (c.f. (6.51)). A special case of Theorem 2 is Arnold's (1966) variational principle for Euler flows.

Note that (A2.16) also furnishes the governing equation for $\boldsymbol{\eta}(\mathbf{x}, t)$. Substituting for ΔL in (A2.16) yields,

$$\ddot{\boldsymbol{\eta}} + 2\mathbf{u}_0 \cdot \nabla\dot{\boldsymbol{\eta}} = \nabla(\dot{\boldsymbol{\eta}} \cdot \mathbf{u}_0) + \mathbf{F}(\boldsymbol{\eta}) \tag{A2.19}$$

where

$$F_i(\boldsymbol{\eta}) = \frac{\delta\left[d^2L(\boldsymbol{\eta})\right]}{\delta\eta_i} \tag{A2.20}$$

The form of $\mathbf{F}(\eta)$ depends on the nature of the body force. When $\mathbf{f} = \mathbf{J} \times \mathbf{B}$, as in ideal MHD, the **B**-field is frozen in during the perturbation and we have

$$\delta^2 V(\boldsymbol{\eta}) = \frac{1}{2}\int\left[\left(d^1\mathbf{B}\right)^2 + \mathbf{B}_0 \cdot \nabla \times \left(\boldsymbol{\eta} \times d^1\mathbf{B}\right)\right]dV, \qquad d^1\mathbf{B} = \nabla \times (\boldsymbol{\eta} \times \mathbf{B}_0)$$

(This is just $\delta^2 E_B$ given by (6.20).) In this case (A2.20) yields, after a little algebra,

$$\begin{aligned}\mathbf{F} = \mathbf{u}_0 \times \left[\nabla \times \left(d^1\mathbf{u}\right)\right] + d^1\mathbf{u} \times [\nabla \times \mathbf{u}_0] \\ - \mathbf{B}_0 \times \left[\nabla \times (d^1\mathbf{B})\right] - d^1\mathbf{B}) \times [\nabla \times \mathbf{B}_0] + \nabla(\sim)\end{aligned} \tag{A2.21}$$

which is identical to (6.45).

We conclude by showing that the Kelvin–Arnold variational principle, as applied to Euler flows, is a special case of Theorem 2. We start by noting that, when $\mathbf{f} = 0$, (A2.19) becomes

$$\ddot{\boldsymbol{\eta}} + 2\mathbf{u}_0 \cdot \nabla\dot{\boldsymbol{\eta}} = \mathbf{u}_0 \times \left(\nabla \times d^1\mathbf{u}\right) + d^1\mathbf{u} \times (\nabla \times \mathbf{u}_0) + \nabla(\cdot)$$

This may be integrated once to give

$$\dot{\boldsymbol{\eta}} = \boldsymbol{\eta} \times \boldsymbol{\Omega}_0 - \nabla \times (\boldsymbol{\eta} \times \mathbf{u}_0) + \mathbf{m} + \nabla(\cdot)$$

where $\mathbf{m}$ is independent of $\boldsymbol{\eta}$ and is governed by

$$\partial\mathbf{m}/\partial t = \nabla \times (\mathbf{u}_0 \times \mathbf{m})$$

It follows from (A2.9) that

$$\delta^1\mathbf{u} = \boldsymbol{\eta} \times \boldsymbol{\Omega}_0 + \mathbf{m} + \nabla(\cdot)$$

If, at $t = 0$, we specify that $\mathbf{m} = 0$, then $\mathbf{m}$ will be zero for all time. In such a case

$$\delta^1\boldsymbol{\Omega} = \nabla \times (\boldsymbol{\eta} \times \boldsymbol{\Omega}_0)$$

Evidently, this is a perturbation in which the $\boldsymbol{\Omega}$-lines are frozen into the fluid – an *isovortical perturbation*. The Kelvin–Arnold principle states that a steady Euler flow is stable provided that $\delta^2 T$ is positive definite or negative definite under an isovortical perturbation. Let us denote such a perturbation by $\hat{d}$, to distinguish it from a general perturbation, δ. However, using (A2.9) it is readily confirmed that

$$\hat{d}^2 T = \frac{1}{2}\int \dot{\boldsymbol{\eta}}^2 dV - d^2 T = e$$

Thus the Kelvin–Arnold principle is simply a special case of Theorem 2.

Appendix 3

Physical Properties of Liquid Metals

Metal	Melting point (°C)	Reference temperature (°C)	Density (10^3 kg/m^3)	Kinematic viscosity (10^{-6} m^2/s)	Electrical conductivity ($10^6 \Omega^{-1}$m^{-1})	Thermal conductivity (Wm^{-1}C^{-1})
Titanium	1685	1700	4.1	1.3	0.58	–
Steel[1]	1495	1600	7.0	0.88	0.71	26
Iron	1535	1600	7.0	0.80	0.72	41
Nickel	1454	1500	7.9	0.62	1.2	–
Copper	1083	1100	7.9	0.51	4.8	160
Aluminium	660	700	2.4	0.60	4.1	95
Magnesium	650	700	1.6	0.80	3.6	81
Tin	232	280	6.9	0.28	2.1	31
Lithium	181	200	0.51	1.2	4.0	47
Sodium	98	100	0.92	0.68	10	89
Woods metal	70	100	9.7	0.29	0.98	8.0
Potassium	64	70	0.82	0.58	7.0	52
Galium	30	70	6.1	0.31	3.8	30
NaK[2]	−12	40	0.87	0.86	2.6	22
Mercury	−38	30	13.5	0.12	1.0	8.0

Notes: [1] Approximate values for steel with .2% carbon.
[2] Sodium–potassium eutectic.

Appendix 4

MHD Turbulence at Low R_m

We have commented on MHD turbulence in a number of places in this book. In Chapter 7 we discussed the decay laws for freely evolving MHD turbulence, while in Chapter 9 we examined the influence of an intense magnetic field on isolated vortices. The purpose of this appendix is to pull together these various threads and to produce a coherent picture of MHD turbulence at low R_m. We shall restrict ourselves to statistically homogeneous turbulence, so that the influence of boundaries may be ignored. We shall assume that there is no mean motion.

We are interested in the evolution of turbulence in a uniform, imposed magnetic field, $\mathbf{B}_0$. For simplicity, the initial conditions are taken to be statistically isotropic and R_m is assumed to be small. This latter condition implies that the induced magnetic field is negligible by comparison with the imposed field.

The nature of MHD turbulence depends crucially on the initial value of the interaction parameter, $N = \sigma B_0^2 l/\rho u$, where l is the integral scale of the turbulence and u is a typical velocity fluctuation, say $u = \left(\langle u_x^2 \rangle\right)^{1/2}$. When N is initially small, $\mathbf{J} \times \mathbf{B}_0$ is negligible by comparison with inertia and the turbulence evolves as discussed in Section 1.5 of Chapter 7. We then have conventional, decaying turbulence. This is governed by two equations:

$$\frac{du^2}{dt} = -\alpha \frac{u^3}{l}$$

$$\int r^2 \langle \mathbf{u} \cdot \mathbf{u}' \rangle d\mathbf{r} = \text{constant}$$

The first of these describes the rate at which energy is lost by the large eddies to the energy cascade, the large eddies breaking up on a timescale of l/u, the eddy turn-over time. The coefficient α is found experimentally

to lie in the range $a = 1.0 \rightarrow 1.2$. The second equation represents the conservation of Loitsyansky's integral and implies that

$$u^2 l^5 = \text{constant}$$

These equations may be combined to yield Kolmogorov's decay laws

$$u^2 = u_0^2[1 + (7\alpha/10)(u_0 t/l_0)]^{-10/7}, \qquad l = l_0[1 + (7\alpha/10)(u_0 t/l_0)]^{2/7}$$

where u_0 and l_0 are the initial values of u and l.

When N is very large, on the other hand, the turbulence is governed by the linearised equation of motion

$$\rho \frac{\partial \mathbf{u}}{\partial t} = -\nabla(P) + \mathbf{J} \times \mathbf{B}_0$$

(Recall that $\mathbf{J}$ is linear in $\mathbf{u}$.) In view of the linearity of this equation, we might regard the turbulence as an ensemble of independent eddies. Some of the eddies will have an axis of rotation which is more or less aligned with $\mathbf{B}_0$. Some will be non-aligned. These eddies will evolve in a manner not unlike those described in Section 4 of Chapter 9. Vortices whose axes of rotation are initially aligned with $\mathbf{B}_0$ will develop into long, columnar structures, with characteristic length scales, $l_{//}$ and $l_\perp$, evolving as $l_\perp \sim l_0$ and $l_{//} \sim l_0(t/\tau)^{1/2}$, where τ is the Joule damping time, $(\sigma \mathbf{B}_0^2/\rho)^{-1}$. The energy of such an eddy declines as $u^2 \sim u_0^2(t/\tau)^{-1/2}$. Vortices which are initially perpendicular to $\mathbf{B}_0$, on the other hand, will develop into sheet-like structures consisting of thin, interwoven layers of oppositely signed vorticity (see Chapter 9, Section 4). The dominant velocity component in these sheets is $\mathbf{u}_{//}$. Like the columns, we find $l_\perp \sim l_0$, $l_{//} \sim l_0(t/\tau)^{1/2}$ and $u^2 \sim u_0^2(t/\tau)^{-1/2}$. Thus, as long as N remains large, we expect two distinct types of structures to emerge from isotropic initial conditions: columns and sheets. We might anticipate that more sheets than columns will develop since relatively few vortices will have their axis of rotation aligned with $\mathbf{B}_0$ at $t = 0$. If this is the case, we might expect $\mathbf{u}_{//}^2$ gradually to exceed $\mathbf{u}_\perp^2$ as the anisotropy develops. In fact, this is exactly what is observed in numerical experiments, with $\mathbf{u}_{//}^2 \sim 2\mathbf{u}_\perp^2$ at large times.

The energy equation governing high-N turbulence is the Joule dissipation equation (5.7)

$$\frac{d}{dt}\left[\frac{1}{2}\rho < u^2 >\right] = - < J^2 > /\sigma$$

Using (5.6b) to estimate $\langle J^2 \rangle$, this yields

$$\frac{du^2}{dt} \sim -\frac{1}{\tau}\left(\frac{l_\perp}{l_{//}}\right)^2 u^2$$

which we might rewrite as

$$\frac{du^2}{dt} = -\beta\left(\frac{l_\perp}{l_{//}}\right)^2 \frac{u^2}{\tau}$$

where β is a coefficient of order unity. (For isotropic turbulence it is possible to show that $\beta = \frac{2}{3}$.) In addition, conservation of the Loitsyansky integral for MHD turbulence yields (see equation 7.49)

$$u^2 l_{//} l_\perp^4 = \text{constant}$$

Moreover, when N is large, we know from our analysis of individual vortices that $l_\perp = \text{constant}$ on a time scale of τ. It follows that the two expressions above may be combined to yield

$$u^2 = u_0^2[1 + 2\beta t/\tau]^{-1/2}$$

$$l_{//} = l_0[1 + 2\beta t/\tau]^{1/2}$$

$$l_\perp = l_0$$

Let us now consider the case where N takes some intermediate value, perhaps of order unity. The energy equation must now combine the influence of the energy cascade and Joule dissipation. From (7.48) we have

$$\boxed{\frac{du^2}{dt} = -\alpha\frac{u^3}{l_\perp} - \beta\left(\frac{l_\perp}{l_{//}}\right)^2 \frac{u^2}{\tau}} \qquad \text{(A4.1)}$$

Moreover, we still have conservation of Loitsyansky's integral for MHD turbulence:

$$\boxed{u^2 l_{//} l_\perp^4 = \text{constant}} \qquad \text{(A4.2)}$$

Unfortunately, these two equations are insufficient to determine the three unknowns $l_{//}$, $l_\perp$ and u. Let us introduce a third, heuristic equation for $l_{//}/l_\perp$. When N is small we have $l_{//} \sim l_\perp$ on a timescale of l/u. Conversely, when N is large, we have $l_{//}/l_\perp \sim (1 + 2\beta t/\tau)^{1/2}$. Both extremes ($N \gg 1$ and $N \ll 1$) satisfy

$$\frac{d}{dt}\left(\frac{l_{//}}{l_\perp}\right)^2 = \frac{2\beta}{\tau} \tag{A4.3}$$

Let us suppose that the heuristic equation (A4.3) also applies for intermediate values of N. Then (A4.1)–(A4.3) provides a closed system of equations for u, $l_{//}$ and $l_\perp$. For simplicity we shall take $\alpha = \beta = 1.0$ and $l_{//} = l_\perp = l_0$ at $t = 0$. The general solution to these equations is then

$$\boxed{u^2/u_0^2 = \hat{t}^{-1/2}\left[1 + (7/15)\left(\hat{t}^{3/4} - 1\right)N_0^{-1}\right]^{-10/7}} \tag{A4.4}$$

$$\boxed{l_\perp/l_0 = \left[1 + (7/15)\left(\hat{t}^{3/4} - 1\right)N_0^{-1}\right]^{2/7}} \tag{A4.5}$$

$$\boxed{l_{//}/l_0 = \hat{t}^{1/2}\left[1 + (7/15)\left(\hat{t}^{3/4} - 1\right)N_0^{-1}\right]^{2/7}} \tag{A4.6}$$

where N_0 is the initial value of N and $\hat{t} = 1 + 2(t/\tau)$. The high- and low-N results given above are special cases of (A4.4)–(A4.6). Note that, in general, u^2, $l_{//}$ and $l_\perp$ do not obey simple power laws. However, for the special case of $N_0 = 7/15$ we have,

$$u^2/u_0^2 = \hat{t}^{-11/7}, \qquad l_{//}/l_0 = \hat{t}^{5/7}$$

The dependence $u^2 \sim t^{-11/7}$ is not far out of line with the experimental data for $N_0 \sim 1$, which suggests $u^2 \sim t^{-1.6}$.

Bibliography

Suggested Books on Fluid Mechanics

D J Acheson, *Elementary fluid dynamics*, 1990. Clarendon Press. (An excellent introductory text.)

G K Batchelor, *An introduction to fluid mechanics*, 1967. Cambridge University Press. (More than just an introduction. See Chapter 7 for vortex dynamics.)

G K Batchelor, *The theory of homogeneous turbulence*, 1953. Cambridge University Press. (A useful reference text on turbulence which is remarkably undated. See Chapter 3 for velocity correlation functions and Chapter 5 for the dynamics of decaying turbulence.)

S Chandrasekhar, *Hydrodynamic Stability*, 1981, Dover. (*The* classic text on stability theory. See Chapters 2 and 4 for Bénard convection.)

Feynman, Leighton & Sands, *The Feynman lectures on physics*, vol. II, 1964. Addison–Wesley. (Chapters 40, 41 provide a nice introduction to fluid mechanics).

J O Hinze, *Turbulence*, 1959. McGraw-Hill Co. (A useful reference text on turbulence. See Chapter 1 for the properties of velocity correlation functions, Chapter 3 for isotropic turbulence.)

L D Landau & E M Lifshitz, *Course of theoretical physics, vol. 6, Fluid mechanics*. 2nd Edition, 1987. Butterworth–Heinemann Ltd. (Chapter 3 gives a nice discussion of the general structure of turbulence.)

M Lesieur, *Turbulence in Fluids*, 1990. Kluwer Acad. Pub. (See Chapter 9 for a detailed discussion of two-dimensional turbulence.)

H Tennekes & J L Lumley, *A first course in turbulence*, 1972, The MIT Press. (Chapters 1–3 give an excellent introduction to the general structure of turbulence.)

Suggested Books on Electromagnetism

Feynman, Leighton & Sands, *The Feynman lectures on physics, Vol. II, 1964* Addison–Wesley. (Chapters 13–18 provide one of the clearest introductions to Maxwell's equations).

J D Jackson, Classical Electrodynamics. 1962. John Wiley & Sons. (A first class reference text.)

P Lorrain & D Corson, *Electromagnetism Principles and Applications*, W H Freeman & Co. (A popular, all-round introductory text on electricity and magnetism.)

Suggested Books on MHD

D Biskamp, *Nonlinear magnetohydrodynamics*, 1993. Cambridge University Press. (See Chapter 4 for stability theory and Chapter 7 for MHD turbulence at high *Rm*.)

H K Moffatt, *Magnetic field generation in electrically conducting fluids*, 1978. Cambridge University Press. (See Chapter 3 for kinematics, Chapter 5 for sunspots, and Chapters 6–12 for a detailed discussion of dynamo theory.)

R Moreau, *Magnetohydrodynamics*, 1990. Kluwer Acad. Pub. (See Chapter 4 for Hartmann layers, Chapter 5 for damping of jets, Chapter 6 for rotating flow and for the point electrode problem, and Chapter 7 for MHD turbulence at low R_m.)

M R E Proctor and A D Gilbert, *Lectures on solar and planetary dynamos*, 1994. Cambridge University Press. (See Chapter 1, by P H Roberts, for an introduction to geodynamo theory and Chapter 2, by N O Weiss, for solar MHD.)

P H Roberts, *An introduction to magnetohydrodynamics*, 1967, Longmans. (See Chapter 3 for dynamo theory (without the α-effect), Chapter 5 for Alfvèn waves and Chapters 8 & 9 for stability theory.)

J A Shercliff, *A textbook of magnetohydrodynamics*, 1965, Pergamon Press. (An excellent introductory text.)

Journal References for Part B and Appendix 2

Birat J & Chone J. 1983. 4th International Iron Steel Congress, London.

Bojarevics V & Romerio M V. 1994. Long waves instability of liquid metal–electrolyte interface in aluminium electrolysis cells: a generalisation of Sele's criterion. *Eur. J. Mech. B*, **13**: 33–56.

Bojarevics V & Millere R. 1982. Amplification of azimuthal rotation in a meridional electric vortex flow in a hemisphere. *Magnetohydrodynamics* **18**, 373.

Bojarevics V, Freidbergs Y, Shilova E I & Shcherbinin E V. 1989. Electrically Induced Vortical Flows. *Kluwer*.

Davidson PA. 1992. Swirling flow in an axisymmetric cavity or arbitrary profile driven by a rotating magnetic field. *J. Fluid Mech.* **245**: 660–99.

Davidson P A. 1995. Magnetic damping of jets and vortices. *J. Fluid Mech.* **299**: 153–86.

Davidson P A. 1997. The rôle of angular momentum in MHD turbulence. *J. Fluid Mech.*, **336**: 123–50.

Davidson P A. 1998. On the application of the Kelvin–Arnold energy principle. *J. Fluid Mech.* **356**, 221–257.

Davidson, P A & Flood, S C. 1994. *Metallurgical and Materials Trans. B* **25B**, 293.

Davidson P A & Hunt J C R. 1987. Swirling, recirculating flow in a liquid metal column generated by a rotating magnetic field. *J. Fluid Mech.* **185**: 67–106.

Davidson P A & Lindsay R I. 1998. Stability of interfacial waves in aluminium reduction cells. *J. Fluid Mech.* **362**, 273–295.

Davidson P A, Short D J & Kinnear D. 1995. The rôle of Ekman pumping in confined electromagnetically driven flows. *European Journal of Mechanics, B/Fluids.* **14** (6)

Davidson, P A et al. 1999. The role of Ekman pumping and the dominance of swirl in confined flows driven by Lorentz forces. *European J. Mech. B*, **18**,

Harada H, Okazawa K, Tanaka M Takeuchi E. 1994. The MHD counterflow around a jet from a nozzle under a DC magnetic field. *Proc. Intl. Symp. on Electromagnetic Processing of Materials, Nagoya, Japan.* Iron & Steel Institute of Japan.

Hunt J C R & Maxey, M R. 1980. Proc. 2nd Beer-Sheeva Seminar on MHD Flows and Turbulence, eds. H H Branover and A Yakhot, *Israel Univ. Press.* p 249.

Iron & Steel Institute of Japan. 1994. *Proc. Int. Symp. on Electromagnetic Processing of Materials.* Nagoya, Japan.

Kinnear D & Davidson P A. 1998. *J. Fluid Mech.*, **375**, p 319

Marr H S. 1984.. Electromagnetic stirring in continuous casting of steel. In: Proctor M R E & Moffatt H K (eds.) *Proc. Metallurgical Applications of MHD,* Cambridge, The Metals Society, 143–53.

Moffatt H K. 1967. On the suppression of turbulence by a uniform magnetic field. *J Fluid Mech.* **28.**

Moffatt H K & Proctor M R E. 1984. Metallurgical Applications of magneto-hydrodynamics. The Metal Society, London.

Moreau R. 1984. Magnetohydrodynamics. *Kluwer.*

Morrison P J. 1998. Hamiltonian description of ideal fluids. *Rev. Modern Phys.* **70**(2).

Muizhnieks A R, & Yakovich A T. 1988. Numerical study of closed axisymmetric MHD rotation in an axial magnetic field. *Magnetohydrodynamics.* **24**.

Muller G, Neumann G & Weber W. 1984. Natural convection in vertical Bridgman configurations. *J. Cryst. Growth* **70**: 78–93.

Nakamura S, Hibiy T, Yokota T & Yamamoto F. 1990. Thermal conductivity measurements of mercury in a magnetic field. *Intl. J. Heat Mass Transfer* **33**: 2609–13.

Roberts P H. 1967. An Introduction to Magnetohydrodynamics. *Longmans.*

Shercliff J A. 1970. *J. Fluid Mech.* **40**, 241.

Shtern, V & Barrero A. 1995. *J. Fluid Mech.* **300**, p 169.

Sneyd A D & Moffatt H K. 1982. *J. Fluid Mech.* **117**, p 45.

Sneyd AD & Wang A. 1994. Interfacial instability due to MHD mode coupling in aluminium reduction cells. *J. Fluid Mech.* **263**: 343–59.

Taberlet E & Fautrelle Y. 1985. Turbulent stirring in an experimental induction furnace. *J. Fluid Mech.* **159**, p 409.

Tacke K H & Schwerdtfeger K. 1979. Stirring velocities in continuously cast round billets as induced by rotating electromagnetic fields. *Stahl und Eisen* **99**: 7–12.

Takeuchi E, Masafumi Z, Takehiko T Mizoguchi S. 1992. Applied MHD in the process of continuous casting. In: *Magnetohydrodynamics in Process*

Metallurgy. Szekely J, Evans J W, Blazek K & El-Kaddah N (Eds.) *The Minerals, Metals and Materials Soc. of USA*.

Ungarish M. 1997. The spin-up of a liquid metal driven by a rotating magnetic field. *J. Fluid Mech.* **347**: 105–18.

Vlasyuk V K & Sharamkin V I. 1987. Effect of vertical magnetic field on heat and mass transfer in a parabolic liquid metal bath. *Magnetohydrodynamics* **23**.

Zibold A F et al. 1986. Hydraulic phenomenon accompanying the growth of single crystals by Czochralski's method. *Magnetohydrodynamics* **22**.

Subject Index